Atlantic Geoscience

Journal of the Atlantic Geoscience Society
V. 58 2022

Revue de la Société Géoscientifique de l'Atlantique
V. 58 2022

Atlantic Geoscience

(*formerly* Atlantic Geology)

VOLUME 58 – 2022

Published by The Atlantic Geoscience Society

Back issues are available for $15 per issue. Subscriptions, requests for back issues and remittances made payable to Atlantic Geology should be sent to Box 116, Acadia University, Wolfville, NS B4P 2R6, Canada.

Complete archives of Atlantic Geoscience are available online at: *http://journals.hil.unb.ca/index.php/AG*

ISSN 2564-2987

Printed and bound in Canada by Gaspereau Press, 47 Church Avenue, Kentville, Nova Scotia, B4N 2M1

Atlantic Geoscience

VOLUME 58 – 2022

Complete archives of Atlantic Geology/Geoscience are available online at:

http://journals.hil.unb.ca/index.php/ag

Atlantic Geoscience Society

ABSTRACTS

48th Colloquium & Annual General Meeting 2022

Virtual

The organizers and all AGS members were saddened to learn of the sudden passing of our President, Dr. Anne Marie Ryan, on January 20th, 2022. She will be greatly missed as a vital member of the society for 40 years, especially her dedication and leadership in geoscience education. Hence, this year's Colloquium is dedicated to her memory.

Once again, due to the continued Pandemic circumstances, the 2022 Colloquium & Annual General Meeting was held using the virtual venue Zoom on February 11th and 12th. On behalf of the society, we thank Colloquium organizers David Lentz, Jim Walker, Rob Raeside, Deanne van Rooyen, Alan Cardenas, and Mike Parkhill, as well the numerous session chairs and judges, for facilitating an excellent meeting with about 185 registrants. AGS acknowledges support from the corporate sponsors and partners for the meeting: Nova Scotia Department of Natural Resources and Renewables (Geoscience and Mines Branch), New Brunswick Department Natural Resources and Energy Development (Geological Surveys Branch), Engineers and Geoscientists of New Brunswick, Galway Metals, and Terrane Geoscience Inc.

In the following pages, we are pleased to publish the abstracts of oral and poster presentations from the meeting on a variety of topics. Best undergraduate and graduate student presentations are recognized and indicated by an asterisk in the title. The meeting included five special sessions: (1) Regional geology in the northern Appalachians or development of the northern Appalachians: new data and new thoughts; (2) Current research in Carboniferous geology of the Maritimes; (3) Mineral resources and metallogeny of the northern Appalachians; (4) Trace elements in crystalline rocks: abundances, variation, and geochemical interpretation; (5) Advances in paleontology; (6) Resources, remediation, and environmental protection: surficial geochemistry and geology studies; (7) The 8Gs: a new paradigm in our geologic heritage; (8) Modern surface processes and sedimentary record: linking geomorphic processes through time and a general session on geoscience research developments.

The traditional Saturday evening banquet and social were replaced by a virtual Awards Banquet at which society awards were announced, as well as student prizes for best poster and oral presentation. The student award winners are noted at the end of the appropriate abstract.

Although the abstracts have been edited as necessary for clarity and to conform to Atlantic Geoscience format and standards, the journal editors do not take responsibility for their content or quality.

THE EDITORS

ATLANTIC GEOSCIENCE 58, 1 - 41 (2022) doi: 10.4138/atlgeo.2022.001
2564-2987|22|00001-041 $7.15|0

Impurities in uraninite: examples of crustal uranium cycling in the Nonacho Basin, Northwest Territories, Canada

Erin Adlakha and Kerstin Landry

Department of Geology, Saint Mary's University, Halifax, Nova Scotia B3H 3C3, Canada <erin.adlakha@smu.ca>

Uraninite (UO_2) is the main ore of uranium and, like all minerals, pure UO_2 rarely occurs in nature. Other elements ("impurities") in major to trace abundances can substitute for U^{4+} and O^{2-} in uraninite); the charge and ionic radius of the impure elements control whether they can be incorporated in the structure of a mineral. For uraninite, these impurities are commonly Th^{4+}, Y^{3+}, REE^{3+}, Ca^{2+}, and Fe^{2+}. The abundances of these impurities in uraninite reflect the origin and environment of uraninite formation. However, the production of Pb^{4+}, a strong oxidizer, from the decay of U^{4+} complicates elemental substitution in uraninite. Tetravalent Pb oxidizes U^{4+}, producing Pb^{2+} and U^{6+}, when accumulated over time leads to the destabilization of the uraninite structure and alteration during later thermotectonic events and hydrothermal activity.

This presentation examines the impurities in different styles of U mineralization of the Paleoproterozoic Nonacho Basin of the Rae Craton, a lithotectonic segment of the Canadian Shield that hosts abundant and prolific uranium deposits (e.g., unconformity-type uranium, albitite-hosted uranium). Coupled with U–Pb geochronology, these data are used to comment on the cycling of uranium during the early assembly of Laurentia and processes responsible for its enrichment in the Rae Craton.

A diverse Late Carboniferous vertebrate and invertebrate ichnofaunal assemblage from Smith Point, Nova Scotia, Canada: implications for local stratigraphic mapping

Luke F. Allen[1], Matthew R. Stimson[2,3], John H. Calder[3,4], Tim J. Fedak[5], and Rowan E. Norrad[1]

1. Citadel High School, Halifax, Nova Scotia B3H 0A4, Canada <alf351678@gnspes.ca>;
2. Natural History Department, New Brunswick Museum, Saint John, New Brunswick E2K 1E5, Canada;
3. Department of Geology, Saint Mary's University, Halifax Nova Scotia B3H 3C3, Canada;
4. John Calder Earthworks, Halifax Central, Halifax, Nova Scotia B3J 2L4, Canada;
5. Nova Scotia Museum, Halifax, Nova Scotia B3H 3A6, Canada

The Maritimes Basin of Atlantic Canada is well known for its rich ichnological resources that span the Mississippian through earliest Permian periods. Upper Pennsylvanian strata along the Northumberland Strait of Nova Scotia have yielded large *Arthropleura* tracks at Cape John and Pugwash, as well as the first in-situ walchian conifer forest associated with a diverse tetrapod ichnofauna assemblage at Brule. Smith Point has previously yielded an articulated tetrapod skeleton (nicknamed "superstar") that is part of a concurrent project by another research group. *Arthropleura* tracks were first documented at Smith Point in the 1980s. They are the first occurrence of tetrapod tracks from that locality, associated with arthropod trackways, rare vertebrate remains, infaunal burrows, and macrofloral elements.

Exposed on the wave-cut platform, two primary sandstone horizons, interpreted as the tops of prograding channel bars, each preserve circa 25 and 40 individual *Arthropluera* trackways (*Diplichnites*). Although *Arthropleura* trackway-bearing strata are well known in Atlantic Canada, this outcrop is perhaps one of the most extensive exposures of *Arthropleura* derived *Diplichnites* tracks in the fossil record, based on trackway length and extent of the trackway surface. The adjacent cliff section exposes abundant fine-grained sandstone and mudstone interpreted as floodplain deposits. These strata commonly preserve small *Diplichnites*, infaunal meniscate backfilled burrows assigned to *Taenidium* and rare examples of *Kouphichnium*. Tetrapod tracks derive from red, flat-bedded sandstones in convex hyporelief, and convex epirelief impressions imprinted into the underlying red mudstone. The high-diversity tetrapod ichnoassemblage includes trackways that are interpreted to have been produced by pelycosaur-grade synapsids (*Dimetropus*), captorhinids (*Varanopus*), seymouriamorphs (*Amphisauropus*), temnospondyl amphibians (*Limnopus*, *Batrachichnus*), and parareptiles (*Dromopus*). Isolated bone fragments of unidentified tetrapods and xenacanthid shark teeth have also been recovered from intraformational mud chip conglomerate. This vertebrate and invertebrate ichnofaunal assemblage is inferred to have been preserved within an upland river system. Semi-articulated paleofloral elements include cordaitaleans, pecopterid tree ferns and walchian conifers which all point to a climate shift favouring drought-tolerant vegetation, consistent with the collapse of coal-forming peatland ecosystems late in the Carboniferous. Geological mapping has assigned strata at Smith Point to the Malagash Formation of the upper Cumberland Group (late Moscovian stage). However, the lithology, ichnofauna, and paleoflora all bear striking resemblance to the Brule fossil site as well as early Permian Euramerican localities, suggesting that the Smith Point strata be reassigned to the Pictou Group (late Gzhelian or younger).

Geophysical and geomorphological monitoring of coastal erosion of Bread and Cheese site, Bay Bulls town, Newfoundland, Canada

Marzieh Arshian and Alison Leitch

Department of Earth Sciences, Memorial University, St. John's, Newfoundland and Labrador A1B 3X5, Canada <marshian@mun.ca>

Coastal erosion can be a serious issue requiring accurate observation to evaluate vulnerable areas and determine the subsequent actions to address this problem. The Town of Bay Bulls, about 29 km south of St. John's, Newfoundland and Labrador, has coastal areas prone to erosion, and an important aim for the Town municipality is to reinforce these areas to avoid future road collapse. An inspection to describe an areas' geomorphological characteristics and a ground-penetrating radar (GPR) investigation were carried out along the Bay Bulls northern shoreline at the 'Bread and 'Cheese' site. To thoroughly assess an area's erosion potential, it is essential to evaluate the coastal geomorphology. Information about the geomorphological variations like wave characteristics, wind direction, fracture plane strike, slope, and beach elevation were acquired. Identifying if the beach is a steep reflective beach or flat dissipative one. can facilitate assessing the areas prone to erosion in shorelines. The shoreline at the Bread and Cheese site has steep cliffs subject to erosion by terrestrial and marine processes. The tilted bedrock is mainly light-grey sandstone, locally thinly bedded, greenish-grey to red sandstone, and siltstone. Regarding the cliff face and toe erosion, a noticeable downward dip is apparent in the cliff face due to soil creep or the slumping of the Quaternary cover including glacial diamicton. This occurrence would probably be considered a rotational slump, a common slumping type. The GPR survey was conducted along the road on a clifftop using 250 antennae, providing useful information about the underground structure. The GPR result at the Bread and Cheese area depicts the subsurface culverts, bedrock location, and highly fractured regions corresponding with the geomorphology observations.

A review of recent research relating to the Grande Anse Formation, Cumberland Basin, eastern Canada

Fadel Bahr and Dave Keighley

Department of Earth Sciences, University of New Brunswick, Fredericton, New Brunswick E3B 5A3, Canada <keig@unb.ca>

The Grande Anse Formation crops out in the Cumberland Basin north of the Minudie Anticline on the Maringouin Peninsula of southeastern New Brunswick, and in northernmost Nova Scotia. Previous biostratigraphic work indicated a temporal equivalence to some part of the Lower Pennsylvanian succession south of the Minudie Anticline in the Athol Syncline and exposed along Joggins Fossil Cliffs. Other work identified the Minudie Anticline to be a salt wall, the formation of which had a major influence on Lower Pennsylvanian sedimentation in the basin. Sedimentological studies identify similarities between facies of the Grande Anse and Ragged Reef formations south of Joggins. Both contain an abundance of red mudstone, of (semi-) humid climate, well-drained floodplain origin, interbedded with red and grey sandstone of braided, east flowing, fluvial origin. Geochemical investigation of coarse clastic deposits in the two units indicates no statistical difference in their elemental compositions. In contrast, underlying units along the Joggins coast (Little River, Joggins, and Springhill Mines formations) have visibly different facies, and many statistically significant differences in composition. The resulting working hypothesis is that salt tectonics produced oblique-to-the-north evacuation of Windsor Group (Mississippian) evaporites. This created the space that accommodated the thick succession of strata (Little River, Joggins, and Springhill Mines formations) in the developing Athol Syncline. Contemporaneously, to the north of the salt wall there was no net deposition, but uplift and folding of post-Windsor Group strata. As salt tectonism waned, any extrusive salt was then buried under strata of the Grande Anse and Ragged Reef formations. It remains unclear whether these latter two units formed contemporaneously and in disconformity to angular unconformity on older units (in which case the Ragged Reef Formation could be considered the junior synonym of the Grande Anse Formation), or whether deposition of the Ragged Reef Formation gradually onlapped both the salt wall and the folded strata further north. In the latter case, only the Spicers Cove Member of the Ragged Reef Formation might be directly equivalent, and reassignable, to the Grande Anse Formation. Petrographic studies of the Grande Anse Formation indicate that lithification was dominated by eodiagenetic processes. Several mineral phases are typical of shallow subsurface changes that would be expected in the (semi-) humid environment indicated by the sedimentology and geochemistry. However, other very distinct phases might be considered indicative of arid, evaporitic conditions; but for our understanding of the recently buried salt-wall that was likely influencing shallow groundwater chemistry.

Potential for post-glacial submarine landslides on Orphan Spur, offshore northeastern Newfoundland, Canada

Laura Broom, Vladimir Kostylev, Alexandre Normandeau, and Gordon Cameron

Geological Survey of Canada, Dartmouth, Nova Scotia B2Y 4A2, Canada <laura.broom@NRCan-RNCan.gc.ca>

Orphan Spur is a large sediment drift deposit located offshore northeastern Newfoundland. It is part of the Northeast Newfoundland Slope Closure which is closed to ground fishing to protect cold-water corals and sponges; however, it is also a region of potential hydrocarbon exploration. With competing interests involving the seabed, it is critical to assess the potential geohazards of this region. Previous studies based on limited hydroacoustic data have suggested that there are few post-glacial landslides in the area. Newly acquired hydroacoustic data including multibeam bathymetry and 3.5 kHz sub-bottom profiles reveal previously unidentified submarine landslides in the region. Some of the submarine landslides closer to the continental shelf appear relatively "fresh" in multibeam bathymetric data and the escarpments surrounding the failures appear sharp. No younger sediment cover has been resolved overlying these failures by the acoustic data. Piston and box cores were collected on the submarine landslide deposits in an attempt to constrain their timing. Preliminary results from radiocarbon dates suggest that some of the shallow submarine landslides were triggered during the Holocene. In addition, the headscarps of some of the largest failures appear to have been reactivated, probably locally, during post-glacial times. The submarine landslide hazard for Orphan Spur could therefore be underestimated and further examination into the timing of these deposits is underway.

Detection of buried rare metal mineralization in a glaciated landscape at Brazil Lake, southwestern Nova Scotia, Canada

Denise M. Brushett[1], M. Beth McClenaghan[2], and Roger C. Paulen[2]

1. Nova Scotia Geological Survey, Nova Scotia Department of Natural Resources and Renewables, Halifax, Nova Scotia B3J 2T9, Canada <denise.brushett@novascotia.ca>;
2. Geological Survey of Canada, Natural Resources Canada, Ottawa, Ontario K1A 0E8, Canada

The variable nature and thickness of glacial sediments affect the characteristics of mineralized dispersal trains in the Brazil Lake Li-Cs-Ta- (LCT) pegmatite district of southwestern Nova Scotia, an area currently being explored for its critical and rare-metal potential. The areal extent of the pegmatites at Brazil Lake are not well known because of their small size (less than 20 m wide), and extensive till cover that limits outcrop exposure. In southwestern Nova Scotia, glacial sediments blanket the region deposited over multiple glaciations throughout the Pleistocene. Thick sequences of glacial sediments coupled with multiple glacial flow trajectories have made bedrock mapping and exploration for buried mineralization in the region challenging.

A multi-year surficial mapping and till-sampling program was initiated by the Nova Scotia Geological Survey in 2019 employing till geochemistry and indicator minerals, aided by recently released LiDAR (Laser imaging, Detection, and Ranging) elevation data, and sediment thickness modelling. The goals of these activities are to: (1) better understand the effects of multiple glaciations on till provenance, depositional history, and net glacial dispersal in the region; (2) to assess the potential for additional rare- and base-metal mineralization; and (3) to document the geometry of glacial dispersion trains using till geochemistry and indicator minerals. The ultimate objective is to increase exploration success by providing advanced exploration models that can be applied to not only the Brazil Lake study area, but other regions of the province draped by thick Quaternary cover. This presentation will include an overview of these methods applied to surficial geological research in southwestern Nova Scotia, as well as preliminary results to date.

Multiple pyrite generations in mineralization of the Elmtree Gold Deposit, northeastern New Brunswick, Canada

Aaron L. Bustard[1,2], David R. Lentz[2], and James A. Walker[1]

1. Geological Surveys Branch, New Brunswick Department of Natural Resources and Energy Development, South Tetagouche, New Brunswick E2A 7B8, Canada <aaron.bustard@gnb.ca>;
2. Department of Earth Sciences, University of New Brunswick, Fredericton, New Brunswick E3B 5A3, Canada

Northern New Brunswick hosts several shear zone-hosted gold occurrences associated with regional-scale faults and tectonism during the Salinic and Acadian orogens. Of these, the Elmtree deposit is the largest with a current resource estimate of 300 000 ounces of gold and subordinate polymetallic (Ag, Zn, Pb, and Sb) sulfide mineralization. The deposit straddles a locally sheared angular unconformity

separating an accretionary wedge complex (Elmtree Inlier) from unconformably overlying syn-orogenic sedimentary clastic and subordinate carbonate rocks of the Quinn Point Group.

Gold is hosted in three zones: the West Gabbro, South Gold, and Discovery zones. The West Gabbro Zone is the largest with mineralization occurring in a gabbro to anorthosite dyke/sill hosted by argillite of the Elmtree Formation, within the Belledune River Mélange. Mineralization at the South Gold Zone occurs within unconformably overlying Silurian conglomerate, calcareous siltstone/sandstone, and minor volcaniclastic rocks within approximately 40 m of the unconformity. The Discovery Zone is situated along the sheared unconformity and is host to both gold and the bulk of the later, cross-cutting, polymetallic mineralization.

Gold is primarily refractory in arsenopyrite precipitated during the sulfidation of iron-bearing phases including ilmenite, titanomagnetite, and Fe-silicates. Prismatic to acicular arsenopyrite occurs as the earliest ore phase sulfide and is later coeval with pyrrhotite in gabbro hosted mineralization (West Gabbro Zone) and pyrite in anorthositic gabbro, mafic dyke, and sedimentary rock hosted mineralization (West Gabbro, South Gold, and Discovery zones). Pyrite can be divided into at least four phases based on morphology: (1) a pre-ore phase; (2) early, spongy, euhedral cores that locally overgrow pre-ore pyrite; (3) inclusion-free overgrowths of earlier phases; and (4) inclusion-rich overgrowths or individual anhedral grains. Compositional variation occurs in pyrite precipitated over multiple stages in both backscatter electron imaging and micro-XRF compositional maps, where pyrite is enriched in arsenic relative to other phases. Pyrite is locally partially to completely desulfidized to pyrrhotite in portions of the deposit, and this desulfidation is sometimes associated with decorations of Ni-Sb alloys, gersdorffite, ullmannite, cobaltite, galena, chalcopyrite, and rare electrum. Electrum occurs as free grains; inclusions in arsenopyrite, pyrrhotite, and pyrite; and along grain boundaries.

Trace element mapping of pyrite using laser ablation inductively coupled plasma-mass spectrometry is ongoing to further characterize sulfide generations, and results will be integrated with geochronological and isotopic analyses to refine the petrogenesis of the Elmtree deposit and identify potential sources of mineralization.

Critical metals in the Cobequid Highlands, Nova Scotia, Canada: resolving the host rock, mineralogy, paragenesis, and controls of cobalt mineralization of the Bass River magnetite prospect

Aidan Buyers[1], Erin Adlakha[1], John Shurko[2], and Mark Graves[3]

1. Saint Mary's University Halifax, Nova Scotia B3H 3C3, Canada <aidan.buyers97@gmail.com>;
2. Spark Minerals Inc., Chester, Nova Scotia B0J 1J0, Canada;
3. Independent Consultant, Halifax, Nova Scotia, Canada

The Cobequid Highlands have a long and productive history as a region with a great endowment of mineral deposits hosting many commodities (e.g., Fe, Ba, Cu, Co, Ni, and Au). In the past 15 years, there has been a concerted effort to investigate Nova Scotia's IOCG (iron oxide copper gold) prospects along the Minas Fault Zone (MFZ), more recently focusing on critical metals like Co. The focus of this study is to use detailed petrography, micro-X-ray fluorescence (XRF) mapping, and scanning electron microscope (SEM) techniques on mineralized drill-core of the Bass River IOCG Prospect to determine the host rock, mineralogy, paragenesis, and mineralogical controls of critical metals.

Previous work done on the Bass River magnetite prospect include a regional gravity survey, a versatile time domain electromagnetic (VTEM) survey, an induced polarization (IP) survey, soil, till, and stream sediment sampling, prospecting, and mapping as well as several diamond drill programs. Most recent drilling by Spark Minerals in 2021 shows that the Bass River prospect is a magnetite breccia with clasts of feldspar-phyric to aphanitic mafic and felsic volcanic rocks, and massive to laminated, fine-grained, dark grey-black sedimentary rocks. The clasts in places show replacement by magnetite. The matrix is dominantly massive magnetite with fine- to coarse-grained, blebby to euhedral pyrite. The degree and coarseness of pyrite mineralization increases downhole. The matrix and clasts are crosscut by late carbonate veins, which are often vuggy close to the top of hole. Chalcopyrite stringers were also observed associated with vuggy carbonate. Representative mineralized samples are currently being analyzed using micro-XRF to map elemental distribution, including critical metals. Targeted samples will then be analyzed using classical petrographic techniques and SEM.

The acceptance and growth of the concept of geoheritage in Atlantic Canada and beyond

John Calder[1], Rob Fensome[2], Jason Loxton[3], Jeff Poole[4], and Matthew Stimson[5]

1. John Calder Earthworks, P.O. Box 43, Halifax Central, Halifax, Nova Scotia B3J 2L4, Canada <johncalder99@gmail.com>;
2. Geological Survey of Canada (Atlantic), Dartmouth, Nova Scotia B2Y 4A2, Canada;
3. Cape Breton University, Sydney, Nova Scotia B1P 6L2, Canada;
4. Nova Scotia Department of Natural Resources and Renewables,

Halifax, Nova Scotia B3J 2T9, Canada;
5. Natural History Department, New Brunswick Museum, Saint John New Brunswick E2K 1E5, Canada

The concept of geoheritage, born at the 1991 meeting of ProGeo in Digne, France, was captured eloquently in the *Declaration of the Rights of the Memory of the Earth*. Geoheritage has grown in the past decade from a concept whose worth was questioned and even derided by some established geoscientists to one fully embraced at the highest levels of the geoscientific community, including at the Geological Society, GSA, USGS, IUGS, IGCP, and even the IUCN, which is traditionally biologically and ecologically focused. The idea of geoheritage is very much rooted in inviting the public to consider the incredible story of our planet as recorded in the geologic record: in other words, to build an appreciation for geology and Earth history. It is public facing, and at its core is bringing to public attention, sites (geosites, geoheritage sites) where the Earth's history is well told. The construction of Geoheritage site lists will always be a source of contention but is fundamental to pointing the public (as well as geologists) to places where they can learn or simply marvel at the Earth's remarkable processes and history. Although perhaps unintentional, the list of sites featured on the Nova Scotia Geological Highway Map provided a starting point for Nova Scotia's Geoheritage Sites List, the first such list in Canada. Currently, international standards for recognition of global geosites are being developed under IGCP Project 731 and select geosites in Atlantic Canada will be considered as examples. Geosites are key to defining Global Geoparks, a growing designation now recognized at 169 regions in 45 countries, and a leading factor in geotourism.

In parallel to the concept of geoheritage is the concept of geodiversity, a concept and term consciously positioned to challenge non-geologists to consider how geology underpins Earth systems and gives rise to biodiversity. This year will see recognition of the first International Day of Geodiversity, endorsed by the United Nations. The first International Day for Geodiversity in October presents an opportunity for the Atlantic Geoscience Society to shine a spotlight on the rich geoheritage of Atlantic Canada and the concentration here of UNESCO World Heritage Sites and Global Geoparks, a legacy of our plate tectonic history and exceptional coastal exposures.

Using fluoride analysis in till to assist in identifying the bedrock potential for critical minerals in central Newfoundland, Canada

Heather Campbell[1], Steve Amor[2], Zsuzsanna Magyarosi[1], Chris Finch[1], and Rosauro Roldan[1]

1. Geological Survey of Newfoundland and Labrador, St. John's, Newfoundland and Labrador A1B 4J6, Canada <heathercampbell@gov.nl.ca>;
2. Geological Consultant, St. John's, Newfoundland and Labrador A1A 3C5, Canada

Fluoride analysis has successfully located previously unrecognized mineralization associated with Li-Cs-Ta (LCT) pegmatites in sandy, bouldery, variably eroded, and dispersed till overlying granites and metasedimentary rocks in the Snowshoe Pond region of the Meelpaeg Subzone in central Newfoundland. Fluoride, measured by Ion Selective Electrode (ISE), is a component of the analytical suite for till-geochemical samples in the province of Newfoundland and Labrador. In central Newfoundland, fluoride in till is thought to be derived from apatite that typically occurs in LCT pegmatites (up to 5%). Fluoride anomalies in till samples are more effective in defining the extent and locale of the underlying pegmatites than other geochemical indicators associated with mineralization (e.g., Cs, Li, Nb), as the fluorine-bearing apatites are; (1) relatively abundant in the source rocks, and (2) sufficiently resistant to reside in dispersed and eroded tills. Based on this study, the use of fluoride analysis in till is highly recommended in other areas with potential for rare element mineralization. More studies are being conducted to assess the potential of fluoride in till in exploring for other types of deposits, such as rare earth elements (REE) that are also typically associated with F-rich rocks.

Petrology, geochemistry, and geochronology of aplite dykes in the Cape Spencer area, southern New Brunswick, Canada

Alan Cardenas[1], David R. Lentz[1], Chris R.M. McFarlane[1], and Kathleen G. Thorne[2]

1. Department of Earth Sciences, University of New Brunswick, Fredericton, New Brunswick E3B 5A3, Canada <alan.cardenas@unb.ca>;
2. Geological Surveys Branch, New Brunswick Department of Natural Resources and Energy Development, Fredericton, New Brunswick E3B 5H1, Canada

The Cape Spencer area is located 15 km southeast of Saint John, New Brunswick. Gold mineralization has been identified mainly in illitized (illite-carbonate ± quartz ± pyrite ± chlorite ± specularite), pyrite-rich rocks of the Millican Lake Granite and the Cape Spencer Formation, along thrust faults and folds, and in quartz ± carbonate veins with sulphides (pyrite ± chalcopyrite ± galena ± arsenopyrite). Other units of Carboniferous age present in

the area are the Balls Lake and the Lancaster formations. A penetrative S1 cleavage is seen in all the lithologies, and a second, spaced crenulation cleavage can be observed in the finest sedimentary units. Previous $^{40}Ar/^{39}Ar$ geochronology (276.6 ± 0.9 and 283.7 ± 0.8 Ma) on illites defining these fabrics and related to the alteration event linked to gold deposition were considered "cooling ages" and constrained the timing of gold mineralization between those ages and the age of the youngest rocks affected by the illitic alteration (Lancaster Formation - Bashkirian).

Leucocratic non-foliated aplitic dykes are comprised of quartz, orthoclase, and plagioclase (An_{10-20}), and minor secondary epidote, specularite, and pyrite, intrude both the Millican Lake Granite and the Cape Spencer Formation. These bodies, varying mainly from 10–50 cm to several metres thick, occur both parallel and crosscutting the foliation in the host rocks, and exhibit a secondary earthy hematization that results in a pink colouration. Whole rock major- and trace-element lithogeochemistry together with U–Pb geochronology (zircon) were employed to evaluate the petrogenesis of these aplitic bodies to build on the understanding of the mineralizing system and the geological evolution of the region.

The aplitic dykes are metaluminous (A/CNK = 0.74–0.92) with SiO_2 content varying between 58.9 and 79.2 wt% and can be subdivided according to their Nb/Ta and Zr/Hf ratios into two groups. The first group has higher Nb/Ta (10.87–11.47) and Zr/Hf (43.8–44.6) ratios than the second group (Nb/Ta = 1.77–10, Zr/Hf = 22.1–30). Low Nb, Ta, Y, Yb, and Rb indicate an I-type affinity. The presence of microfracturing and textural setting (i.e., zircon sitting along grain boundaries vs. included in phenocryst phases), in addition to critical radiation damage threshold in zircon makes geochronological analysis complicated. Preliminary U–Pb zircon ages define two clusters around 275 and 350 Ma. The 350 Ma cluster is considered to be the crystallization age, whereas the 275 Ma cluster is related to hydrothermal alteration and complete resetting of the most heavily radiation-damaged grains.

Lithogeochemical and petrological constraints on the environment of deposition of the Nicola Group volcano-sedimentary rocks about the Copper Mountain alkalic Cu-Au porphyry deposit, Princeton, British Columbia, Canada

Nathan Carter[1], Cliff Stanley[1], and Peter Holbek[2]

1. Department of Earth and Environmental Science, Acadia University, Wolfville, Nova Scotia B4P 2R6, Canada <14282c@acadiau.ca>;

2. Copper Mountain Mining Corporation, Vancouver, British Columbia V6C 1G8, Canada

The upper Triassic Nicola Group is an economically important succession of volcano-sedimentary rocks that host the Copper Mountain alkalic Cu-Au porphyry deposit. All known mineralization at Copper Mountain appears to be associated with Lost Horse intrusive dykes and stocks of diorite to monzonite composition, and these intruded rocks of the Wolf Creek Formation within a 1000 by 4300 m NE-SW trending belt bounded on the south by the Copper Mountain Stock and on the north by the Smelter Lake and Voigt stocks. Discovery of additional copper resources in the camp will likely rely on a better understanding of the stratigraphy of the Wolf Creek Formation, and the environment it was deposited in. Consequently, mapping of Nicola Group rocks south and east of the Copper Mountain Stock and west of the Smelter Lake stock was undertaken, revealing the presence of flows, breccias, volcaniclastic sedimentary rocks, and dykes. One hundred and thirteen flow and volcaniclastic sedimentary rock samples were analyzed lithogeochemically and evaluated using molar element ratio analysis. Fifty-four of these samples were cut into thin sections for petrographic examination.

Wolf Creek Formation rocks from west of the Smelter Lake Stock appear to be less green and less altered than those elsewhere in the camp, containing measurably less chlorite and epidote, more calcite (in amygdales), and hosting exotic clasts of limestone. This suggests that these rocks were deposited in a subaerial environment. In contrast, Wolf Creek Formation rocks from south and east of the Copper Mountain Stock are demonstrably greener, more altered to chlorite and epidote, and interbedded with volcaniclastic siltstones and sandstones. They were likely deposited sub-aqueously.

Molar element ratio analysis indicates that Wolf Creek Formation rocks have a primary composition consistent with the presence of plagioclase, clinopyroxene, and biotite, a conclusion consistent with petrographic observations. In contrast, compositional variability was controlled only by plagioclase and clinopyroxene sorting. These rocks have also been variably altered to a likely low temperature assemblage of chlorite, epidote, albite, and calcite, and molar element ratio constraints suggest that this alteration was largely isochemical, with the exception of water and CO_2. Consequently, mapped rocks were likely subjected to only seafloor alteration, as they do not exhibit evidence of higher temperature potassic and albitic alteration and metasomatism associated with Cu mineralization elsewhere in the camp.

Trace element geochemistry of biotite from the Scrag Lake and New Ross plutons of the South Mountain Batholith, Nova Scotia, Canada: implications for magma differentiation

Kathleen Clark and James Brenan

Department of Earth and Environmental Science, Dalhousie University, Halifax, Nova Scotia B3H 4R2, Canada <kt747032@dal.ca>

The South Mountain Batholith (SMB) is a 7300 km^2, peraluminous, felsic intrusion that occurs in southwestern Nova Scotia and consists of 13 plutons that were emplaced in two different phases between ~385 and ~368 Ma. Previous research revealed that samples from phase 2 plutons show significant trace element variability in biotite compared to phase 1 plutons. Since phase 2 plutons tend to be more geochemically evolved, it is not clear if this difference arises due to sampling bias or is an intrinsic property of the second stage of batholith emplacement. Therefore, the goal of this work is to better characterize biotite compositions across a broad compositional range of representative phase 1 and phase 2 plutons. This work focuses on samples from the phase 1 Scrag Lake pluton (SGP) and the phase 2 New Ross pluton (NRP). An electron microprobe and laser ablation ICP-MS have been used to collect major and trace element data on biotite from a suite of 5 samples from each pluton covering a compositional range of ~68 to ~75 wt% SiO_2. In addition to spot analyses, major and trace element maps have been obtained from select biotite crystals to assess internal zonation. Although data for 34 trace elements were obtained, the current focus is on the critical metals Nb, Ta, Sn, and W. Preliminary results show continuous zoning in trace elements from core to rim in biotite grains in both pluton phases. The concentrations of Nb, Ta, Sn, and W all increase from core to rim, while the Nb/Ta ratio decreases from core to rim, which is expected with the crystallization of the assemblage biotite-quartz-plagioclase-k-feldspar. For similarly-sized grains and similar whole-rock wt% SiO_2, phase 1 samples show within grain variation from 10–100s mg/g, while variation within phase 2 biotites is 10–1000s mg/g. This indicates that the more extreme extent of trace element variation is an intrinsic property of stage 2 plutons. As both phase 1 and phase 2 samples show similar trace element concentrations in the cores of the biotite grains, the difference in variability is due to more extreme extents of crystallization, and not due to differences in starting compositions. This extreme crystallization could be due to the addition of a flux that lowers the solidus (B, Li). The data shows that Li concentrations are higher in phase 2 biotites, and B will be measured to investigate this potential explanation further.

The first description of vertebrate and invertebrate ichnofossils in the Stellarton Basin (Westphalian C), Nova Scotia, Canada*

Logan M. Cormier[1], Matthew R. Stimson[1,2], Olivia A. King[1,2], John H. Calder[1], Janey MacLean[3], Lorenzo Marchetti[4], Spencer G. Lucas[5], and R. Andrew McRae[1]

1. Department of Geology, Saint Mary's University, Halifax, Nova Scotia B3H 3C3, Canada <logan.cormier@smu.ca>; 2. Steinhammer Paleontological Laboratories, Geology/ Paleontology section, Natural History Department, New Brunswick Museum, Saint John New Brunswick E2K 1E5, Canada; 3. 4621 Trafalgar Road, Hopewell, Nova Scotia B0K 1C0, Canada; 4. Museum für Naturkunde Berlin, Leibniz-Institut für Evolutions- und Biodiversitätsforschung, Berlin, Germany; 5. New Mexico Museum of Natural History, Albuquerque, New Mexico 87104, USA

Newly discovered tetrapod and invertebrate ichnofossils from the Pennsylvanian (Westphalian C) Stellarton Formation represent the first ichnofossil assemblage to be described in the Stellarton Basin of Nova Scotia. The Stellarton Basin is well known for its economic deposits of coal, yet apart from paleobotanical records and the exceptional discovery by Sir William Dawson of the tetrapod *Baphetes*, little paleontological work has been formally documented in the literature prior to this study. This is the first discovery of tetrapod traces from the Stellarton Formation. The tetrapod trackway-bearing Plymouth Member is exposed in an aggregate quarry near the town of Stellarton. The Plymouth Member is composed of fluvial sandstones and is interpreted to conformably overlie the lacustrine deposits of the Westville Member that crop out just east of the quarry along the East River of Pictou. The well-preserved, plantigrade tetrapod tracks within the Plymouth Member are identified as *Batrachichnus salamandroides* and *Matthewichnus* cf. *M. velox*, ichnotaxa that are often attributed to temnospondyl or microsaurian trackmakers. Of greater abundance and diversity is the invertebrate trace fossil assemblage of the Westville Member, which consists of *Cruziana* isp., *Monomorphichnus* isp., *Lockeia* isp. and various morphologies of *Rusophycus* tentatively assigned to various ichnospecies. They have been attributed to freshwater crustacean and molluscan tracemakers. In addition, a previously undescribed cubichnia morphotype shows morphologic features that may justify the erection of a possible new ichnogenus and is interpreted to have been produced by an isopod-like invertebrate. The marginal lacustrine depositional setting at this site encompasses a diverse invertebrate ichnoassemblage within the *Mermia*

Ichnofacies and a low diversity tetrapod ichnoassemblage of the *Batrachichnus* Ichnofacies.

**Winner: AGS Rupert MacNeill Award for best undergraduate student oral presentation*

Geothermal potential of New Brunswick, Canada: "Salt Chimneys"

Joseph de Luca and Dave Keighley

Department of Earth Sciences, University of New Brunswick, Fredericton, New Brunswick E3B 5A3, Canada <pdeluca@unb.ca>

Geothermal energy provides a clean source of reliable electricity that may help provide energy security and reduce CO_2 emissions. The economical application of geothermal electricity requires sufficiently elevated subsurface thermal gradients to minimize costs associated with industrial development and production. Consequently, global focus for geothermal energy has traditionally been on areas with active tectonism and volcanism, where geothermal gradients easily meet conditions for cost-effective power stations. More recently, attention has been given to evaluating the potential for sedimentary basin geothermal production in strategic areas. While New Brunswick has not historically been such an area for inquiry, subsurface thermal-gradient contour maps have recently been updated for the southeastern half of the province. Updated maps show that New Brunswick has mostly low-potential geothermal gradients of around 20°C/km, but revealed areas of anomalously high gradients, relative to the provincial background, primarily associated with known subsurface Mississippian (Carboniferous) evaporites of the Gautreau Formation and the Windsor Group. Where geothermal gradients appear more prospective, exceeding 30°C/km, their values are being further assessed for their validity. The stratigraphy of 12 boreholes were divided into sections based on the dominant lithologies of lithostratigraphic units. Among the 12 boreholes, four terminate in the Windsor Group, one terminates below the Windsor Group, one cuts through a section of the Gautreau Formation but does not encounter the Windsor Group, and the remaining six have no direct contact with evaporitic bodies in the subsurface. Heat flow (q) was calculated using the equation

$$q = \frac{\Delta T \times k \times A}{L}$$

where ΔT = temperature difference between the top and bottom of a stratigraphic column or unit, A = cross-sectional area of a unit, and L = unit thickness. Thermal conductivity (k) of the units was experimentally determined in earlier work from rock samples of different lithologies, which had been taken from drill cores around the region. Preliminary calculations suggest that, in most cases where the Windsor Group is present, temperatures at the top of Windsor Group halite show the greatest positive separation from expected temperatures versus other contact points in the column. Elsewhere, this has been termed the "salt chimney effect" because of the inherently high thermal conductivity of halite, which when present in the subsurface brings higher temperatures closer to the surface.

Integrative geophysical analysis and characterization of prospective hydrocarbon seepage sites on the southwestern to central Scotian Slope, Canada

John Dooma[1], Natasha Morrison[2], Adam Macdonald[2], and G. T. Ventura[1]

1. Department of Geology, Saint Mary's University, Halifax, Nova Scotia B3H 3C3, Canada <John.Mishael.Dooma@smu.ca>;
2. Nova Scotia Department of Natural Resources and Renewables, Halifax, Nova Scotia B3J 3P7, Canada

Nova Scotia has potential for undiscovered hydrocarbon reservoirs in the deep-water portion of the Scotian Margin. However, exploration in these environments involves major challenges and geological risks. As the presence, quality, size, and distribution of source and reservoir rocks are relatively still unknown, the cost of exploration and the risk multiplies. Therefore, new data are needed to de-risk offshore exploration to achieve the next generation of discoveries. This research project investigates the shallow depth (0 to 3000 m) of BP's 3-D Tangier seismic survey to better constrain the subsurface geology in regions where prospective hydrocarbon seep sites have been found. The 3-D Tangier seismic survey marks one of the most geologically complex regions of the slope and its shallow stratigraphy has not yet been fully understood. Seven key seismic horizons were interpreted and subsequent seismic attribute analysis using root-mean square (RMS) and coherence was completed, resulting in several depth structure and geophysical maps. Initial interpretation of these results indicates the region hosts a complex subsurface geology comprised of well-stratified sediments from draping and hemipelagic deposition incised by paleo-channels and mass transport complexes that are associated with localized slope failure. In some parts of the survey, these subsurface features are incised by deep submarine canyons. Direct hydrocarbon indicators (DHIs), which are anomalous amplitudes that mark potential sites of hydrocarbon migration and accumulation are identified in the seismic interpretation and further resolved with the RMS attribute extraction. Thus far, most identified DHIs lie within a shallow band

of ~2300 to ~2500 m below sea level. These DHIs are commonly located in sediments above salt diapir structures. The presence of shallow DHIs in the survey, combined with geochemical data from coring of potential seeps, suggests they are formed from migrating deeper fluids from either a reservoir or directly from a source interval. For future work, this project will investigate the deeper lithostratigraphic intervals below selected DHIs to locate a potential source and migration pathways of contributing fluids. The results of this study will then be further compared to the Play Fairway Analysis, high-resolution multi-beam bathymetric maps of prospective seeps within the seismic data block, as well as core geochemistry and genomic data to confirm and produce robust interpretation and results.

An experimental study of the effect of pressure on the formation of chromite deposits

Natashia Drage and James Brenan

Department of Earth and Environmental Sciences, Dalhousie University, Halifax, Nova Scotia B3H 4R2, Canada <Natashia.drage@dal.ca>

Despite extensive research on the Bushveld Complex chromitites, the mechanism(s) that form such anomalous chromite segregations remains uncertain. Recent work applying the MELTS thermodynamic model proposed that reduction of pressure upon magma ascent shifts the silicate-in temperature to lower values, with the chromite-in temperature remaining unchanged, resulting in chromite-alone crystallization and formation of massive chromitites. Evaluation of this hypothesis is by laboratory phase equilibrium experiments conducted at 0.1 MPa, 0.5 GPa, and 1 GPa, employing two bulk compositions. Composition 1 (C1) corresponds to a widely accepted parental magma of Bushveld chromitites, termed B1. Composition 2 (C2) is the same used in the MELTS modelling study, which contrasts with C1 most significantly in Al_2O_3 (17.4 wt% vs 11.8 wt% in C1), MgO (6.7 wt% vs 11.9 wt% in C1), and Cr (680 μg/g vs 970 μg/g in C1) contents. Experiments were conducted at 0.1 MPa by equilibrating synthetic starting materials on Fe-Ir alloy wire loops over the temperature interval of 1170–1300°C in a vertical-tube, gas-mixing furnace for 12–48 hours, at FMQ and FMQ-0.4. Experiments at 0.5 GPa and 1 GPa were conducted with a piston-cylinder apparatus using Fe-Ir alloy capsules to buffer fO_2 at FMQ-0.4 at 1230°C and 1280°C for 4–12 hours. Results indicate that there is no significant change in Cr content of the melt at chromite saturation with pressure. For C1, the average Cr content of the melt over the pressure interval studied is 439 ± 22 μg/g at 1230°C and 799 ± 100 μg/g at 1280°C. The average Cr content for C2 is 417 ± 17 μg/g at 1230°C and 704 ± 48 μg/g at 1280°C. Results from C1, where pyroxene crystallizes at all pressures, show modal abundance and Cr content of pyroxene increasing with rising pressure. Using pressure and temperature trends for Cr content at chromite saturation and $D_{Cr(px/liq)}$ from experiments, chromite-in temperatures were modelled for different total Cr contents in the melt. Chromite-alone crystallization between 0.1–0.3 GPa occurs in C1 only for above average total Cr levels for this composition (>1100 μg/g). In C2, results predict a higher chromite-in temperature and therefore, larger interval of chromite-alone crystallization at low pressure compared to MELTS. For the same total Cr content as the initial MELTS model, the results show that chromite is dropped from the C2 assemblage above 0.5 GPa due to appearance of pyroxene, which differs from MELTS as Cr is not included in their pyroxene model.

Age, zircon chemistry, and petrogenesis of voluminous extension-related late Ediacaran silicic magmatism in the Coldbrook Group, southern New Brunswick, Canada

Alicia P. Escribano[1], Sandra M. Barr[2], and James L. Crowley[3]

1. Department of Earth Sciences, Memorial University, St. John's, Newfoundland and Labrador A1B 3X5, Canada <adpescribano@mun.ca?;
2. Department of Earth and Environmental Science, Acadia University, Wolfville, Nova Scotia B4P 2R6, Canada;
3. Boise State University, Boise, Idaho 83725-1535, USA

The Coldbrook Group is a unique suite of Late Ediacaran volcanic and epiclastic rocks that together with related plutons was emplaced in the Avalonian Caledonia terrane of southern New Brunswick. The suite is topped by the mainly rhyolitic Silver Hill Formation that has been recognized in five different areas of the Caledonia Highlands, each with distinct petrographic textures: Silver Hill, Coastal Fundy Park, Fundy Park, Vernon Mountain, and Blackall Lake. The coeval felsic Bonnell Brook pluton is represented by a medium- to coarse-grained granite and a fine-grained granitic dome. Whole-rock chemistry, zircon chemistry (LA-ICP-MS), and U–Pb dating (LA-ICP-MS and CA-TIMS) were used to study the relationship between the felsic volcanic and plutonic rocks and to constrain their age and tectonic setting. Transitional felsic I- to A-type chemical signatures in both volcanic and plutonic rocks suggest that magmatism occurred in an extensional within-plate setting, consistent with the tectonic regime at that time throughout Avalonia. Whole-rock chemistry shows that, although coeval, the medium- to coarse-grained granite was emplaced

at a deeper level and is not cogenetic with the fine-grained granite and rhyolite of the Silver Hill Formation. Rhyolite in the Silver Hill area yielded a weighted mean $^{206}Pb/^{238}U$ age of 551.65 ± 0.15 Ma, similar within error to the age of 551.71 ± 0.15 Ma for the fine-grained granite. Furthermore, zircon grains of the Silver Hill rhyolite and fine-grained granite have similar chemical compositions and morphology suggesting rhyolite and granite are comagmatic. However, the main belt of rhyolite in the Coastal Fundy and Fundy Park areas is younger at 549.18 ± 0.07 Ma, consistent with the older age of 551.19 ± 0.20 Ma obtained for an underlying lithic tuff unit. Stratigraphic relationships and petrography suggest that the rhyolite of the Coastal Fundy and Fundy Park areas formed in one event that commenced with pyroclastic flows and progressed to calmer eruptions, represented by rhyolitic lava flows. Younger dates of 540–520 Ma obtained from zircon grains in the same samples by LA-ICPMS indicate that the zircon experienced cryptic alteration and Pb loss and demonstrate the importance of combining LA-ICP-MS dating with CA-TIMS from the same zircon populations.

Ice dynamics and deglacial history of the northeast Newfoundland Ice Sheet

Sef C. Everest, John C. Gosse, Sophie L. Norris, and Arthur S. Dyke

Department of Earth and Environmental Sciences, Dalhousie University, Halifax, Nova Scotia B3H 4R2, Canada <everest@dal.ca>

The timing and dynamics of deglaciation of the Newfoundland Ice Sheet (NIS) represents a complex and poorly resolved portion of the North American Ice Sheet Complex. Establishing the flow dynamics of the NIS precisely is useful to minimize risk for mineral exploration through drift prospecting on the island, and is important to paleoclimatic, paleoceanographic, and glaciologic research owing to its proximity to the shelf-edge limit of the LIS and the interpreted occurrence of numerous ice streams juxtaposed with cold basal thermal regimes. High-quality surface exposure ages representing onshore ice margin retreat in Newfoundland are also needed for ongoing studies of subglacial erosion rates beneath warm-based and cold-based ice. Existing deglacial chronologies in northeastern Newfoundland are lacking input from onshore dates, and surface exposure dating methods are underutilized across the NIS. As a result, ice extent during the last glacial maximum is poorly constrained in Newfoundland and is the subject of ongoing debate. Marine evidence shows ice extending almost to the continental shelf-edge at the Last Glacial Maximum (LGM) but opposing models have argued for ice only reaching modern shorelines in Newfoundland, based on biological refugia evidence that certain uplands were ice-free. This study helps constrain ice sheet dynamics in central-eastern Newfoundland and contribute to the data gap in a critical region of Newfoundland. Ten new terrestrial cosmogenic nuclide ages were obtained spanning three strategic locations in northeastern Newfoundland. These data combined with previous published geomorphic maps, as well as new interpretations and synthesis provide an updated deglacial model for the region. The summary exposure age of the three sites selected for Be-10 dating are 13.3 ± 0.8 ka near New-Wes-Valley, NL; 12.7 ± 0.8 ka near Gander, NL; and 12.2 ± 1.0 ka near Glovertown, NL (errors are 1σ total external uncertainty). These ages are consistent with calibrated radiocarbon ages in the region. This record of deglaciation and new constraints demonstrate deglaciation at these sites was 1–2 ka later than in previous models, and this study will explore the potential effect of the Younger Dryas stadial on readvance or stagnation of the ice margin. Reconstructions of ice dynamics will also refine existing estimates of the location of ice divides in the northeast NIS.

Reaction rims on ilmenite macrocrysts from kimberlite as a proxy of kimberlite emplacement process

Lydia Fairhurst[1], Yana Fedortchouk[1], Ingrid Chinn[2], and Philippe Normandeau[3]

1. Department of Earth and Environmental Sciences, Dalhousie University, Halifax, Nova Scotia B3H 4R2, Canada <lydiafairhurst@dal.ca>;
2. DeBeers Group, Johannesburg, Gauteng, South Africa;
3. Northwest Territories Geological Survey, Northwest Territories, Canada

Kimberlites are mantle-derived magmas often emplaced in the upper crust as pipe-shaped structures. Large multi-phase bodies of class 1 consist of coherent kimberlite (CK) and different pyroclastic facies, including diatreme Kimberley-type pyroclastic kimberlite (KPK). The composition, crystallization conditions and emplacement processes of these kimberlites are poorly understood, especially the formation of KPK. CK facies include hypabyssal kimberlite (HK) and ambiguous partially fragmented CK. Ilmenite macrocrysts from some Orapa kimberlites show reaction rims developed due to a reaction with the kimberlite magma. The composition of these rims correlates with kimberlite facies and may provide information about their crystallization conditions. The goal of this study is to use the reaction products on ilmenite from different kimberlite facies in order to examine variation in crystallization temperature (T), oxygen fugacity (fO_2), and

silica activity (αSiO_2) during the emplacement of large kimberlite pipes. fO_2 is also important for assessment of diamond preservation in kimberlites as more oxidized conditions promote diamond resorption.

This study used thin sections from known depth intervals in drillholes from the AK15 and BK1 kimberlites from the Orapa kimberlite cluster (Botswana). The AK15 intrusion consists of a single phase of CK facies. The BK1 pipe consists of two CK facies (CK-A and CK-B) and one KPK facies. CK-B is a HK and CK-A shows areas of partial fragmentation. Secondary phases in ilmenite reaction rims were identified with SEM. The composition of perovskite, ilmenite, and magnetite was obtained from EMP analyses and used for T and fO_2 calculation. The ilmenite macrocrysts are unstable and develop magnetite-perovskite symplectite aggregate in the magmatic CK-B facies. Ilmenite macrocrysts are well-preserved in in CK-A and KPK and develop rims composed of magnetite and rutile in CK-A and highly variable mineralogy distinguished by the presence of titanite in KPK. In AK15, ilmenite macrocrysts have magnetite and perovskite rims. Perovskite crystallization conditions are estimated to vary from DNNO -5.74 to -1.30 and 560–700°C based on the ferric iron content in perovskite. Magnetite crystallization conditions are estimated to vary between ΔNNO -1.6 to 0.5 and 850–1200°C based on Fe-Ti exchange in magnetite and ilmenite. fO_2 estimates vary between facies with magmatic CK-B showing the narrowest range and a slight oxidation towards the surface, and KPK showing the largest range and no correlation with depth. In KPK, an increase in αSiO_2 is evidenced through the development of titanite ($CaTiSiO_5$) while perovskite ($CaTiO_3$) becomes unstable.

3D modelling of the Key Anacon Titan deposit near Bathurst, New Brunswick, Canada using ELF-EM data and open-source inversion software

Alex Furlan

Department of Earth Sciences, Brock University, St Catharines, Ontario L2S 3A1, Canada <afurlan@brocku.ca>

The Key Anacon Titan deposit is a Bathurst-type volcanogenic massive sulfide (VMS) hosted in the same stratigraphic horizon as the well-known Brunswick No. 12 mine. The current mineral resource reported by AGP Mining Consultants Inc. indicates 0.3 million tonnes of material with ~4.4% Zn, ~1.6% Pb, ~0.7% Cu, and ~39 g/t Ag. Exploration and development of the Key Anacon deposit were stunted by falling zinc prices in the 1950s and 1960s and since then, only two major exploration programs have occurred. While Osisko waits for the deposit to become economically viable (zinc was recently listed as a critical mineral by the USGS), it provides a great location to test new exploration methods. In 2012, the Extremely Low Frequency (ELF) EM survey system was developed as a ground-based version of Z-axis Tipper Electromagnetics (ZTEM). By measuring in the 1–1440 Hz frequency range, the ELF-EM system can see ~2 km into the ground depending on subsurface conductivity. This system makes use of a transfer function which relate the horizontal and vertical magnetic field components to subsurface conductivity changes. The resulting data are known as tippers (T_{zx} and T_{zy}), dimensionless ratios which get their name by 'tipping' the magnetic field vector away from horizontal in response to 3D conductivity variations. In 2019, an ELF survey was collected over the Key Anacon Titan deposit to test the systems ability to resolve conductivity changes in the subsurface. The data collected agreed with previous findings but at the time of the survey, 3D modelling ELF-EM data was an arduous task. Recent developments in SimPEG (Simulation and Parameter Estimation in Geophysics), an open-source Python package, provides tools for users to create their own inversion workflow. This package was used to write a new 3D ELF inversion script that could run on modern hardware without the need to license any software. The Key Anacon ELF survey was a perfect test candidate due to its small footprint allowing it to be run quickly and repeatedly with tweaks in parameters. The inversion models produced by ELF tipper data are conformable to 3D geological wireframe models independently derived from other geophysical surveys as well as borehole logs. With this recent improvement to 3D modelling, the ELF-EM system shows great potential to be a reconnaissance tool for deep conductive structures in both greenfield and brownfield exploration projects.

Composition of mafic minerals from intrusive rocks near the Teahan Mine, Caledonia Highlands, southern New Brunswick, Canada: implications for mineralization and conditions of magma solidification

Ayalew Gebru

New Brunswick Department of Natural Resources and Energy Development, Fredericton, New Brunswick E3B 5H1, Canada <Ayalew.gebru@gnb.ca>

Using Electron Probe Microanalysis, the composition of biotite was determined for the Teahan area granitoids (Pollett River Granodiorite and Rat Tail Brook Granodiorite) along with amphibole and chlorite compositions of the nearby Pollett River Gabbro/Gabbroic Diorite, Caledonia Road Diorite/Gabbroic Diorite, Kent Hills Granodiorite, Forty Five River Granodiorite, Teahan Mine Granodiorite,

and a "younger" sheared gabbro. On the Al^{iv} vs Mg/(Mg + Fe) and Fe/(Fe + Mg) compositional fields, the biotite grains both from the Pollett River and Rat Tail Brook granodiorites plot within the biotite field, near the biotite-phlogopite field boundary close to the Annite–Phlogopite binary. Relatively high TiO_2, MnO, MgO, CaO, K_2O, BaO, F, and Cl, and low Na_2O, Al_2O_3, and H_2O contents distinguish the biotite of the Pollett River Granodiorite from that of the Rat Tail Brook Granodiorite. The X_{phl} versus $\log(X_F/X_{Cl})$ compositions of biotite from these granitoids indicate an I-type magmatic composition, whereas on the $\log(X_F/X_{OH})$ versus $\log(X_{Mg}/X_{Fe})$ discrimination diagram, the biotite compositions indicated a weakly contaminated I-type granitoid source composition. The Mg versus Al binary plot (apfu) demonstrates the peraluminous affinity of the Rat Tail Brook Granodiorite, and the calc-alkaline nature of the Pollett River Granodiorite. The FeO_t–MgO–Al_2O_3 composition of biotite from the Pollett River Granodiorite also supports the calc-alkaline nature of the source magma, whereas the source for the Rat Tail Brook Granodiorite plots close to the calc-alkaline-peraluminous granite boundary.

The IV (F/Cl) versus IV(F) data distribution of biotite from the granitoids is transitional between the porphyry copper and W-(Cu-Au-Bi) magmatic systems. They have higher IV(F) values relative to porphyry Mo and Sn-W-Be mineralizing systems. From additional petrological information (i.e., ore element ratios such as Mo/Cu, Rb/Sr, Cu/Mo, Cu/Sn), the Pollett River Granodiorite is the most favourable for potential porphyry copper and W-(Cu-Au) skarn mineralization, provided there is a favorable host lithology in the latter case.

The temperature of biotite crystallization was determined using the Ti-in-biotite thermometry; the Pollett River Granodiorite yielded a temperature of 600–720°C, whereas the Rat Tail Brook Granodiorite yielded 500°C with the latter temperature possibly being a result of re-equilibration. The apfu composition of amphiboles from the Pollett River gabbroic diorite correspond to titanian and ferrian tschermakitic hornblende, ferrian-tschermakite, ferri-titanian-tschermakitic hornblende, and magnesio-hornblende composition. Pressures of equilibration of the titanian, ferrian tschermakite and the titanian and ferrian tschermakitic hornblende group of minerals range from 4.8 to 6.5 kb, from the mean of various barometric determinations. Magnesio-hornblende equilibrated from 2.4 to 3.1 kb. Amphiboles from the Caledonia Road gabbroic diorite are ferri-magnesio-hornblende to ferrian-magnesio-hornblende in composition and equilibrated at pressures around 2 kb.

The chlorite in the Kent Hills Granodiorite is of brunsvigite composition, whereas the Pollett River Diorite/Gabbroic Diorite and the Caledonia Road gabbroic diorite have pycnochlorite compositions. The Forty Five River Granodiorite, the Teahan Mine Granodiorite and a highly sheared gabbroic diorite intruding the Teahan Formation west of the Kent Hills contain chlorite of ripidolite composition.

Using pXRF to differentiate igneous rocks in the Bermuda volcanic basement

Wednesday Gillespie, Emma Stainsforth, Alex Hancock, and Lexie Arnott

Department of Earth and Environmental Science, Dalhousie University, Halifax, Nova Scotia B3H 4R2, Canada <Wednesday.Gillespie@dal.ca>

The island of Bermuda is unique because its geology is inconsistent with established theories on the formation of volcanic seamounts. Research into the formation of the Bermuda rise began in the early 20th century with the emergence of the theory of plate tectonics. The 1972 Deep Drill core is 802 m with almost all of it intersecting the igneous basement. Since then, little has been done to geochemically analyze the samples, which were visually classified on site as containing alternating ultramafic intrusions and mafic lavas. In this study, a portable X-ray fluorescence (pXRF) spectrometer was used to geochemically analyze samples from the drill core. The samples showed that there is a significant variation in the SiO_2 content between sheets and lavas, with intrusions having a mean of 41.8% and lavas having a mean of 52.0%. Based on the project results, using pXRF to measure the SiO_2, TiO_2, and P_2O_5 found in rock samples of the Bermuda rise is a valid technique for efficiently differentiating between intrusions and lavas in the field. However, further analysis is needed to quantify this. Traditional X-ray fluorescence analysis should be conducted to confirm the major element geochemistry.

An evaluation of magmatic processes responsible for tungsten enrichment in the Canadian Tungsten Belt: evidence in melt inclusions of granitoids associated with the Cantung and Mactung W-Cu deposits

Gabriel Gomez Garcia[1], A. Wagner[1], E. Adlakha[1], J.J. Hanley[1], P. Lecumberri-Sanchez[2], K.L. Rasmussen[3], and H. Falck[4]

1. Department of Geology, Saint Mary's University, Halifax, Nova Scotia B3H 3C3, Canada <Gabriel.Gomez.Garcia@smu.ca>;
2. Department of Earth and Atmospheric Sciences, University of Alberta, Edmonton, Alberta T6G 2E3, Canada;
3. Department of Earth, Ocean and Atmospheric Sciences,

University of British Columbia, Vancouver, British Columbia V6T 1Z4, Canada; 4. Northwest Territories Geological Survey, Yellowknife, Northwest Territories X1A 2L9, Canada

The world-class Cantung and Mactung W-Cu-Au skarn deposits are hosted in limestone of the Selwyn Basin, where it is intruded by a series of Cretaceous-aged granitoids known as the Tungsten plutonic suite. Tungsten and the associated metals (e.g., Au, Cu, Mo, Sn) in W skarn settings are thought to be provided and transported by exsolved magmatic-hydrothermal fluids from the granitoids. Several mechanisms for W enrichment in fertile magmas have been proposed, all of which focus on the incompatible element (IE) behaviour of W during protracted fractional crystallization due to (i) mid-crustal depths of magma staging and emplacement, and/or (ii) high dissolved volatile content, and/or (iii) reduced oxidation conditions that prevented fractionation of W in phases such as magnetite.

This study aims to determine the major and trace element concentrations of apatite-hosted silicate melt inclusions (SMI) from the Mine Stock and associated aplite dykes at the Cantung deposit, as well as the Cirque Lake and Rockslide Mountain Stocks and leucocratic dykes at the Mactung deposit. The major element composition of homogenized SMI will be gathered via electron probe microanalysis (EPMA) to classify the tectonic environment of the magmas. The trace element abundances of homogenized and non-homogenized SMI will be acquired via laser-ablation inductively coupled plasma mass spectrometry (LA-ICP-MS) to determine the W and other important ore elements concentrations of the melts during different stages of fractional crystallization. The data will also be used to model the behaviour of the trace elements during fractional crystallization by using the petrography results and mineral-melt partition coefficients of the minerals in the rock samples in batch crystallization calculations.

Preliminary data show a wide range in compositions from intermediate to felsic reflecting the trapping of melts at different stages of fractional crystallization. The transition from syn- to post-collisional may also reflect the entrapment at different stages. Tungsten content in the most evolved melts is up to three orders in magnitude higher than the average crustal values as well as the whole rock. The inclusions with the lower IE represent melts trapped during the earliest stages of fractional crystallization. Positive correlations between Zr/Hf and Nb/Ta indicate the preferred fractionation of Nb and Zr in biotite and zircon, respectively. The negative correlation between Nb/Ta and Ta indicate the incompatible behaviour of Ta during biotite crystallization. When compared to the concentrations of Ta and other IE, W shows enrichment during fractional crystallization reflecting its incompatible behaviour with crystallizing phases.

Sulfur isotope and trace element systematics of pyrite and marcasite associated with epithermal gold mineralization in the northeastern Cobequid Highlands, Nova Scotia, Canada

Jacob Hanley[1], Kevin Neyedley[1,2], Ryan Sharpe[3], Mostafa Fayek[3], and Brandon Boucher[4]

1. Department of Geology, Saint Mary's University, Halifax, Nova Scotia B3H 3C3, Canada <jacob.hanley@smu.ca>; 2. Nova Scotia Department of Natural Resources and Renewables, Halifax, Nova Scotia B3J 2T9, Canada; 3. Department of Earth Sciences, University of Manitoba, Winnipeg, Manitoba R3T 2N2, Canada; 4. Department of Earth Sciences, University of New Brunswick, Fredericton, New Brunswick E3B 5A3, Canada

The chemistry and S isotope composition of pyrite and marcasite from silicified and sulphidized, variably Au-As-Sb-Hg-enriched and barren, Late Devonian to Early Carboniferous bimodal volcanic rocks in the Nuttby and Warwick Mountain areas were investigated by in-situ microanalytical methods (SIMS, LA-ICPMS, EPMA). The aim of the ongoing study is to determine if S isotopic and trace element systematics of Fe sulfide minerals can be used to recognize zones of hydrothermal fluid flow tied to epithermal mineralization, differentiating those from pyritic zones related to other geological processes, unrelated to Au mineralization.

Petrography (optical, SEM) coupled with LA-ICP-MS trace element mapping (14 areas) and $\delta^{34}S$ analysis by SIMS (n = 190 spots) identified 4 stages of pyrite/marcasite. The earliest (type 1 pyrite) comprises ^{34}S-depleted ($\delta^{34}S_{VCDT}$ = -6.4 to -5.4 ‰), metal-poor (based on SEM-EDS) pyrite within sedimentary enclaves enclosed within felsic volcanic rocks. Incorporation of this pyrite into the volcanic rocks did not contribute metals but may have been an important S contaminant. Following this stage, two stages of epithermal pyrite are recognized: Early marcasite and pyrite (type 2), forming the cores of pyrite grains show enrichment in Co-Ni-Cu-Ag-Hg-Cd-Bi-Sb (±Au, As); these cores have $\delta^{34}S_{VCDT}$ from -2.0 to 6.0 ‰ with 90 % of values between -1.5 and 2.0 ‰. Later pyrite (type 3; occurring as rims and oscillatory zones overgrowing type 2) shows enrichment in As-Sb-Mo-Cu-Se (±Au, Ag, Co); the dominant Au-enrichment stage in all pyrites examined occurs in type 3 rims. Type 3 pyrite has $\delta^{34}S_{VCDT}$ values from -6.8 to 2.0 ‰ with 90 % of values between -3 and 1 ‰. Core to rim transitions from type 2 to 3 pyrite generally show a shift to lower $\delta^{34}S_{VCDT}$ values, likely reflecting isotope fractionation during transient fluid boiling. Finally, a late pyrite generation (type 4) shows minor enrichment in Hg-Sb-Ag-Mo and occurs as overgrowths on type 3 pyrite; these overgrowths yield very high $\delta^{34}S_{VCDT}$

values (17.9–23.8 ‰) interpreted to reflect incursion of a fluid containing S derived from the reduction of seawater sulphate at the cessation of epithermal mineralization.

Although there were likely multiple sources of S, overall, the study of pyrite/marcasite indicates that the most important stage of Au enrichment is late in the paragenesis and is most closely correlated to As-Sb-Mo-Cu-Se-Ag enrichment. Some of these metals, including Au, may have been remobilized from earlier pyrite. Incursion of cooler, marine-derived fluids and transient boiling were likely triggers for late Au deposition.

Relationship between gold mineralization in the Annidale and Clarence Stream areas of southern New Brunswick, Canada

Hassan Heidarian[1], David R. Lentz[1], and Kathleen Thorne[2]

1. Department of Earth Sciences, University of New Brunswick, Fredericton, New Brunswick E3B 5A3, Canada <Ha.heidarian@unb.ca>;
2. Geological Surveys Branch, New Brunswick Department of Natural Resources and Energy Development, Fredericton, New Brunswick E3B 5H1, Canada

Tectonically, the various types of hydrothermal gold deposits form progressively through the evolution of subduction-related processes along convergent margins. The orogenic and intrusion-related gold deposits in the Annidale and Clarence Stream areas are interpreted to be different in terms of geological environment, tectonic setting, ore formation system, and timing of mineralization. Since these areas are parallel to each other and formed close to the margin of the subducted zone of Avalonia under Ganderia, gold-forming processes in these two different regions may still have formed in a common geodynamic environment.

The Annidale Belt, along with the Miramichi and St. Croix belts, were accreted onto the New River terrane on the trailing edge of Ganderia during the Early Ordovician closure of the Penobscot back-arc basin. Orogenic gold was formed during the Penobscot orogeny in the Annidale and New River belts. Ordovician orogenic gold was preserved in the Annidale area as no later major magmatic activities occurred in these belts. It is probable that similar orogenic gold mineralization was formed in the southwestern part of the New River Belt (Clarence Stream area) at the same time as in the northeastern part of this belt. The New River Belt was covered by sedimentary sequences of the Ordovician St. Croix and Silurian Mascarene belts in southwestern New Brunswick. Partial melting of the lower Avalonian lithosphere during subduction close to the convergent margin between the Avalonia and Ganderia zones caused extensive magmatic activity, generating the multi-phase Saint George Batholith; this protracted magmatic activity (during the Neoacadian orogeny) digested (assimilated and/or sequestered) parts of the New River and Mascarene belts during emplacement of several phases of the Saint George Batholith. In the Clarence Stream area, the emplacement of the Early Devonian Magaguadavic Granite was followed by thermal events, such as contact metamorphism and fluid circulation. The advanced hydrothermal activities related to emplacement of the Magaguadavic Granite recycled and may have remobilized pre-existing auriferous systems, including orogenic lode gold deposits. These activities ultimately led to the precipitation of gold as several intrusion-related deposits in the shear zones related to the Sawyer Brook Fault. The combination of several factors, including pre-existing orogenic gold deposits, advanced hydrothermal activities related to the Magaguadavic Granite, and the presence of local brittle-ductile shear zones, were crucial and explain the greater concentration of gold in intrusion-related deposits in the Clarence Stream area relative to the orogenic gold deposits in the Annidale area.

Paragenesis of mineralized South Mountain Batholith granitoid rocks at the Castle Frederick prospect, Upper Falmouth, Nova Scotia, Canada

Luke Hilchie[1] and Fergus Tweedale[2]

1. Earthbound Eyes Consulting, East Lawrencetown, Nova Scotia B2Z 1V1, Canada <EarthboundEyes@gmail.com>;
2. Department of Geology, Saint Mary's University, Halifax, Nova Scotia B3H 3C3, Canada

The Castle Frederick prospect is a Pb-Zn play hosted in the granitoid rocks of the Late Devonian (~380–365 Ma) South Mountain Batholith (SMB), within the Meguma terrane, near Upper Falmouth, Nova Scotia. The geochemical anomalies of economic interest (Pb, Zn) and reported mineralogy (sphalerite, galena, pyrite, barite, calcite) bear resemblance to Pennsylvanian (~320–300 Ma), low-temperature epigenetic ores within mineralized sedimentary carbonates of the Windsor Group, a major proportion of the infill of the Maritimes Basin. The base of the Maritimes Basin (i.e., the Devonian–Carboniferous unconformity) is exposed near the prospect, where Horton Group clastic rocks overlie the eroded SMB, and the world-class Walton barite-Pb-Zn-Cu-Ag deposit lies ~30–40 km northeast. The purpose of this research was to test whether mineralization at Castle Frederick is an expression of the same hydrothermal system that produced Maritimes Basin-associated Pennsylvanian

hydrothermal deposits. The work focused on petrographic characterization of several samples selected from drill core, and isotopic microanalytical characterization of minerals associated with the late hydrothermal paragenesis to either date the mineralization or establish an isotopic affinity with the overlying Pennsylvanian hydrothermal deposits. Three parageneses: magmatic crystallization products, hydrothermal "autometamorphic" alteration associated with magmatism, and late hydrothermal mineralization were identified. Magmatic mineralogy is typical of the SMB (cordierite-bearing two-mica monzogranite/granodiorite with accessories of apatite zircon, monazite, TiO_2), as is the autometamorphic suite (alkali feldspar exsolutions, myrmekite intergrowths, sericite after plagioclase, chlorite [with brookite] after biotite, and rare molybdenite). The late hydrothermal suite differs, featuring veins of pyrite (with anatase), calcite, and barite with fine SMB rock fragments, and grain-boundary network replacements/overgrowths (phengite rims on chlorite, calcite-anatase after chlorite-brookite) and disseminations (pyrite, anatase, chalcopyrite, galena, sphalerite) commonly associated previously biotite-rich domains. Pending laser ablation inductively coupled plasma mass spectrometry studies will attempt to date hydrothermal anatase and brookite, and/or examine changes in radiogenic Pb isotope ratios in sheet silicates across the parageneses and in late sulphides to probe connections to the regional Pennsylvanian hydrothermal system associated with the Maritimes Basin.

The Visean to Serpukhovian Millstream Subbasin within the Midland to Lower Millstream areas: implications for Carboniferous regional tectonics of southern New Brunswick, Canada

Steven Hinds[1], Matthew Stimson[2,3], Olivia King[2,3], Duncan McLean[4], and Adrian Park[1]

1. New Brunswick Department of Natural Resources and Energy Development, Geological Surveys Branch, Fredericton, New Brunswick E3B 5H1, Canada <steven.hinds@gnb.ca>;
2. Department of Natural History, New Brunswick Museum, Saint John, New Brunswick E2K 1E5, Canada;
3. Department of Geology, Saint Mary's University, Halifax, Nova Scotia B3H 3C3, Canada;
4. MB Stratigraphy Ltd., Sheffield, S9 5EA, UK.

Recent integration of seismic profiles, palynology, industry reports, boreholes, and field interpretation has confirmed the existence of the Millstream Subbasin, an approximately 80 km^2 pull-apart basin within the Midland area of southern New Brunswick. From the late Tournaisian (?) to Visean–Serpukhovian, the Millstream Subbasin was deposited as a pull-apart basin resulting from differential rates of strike-slip movement along the Belleisle Fault to the north, and the Kennebecasis Fault to the south, which were both intermittently active as dextral strike-slip systems during this time range. The age justification is from palynology samples collected from boreholes and outcrops within the basin. The Millstream Subbasin is bounded by a minor system of normal faults; the Lower Millstream–Parleeville faults to the north and the Dickie Mountain–Peekaboo faults to the south. An initial episode of fault activity caused the opening of the basin by movement on the Lower Millstream and Dickie Mountain faults, which allowed for deposition of a thick, basal red bed clastic sequence of probable Late Tournaisian (?) age, and the subsequent deposition of Visean limestone and evaporite facies. After a period of quiescence, renewed transtension initiated movement on the Parleeville and Peekaboo normal faults, resulting in the deposition of a red clastic sequence above the evaporites and the down-dropping of the central part of the basin until fault movement waned during the early Serpukhovian. Activation of the late normal faults is most likely due to the differential rotation of the Midland area between the Belleisle and Kennebecasis faults, and/or the transfer of dextral movement from the Belleisle Fault to the Kennebecasis Fault. Limited field mapping to the east in the Smiths Creek area suggests the current understanding of the dextral displacement kinematics of the Kennebecasis Fault during the Visean–Serpukhovian needs revision, however additional field studies and palynology will be required to improve the confidence level of these initial observations.

Modelling the pressure-temperature-time evolution of in situ shock veins from the Manicouagan impact structure

Randy G. Hopkins and John G. Spray

Planetary and Space Science Centre, University of New Brunswick, Fredericton, New Brunswick E3B 5A3, Canada <rhopkins@unb.ca>

The Manicouagan impact structure is one of three terrestrial craters in which in situ shock veins have been identified. Shock veins are thin (<2 mm) shock-induced frictional-melt bodies that form syn-shock during the early compression stage of impact crater formation. Their formation has been attributed to pressure excursions within the target rock leading to the presence of high-pressure polymorphs within shock vein matrices, with less regard for the effect that temperature may play in these transitions.

This work utilizes numerical computing software (via MathWorks MATLAB), which has been developed to understand the relationship between shock wave passage

in geological targets (i.e., heterogeneous media) and the formation of shock veins (and associated high pressure/temperature polymorphs) within the target rock. This approach takes into consideration the pressure due to the passage of the shock front, subsequent rarefaction unloading pressures, and associated heating and cooling rates. The model is applied to calculate pressure-temperature-time conditions for hollandite-structured plagioclase and stishovite-bearing shock veins within the central uplift of the Manicouagan impact structure of Quebec.

Modelling reveals that: (1) at the time of shock vein formation (1.5 s following the initial contact of the projectile), the shock front pressure was 10.5 GPa and the width of the shock wave was 7.9 km; and (2) the melt within the shock veins initially reached ~2200°C, which corresponds to the melting temperature of the target rock at 10.5 GPa. These conditions are sufficient for hollandite and stishovite formation. Thus, pressure excursions beyond the peak shock pressure of the shock wave are not required for the shock veins to enter the appropriate stability fields. This work suggests that high pressure phases within the shock vein system are not the result of pressure excursions but rather are facilitated by localized high temperatures realized by the shock vein system.

A new exhibit at the Quartermain Earth Science Centre: bridging geology with biology celebrating paleontology and ornithology of Atlantic Canada. Honouring the work of paleontologist Dr. Ronald Pickerill

Grace Jackson, Ethan Mcdonald, and Ann C. Timmermans

Quartermain Earth Science Centre, University of New Brunswick, Fredericton, New Brunswick E3B 5A3, Canada <quartermain@unb.ca>

A new interactive exhibit bridging the disciplines of biology and earth science is near completion at the Quartermain Earth Science Centre (QESC), located at the University of New Brunswick. Phase I of the project is dedicated to paleontologist Dr. Ronald Pickerill in recognition of his important contribution to the field of ichnology. Three robust collapsible cabinets contain six dioramas, representing the six periods of the Paleozoic Era and are QESC's first transportable exhibit. Each diorama features colourful landscapes with paleontological and ichnological fossils from targeted locations around Atlantic Canada. The exhibit includes informative legends for the various invertebrate, vertebrate, and plant fossils, plexiglass-covered drawers with additional specimens, and four introductory panels. Each cabinet can be easily disassembled into five pieces for transport. Transitioning to the Mesozoic Era, Phase II of the project focuses on several theropod dinosaurs from the Triassic to Cretaceous periods. A series of interactive displays including floor mounted trackways have been established along a high-traffic route between the Forestry and Geology Building, through the Science Concourse, culminating at the Biology Greenhouse. Informative display panels covering example fossil discoveries as well as phylogenetic and macroevolutionary studies are presented alongside the trackways. Seven evolutionary jumps are represented along the journey, from the theropod's earliest ancestor (*Herrerasaurus* sp.), to the earliest recognizable bird (*Archaeopteryx* sp.), to the more recent giant flightless bird of the Cenozoic Era (*Gastornis* sp.). The exhibit ends with Phase III, inside the entrance lobby to Loring Bailey Hall. Presented in the form of a wall-size phylogeny graphic opposite of a large diorama case of taxidermized avian, visitors can examine the diversity, detail, and delicate beauty of Neornithes (modern birds), from New Brunswick and around the world. This exhibit has been designed so that students, educators, and visiting groups can engage with and learn about many fields of science, including ichnology, taphonomy, invertebrate and vertebrate paleontology, paleoenvironmental geology, phylogeny, biophysics, biomechanical engineering, and ornithology. This project is made financially possible through gracious funding by the Canadian Geological Foundation, the Quartermain Earth Science Centre, and the department of Biology at the University of New Brunswick. Presenters will share the highlights of the exhibit and the applications to education.

Nova Scotia basalt as a soil additive for CO_2 capture and fertilizing crops

Christopher D. Jauer

Geological Survey of Canada (Atlantic), Bedford Institute of Oceanography, Dartmouth, Nova Scotia B2Y 4A2, Canada <chris.jauer@NRCan-RNCan.gc.ca>

Recent work on Enhanced Rock Weathering (ERW) shows that pulverized basalt spread over croplands is not only an effective crop fertilizer but also a stand-alone CO_2 sink. Airborne carbon dioxide mineralizes upon contact with the various minerals in pulverized basalt. Compared to subsurface CO_2 injection, this method of capture is inexpensive and simple to regulate and has the added benefit that the resulting basalt fertilizer runoff can ultimately contribute to the amelioration of ocean acidification.

Nova Scotia has an abundance of basalt deposits, both exposed and buried. The chemical storage of carbon dioxide

in basalt is reasonably established, however the use of these deposits as fertilizer for agriculture is not widely known. The North Mountain Basalt from Nova Scotia also hosts zeolites that act as a cation intensive agent that when added to soil makes an excellent supplement for enhanced plant growth.

It has been estimated that the volume of North Mountain Basalt accessible onshore is over 2300 km^3, spread over some 9400 km^2. Given the relative potential ease of extracting and transporting this rock, much of which is exposed along the southern coast of the Bay of Fundy, it could represent a new "green industry" working to apply ERW methods using agriculture on a regional scale to help meet Canadian CO_2 emission limits. Mapping the North Mountain Basalt and similar basalt formations in the Maritime Provinces with respect to their suitability for ERW development is a necessary first step, which can be achieved with archival data sets. An initial laboratory proof-of-concept test for ERW in a laboratory setting could be arranged with the Centre for Sustainable Soil Management, Department of Plant, Food, and Environmental Sciences at Dalhousie University. This step would add credibility in a Canadian context toward the application of this new method of carbon sequestration.

The work described here is being carried out under the Carbon Capture Utilization and Storage section within the Marine Geoscience for Marine Spatial Planning program of the Geological Survey of Canada.

A targeting tool for gold mineralization in the Williams Brook epithermal system northern New Brunswick, Canada: insights from compositional geochemical balances

Farzaneh Mami Khalifani[1], David R. Lentz[1], Mohammad Parsa[1], and James A. Walker[2]

1. Department of Earth Sciences, University of New Brunswick, Fredericton, New Brunswick E3B 5A3, Canada <farzaneh.mamikhalifani@unb.ca>;
2. New Brunswick Department of Natural Resources and Energy Development, South Tetagouche, New Brunswick E2A 7B8, Canada

The Williams Brook property, located in the northwestern part of the Chaleur Bay Synclinorium of northern New Brunswick, hosts gold mineralization within Silurian–Devonian, bimodal volcano-sedimentary rocks of the Wapske Formation (Tobique Group). The Tobique Group is bounded to the north and west by the Rocky Brook–Millstream Fault, and to the south and to the east where it lies unconformably on the Miramichi Inlier. The fault-controlled mineralization at Williams Brook is a low-sulfidation epithermal style system, hosted by quartz veins cross cutting flow-layered K-feldspar porphyritic rhyolite. Preliminary studies indicate that dextral movement along the Rocky–Brook–Millstream fault system during Early Devonian Acadian orogenesis exerts substantial control over gold mineralization at Williams Brook. Despite the similarities in the processes that trigger ore-metal deposition among various systems variation in local geological settings render differences in grade, shape, geochemical, and geophysical features of individual deposits. Consequently, a solid understanding of individual mineral deposits in a specific area is critical to future exploration success. Although pathfinders have been applied to constrain gold deposits geochemically, it is challenging to identify a unique suite of pathfinder elements for use as a vectoring tool exclusively for gold exploration. This study seeks to (i) address the question as to which elements can be regarded as pathfinders at the Williams Brook deposit and (ii) define a geochemical targeting tool for similar style mineralization. Geochemical samples (n = 1153) collected from trenches and outcrops underwent multi-element analysis. Grab samples collected from quartz veins were commonly anomalous in Au (128, 44.4, 38.8, 21, 15.95, 7.38, 6.63, 5.55, 2.94, and 1.14 ppm). In addition, the rhyolite, which contained a network of quartz veinlets to stockwork, contained several significant gold results. These were subjected to compositional data analysis (CODA) techniques, namely CODA-based principal component analysis, compositional balance analysis, and element association analysis. The compositional data includes information about relative magnitudes. Analyzing the covariance structures of the log ratios can inquire about the relationship between compositional variables. These techniques help reveal the interconnection between various element associations at the Williams Brook property as either uni- or multi-element geochemical signatures. Subsequent mapping of these signatures using CODA-based geochemical tools and measuring their spatial association with gold mineralization was conducted. The results of this study can help assist further exploration and finding promising area in the Williams Brook area. The methodology adopted herein can be applied to other gold deposits/occurrences, especially epithermal systems, for unraveling the interrelationship between different elements and gold mineralization.

Palynology of the Albert Formation of New Brunswick, Canada

Olivia King[1, 2], R. Andrew MacRae[2], Matthew Stimson[1, 2], Steven Hinds[3], Adrian Park[3], and Duncan McLean[4]

1. Department of Natural History, New Brunswick Museum, Saint John, New Brunswick E2K 1E5, Canada <olivia,king@smu.ca>;

2. Department of Geology, Saint Mary's University, Halifax, Nova Scotia B3H 3C3, Canada;
3. New Brunswick Geological Survey, New Brunswick Department of Natural Resources and Energy Development, Fredericton, New Brunswick E3B 5H1, Canada;
4. MB Stratigraphy Ltd., Sheffield, S9 5EA, UK.

A palynological (plant spores) biostratigraphic study of the Tournaisian (Early Carboniferous) aged sites between the townships of Bloomfield and Norton, New Brunswick is being conducted. Newly collected and historical samples are being used to study the subdivisions within the *Vallatisporites vallatus* zone: *Claytonispora distincta* (formerly *Dibolisporites distinctus*) and *Speleaotriletes cabotii* subzones (informally NB Spore Zone 2 and 3).

The Tournaisian and Visean stages of the Mississippian Period are considered part of 'Romer's Gap', an interval of time when tetrapods diversified and made the transition from aquatic into terrestrial environments. Three fossil locations are known to yield fossil evidence of tetrapods from Romer's Gap: Scotland; Horton Bluff, Nova Scotia; and the newly discovered tetrapod tracks preserved in sites around Norton, New Brunswick. Interest in the relative age of these fossil-bearing strata arose due to the discovery of these important tetrapod ichnofossils as they could represent some of the earliest evidence of terrestrial tetrapods within this hiatus. Refining the age of the fossil bearing strata is important to better understand how the recently discovered sites near Norton compare to the broader evolutionary story of vertebrate life on land. A lack of marine biota, datable macrofossils or radiometrically-dateable volcanic rocks leaves palynology as the sole tool to assess the relative timing of the New Brunswick stratigraphy.

The historical palynological framework (biozonations) applied to the Tournaisian in the region is based on sites along the Horton Bluff shoreline and surrounding area in Nova Scotia (including Blue Beach). This biozonation framework has been widely accepted and applied across Atlantic Canada. Upon further inspection of the original literature and sampled sites, questions have been raised about the *Claytonispora distincta* (formerly *Dibolisporites distinctus*) and *Speleaotriletes cabotii* biozones at the Blue Beach tetrapod locality. Once fully unravelled, this new information may affect how to determine the relative age of similar sites in Atlantic Canada. Better understanding of this original palynological framework will allow for better correlation of sites within Romer's Gap, both locally and globally.

Survey of porewater geochemistry within deep marine hydrocarbon seep sediments of the Scotian Slope, Nova Scotia, Canada*

Nikita Lakhanpal[1], Venus Baghalabadi[1], Natasha Morrison[2], Adam MacDonald[2], and G. Todd Ventura[1]

1. Department of Geology, Saint Mary's University, Halifax, Nova Scotia B3H3C3, Canada <nikita.nikita@smu.ca>;
2. Nova Scotia Department of Natural Resources and Renewables, Halifax, Nova Scotia B3J 3J9, Canada

The ocean floor surface sediments of the Scotian Slope, Nova Scotia are host to a complex network of microbially mediated reactions that knit together the carbon, sulfur, and nitrogen biogeochemical cycles. Limited diffusion between the upper water column and ocean floor muds pore space, coupled with competitive microbial ecological niche partitioning, leads to the formation of biogeochemically controlled redox gradients. The energetics of such gradients are further governed by microbial heterotrophy with the deposition of detrital organic matter that is primarily sourced from terrestrial runoff and upper water column productivity. However, these microbial biogeochemical zones will likely change if surface sediments are impregnated by hydrocarbon seepage that migrates up from deeper within the basin. Extracting the porewaters anions, such as sulfate, carbonate, nitrate, nitrite, from frozen marine sediment cores located in prospective hydrocarbon seep sites is proposed to reconstruct biogeochemical stratification depth profiles that can provide additional evidence for active seepage events. These profiles define microbial metabolic processes within the sediment subsurface. To test this hypothesis, a total of 28 samples across 7 sediment cores were collected, separated, centrifugated, and analyzed using ion chromatography. Systematic stratigraphic trend of anions was observed in the sampled cores. For example, carbonate porewater concentrations increase with sediment burial depth. Sulfate concentrations, however, systematically decrease with depth. Additionally, seep locations will be examined as this study progresses. When complete, it is expected that the results will help constrain the depth and extent to which biogeochemical cycles change within the Scotian Slope surface sediments.

**Winner: AGS Rob Raeside Award for best undergraduate student poster*

Seeking seeps with geophysics in the Blow Me Down Massif, western Newfoundland, Canada

Alison Leitch

Department of Earth Sciences, Memorial University of Newfoundland, St John's, Newfoundland and Labrador A1B 3X5, Canada <aleitch@mun.ca>

The Bay of Islands Ophiolite (BIOC) in western Newfoundland consists of four massifs, blocks of oceanic lithosphere that were obducted onto the margin of Laurentia during the Taconic orogeny (~ 470 Ma). Chemical reactions between meteoric waters and peridotite result in the serpentinization of the rock and highly reducing spring water. Also produced are hydrogen and methane which may support extreme life, which in turn is of interest to biogeochemists and astrobiologists. The small springs, or more often seeps, are difficult to detect, and they are usually found by ground searches for associated travertine deposits. However, the reactions involve strong electrical potentials and result in the production of magnetite, therefore they may be detected by geophysical surveys. Previous studies in Winterhouse Canyon, within the ultramafic Tablelands Massif, were successful in correlating known seeps with strong magnetic and self-potential (electrical) anomalies and identifying a further potential occurrence. In the summer of 2021, magnetic and self-potential surveys were carried out along a section of a canyon within the more southerly Blow Me Down Massif. In this location, electrical and magnetic anomalies of similar magnitude to the Tablelands sites were observed, though their relationship to observed seeps was more enigmatic, possibly due to more complex geological structure.

Reconciling adakite geochemical systematics: a review

David R Lentz and Fazilat Yousefi

Department of Earth Sciences, University of New Brunswick, Fredericton, New Brunswick E3B 5A3, Canada <dlentz@unb.ca>

Since 1978, adakitic volcanic and subvolcanic rocks have been recognized from the Island of Adak in the Andreanof Islands (Aleutians chain); they have enrichment in LILE, LREE, with high La/Yb, but also high Sr/Y and are low in HREE, Y (<18 ppm), and Yb (<1.8 ppm). Since the 1990s, adakites have been recognized worldwide, with similar geochemical characteristics, from recent to Archean TTGD magmatic suites. Based on GEOROC data, the geochemical composition of adakite rocks are divided into two types; high-SiO_2 adakites (HSA; SiO_2>60 wt%) and low-SiO_2adakites (LSA; SiO_2<60 wt%), although they should be redefined to be high-SiO_2 adakites (HSA; SiO_2>63 wt%), with low-SiO_2 adakites (LSA; SiO_2 57–63 wt%) and basaltic andesite adakites (BAA; SiO_2 52–57 wt%), which are similar to high Mg adakites (MgO>3 wt%). These rocks are subalkalic on the TAS diagram, and the boundary between sodic (Na), sodic-potassic (Na-K), and potassic (K) should follow the lower and upper boundary of the calc-alkaline series. The ASI is typical of metaluminous compositions and I-type suites (<1.1). The FeOt/MgO is <4, but typically ranges between 1.0 and 2.5 depending on redox and fractionation. The MnO is low (<0.15 wt%) with low FeOt/MnO ranging between 20–120, again reflecting higher redox. TiO_2 ranges from 0.15 to 1.15 wt%, V is 25 to 250 ppm, and the Ti/V <100, typical of transitional to calc-alkaline compositions reflecting higher redox. As many major elements are mobile in altered rocks, like porphyry environments, Zr/Ti is used as proxy for SiO_2 with a direct correlation. Immobile high field strength element and immobile element ratio diagrams are very useful; the Zr/Ti vs Nb/Y diagram that is a popular compositional discriminant has issues with anomalously low Y, i.e., the Nb/Y is over 0.7, even though these are all subalkaline rocks. The Nb + Y are like volcanic arc rocks (I-type) (<<50 ppm) and does not vary systematically with Zr/Ti. The Th abundance of suites varies with Zr/Ti, with multiple trends reflecting fractionation, and possibly magma mixing or contamination by subducting sediments or continental crust. The La/Yb (>2.6), Zr/Y (>2.8), Th/Y (>2.0), Th/Yb (>0.35), Zr/Nb (>5), and Th/Nb (>0.2) are all consistent with transitional to calc-alkaline signatures. Other than higher redox due to subduction metasomatism, the discrimination of various melt sources, like oceanic slab (very low Th), supra-subduction zone mantle (low Th), and crust (via AFC) (higher Th) relative to fractionation can only be discriminated by certain LILE like Th and Nb.

The impact of submarine canyons and channels on primary productivity dynamics in the Lower St. Lawrence Estuary, eastern Canada

Audrey Limoges[1], Jean-Carlos Montero-Serrano[2], Alexandre Normandeau[3], David Didier[4], Daniel Bourgault[2], Camille Deslauriers[5], Michel Gosselin[2], Patrick Lajeunesse[6], Catherine Lalande[7], Kateri Lemmens[5], Urs Neumeier[2], André Rochon[2], Owen Sherwood[8], Guillaume St-Onge[2], Pascal Bernatchez[4], Danny Rondeau[9], Khouloud Baccara[2], Camille Bernier[8], Florian Jacques[2], Tina Laphengphratheng[5], and Hannah Sharpe[1]

1. Department of Earth Sciences, University of New Brunswick, Fredericton, New Brunswick E3B 5A3, Canada <alimoges@unb.ca>;
2. Institut des Sciences de la mer de Rimouski, Université du Québec à Rimouski, Rimouski, Québec G5L 2Z9, Canada;
3. Geological Survey of Canada (Atlantic), Dartmouth, Nova Scotia B2Y 4A2, Canada;
4. Département de Biology, Chimie and Géographie, Université du Québec à Rimouski, Rimouski, Québec G5L 3A1, Canada;
5. Département des lettres et humanités Université du Québec à Rimouski, Rimouski, Québec G5L 3A1, Canada;
6. Département de Géographie, Université Laval, Québec, Québec G1V 0A6, Canada;
7. Amundsen Science, Université Laval, Québec, Québec G1V 0A6, Canada;
8. Department of Earth and Environmental Sciences, Dalhousie University, Halifax, Nova Scotia B3H 4R2, Canada;
9. Département d'Éthique et Philosophie Pratique, Université du Québec à Rimouski, Rimouski, Québec G5L 3A1, Canada

The complex topography surrounding submarine canyons influences local hydrodynamics. For example, canyon-induced upwelling can supply nutrients to the surface waters and stimulate biological productivity. Canyons may also represent hazard hotspots by acting as preferential pathways for turbidity currents traveling down to deeper marine basins. The glacial history of the Lower St. Lawrence Estuary (LSLE), Quebec, created a deep and steep estuary that now hosts several submarine canyon and channel systems. While these canyons may provide numerous ecosystem services, it is hypothesized that they may also be pathways for the dispersion of toxic algae, notably the dinoflagellate *Alexandrium catenella* for which sedimentary seedbeds are documented regionally.

This highly multidisciplinary project aims to assess the impact of hydrodynamic processes occurring in submarine canyons located off Pointe-des-Monts on primary production in the LSLE. Coastal sediment budgets around Pointe-des-Monts were monitored and current profilers were deployed along with sediment traps inside and outside the Pointe-des-Monts canyon system. Coastal and nearshore imagery shows that sediments are stored on the shelf, in small, ponded basins. During intense storms, increased wave heights sometimes lead to shelf-sediment resuspension and trigger turbidity currents. Other hydrodynamic processes including internal tides and internal waves also remobilize near-bed sediment and cause vertical mixing. Chlorophyll-a data from the sediment traps suggest that these processes impact primary production, as unpredictable phenological patterns of pelagic primary production are recorded in the canyon compared to background LSLE conditions. Finally, this research animates literary creations that will be combined into a logbook for the large public.

Save paper, save time? Digital answer entry during in-person geology labs (a pilot study)

Jason Loxton and Lilian Navarro

Department of Mathematics, Physics, and Geology, Cape Breton University, Sydney, Nova Scotia B1P 6L2, Canada <Jason_loxton@cbu.ca>

The shift to online learning in Nova Scotia during the 2020–2021 academic year forced faculty to digitize activities that would traditionally be done using paper and pen. This included geology labs, which needed to be completed using a digital interface, even where physical specimens were provided by mail. While adopted by necessity, digital data entry offered several significant advantages over paper and pen: (1) many questions can be set for automated grading, allowing for real time feedback to support student learning; (2) automated marking of fact-based questions frees up instructor time, allowing them to concentrate on more intellectually taxing activities; (3) digital entry eliminates the risk of misplaced labs; and (4) digital entry significantly reduces the paper required (a positive environmental step). The transition back to in-person learning provided an opportunity to test whether these benefits could be retained by having students enter answers using a digital device, while working in a laboratory setting with physical specimens. The results of a pilot study of digital answer entry, conducted in an introductory Engineering Geology lab over the 2021 fall semester at Cape Breton University (n = 30) are reported. This pilot demonstrated the feasibility of utilizing digital entry, using the tools offered by the Moodle learning management system; general acceptance of a digital interface (69% preferred digital entry or were neutral); and—somewhat surprisingly—student tolerance for smart phone-only data entry. However, it also highlighted limitations, including periodic technical glitches, high initial instructor effort (during lab buildout), and difficulty accommodating short answer questions.

The Signal Hill Group, Newfoundland, Canada: a record of pre-vegetated fluvio-deltaic response to progressive Neoproterozoic deformation during the Avalonian orogeny

David G. Lowe[1], Santiago Serno Ortiz[1], Andrea Mills[2], Benjamin F. Stanley[1], and Grace Khatrine[1]

1. Department of Earth Sciences, Memorial University, St. John's, Newfoundland and Labrador A1B 3X7, Canada <dlowe@mun.ca>;

2. Geological Survey of Newfoundland and Labrador, St. John's, Newfoundland and Labrador A1B 4J6, Canada

The Signal Hill Group consists of the youngest Neoproterozoic strata in the Newfoundland Avalon Zone. It records sedimentation coeval with the ca. 560–555 Ma Avalonian orogeny, defined by local deformation of west Avalonia, including metamorphism, faulting, and folding coinciding with the shutdown of arc magmatism and initiation of local extensional magmatism. The regional tectonic significance of this orogeny is equivocal, attributed to either oceanic trench subduction or terrane collision. Nevertheless, the Signal Hill Group provides a record of clastic progradation during the Avalonian orogeny, details of which can resolve the near-surface effects and kinematics of the Avalonian orogeny and provide an excellent example of the response of pre-vegetated fluvio-deltaic systems to progressive deformation. The Signal Hill Group conformably overlies fine-grained shelf and pro-deltaic strata of the St. John's Group, forming a north-south oriented folded succession exposed along the eastern edge of the Avalon Peninsula. At the base of Signal Hill, the Gibbet Hill Formation and overlying Quidi Vidi Formation record southward progradation of a sandy delta front environment dominated by mouth bars and distributary channel networks. Preliminary structural and stratigraphic evidence suggests blind faulting, folding, unconformity development, and basin reconfiguration between these units, supported by locally intense soft-sediment deformation along their contact. Conformably overlying the Quidi Vidi Formation are gravelly braided fluvial deposits of the Cuckhold Formation, recording amalgamation of alluvial channel belts with overall coarsening-up to pebble-cobble conglomerate followed by fining-up to pebbly sandstone.

In the northern (proximal) Signal Hill basin, subsequent folding of the Signal Hill Group coincided with erosion that locally removed the Cuckhold Formation, with subsequent onlap of gravelly braded fluvial growth strata of the Flatrock Cove Formation. Here, progressive fault propagation then resulted in a change from braided channel belt to alluvial fan floodplain conditions. Conversely, in the southern (distal) part of the Signal Hill basin, the Cuckhold Formation is conformably overlain by the Blackhead Formation, recording anomalous overbank mudstone preservation under conditions of high sediment accommodation. It is not understood if or how these post-Cuckhold proximal and distal events were related; however, it is possible that renewed thrust propagation and orogenic loading led to proximal deformation and growth stratification (Flatrock Cove Formation), with coinciding reciprocal foredeep subsidence and preservation of overbank strata farther south (Blackhead Formation). Ongoing facies, stratigraphic, provenance, and geochronology investigations will test this hypothesis and resolve details of pre-vegetated fluvio-deltaic sedimentation and its response to orogenesis in the Signal Hill Group.

New insights about Ganderian accretion to Laurentia and post-accretion tectonism from the southern end of the Miramichi inlier, east-central Maine, USA

Allan Ludman

School of Earth and Environmental Sciences, Queens College (CUNY), Flushing New York 11367, USA <allan.ludman@qc.cuny.edu>

The Miramichi inlier is the largest Ganderian Cambrian–Ordovician belt in New Brunswick, extending 250 km from Chaleur Bay to the Maine border. It is also the northwesternmost Ganderian belt in New Brunswick, and tectonic models for its middle Ordovician accretion to Laurentia have been based almost entirely on decades of intense studies from Bathurst to the Eel River area. Results of recent mapping and volcanic geochemical and geochronologic studies of the ~100 km long continuation of the inlier in Maine support some aspects of the tectonic model but require rethinking of others.

As in New Brunswick, a continental arc is suggested by a siliciclastic substrate beneath a calc-alkaline basalt-andesite-rhyolite suite and confirmed by trace element discrimination diagrams. Ages of the Maine (469 Ma) and most likely correlative Meductic Group volcanic rocks in New Brunswick (480 Ma) suggest active subduction related volcanism over at least 11 million years. Stratigraphic and lithologic differences in the volcanic suites along the length of the inlier probably result from eruptions at multiple volcanic centres.

Volcanic rocks in the Munsungun–Winterville and Weeksboro–Lunksoos Lake inliers in northeastern Maine provide information as much as 150 km (present distance) closer to the leading edge of Ganderia than those in the Miramichi. Current work, the first in those areas in the plate tectonic era, reports ages that indicate eruptions coeval with those in the Miramichi inlier in Maine and New Brunswick (Meductic Group). This is not consistent with models positing progressive northwest migration of volcanism in a single arc and suggests that a multiple arc model is more likely.

The Miramichi inlier is separated by faults from adjacent cover rocks – in Maine the Fredericton trough to the southeast and Central Maine/Aroostook–Matapedia basin (CMAM) to the northwest. Map relationships suggest a complex, multi-phase history for the northwestern boundary, beginning with large-scale pre-Acadian thrusting of CMAM strata onto and in some places over their Miramichi source.

Those strata are preserved in a small klippe near the New Brunswick border, and the southwestern segment of the inlier in Maine appears to be a window through the thrust sheet.

The Miramichi inlier terminates abruptly in east-central Maine at the intersection of its northwest and southeast boundary faults. Southwest of the termination, similar Fredericton and CMAM strata are juxtaposed, but their similarity obscures the continuation of the fault that separates them.

Geogenic sources of arsenic in well water related to granites from southwestern Nova Scotia, Canada

Bryan J. Maciag and James M. Brenan

Department of Earth and Environmental Sciences, Dalhousie University, Halifax, Nova Scotia B3H 4R2, Canada <bmaciag@dal.ca>

Arsenic toxicity in drinking water sourced from groundwater is a global concern. Elevated arsenic in Nova Scotia well water is typically drawn from aquifers with metamorphic or granitic bedrock. In southwestern Nova Scotia, the granitic bedrock is divided into two geochemical and petrological affinities, central (South Mountain and Musquodoboit batholiths) and southern (Port Mouton, Shelburne, and Barrington Pass plutons). Arsenic concentrations in 84% of well water samples taken from the central batholiths are greater than the highest concentrations observed in the southern plutons. Since well water arsenic content does not scale with the whole-rock arsenic concentrations, it is thought the origin of this discrepancy is mineralogical. This study examines the arsenic content of the major and accessory phases of central and southern granites, as well as evaluates the susceptibility of these phases to weathering by calculating the saturation index (SI) of each mineral in the local well water. Analysis by laser ablation ICP-MS was performed on over 292 grains from 8 samples from the central granites (with an additional 472 analysis of primarily apatite and biotite from another 45 samples from a separate study) and 79 grains from 4 samples of the Port Mouton Pluton which represents the southern granites.

The major rock-forming silicates contain over 50% of the arsenic in all Nova Scotia granites. In the central granites, monazite, pyrite, and cordierite, along with its alteration products, contain 5–9%, 5–8% and, 9–27% of the total arsenic budget, respectively. Additionally, ferric hydroxide and hydrous oxide (FOH) oxidation products of pyrite may contain 0.5–6% of the arsenic budget. Mineral saturation index and Eh-pH calculations show that both monazite and the rock-forming silicates are stable in the local groundwater, whereas pyrite and cordierite are unstable and therefore release arsenic upon dissolution. In the southern granitic bodies, pyrite is the only significant source of arsenic other than the rock-forming silicates. This pyrite is largely pristine rather than oxidized, in contrast to the central plutons. The absence of FOH replacement of pyrite suggests that pyrite does not contribute significant arsenic to the local well water. Thus, the difference in well water arsenic concentration between the southern and central granites is attributed to (1) the absence of cordierite in the southern plutons and (2) different degrees of pyrite oxidation. The lower degree of pyrite oxidation in the southern granites suggests that the sulphides have not reacted with groundwater, likely due to lower rock permeability.

The paleobiogeographic distribution of graptolites in the earliest Silurian following the Late Ordovician mass extinction event

Bailey Malay

Department of Earth Sciences, St. Francis Xavier University, Antigonish, Nova Scotia B2G 2W5, Canada <bmalay@stfx.ca>

The Late Ordovician Mass Extinction Event (LOME) was the world's first major mass extinction of the Phanerozoic, which killed an estimated 80 percent of global species. The immediate aftermath of the LOME is well documented in the earliest Silurian, as it was a time of anoxia that readily fossilized deep marine organisms. One group of organisms that were incredibly helpful in documenting the aftereffects of the LOME are the graptolites. Globally well preserved in black shales during the Rhuddanian (the earliest Silurian), these zooplankton were geographically widespread and make excellent biostratigraphic index taxa. Samples taken from the Road River Group in the Peel River area of the Yukon Territory, along with samples taken from Cape Phillips South on Cornwallis Island, part of the Canadian Arctic Islands, have been identified and documented. These taxa belong to the earliest Silurian, specifically the *Akidograptus ascensus – Parakidograptus acuminatus* Biozone, a biozone that is globally correlative as there are a significant number of graptolitic black shales of this age preserved. A quantitative global paleobiogeographic analysis has been undertaken using data from this study, together with global data available from critically reassessed published and unpublished studies. These results will help determine the changes in paleobiogeography of the graptolites following the LOME in the earliest Silurian. Cluster analyses, specifically using the Unweighted Pair Group Method algorithm and non-metric multidimensional scaling (NMDS), were implemented to analyze the data. Together

these analyses show that graptolites underwent little change in paleobiogeographic distribution between the *ascensus* to *acuminatus* biozones. The assemblages of South China and northern Canada cluster together, as both were on the outer edge of the Panthalassic Ocean in the northern paleotropics. The assemblages from peri-Gondwanan Europe cluster closely with those of Scotland, England, Wales, and Baltica, as these were all located in the closing Iapetus Ocean in the southern subtropics to middle-paleolatitudes. Comparison with published paleoceanographic studies suggest that ocean circulation kept these two clusters mostly separate. Faunas of northern Africa were found to be separate from all other assemblages, likely due to their location in Gondwanan deep epicontinental basins.

Automated sinkhole delineation using LiDAR in the Cumberland Basin, Nova Scotia, Canada

Mitch Maracle[1], Morgan Snyder[1], and Peter Opra[2]

1. Department of Earth and Environmental Science, Acadia University, Wolfville, Nova Scotia B4P 2R6, Canada <159979m@acadiau.ca>;
2. 34 Agincourt Crescent, Dartmouth, Nova Scotia B2V 1J1, Canada

The Maritimes Basin is composed of multiple intra-basin depocentres each with variable structural and depositional regimes related to halokinesis. The Cumberland Basin, in northwestern Nova Scotia, is one such depocentre oriented parallel to the east-west striking Cobequid–Chedabucto fault system. Stratigraphy in the Cumberland Basin is dominantly terrestrial; however, does include marine rocks of the Visean Windsor Group. Evaporites of the Windsor Group, including halite, anhydrite, and gypsum, accumulated in marine supersaline water bodies during a period of transtensional rifting. Windsor Group evaporites in the Cumberland Basin are abundant; however, because evaporites are highly soluble, very few outcrops are exposed. Karstification of evaporitic rocks can produce solution collapse structures (i.e., sinkholes). Recognition of solution collapse structures on aerial photography is difficult in Nova Scotia due to overburden and vegetation. LiDAR (Light Detection and Ranging) is an active remote sensing system that can model the ground surface with the ability of penetrating the overlying vegetation, allowing for the clear observation of structural geomorphological features, including sinkholes. A model to automatically identify and delineate sinkholes in the Cumberland Basin is here created using ArcGIS software to transform provincial LiDAR data into raster datasets, on which the analysis is conducted. ModelBuilder is an application in ArcGIS that allows geoprocessing tools to be tied together. The model allows an automated workflow that extracts a bare earth model from the input LiDAR data and employs a sink-filling method to locate solution collapse structures systematically and accurately. Map Algebra, and the application of filters, such as low pass and high pass, are the methods investigated to remove insignificant and artefact features. Constructing the geoprocessing model in ModelBuilder results in an intuitive tool that is sharable with other ArcGIS users. To test the model's effectiveness on solution collapse structures in the Cumberland Basin, an area of interest along the Phillip and Pugwash rivers was chosen. The area of interest is a zone with sinkholes atop or adjacent to mapped diapirs. The model identified both known and unknown structures within the study areas, indicating preliminary success in the model's delineation methods, especially when compared to manual visual identification and interpretation. This new model will be used for subsequent studies in sinkhole detection in Nova Scotia as morphometrical variables are further constrained. Identifying the locations of surface collapse structures gives greater insight to both the halokinetic history of the Cumberland Basin and potential risks associated with future sinkhole development.

Influence of tectonically controlled topography on deep-water sedimentation

Vittorio Maselli[1], Aaron Micallef[2,3], Alexandre Normandeau[4], Davide Oppo[5], David Iacopini[6], Andrew Green[7], and Zhiyuan Ge[8]

1. Department of Earth and Environmental Sciences, Dalhousie University, Halifax, Nova Scotia B3H 4R2, Canada <vittorio.maselli@dal.ca>;
2. Marine Geology and Seafloor Surveying, Department of Geosciences, University of Malta, Msida, 1805, Malta;
3. Helmholtz Centre for Ocean Research, GEOMAR, 24148 Kiel, Germany;
4. Geological Survey of Canada, Natural Resources Canada, Dartmouth, Nova Scotia B2Y 4A2, Canada;
5. School of Geosciences, University of Louisiana at Lafayette, Lafayette, Louisiana 70504, USA;
6. DiSTAR, Università di Napoli Federico 11 II, 80138 Naples, Italy;
7. Geological Sciences, University of KwaZulu-Natal, Durban, 4041, South Africa;
8. College of Geosciences, China University of Petroleum, Beijing, 94305, China

Increasing availability of high-resolution bathymetric and seismic data along the slope of continental margins has allowed a step change in understanding processes

and products of turbidity currents. Yet, many questions regarding how such flows interact with tectonic-driven deformation of the seafloor are outstanding. Using 3D seismic reflection data from the Levant Basin (Eastern Mediterranean Sea), the spatial and temporal evolution of bedforms on a deep-water fan cut by an active normal fault was investigated. The goal is to understand how a dynamic knickpoint controls sediment deposition from superficial to transcritical turbidity currents, and how allogenic signals, such as tectonic processes, are preserved in the sedimentary record. Seismic data show that in the footwall the fan comprises cyclic steps and antidunes along its axial and external portions, respectively, which is interpreted to result from the spatial variation in flow velocity due to the loss of confinement at the canyon mouth. Conversely, in the hanging wall, the seafloor is nearly featureless at seismic scale. Numerical modelling of turbidity currents shows that the fault triggers a hydraulic jump that suppresses flow velocity downstream, thus explaining the lack of visible bedforms basinward. This study shows that the topography generated by active normal faulting controls the downslope evolution of turbidity currents and the associated bedforms, and that seafloor geomorphology can be used to evince syn-tectonic deposition.

A novel approach to generating in situ Lu-Hf garnet isochrons using micro-XRF mapping, LA ICP-MS mapping, and MS/MS-ICP-MS

Christopher R.M. McFarlane

University of New Brunswick Department of Earth Sciences, Fredericton, New Brunswick E3B 5A3, Canada <crmm@unb.ca>

Garnet is widely used for Lu–Hf isochron (beta-decay) geochronology because of its strong affinity for HREE and comparatively low initial Hf. The first increments of garnet growth during metamorphism of metasedimentary rocks tend to sequester Y and HREE at the expense of accessory minerals like xenotime ((Y, HREE) PO_4). This typically produces Lu-enriched garnet cores with concentrations sometimes >100 ppm. The corresponding $^{176}Lu/^{177}Hf$ values for core domains can range up to 100 thereby exerting considerable leverage on the age and error produced using isochron methods. Conventional bulk dissolution approaches typically produce Lu/Hf <1.0. Finding and targeting these Lu-rich domains for in situ Lu–Hf garnet geochronology is the focus of this study. Assessing the impact of other mineral inclusions (e.g., zircon, ilmenite, apatite) is also possible using this approach. The dataset also demonstrates the ability to eliminate ^{176}Yb interference from ^{176}Hf using NH_3 reaction gas to mass-shift Hf isotopes.

The first step in this process is to produce high-resolution (20 μm/pixel) micro-XRF maps for several 100 μm thick polished thin sections of garnet-rich target rocks. Doing so reveals which garnets expose near-central sections as defined by elevated zoning in Mn and Y. Conventional LA ICP-MS is then used to rapidly map (10 μm/pixel) the core regions of target grains to reveal Lu distribution and assess inclusion suites. The LA ICP-MS maps are added as overlays in the laser software to guide the position of spots for LA MS/MS-ICP-MS using a crater size of >100 μm if possible. The MS/MS-ICP-MS setup includes inclusion monitors ^{90}Zr, ^{49}Ti, ^{31}P, and ^{89}Y to assess the impact on Lu–Hf isochrons of inadvertent ablation of zircon, FeTi-oxides, and phosphates. Two previously dated rocks, a 2650 Ma paragneiss and a 400 Ma metapelitic schist, establish the veracity of the technique and define target precision required to achieve 1% (2σ) error on final isochron ages. By anchoring at an initial $^{176}Hf/^{177}Hf$ of 0.282 ± 0.004, precise isochrons are obtained for 2–3% (2σ) error on $^{176}Lu/^{177}Hf$ and 1% error $^{176}Hf/^{177}Hf$. A similar approach is applicable to other beta-decay chronometers such as Rb/Sr and K/Ca in micas.

Petrology, age, and tectonic setting of mafic-intermediate intrusions in the northeastern Meguma terrane, Nova Scotia, Canada*

Shae J. Nickerson[1], Sandra M. Barr[1], Donnelly B. Archibald[2], and Chris E. White[3]

1. Department of Earth and Environmental Science, Acadia University, Wolfville, Nova Scotia B4P 2R6, Canada <shaenickerson@acadiau.ca>;
2. Department of Earth Sciences, St. Francis Xavier University, Antigonish, Nova Scotia B2G 2W5, Canada;
3. Nova Scotia Department of Natural Resources and Renewables, Halifax, Nova Scotia B3J 2T9, Canada

Small plutons of mafic to intermediate composition are locally associated with the abundant Devonian granitic plutons that intruded the Goldenville and Halifax groups in the eastern Meguma terrane of mainland Nova Scotia. In addition, a swarm of mafic-intermediate dykes, here termed the Eastern Shore dykes, occur in the coastal part of that area. The purpose of this study is to investigate the age, petrology, and tectonic implications of these mafic-intermediate plutons and mafic dykes. Understanding the petrogenesis of these mafic-intermediate rocks provides sights into their genetic relationship with granitic magmatism, the origin and tectonic significance of the coeval granitic plutons, and a better understanding of the tectonic evolution of the Meguma terrane. The mafic-intermediate plutons in the Forest Hills and Cranberry

Lake areas are of tonalite to quartz diorite composition and occur close to the Cobequid–Chedabucto Fault System that separates the Meguma terrane from Avalonia. They range from undeformed to proto-mylonitic, contain abundant metasedimentary xenoliths, and show magma mingling textures with their adjacent granitic plutons. The Melrose dioritic dyke intruded the Cranberry Lake pluton because it contains granodiorite xenoliths from that pluton. Farther west, mafic-intermediate plutons (Porcupine Lake, Bog Island Lake, Mink Lake, and Ten Mile Lake) form part of the Trafalgar Plutonic Suite. They range in composition from tonalite to gabbronorite, contain mafic enclaves, and metasedimentary xenoliths, and are mostly undeformed. The Eastern Shore dykes range in width from ~10 cm to ~15 m and consist of lamprophyre (variety spessartite) based on their dominant mineralogy of plagioclase and amphibole with K-feldspar in the groundmass. They are subdivided into two groups based on the presence or absence of xenoliths and on geochemical data. Group one dykes lack xenoliths and show convex rare-earth-element (REE) patterns. Group two dykes contain xenoliths, have higher Sr and Zr, and show more sinuous REE patterns. Chemical compositions of the mafic-intermediate rocks from the Forest Hills, Cranberry Lake, Melrose, and Trafalgar areas range in SiO_2 from ~50 to ~70 wt%. They display light REE-enriched patterns with both negative and positive Eu anomalies, and have high Al_2O_3 and low Cr and Sr. In contrast, the Eastern Shore mafic-intermediate dykes have lower SiO_2 (~50 to 57 wt%) and higher MgO, Cr, and Ni. Zircon U–Pb dating and isotopic data will better constrain the ages and assist in evaluating crustal and mantle components in these rocks.

**Honourable Mention: AGS Graham Williams Award for best graduate student poster*

A new approach for investigating thermal and fluid evolution in critical mineral deposits of southern Nova Scotia via paired in situ Rb/Sr and Ar/Ar geochronology of micas

Adam Nissen[1], Dawn Kellett[1,2], and Jacob Hanley[1]

1. Department of Geology, Saint Mary's University, Halifax, Nova Scotia B3H 3C3, Canada <Adam.Nissen@smu.ca>;
2. Geological Survey of Canada, Atlantic, Natural Resources Canada,Dartmouth, Nova Scotia B2Y 4A2, Canada.

Paleozoic granite-hosted ore systems in southern Nova Scotia have complex thermal and fluid histories, including a post-magmatic, major regional tectonothermal event that disturbed geochronometers at ca. 315 Ma. As such, reconstructing the timing of mineralization and alteration events in these systems is challenging, particularly when using standard bulk mineral separate analysis. The spatial resolution made available by evolving in situ methods for geochronology can reveal multiple age domains in targets with multiphase thermal histories. The challenge presented by the complexities in these ore systems presents the opportunity to compare two modern in situ methods for mica geochronology. This project will compare in situ $^{40}Ar/^{39}Ar$ mapping of micas with newly developed in situ Rb/Sr age mapping of the same grains to characterize the mica geochronology of two mineralized systems, the Brazil Lake lithium-cesium-tantalum pegmatite, Yarmouth County, Nova Scotia, and the East Kemptville tin greisen complex, Yarmouth County, Nova Scotia. The proposed work will include full chemical and textural characterization of the minerals to be dated, and initial dating results. Geochronology data will be reconciled with fluid inclusion systematics to resolve the nature of mineralizing or post-mineralization fluids. Major contributions from the ongoing work will: (1) provide insight into the use of in situ Rb/Sr geochronology, an emerging method that makes use of state-of-the-art tandem mass spectrometers separated by a reaction cell; (2) inform critical mineral exploration and mining in the Canadian Appalachians; and (3) produce a framework for interpreting mica geochronology in systems with complex thermal histories.

An Early Carboniferous strike-slip duplex in the Belleisle Fault zone, southwestern New Brunswick, Canada, (or 'The secrets of Deadmans Harbour')

Adrian F. Park[1], Steven J. Hinds[1], and Susan C. Johnson[2]

1. Geological Surveys Branch, Department of Natural Resources and Energy Development, Fredericton, New Brunswick E3B 5H1, Canada <Adrian.Park@gnb.ca>;
2. Geological Surveys Branch, Department of Natural Resources and Energy Development, Sussex, New Brunswick E4E 7H7, Canada

The Belleisle Fault (Lubec Fault in southeast Maine) is one of several large strike-slip faults in the Appalachians of Maritime Canada. For much of its length, the Belleisle Fault is a relatively simple structure marked by mylonite-bearing high strain zones and brittle structures, such as between the Pocologan River and Loch Alva in southwest New Brunswick, and southwest from Eastport in Maine. Between the Pocologan River and the west end of Campobello Island, the Belleisle Fault zone consists of major splays defining a strike-slip duplex. Within the duplex occur fault-bounded 'horses' of units seen to the northwest in the New River

terrane, namely: (1) The early Ediacaran (ca. 625 Ma) Blacks Harbour granite and its thermal aureole, (2) The late Ediacaran to earliest Cambrian Belleisle Bay Group of volcanic and sedimentary rocks and related granites, (3) The Cambrian Saint John Group, including the mafic volcanic Waites Lane Formation, (4) The late Ordovician–Silurian Mascarene Group and, 5. The late Devonian Perry Formation. The early Silurian Kingston terrane forms the southeast margin of the duplex (as well as the southeast side of the Belleisle Fault in general), and its rocks are not found within the duplex. Older units within the duplex generally display more deformation, and within the structure there are extensive zones of tectonic mélange. Primary relationships, such as the intrusion of Blacks Harbour granite into its aureole and the non-conformity of Perry Formation on the Blacks Harbour granite are preserved, but most contacts are tectonic, and some fault-bound enclaves are merely metres long and less than a metre thick. The duplex is overstepped by a Carboniferous sequence forming the Cripps Stream and Russels Point formations (Beaver Harbour Group). Good miospore assemblages acquired from the Perry Formation (middle Famennian, youngest unit in the duplex) and Russels Point Formation (lower Visean, oldest overstepping unit) constrain a major period of strike-slip displacement along the Belleisle Fault to the Tournaisian interval.

Exploiting the potential of legacy data with artificial intelligence for renovating VMS mineral prospectivity models of the renowned Brunswick Belt, Canada

Mohammad Parsa[1], David Lentz[1], and James Walker[2]

1. Department of Earth Sciences, University of New Brunswick, Fredericton, New Brunswick E3B 5A3, Canada <m.parsa@unb.ca>;
2. New Brunswick Department of Natural Resources and Energy Development, South Tetagouche, New Brunswick E2A 7B8, Canada

The renowned Brunswick belt (BB) that hosts the Brunswick Horizon (BH), the stratigraphic sequence constituting the upper contacts of the Nepisiguit Falls Formation (NFF) with the overlying Flat Landing Brook Formation (FLBF), is associated with several well-known massive sulphide deposits and some mineral occurrences. These include the supergiant Brunswick No. 12, the Brunswick No. 6, Key Anacon, and Austin Brook deposits. Historically, this belt has been subjected to various geophysical, geochemical, and geological surveys by governments and private companies, making it a data-rich zone. However, these data have never been exploited to their full potential, and to the best of the authors' knowledge, there is no publicly available renovated mineral prospectivity model for this belt or the Bathurst Mining Camp as a whole. This study seeks to bridge this knowledge gap by adopting AI-based techniques for developing renovated predictive models of volcanic-hosted massive sulphide mineralization for this well-endowed belt, that will then serve to build better models for the Bathurst Mining Camp.

Aiming to achieve the above goal, two sets of exploration targeting criteria, namely the one used for deposits hosted by the NFF and the other used for deposits hosted by the FLBF, were adopted to distill the legacy geoscientific data available into predictor models using state-of-the-art machine-learning techniques. In the context of this study, major differences considered in these sets are: (i) whereas the presence of iron-rich chemically derived sedimentary rocks, known as iron formations (BH), is intrinsic to the deposits hosted by the NFF, the deposits hosted by the FLBF predominantly lack this feature; and (ii) in contrast to the deposits hosted by the FLBF, the deposits hosted by the NFF show lateral chemical zonation. The legacy data employed in this study are the results of aeromagnetic, airborne electromagnetic, airborne radiometric, till geochemical, and bedrock mapping surveys. Based on the exploration targeting criteria defined, these data were reprocessed and re-analyzed to highlight the subtle patterns linked to these data that might represent mineralized horizons.

This study started by recognizing that the process of developing a probability map pointing to the location of possible mineralized zones can be deemed a type of regression analysis. Employing the recently developed regularized regression techniques were based on this premise, namely Ridge and Lasso. The results of this study were further compared to the previously developed BB and BH prospectivity models. Given a set of spatial/statistical methods commonly used to compare prospectivity models, the models developed in this study are more robust than those developed earlier. A further step in this study is a risk-return analysis applied to predictive models to prioritize prime exploration targets based on their uncertainty. This procedure estimates the stochastic uncertainty of predictor models and links the estimated values to selecting low-risk, confident exploration targets. The outcome of this preliminary reanalysis is an exploration targeting model that effectively reduces the search space for exploration in the BB and can be used by decision makers and exploration campaigns.

Late Devonian deformation and exhumation in the northern Appalachian orogen: a syntaxial origin?*

Nicolas Piette-Lauzière[1], Kyle P. Larson[1], Dawn A. Kellett[2], Lyal B. Harris[3], Nathan R. Cleven[4], and Neil Rogers[5]

1. Earth and Environmental Sciences, IKBSAS, University of British Columbia Okanagan, Kelowna, British Columbia V1V 1V7, Canada <nicolas.piette-lauziere@alumni.ubc.ca>;
2. Geological Survey of Canada (Atlantic), Natural Resources Canada, Dartmouth, Nova Scotia B2Y 4A2, Canada;
3. Institut National de la Recherche Scientifique, Centre Eau Terre Environnement, Québec, Québec G1K 9A9, Canada;
4. Geological Survey of Canada, Vancouver, British Columbia V6B 5J3, Canada;
5. Geological Survey of Canada – Central, Natural Resources Canada, Ottawa, Ontario K1A 0G1, Canada

The pre-accretionary shape of the eastern Laurentian margin with promontories and re-entrants, in conjunction with the obliquity of the collision of the various crustal fragments, primarily control the timing, kinematics, and intensity of deformation related to accretionary events in the northern Appalachian orogen. When considering the progressive accretion of oceanic arcs and microcontinents to the composite Laurentian margin, it is often difficult to determine which tectonic setting controlled the deformation or reactivation of shear zones not located in the immediate vicinity of the active suture. This problem is best represented by the lack of tectonic interpretation for the regional deformation occurring during the Late Devonian oblique collision of Meguma leading to the Neoacadian orogeny.

Modern collisional settings provide a conceptual framework to investigate the Late Devonian to Mississippian deformation inboard of the Neoacadian suture. In active mountain belts, accreted promontories can form syntaxes characterized by rapid crustal deformation, high elevation, and fast erosional exhumation with abundant sedimentation. Compiled new and published shear zone kinematic interpretations, deformation ages, and regional $^{40}Ar/^{39}Ar$ cooling ages was compared and integrated with structural interpretation of aeromagnetic and gravimetric depth slices covering the northern Appalachians.

Results indicate that between the Late Devonian and Mississippian, regionally extensive NE-SW and ENE-WSW oriented shear zones such as the Cobequid–Chedabucto suture, the Hermitage Bay–Dover shear zone, the Norumbega fault zone, the Pocologan–Kennebecasis shear zone, and the Catamaran fault were formed or reactivated with a dextral strike-slip shear sense consistent with a large-scale C-C' system. Depth slices of aeromagnetic and gravity geophysical data indicate that several of these structures are listric, and thus formed a lateral succession of transpressive and transtensive segments crosscut by antithetic sinistral shear zones. At the apex of the collision between Meguma terrane and the composite Laurentian margin of New England, $^{40}Ar/^{39}Ar$ cooling age transects highlight large regions of focused Neoacadian cooling and exhumation. These regions spatially correlate with an area of contemporaneous high paleoelevation flanked by the opening of the Maritimes and Catskills basins. A regional structure with a component of Neoacadian southeast-side up motion, tentatively named the Honey Hollow fault, forms the back-thrust that accommodated this uplift, while the Norumbega fault zone (northern New England) and the Clinton Newbury fault (southern New England) appear to have accommodated the frontal uplift. Such a setting is potentially similar to transpressive syntaxes such the present-day oblique collision of the Yakutat terrane to North America.

**Winner: AGS Sandra Barr Award for best graduate student oral presentation*

Resolution of the hydrocarbon molecular matrix by comprehensive two-dimensional gas chromatography as evidence of hydrocarbon sources of the Scotian Margin, offshore Nova Scotia, Canada

Elish Redshaw[1], Anirban Chowdhury[1], Jeremy N. Bentley[1], Adam MacDonlad[2], Natasha Morrison[2], and G. Todd Ventura[1]

1. Department of Geology, Saint Mary's University, Halifax, Nova Scotia B3N 3C3, Canada <elish.redshaw@smu.ca>;
2. Nova Scotia Department of Natural Resources and Renewables, Halifax, Nova Scotia B3J 3J9, Canada.

Shallow deep marine surface sediments often contain hydrocarbons that do not have a well-constrained point of origin. Over the course of three cruises (2015, 2016, and 2018) subsurface sediment samples of piston and gravity cores were collected over prospective hydrocarbon seep sites. These cores have been classified based on petroleum geochemistry as being either positive or negative for containing hydrocarbon that have migrated up from deeper within the Scotian Basin. The extractable hydrocarbon matrix of the shallow sediments may represent a mix of organic matter having different origins. This study will examine the hydrocarbon matrix of 8 sediment cores (n = 37). Hydrocarbon extraction involved isolation of organic matter (OM) from the sediment by means of sonication and separation of apolar and polar fractions in organic solvents. Comprehensive two-dimensional gas chromatography, coupled with high-resolution mass spectral data, will be used to resolve these hydrocarbon matrices. The produced two-dimensional chromatograms will be used to map down core variations in the absolute abundance of compounds in the hydrocarbon matrix. A background hydrocarbon fingerprint will be formulated from an average chromatographic trace that will further be subtracted from individual sample chromatograms.

The resulting mean difference chromatograms will be used to identify downcore matrix attenuation and evaluate point sources from the multimolecular composition in the sediment strata. Bulk extract data, including total lipid extracts, apolar, and polar fractions, along with sediment TOC and their associated multi-molecular difference chromatograms will further the support downcore mapping. Through this methodology, the project aims to provide evidence for sources of hydrocarbon production by differentiating native and migrated hydrocarbons.

Geoscience through the lens of heritage: virtual geoheritage education at Stonehammer UNESCO Global Geopark, New Brunswick, Canada

Catrina Russell

Stonehammer UNESCO Global Geopark, Saint John, New Brunswick E2L 4Z6, Canada <catrina@stonehammergeopark.com>

Geoscience education in New Brunswick is often hindered by a lack of process and understanding on the part of school boards and a lack of training and comfort level on the part of many teachers assigned to instruct on it. In New Brunswick, the curriculum calls for geoscience topics to be discussed in Grades 4 and 7. Stonehammer has long delivered hands-on programming geared specifically at these grades, as well as workshops for teachers instructing at these levels. As the Global Pandemic has put a hiatus on in class programming, Stonehammer has gone virtual, developing new strategies to build upon these initial offerings using a more holistic approach. Exploring multidisciplinary topics throughout the geopark that link to curricula across all grade levels has proven extremely engaging for students. This content acts as a gateway, leading to opportunities to delve deeper into and foster greater understanding of more specific geoscience topics. The subject of geoheritage has long fascinated this author, and recent initiatives to better acknowledge and celebrate indigenous cultures throughout the region have inspired the creation of a virtual program that ties together themes of indigenous culture and custom with the region's geological history. This session will outline best practices within Stonehammer Geopark to deliver geoscience and geoheritage content to all ages.

Seasonal and spatial changes in vertical export and deposition of productivity tracers in a submarine canyon system of the Lower St. Lawrence Estuary, eastern Canada

Hannah Sharpe[1], Audrey Limoges[1], Michel Gosselin[2], Catherine Lalande[3], Jean-Carlos Montero-Serrano[2], and Owen Sherwood[4]

1. Department of Earth Sciences, University of New Brunswick, Fredericton, New Brunswick E3B 5A3, Canada <hsharpe@unb.ca>; 2. Institut des sciences de la mer de Rimouski, Université du Québec à Rimouski, Rimouski, Québec G5L 3A1, Canada; 3. Amundsen Science, Université Laval, Québec, Québec G1V 0A6, Canada; 4. Department of Earth and Environmental Sciences, Dalhousie University, Halifax, Nova Scotia B3H 4R2, Canada

The coastal shelf of Pointe-des-Monts (PDM), located on the northern shore of the Lower St. Lawrence Estuary (LSLE), is characterized by active submarine canyons. Despite the presence of regional biological hotspots, there is a lack comprehensive understanding of the relationship between canyon processes and surface primary production (i.e., conversion of inorganic material into energy-bearing organic material). This study documents seasonal and spatial variations in primary production based on the analysis of 29 surface sediment samples and 72 sequential sediment trap samples over the span of an annual cycle, from within and outside the canyon system. A particular focus is placed on potentially harmful taxa, including the toxic dinoflagellate *Alexandrium catenella*, which has been associated with regional mass mortality events in the past.

Preliminary analyses show that the surface sediments contain well-preserved organic-walled dinoflagellate cysts with an average concentration of 54 000 cysts dry g^{-1} inside the PDM canyons and 99,000 cysts dry g^{-1} outside the canyons. A clear pattern of increasing dinoflagellate cyst concentrations with distance from the shore is observed. Surface sediments have nitrogen isotopic ($\delta^{15}N$) and carbon isotopic ($\delta^{13}C$) values ranging between 5.1 and 6.3‰, and -23.2 and -25.6‰, respectively. Indeed, nearshore samples contain more terrestrially derived organic carbon with an increasing proportion of marine organic carbon with distance from the shore. Total particulate matter (TPM) fluxes in the sediment trap samples were significantly greater at PDM (maximum 7.9 g m^{-2} d^{-1}) than outside the canyons (maximum 1.1 g m^{-2} d^{-1}). Chloropigment fluxes (maximum 1.6 mg m^{-2} d^{-1}) indicate a typical seasonal production cycle over the course of one year outside the canyons, while this pattern is not observed at PDM. During the spring bloom, chloropigment and TPM fluxes are coupled outside the canyons and decoupled at PDM. Subsequent enumeration of phytoplankton cells (dinoflagellates and diatoms), along with compound specific carbon isotope analyses, will provide information about variations in the taxonomic composition and sinking fluxes of primary producers. This project will help to identify the relative importance of key forcing mechanisms for the preconditioning of harmful algal blooms, thereby improving coastal management strategies in the LSLE and directly influencing public health, marine life, and the economy.

Application of ore deposit models for critical mineral assessments: examples from Maine, USA

John F. Slack[1,2]

1. U.S. Geological Survey (Emeritus), National Center, MS 954, Reston, Virginia 20192, USA <jfslack@usgs.gov>;
2. Department of Earth Sciences, Memorial University of Newfoundland,St. John's, Newfoundland and Labrador A1B 3X5, Canada

Evaluation of undiscovered resources of critical minerals and metals is greatly enhanced by the use of current ore-deposit models. Such models are crucial for the understanding of geological settings in which various deposits may occur, and how the presence of even small deposits and prospects can be highly prospective, when their settings are compared to those of major deposits elsewhere. Analysis of the potential in Maine is divided into two groups of deposits based on metal signature and geological setting. One group consists of known deposits (sediment-hosted Mn, volcanogenic massive sulphide, porphyry Cu-Mo, mafic- and ultramafic-hosted Ni-Cu[-Co-PGE], pegmatitic Li-Cs-Ta) that are in most cases relatively large, well-documented, and explored extensively. The second and much larger group of commodities comprises small deposits, prospects, and occurrences that are minimally explored or unexplored.

The qualitative assessment used here relies on three key criteria: (1) the presence of known deposits, prospects, or mineral occurrences; (2) geological settings that are favorable for containing certain deposit types based on descriptive and genetic ore-deposit models; and (3) geochemical anomalies in rocks or stream sediments, including panned concentrates. Geophysical data may be relevant in some cases. Among the 20 deposit types considered, a high resource potential is assigned to only three: (1) sediment-hosted Mn, within and near the large (~327 Mt @ 9.0 wt% Mn) Silurian deposits in northeastern Maine that constitute the largest resource of this metal known in the US; (2) mafic- and ultramafic-hosted Ni-Cu(-Co-PGE), represented chiefly by deposits within the Moxie mafic-ultramafic pluton of Devonian age in central Maine; and (3) pegmatitic Li-Cs-Ta, the largest being the Plumbago Mountain Li deposit (~10 Mt @ 4.68 wt% Li_2O_3) hosted by Permian(?) pegmatite in western Maine. In the Silurian sediment-hosted Mn-Fe deposits higher grades may occur in euxinic facies of the host black shales thus minimizing the Fe present in the deposits and in weathered Mn-rich oxide zones, such as exist in the giant orebodies of Groote Eylandt in Australia and Moanda in Gabon, respectively. The Moxie pluton is considered especially prospective because its elongate shape suggests formation in a magma conduit, like the dyke-sill complexes that host world-class Ni-Cu(-Co-PGE) deposits such as Noril'sk in Russia and Voisey's Bay in Labrador. Potential for pegmatitic Li deposits in Maine can be assessed by integrating relevant occurrences of spodumene and other Li-rich minerals with favorable geology including evidence of post-Acadian anatectic felsic magmatism.

Petrology and tectonic setting of the Park Spur pluton, central Cape Breton Highlands, Nova Scotia, Canada

Amanda M. Smith[1], Sandra M. Barr[1], and Chris E. White[2]

1. Department of Earth and Environmental Science, Acadia University, Wolfville, Nova Scotia B4P 2R6, Canada <160000s@Acadiau.ca>;
2. Nova Scotia Department of Natural Resources and Renewables, Halifax, Nova Scotia B3J 2T9, Canada

The Park Spur pluton (PSP) is located in the central Cape Breton Highlands, near the eastern margin of the Aspy terrane and its tectonic contact with the adjacent Bras d'Or terrane. The PSP has not previously been the focus of a petrological study, and hence this study was undertaken to determine the petrological characteristics of the pluton, including its potential for critical element mineralization, and to compare the pluton to the Black Brook Granitic Suite (BBGS) to the northeast and the Bothan Brook–West Branch North River granite (BB–WBNRG) to the south. Based on previously published U–Pb zircon ages, all three plutons have similar middle-to late Devonian ages of about 373 Ma, but their relationship to one another and tectonic setting are not well understood.

Thirty-seven samples were collected for petrographic study and a subset of twenty were submitted for whole-rock chemical analysis, including critical elements. As a result of field work and petrographic study, the extent of the pluton has been modified compared to published maps, and the pluton has been subdivided into three units. Most widespread is medium-grained muscovite-biotite monzogranite, intruded in places by pegmatite and aplite dykes. The northwestern tip of the pluton consists of finer-grained garnet-bearing muscovite monzogranite. An area of protomylonitic granite occurs along the southwestern margin of the of the PSP, near its contact with metamorphic rocks of probable Ordovician–Silurian age. Deformed granitic dykes occur in metamorphic units adjacent to the southeastern margin of the pluton. Both the dykes and deformed pluton margin are characterized by large K-feldspar grains with anastomosing texture of the surrounding quartz and plagioclase grains.

Most samples from the PSP contain 70–73% SiO_2 but the fine-grained muscovite monzogranite is more evolved,

with 74–75% SiO_2. Variations in major element oxides with SiO_2 suggest that petrological variations were caused by fractional crystallization, an interpretation supported by negative Eu anomalies indicative of plagioclase removal. The rocks are enriched in light rare-earth elements up to 300 times chondritic values with flat heavy REE, although anomalous trends in some samples suggest involvement of accessory phases such as garnet and zircon. Comparison to the BBGS and BB–WBNRG shows that all three plutons are peraluminous with trace element compositions consistent with those of volcanic-arc to syn-collisional granites formed in association with slab breakoff. However, the BB–WBNRG lacks muscovite and shows chemical differences such as higher SiO_2, K_2O, Th, and Nb compared to both PSP and BBGS.

Bay St. George subbasin, Newfoundland, Canada: deformation of evaporites and wet sediment in a tectonically active basin

Morgan E. Snyder[1], John W.F. Waldron[1,2], and Paul Durling[3]

1. Department of Earth and Environmental Science, Acadia University, Wolfville Nova Scotia B4P 2R6, Canada <mesnyder@ualberta.ca>;
2. Department of Earth and Atmospheric Sciences, Edmonton, Alberta T6G 2E3, Canada;
3. Geological Survey of Canada (Atlantic), Dartmouth, Nova Scotia B2Y 4A2, Canada

The Bay St. George subbasin of SW Newfoundland, part of the larger late Paleozoic Maritimes basin, formed under the influence of strike-slip faulting and the movement of evaporites. New stratigraphic correlations between Newfoundland and other late Paleozoic subbasins illustrate the effects of both basement and salt movement. Coastal outcrops show complex combinations of synsedimentary, salt-related, and tectonic structures.

Map relationships and dramatic thickness contrasts in the Tournaisian Anguille Group indicate that a large, concealed, northeast–striking normal growth fault (here termed the Ship Cove fault) controlled sedimentation. An exposed structure, the Snakes Bight fault, originated as a hanging wall splay. Structures formed during, or soon after deposition in the Anguille Group include soft-sediment folds, boudins, clastic dykes, and millimetre-scale diapiric bulb structures formed by overpressuring and liquidization of sediment. These suggest that the subbasin was tectonically active throughout deposition of the Anguille Group, and that tectonic disturbance of sediment continued into the Visean, when the overlying Codroy Group was deposited. The Codroy Group originally contained thick salt units, interbedded with clastic and carbonate sediment. Former evaporite units are represented in outcrop by mudstone breccias, the residues of salt solution. Complex outcrop relationships indicate salt welds and suggest that units of the upper Codroy and overlying Barachois groups represent fills of minibasins that subsided into thick evaporites. Early expulsion of evaporites can explain otherwise enigmatic contrasts between laterally equivalent units.

Field relationships suggest tectonic inversion deposition related to E-W dextral strike-slip motion that affected the entire Maritimes basin in the Serpukhovian, producing reverse-sense offsets and contractional folds. Many of the structures in the Bay St. George subbasin, previously interpreted as post-depositional and purely tectonic, were formed by deformation of unlithified sediment and ductile evaporites during basin development and subsequent shortening.

Six years at Boat Harbour, Pictou County, Nova Scotia, Canada: a review of research on the spatiotemporal distribution of contaminants in pulp mill stabilization basin sediments

Ian Spooner[1], Kirklyn Davidson[2], Ballie Holmes[3], Dewey Dunnington[4], Tony Walker[5], and Craig Lake[3]

1. Department of Earth and Environmental Science, Acadia University, Wolfville, Nova Scotia B4P 2R6, Canada <ian.spooner@acadiau.ca>;
2. SGC Industries, Saint John, New Brunswick E2M 5Y5, Canada;
3. Centre for Water Resources Studies, Department of Civil and Resource Engineering, Dalhousie University, Halifax, Nova Scotia B3H 4R2, Canada;
4. Voltron Data, San Francisco, California 94041, USA;
5. School for Resource and Environmental Studies, Kenneth C. Rowe Management Building, Halifax, Nova Scotia B3H 4R2, Canada

Boat Harbour is a sediment stabilization basin located in Pictou County, Nova Scotia that has been impacted by industrial effluents discharged by a bleached kraft pulp mill (1967 to 2019) and a chlor-alkali plant (1971 to 1992). The former estuary now contains >577,000 m^3 of unconsolidated sediment, impacted by inorganic and organic contaminants, including metal[loid]s and polychlorinated dibenzofurans (PCDD/Fs).

In the past 6 years over 100 gravity, percussion and piston core samples have been taken to determine contaminant spatiotemporal distribution of As, Cu, Pb, and Zn sediment concentrations which consistently exceeded guidelines for aquatic sediments. Results demonstrate that

there is no distinct spatial trend in metal concentrations though effluent is introduced from a point source. High and variable concentrations of Cu and Zn in the contaminated sediment likely represent a combination of cation capture by the highly organic sediment and influence of the effluent from the pulp mill on lakebed sediment chemistry. Elevated Pb in the contaminated sediment is the result of atmospheric deposition from combustion of fossil fuels and bioaccumulation in the effluent feedstock. Temporal trends reflect changes in effluent treatment procedures as well as composition of effluent solids. Comparison of geochemistry of effluent influenced sediment and pre-effluent substrate sediment at Boat Harbour to freshwater and marine reference was required to understand the degree to which geogenic and anthropogenic sources of metal(loids) have influenced effluent chemistry. This research demonstrates that undisturbed, time transgressive samples from both impacted sites and reference sites combined with non-destructive, rapid, small sample analytical techniques such as X-ray fluorescence, provide an accurate assessment of sediment metal contaminant distribution, data required to guide remediation and environmental effects monitoring and compliance.

Petrology and lithogeochemistry of the Wildcat Brook Mo-W deposit, Charlotte County, New Brunswick, Canada

Cliff Stanley[1], Jacob Hanley[2], Abdul Asfour[2], and Patrick Crouse[2]

1. Department of Earth and Environmental Science, Acadia University, Wolfville, Nova Scotia B4N 2R6, Canada <cliff.stanley@acadiau.ca>;
2. Department of Geology, Saint Mary's University, Halifax, Nova Scotia B3H 3C3, Canada

The Wildcat Brook Mo-W deposit is located approximately 9 km east of the former Mt. Pleasant Sn-W-Mo mine in Charlotte County, New Brunswick. It is hosted by a leucocratic, quartz-feldspar porphyritic-to-aplitic, peraluminous, EW-striking, moderately north-dipping dyke. This intrudes turbiditic metasedimentary wackes and argillites of the Digdeguash Formation of the Fredericton Trough immediately north of the Magaguadavic granite of the St. George batholith. High-grade Mo mineralization up to +4% over one metre consists of molybdenite blebs up to 4 mm in diameter disseminated in small miarolitic cavities within albite- and muscovite-altered dyke, and medium-grade Mo mineralization at the margins or cores of 2–5 cm wide quartz veins cutting altered or unaltered dyke and adjacent metasedimentary rocks. Wackes adjacent to the dyke also contain up to 2 cm diameter rare white orbs of radially arrayed acicular crystals of powellite ($CaWO_4$) replacing the matrix and clastic grains. At present, the dyke has been intersected by 17 diamond drill cores spanning approximately 250 m along strike and dip. Dyke thickness ranges from 17 to 42 metres (averaging 27 m thick), and the dyke contains a sample length-weighted average grade of 0.27% Mo, and sample length-weighted average grade-meter product of 5.76% Mo x m, calculated from 325 samples, 25 of which have assigned grades of 0.4001% Mo, as their upper detection limit concentrations (>4000 ppm) have yet to be updated via re-assay.

Two styles of hydrothermal alteration occur in the dyke: albite-minor epidote, and muscovite-quartz. Molar element ratio analysis of 110 drill core samples, constrained by petrography, reveal that the addition of Na and loss of K accompanied albite alteration: Microcline + Na^+ => Albite + K^+ (-8 vol.%), and 4 Anorthite + 4 Quartz + 2 Water + 2 Na^+= >2 Clinozoisite + 2 Albite + 2 H^+ (+26 vol.%), and inverse material transfers, plus Ca loss, accompanied muscovite plus quartz alteration: 3 Albite + K^+ + 2 H^+ = >Muscovite + 6 Quartz + 3 Na^+ (-7 vol.%), and Clinozoisite + K^+ + 3 H^+=> Muscovite + Water + 2 Ca^{+2} (-0 vol.%). These alteration styles principally affect the dyke, but several greisenized hydrothermal compartments up to several metres width, bounded by quartz veins and containing coarse muscovite and minor Mo mineralization, occur above the dyke in drill core. Isolated high-grade wolframite-bearing quartz veins 4–8 cm thick also occur sporadically above the felsic dyke.

Discovery of Visean to early Serpukhovian (Mississippian) aged tetrapod burrows from Midland and Lepreau Falls, New Brunswick, Canada: an ichnological, palynological and seismic investigation of the Millstream Subbasin

Matthew Stimson[1,2], Steven Hinds[3], Olivia King[1,2], Duncan McLean[4], Lynn Dafoe[5], R. Andrew MacRae[2], and Adrian Park[3]

1. Department of Natural History, New Brunswick Museum, Saint John, New Brunswick E2K 1E5, Canada <mstimson29@gmail.com>;
2. Department of Geology, Saint Mary's University, Halifax, Nova Scotia B3H 3C3, Canada;
3. New Brunswick Geological Survey, New Brunswick Department of Natural Resources and Energy Development, Fredericton, New Brunswick E3B 5H1, Canada;
4. MB Stratigraphy Ltd., Sheffield, S9 5EA, UK;
5. Geological Survey of Canada (Atlantic), Dartmouth, Nova Scotia B2Y 4A2, Canada

During the spring of 2018, residents Gary, David, and Rick Leblanc, found a near-horizontal burrow fossil within red sandstone along a ditch outcrop at Midland, New Brunswick. These red sandstones, minor conglomerates, and mudrocks are considered part of the undivided Mabou Group, which is Visean to Serpukhovian in age. This fossil burrow is about 50 cm long, has a maximum width of 10 cm, and is tentatively assigned to the ichnogenus *Katarrhedrites*, which is commonly ascribed to tetrapod burrowing activities. Other features of the burrow include an entry chamber, a complex tunnel structure with preserved digging scratches along the sides, and a terminal living chamber. A second, 50 cm scale, subhorizontal burrow structure was found within unnamed red beds of the "Mabou Group" at Lepreau Falls in 2020. This feature has no ichnological designation at present and is interpreted as a tetrapod burrow. In general, tetrapod burrows are extremely rare in the fossil record during the Carboniferous Period, limiting the knowledge of tetrapod dwellings (domichnia) during this interval. The only known occurrence of a Mississippian fossil tetrapod burrow occurs in the Mauch Chunk Formation (Chesterian or Arnsbergian), near Pottsville, eastern Pennsylvania, USA. The Mauch Chunk burrow appears to be near vertical, has no ichnological taxonomic assignment, and is approximately five times the size and diameter of the New Brunswick burrows. The age of the Mauch Chunk Formation was determined through paleobotany. Both palynology and macrofossil analyses from outcrop and boreholes were used at the Midland and Lepreau Falls fossil sites to determine their relative age. Using seismic and recent field mapping in Midland, shallow cross-sections were created that allowed the successful correlation of the fossil burrow locality to outcrops and adjacent boreholes over 20 kilometres northeast from the fossil burrow site along the axis of the Millstream Subbasin. The age of the Midland burrow (*Katarrhedrites*) can be constrained to Arnsbergian and younger; approximately time-equivalent to the Mauch Chunk Formation burrow. The tetrapod burrow from Lepreau Falls is assigned a Visean age and is older than the Mauch Chunk burrow. The presence of Visean burrows in the Maritimes Basin has ethological and paleoecological implications for the timing of fossorial tetrapods. The detailed stratigraphic work, palynology analysis, and geological mapping from boreholes and seismic profiles confirms the existence of the Millstream Subbasin, which was only inferred in previous literature.

Extent and timing of deformation and metamorphism associated with the Eastern Highlands shear zone, central Cape Breton Highlands, Nova Scotia, Canada*

Evelyne Sunatori[1], Deanne van Rooyen[2], Sandra M. Barr[1], and Chris E. White[3]

1. Department of Earth and Environmental Science, Acadia University, Wolfville, Nova Scotia B4P 2R6, Canada <evelynesunatori@acadiau.ca>;
2. Department of Mathematics, Physics, and Geology, Cape Breton University, Sydney, Nova Scotia B1P 6L2, Canada;
3. Nova Scotia Department of Natural Resources and Renewables, Halifax, Nova Scotia B3J 2T9, Canada

The Aspy and Bras d'Or terranes in northern Cape Breton Island are both interpreted as part of Ganderia in the northern Appalachian orogen but contrasts in rock types, ages, and magmatic, metamorphic, and tectonic history make their original relationship difficult to interpret. The two terranes were juxtaposed along the Eastern Highlands shear zone (EHSZ). In its northern part, the EHSZ strikes northeast and previous structural studies documented evidence for three deformational events between 424 Ma and 375 Ma and Bras d'Or-over-Aspy terrane sense of motion. The purpose of this study is to determine the extent and timing of deformation and metamorphism in the rocks within and adjacent to the EHSZ father south in the central Cape Breton Highlands where its location and history are less well constrained. Four main units occur in the study area: the Ordovician to Silurian Calumruadh Brook Formation (CBF) and Middle River metamorphic suite (MRMS) in the Aspy terrane, and the Neoproterozoic McMillan Flowage Formation (MFF) and Kathy Road dioritic suite (KRDS) in the Bras d'Or terrane. In the NE part of the study area (CBF in contact with MFF) the deformation is strongly partitioned into the CBF, and most foliations dip steeply to the NW. Lineations are variable so sense of motion is cryptic, but C-S fabrics suggest that the main shear plane is roughly E-W, with a moderate dip to the N. In the central part of the study area the KRDS is variably deformed, and deformation is most intense along its western margin where rocks are strongly lineated and foliated (L>S) for about 1.5 km into the diorite. The foliations dip moderately to the NW and lineations plunge moderately to the NW, suggesting that the main shear direction is top-to-the-SE (Aspy over Bras d'Or). In the south foliations in the MRMS and CBF dip very steeply to the W and kinematic indicators and mineral lineations suggest the main shear plane is oriented roughly N-S and the major S-directed motion was dextral in a transpressional setting. The metamorphic minerals in the rocks affected by the movement on the EHSZ are limited to chlorite (overprinting pre-existing amphibolite-facies metamorphism in the MRMS and upper greenschist facies metamorphism in the CBF), indicating that the activity on the shear zone in this area represents lower greenschist conditions and suggesting that rocks currently at the surface were buried <7 km when the shear zone was last active.

**Winner: AGS Graham Williams Award for best graduate student poster*

The application of melt inclusions to evaluate magma ore metal fertility, oxidation state, sulfur saturation, and volatile contents in the South Mountain Batholith, Nova Scotia, Canada

Anna Terekhova[1], Jacob Hanley[1], and Kevin Neyedley[1,2]

1. Department of Geology, Saint Mary's University, Halifax, Nova Scotia B3H 3C3, Canada <anna.terekhova@smu.ca>; 2. Nova Scotia Department of Natural Resources and Renewables, Halifax, Nova Scotia B3J 2T9, Canada

The South Mountain Batholith (SMB), the largest granitoid body in the Appalachian orogen, outcrops over a large portion of central and western Nova Scotia. The SMB has been the target of sporadic mineral exploration since the late 1800s and mining in the 1980s (e.g., Sn greisen deposit at the East Kemptville Mine) while extensive research has yielded a comprehensive geochemical classification of the granitoids, with the distinction made between Phase 1 and Phase 2 plutons. However, there are no comparative studies that focus on the metal and volatile "fertility" of magmas associated with the formation of dominantly barren Stage 1 and commonly mineralized Stage 2 plutons in the SMB. Additionally, there have been no studies of melt inclusions in those intrusive rocks. This study will aim to quantify and compare the metal and volatile content, and oxygen fugacity of magmatic liquids from Stage 1 and Stage 2 plutons in the SMB. This will be done by analyzing aliquots of the former magmatic liquids directly from preserved silicate and sulfide melt inclusions (trapped samples of crystallized melt) hosted in zircon and combining high spatial resolution microanalytical methods (laser ablation-inductively coupled plasma mass spectrometry, scanning electron microscopy, Raman spectroscopy, electron microprobe analysis, and cathodoluminescence) with detailed zircon and inclusion petrography. Through the analysis of melt inclusions in zircon, and evaluation of associated physicochemical conditions, comparison of melt inclusion parameters within and between Stage 1 and 2 plutons will aim to identify differences in magmatic parameters that may have led to the differential metal associations and tenors of these plutons. The project will also aim to establish the temporal variations in melt and volatile composition, and associated entrapment conditions, as well as develop exploration indicators and mass balance constraints for the mineralized systems within Stage 2 plutons. The planned integration of coupled zircon-melt inclusion analysis to define the above parameters is innovative and will lead to quantitative, predictive criteria for differentiating barren or sub-economic from well-endowed plutonic suites.

Physical Geography 110: a new course for New Brunswick high school learners

Ann C. Timmermans[1] and Ryan Jones[2]

1. Department of Earth Sciences, University of New Brunswick, Fredericton, New Brunswick E3B 5A3, Canada <ann.timmermans@unb.ca>; 2. New Brunswick Department of Education and Early Childhood Development, Fredericton, New Brunswick E3B 5H1, Canada

A new Physical Geography 110 high school course for New Brunswick learners is nearing completion. This endeavor has been co-led by the Department of Earth Sciences at UNB and seeks to replace the current course published in the middle 1990s. New curriculum writing supports the International Geoscience Syllabus and is consistent with the Earth Science Literacy initiative outlined by the National Science Foundation. The curriculum embeds the New Brunswick Global Competencies and United Nation's Sustainable Development Goals. Aspirational ideas for the enactment of this course include aspects of human knowledge, culture, and equity. For the final summative assessment, educators will be encouraged to engage learners in a comprehensive field project instead of a traditional paper-based exam. The new positioning of the Physical Geography 110 course will provide a science credit for graduation and the acquisition of science skills, and appeal to a broader range of learners and interests. Presenters will share aspects of the curriculum writing journey, gather feedback, and facilitate general Science Education discussion.

Dissolution features on diamonds from hypabyssal kimberlite facies and the effect of melt composition on diamond resorption

Rosa Toutah and Yana Fedortchouk

Department of Earth and Environmental Sciences, Dalhousie University, Halifax, Nova Scotia B3H 4R2, <Canada rosa@dal.ca>

Diamonds can preserve features from their time deep in the Earth's mantle and their ascent from the mantle to the Earth's surface in hot kimberlite magma due to their high stability. The record of dissolution textures on diamond surfaces opens a window into the history of the diamonds journey through the kimberlite. Composition of kimberlitic fluid affects dissolution textures on diamonds from volcaniclastic kimberlite facies. The focus of this study is to identify different resorption styles of diamonds from hypabyssal kimberlite facies and use experiments in

volatile-undersaturated melt to determine the effect of melt composition on diamond resorption features. The study uses 1300 diamonds from 16 kimberlites from the Ekati Mine, selected hypabyssal dykes, and sills. This data obtained for class 3 kimberlites will be compared to the existing data on diamonds from class 1 kimberlites. SEM, AFM, and microscope imaging will be utilized for analysis of surface features. Secondary dissolution corrosion sculpture (CS) features seen on tetrahexahedra (THH) diamond faces will act as a proxy for kimberlite melt composition to allow for the identification of kimberlitic conditions in class 1 and 3 hypabyssal kimberlites. Experiments in a Piston-cylinder apparatus will quantify the effect of melt composition and temperature/pressure variation on the diamond dissolution features. The experiments are conducted between 1000–1200°C in silicate, carbonate, and silicate-carbonate melts at 1 GPa in "dry" or H_2O-undersaturated conditions. Experiments done in exact temperature pressure conditions with either silicate or carbonate melts have shown drastic differences in resorption styles and features. Diamonds in silicate rich melts under 1 GPa of pressure at 1100°C demonstrate strong resorption on the {111} and {012} faces whereas the same experiment in a carbonate melt demonstrates strong graphitization and little resorption. The established relationship between dissolution features on diamonds and composition of kimberlitic melt will allow a long-standing question to be addressed; if different kimberlite classes are formed by a uniform kimberlite melt due to difference in the country rock characteristics or due to compositional differences in kimberlite melt. In addition, use of surface features on microdiamonds from hypabyssal kimberlite facies for early identification of kimberlite class will help better planning for drilling programs and diamond grade assessment. This allows for saving on drilling costs and improves the modelling of kimberlite emplacement.

Geophysical exploration at Castle Frederick prospect, Upper Falmouth, Hants County, Nova Scotia, Canada

Fergus Tweedale[1] and Charles Banks[2]

1. Department of Geology, Saint Mary's University, Halifax, Nova Scotia B3H 3C3, Canada <fergus.tweedale.gmail.com>;
2. 70 Country Club Lane, Falmouth Nova Scotia, B0P 1L0

A road-accessible aggregate quarry situated on crown land, 4.5 km west of Windsor Junction, exposes mineralization and is the designated geographic centre of Castle Frederick (CF) prospect. The east-facing quarry headwall strikes N-S, is 130 m in length and up to 3.5 m in height. Centimetre-scale sulphide (pyrite-galena-sphalerite)-barite veins of unknown lateral extent are hosted in megacrystic biotite-rich granitic phases of the South Mountain Batholith (SMB). The veins are spatially associated with brecciation and fault gouge, clearly not magmatic and considered hydrothermal in origin. Observations of drill core extracted from beneath the quarry confirm the sporadic occurrence of sulphide veining and carbonate veinlets to at least 125 metres depth. Presently, relative age of sulphides and carbonates is indeterminate. The CF quarry is situated <1 km from an unexposed late Devonian-Carboniferous contact, suggesting an unconformity cuts through the property. Proximal location of CF prospect to Walton Mine (barite-galena-sphalerite-chalcopyrite-silver) and the Millet Brook uranium showing further suggest prospective potential in Hants County. Sporadic drilling throughout the county and local magnetic anomalies identified in small-scale aeromagnetic surveys support this claim. An exploration tool suited specifically to areas around Windsor, Falmouth, and Windsor Junction would help clarify questions about potential mineralization, and the objective of this work is to determine if ground-based magnetic surveying is an appropriate exploration tool. Magnetometer data (nanotesla units) collected during repeat walking transects along a bisecting quarry road is interpreted to reveal a measurable magnetic-field-intensity anomaly associated with sulphide veining. Graphical representation of this data provides a visual reference for the interpretation of other field data collected in an unexplored 2 km^2 forested area. Except for a few metasedimentary rocks, boulders and outcrop in the study area are granitic. A second quarry, intersected by a transect path, exposes SW dipping mudstones and medium- to coarse-grained sandstones, confirming the presence (but not the location) of an unconformable contact. Conspicuous hematite veining cutting at least one sedimentary horizon suggests late Devonian–Pennsylvanian hydrothermal fluid circulation was not spatially restricted to the SMB.

The energy transition - our winter of discontent

Grant D. Wach

Basin and Reservoir Lab, Department of Earth and Environmental Sciences, Dalhousie University, Halifax, Nova Scotia B3H 4R2, Canada <grant.wach@dal.ca>

Access to energy has been recognized by The United Nations Economic Commission for Europe (UNECE) as "critical for assuring quality of life", and at present 80 per cent of the energy usage in the UNECE region is fossil-fuel based. Many countries are reliant on non-renewable sources for their energy security and economic well-being, yet there is a growing global urgency to transition to a more sustainable energy future with increased dependence

on renewable energy sources, improved energy efficiency, and reduced global carbon emissions but at present this is being disrupted by severe spikes in energy prices, delivery networks, and the supply of both fossil and renewable energy systems.

Canada also has carbon reduction targets that the energy transition must help achieve. In Atlantic Canada, the provinces are in a unique position to become a green energy powerhouse, with reduced dependence on fossil fuels and to help lead Canada, and the World, in the transition to clean energy. An area tentatively called the Energy Corridor, straddling the New Brunswick and Nova Scotia boundary, has all the components for green energy success, including regular wind patterns in the nearby Gulf of St. Lawrence, salt deposits suitable for energy storage, and a central location with power links to the northeastern U.S.A.

Research into the Scotian and Sydney basins for carbon capture and storage (CCS) for emission reduction, renewable energy sources such as biomass, geothermal, tidal, hydrogen, and wind energy, and the energy storage potential in salt caverns will be discussed with other issues contributing to the overall energy situation in Atlantic Canada. This lecture will present an overview of the 'greening' of the Atlantic Canada provinces, review the vision for the energy future, and highlight opportunities to improve energy sustainability in the region. With energy costs spiking around the world, and a "winter of discontent" upon us, the Energy Transition is very important for Atlantic Canada and the World.

Stirring the Maritimes Basin: more than a pinch of salt

John W.F. Waldron[1,3], Alison Thomas[2], and Morgan E. Snyder[3]

1. Department of Earth and Atmospheric Sciences, University of Alberta, Edmonton, Alberta T6G 2E3, Canada <john.waldron@ualberta.ca>;
2. Department of Mathematics, Physics, and Geology, Cape Breton University, Sydney, Nova Scotia B1P 6L2, Canada;
3. Department of Earth and Environmental Science, Acadia University, Wolfville, Nova Scotia B4P 2R6, Canada

The Maritimes Basin of Atlantic Canada is a large and deep sedimentary basin underlying large parts of Atlantic Canada. The basin fill is predominantly late Paleozoic (Devonian–Permian) non-marine clastic sedimentary rocks, but the Visean Windsor Group, and the correlative Codroy Group of Newfoundland, contain substantial evaporites, including gypsum and anhydrite, halite, and potash. Laterally correlative limestone-evaporite-shale cycles have been traced throughout the middle and upper parts of the Windsor Group.

The role of Windsor evaporites in the tectonics of the Maritimes Basin has long been recognized. In addition to diapiric features generated by primarily vertical tectonics, there are extensive low-angle deformation surfaces characterized by anomalous breaks in the basin-wide stratigraphic succession. These breaks were originally interpreted as thrust faults, but later investigations, noting substantial omission of stratigraphy, led to their re-interpretation as a single low-angle detachment - the Ainslie Detachment. The availability of industry seismic reflection data allows these structures to be again reinterpreted as salt welds, in the light of recent advances in evaporite tectonics on passive continental margins.

For example, the famous Joggins Pennsylvanian succession was rapidly deposited in accommodation space created by salt expulsion, showing that Windsor Group salt remained in place until the Pennsylvanian before rapidly moving into diapiric salt walls. In contrast, in the eastern Cumberland subbasin, evaporite expulsion was already controlling sedimentation during Mississippian deposition of the Windsor and Mabou groups. Field relations in other parts of the Maritimes Basin suggest that this history of early evaporite expulsion is more usual.

These observations suggest an interpretation in which movement of the thick lower Windsor evaporites began within a few million years of their deposition. Feedback between halokinesis and sedimentation occurred from middle Visean onward. Multiple minibasins were simultaneously flooded by eustatic sea-level rises, related to glacial cycles on Gondwana, accounting for the laterally correlative limestones. Differences in the overlying stratigraphic successions are best explained, therefore, by deposition above a changing configuration of moving evaporite bodies that culminated in complete expulsion of salt beneath some minibasins.

The tops of evaporite diapirs have probably remained near the surface, producing areas of subsidence and karst development, throughout much of Nova Scotia's subsequent history. The distribution of near-surface evaporites continues to be marked by widespread development of sinkholes at the present day.

What drove the Acadian orogeny?

John W.F. Waldron[1,2]

1. Department of Earth and Atmospheric Sciences, University of Alberta, Edmonton, Alberta T6G 2E3, Canada <john.waldron@ualberta.ca>;
2. Department of Earth and Environmental Science, Acadia University, Wolfville, Nova Scotia B4P 2R6, Canada

Most orogenic events in the northern Appalachians and the Caledonides have relatively clear tectonic drivers. The Taconian–Grampian orogeny (latest Cambrian to Ordovician) represents a collision of the hyperextended Laurentian margin with a SE-dipping subduction zone. Salinian deformation (mainly Silurian) recorded accretion of Ganderian fragments at the now-active Laurentian margin, culminating in the Scandian collision of Baltica (already connected to East Avalonia along the 'Tornquist line'). Late Paleozoic Alleghanian deformation resulted from the arrival of Gondwana.

The Silurian (~423 Ma) to Devonian (~385 Ma) Acadian orogeny is more difficult to interpret. It is widely attributed to collision of Avalonia with Laurentia, following NW-dipping subduction recorded by the coastal igneous belt (Maine, New Brunswick, Cape Breton Island, and southern Newfoundland). Nonetheless the major nappes in the Acadian orogen in southern New England are rooted to the SE. The Acadian orogeny has been interpreted to involve major transpression, but authors have been divided as to whether that transpression was dextral or sinistral. Further complicating the issue is the 'Neoacadian' orogeny, a term used to describe shortening both in the Meguma terrane (~400 Ma), and much later (370–355 Ma) in New England, coincident with early extension in the Maritimes Basin in Atlantic Canada.

Transpression provides a potential solution to the enigma. In Scotland, a major tectonic mismatch occurs across the Great Glen Fault. To the NW, major Silurian Scandian deformation affected the Northern Highlands, where Grampian deformation was insignificant. In contrast the Grampian Highlands, to the SE, underwent major Ordovician Grampian tectonism, but were little deformed in the Silurian. British geologists have suggested up to 1000 km of sinistral slip, bringing these disparate terranes together in the Late Silurian to Early Devonian. Acadian sinistral transpression is widely reported through southern Britain, though overprinted by dextral shear in the Carboniferous.

Because of the shape of the Laurentian margin, sinistral deformation of this magnitude would have led to transpression in the Appalachians, consistent with sinistral Acadian shear zones in Newfoundland (Gander terrane), Cape Breton Island, northern Maine, and southern New England. This convergence may have brought West Avalonia into oblique collision with the NW-dipping subduction zone that fueled the coastal igneous belt. Collapse of the Mascarene backarc led to the vergence change responsible for the southern New England nappe pile. A change to dextral motion in the Middle Devonian overprinted Acadian structures, leading to Neoacadian transpression in New England but transtension in Atlantic Canada.

Introducing a new addition to the Atlantic Geoscience Society's geological highway map series: *'Journey through time: places of geological significance in New Brunswick and Prince Edward Island'*

Jim Walker[1], Erin Keith[2], Jolane Sorge[2], and Kathleen Thorne[2]

1. New Brunswick Department of Natural Resources and Energy Development,South Tetagouche, New Brunswick E2A 7B8, Canada <jim.walker@gnb.ca>;
2. New Brunswick Department of Natural Resources and Energy Development, Fredericton, New Brunswick E3B 5H1, Canada

The Atlantic Geoscience Society (AGS) undertakes a wide range of communication and educational activities and projects, one of which is the publication of geological highway maps. One of the newest (soon to be released) maps in this series, entitled: *'Journey through time: places of geological significance in in New Brunswick and Prince Edward Island'* is an updated version of the 'Geological Highway Map of New Brunswick and Prince Edward Island' (AGS Special Publication Number 2) that was published in 1985. Since that time, substantial advances have been made in the understanding of New Brunswick's geology; primarily due to work carried out by the province's Geological Survey but also with significant contributions from researchers at local universities and colleagues with the Geologic Survey of Canada. It is for this reason that the decision was made to release this new map.

The new map will be a digital product measuring 68.5 x 99 cm (27″ by 39″) from which hard copies can be printed. The front side of the map presents New Brunswick's geology at the Group level with a shaded relief background and includes an up to date (somewhat simplified) provincial road network, and major water courses. The map highlights points of geological interest (84 in New Brunswick and 7 in Prince Edward Island) that are accompanied by short descriptions of their geological attributes. These sites were selected on the basis of geologic interest, geographical distribution, ease of access and safety. The reverse side of the map is divided into 16 sections providing more detailed information on a variety of topics including the geological-tectonic history of the region, specific metallic and industrial minerals and petroleum resources, the geology of New Brunswick's parks (e.g., Mount Carleton Provincial, Fundy National, Stonehammer Geopark, and Hopewell), the paleontological riches, glacial geology, and coastal zone issues pertaining to climate change. Many of the points of interest or back panel sites are described in greater detail in the 'Geology of New Brunswick and Prince Edward Island' field guide published by Hickman Hild and Barr in 2020, and are identified as such for those searching for more in-depth descriptions.

The map is intended to provide the neophyte a rudimentary understanding of the complex bedrock and glacial geology and how that geology relates to landforms and mineral endowment. It is anticipated that this map will be popular with the public, used in schools and university earth science classes, and will increase the profile of geoscience in New Brunswick, Prince Edward Island, and beyond. It will also serve as the base for a proposed extended digital version (downloadable app) of New Brunswick's geological points on interest.

Progress report on northern Maine geology: new data and thoughts on the extent and geologic history of the Munsungun–Winterville Belt

Chunzeng Wang

University of Maine at Presque Isle, Presque Isle, Maine 04769, USA <chunzeng.wang@maine.edu>

The Munsungun–Winterville Belt (MWB) is a major Ordovician lithotectonic belt developed on the leading edge of the ensialic Ganderia in northern Maine. Recent mapping reveals a much wider extent of the belt, and the belt includes 11 inliers of various sizes. In addition to the Munsungun, Winterville, Portage Lake, Haystack Mountain, and York Ridge inliers, the belt also contains several much smaller ones, including the small inliers in the headwater of the East Branch Penobscot River and Aroostook River. The MWB is believed to connect the Caucomgomoc inlier, Chesuncook "dome", and Lobster Mountain "anticlinorium" in the SW, as part of the Bronson Hill–Popelogan arc. The MWB and the overlying cover strata occur as a widespread imbricated stack of multiple NE-striking reverse-thrust faults that resulted from a prolonged faulting history starting from the earliest phase of Salinic orogeny to the Neoacadian–Alleghanian orogenies. Several small inliers even occur entirely as fault blocks. The MWB is composed predominantly of several NE-striking petrographically and geochemically distinct volcanic units that were formed in different tectonic settings. Most of them exhibit calc-alkaline or tholeiitic arc signatures, with the remaining lesser ones having tholeiitic non-arc affinity. Zircon U–Pb ages of the calc-alkaline and tholeiitic arc volcanic rocks show a generally NW-younging trend across the MWB, from 471 Ma to 451 Ma, probably indicative of northwestward trench-arc migration, likely associated with a prolonged SE-dipping, retreating subduction system between Laurentia and Ganderia. The tholeiitic non-arc volcanic rocks were produced in extensional setting (back-arc or intra-arc rifts) and probably associated with the NW-directed Brunswick Subduction System from Late Ordovician to Early Silurian. Detrital zircon age spectra and sedimentary features of several minor Upper Ordovician syn-tectonic forearc formations deposited along the MWB indicate a Laurentian provenance, suggesting that, immediately after the accretion of the Munsungun–Winterville arc to the Laurentia margin during closure of the Iapetus Ocean during the Late Ordovician, the rapid exhumation facilitated the deposition of the detritus derived from the accreted Laurentia over the MWB. Subsequent Salinic and Acadian orogeneses significantly reshaped the MWB as indicated by the widespread unconformities of the foreland Silurian formations and Devonian Seboomook Group and the large-scale reverse/thrust faults. The large post-Acadian, plant fossil-rich molasse basins (aged Emsian) discovered recently marked the end of the Acadian orogeny, but a NE-striking, SE-directed reverse/thrust fault system significantly displaced the basins, indicating a remarkable Neoacadian–Alleghanian faulting event in the northern Maine Appalachians.

Late-Triassic epithermal polymetallic Sb-Au (-Pb-Zn-Co-Ag) veins, Meguma terrane, Canadian Appalachian orogen: a new critical metal deposit type in Nova Scotia

Naomi Welt[1], Joshua Jackman[1], Erin Adlakha[1], Jacob Hanley[1], Mitchell Kerr[1], Robert Creaser[2], and Geoffrey Baldwin[3]

1. Department of Geology, Saint Mary's University, Halifax, Nova Scotia B3H 3C3, Canada <naomi.welt@smu.ca>; 2. University of Alberta, Department of Earth and Atmospheric Sciences, Edmonton, Alberta T6G 2R3, Canada; 3. Nova Scotia Department of Natural Resources and Renewables, Halifax, Nova Scotia B3J 2T9, Canada

A multi-analytical approach has been applied to the characterization of a little-known polymetallic (As-Sb-Zn-Pb-Fe-Cu-Co-Au-Ag) vein-hosted occurrence in the Digby area of southwestern Nova Scotia, called the Lansdowne occurrence. This occurrence has been selected as a case-study to further understand critical metal endowment of the Meguma terrane, the outward-most terrane of the Canadian Appalachians. Detailed petrography along with mineral chemistry, and Re–Os geochronology of arsenopyrite in mineralized zones constrain two distinct periods of mineralization: the early stage (composed of arsenopyrite), which formed at ~365 Ma, and the more dominant late stage (composed of early sphalerite, chalcopyrite, and pyrrhotite, followed by later arsenopyrite, galena, and Sb-Pb sulfosalts boulangerite and jamesonite), which formed at ~214 Ma. These two mineralizing stages coincide temporally with major tectono-magmatic events affecting the Meguma

terrane: (i) the waning stages of the Neoacadian orogeny and emplacement of the South Mountain Batholith (early stage), and (ii) rifting of the Bay of Fundy, due to the opening of the Atlantic Ocean from the breakup of Pangea (late stage). Results of Al-in-chlorite thermometry associated with early sphalerite of the late stage indicates chlorite formation at 350 to 390°C. Fluid inclusion petrography, microthermometry, and Raman spectroscopic analyses indicate two mingling fluids during the Sb-Pb sulfosalt stage: a variable salinity (6.16 – 27.35 wt% eq. NaCl) aqueous brine and a methane dominated fluid. Isochore calculations suggest epithermal conditions for Sb-Pb mineralization (approximately 165°C and 15 bars). High and positive S isotope values of sulfides ($\delta^{34}S$ = 14.7‰ to 25.1‰) suggest a sulfate source for S. An increase in $\delta^{34}S$ values from early to late stage arsenopyrite (15.30‰ to 23.95‰) suggests recycling and re-precipitation of early-stage sulfides (up to 30%) to form the late-stage sulfides. Base metals are likely sourced from surrounding country rock (mafic sills and host metasedimentary rocks) because of their alteration to calcite-chlorite, but sources of As and Sb remain unknown. Comparisons can be drawn between the Lansdowne occurrence to other Au deposits in the Meguma terrane (e.g., West Gore deposit), as well as other epithermal Sb-Au vein-type occurrences worldwide, such as those of the Variscan orogen in western Europe (e.g., the Berga Antiform of eastern Germany or the Biards Sb-Au-bearing shear zone in central France). The results of this project support exploration of this newly classified deposit type for critical metals in Nova Scotia.

A new edition of Atlantic Geoscience Society's Geological Highway Map of Nova Scotia

Chris E. White[1], Angie Barras[1], Sandra M. Barr[2], Jeff Poole[1], and Robert Raeside[2]

1. Nova Scotia Department of Natural Resources and Renewables, Halifax, Nova Scotia B3J 2T9, Canada <christopher.e.white@novascotia.ca>;
2. Department of Earth and Environmental Science, Acadia University, Wolfville, Nova Scotia B4P 2R6, Canada

The Atlantic Geoscience Society (AGS) undertakes a wide range of communication and educational activities and projects, one of which is the publication of the Geological Highway Map of Nova Scotia. Three editions of this map have been published previously, in 1980, 1990 (repackaged version in 1994), and 2005 (reprinted in 2014). The maps show the road systems of Nova Scotia and, using colours, the types of bedrock that occur at the surface throughout the province. The map is intended to encourage people to observe and help them to understand the origins of the varied geological features visible from their vehicles as they travel through Nova Scotia or visit coastal sections and viewpoints. The understanding of the bedrock geology has improved since 2005 because of new bedrock mapping by government and university geoscientists combined with other studies, especially geochronology. Hence it is timely to produce a fourth edition of the map that includes not only updated geological interpretations but also the current road network, which has changed since 2005. Like the 2005 edition, the product will be a digital map from which hard copies will be printed on a sheet size of 27″ by 39″; in addition, the option of producing a software application to be accessible on digital devices is being explored. The layout of the map is similar to the 3rd, with one side showing the geological map at the same scale as the third edition. The associated Table of Formations uses the 2021 International Chronostratigraphic Chart as the time scale. Also included is information on how to use the map, a symbols key, representative block diagrams, and a list of geological sites of interest. The reverse side provides more detailed maps and descriptions of particular areas that are well known and accessible, including Joggins, the Cabot Trail, the Parrsboro–Five Islands area, Scots Bay–Burntcoat Head, Yarmouth–Cape St. Marys, Arisaig, Halifax, and Louisbourg. The descriptions emphasize rock types, minerals, fossils, structural features, landforms, and glacial history. It is anticipated that the 2022 edition of the Geological Highway Map of Nova Scotia will continue to be used in schools and university earth science classes as part of the course material, an integral part of the annual EdGeo Workshops, and a product sought by residents and visitors to the province.

Characteristics of metamorphic textures of the Loch Eil Group of the Moine Highlands

Julie Woods and Richard Cox

Department of Earth Sciences, Dalhousie University, Halifax, Nova Scotia B3H 4R2, Canada. <jl569631@dal.ca>

Recent studies on the Moine Supergroup suggests that ages over a large extent have been poorly constrained, and lack of research conducted is a result of structural complexity and mineralogical monotony. The purpose of this research is to fill in said gaps in knowledge and data, with the following research question: how many metamorphic events are being recorded in the rocks of the southern Moine Highlands. It is hypothesized that there are 2 events at 800 Ma, caused by different phases of the Knoydartian event, 1 event at 450 Ma, caused by the Caledonian event, and possible contact metamorphism at 425 Ma, caused by the Strontian granitic intrusions. The methodology being implemented

consists of microscope analysis to broadly identify mineral assemblages and metamorphic textures in the samples, followed by major element analysis conducted on an electron microprobe, which is then proceeded by X-ray mapping of garnet grains present in the samples, U-Th-Pb analysis of monazite grains to help establish a range of ages, and geothermobarometric modelling to establish temperature and pressure conditions of the samples. For this research, garnet geothermobarometers such as GASP, GMBP, and garnet-biotite-plagioclase-quartz will be used, and the data being inputted into the models will be extracted from major element analysis. The mineral assemblages present in the four samples used in this study show varying percentages of quartz, feldspars, and micas, with garnet and monazite having abundance in one sample. Primary metamorphic textures present are symplectite, undulatory extinction, and schistosity. Current limitations are due to; overprinting, which affects age precision; distinguishing between older and younger fabrics; deciphering between competing P-T paths; and a lack of aluminosilicates in the samples.

Biogeochemical cycling within the Grand Lake Meadows floodplain. New Brunswick, Canada

Regan Worden and Allison Enright

Department of Earth Sciences, University of New Brunswick, Fredericton, New Brunswick E3B 5A3, Canada <regan.worden@unb.ca>

Grand Lake Meadows is Atlantic Canada's largest freshwater wetland, providing flood storage for the lower Saint John River basin. Each spring, the spring freshet submerges the 5000ha floodplain with high stand floodwater that transports essential particulate and dissolved nutrients to the wetland. These nutrients supply the sediment-hosted microbial community with organic carbon and other reduced ions which are energy sources for chemotrophic metabolic processes. The microbial consortium performs a variety of critical biogeochemical tasks, such as fixing N, C, and S that are used by higher trophic level organisms. In this way, microbial processes underpin the distribution of elements and energy for the entire ecosystem. Thus, the annual flooding cycle and associated transportation of nutrients are important energy sources to the floodplain. As New Brunswick experiences more frequent and severe flooding due to climate change, the timing and volume of the spring freshet becomes increasingly unpredictable. In high-water level years, such as 2018, floodwater reaching industrialized areas could negatively influence the chemical characteristics of the incoming water.

By creating a multivariate geochemical dataset of the Grand Lake Meadows floodplain, the aim is to determine a healthy geochemical baseline against which the geochemical and ecological impacts of future extreme floods can be measured. Providing a healthy baseline reference of this wetland aids as a protective strategy to quantify the effects of flooding on the wetland and critical biogeochemical cycling occurring. The study focuses on the microbially-mediated redox chemical reactions that fix critical nutrients (i.e., N, C, S) into the biosphere, over the duration of a flood pulse to determine modes of biogeochemical cycling within Grand Lake Meadows. By providing this knowledge, a baseline assessment will make it possible for investigators to mitigate negative impacts of flooding and climate change on freshwater wetlands in New Brunswick.

Petrogenesis and geochemistry of the Late Devonian Eagle Lake Granite and its association with Cu-Au-Mo mineralization in southwestern New Brunswick, Canada

Fazilat Yousefi[1], David R. Lentz[1], and Kathleen G. Thorne[2]

1. Department of Earth Sciences, University of New Brunswick, Fredericton, New Brunswick E3B 5A3, Canada <fazilat.yousefi@unb.ca>;
2. Geological Surveys Branch, Department of Natural Resources and Energy Development, Fredericton, New Brunswick E3B 5H1, Canada

The Late Devonian Eagle Lake Granite is an elongate 1.2 km-long hypabyssal stock located in southwestern New Brunswick just south of the Belleisle Fault. Copper, Mo, and Au mineralization is associated with this pluton and related dykes (15 cm to <1 m in width) that intruded Silurian meta-basic units of the Kingston Group. The granite comprises phenocrysts and microcrystalline groundmass of quartz, K-feldspar, and plagioclase (exhibiting oscillatory zoning), with minor biotite (primary, re-equilibrated, and secondary), magnetite, titanite, and apatite. The groundmass of these variably porphyritic rocks is medium-grained hypidiomorphic granular with an average grain size of two millimetres, whereas the fine-grained variety averages 0.05 mm in size. A zircon U–Pb age of 363.2 ± 4.2 Ma was determined for this granite using laser ablation methods. Based on the SiO_2 content, the Eagle Lake Granite can be further subdivided into three groups: (a) 69–70% SiO_2; (b) 71–73% SiO_2; and (c) 75–76% SiO_2 with group (a) consisting of porphyritic varieties restricted to the external parts of the stock; these three phases are peraluminous magnesian I-type granite (A/CNK = 1.0–1.3). In these rocks the ratio of Fe_2O_3/FeO is about 1.11 and Mg/(Fe + Mg) is 0.09–0.60. Based on the Na_2O + K_2O-CaO versus SiO_2 diagram, they plot in the range of calc-alkaline and alkali-calcic field. Electron microprobe analyses of biotite crystals indicates

the calc-alkaline nature of the Eagle Lake rocks.

The Eagle Lake rocks are enriched in large ion lithophile elements (LILE), depleted in high field strength elements (HFSE) with positive anomalies of K, Rb, and negative anomalies in Ti and Nb. The Zr content of the Eagle Lake samples ranges from 15 to 170 ppm and Nb contents range from 7.2 to 9.2 ppm. The Zr/Ti, Zr/Y, and Nb/Y ratios are consistent with calc-alkalic granites. The mineralogical, petrographic, and geochemical characteristics of the three phases are consistent with volcanic arc granites; these are consistent with the NB-2 granites in the region that are associated with Cu-Mo mineralization. Their magnesian bulk composition and magnetite-titanite assemblage with Mg-biotite are consistent with a higher oxidation potential, although local ilmenite with sulfides supports local reduction, possibly via assimilation. The similarity in age and composition to the DMd1 phase of the Mount Douglas Granite suggests a related late tectonic origin. These Late Devonian intrusions have an elongated shape, somewhat parallel to the regional faults, suggesting that faulting played a role in their high-level emplacement.

Feldspar, biotite, and magnetite phenocrysts with groundmass compositions from the Benjamin River South Porphyry Cu-Mo-Au deposits, northeastern New Brunswick, Canada: analysis of primary, re-equilibrated, and hydrothermal forms

Fazilat Yousefi[1], David R. Lentz[1], and James Walker[2]

1. Department of Earth Sciences, University of New Brunswick, Fredericton, New Brunswick E3B 5A3, Canada <fazilat.yousefi@unb.ca>;
2. Geological Surveys Branch, Department of Natural Resources and Energy Development, South Tetagouche, New Brunswick E2A 7B8, Canada

The Early Devonian (400 Ma) Blue Mountain Granodiorite Suite (BMGS) underlies an area of approximately 80 km^2 in the Benjamin River South area of northeastern New Brunswick. Porphyry-related copper and molybdenum deposits occur in the northeastern part of BMGS; these hypabyssal intrusive rocks range in composition from tonalitic to granodioritic. These rocks contain phenocryst to phenoclasts of subhedral hornblende (2%), subhedral biotite (8–12%), euhedral and subhedral prismatic plagioclase (42–47%), and anhedral magnetite (≤ 0.5%) in a fine- to medium-grained granular groundmass consisting of anhedral quartz (25–27%) and subhedral alkali feldspar (6–11%). Partial chloritization of some biotite is evident. These intrusions have an adakitic affinity.

In addition to the lithogeochemical data, biotite chemistry supports a calc-alkaline orogenic affinity. Furthermore, a range of Fe-biotite compositions, that fall mostly in the re-equilibrated biotite field on the FeO^{tot} + MnO - ($10*TiO_2$) - MgO discrimination diagram, confirms that both phenocryst and groundmass biotite formed over a protracted period in an evolving magmatic-hydrothermal system. These data indicate primary or modified primary igneous biotite compositions as well as hydrothermally generated compositions. Plagioclase in the BMGS is mostly anorthite, which is indicative of Ca-metasomatism. Quartz is released and anorthitic feldspar is formed in solid solution in plagioclase: $2(K,Na)AlSi_3O_8 + Ca^{2+} \rightarrow CaAl_2Si_2O_8 + 4SiO_2 + 2K(Na)^+$

The composition of iron and titanium oxide minerals is between magnetite and ilmenite. Magnetite is a common accessory phenocryst and is stable over a wide range of conditions in igneous rocks and in a diversity of ore deposit types. An initially oxidized I-type magma can generate features of ilmenite-series (reduced) intrusions if the magma is subsequently emplaced into rocks with low redox potential. The presence of pyrrhotite in some samples is an indicator of increasing fH_2S with decreasing T of the hydrothermal fluid. The formation of ilmenite exsolutions is controlled by the oxidation of ulvospinel at temperatures above the magnetite-ulvospinel solvus: ($6Fe_2TiO_4 + O_2 \rightarrow 2Fe_3O_4 + 6FeTiO_3$). In the BMGS, hydrothermal alteration is widespread and commonly zoned on the deposit scale, as well as around individual veins and fractures. Porphyry deposits commonly exhibit an inner potassic zone characterized by K-feldspar and/or biotite, thence outward into a zone of phyllic alteration (quartz, pyrite, and phengite), and finally an outer most zone propylitic alteration (epidote, chlorite, and carbonate); sulphides and biotite form along micro-fractures, with the chalcopyrite-pyrite mineralization (up to 5%, with molybdenite), occurring as disseminations in potassically altered upper part of the cupolas and is consistent with the mineralization and alteration of the potassic zone of many porphyry systems.

Geological Association of Canada, Newfoundland and Labrador Section

ABSTRACTS

2022 Technical Meeting

Virtual

The Annual Technical Meeting was held virtually on February 21 and 22, 2022, from various home offices, dens, and bedrooms across St. John's, Newfoundland and Labrador, and beyond.

This year the meeting kicked off on Monday with introductory remarks from the GAC-NL President, Anne Westhues, followed by a tribute to Dave Liverman who passed away earlier this year. The rest of the conference was taken up by presentations on a wide range of geoscience topics. Monday afternoon featured a Special Session on New Developments in Mineral and Petroleum Exploration. In the following pages, we are pleased to publish the abstract from the oral presentations. The best student presentations are recognized and receive the "Outstanding Student Presentation Award" which consists of $100 and a certificate. The award winners are indicated by an asterisk in the title.

As always, this meeting was brought to participants by volunteer efforts and would not have been possible without the time and energy of the executive and other members of the section such as Anne Westhues, Jared Butler, James Conliffe, Shawn Duquet, Sarah Hashmi, Zsuzsanna Magyarosi, Annie Parrell, and Karen Waterman. We are also indebted to our partners in this venture, particularly the Geological Association of Canada, Department of Earth Sciences (Memorial University of Newfoundland), and the Geological Survey of Newfoundland and Labrador, Department of Energy, Industry, and Technology. We are equally pleased to see the abstracts published in Atlantic Geoscience. Our thanks are extended to all the speakers and the editorial staff of the journal.

Although the abstracts are modified and edited as necessary for clarity and to conform to Atlantic Geoscience format and standards, the journal editors do not take responsibility for their content or quality.

THE EDITORS

ATLANTIC GEOSCIENCE 58, 43 - 54 (2022)
2564-2987|22|00043-054 $2.80|0
doi: 10.4138/atlgeo.2022.002

Combining high resolution seismic sub-bottom imagery with magnetometer data to identify potential UXOs: a case study off the Danish coast

Stephanie M. Abbott, Maria Kotsi, Ryan Laidley, and Jacques Y. Guigne

PanGeo Subsea, A Kraken Robotics Company, St. John's, Newfoundland and Labrador A1G 1A1, Canada

The aim of this project was to acquire Sub-Bottom Imager (SBI) and magnetometer data to identify shallow sub-surface geohazards, particularly potential Unexploded Ordinances (pUXOs). The Sub-Bottom Imager, developed by PanGeo Subsea, is a novel system that provides high-resolution near-surface investigations with real-time 3D imaging. Its novelty relies on the combination of near-field beamforming with synthetic aperture sonar (SAS) processing tools, and the use of an Inertial Navigation System (INS) that allows for accurate source and receiver positioning and orientation. PanGeo's SeaKite deployment method was used to equip and acquire the SBI and magnetic data simultaneously. The survey area was 2480 m by 150 m, and the geological composition was primarily fine-grained sand or silt. Initial processing involved identification and interpretation of acoustic anomalies suggestive of pUXOs. This interpretation included associated attributes such as location, depth of burial, shape, and size meeting the minimum criteria of 0.60 m by 0.30 m. The magnetic processing was completed using the UXO Marine extension of Oasis Montaj, and targets were picked using the analytical signal (nT/m) grid. A target list was compiled with the information of target_ID, easting, northing, altitude, anomaly amplitude, and depth to target. Together with the target list, the residual field (nT) maps of magnetic anomalies displaying their shape and amplitude were used to correlate with the acoustic anomalies. Specifically, the SBI data was assessed for the presence of acoustic anomalies at the provided magnetic anomaly locations, and these correlations were delivered to the offshore renewable energy developer. Utilizing our results, the energy developer was able to assess the risk associated with these pUXOs and plan to safely remove them as deemed necessary.

Geophysics over a vulnerable cliff-side road, Bay Bulls, Newfoundland, Canada

Marzieh Arshian and Alison Leitch

Department of Earth Sciences, Memorial University of Newfoundland, St. John's, Newfoundland and Labrador A1B 3X5, Canada

Coastal erosion can be a serious issue requiring accurate observations in order to evaluate vulnerable areas and determine the subsequent actions to address this problem. The Town of Bay Bulls, about 29 km south of St. John's, Newfoundland, has coastal areas prone to erosion, and an important aim for the Town municipality is to reinforce these areas to avoid future road collapse. The Cliff site is over Northside Road, near the northwest end of the bay on the side of a steep incline, facing the marine terminal. The road here was widened in the 1960s, involving the construction of a wooden retaining wall infilled with earth materials. Slumping of the road surface and outward displacement of some parts of the wall are observed today.

Two geophysical methods were employed to image the surface and subsurface of the vulnerable stretch of road 140 m long. The methods were ground penetrating radar (GPR) and direct current resistivity/induced polarization (DCR/IP). A GPR investigation was carried out to examine about a 5-metre depth of subsurface. The GPR survey used 250 antennae, providing useful information about the shallow underground structure. GPR results of the Cliff area depict the subsurface wooden braces for the wall, culverts, and bedrock.

To thoroughly assess an area's vulnerability, it is essential to evaluate the deeper subsurface using DCR method. Combining two different DCR configurations, Schlumberger-Wenner and Dipole-Dipole, helped us achieve a two-dimensional model to a depth of about 17 m. Two overlapped DCR profiles were performed along the north side of Northside Road in the Cliff area.

St. John's urban flooding – The Rennies River experience: can we or should we try to tease modern global change phenomena from city-orchestrated urbanization (building and paving)?

Elliott Burden

Department of Earth Sciences, Memorial University of Newfoundland, St John's, Newfoundland and Labrador A1B 3X5, Canada

The Rennies River watershed, a small network of streams and ponds draining a little more than 30 km^2 in St. John's, Newfoundland, has a history and prehistory extending back to end of the last ice age. Throughout most of that time the river has behaved as a misfit s tream fed from a marshy landscape perfectly adapted to our boreal oceanic climate. Late 19th and early 20th century agriculture had a modest impact on improving river fitness with much more sediment entering Quidi Vidi Lake, but air photo coverage from the mid 20th century indicates that the large

marshlands of the Ken Brook and Yellow Marsh Brook tributaries basically remained intact until more recent times. The city's own poster board displayed on the Rennies River trail shows a river flood in 1948. In 1986, and now some years after Ken Brook and Yellowmarsh Brook wetlands were being developed a significant late fall rainfall event led to flooding of many downstream homes and the "Mall". By the early 2000s, when hurricanes Gabrielle and Igor indeed touched upon Newfoundland shores, climate researchers were beginning to sound the alarm about global change. And so too, development of the upland marshlands continued. During our most recent event – a rainfall/snow melt upon frozen ground, can we really blame climate change, or is this a function of our growing lack of wetlands to absorb precipitation? I am not a lawyer, and there may yet be other issues at play if flooding is not simply explained as a random act of nature. Solutions are possible, but none are without costs to people and governments.

Using fluoride analysis in till to assist in identifying the bedrock potential for critical minerals in central Newfoundland, Canada

Heather Campbell[1], Steve Amor[2], Zsuzsanna Magyarosi[1], Chris Finch[1], and Rosauro Roldan[1]

1. Geological Survey, Department of Industry, Energy and Technology, Government of Newfoundland and Labrador, St. John's, Newfoundland and Labrador A1B 4J6, Canada; 2. Geological Consultant, St. John's, Newfoundland and Labrador A1A 3C5, Canada

Fluoride analysis has successfully located previously unrecognized mineralization associated with Li-Cs-Ta (LCT) pegmatites in sandy, bouldery, variably eroded, and dispersed till overlying granite and metasedimentary rocks in the Snowshoe Pond region of the Meelpaeg Subzone in central Newfoundland. Fluoride, measured by Ion Selective Electrode (ISE) analysis, is a component of the analytical suite for till-geochemical samples in the province of Newfoundland and Labrador. In central Newfoundland, fluoride in till is thought to be derived from apatite that typically occurs in LCT pegmatites (up to 5%). Fluoride anomalies in till samples are more effective in defining the extent and locale of the underlying pegmatites than other geochemical indicators associated with mineralization (e.g., Cs, Li, Nb), as the fluorine-bearing apatites are: (1) relatively abundant in the source rocks, and (2) sufficiently resistant to reside in dispersed and eroded tills. Based on this study, the use of fluoride analysis in till is highly recommended in other areas with potential for rare element mineralization. More studies are being conducted to assess the potential of fluoride in till in exploring for other types of deposits, such as rare earth elements (REE) that are also typically associated with F-rich rocks.

A review of the structural controls on mineralization at the Valentine Gold Project, Central Newfoundland, Canada

Nic Capps

Marathon Gold Corporation, 36 Lombard Street, Toronto, Ontario M5C 2X3, Canada

The Valentine Gold Project, located in central Newfoundland, is a structurally-controlled orogenic gold deposit consisting of quartz-tourmaline-pyrite-Au (QTP-Au) veining hosted in the Valentine Lake Intrusive Suite (VLIS; 575–565 Ma). The VLIS lies in unconformable contact with the Silurian-aged Rogerson Lake Conglomerate (RLC) along the NE-SW trending Valentine Lake Shear Zone (VLSZ). Five phases of Acadian-aged deformation have been identified on the property, with gold mineralization associated with up to four orientations of QTP-Au veining, the dominant set being SW-dipping, and infilling extensional brittle fractures. Individual extensional fractures, as exposed at surface, can have a lateral extent of up to 50m.

The project currently hosts five deposits with mineral resource estimates, two of which, Leprechaun and Marathon, form the basis of an open-pit mining proposal currently undergoing provincial and federal environmental assessment. Once operational, the Valentine Gold Project is expected to produce approximately 2 million ounces of gold over a 13-year life, with an average gold production of 173 000 ounces a year for the first 9 years. This makes it the largest undeveloped gold project in Atlantic Canada.

Current exploration is focused on the newly discovered Berry Deposit. At Berry, as well as at Leprechaun, gold mineralization within the QTP veins appears controlled by large-scale (>20 m) mafic dykes which run sub-parallel to the VLSZ, causing the mineralization to accrete in a concentrated band between these dykes and the Rogerson Lake Conglomerate to the SE. The Marathon deposit, which is the largest deposit currently on the property, hosts much more irregular, discontinuous mafic dykes. This appears to dictate a broader distribution of brittle deformation and QTP-Au veining, at a modestly lower average grade.

The Valentine Gold Project is a large scale, bulk-mineable gold deposit of a type generally new to Newfoundland. Understanding the genesis of the project's multiple mineral deposits, the detailed structural and geological controls on mineralization, and the similarities and differences of one deposit to the next,

is key to the further discovery and development of additional large scale gold projects across the island.

Predictive lithology mapping using machine learning: practical insights

Michael W. Dunham[1,2], Alison Malcolm[1], and J. Kim Welford[1]

1. Department of Earth Sciences, Memorial University of Newfoundland, St. John's, Newfoundland and Labrador A1B 3X5, Canada;
2. Goldspot Discoveries Corporation, Toronto, Ontario M5E 1K3, Canada

A popular use for machine learning in the mineral exploration industry is predictive mapping, where remote sensing data are combined with our limited observations on the ground to make lithology predictions for an entire region of interest. These machine learning predictions can produce a starting geologic map or enhance existing geologic maps. Over the past decade, supervised learning (SL) methods have become the common approach for predictive lithology mapping. In essence, SL methods learn a relationship between the co-located remote sensing observations and training targets (e.g., lithologies from outcrops, grab samples, etc.) in order to make predictions for where the lithology is unknown. Arguably, the biggest challenge with these problems is that the amount of training data is inherently limited (e.g., minimal outcrop exposure), which can lead to a phenomenon called overfitting; this translates to the SL model generalizing poorly to the data where the lithology is unknown (i.e., the unlabeled data). Semi-supervised learning (SSL) is a different machine learning approach that is better designed for these minimal training data situations. The advantage of SSL techniques is that they incorporate all the information (i.e., the training data and all the unlabeled data) during the learning process, which can provide improved predictions compared to SL methods.

We explore the effectiveness of SSL methods using a dataset from New South Wales, Australia, where the geologic map, and radiometric and magnetic data are provided. We simulate multiple exploration scenarios where the *a priori* knowledge of lithology is limited, and the task is to predict the lithology for the remaining majority of the map. Our results show that SSL can be 5–10% more accurate than SL, which means that lithology predictions from SSL can further reduce our risk when identifying exploration targets.

Ground penetrating radar observes forest hillslope soil trends in Pynn's Brook, Newfoundland, Canada

Zachary X. Gates[1], Lakshman Galagedara[2], and Susan Ziegler[1]

1. Department of Earth Sciences, Memorial University of Newfoundland, St. John's, Newfoundland and Labrador A1B 3X5, Canada;
2. School of Science and the Environment, Memorial University of Newfoundland, Corner Brook, Newfoundland and Labrador A2H 5G4, Canada

Soil property measurements to determine carbon (C) stocks are traditionally collected using physical samples or excavation practices which rely on small scale interpretations for sitewide averages. Such methods are limited in capturing soil distribution and landscape variance across heterogenous forests, as seen in estimates of 384 ± 214 Pg C in the top 1 m of Canadian forest soils and 1500–2400 Pg C globally at 30 cm deep.

Ground penetrating radar (GPR), a continuous, non-destructive geophysical tool for measuring subsurface reflection patterns, can expand boreal forest soil investigations past limited spatial scales. We have demonstrated through soil sampling and GPR surveying in Pynn's Brook, Newfoundland, Canada, at small pit (<1000 m^2) and large plot (>1000 m^2) scales that GPR measurements of soil horizon thickness, bulk density, and C stocks observe landscape trends across a hillslope site not previously captured by soil sampling methods.

GPR measurements across landscape scales suggest variable mineral soil horizon thickness sitewide (±4 cm) with thicker horizons accumulating downslope, following expected sediment transport and deposition mechanics. Soil bulk density measurements by GPR were consistently lower than soil estimates which suggests that traditional methods may overestimate soil content due to sampling bias. These differences in soil horizon thickness and bulk density measurements contributed to lower soil C stock calculations by the GPR method across scales. Overall, analogous GPR measurements for sitewide soil C stocks showed that increasing spatial data capture across gradients like a hillslope can significantly impact interpretations of sitewide soil and thus C content. As such, GPR's high resolution spatial sampling (5 cm sampling interval) and sitewide data collection capabilities expanded previous soil and C estimates to incorporate measurements across the full slope for a better understanding of landscape soil trends.

Natural CO_2 sequestration and mineralization in the Bay of Islands Ophiolite Complex, Newfoundland, Canada

Matthew J. Gill and Penny L. Morrill

Department of Earth Sciences, Memorial University of Newfoundland, St. John's, Newfoundland and Labrador A1B 3X5, Canada

The high reactivity and unique chemistry of ophiolites make them ideal sites for carbon mineralization. At elevated pH values, dissolved CO_2 in the water can dissociate to form CO_3^{2-} ions which readily bonds with Mg^{2+} and Ca^{2+} which are present in ophiolite groundwater. While this process has been proposed as a unique method to combat climate change the kinetics of these reactions and the impact that they could have on the atmosphere has not been quantified experimentally.

Experiments reported here were performed on rocks from the Bay of Islands Complex (BOIC) an ophiolite in Western Newfoundland. Crushed rock (<7 mm) was combined with simulated basic and ultra-basic groundwaters in a closed-batch chamber. A CO_2 analyzer was connected to the chamber headspace which monitored CO_2 concentrations over a 4-hour period. Conductivity, pH, ion concentrations, and total inorganic carbon (TIC) were measured before and after each observation. A total of 6 experiments were completed (in triplicate), one for each water type with and without the addition of crushed peridotite.

In all experiments, except for the control group, the CO_2 concentration decreased in the chamber headspace over the four-hour period. The addition of crushed ultramafic rock to deionized water had a CO_2 flux of -1.26×10^{-5} mol/m^{2}min ($\pm 4.5 \times 10^{-6}$ mol/m^{2}min, 1σ, $n = 3$). Basic waters and deionized water with rock had similar CO_2 fluxes while ultra-basic waters had the greatest CO_2 flux of all experiments at -7.05×10^{-5} mol/m^{2}min ($\pm 1.4 \times 10^{-6}$ mol/m^{2}min, 1σ, $n = 3$). The data here suggest that ultramafic rock in the presence of H_2O can sequester carbon dioxide. At a greatly elevated pH (>12), some of the CO_2 removed from the headspace precipitates out of solution as solid carbonate minerals. Our results indicate that this process could have a substantial impact on the Earth's atmosphere.

Volcanism associated with edge-driven convection preserved in the Deer Lake Basin, Newfoundland, Canada

Alana M. Hinchey, Ian Knight, Hamish A. Sandeman, and John G. Hinchey

Geological Survey, Department of Industry, Energy and Technology, Government of Newfoundland and Labrador, St. John's, Newfoundland and Labrador A1B 4J6, Canada

During the Carboniferous, the assembly of the supercontinent Pangea periodically reactivated strike-slip faults and shear zones that transect the northern Appalachian orogen. These strike-slip deformation zones represent crustal-scale tectonic boundaries that likely originated in association with Paleoproterozoic rifting of the paleo-Laurentian margin and have long-lived and complex kinematic histories. Their periodic reactivation controlled the evolution of the transtensional sedimentary basins of the region. The continuous interplay between the lithospheric plates, their subcontinental lithospheric mantle, and surficial processes (i.e., oceanic/riverine, biological, atmospheric, gravitational, erosional) controlled the development of the Deer Lake Basin (DLB) in western Newfoundland. The Saltwater Cove Formation of the DLB is a late Tournaisian deltaic succession where sedimentation was interrupted by minor intervals of basalt flows and pyroclastic deposits. The basalt samples have E-MORB (enriched mid-ocean ridge basalt) to OIB (ocean island basalt) chemical affinities, i.e., enriched LREE to HREE, and have $\varepsilon Nd_{(t=345\ Ma)}$ values between +2.8 and +6.4. Pyroclastic deposits include mafic lapilli tuff and intermediate tuff, and have compositions similar to CAB (continental arc basalt), with steep LREE relative to HREE patterns, negative Nb and Ti anomalies, and have $\varepsilon Nd_{(t=345\ Ma)}$ ranging from -6.1 to -1.0. Geochemical variation within the mafic rocks is explained by an E-MORB source variably influenced by crustal contamination processes. Coupled with field evidence, the geochemical and isotopic data support their emplacement in a transtensional, intra-orogenic basin setting that formed during the assembly of Pangea. Their m oderately primitive chemistry supports the interpretation that faulting associated with transtensional basin development facilitated asthenosphere upwelling via edge-driven convection.

Critical minerals in Newfoundland and Labrador: a review of concepts and a preliminary inventory of potential resources

Andrew Kerr

Department of Earth Sciences, Memorial University of Newfoundland, St. John's, Newfoundland and Labrador A1B 3X5, Canada

Critical Minerals is now a widely used phrase in the Minerals Industry, but it is hardly a new concept. During the Cold War, critical minerals were initially defined as materials important to national objectives that might encounter

supply disruptions by military or political conflicts, but the term is now much broader. Canada has a list of 31 critical minerals, but this includes several with widespread global production and some (e.g., nickel, uranium, and potash) that we produce ourselves. There is limited supply risk for these, but they are important to the economy.

All present lists of critical minerals feature commodities linked to the much-heralded *Energy Transition*. These include cobalt, lithium, manganese, nickel, graphite, and vanadium (for batteries in electric vehicles and energy-storage systems), the Rare Earth Elements (REE: for high-strength magnets in EV motors and wind-turbines) and some truly rare elements (e.g., cadmium, germanium, gallium, indium and tellurium) used in high-efficiency photovoltaic (solar) energy systems. Some of these (e.g., cobalt and the REE) are important in more than one sector or have other diverse applications in modern technology. Although some are primary commodities, many critical minerals (e.g., cobalt and "photovoltaic" elements) are by-products.

Exploration and development for many critical minerals will likely be very different from what we are used to. Future trends are hard to predict because end-use technology evolves on a scale of years, but exploration and development typically takes decades. There is much research aimed at material substitutions, which can quickly change requirements. Conversely, optimistic projections predicated on new research may be derailed if such innovations cannot be commercialized. Forecasts of demand growth made on a percentage basis often obscure the reality that global production of some commodities will remain small in *absolute* terms, which limits options for new producers. The geometallurgy of some such deposits (notably for REE) is complex, so custom process development adds another layer of cost and risk to any new project. Valuable by-product commodities are commonly extracted during smelting or refining, which may be in another jurisdiction. Finally, if such new operations are claimed to have climate mitigation benefits, their own environmental and energy footprints will require careful auditing.

Setting aside these multiple uncertainties, Newfoundland and Labrador has a promising inventory of known and potential critical minerals resources, including nearly half of the entries on Canada's current list. In Labrador, nickel and copper are produced at Voisey's Bay, and its by-product cobalt will be increasingly important. Significant manganese and uranium resources exist elsewhere in Labrador, and the Strange Lake Deposit is a world-class undeveloped resource of REE and associated elements. Other smaller REE and Be resources may also have future importance. Newfoundland hosts important antimony and fluorite producers, and also undeveloped resources of molybdenum and tungsten. Our knowledge of the abundance of other critical minerals such as graphite, lithium and vanadium is more limited, but our varied geology implies that potential exploration environments exist in both regions of the Province.

Reconstructing the southern North Atlantic Ocean back through time using deformable plate tectonic models*

Michael King and J. Kim Welford

Department of Earth Sciences, Memorial University of Newfoundland, St. John's, Newfoundland and Labrador A1B 3X5, Canada

The offshore rifted margins of the southern North Atlantic Ocean have been demonstrated to have a complex present-day crustal structure comprised of sedimentary basins, inherited structures, variable basement affinities, and continental blocks. Consequently, this has led to challenges when studying the crustal evolution of the southern North Atlantic. In particular, the kinematic history of continental blocks (e.g., Flemish Cap) and micro-plates (e.g., Iberia) and their subsequent impact on strain-partitioning during poly-phase rifting experienced along the Newfoundland, Irish, and West Iberian margins. Recently, deformable plate tectonic models, built using the GPlates software, have proven to be an advantageous method for investigating the interplay between plate kinematics and deformation experienced throughout the North Atlantic. Furthermore, their ability to calculate temporal variations in strain rate and crustal thickness provides a quantitative method of comparison with present day crustal thickness estimates calculated by gravity inversion and interpretations made from offshore seismic and well data. However, previous deformable plate models of the North Atlantic have included assumptions that are geologically problematic. Examples of assumptions include, but are not limited to, the rigid nature of continental blocks and model boundaries, and the specification of uniform crustal thicknesses within pre-rift templates.

In this study, we present a new deformable plate modelling approach using GPlates and its python programming module, pyGPlates, which aims to address these limitations by reconstructing present-day crustal thicknesses back through time. Using previously published and newly presented models, our results demonstrate the pre-rift crustal thickness template of the southern North Atlantic and the crustal thickness evolution of continental blocks and sedimentary basins within. In addition, this study highlights the potential impact of Appalachian and Caledonian terrane boundaries on the crustal segmentation observed within pre-rift templates and subsequent rift events.

**Honourable Mention: Outstanding Student Presentation Award*

Lithological controls on freshwater dissolved ultra-trace element signatures: examples from small catchments in Northern Ireland and Newfoundland and Labrador, Canada

Gabrielle M. Ledesma[1], Michael G. Babechuk[1], and Saskia E. Ryan[2]

1. Department of Earth Sciences, Memorial University of Newfoundland, St. John's, Newfoundland and Labrador A1B 3R5, Canada;
2. Archéozoologie, Archéobotanique: Sociétés, Pratiques et Environnements (AASPE, UMR 7209), Muséum national d'Histoire naturelle, CNRS, 75005 Paris, France

The global cycling of dissolved elements from land to sea is broadly controlled by relative element solubility and bulk crustal element abundance, as reflected in the geochemical signatures of major rivers. However, smaller rivers and streams within a catchment that contain predominantly one lithological rock type can provide a more detailed reconstruction of the biogeochemical factors governing the soil-to-aquatic transport of elements. Dissolved low abundance trace and ultra-trace elements (UTEs) within the freshwaters draining these smaller, monolithological catchments are especially powerful tools that can be used as indicators to link anomalous signatures to geological (e.g., mineralization, rock provenance) or anthropogenic point sources. Due to analytical challenges in quantifying UTEs in natural water, studies that contain full UTE characterization in monolithological catchments are rare, consequently resulting in poor understanding of the abundance and biogeochemical cycles of many element groups such as rare earth elements (REE), Zr, Nb, Mo, W, and Tl.

This study aims to characterize UTEs in rivers/streams in three areas, each with a different predominant bedrock lithology: Northern Ireland, UK (mafic volcanic rock); Bay of Islands, Newfoundland and Labrador (NL) (mafic-ultramafic plutonic rock); and St. Lawrence, NL (evolved felsic plutonic rock). Selected geochemical signatures of the Northern Ireland samples that cover standalone streams and a freshwater-to-seawater estuary transect will be the focus of this presentation. These results demonstrate that freshwaters draining mafic volcanic rock, despite being low in UTE abundance, develop consistent and geologically controlled signatures that diverge from major river patterns, with some signatures (e.g., REE patterns) being unexpectedly coherent, for particle-reactive elements, across wide salinity gradients. The NL study sites are part of a planned sampling excursion in 2022, with samples to be measured in the new low-metal clean laboratory facility at Memorial University and resulting in a dataset, the first of its kind, for NL freshwaters.

The Signal Hill Group: a record of fluvio-deltaic response to progressive Neoproterozoic deformation during the Avalonian Orogeny

David G. Lowe[1], Santiago Serna Ortiz[1], Andrea Mills[2], Benjamin F. Stanley[1], and Grace Khatrine[1]

1. Department of Earth Sciences, Memorial University of Newfoundland, St. John's, Newfoundland and Labrador A1B 3X7, Canada;
2. Geological Survey, Department of Industry, Energy and Technology, Government of Newfoundland and Labrador, St. John's, Newfoundland and Labrador A1B 4J6, Canada

The Signal Hill Group consists of the youngest Neoproterozoic strata in the Newfoundland Avalon Zone. It records sedimentation coeval with the ca. 560–555 Ma Avalonian orogeny, defined by local deformation of West Avalonia, including metamorphism, faulting, and folding coinciding with the shutdown of arc magmatism and initiation of local extensional magmatism. The Signal Hill Group provides a record of clastic progradation during the Avalonian Orogeny, details of which can resolve the near-surface effects and kinematics of deformation. At the base of Signal Hill, the Gibbet Hill Formation and overlying Quidi Vidi Formation record southward progradation of a sandy delta front environment dominated by mouth bars and distributary channel networks. Structural and stratigraphic evidence suggests blind faulting, folding, unconformity development, and basin reconfiguration between these units, supported by locally intense soft-sediment deformation along their contact. Conformably overlying the Quidi Vidi Formation are gravelly braided fluvial deposits of the Cuckhold Formation, recording amalgamation of alluvial channel belts with overall coarsening-up to pebble-cobble conglomerate followed by fining-up to pebbly sandstone. In the northern (proximal) Signal Hill basin, subsequent folding of the Signal Hill Group coincided with erosion that locally removed the Cuckhold Formation, with subsequent onlap of gravelly braded fluvial growth strata of the Flatrock Cove Formation. Here, progressive fault propagation then resulted in a change from braided channel belt to alluvial fan floodplain conditions. Conversely, in the southern (distal) part of the Signal Hill basin, the Cuckhold Formation is conformably overlain by the Blackhead Formation, recording anomalous overbank mudstone preservation under conditions of high sediment accommodation. It is not understood if or how these post-Cuckhold proximal and distal events were related; however, it is possible that renewed thrust propagation and orogenic loading led to proximal deformation and growth stratification coincided with reciprocal foredeep subsidence and preservation of overbank strata farther south.

Computer modelling of electromagnetic and direct-current resistivity data for mineral exploration

Xushan Lu[1,2], Colin Farquharson[2], and Peter Lelièvre[1]

1. Department of Mathematics and Computer Science, Mount Allison University, Sackville, New Brunswick E4L 1E4, Canada; 2. Department of Earth Sciences, Memorial University of Newfoundland, St. John's, Newfoundland and Labrador A1B 3X5, Canada

Three-dimensional (3D) computer geological models created by integrating various types of geological, geophysical, and geochemical datasets are widely used in mineral exploration projects to help find and delineate ore deposits. Electromagnetic (EM) and direct-current resistivity (DCR) methods are extensively used geophysical methods in mineral exploration, and they are becoming increasingly more important as exploration requires more accurate imaging at depth. Forward and inverse modelling of EM and DCR data can help refine the 3D geological model which is then used for drill targeting. Consequently, it is of vital importance to be able to perform the modelling accurately and efficiently. Realistic geological models can be complex, with topography and irregular geometric interfaces between distinct geological units. Traditional modelling algorithms which use structured rectilinear meshes to discretize realistic geological models can be inaccurate unless extremely small cells are used to discretize the model, which inevitably leads to poor modelling efficiency.

We have developed numerical algorithms for the forward and inverse modelling of various types of geophysical data including EM and DCR data using unstructured tetrahedral meshes. Compared with rectilinear meshes, unstructured meshes can more faithfully conform to complex geometric features in the geologic model and topography. The modelling efficiency is also significantly better because local refinements in key regions of the geological model can be easily introduced while keeping the total number of cells small. To facilitate the process of mesh creation, we have also developed software (FacetModeller) to create wireframe models representing arbitrarily complex geological models within a graphical user interface environment.

We have applied our modelling codes to real EM and DCR datasets, and to realistic, challenging test scenarios representing a range of ore deposit types and hosts. Our computer modelling algorithms have been shown to be accurate and efficient, and can greatly contribute to a better understanding of subsurface geology.

Li-Cs-Ta pegmatites in Newfoundland, Canada

Zsuzsanna Magyarosi and Heather Campbell

Geological Survey, Department of Industry, Energy and Technology, Government of Newfoundland and Labrador, St. John's, Newfoundland and Labrador A1B 4J6, Canada

Pegmatites are a significant source of several critical elements including REE, Li, Cs, Ta, and Nb, and also a source of gemstones, high-quality feldspar, quartz and mica. Most economic pegmatites are derived from evolved granites with numerous magmatic phases representing varying degrees of fractionation. In the late stages of crystallization of the main granite, a residual melt enriched in incompatible elements, such as Li, Cs, REE, Nb, Ta and volatiles, separates and crystallizes as pegmatite dykes.

Based on their trace element enrichments, pegmatites are subdivided into Li-Cs-Ta (LCT) and Nb-Y-F (NYF) types. NYF pegmatites are associated with A-type granites, are enriched in REE and occur within their parent granite. LCT pegmatites are usually associated with S-type granites, having formed as a result of anatexis of metasedimentary rocks, and occur in the surrounding rocks up to ~10 km from the parent granite. The degree of fractionation is directly correlated with their economic potential and increases with increasing distance from the parent granite. LCT pegmatites are located along major tectonic boundaries, typically within metasedimentary dominated areas, where the grade of metamorphism ranges between greenschist and amphibolite facies. The host rocks are metasomatized around the pegmatite dikes with elevated Li, Rb, Cs, B and F contents and the occurrence of minerals such as tourmaline, holmquistite, muscovite and garnet.

In Newfoundland, the Gander Zone and surrounding areas represent an ideal geological setting for LCT pegmatites and show many similarities to the well-known pegmatite fields in the Superior Province. Pegmatites have been identified in central Newfoundland, but their economic potential has only recently been recognized. Further exploration should include till and bedrock sampling to identify fertile granites and metasomatic alteration associated with unexposed pegmatites, and mapping metamorphic grades to identify the contact metamorphic aureole from underlying intrusions. Once fertile granites or pegmatites are identified, further work should concentrate on determining fractionation trends with whole-rock and mineral chemistry.

Assessing the CO_2 sequestration potential of serpentinized ultramafic rocks of Baie Verte, Newfoundland, Canada*

Timilehin A. Oguntuyaki and Penny L. Morrill

Department of Earth Sciences, Memorial University of Newfoundland, St. John's, Newfoundland and Labrador A1B 3X5, Canada

The increasing need to mitigate the effects of climate change has necessitated CO_2 sequestration using ultramafic rocks. Despite numerous studies on the use of ultramafic rocks, highly altered forms of these rocks in Baie Verte have not been assessed for their potential to sequester CO_2. This study focused on using serpentinized ultramafic rocks of the Baie Verte Oceanic Tract (BVOT) to trap atmospheric CO_2 and potentially use it to mineralize carbonate.

Rocks from the BVOT, which primarily comprise peridotites with compositions ranging from serpentinized mantle harzburgite to dunite, were crushed into two sample groups of distinct grain sizes; crushed rock (CR) and powdered rock (PR), each of which was reacted with two water types; deionized (DI) water and magnesium-rich water, and a known concentration of CO_2 in a LiCor Flux Chamber and CO_2 Gas Analyzer for 4 hours. Water-only experiments were also conducted in the same manner for the two types of water. After the 4-hour experiments, observations were made for the change in concentration of CO_2 in the system, changes in dissolved ions (Mg^{2+}) concentration, and change in Total Inorganic Carbon (TIC).

Results showed that CO_2 concentration in the system decreased in all experiments; 300 g of CR + 300 mL of Mg-rich water had the most significant average CO_2 sequestration rate of $1.69\times10^{-7} \pm 1.40\times10^{-8}$ mole/min. The DI water + PR experiment also had the most significant increase in TIC (about 9.8 ppm of carbon) after 4 hours of reaction. The DI water-only experiments had the slightest decrease in CO_2 concentration and the lowest change in TIC.

The change in CO_2 concentration results suggests that serpentinized ultramafic rocks in BVOT could sequester CO_2, while the TIC and dissolved ion analyses showed that the rocks could convert the sequestered CO_2 into more stable carbonates.

**Winner: Outstanding Student Presentation Award*

Quaternary mapping and stratigraphy of northwest Gander, Newfoundland, Canada, and implications for regional ice dynamics and mineral exploration

Jennifer S. Organ[1], Daniela Mendoza-Marin[2] and Heather E. Campbell[1]

1. Geological Survey, Department of Industry, Energy and Technology, Government of Newfoundland and Labrador, St. John's, Newfoundland and Labrador A1B 4J6, Canada; 2. Department of Earth Sciences, Memorial University of Newfoundland, St. John's, Newfoundland and Labrador A1B 3X5, Canada

The northwest Gander region has a complex glacial history influenced by multiple ice flows including an ice streaming event, and marine incursion as ice retreated during deglaciation. This complexity is identified in landforms, surface morphology, and underlying stratigraphy. The regional ice-flow chronology is identified by relative age relationships found at multidirectional striation sites. It indicates that the region was influenced by three phases of ice flow: Phase (1) an early east-southeast flow; Phase (2) a pervasive north to northeast flow that is also recorded by streamlined landforms; and Phase (3) a local northwest flow observed in the northwestern part of the study region.

Surficial units include till, organic deposits, glaciofluvial sediments (particularly in the Gander River Valley and its tributaries), and sparse marine sediments near the coast and along the Gander River. Till is the most dominant surficial unit identified. It has a varying thickness (1–5 m) and is thinner towards the coast. It forms different morphologies, including veneers, blankets, ridges, and hummocky, eroded, lineated (streamlined) or glaciotectonized till. Subglacial till is typically more useful for delineating mineral dispersal than other till types.

Preliminary investigations have exposed multiple till units (e.g., three till units were identified at one site in 2021) and provided insight into their stratigraphic relationships, although their lateral extent is unknown. The upper two tills were identified in 30% of sites visited during the 2021 field season, indicating that multiple-till preservation is more widespread than previously thought. The uppermost unit varies in thickness from 30–90 cm, which may have implications for mineral exploration using till geochemistry; knowledge of till units and their stratigraphic relationships are paramount when conducting sampling programs. Future work includes continued detailed mapping and examining the textural, mineralogical, and geochemical variation of each regional till unit through laboratory analyses, pebble counts, and mineral indicator studies. This future work will assist in providing constraints on material transport distances in a subglacial regime.

Topographic controls on soil organic carbon in moist boreal forest mineral soils*

Mackenzie Patrick, Zach Gates, and Susan Ziegler

Department of Earth Sciences, Memorial University of Newfoundland, St. John's, Newfoundland and Labrador A1B 3X5, Canada

Boreal forests contain ~30% of the global soil organic carbon (SOC) stock within a region vulnerable to climate change, yet detailed studies on the controls of this large reservoir are lacking. In these moist acidic soils, soil forming processes link C dynamics and chemical weathering via organo-metal complexes (OMC), which are important weathering products that stabilize C in the surface mineral soil. At the continental scale, climate and parent material control OMC abundance, but within a climate region, the influence of slope on hydrological and erosional processes may impact OMC formation and stability, and subsequently SOC content.

To investigate the role of topography on SOC, changes in particulate and dissolved organic carbon (POC and DOC, respectively) were measured experimentally using soil columns built from mineral horizon soils collected from different depth and slope positions within an experimental watershed in the Pynn's Brook region of Newfoundland. The gentle-sloped (6°) upslope soils had greater SOC and OMC, while the steeper (12°) downslope soils had higher bulk density and sand, consistent with a footslope depositional zone. Dissolved organic matter, a primary source of SOC to these mineral soils, was collected in passive pan lysimeters and applied to the experimental soil columns. Uptake of C was dependent on the degree to which OMC were saturated with SOC, where undersaturated deep horizons sequestered more C while saturated surface soils exhibited little change. The footslope had greater POC loss while upslope was relatively stable. Overall, vertical flow promoting OMC formation-controlled SOC content and C uptake in the gentle-sloped soils, while lateral flow and depositional processes of erosion dominated in steeper soils resulting in less OMC, easily mobilized POC, and consequently, lower SOC. These results highlight the importance of slope on SOC content through interacting hydrological and erosional processes, and the high potential for C uptake at depth in these forest landscapes.

**Winner: Outstanding Student Presentation Award*

Stable Isotope Precipitation Sampling (SIPS): determining the local meteoric water line using seasonal precipitation samples across the island of Newfoundland, Canada*

Kendra R. Revoy, Michael G. Babechuk, and Penny L. Morrill

Department of Earth Sciences, Memorial University of Newfoundland, St. John's, Newfoundland and Labrador A1B 3X7, Canada

The aim of this study, known as the Stable Isotope Precipitation Sampling (SIPS) project, was to define a local meteoric water line (LMWL) for the island of Newfoundland using seasonal precipitation samples gathered during the 2021 calendar year. Meteoric water lines are linear relationships of the stable isotope values of hydrogen (H) and oxygen (O), derived empirically from isotopic measurements of precipitation in a defined region. Stable isotope values of H and O in meteoric waters vary with latitude, temperature, or any combination of these and other factors. This leads to variations in reported slope and intercept values for different geographic locations. While LMWLs have been calculated for the Corner Brook and the Bay d'Espoir regions, Newfoundland lacks a line that represents the whole island.

For this study, samples were collected through a community science network facilitated between Memorial University and the Newfoundland and Labrador English School District (NLESD). High school science students across Newfoundland's three primary regions (Eastern, Central, and Western) collected recent precipitation, recorded accompanying weather conditions, and applicable geographic information. The samples and field data were sent to Memorial University to arrange for isotopic analysis. While samples are still being received, to date, the H and O isotope data (n = 21) are well described by linear regression ($r^2 = 0.9864$) of $\delta^2H = 7.4919(\delta^{18}O) + 5.5348$.

The development of a unique slope and intercept for Newfoundland will allow for more accurate interpretations of water samples on the island, including those used for environmental, meteorological, or climatological studies. Unlike previous LMWLs from Corner Brook and Bay d'Espoir that address H-O isotopic variability in a specific area and/or over a long time period, the island-wide LMWL being reconstructed for this study allows for further evaluation of how factors such as latitude and temperature control variability on a wider spatial scale.

**Winner: Outstanding Student Presentation Award*

An overview of geochronological constraints on gold mineralization on the Island of Newfoundland, Canada, and their implications

Hamish Sandeman[1] and Ian Honsberger[2]

1. Geological Survey, Department of Industry, Energy and Technology, Government of Newfoundland and Labrador, St. John's, Newfoundland and Labrador A1B 4J6, Canada; 2. Geological Survey of Canada, Ottawa, Ontario K1A 0E8, Canada

Although gold exploration on the island of Newfoundland started in the early 1900s, it did not gain significant momentum until the 1977 discovery of gold along the Cape Ray Fault Zone. Exploration in the late 1980s and 1990s led to many new discoveries; however, until the recent exploration boom only a select few gold-related projects had been episodically explored. These were largely restricted to the known auriferous areas of western Newfoundland and on the Avalon Peninsula.

The emerging Newfoundland gold district contains numerous gold occurrences spatially associated with Paleozoic crustal-scale fault zones and their subsidiaries. These encompass a number of mined deposits and developed prospects having variably developed resources, and include: (1) Pine Cove Mine (3.63 Mt at 1.3–2.0 g/t for 154 132 oz Au mined); (2) Valentine Lake (~86 Mt at 1.72 g/t Au for ~4.7 Moz Au, measured and indicated); (3) Cape Ray (3.5 Mt at 3.15 g/t for 0.918 Moz Au; measured and indicated); (4) Reid Zone (9.75 Mt at 0.56 g/t for 176 000 oz Au, indicated); (5) Nugget Pond Mine (0.43 Mt at 10.5 g/t, 168 748 oz mined); (6) Hammerdown Mine (291 400 t at 15.83 g/t Au for143 000 oz Au mined); (7) Rattling Brook (5.46 Mt at 1.45 g/t for 255 000 oz; indicated); (8) Mosquito Hill (4.47 Mt at 0.53 g/t for 75 600 oz Au, indicated); (9) Thor (0.357Mt at 3.19 g/t for 36 600 oz Au, indicated); (10) Argyle (0.529 Mt at 1.99 g/t for 33 850 oz Au, probable) and; (11) Stog'er Tight (191 500 oz at 2.39 g/t for 14 740 oz Au, probable). In addition to these deposits there are numerous other, in some cases newly discovered, gold discoveries in the central Newfoundland Appalachians including, for example, those associated with the Queensway, Moosehead, Kingsway and Toogood exploration projects; extensive drilling is underway on these targets.

This contribution summarizes current geochronological constraints on gold mineralization on the Island, evaluates their type and dependability and discusses their implications with respect to our current knowledge of the timing, and broad kinematics, of the geotectonic controls on orogenesis and mineralization. Future research must emphasize the integration of diverse datasets, including regional and local geological observations, ore parageneses, fluid inclusion analyses, stable and radiogenic isotopic analyses, sulphide trace element analyses, geochronological studies, and ore-host rock lithogeochemical investigations to better constrain the origin of the individual gold mineralized zones.

Application of ore deposit models for critical mineral assessments: examples from Maine, USA

John F. Slack

U.S. Geological Survey (Emeritus), National Center, MS 954, Reston, Virginia 20192, USA

This talk highlights the use of descriptive and genetic models, together with grade-tonnage data, in assessing the potential for undiscovered deposits that contain critical minerals and metals. Emphasis is on areas of known deposits having high potential, including sediment-hosted Mn, magmatic Ni-Cu(-Co-PGE), and pegmatitic Li-Cs-Ta. Also briefly discussed is the potential for other deposit types such as ophiolite-hosted PGE, orogenic Sb(-Au), and skarn W, and black shale-hosted V.

Seeking hot and cold water in the Sandıklı graben, Turkey

Fethi Tayfun Turanli and Alison Leitch

Department of Earth Sciences, Memorial University of Newfoundland, St. John's, Newfoundland and Labrador A1B 3X5, Canada

The country formerly known as Turkey has extensive geothermal and agricultural resources. It lies within the Alpine–Himalayan orogenic belt, and its interior is characterized by rugged mountainous terrain interspersed with cultivated valleys. It's generally high elevation, recent volcanism, and high heat flow is attributed to delamination of the mantle lithosphere about 10 Ma, and subsequent upwelling of the asthenosphere and crustal anatexis.

The Sandikli graben, west central Anatolia, is one of the largest agricultural areas in the region and features 1500 wells tapping fresh water from shallow aquifers for domestic and agricultural use. It is also the site of the Hudai-Sandikli geothermal field, which provides heat to spas and greenhouses from 23 deeper thermal wells.

We analyzed data from geophysical resistivity surveys covering an area of 36 km × 10 km and extending to 1 km depth in the Sandikli graben, including the geothermal field. The aim was to characterize the subsurface structure throughout the graben, looking for hot and

cold aquifers and for fault structures which may be related to the upward transfer of geothermal waters. Low resistivity values are generally associated with aquifers, and large changes with faults.

We found resistivity near the surface followed topography and drainage patterns, and that known faults produced varied results. Low resistivity layers, signifying aquifers, were common, although limited in horizontal extent to 1 or 2 km. Raw data in the geothermal field showed large jumps which may be a characterizing feature. We discovered the limitations of the data set: without additional data (e.g., well temperatures, heat flow) we could not determine the temperature of the aquifers.

Regional shear zones and faults in the Baie d'Espoir Group, south central Newfoundland Appalachian orogen, Canada

Anne Westhues

Geological Survey, Department of Industry, Energy and Technology, Government of Newfoundland and Labrador, St. John's, Newfoundland and Labrador A1B 4J6, Canada

The Bay d'Espoir area straddles the boundary between rocks traditionally assigned to the Dunnage (Exploits Subzone) and Gander zones in Newfoundland (equivalent to the Tetagouche-Exploits Backarc Basin (BAB) and the Gander margin of the microcontinent Ganderia, respectively). The contact between the Baie d'Espoir Group (Exploits–BAB) and the Little Passage Gneiss (Gander margin) was originally mapped as a thrust in early studies of the St. Alban's map area. However, wide mylonite zones and mylonitic fabrics reported along coastal outcrops of Bay d'Espoir indicate a ductile shear zone with a sinistral sense of shear. In the St. Alban's map area, the contact is often expressed as a topographic depression and a change in lithology and metamorphic grade over a relatively short distance. Rocks of both the Baie d'Espoir Group and the Little Passage Gneiss are mylonitized for several hundred metres or more, which supports the interpretation of a ductile shear zone. This zone is fairly well traceable in a detailed airborne geophysical survey.

Another prominent magnetic lineament relating to a potentially regional fault zone is the stark contrast between Salmon River Dam (low) and St. Joseph's Cove (high) formations of the Baie d'Espoir Group. In the northwest of the St. Alban's map area, part of this sharp contrast coincides with the Salmon River Dam Fault. However, this feature continues to the northeast for more than 50 km and connects with a fault in the Hungry Cove Pond map area, representing the contact between the North Steady Pond and St. Joseph's Cove formations of the Baie d'Espoir Group. Along this fault, small bodies of sheared serpentinizied peridotite are exposed. The lithological and tectonic relationships along this magnetic lineament require further examination, especially in the Twillick Brook map area, but it potentially represents a large-scale structure within in the Baie d'Espoir Group.

Jurassic palynoevents in the circum-Arctic region

Jonathan Bujak[1*], Manuel Bringué[2], Anna A. Goryacheva[3,4], Natalia K. Lebedeva[3], Ekaterina B. Pestchevitskaya[3], James B. Riding[5] and Morten Smelror[6]

1. Bujak Research International, Burbage Lodge, 200 Queens Promenade, Blackpool, Lancashire FY2 9JS, UK
2. Geological Survey of Canada, 3303–3333 Street NW, Calgary, Alberta T2L 2A7, Canada
3. Trofimuk Institute of Petroleum Geology and Geophysics, Siberian Branch of the Russian Academy of Sciences, pr. Akademika Koptyuga 3, 630090 Novosibirsk, Russia
4. Novosibirsk State University, ul. Pirogova 2, 630090 Novosibirsk, Russia
5. British Geological Survey, Keyworth, Nottingham NG12 5GG, UK
6. Geological Survey of Norway, Leiv Eirikssons vei 39, 7040 Trondheim, Norway
*corresponding author: jonathanbujak@outlook.com

Date received:10 December 2021 ¶ Date accepted 25 February 2022

ABSTRACT

Successions of Jurassic strata located in the Arctic region normally yield rich assemblages of terrestrially-derived and marine palynomorphs, reflecting relatively warm air and sea-surface temperatures. The land plant floras were prone to the development of local communities and regional provincialism, whereas the marine biotas thrived across extensive open marine areas with high productivity, resulting in the rapid evolution of dinoflagellate cysts (dinocysts) following their earliest fossil record in the Triassic. Dinocysts exhibit low taxonomic richness and provide low biostratigraphic resolution throughout the Lower Jurassic sections. By contrast, they are diverse in Middle and Upper Jurassic strata where they provide excellent biostratigraphic markers for correlating and dating both surface and subsurface sections. Over twenty formal and informal biozonations based on the first and last occurrences of dinocysts have been erected in Alaska, Arctic Canada, the Barents Sea region, Greenland and northern Russia, many of which are correlated with macrofossils, including ammonites, that occur in the same sections. This paper presents a compilation of 214 Jurassic palynostratigraphic events (118 first occurrences and 96 last occurrences) that have regional chronostratigraphic value in the Circum-Arctic, based on their published records. Each event is correlated with the base of a chronostratigraphical unit (including formal stages and sub-Boreal ammonite zones), or as an estimated percentage above the base of the chronostratigraphical unit relative to the entire unit. The relationships of each event to stages and key fossil zonal schemes is shown on chronostratigraphic plots using the 2020 version of TimeScale Creator®.

RÉSUMÉ

Les successions de strates jurassiques dans la région de l'Arctique recèlent normalement de riches assemblages de palynomorphes d'origine terrestre et marins reflétant les températures relativement chaudes de l'air et à la surface de la mer. Les flores de plantes terrestres étaient susceptibles de favoriser l'épanouissement de communautés locales et d'un provincialisme régional, alors que les biotes marins se développaient sur de vastes secteurs marins ouverts à un rythme de productivité élevé, ce qui a entraîné l'évolution rapide de kystes de dinoflagellés (dinokystes) d'après leur plus récents enregistrements fossiles au cours du Trias. Les dinokystes affichent une faible richesse taxonomique et produisent une faible résolution biostratigraphique dans toutes les sections du Jurassique inférieur. Par contre, ils se diversifient dans les strates du Jurassique moyen et supérieur, où ils représentent d'excellents repères biostratigraphiques pour la corrélation et la datation de sections de surface et de subsurface. Plus d'une vingtaine de biozonations officielles et officieuses basées sur les premières et dernières manifestations de dinokystes ont été établies en Alaska, dans l'Arctique canadien, dans la région de la mer de Barents, au Groenland et dans le nord de la Russie, lesquelles sont dans de nombreux cas corrélées avec des macrofossiles, notamment des ammonites, présents dans les mêmes sections. Le présent article présente une compilation de 214 phénomènes palynostratigraphiques du Jurassique (118 premières manifestations et 96 dernières manifestations) ayant une valeur chronostratigraphique régionale dans la région circumarctique, d'après les documents pertinents publiés. Chaque phénomène est corrélé avec la base d'une unité chronostratigraphique (notamment les stades et les zones d'ammonites subboréales officielles), ou sous forme d'un pourcentage estimatif au-dessus de la base de l'unité chronostratigraphique par rapport à l'ensemble de l'unité. Les liens entre chaque phénomène et les stades et principaux mécanismes zonaux fossiles sont illustrés dans les schémas chronostratigrapiques au moyen de la version de 2020 de TimeScale Creator®.

[*Traduit par la redaction*]

doi:10.4138/atlgeo.2022.003

INTRODUCTION

This article is a contribution to the Circum-Arctic Palynological Events (CAPE) project, providing a scheme of selected bioevents for the Jurassic Period. The Jurassic extended from 201.36 to 143.10 Ma according to the timescale of Gradstein *et al.* (2021). The Jurassic Period is divided into three epochs, Early Jurassic, Middle Jurassic (with a base at 174.70 Ma) and Late Jurassic (with a base at 161.53 Ma).

The present Jurassic compilation will be added to others from the CAPE series of articles in *Atlantic Geology* (now *Atantic Geoscience*), which will contribute ultimately (when all articles in the series are complete) to the "CAPE datapack" in TimeScale Creator® (TSC; https://timescalecreator.org/index/index.php) and thus can be used with other data in TSC to make plots such as that shown in Figures 1–9. The latter diagrams include age calibrations in millions of years ago (Ma) according to the 2020 version of TSC and in Gradstein *et al.* (2021). Similar compilations for the Early, Middle and Late Jurassic are provided in the Supplementary Data (*see URL links after References*). The main Jurassic locations discussed in this paper are shown in Figure 10.

The events compiled herein include last occurrences (LOs), first occurrences (FOs), and some abundance events. Their relationship to other fossil zonal schemes is shown in Figures 1–9. Where possible, each event is correlated with the base of a chronostratigraphic unit, for example a Sub-Boreal ammonite zone or a formal stage. If the event is not equivalent to the base of such a unit, then an estimation is given as a percentage above the base of the chronostratigraphic unit relative to the entire unit. Details of how a biostratigraphic datapack is constructed in TSC from such information are given in Bringué *et al.* (in press).

PALYNOSTRATIGRAPHY

Background

The transition from the Triassic to the Jurassic at 201.36 Ma was followed over time by major changes in the continental configuration, seaway connections and climate. Pangaea fragmented and North America drifted away from Africa, the North Atlantic Ocean opened, and major tectonic changes led to transgressions over extensive shelf and land areas in the circum-Arctic region (Blakey 2021). These profound changes brought about the development of various phytogeographic marine and terrestrial provinces, with diachronous originations and extinctions, and the evolution of endemic taxa. During the Jurassic, significant radiations of marine taxa occurred, principally dinoflagellate cysts (dinocysts) which became more diverse and abundant. As a consequence, biostratigraphic ranges and biozonations established in the formal or proposed stage type areas in the Tethyan and Sub-Boreal realms may be based on species not found in the Boreal/Arctic Realm or defined by species that may have diachronous stratigraphic ranges within different biogeographic provinces. Equally, palynostratigraphic zonations defined in the Boreal Realm may not be readily applicable farther south.

There have been several Jurassic palynostratigraphic zonations established which are based on records from different areas in the Arctic region. Several of them are calibrated to established Boreal and Sub-Boreal ammonite zonations, but some discrepancies and uncertaincies still exist with respect to correlation to the latest Geological Time Scale (Gradstein *et al.* 2021). In the present study, the first and last occurrences of the listed species calibrated to the 2020 Geological Time Scale are shown in Figures 1–9.

Jurassic dinocysts of the Canadian Arctic and Alaska

In the Canadian Arctic, the first biostratigraphic zonation for the Jurassic based on dinocysts was from the Sverdrup Basin (Johnson and Hills 1973). This landmark study comprised four range-zones, four range-subzones, one concurrent range-zone and one peak-zone, and was established on three sections of the Savik and Awingak formations on Axel Heiberg, Bjarnason and Ellesmere islands (Fig. 10). In general, these sections were characterized by poor preservation and low species richness. This material was also described by Johnson (1974). Subsequently, Pocock (1976) presented a preliminary zonation for the uppermost Jurassic to Lower Cretaceous of the Canadian Arctic based on material from the Awingak and Deer Bay formations on Amund Ringnes Island (Fig. 10), and Tan and Hills (1978) documented the dinocyst succession of the Ringnes Formation (Oxfordian–Kimmeridgian), calibrated with ammonite faunas.

A more comprehensive dinocyst zonation of the Jurassic and Lower Cretaceous successions in the Sverdrup Basin was defined by Davies (1983), who erected 17 Oppel zones. Twelve of these Oppel-zones (A–L) cover the Jurassic part of the succession. Comparisons of the zonations of Johnson and Hills (1973) and Davies (1983) were made by Davies (1983) and Smelror and Below (1992). The latest contribution on the dinocyst zonation of the Canadian Arctic was by Ingrams *et al.* (2021). These authors studied the Upper Jurassic and Lower Cretaceous (Oxfordian–lower Valanginian) succession of the Rollrock section, northern Ellesmere Island, a largely complete and expanded section for which they established seven dinocyst biozones. Their zones H to L/M cover the Oxfordian to Tithonian interval and have substantial calibration to macrofossil biostratigraphy.

Several other publications have recorded Jurassic dinocysts from Arctic Canada, but no additional formal zonations have been proposed. These works include Brideaux (1975, 1976), Brideaux and Myhr (1976), van Helden (1977), Pocock (1980), Poulton *et al.* (1982), Poulton (1989),and Pimpirev and Pavlishina (2005a, b)..

By contrast with the Canadian Arctic, the literature on Jurassic dinocysts from Alaska is relatively sparse. The most detailed publication, by Wiggins (1973), is a comprehensive systematic treatment of the family Pareodiniaceae from the Middle Jurassic to Early Cretaceous of northern and south-

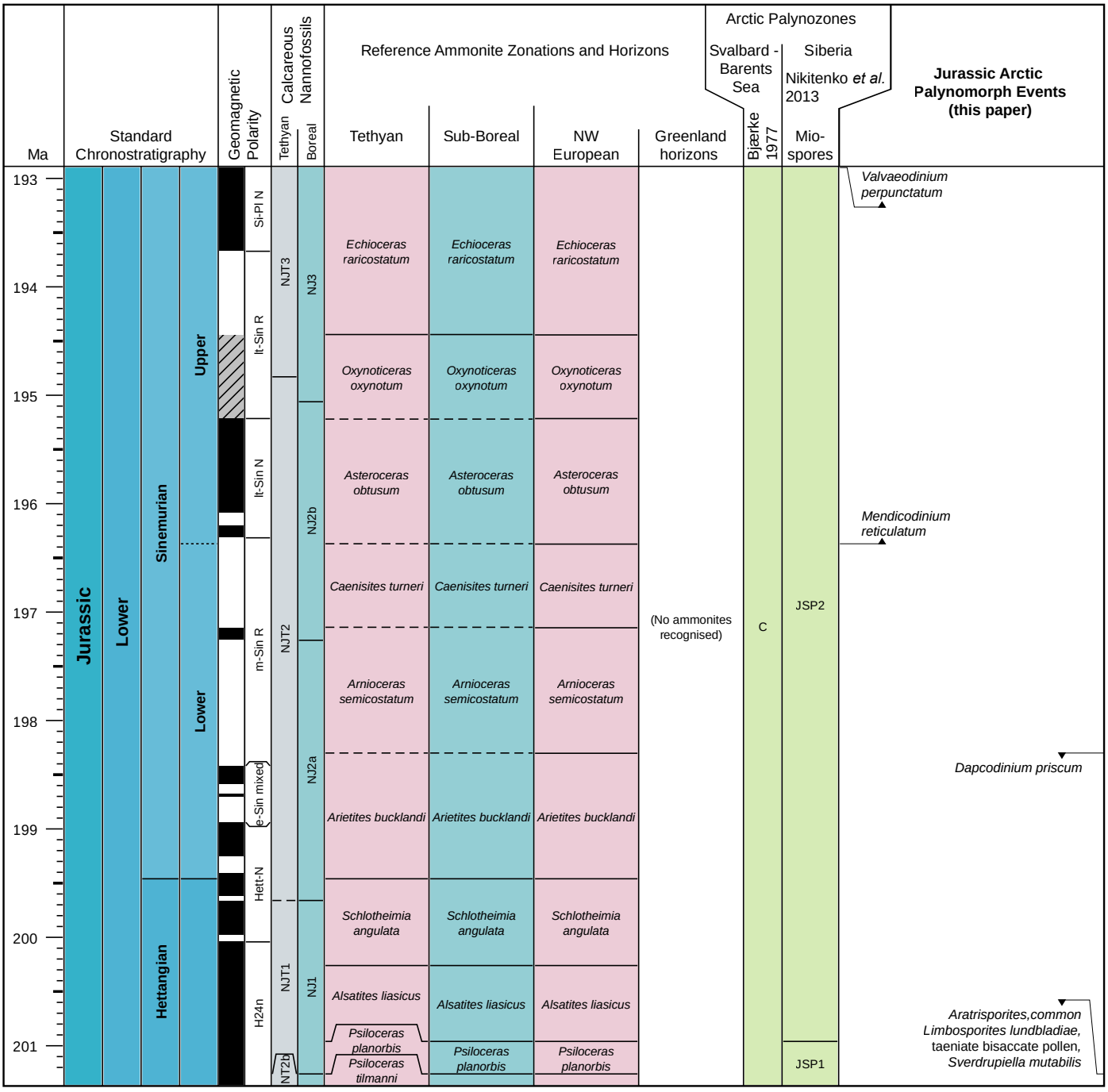

Figure 1. Stratigraphic chart for the Hettangian–Sinemurian showing palynomorph bioevents compiled in this paper, in the context of geomagnetic polarity, standard calcareous nannofossil zones, reference ammonite zonations and horizons and published Arctic palynomorph zonations. The chart was generated using TimeScale Creator®. Standard chronostratigraphy and reference data from Gradstein *et al.* (2021).

ern Alaska. Albert *et al.* (1986) made a later taxonomic contribution, but other records in the public domain are abstracts (e.g., Wharton 1988), doctoral dissertations (e.g., Albert 1988), and unpublished reports (e.g., Bjærke 1993; Witmer *et al.* 1981).

Jurassic dinocysts of northern Russia

In Russia, a Boreal Lower–Middle Jurassic dinocyst biostratigraphy was published by Ilyina *et al.* (1994) and subsequently presented in Zakharov *et al.* (1997). This dinocyst zonation was later refined by Riding *et al.* (1999) and Shurygin *et al.* (2000), and the ages of some of the biostratigraphic

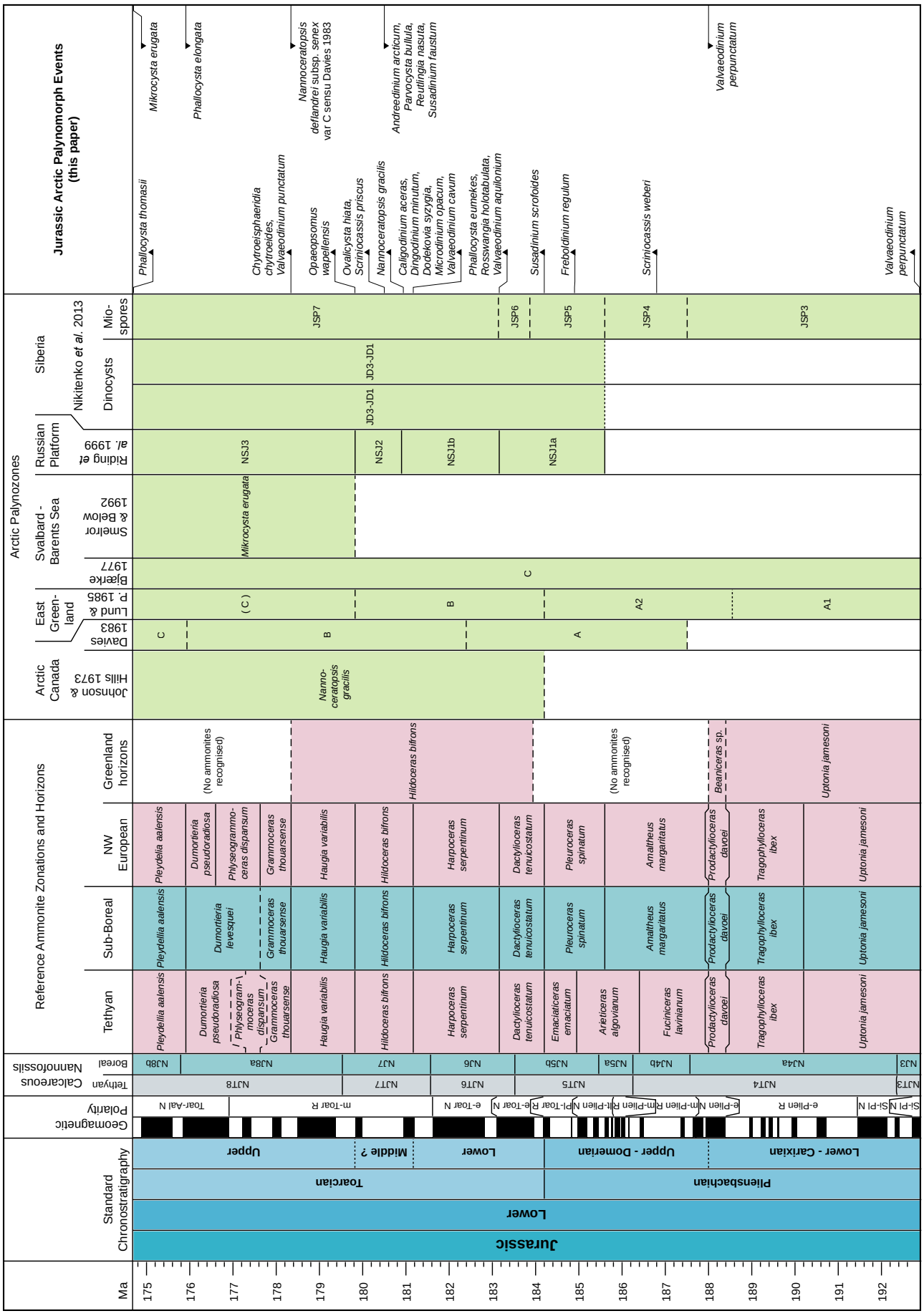

Figure 2. Stratigraphic chart for the Pliensbachian–Toarcian; details as for Figure 1. Lund & P. 1985 - Lund and Pedersen (1985).

units have been revised in light of new data on index species from sections in northern East Siberia (Nikitenko *et al.* 2011; Goryacheva 2017).

The uppermost Pliensbachian to upper Toarcian of northern East Siberia was studied by Riding *et al.* (1999), who subdivided the interval into three dinocyst biozones, of which one is subdivided into two interval subbiozones. Later Ilyina *et al.* (2005) presented a Middle and Upper Jurassic dinocyst zonation comprising 11 interval zones for the Boreal zonal standard scheme in Zakharov *et al.* (1997), with new data on the dinocyst stratigraphic distributions for the Callovian to Volgian strata of West Siberia. The material for these studies was obtained from a study of the Tyumenskaya superdeep well (SDW-6; Ilyina *et al.* 2005). This zonation was correlated to time-equivalent Callovian to Volgian dino cyst zonations of West Siberia, the Russian Platform and northwestern Europe by Ilyina *et al.* (2005).

Riding *et al.* (1999) also included a comprehensive record from the Jurassic and lowermost Cretaceous of the Russian Platform. In parts of the Jurassic, the dinocyst assemblages from northeast Siberia exhibit significant provincial differences from those of the Pechora Basin (Meledina *et al.* 1998; Riding *et al.* 1999); consequently, the assemblages from, and the zonation of, the Russian Platform are not further discussed herein. References to additional publications on Jurassic dinocysts from Siberia can be found in Riding *et al.* (1999), Ilyina *et al.* (2005) and Riding (2019).

Pestchevitskaya *et al.* (2011) identified a series of Volgian to Berriasian palynostratigraphic events based on a substantial database. The data comprises material from Nordvik on the Laptev Sea coast (Nikitenko *et al.* 2008; Nikitenko *et al.* 2011); the Severo-Vologochanskaya-18 well at the mouth of the Yenisei River and the Zapadno-Purpeiskaya-710 well in northwestern Siberia (Beisel *et al.* 2002); the River Yatriya in the Subarctic Urals (Lebedeva and Nikitenko 1998, 1999); and Kashpir located in the middle reaches of the River Volga (Riding *et al.* 1999; Harding *et al.* 2011). Of particular relevance herein are the data from the several outcrops on the Nordvik Peninsula (Nikitenko *et al.* 2008; Nikitenko *et al.* 2011; Pestchevitskaya *et al.* 2011). Pestchevitskaya *et al.* (2011) compared their results to existing palynological data from America, Antarctica, Australia and Europe using first and last appearances of selected key species and evolutionary trends of dinocyst floras. They defined four correlative horizons in the Volgian and Berriasian, thus providing interregional correlation of the dinocyst successions.

In an integrated study of the Jurassic and Cretaceous of the Anabar Bay area on the Laptev Sea coast, Nikitenko *et al.* (2013) provided a comprehensive review of the Jurassic and Cretaceous dinocyst zones of pan-northern Siberia correlated to the Boreal ammonite standard and to coeval belemnite, bivalve, ostracod and spore–pollen (miospore) zones. Due to lack of data, these authors defined no dinocyst zones for the Hettangian to Pliensbachian and Aalenian to Bathonian intervals. Later, Nikitenko *et al.* (2017, 2018a) made comprehensive studies of the Jurassic–Cretaceous paralic successions of the New Siberian Islands based on dinocysts, foraminifera, ostracods, and miospores.

Nikitenko *et al.* (2015a, b) described the dinocyst biostratigraphy and paleoecology of the upper Oxfordian to middle Volgian interval of the Paksa section in Nordvik. These studies provided comprehensive information on the Upper Jurassic marine microfloras of the Laptev Sea region compared to previous works such as Ilyina (1986, 1988). Nikitenko *et al.* (2018b) also studied rich dinocyst assemblages from the Volgian–Hauterivian of the River Olenek region of northern Siberia. The investigations of Nikitenko *et al.* (2015a, b; 2018b) included detailed biozonations based on the dinocyst assemblages, specifically FOs and LOs of key geographically widespread species that are also recorded from North America, northwest Europe and the Russian Platform. The dinocyst zones were all calibrated against biostratigraphic scales based on ammonites and foraminifera.

Jurassic dinocysts of the Barents Sea and Svalbard

In the Barents Sea area and Svalbard, dinocyst zonations covering the whole or parts of the Jurassic include Bjærke (1977), Smelror and Below (1992), Dalseg *et al.* (2016) and Rismyhr *et al.* (2019). Bjærke (1977) introduced an informal palynomorph zonation scheme comprising associations A–F for the uppermost Triassic (Rhaetian) to Lower Cretaceous of Kong Karls Land. Smelror and Below (1992) proposed a dinocyst zonation for the Toarcian to lower Oxfordian of the Barents Sea region. This zonation comprises seven dinocyst zones and is based on the stratigraphic distribution of ninety Toarcian to early Oxfordian dinocyst species from outcrops from Svalbard and Franz Josef Land, as well as from boreholes in the Nordkapp and Hammerfest basins. Dalseg *et al.* (2016) introduced a scheme of informal dinocyst zones for the Upper Jurassic and Lower Cretaceous of central Spitsbergen. Rismyhr *et al.* (2019), a major work on the palynology and sedimentology of the Late Triassic (Carnian) to Middle Jurassic (Callovian) of west-central Spitsbergen, established ten composite assemblage zones based on palynomorphs, six of which are based on dinocysts (Rismyhr *et al.* 2019, fig. 3).

In addition to the works cited above, several other studies treat the dinocyst biostratigraphy of the Barents Sea region, most of which have ranges calibrated to ammonite zones, but lack formal palynological zonation schemes. These include Bjærke *et al.* (1976), Thusu (1978), Bjærke and Dypvik (1977), Bjærke (1980a, b), Dypvik *et al.* (1985), Smelror (1988a, 1991, 1994), Wierzbowski and Århus (1990), Smelror *et al.* (1998, 2018), Wierzbowski *et al.* (2002), Smelror and Dypvik (2005), Koevoets *et al.* (2018), Olaussen *et al.* (2018) and Turner *et al.* (2019).

Jurassic dinocysts of Greenland

Jurassic marine faunas (e.g., ammonites and bivalves) and microfloras of Greenland are more similar in overall character to Boreal faunas, than to, for example, those of Sub-Boreal northern Europe. Several comprehensive palynological

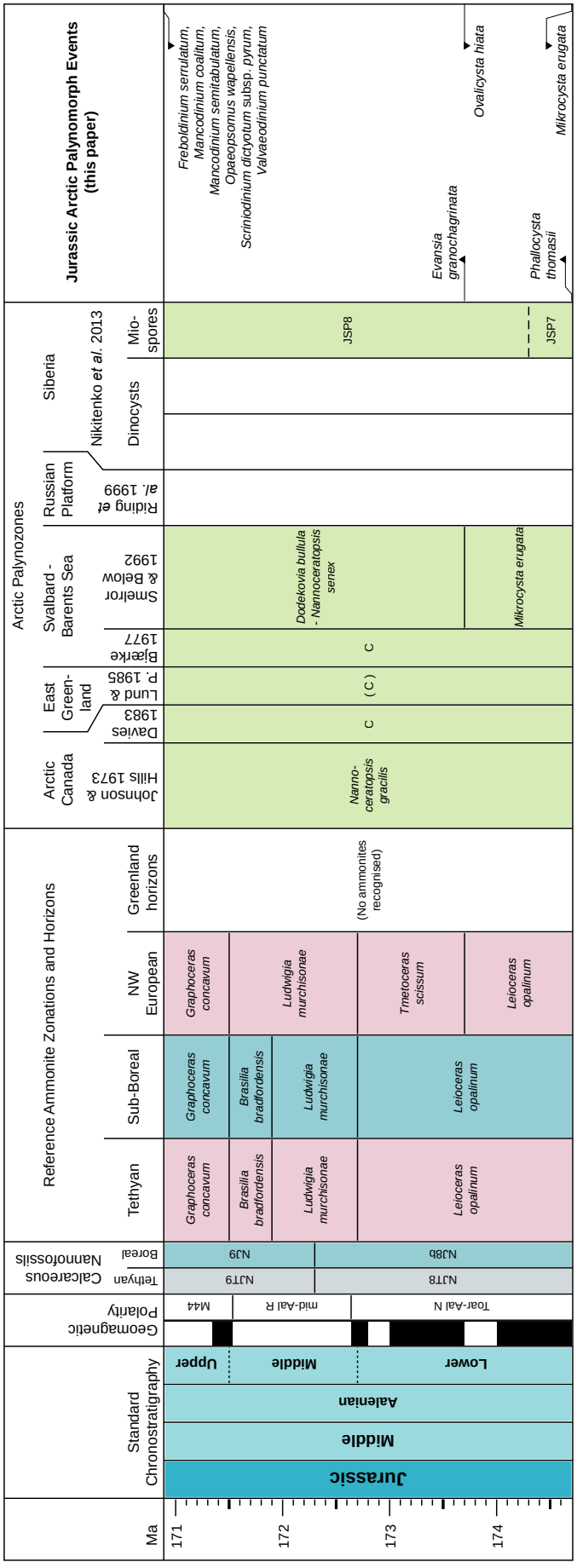

Figure 3. Stratigraphic chart for the Aalenian; details as for Figure 1. Lund & P. 1985 - Lund and Pedersen (1985).

contributions from Greenland have been published (e.g., Sarjeant 1972; Fensome 1979), although not all of them include zonation schemes. Studies with biozonations include the unpublished doctoral thesis by Piasecki (1980) on Milne Land and his subsequent publication (Piasecki 1996). Other publications on Jameson Land include those by Poulsen (1985), Smelror (1988b) and Milner and Piasecki (1996). Smelror (1988b) defined six dinocyst zones and five subzones for the upper Bathonian to lower Oxfordian successions of East Greenland. The proposed dinocyst zones were all correlated to the ammonite zonation for this region (Callomon and Birkelund 1980). Contributions on Jurassic dinocysts from northeast Greenland include Piasecki *et al.* (2004a) on Hold with Hope, Piasecki and Stemmerik (2004) on Hochstetter Foreland, and Piasecki *et al.* (2004b) on Store Koldewey. These papers document the dinocyst distributions calibrated with relatively few Bathonian to Kimmeridgian ammonite records, but lack a unifying palynological zonation scheme. Other relevant papers on the Jurassic dinocysts of Greenland include Pocock and Sarjeant (1972), Håkansson *et al.* (1981), Lund and Pedersen (1985), Poulsen (1991), Piasecki (2001), Koppelhus and Dam (2003), Koppelhus and Hansen (2003), Kelly *et al.* (2015).

Jurassic miospores of northern Russia

Whereas dinocysts have proved to be reliable biostratigraphic markers for the marine Middle and Upper Jurassic throughout the Circum-Arctic, correlations and relative age assessments based on miospores are frequently used for Lower and Middle Jurassic non-marine strata. The Boreal standard presented by Zakharov *et al.* (1997) incorporated the Lower and Middle Jurassic (excluding Callovian) miospore palynostratigraphic scheme for Siberia published by Ilyina (1985). This Boreal standard does not contain data on terrestrially derived palynomorphs for the Upper Jurassic (Zakharov *et al.* 1997). Subsequently, a palynozonation for the Lower and Middle Jurassic (excluding the Callovian) for Western Siberia was published by Gurari and Mogucheva (2004). A succession of palynostratigraphic units for the uppermost Middle Jurassic (Callovian) and Upper Jurassic of northeastern Siberia based on the studies of key sections of Jurassic marine sediments was established by Shurygin *et al.* (2000). The study areas for that major work were the coast of Anabar Bay, the banks of the River Anabar, Bol'shoi Begichev Island, the lower reaches of the River Lena, and the Nordvik Peninsula.

Miospore palynostratigraphic units are well defined for the Callovian–Oxfordian and middle–upper Volgian, whereas assemblages from the Kimmeridgian, lower Volgian, and part of the middle Volgian in northeastern Siberia have been barely studied. The Callovian to Volgian miospore units have been calibrated against local ammonite faunas. The proposed zonation by Ilyina (1985, 1988) and Shurygin *et al.* (2000) covers a virtually continuous succession of six palynostratigraphic units.

In their comprehensive review of the Jurassic and Cretaceous stratigraphy of the Anabar Bay area on the Laptev Sea coast, Nikitenko *et al.* (2013) presented a review of the Jurassic and Cretaceous miospore zones of Arctic Siberia correlated to the Boreal ammonite standard and to coeval belemnite, bivalve, ostracod and dinocyst zones. Twenty-one zones were defined covering the Early and Middle Jurassic, and five zones were established for the Late Jurassic. No mio spore zones were erected for the middle Oxfordian and Kimmeridgian to middle Volgian (Nikitenko *et al.* 2013).

Further investigations have contributed to the miospore zonation of the Jurassic of northern Russia. Four miospore zones were proposed for the upper Oxfordian to middle Volgian of Arctic Siberia based on analysis of terrestrially derived palynomorphs from the Nordvik (Paksa) section by Nikitenko *et al.* (2015a, b). Two miospore zones were later defined for the Volgian to lowermost Berriasian of the Olenek River section (Nikitenko *et al.* 2018b). The bioevents used for the definition of the boundaries of Siberian miospore zones are mainly applicable to local to sub-regional correlations.

Dzyuba *et al.* (2018) proposed the first formal biostratigraphy for the upper Volgian to lower Ryazanian of the Northern Urals, defining two miospore zones. In addition to regional correlations, the key taxa from the upper Volgian interval enabled these authors to make a biostratigraphic comparison with coeval successions of terrestrially derived palynomorphs from Australia.

Jurassic miospores of the Arctic excluding Russia

No miospore zonations have been established for the Jurassic of the Barents Sea. Lund and Pedersen (1985), Koppelhus and Dam (2003) and Koppelhus and Hansen (2003) used pollen, spores and dinocysts, to subdivide the Lower and Middle Jurassic successions of northeast Greenland. In the most detailed of these studies, Koppelhus and Dam (2003) identified four assemblage zones (AZ1–4) for the Pliensbachian of Jameson Land.

There are several records, including some relatively comprehensive accounts, of Jurassic miospores from the Canadian Arctic (e.g., Davies 1983 and references therein). Detailed descriptions of various assemblages have been reported, but formal zonations are lacking. Galloway *et al.* (2013) applied a multivariate statistical approach to long-ranging miospore taxa from the Aalenian to the Albian, and defined four palynomorph assemblages in the Hoodoo Dome H-37 well drilled on southern Ellef Ringnes Island, near the centre of the Sverdrup Basin. They also characterized their as-semblages in terms of Middle Jurassic to Early Cretaceous pan-hemispherical paleoclimate events.

ARCTIC JURASSIC PALYNOEVENTS

A summary of the following events in spreadsheet format is provided as Appendix B. All taxon names with authors are

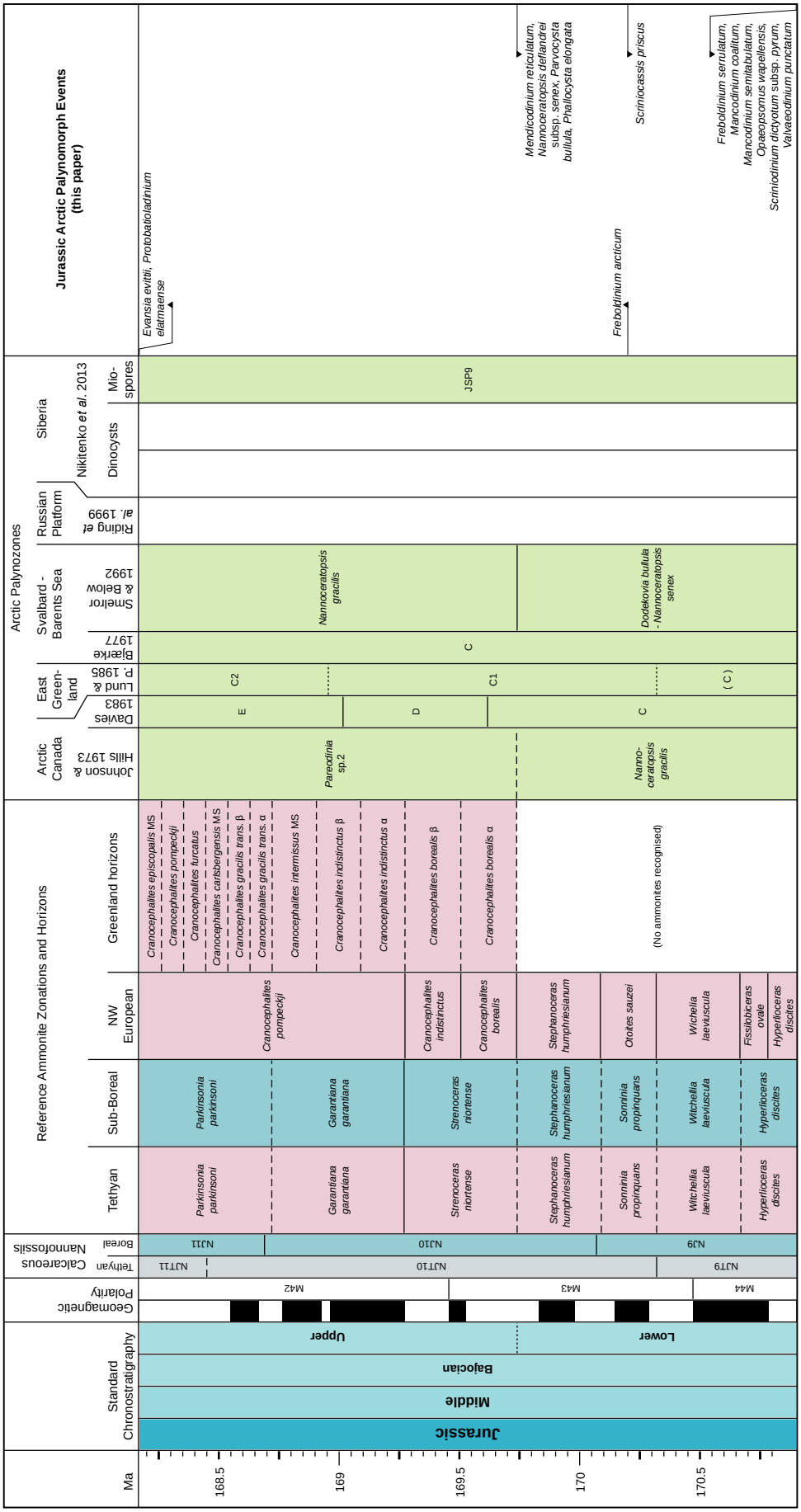

Figure 4. Stratigraphic chart for the Bajocian; details as for Figure 1. Lund & P. 1985 - Lund and Pedersen (1985).

listed in Appendix A. Events that occur at the Triassic/Jurassic boundary were defined in Mangerud *et al.* (2021) and are grouped below in the LO of *Sverdrupiella mutabilis*. Appendix C includes the Beechey Point State 1 reference well plus three other reference wells reproduced from Mangerud *et al.* (2021): Fireweed 1 (offshore northern Alaska), Klondike OCS-Y-1482 (Chukchi Sea) and Romulus C-67 (Sverdrup Basin) as they include the Triassic/Jurassic boundary. All palynoevents are shown in Figures 1–9.

LO of *Sverdrupiella mutabilis* and other taxa listed below

Sverdrupiella mutabilis has a longer stratigraphic range than other species of *Sverdrupiella*. The LO is based on its occurrence relative to miospore LOs in the Fireweed 1 well, offshore northern Alaska, the Klondike OCS-Y-1482 well in the Chukchi Sea and the Romulus C-67 well in the Sverdrup Basin, plus outcrops and wells documented by Mangerud *et al.* (2021).

The LO of the spore genus *Aratrisporites* occurs at the Triassic/Jurassic transition, within the Heiberg Formation, in the Sverdrup Basin (Felix 1975; Suneby and Hills 1988) Vigran *et al.* (2014) also listed several species of *Aratrisporites* with LOs at the top of the Triassic. Paterson and Mangerud (2015) recorded several *Aratrisporites* species in their uppermost samples from the Svenskøya Formation on Hopen, including *Aratrisporites scabratus, Aratrisporites laevigatus*, *Aratrisporites macrocavatus* and *Aratrisporites tenuispinosus*. Mangerud *et al.* (2021) commented that no records of *Aratrisporites* occur younger than Triassic in the circum-Arctic region.

Suneby and Hills (1988) reported the LO of common *Limbosporites lundbladiae* at the top of their *Limbosporites lundbladiae–Ricciisporites tuberculatus* Zone and tentatively suggested its age as latest Norian or early Rhaetian. Vigran *et al.* (2014) reported the LO of common *Limbosporites lundbladiae* as an intra-Rhaetian event. Paterson and Mangerud (2015) defined their *Limbosporites lundbladiae–Quadraeculina anellaeformis* Assemblage from the Svenskøya Formation and recorded common *Limbosporites lundbladiae* in the uppermost part of this unit. Since *Limbosporites lundbladiae* has not been reported from the Jurassic, this LO is inferred to coincide with the base of the Jurassic.

The LO of taeniate bisaccate pollen has been reported from multiple localities in the Arctic. Vigran *et al.* (2014) used the LO of taeniate bisaccate pollen as a top Triassic event. Suneby and Hills (1988) stated that *Lunatisporites rhaeticus* (as *Taeniasporites rhaeticus*) extends to the top of the Triassic in the Sverdrup Basin. *Lunatisporites rhaeticus* was also recorded by Felix (1975) and Paterson and Mangerud (2015), the latter authors recording it as a single specimen in their uppermost sample from the Norian–Rhaetian Svenskøya Formation on Hopen.

The LOs of *Sverdrupiella mutabilis, Aratrisporites*, common *Limbosporites lundbladiae,* and taeniate bisaccate pollen are taken as the base of the ammonite *Psiloceras planorbis* Zone (i.e., at the base of the Hettangian).

LO of *Dapcodinium priscum*

The LO of *Dapcodinium priscum* occurs within the ammonite *Arnioceras semicostatum* Zone in the Barents Sea and on Svalbard (Feist-Burkhardt 1994, based on Below 1987a, 1990).

The LO of *Dapcodinium priscum* is taken as the base of the ammonite *Arnioceras semicostatum* Zone (i.e., earliest Sinemurian).

FO of *Mendicodinium reticulatum*

The FO of *Mendicodinium reticulatum* occurs at the base of beds with *Mendicodinium* spp. in the Middle-Nakynskaya 360 Borehole, northeastern Siberia, at the base of the ammonite *Asteroceras obtusum* Zone and the foraminiferal *Trochammina inusitata–Turritellella volubilis* Zone (Nikitenko 2009; Goryacheva and Nikitenko 2016).

The FO of *Mendicodinium reticulatum* is taken as the base of the ammonite *Asteroceras obtusum* Zone (i.e., the base of the upper Sinemurian).

FO of *Valvaeodinium perpunctatum*

The FO of *Valvaeodinium perpunctatum* occurs at the base of the early Pliensbachian as extrapolated from a compilation of Pliensbachian to early Toarcian dinocysts from the Tethyan and Boreal realms by Bucefalo Palliani and Riding (2003). These authors concluded that *Valvaeodinium perpunctatum* is confined to the early Pliensbachian in the Boreal Realm.

The FO of *Valvaeodinium perpunctatum* is taken as the base of the ammonite *Uptonia jamesoni* Zone (i.e., the base of the early Pliensbachian).

LO of *Valvaeodinium perpunctatum*

The LO of *Valvaeodinium perpunctatum* occurs at the base of the late Pliensbachian as extrapolated from a compilation of Pliensbachian to early Toarcian dinocysts from the Tethyan and Boreal realms by Bucefalo Palliani and Riding (2003), who concluded that *Valvaeodinium perpunctatum* is confined to the early Pliensbachian in the Boreal Realm.

The LO of *Valvaeodinium perpunctatum* is taken as the base of the ammonite *Almaltheus margaritatus* Zone (i.e., the base of the late Pliensbachian).

FO of *Scriniocassis weberi*

The FO of *Scriniocassis weberi* occurs at the base of the Toarcian in the Barents Sea area and on Svalbard (Feist-Burkhardt 1994, based on data from Below 1987a, b, 1990). However, this range base is of late Pliensbachian (ammonite *Amaltheus margaritatus* Zone) age throughout the Sub-Boreal and Boreal relams according to, for example,

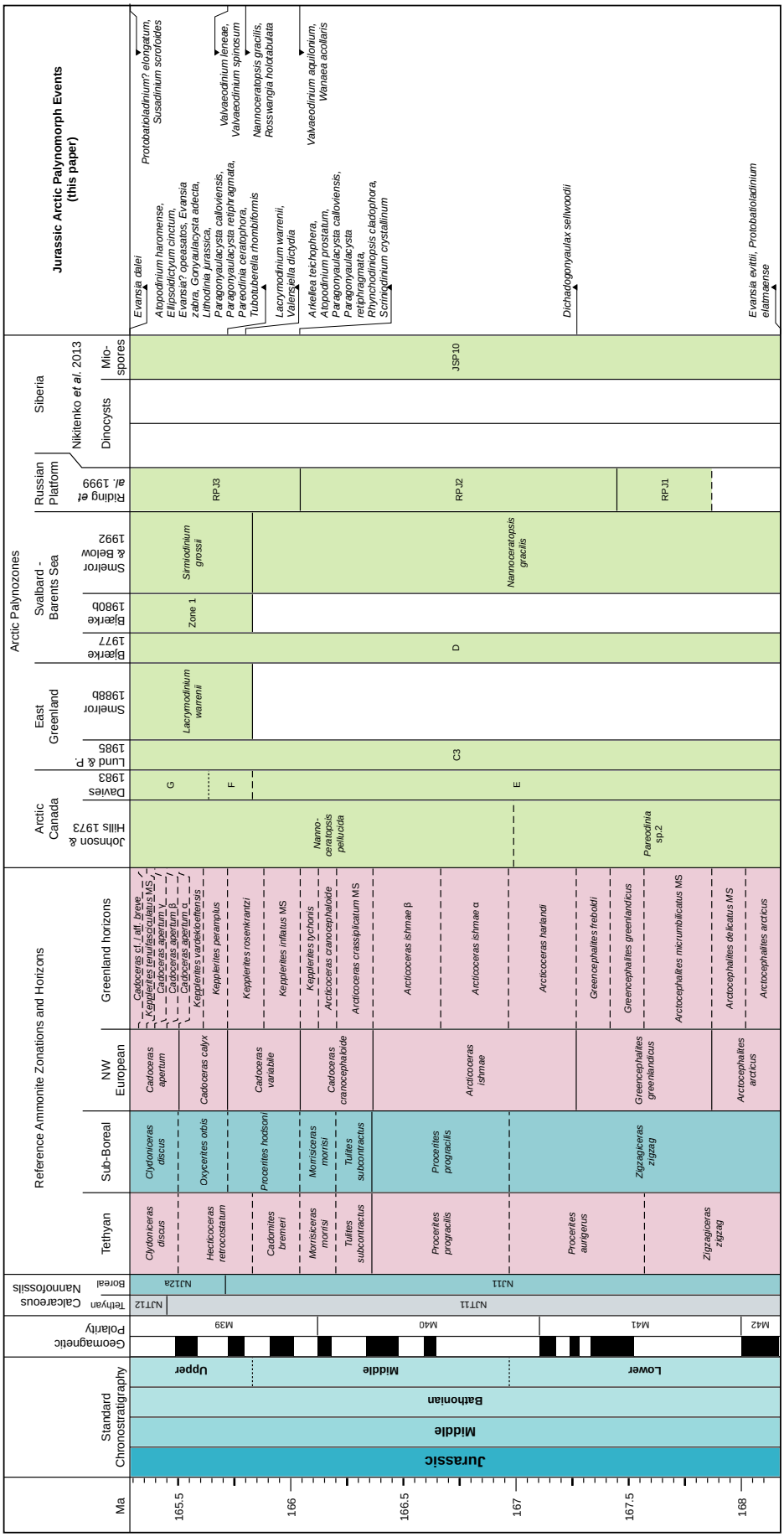

Figure 5. Stratigraphic chart for the Bathonian; details as for Figure 1. Lund & P. 1985 - Lund and Pedersen (1985).

Morgenroth (1970) and Riding and Thomas (1992).

The FO of *Scriniocassis weberi* is taken as 50% up from the base of the ammonite *Amaltheus margaritatus* Zone (i.e., late Pliensbachian).

FO of *Freboldinium regulum*

The FO of *Freboldinium regulum* occurs in the latest Pliensbachian ammonite *Pleuroceras spinatum* Zone on Svalbard (Feist-Burkhardt 1994, based on data from Below 1987a, b, 1990).

The FO of *Freboldinium regulum* is taken as 50% up from the base of the ammonite *Pleuroceras spinatum* Zone (i.e., latest Pliensbachian).

FO of *Susadinium scrofoides*

The FO of *Susadinium scrofoides* occurs at the base of dinocyst Oppel Zone B of Davies (1983), which was assigned to the early Toarcian based on the presence of the marker ammonites *Dactylioceras commune, Peronoceras spinatum*, *Peronoceras polare* and *Pseudoleoceras* aff. *compactile* in the Sverdrup Basin (Davies 1983). The FO of *Mancodinium semitabulatum* also occurs within the Pliensbachian–Toarcian dinocyst *Nannoceratopsis deflandrei* Zone and the Pliensbachian–Toarcian dinocyst *Nannoceratopsis deflandrei* subsp. *anabarensis* Subzone defined in northern East Siberia by Riding *et al.* (1999), equivalent to the base of the ammonite *Dactylioceras tenuicostatum* Zone. However, van de Schootbrugge *et al.* (2020) reported *Mancodinium semitabulatum* from the upper Pliensbachian of northeast Russia.

The FO of *Susadinium scrofoides* is taken as the base of the ammonite *Dactylioceras tenuicostatum* Zone (i.e., the base of the early Toarcian).

FOs of *Phallocysta eumekes* and other taxa listed below

The FOs of *Phallocysta eumekes* and *Valvaeodinium aquilonium* occur at the base of the ammonite *Harpoceras falciferum* Zone at the Kelimyar River, northeastern Siberia. These biovents are within the foraminiferal *Ammobaculites lobus–Trochammina kisselmani* Zone (Nikitenko *et al.* 2013). The FO of *Rosswangia holotabulata* is also placed, albeit tentatively, at the base of the ammonite *Harpoceras falciferum* Zone based on regional synthesis of Tethyan to Boreal dinocyst events by Goryacheva (2017, fig. 14). The latter work incorporated data from Davies (1983, 1985) from Arctic Canada.

The FOs of *Phallocysta eumekes, Rosswangia holotabulata* and *Valvaeodinium aquilonium* are taken as the base of the ammonite *Harpoceras serpentinum* Zone (i.e., early Toarcian).

FOs of *Caligodinium aceras* and other taxa listed below

The FOs of *Caligodinium aceras*, *Dingodinium minutum*, *Dodekovia syzygia*, *Microdinium opacum* and *Valvaeodinium cavum* occur at base of Zone B of Davies (1983), which was assigned to the Toarcian of the Sverdrup Basin, interpreted here as the base of the ammonite *Hildoceras bifrons* Zone.

The FOs of *Caligodinium aceras*, *Dingodinium minutum*, *Dodekovia syzygia*, *Microdinium opacum* and *Valvaeodinium cavum* are taken as the base of the ammonite *Hildoceras bifrons* Zone (i.e., the base of the middle Toarcian).

FO of *Nannoceratopsis gracilis*

The FO of *Nannoceratopsis gracilis* occurs in the lower parts of the ammonite *Hildoceras bifrons* Zone and the foraminiferal *Ammobaculites lobus–Trochammina kisselmani* Zone in the Kelimyar River area, northeastern Siberia (Nikitenko *et al.* 2013).

The FO of *Nannoceratopsis gracilis* is taken as 17% up from the base of the ammonite *Hildoceras bifrons* Zone (i.e., middle Toarcian).

LOs of *Andreedinium arcticum* and other taxa listed below

The LOs of *Andreedinium arcticum*, *Parvocysta bullula*, *Reutlingia nasuta* and *Susadinium faustum* occur in the Toarcian ammonite *Porpoceras polare–Pseudolioceras rosenkrantzi* Zone on Svalbard (Feist-Burkhardt 1994, based on data from Below 1987a, 1990).

The LOs of *Andreedinium arcticum*, *Parvocysta bullula*, *Reutlingia nasuta* and *Susadinium faustum* are taken as 50% up from the base of the ammonite *Hildoceras bifrons* Zone (i.e., middle Toarcian).

FOs of *Ovalicysta hiata* and *Scriniocassis priscus*

The FOs of *Ovalicysta hiata* and *Scriniocassis priscus* occur in the Toarcian ammonite *Porpoceras polare–Pseudolioceras rosenkrantzi* Zone in the Barents Sea region (Feist-Burkhardt 1994, based on data from Below 1987a, 1990).

The FOs of *Ovalicysta hiata* and *Scriniocassis priscus* are taken as 50% up from the base of the ammonite *Hildoceras bifrons* Zone (i.e., middle Toarcian).

FO of *Opaeopsomus wapellensis*

The FO of *Opaeopsomus wapellensis* occurs within dinocyst Oppel-Zone B of Davies (1983), which was assigned to the Toarcian to early Bajocian in the Sverdrup Basin, interpreted here as the base of the ammonite *Haugia variabilis* Zone.

The FO of *Opaeopsomus wapellensis* is taken as the base of the ammonite *Haugia variabilis* Zone (i.e., the base of the late Toarcian).

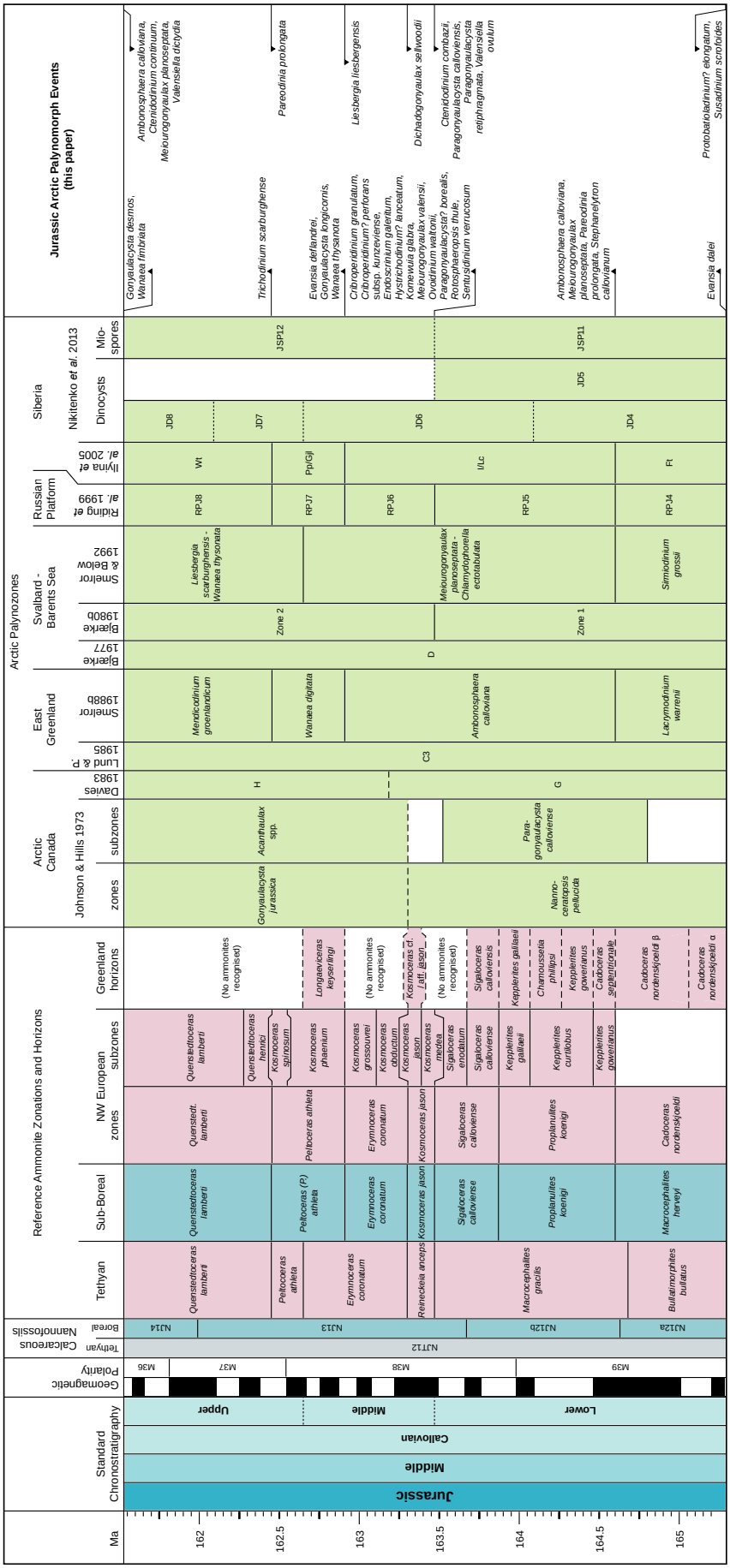

Figure 6. Stratigraphic chart for the Callovian; details as for Figure 1. Lund & P. 1985 - Lund and Pedersen (1985).

LO of *Nannoceratopsis deflandrei* subsp. *senex* var. C sensu Davies 1983

The LO of *Nannoceratopsis deflandrei* subsp. *senex* var. C sensu Davies 1983 occurs at base of dinocyst Oppel-Zone C of Davies (1983) which was assigned to the Toarcian to Early Bajocian in the Sverdrup Basin.

The LO of *Nannoceratopsis deflandrei* subsp. *senex* var. C sensu Davies 1983 is taken as the base of the ammonite *Grammoceras thouarsense* Zone (i.e., late Toarcian).

FOs of *Chytroeisphaeridia chytroeides* and *Valvaeodinium punctatum*

The FOs of *Chytroeisphaeridia chytroeides* and *Valvaeodinium punctatum* occur at base of dinocyst Oppel-Zone C of Davies (1983) which was assigned to the Toarcian to early Bajocian in the Sverdrup Basin.

The FOs of *Chytroeisphaeridia chytroeides* and *Valvaeodinium punctatum* are taken as the base of the ammonite *Grammoceras thouarsense* Zone (i.e., late Toarcian).

LO of *Phallocysta elongata*

The LO of *Phallocysta elongata* occurs at the top of the Toarcian dinocyst *Phallocysta eumekes* Zone defined in northern East Siberia by Riding *et al.* (1999); this horizon is coeval with the top of the ammonite *Dumortieria levesquei* Zone and is overlain by an Aalenian to Bajocian interval in northern East Siberian sections devoid of dinocysts (Riding *et al.* 1999).

The LO of *Phallocysta elongata* is taken as the base of the ammonite *Pleydellia aalensis* Zone (i.e., latest Toarcian).

LO of *Mikrocysta erugata*

The LO of *Mikrocysta erugata* occurs close to the base of the Aalenian, based on its occurrence near the top of the dinocyst *Mikrocysta erugata* Zone of Smelror and Below (1992, fig. 4). This zone was assigned to the Toarcian in the Arctic Norway/Barents Sea region.

The LO of *Mikrocysta erugata* is taken as the base of the ammonite *Leioceras opalinum* Zone (i.e., the base of the Aalenian).

FO of *Phallocysta thomasii*

The FO of *Phallocysta thomasii* occurs at the base of the Aalenian, based on its occurrence close to the top of the dinocyst *Mikrocysta erugata* Zone of Smelror and Below (1992, fig. 4), which these authors assigned to the Toarcian in the Arctic Norway–Barents Sea region.

The FO of *Phallocysta thomasii* is taken as the the base of the ammonite *Leioceras opalinum* Zone (i.e., the base of the Aalenian).

LO of *Ovalicysta hiata*

The LO of *Ovalicysta hiata* occurs in the Toarcian ammonite *Porpoceras polare–Pseudolioceras rosenkrantzi* Zone in the Barents Sea and on Svalbard (Bjærke 1980a).

The LO of *Ovalicysta hiata* is taken as at 50% up from the base of the ammonite *Leioceras opalinum* Zone (i.e., earliest Aalenian).

FO of *Evansia granochagrinata*

The FO of *Evansia granochagrinata* occurs in the latest Pliensbachian ammonite *Pleuroceras spinatum* Zone on Svalbard (Feist-Burkhardt 1994, based on data from Below 1987a, 1990).

The FO of *Evansia granochagrinata* is taken as 50% up from the base of the ammonite *Leioceras opalinum* Zone (i.e., earliest Aalenian).

LOs of *Freboldinium serrulatum* and other taxa listed below

The LOs of *Freboldinium serrulatum, Mancodinium coalitum*, *Mancodinium semitabulatum*, *Opaeopsomus wapellensis*, *Scriniodinium dictyotum* subsp. *pyrum* and *Valvaeodinium punctatum* occur at the base of dinocyst Oppel-Zone D of Davies (1983), which was assigned to the early Bajocian. The age of this zone was calibrated to the early Bajocian by Davies (1983) due to the presence of the ammonite *Leioceras opalinum* near its base on Ellef Ringnes Island (Fig. 10). This distinctive mollusk is the only age-diagnostic macrofossil in this zone. Strata immediately above this zone at Vantage Point, Axel Heiberg Island, have yielded the middle Bajocian ammonite *Arkelloceras mclearni* (Davies 1983).

The LOs of *Freboldinium serrulatum, Mancodinium coalitum*, *Mancodinium semitabulatum*, *Opaeopsomus wapellensis*, *Scriniodinium dictyotum* subsp. *pyrum* and *Valvaeodinium punctatum* are taken as the base of the ammonite *Hyperlioceras discites* Zone (i.e., the base of the Bajocian).

LO of *Scriniocassis priscus*

The LO of *Scriniocassis priscus* occurs in the Aalenian to early Bajocian ammonite *Leioceras opalinum–Hyperlioceras discites* Zone in the Barents Sea and on Svalbard (Feist-Burkhardt 1994, based on data from Below 1987a, 1990).

The LO of *Scriniocassis priscus* is taken as 50% up from the base of the ammonite *Sonninia propinquans* Zone (i.e., early Bajocian).

FO of *Freboldinium arcticum*

The FO of *Freboldinium arcticum* occurs in the Toarcian ammonite *Porpoceras polare–Pseudolioceras rosenkrantzi* Zone in the Barents Sea region and Svalbard (Feist-Burkhardt 1994, based on data from Below 1987a, 1990).

The FO of *Freboldinium arcticum* is taken as 50% up from

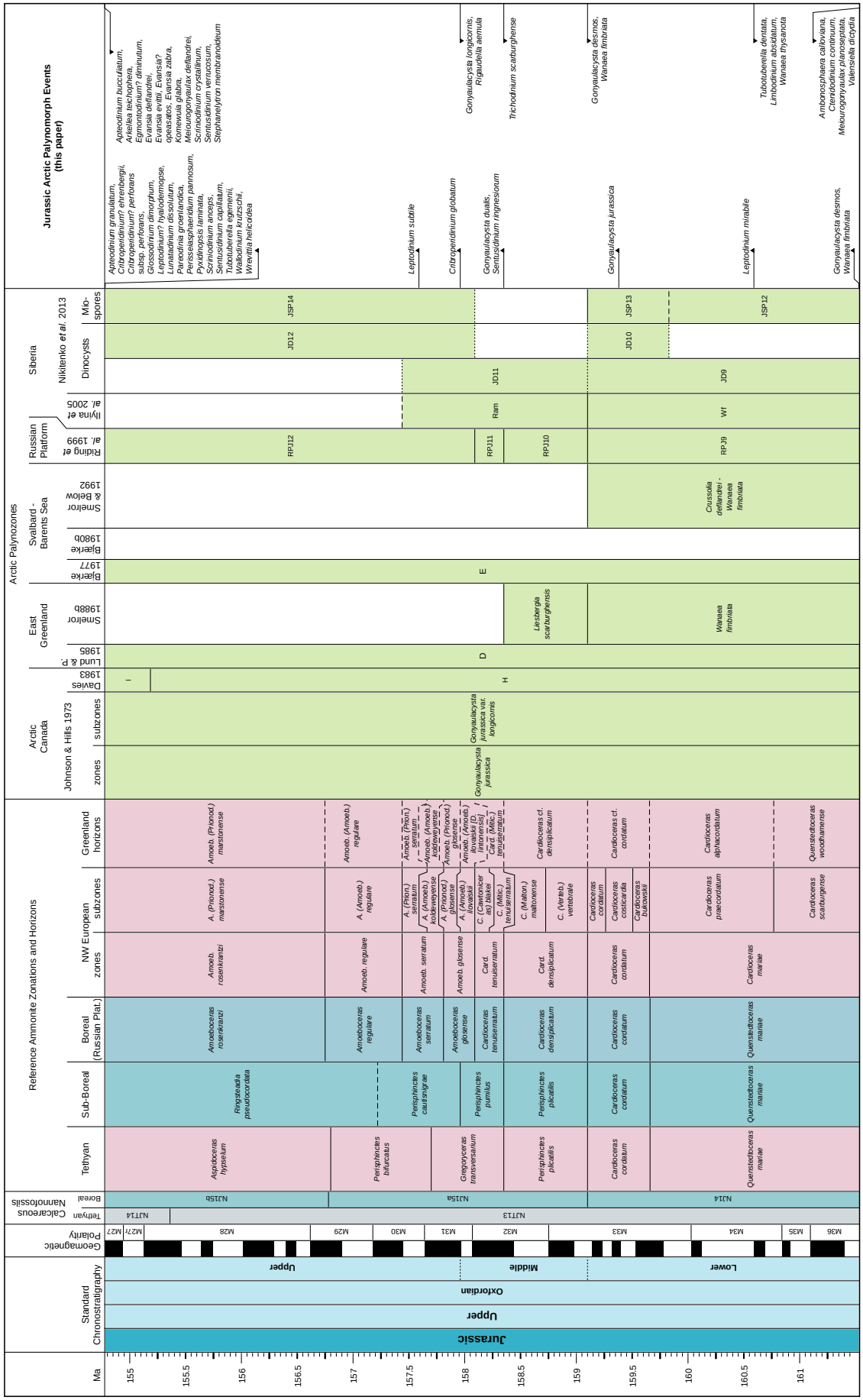

Figure 7. Stratigraphic chart for the Oxfordian; details as for Figure 1. Lund & P. 1985 - Lund and Pedersen (1985).

the base of the ammonite *Sonninia propinquans* Zone (i.e., early Bajocian).

LOs of *Mendicodinium reticulatum* and other taxa listed below

The LOs of *Mendicodinium reticulatum* and *Phallocysta elongata* occur at the base of dinocyst Oppel-Zone E of Davies (1983), which was dated as late Bajocian to middle Bathonian in the Sverdrup Basin. The presence of the ammonite *Arkelloceras mclearni* at the base of Oppel-Zone E at Vantage Point, Axel Heiberg Island, indicates a middle Bajocian age (Frebold in Tozer 1963; Frebold 1964; Frebold *et al.* 1967; Davies 1983). Stratigraphically higher in Oppel-Zone E the ammonite *Arctocephalites elegans* is present and indicates a middle Bathonian age (Davies 1983). The LOs of *Nannoceratopsis deflandrei* subsp. *senex* and *Parvocysta bullula* are correlated with the base of the late Bajocian based on its occurrence near the top of the dinocyst *Dodekovia bullula–Nannoceratopsis senex* Zone of Smelror and Below (1992, fig. 4), which they assigned to the Aalenian and early Bajocian in the Barents Sea region.

The LOs of *Mendicodinium reticulatum*, *Nannoceratopsis deflandrei* subsp. *senex*, *Parvocysta bullula* and *Phallocysta elongata* are taken as the base of the late Bajocian.

FOs of *Evansia evittii* and *Protobatioladinium elatmaense*

The FOs of *Evansia evittii* and *Protobatioladinium elatmaense* occur at the base of the Bathonian dinocyst *Evansia evittii* Zone defined in the Russian Platform by Riding *et al.* (1999). This is equivalent to the top of the ammonite *Parkinsonia parkinsoni* Zone which is at the Bajocian–Bathonian transition. This interval is underlain by an Aalenian–Bajocian interval in northeastern Siberia, which is devoid of dinocysts (Riding *et al.* 1999).

The FOs of *Evansia evittii* and *Protobatioladinium elatmaense* are taken as the base of the ammonite *Zigzagiceras zigzag* Zone (i.e., the base of the Bathonian).

FO of *Dichadogonyaulax sellwoodii*

The FO of *Dichadogonyaulax sellwoodii* occurs at the top of the Bathonian dinocyst *Evansia evittii* Zone defined in the Russian Platform by Riding *et al.* (1999), and thus within the earliest Bathonian ammonite *Zigzagiceras zigzag* Zone.

The FO of *Dichadogonyaulax sellwoodii* is taken as 75% above the base of the ammonite *Zigzagiceras zigzag* Zone (i.e., earliest Bathonian).

FOs of *Arkellea teichophera* and other taxa listed below

The FOs of *Arkellea teichophera*, *Atopodinium prostatum*, *Paragonyaulacysta calloviensis*, *Paragonyaulacysta retiphragmata*, *Rhynchodiniopsis cladophora* and *Scriniodinium crystallinum* occur at the base of dinocyst Oppel-Zone F of Davies (1983), which was assigned to the late Bathonian in the Sverdrup Basin. No index macrofossils occur in strata correlative with Oppel-Zone F. This Oppel-Zone, however, is bracketed by the middle Bathonian ammonite *Arctocephalites elegans* in Oppel-Zone E and the early Callovian ammonite *Cadoceras bodylevski* in Oppel-Zone G. The age of Oppel-Zone F is probably late Bathonian based on the ammonites *Arcticoceras ishmae* and *Arcticoceras kochi* (Davies 1983). The FOs occuring at this horizon are interpreted to occur at the base of the middle Bathonian ammonite *Procerites hodsoni* Zone.

The FOs of *Arkellea teichophera*, *Atopodinium prostatum*, *Paragonyaulacysta calloviensis*, *Paragonyaulacysta retiphragmata*, *Rhynchodiniopsis cladophora* and *Scriniodinium crystallinum* are taken as the base of the ammonite *Procerites hodsoni* Zone (i.e., middle Bathonian).

LOs of *Valvaeodinium aquilonium* and *Wanaea acollaris*

The LO of *Valvaeodinium aquilonium* occurs at base of dinocyst Oppel-Zone F of Davies (1983) which was assigned to the late Bathonian in the Sverdrup Basin. The LO of *Wanaea acollaris* is coeval with the LO of *Valvaeodinium aquilonium* based on the co-occurrence of these species in northern Alaska and the Sverdrup Basin (see the Beechey Point State 1 reference well in Appendix C).

The LOs of *Valvaeodinium aquilonium* and *Wanaea acollaris* are taken as the base of the ammonite *Procerites hodsoni* Zone (i.e., middle Bathonian).

LOs of *Nannoceratopsis gracilis* and *Rosswangia holotabulata*

The LOs of *Nannoceratopsis gracilis* and *Rosswangia holotabulata* are correlated with the boundary between the dinocyst *Nannoceratopsis gracilis* and *Sirmiodinium grossii* zones of Smelror and Below (1992), at the base of the late Bathonian in the Barents Sea area. These two LOs are coeval based on data from northern Alaska and the Sverdrup Basin, including the Beechey Point State 1 reference well (Appendix C).

The LOs of *Nannoceratopsis gracilis* and *Rosswangia holotabulata* are taken as 75% up from the base of the ammonite *Procerites hodsoni* Zone (i.e., close to the middle/late Bathonian transition).

FOs of *Lacrymodinium warrenii* and *Valensiella dictydia*

The FOs of *Lacrymodinium warrenii* and *Valensiella dictydia* are assigned to the late Bathonian based on their occurrence at the boundary between the dinocyst *Nannoceratopsis gracilis* and *Sirmiodinium grossii* zones of Smelror and Below (1992) in the Barents Sea region.

The FOs of *Lacrymodinium warrenii* and *Valensiella*

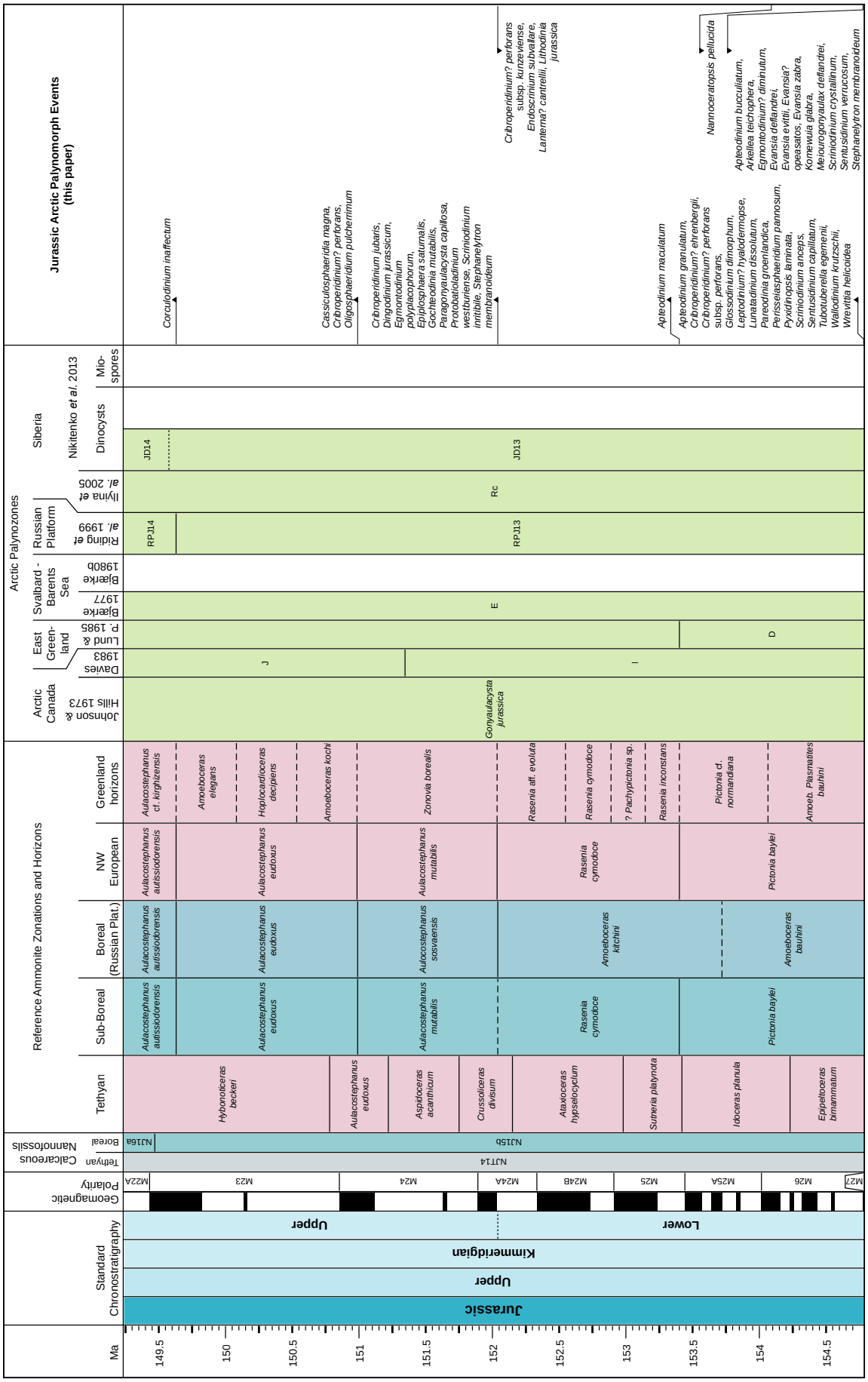

Figure 8. Stratigraphic chart for the Kimmeridgian; details as for Figure 1. Lund & P. 1985 - Lund and Pedersen (1985).

dictydia are taken as 75% up from the base of the ammonite *Procerites hodsoni* Zone (i.e., close to the middle/late Bathonian transition).

LOs of *Valvaeodinium leneae* and *Valvaeodinium spinosum*

The LO of *Valvaeodinium leneae* occurs in the latest Bath-onian ammonite *Cadoceras apertum* Zone in East Green-land (Piasecki 2001). However, the LO of *Valvaeodinium spinosum* is present in the late Bathonian ammonite *Cadoceras calyx* Zone in central Spitsbergen, Svalbard (Koevoets *et al.* 2018), which is coeval with the ammonite *Oxycerites orbis* Zone (Fig. 5).

The LOs of *Valvaeodinium leneae* and *Valvaeodinium spinosum* are taken as the base of the ammonite *Oxycerites orbis* Zone (i.e., late Bathonian).

FOs of *Atopodinium haromense* and other taxa listed below

The FO of *Atopodinium haromense* occurs in the late Bathonian ammonite *Cadoceras calyx* Zone in central Spitsbergen, Svalbard (Koevoets *et al.* 2018) and is interpreted to occur at the base of the ammonite *Oxycerites orbis* Zone. The FOs of *Ellipsoidictyum cinctum*, *Evansia*? *opeasatos*, *Evansia zabra*, *Gonyaulacysta adecta, Lithodinia jurassica*, *Paragonyaulacysta calloviensis*, *Paragonyaulacysta retiphragmata*, *Pareodinia ceratophora* and *Tubotuberella rhombiformis* also occur within dinocyst Zone F of Davies (1983), in the late Bathonian of the Sverdrup Basin.

The FOs of *Atopodinium haromense, Ellipsoidictyum cinctum*, *Evansia*? *opeasatos*, *Evansia zabra*, *Gonyaulacysta adecta, Lithodinia jurassica*, *Paragonyaulacysta calloviensis*, *Paragonyaulacysta retiphragmata*, *Pareodinia ceratophora* and *Tubotuberella rhombiformis* are taken as the base of the ammonite *Oxycerites orbis* Zone (i.e., late Bathonian).

LOs of *Protobatioladinium*? *elongatum* and *Susadinium scrofoides*

The LO of *Protobatioladinium*? *elongatum* occurs at the top of the latest Bathonian dinocyst *Protobatioladinium*? *elongatum* Zone defined in the Russian Platform by Riding *et al.* (1999). Likewise, the LO of *Susadinium scrofoides* occurs at the top of dinocyst Oppel-Zone F of Davies (1983), which was assigned to the late Bathonian. Evidence for the age of Oppel-Zone F is provided by the middle Bathonian ammonite *Arctocephalites elegans* in Oppel-Zone E below, and the early Callovian ammonite *Cadoceras bodylevski* in Oppel-Zone G.

The LOs of *Protobatioladinium*? *elongatum* and *Susadinium scrofoides* are taken as the base of the ammonite *Macrocephalites herveyi* Zone (i.e., at the base of the Callovian).

FO of *Evansia dalei*

The FO of *Evansia dalei* occurs at the base of the early Callovian *Fromea tornatilis* Zone defined by Ilyina *et al.* (2005) in the Tyumenskaya superdeep well-6, West Siberia. This bioevent lies at the base of the ammonite *Macrocephalites herveyi* Zone and the foraminiferal *Kutsevella memorabilis–Guttulina tatarensis* Zone. *Evansia dalei* was also reported from the lowermost Callovian of the Russian Platform by Riding *et al.* (1999).

The FO of *Evansia dalei* is taken as the base of the ammonite *Macrocephalites herveyi* Zone (i.e., at the base of the Callovian).

FOs of *Ambonosphaera calloviana* and other taxa listed below

The FOs of *Ambonosphaera calloviana* and *Meiourogonyaulax planoseptata* occur in the Barents Sea at the boundary of the dinocyst *Sirmiodinium grossii* Zone, and the dinocyst *Meiourogonyaulax planoseptata–Chlamydophorella ectotabulata* Zone of Smelror and Below (1992). These events were assigned to the earliest Callovian. The FOs of *Pareodinia prolongata* and *Stephanelytron callovianum* occur in the Tyumenskaya superdeep well-6, West Siberia at the base of the Callovian dinocyst *Impletosphaeridium* spp.–*Stephanelytron* Zone; this horizon is equivalent to the bases of the earliest Callovian ammonite *Proplanulites koenigi* Zone and the foraminiferal *Dorothia insperata–Trochammina rostovzevi* Zone (Ilyina *et al.* 2005).

The FOs of *Ambonosphaera calloviana*, *Meiourogonyaulax planoseptata*, *Pareodinia prolongata* and *Stephanelytron callovianum* are taken as the base of the ammonite *Proplanulites koenigi* Zone (i.e., earliest Callovian).

LOs of *Ctenidodinium combazii* and other taxa listed below

The LO of *Ctenidodinium combazii* occurs at the top of the early Callovian dinocyst *Lagenadinium callovianum* (now *Stephanelytron callovianum*) zone defined on the Russian Platform by Riding *et al.* (1999). The LOs of *Paragonyaulacysta calloviensis*, *Paragonyaulacysta retiphragmata* and *Valensiella ovulum* are coeval with the LO of *Ctenidodinium combazii* based on their occurrences in northern Alaska and the Sverdrup Basin, for example the Beechey Point State 1 reference well (Appendix C).

The LOs of *Ctenidodinium combazii*, *Paragonyaulacysta calloviensis*, *Paragonyaulacysta retiphragmata* and *Valensiella ovulum* are taken as the base of the ammonite *Kosmoceras jason* Zone (i.e., the base of the middle Callovian).

FOs of *Cribroperidinium granulatum* and the other taxa listed below

The FOs of *Cribroperidinium granulatum*, *Cribroperidinium*? *perforans* subsp. *kunzeviense*, *Endoscrinium galeritum*,

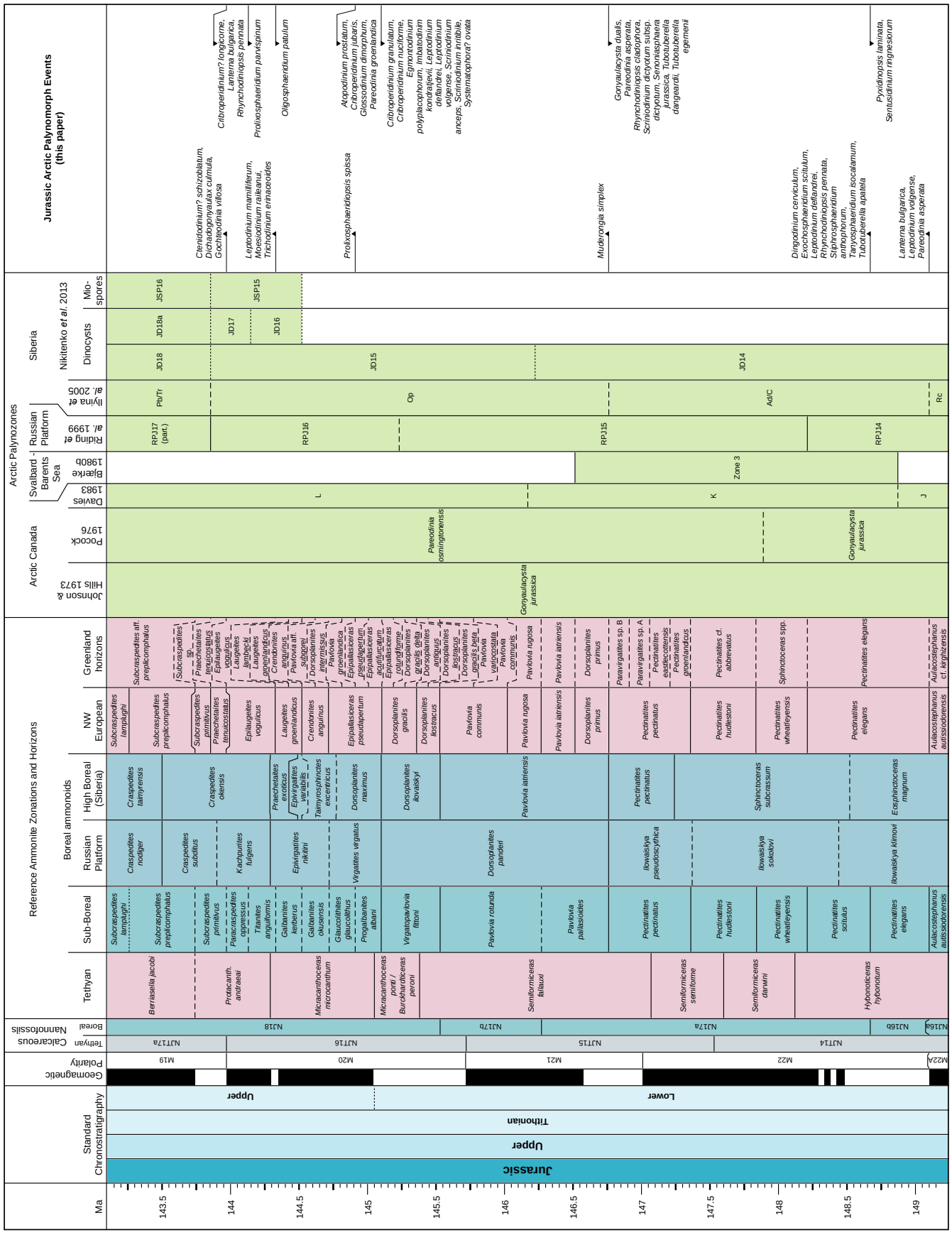

Figure 9. Stratigraphic chart for the Tithonian; details as for Figure 1.

Hystrichodinium? *lanceatum*, *Komewuia glabra*, *Meiourogonyaulax valensii*, *Ovoidinium waltonii, Paragonyaulacysta*? *borealis*, *Rotosphaeropsis thule* and *Sentusidinium verrucosum* occur at base of dinocyst Oppel-Zone H of Davies (1983). This zone was assigned to the middle Callovian–Oxfordian in the Sverdrup Basin and the base of it is interpreted here to represent the base of the ammonite *Kosmoceras jason* Zone.

The FOs of *Cribroperidinium granulatum*, *Cribroperidinium*? *perforans* subsp. *kunzeviense*, *Endoscrinium galeritum*, *Hystrichodinium*? *lanceatum*, *Komewuia glabra*, *Meiourogonyaulax valensii*, *Ovoidinium waltonii, Paragonyaulacysta*? *borealis*, *Rotosphaeropsis thule* and *Sentusidinium verrucosum* are taken as the base of the ammonite *Kosmoceras jason* Zone (i.e., the base of the middle Callovian).

LO of *Dichadogonyaulax sellwoodii*

The LO of *Dichadogonyaulax sellwoodii* occurs within the middle Callovian dinocyst *Kalyptea stegasta* Zone defined in the Russian Platform by Riding *et al.* (1999) at the base of the ammonite *Erymnoceras coronatum* Zone.

The LO of *Dichadogonyaulax sellwoodii* is taken as the base of the ammonite *Erymnoceras coronatum* Zone (i.e., middle Callovian).

LO of *Liesbergia liesbergensis*

The LO of *Liesbergia liesbergensis* occurs in Tyumenskaya superdeep well-6, West Siberia, at the base of the Callovian dinocyst *Gonyaulacysta jurassica* subsp. *adecta* var. *longicornis* Zone (Ilyina *et al.* 2005). The datum corresponds to the base of the ammonite *Peltoceras athleta* Zone on the Russian Platform (Riding *et al.* 1999).

The LO of *Liesbergia liesbergensis* is taken as the base of the ammonite *Peltoceras athleta* Zone (i.e., close to the middle/late Callovian transition).

FOs of *Evansia deflandrei* and the other taxa listed below

The FO of *Gonyaulacysta longicornis* occurs at the base of the late Callovian dinocyst *Gonyaulacysta jurassica* subsp. *adecta* var. *longicornis* Zone defined in the Tyumenskaya SDW-6 borehole of West Siberia by Ilyina *et al.* (2005) and calibrated by ammonites indicative of the ammonite *Peltoceras athleta* Zone. The base of the dinocyst *Gonyaulacysta jurassica* subsp. *adecta* var. *longicornis* Zone of Ilyina *et al.* (2005) is equivalent to the base of the late Callovian dinocyst *Pareodinia prolongata* Zone of Riding *et al.* (1999) of the Russian Platform. Similarly, this bioevent is coeval with the base of the dinocyst *Liesbergia scarburghensis–Wanaea thysanota* Zone of Smelror and Below (1992) in the Barents Sea. The FO of *Evansia deflandrei* occurs at top of the dinocyst *Meiourogonyaulax planoseptata–Chlamydophorella ectotabulata* Zone (= base of the dinocyst *Liesbergia scarburghensis – Wanaea thysanota* Zone) of Smelror and Below (1992), which was assigned by the latter authors to the later early and middle Callovian in the Norwegian Barents Sea region.

The FOs of *Evansia deflandrei, Gonyaulacysta longicornis* and *Wanaea thysanota* are taken as the base of the ammonite *Peltoceras athleta* Zone (i.e., close to the middle/late Callovian transition).

LO of *Pareodinia prolongata*

The LO of *Pareodinia prolongata* occurs at the top of the Callovian dinocyst *Pareodinia prolongata* Zone defined in the Russian Platform by Riding *et al.* (1999), equivalent to the top of the ammonite *Peltoceras athleta* Zone and the base of the ammonite *Quenstedtoceras lamberti* Zone.

The LO of *Pareodinia prolongata* is taken as the base of the ammonite *Quenstedtoceras lamberti* Zone (i.e., late Callovian).

FO of *Trichodinium scarburghense*

The FO of *Trichodinium scarburghense* occurs at the base of latest Callovian dinocyst *Trichodinium scarburghense* Zone of Riding *et al.* (1999) on the Russian Platform, equating with the base of the ammonite *Quenstedtoceras lamberti* Zone.

The FO of *Trichodinium scarburghense* is taken as the base of the ammonite *Quenstedtoceras lamberti* Zone (i.e., late Callovian).

LOs of *Ambonosphaera calloviana* and other taxa listed below

The LOs of *Ambonosphaera calloviana*, *Ctenidodinium continuum*, *Meiourogonyaulax planoseptata* and *Valensiella dictydia* occur at the base of the early Oxfordian. This is based on their occurrences at the base of the dinocyst *Crussolia deflandrei–Wanaea fimbriata* Zone of Smelror and Below (1992) in the Barents Sea, and the base of the dinocyst *Wanaea fimbriata* Zone on the Russian Platform (Riding *et al.* 1999).

The LOs of *Ambonosphaera calloviana*, *Ctenidodinium continuum*, *Meiourogonyaulax planoseptata* and *Valensiella dictydia* are taken as the base of the ammonite *Quenstedtoceras mariae* Zone (i.e., the base of the Oxfordian).

FOs of *Gonyaulacysta desmos* and *Wanaea fimbriata*

Gonyaulacysta desmos is a characteristically Arctic form which is confined to the early Oxfordian (Poulsen 1991; Riding *et al.* 2022). The FO of *Wanaea fimbriata* occurs in the Tyumenskaya superdeep well-6, West Siberia, is close to the base of the early Oxfordian dinocyst *Wanaea fimbriata* Zone in West Siberia (Ilyina *et al.* 2005). This event is also observed in the Barents Sea and the Russian Platform (Smelror and Below 1992; Riding *et al.* 1999).

The FOs of *Gonyaulacysta desmos* and *Wanaea fimbriata*

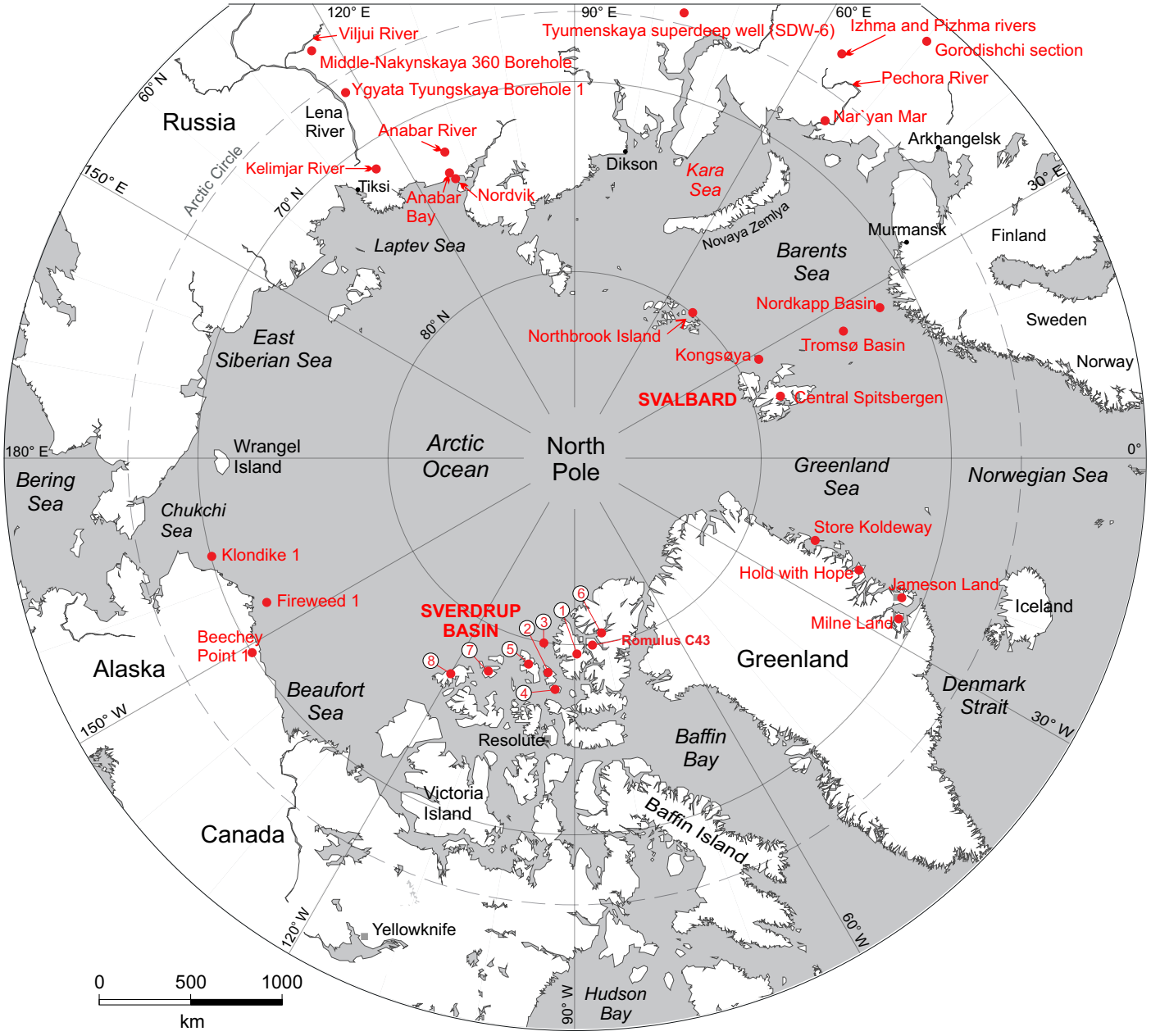

Figure 10. Circumpolar projection map showing the main Jurassic localities discussed in the text. Key to islands in the Sverdrup Basin is as follows: 1= Axel Heiberg; 2 = Amund Ringnes; 3 = Bjarnason; 4 = Cornwall; 5 = Ellef Ringnes; 6 = Ellesmere; 7 = Mackenzie King; 8 = Prince Patrick.

are taken as the base of the ammonite *Quenstedtoceras mariae* Zone (i.e., the base of the Oxfordian).

LOs of *Limbodinium absidatum* and other taxa listed below

The LO of the typically Arctic species *Tubotuberella dentata* occurs within the ammonite *Quenstedtoceras mariae* Zone (Riding 2012a). The LOs of *Limbodinium absidatum* and *Wanaea thysanota* occur in the lower part of the Oxfordian dinocyst *Wanaea fimbriata* Zone defined in the Russian Platform by Riding *et al.* (1999), an interval also within the ammonite *Quenstedtoceras mariae* Zone.

The LOs of *Limbodinium absidatum, Tubotuberella dentata* and *Wanaea thysanota* are taken as 50% up from the base of the ammonite *Quenstedtoceras mariae* Zone (i.e., earliest Oxfordian).

FO of *Leptodinium mirabile*

The FO of *Leptodinium mirabile* occurs in the lower part of the Oxfordian dinocyst *Wanaea fimbriata* Zone defined in the Russian Platform by Riding *et al.* (1999), within the ammonite *Quenstedtoceras mariae* Zone.

The FO of *Leptodinium mirabile* is taken as 50% above the base of the ammonite *Quenstedtoceras mariae* Zone (i.e., earliest Oxfordian).

FO of *Gonyaulacysta jurassica*

The FO of *Gonyaulacysta jurassica* occurs within the upper part of the dinocyst *Wanaea fimbriata* Zone established for the Russian Platform (Riding *et al.* 1999). This event is therefore within the ammonite *Cardioceras cordatum* Zone.

The FO of *Gonyaulacysta jurassica* is taken as 50% above the base of the ammonite *Cardioceras cordatum* Zone (i.e., early Oxfordian).

LOs of *Gonyaulacysta desmos* and *Wanaea fimbriata*

The extinction of *Gonyaulacysta desmos* occurs at the top of the early Oxfordian and has been reported from East Greenland (Poulsen 1991). The LO of *Wanaea fimbriata* occurs at the top of the early Oxfordian dinocyst *Wanaea fimbriata* Zone defined from the Russian Platform by Riding *et al.* (1999), equivalent to the top of the ammonite *Cardioceras cordatum* Zone. This event also occurs at the top of the dinocyst *Wanaea fimbriata* Zone of West Siberia (Ilyina *et al.* 2005), and at the top of the dinocyst *Crussolia deflandrei–Wanaea fimbriata* Zone in the Barents Sea (Smelror and Below 1992). The latter dinocyst zones are of early Oxfordian age.

The LOs of *Gonyaulacysta desmos* and *Wanaea fimbriata* are taken as the base of the ammonite *Perisphinctes plicatilis* Zone (i.e., the base of the middle Oxfordian).

LO of *Trichodinium scarburghense*

The LO of *Trichodinium scarburghense* occurs at the top of the middle Oxfordian dinocyst *Endoscrinium galeritum* subsp. *reticulatum* Zone defined in the Russian Platform by Riding *et al.* (1999). This zone is equivalent to the ammonite *Perisphinctes plicatilis* and *Cardioceras densiplicatum* zones.

The LO of *Trichodinium scarburghense* is taken as the base of the ammonite *Cardioceras tenuiserratum* Zone (i.e., middle Oxfordian).

FOs of *Gonyaulacysta dualis* and *Sentusidinium ringnesiorum*

Sentusidinium ringnesiorum was recorded by Davies (1983) as *Chytroeisphaeridia*? *mantellii* (subsequently *Escharisphaeridia mantellii*), *Escharisphaeridia pocockii* and *Escharisphaeridia rudis*, all of which were considered to be taxonomic junior synonyms of *Sentusidinium ringnesiorum* by Wood *et al.* (2016). The FOs of *Sentusidinium ringnesiorum* and *Gonyaulacysta dualis* occur within dinocyst zone H of Davies (1983) established in the Sverdrup Basin. Both events are interpreted here as representing the top of the ammonite *Perisphinctes plicatilis* Zone.

The FOs of *Gonyaulacysta dualis* and *Sentusidinium ringnesiorum* are taken as the base of the ammonite *Perisphinctites pumilis* Zone (i.e., middle Oxfordian).

LOs of *Gonyaulacysta longicornis* and *Rigaudella aemula*

The LOs of *Gonyaulacysta longicornis* and *Rigaudella aemula* occur at the top of the Oxfordian dinocyst *Gonyaulacysta jurassica* subsp. *adecta* var. *longicornis* Zone defined in the Russian Platform by Riding *et al.* (1999). These events are broadly coeval with the boundary between the ammonite *Perisphinctites pumilis* and *Perisphinctes cautisnigrae* zones.

The LOs of *Gonyaulacysta longicornis* and *Rigaudella aemula* are taken as the base of the ammonite *Perisphinctites cautisnigrae* Zone (i.e., at the base of the late Oxfordian).

FO of *Cribroperidinium globatum*

The FO of *Cribroperidinium globatum* occurs at the top of the Oxfordian dinocyst *Gonyaulacysta jurassica* subsp. *adecta* var. *longicornis* Zone defined in the Russian Platform by Riding *et al.* (1999). This datum is approximately equivalent to the top of the ammonite ammonite *Perisphinctites pumilis* Zone.

The FO of *Cribroperidinium globatum* is taken as the base of the ammonite *Perisphinctites cautisnigrae* Zone (i.e., at the base of the late Oxfordian transition).

FO of *Leptodinium subtile*

The FO of *Leptodinium subtile* occurs in the late Oxfordian ammonite *Amoeboceras serratum* Zone in Jameson Land, East Greenland (Alsen and Pasecki 2018).

The FO of *Leptodinium subtile* is taken as 50% up from the base of the ammonite *Perisphinctites cautisnigrae* Zone (i.e., late Oxfordian).

LOs of *Apteodinium bucculiatum* and other taxa listed below

The LOs of *Evansia deflandrei* and *Scriniodinium crystallinum* occur close to the top of the late Oxfordian dinocyst *Cribroperidinium globatum* Zone defined in the Russian Platform by Riding *et al.* (1999), equivalent to the top of the ammonite *Amoeboceras rosenkrantzi* Zone. LOs of the other species mentioned below occur at base of the early Kimmeridgian dinocyst Oppel-Zone I of Davies (1983) for the Sverdrup Basin. These datums are interpreted herein as representing the Oxfordian/Kimmeridgian transition.

The LOs of *Apteodinium bucculiatum*, *Arkellea teichophera*, *Sentusidinium verrucosum, Egmontodinium*? *diminutum*, *Evansia deflandrei*, *Evansia evittii*, *Evansia*? *opeasatos*, *Evansia zabra, Komewuia glabra*, *Meiourogonyaulax deflandrei*, *Scriniodinium crystallinum* and *Stephanelytron membranoideum* are taken as the base of the ammonite *Pictonia baylei* Zone (i.e., at the base of the Kimmeridgian).

FOs of *Apteodinium granulatum* and other taxa listed below

The FOs of *Apteodinium granulatum*, *Cribroperidinium*? *ehrenbergii*, *Cribroperidinium*? *perforans* subsp. *perforans, Leptodinium*? *hyalodermopse*, *Lunatadinium dissolutum*, *Pareodinia groenlandica*, *Pyxidinopsis laminata*, *Sentusidinium capillatum* (including *Pilosidinium filiatum*, a taxonomic junior synonym according to Wood *et al.* 2016), *Tubotuberella egemenii*, *Wallodinium krutzschii* and *Wrevittia helicoidea* occur at the base of dinocyst Oppel-Zone I of Davies (1983). This horizon is considered here to be coeval with the boundary between the Oxfordian and Kimmeridgian. The FOs of *Glossodinium dimorphum*, *Perisseiasphaeridium pannosum* and *Scriniodinium anceps* occur at the top of the late Oxfordian dinocyst *Cribroperidinium globatum* Zone defined in the Russian Platform by Riding *et al.* (1999), again equivalent to the Oxfordian/Kimmeridgian transition.

The FOs of *Apteodinium granulatum*, *Cribroperidinium*? *ehrenbergii*, *Cribroperidinium*? *perforans* subsp. *perforans*, *Glossodinium dimorphum, Leptodinium*? *hyalodermopse*, *Lunatadinium dissolutum*, *Pareodinia groenlandica*, *Perisseiasphaeridium pannosum*, *Pyxidinopsis laminata*, *Scriniodinium anceps*, *Sentusidinium capillatum*, *Tubotuberella egemenii*, *Wallodinium krutzschii* and *Wrevittia helicoidea* are taken as the base of the ammonite *Pictonia baylei* Zone (i.e., at the base of the Kimmeridgian).

LO of *Nannoceratopsis pellucida*

The LO of *Nannoceratopsis pellucida* was reported by Ilyina *et al.* (2005) in the earliest Kimmeridgian of West Siberia, specifically within the Boreal ammonite *Amoeboceras kitchini* Zone. By contrast, this event occurs in the strata assigned to the upper Oxfordian ammonite *Amoeboceras regulare* Zone in the Barents Sea (MS personal observations).

The LO of *Nannoceratopsis pellucida* is taken as at 50% up from the base of the ammonite *Pictonia baylei* Zone (i.e., earliest Kimmeridgian).

FO of *Apteodinium maculatum*

The FO of *Apteodinium maculatum* occurs within dinocyst Oppel-Zone I of Davies (1983) in the Sverdrup Basin. This zone was dated using evidence from ammonites and bivalves; Davies (1983) interpreted Oppel-Zone I as including the transition of the ammonite *Pictonia baylei* and *Rasenia cymodoce* zones.

The FO of *Apteodinium maculatum* is taken as the base of the ammonite *Rasenia cymodoce* Zone (i.e., early Kimmeridgian).

LOs of *Cribroperidinium*? *perforans* subsp. *kunzeviense* and other taxa listed below

The LOs of *Cribroperidinium*? *perforans* subsp. *kunzeviense*, *Endoscrinium subvallare*, *Lanterna*? *cantrellii* and *Lithodinia jurassica* occur at base of dinocyst Oppel-Zone J of Davies (1983) in the Sverdrup Basin. This intra-Kimmeridgian age is consistent with the presence of the bivalve species *Buchia mosquensis* in the central Amund Ringnes Dome. Furthermore, due to the occurrence of *Buchia jischeriana* in the lowermost part of Oppel-Zone K, (Davies 1983) interpreted his J/K zonal boundary as "middle" Kimmeridgian (top of the ammonite *Rasenia cymodoce* Zone).

The LOs of *Cribroperidinium*? *perforans* subsp. *kunzeviense*, *Endoscrinium subvallare*, *Lanterna*? *cantrellii* and *Lithodinia jurassica* are taken as the base of the ammonite *Aulacostephanus mutabilis* Zone (i.e., the base of the late Kimmeridgian).

FOs of *Cribroperidinium jubaris* and other taxa listed below

The FOs of *Cribroperidinium jubaris*, *Epiplosphaera saturnalis* and *Paragonyaulacysta capillosa* occur at the base of dinocyst Oppel-Zone J of Davies (1983) in the Sverdrup Basin. The Kimmeridgian age of this biozone is based on evidence from the bivalve genus *Buchia*. The FOs of *Dingodinium jurassicum, Gochteodinia mutabilis*, *Protobatioladinium westburiense* and *Stephanelytron membranoideum* occur in the Tyumenskaya superdeep well-6, West Siberia, at the base of the Kimmeridgian dinocyst *Rhynchodiniopsis cladophora* Zone defined by Ilyina *et al.* (2005). Lastly, the FOs of *Egmontodinium polyplacophorum* and *Scriniodinium inritibile* occur in the dinocyst *Pareodinia nuda* (= *Pareodinia ceratophora*) Subzone of Fisher and Riley (1980), equivalent to the boundary between the ammonite *Rasenia cymodoce* and *Aulacostephanus mutabilis* zones.

The FOs of *Cribroperidinium jubaris*, *Dingodinium jurassicum*, *Egmontodinium polyplacophorum*, *Epiplosphaera saturnalis, Gochteodinia mutabilis*, *Paragonyaulacysta capillosa*, *Protobatioladinium westburiense, Scriniodinium inritibile* and *Stephanelytron membranoideum* are taken as the base of the ammonite *Aulacostephanus mutabilis* Zone (i.e., the base of the late Kimmeridgian).

FOs of *Cassiculosphaeridia magna* and other taxa listed below

The FOs of *Cassiculosphaeridia magna*, *Cribroperidinium*? *perforans* and *Oligosphaeridium pulcherrimum* occur at the base of the Boreal dinocyst *Pareodinia nuda* Subzone of Fisher and Riley (1980).

The FOs of *Cassiculosphaeridia magna*, *Cribroperidinium*? *perforans* and *Oligosphaeridium pulcherrimum* are taken as the base of the ammonite *Aulacostephanus eudoxus* Zone (i.e., late Kimmeridgian).

FO of *Corculodinium inaffectum*

The FO of *Corculodinium inaffectum* occurs at the top of the Kimmeridgian dinocyst *Gonyaulacysta jurassica* subsp. *jurassica* Zone defined in the Russian Platform by Riding *et*

al. (1999). This is equivalent to the boundary between the ammonite *Aulacostephanus eudoxus* and *Aulacostephanus autissiodorensis* zones.

The FO of *Corculodinium inaffectum* is taken as the base of the ammonite *Aulacostephanus autissiodorensis* Zone (i.e., latest Kimmeridgian).

FOs of *Lanterna bulgarica* and other taxa listed below

The FOs of *Lanterna bulgarica*, *Leptodinium volgense* and *Pareodinia asperata* occur at the base of the Boreal dinocyst *Gonyaulacysta jurassica* Subzone of Fisher and Riley (1980). The datum approximately correlates with the boundary between the ammonite *Aulacostephanus autissiodorensis* and *Pectinatites elegans* zones.

The LOs of *Lanterna bulgarica*, *Leptodinium volgense* and *Pareodinia asperata* are taken as the base of the ammonite *Pectinatites elegans* Zone (i.e., the base of the Tithonian).

LOs of *Pyxidinopsis laminata* and *Sentusidinium ringnesiorum*

The LOs of *Pyxidinopsis laminata* and *Sentusidinium ringnesiorum* occur at the base of dinocyst zone K of Davies (1983) which was assigned to the earliest Tithonian in the Sverdrup Basin. (*Sentusidinium ringnesiorum* was recorded by Davies as *Chytroeisphaeridia*? *mantellii*, *Escharisphaeridia pocockii* and *Escharisphaeridia rudis*, all of which were considered taxonomic junior synonyms of *Sentusidinium ringnesiorum* by Wood *et al.* 2016.) These events are interpreted herein as being at the transition of the ammonite *Pectinatites elegans* and *Pectinatites scitulus* zones.

The LOs of *Pyxidinopsis laminata* and *Sentusidinium ringnesiorum* are taken as the base of the ammonite *Pectinatites scitulus* Zone (i.e., earliest Tithonian).

FOs of *Dingodinium cerviculum* and the other taxa listed below

The FOs of *Dingodinium cerviculum*, *Exochosphaeridium scitulum*, *Leptodinium deflandrei, Rhynchodiniopsis pennata*, *Stiphrosphaeridium anthophorum*, *Tanyosphaeridium isocalamum* and *Tubotuberella apatela* occur at the base of the dinocyst *Gonyaulacysta pennata* Subzone of Fisher and Riley (1980). These datums correlate roughly with the top of the ammonite *Pectinatites elegans* Zone and the base of the ammonite *Pectinatites scitulus* Zone in the Boreal Realm.

The FOs of *Dingodinium cerviculum*, *Exochosphaeridium scitulum*, *Leptodinium deflandrei*, *Rhynchodiniopsis pennata*, *Stiphrosphaeridium anthophorum*, *Tanyosphaeridium isocalamum* and *Tubotuberella apatela* are taken as the base of the ammonite *Pectinatites scitulus* Zone (i.e., earliest Tithonian).

LOs of *Gonyaulacysta dualis* and other taxa listed below

The LOs of *Gonyaulacysta dualis* and *Pareodinia asperata* occur at the base of the dinocyst *Muderongia simplex* zone defined by Fisher and Riley (1980). These events correlate approximately with the transition between the ammonite *Pectinatites pectinatus* and *Pavlovia pallasioides* zones. Furthermore, the LOs of *Rhynchodiniopsis cladophora*, *Scriniodinium dictyotum* subsp. *dictyotum*, *Senoniasphaera jurassica, Tubotuberella dangeardii* and *Tubotuberella egemenii* are coeval with the range tops of *Gonyaulacysta dualis* and *Pareodinia asperata* based on their occurrences in northern Alaska and the Sverdrup Basin, including the Beechey Point State 1 reference well (Appendix C).

The LOs of *Gonyaulacysta dualis*, *Pareodinia asperata*, *Rhynchodiniopsis cladophora*, *Scriniodinium dictyotum* subsp. *dictyotum, Senoniasphaera jurassica, Tubotuberella dangeardii* and *Tubotuberella egemenii* are taken as the base of the ammonite *Pavlovia pallasioides* Zone (i.e., early Tithonian).

FO of *Muderongia simplex*

The FO of *Muderongia simplex* occurs in the Boreal Realm at the base of the dinocyst *Muderongia simplex* Zone of Fisher and Riley (1980). This horizon approximately correlates with the base of the ammonite *Pavlovia pallasioides* Zone.

The FO of *Muderongia simplex* is taken as the base of the ammonite *Pavlovia pallasioides* Zone (i.e., early Tithonian).

LOs of *Cribroperidinium granulatum* and other taxa listed below

The LOs of *Cribroperidinium granulatum*, *Cribroperidinium nuciforme*, *Egmontodinium polyplacophorum*, *Imbatodinim kondratjevii*, *Leptodinium deflandrei*, *Leptodinium volgense*, *Scriniodinium anceps*, *Scriniodinium inritibile* and *Systematophora*? *ovata* occur at the base of the palynomorph *Pterospermopsis aureolata* Subzone defined in Canada, Greenland and northwestern Europe by Fisher and Riley (1980).

The LOs of *Cribroperidinium granulatum, Cribroperidinium nuciforme*, *Egmontodinium polyplacophorum*, *Imbatodinim kondratjevii*, *Leptodinium deflandrei*, *Leptodinium volgense*, *Scriniodinium anceps, Scriniodinium inritibile* and *Systematophora*? *ovata* are taken as the base of the ammonite *Progalbanites albani* Zone (i.e., the base of the late Tithonian).

LOs of *Atopodinium prostatum* and other taxa listed below

The LOs of *Atopodinium prostatum*, *Cribroperidinium jubaris*, *Glossodinium dimorphum* and *Pareodinia groenlandica* occur at the base of dinocyst Oppel-Zone L of Davies (1983) in the late Tithonian in the Sverdrup Basin. This

horizon is interpreted here as equating with the top of the ammonite *Progalbanites albani* Zone. The LO of *Glossodinium dimorphum* also occurs at the top of the dinocyst *Glossodinium dimorphum* Zone defined in the Russian Platform by Riding *et al.* (1999). This event is coeval with the transition between the ammonite *Progalbanites albani* and *Glaucolithites glaucolithus* zones.

The LOs of *Atopodinium prostatum*, *Cribroperidinium jubaris*, *Glossodinium dimorphum* and *Pareodinia groenlandica* are taken as the base of the ammonite *Glaucolithites glaucolithus* Zone (i.e., late Tithonian).

FO of *Prolixosphaeridiopsis spissa*

The FO of the acritarch species *Prolixosphaeridiopsis spissa* occurs at base of dinocyst Oppel-Zone L of Davies (1983), within the late Tithonian in the Sverdrup Basin, interpreted here as equating with the base of the ammonite *Glaucolithites glaucolithus* Zone.

The FO of *Prolixosphaeridiopsis spissa* is taken as the base of the ammonite *Glaucolithites glaucolithus* Zone (i.e., late Tithonian).

LO of *Oligosphaeridium patulum*

The LO of *Oligosphaeridium patulum* occurs in the late Tithonian, close to the base of the Boreal ammonite *Craspidites okensis* Zone in Andøya, Arctic Norway (MS, personal observations). Ilyina *et al.* (2005) also recorded this event at the base of the ammonite *Craspedites okensis* Zone in West Siberia, approximately coeval with the base of the ammonite *Titanites anguiformis* Zone (Fig. 9).

The LO of *Oligosphaeridium patulum* is taken as the base of the ammonite *Titanites anguiformis* Zone (i.e., late Tithonian).

FOs of *Leptodinium mamilliferum* and other taxa listed below

The FOs of *Leptodinium mamilliferum*, *Moesiodinium raileanui* and *Trichodinium erinaceoides* occur at the base of dinocyst Oppel-Zone M of Davies (1983) in the late Tithonian of the Sverdrup Basin. This horizon is interpreted here as equating with the base of the ammonite *Titanites anguiformis* Zone. The stratigraphic range of *Moesiodinium raileanui* is early Toarcian to earliest Bajocian, i.e., substantially older in northwestern Europe (e.g., Riding and Thomas 1992) than in northern Canada. The occurrences of *Moesiodinium raileanui* reported by Davies (1983) may be either misidentified or reworked. The characteristic hexagonal archaeopyle with geniculate top and base is not visible in the single specimen illustrated by Davies (1983, pl. 6, fig. 23).

The FOs of *Leptodinium mamilliferum*, *Moesiodinium raileanui* and *Trichodinium erinaceoides* are taken as the base of the ammonite *Titanites anguiformis* Zone (i.e., late Tithonian).

LO of *Prolixosphaeridium parvispinum*

The LO of *Prolixosphaeridium parvispinum* occurs in the upper part of the dinocyst *Senioniasphaera jurassica* Zone defined in the Russian Platform by Riding *et al.* (1999). This event is coeval with the transition between the ammonite *Titanites anguiformis* and *Paracraspedites oppressus* zones.

The LO of *Prolixosphaeridium parvispinum* is taken as the base of the ammonite *Paracraspedites oppressus* Zone (i.e., late Tithonian).

LOs of *Cribroperidinium*? *longicorne* and other taxa listed below

The LOs of *Cribroperidinium*? *longicorne*, *Lanterna bulgarica* and *Rhynchodiniopsis pennata* occur at the base of the dinocyst *Dichadogonyaulax culmula* Subzone of Fisher and Riley (1980), which approximately correlates to the top of the ammonite *Paracraspedites oppressus* Zone.

The LOs of *Cribroperidinium*? *longicorne*, *Lanterna bulgarica* and *Rhynchodiniopsis pennata* are taken as the base of the ammonite *Subcraspedites primitivus* Zone (i.e., late Tithonian).

FOs of *Ctenidodinium*? *schizoblatum* and other taxa listed below

The FOs of *Ctenidodinium*? *schizoblatum* and *Dichadogonyaulax culmula* occur in the late Tithonian, at the base of the dinocyst *Dichadogonyaulax culmula* Subzone of Fisher and Riley (1980), which is broadly coeval with the top of the ammonite *Paracraspedites oppressus* Zone. Furthermore, the FO of *Gochteodinia villosa* occurs at the top of the late Tithonian dinocyst *Senoniasphaera jurassica* Zone defined in the Russian Platform by Riding *et al.* (1999). This event also equates to the boundary between the ammonite *Paracraspedites oppressus* and *Subcraspedites primitivus* zones.

The FOs of *Ctenidodinium*? *schizoblatum*, *Dichadogonyaulax culmula* and *Gochteodinia villosa* are taken as the base of the ammonite *Subcraspedites primitivus* Zone (i.e., late Tithonian).

DISCUSSION AND CONCLUSIONS

In this contribution we summarize the Jurassic palynostratigraphy of the circum-Arctic region (i.e., northern North America and Greenland in the west, and arctic Norway, the Barents Sea and northern Russia in the east) with the principal emphasis on dinocyst bioevents. The literature on the marine palynology of the Arctic is mainly centred on the eastern Arctic (Svalbard and northern Russia), with substantially fewer papers on the western Arctic (Canadian Arctic and Greenland). There is relatively little relevant information in the public domain on Alaska. In terms of stratigraphic coverage, most data are from the Upper Jurassic with markedly fewer contributons on Middle Jurassic

successions. The palynology of the Arctic Lower Jurassic has not been extensively researched, and this overall pattern closely follows the global trend in terms of the research effort on Jurassic dinocysts (Riding 2012b).

We document herein a succession of 214 bioevents (FOs and LOs), calibrated to ammonite zones, from the Hettangian to the Tithonian. These biohorizons have been selected to provide a practical succession of datums based on common and easy to recognize taxa that give a high resolution biostratigraphic coverage of the entire Jurassic System in the Arctic. This reflects the typically highly diverse floras during the Jurassic at high northern latitudes, which appear to have been an evolutionary "hotspot" (Mantle *et al.* 2020; van de Schootbrugge *et al.* 2020; Correia *et al.* 2021). The main Arctic Jurassic palynozonations such as those by Johnson and Hills (1973), Fisher and Riley (1980), Davies (1983), Smelror and Below (1992), Riding *et al.* (1999) and Ilyina *et al.* (2005) are referenced extensively.

The parent cells of dinocysts are largely motile and planktonic, and therefore they typically have extensive geographical distributions (Riding and Lucas-Clark 2016). Substantial numbers of cosmopolitan Jurassic taxa occur generally, and many were present in the Boreal, sub-Boreal and Tethyan realms in the northern hemisphere (Riding *et al.* 2010; Mantle and Riding 2012). However, some provincialism did occur and the intensity of this endemism fluctuated during the Jurassic. The diversity of Early Jurassic dinocysts is relatively low compared to the post-Bajocian interval (e.g., Riding and Thomas 1992). Bucefalo Palliani and Riding (2003) demonstrated that Boreal Pliensbachian and Toarcian dinocysts were markedly more species-rich than their Tethyan counterparts. The Bathonian during the Middle Jurassic was a time of relatively high levels of eustatic-driven endemism, prior to substantially more cosmopolitan and diverse floras in the Callovian and onwards (Riding *et al.* 1985, 1991). The latest Jurassic was characterized by very high levels of provincialism largely due to land barriers and low sea levels (e.g., Abbink *et al.* 2001). The provincialism of Lower, Middle and Late Jurassic floras was discussed by, for example, Riding (1984), Smelror (1993), Riding and Ioannides (1996), Riding and Hubbard (1999), Riding *et al.* (1999) and Harding *et al.* (2011). These studies confirm that genera such as *Evansia* and *Paragonyaulacysta* and species such as *Gonyaulacysta dualis* are typically Arctic (Riding *et al.* 1999; Riding and Lucas-Clark 2016; Riding *et al.* 2022). More specifically, Riding and Michoux (2013) discussed the migration southward of Boreal forms such as *Evansia deflandrei, Mendicodinium groenlandicum, Rigaudella aemula, Trichodinium scarburghensis, Tubotuberella dentata* and *Wanaea fimbriata* at the Callovian–Oxfordian transition. These taxa are envisaged as being cold water forms, however it should be borne in mind that seasonality and thermal latitudinal gradients during the Mesozoic greenhouse were generally considerably less than those in today's Quaternary Icehouse (Valdes and Sellwood 1992; Alberti *et al.* 2017).

ACKNOWLEDGEMENTS

We are grateful to Eva Bjørseth and Bill MacMillan who helped draft the figures, to Jan Hennissen who provided advice about key events, and to Vânia Correia who provided feedback on the manuscript. Special thanks to Rob Fensome for editing the paper and his advice on some of the trickier aspects of dinocyst nomenclature and taxonomy. We thank Karen Dybkjær and Dave Shaw for their very useful feedback on the original manuscript. This paper was supported by the Russian Foundation for Basic Research (RFBR) project number 20-05-00076 and the Program of Russian Fundamental Scientific Research project number 0331-2019-0004. It is a contribution to the TransGEM Event Stratigraphy activity of the Geological Survey of Canada's Geo-Mapping for Energy and Minerals Program. James B. Riding publishes with the approval of the Chief Executive Officer, British Geological Survey (NERC).

REFERENCES

Abbink, O.A., Callomon, J.H., Riding, J.B., Williams, P.D.B., and Wolfard, A. 2001. Biostratigraphy of Jurassic–Cretaceous boundary strata in the Terschelling Basin, The Netherlands. Proceedings of the Yorkshire Geological Society, 53, pp. 275–302. https://doi.org/10.1144/pygs.53.4.275

Albert, N.R. 1988. Dinoflagellate cysts from the Early Cretaceous of the Yukon–Koyukuk Basin and from the Upper Jurassic Naknek Formation, Alaska. University Microfilms International (U.M.I.) Dissertation Information Service, Ann Arbor, Michigan, USA, 481 pp.

Albert, N.R., Evitt, W.R., and Stein, J.A. 1986. *Lacrymodinium,* n. gen., a gonyaulacoid dinoflagellate with intercalary archeopyle from the Jurassic and Early Cretaceous of California and Alaska. Micropaleontology, 32, pp. 303–315. https://doi.org/10.2307/1485724

Alberti, M., Fürsich, F.T., Abdelhady, A.A., and Andersen, N. 2017. Middle to Late Jurassic equatorial seawater temperatures and latitudinal temperature gradients based on stable isotopes of brachiopods and oysters from Gebel Maghara, Egypt. Palaeogeography, Palaeoclimatology, Palaeoecology, 468, pp. 301–313. https://doi.org/10.1016/j.palaeo.2016.11.052

Alsen, P. and Piasecki, S. 2018. Biostratigraphy of the Hareelv Formation (Upper Jurassic) in the Blokelv-1 core, Jameson Land, East Greenland. Geological Survey of Denmark and Greenland Bulletin, 42, pp. 15–37. https://doi.org/10.34194/geusb.v42.4308

Beisel, A.L., Zanin, Y.N., Zamirailova, A.G., Ilyina, V.I., Lebedeva, N.K., Levchuk, L.K., Levchuk, M.A., Meledina, S.V., Nikitenko, B.L., Shurygin, B.N., and Yan, P.A. 2002. Reference section for the Upper Jurassic and Callovian in northern West Siberia. Russian Geology and Geophysics, 43, pp. 811–825.

Below, R. 1987a. Evolution und Systematik von Dinoflagellaten-Zysten aus der Ordnung Peridiniales. I. Allgemeine

Grundlagen und Subfamilie Rhaetogonyaulacoideae (Familie Peridiniaceae). Palaeontographica Abteilung B, 205, pp. 1–164.

Below, R. 1987b. Evolution und Systematik von Dinoflagellaten-Zysten aus der Ordnung Peridiniales. II. Cladopyxiaceae und Valvaeodiniaceae. Palaeontographica Abteilung B, 206, pp. 1–115.

Below, R. 1990: Evolution und Systematik von Dinoflagellaten-Zysten aus der Ordnung Peridiniales. III. Familie Pareodiniaceae. Palaeontographica Abteilung B, 220, pp. 1–96.

Bjærke, T. 1977. Mesozoic palynology of Svalbard II. Palynomorphs from the Mesozoic sequence of Kong Karls Land. Norsk Polarinstitutt, Årbok 1976, pp. 83–120.

Bjærke, T. 1980a. Mesozoic palynology of Svalbard IV. Toarcian dinoflagellates from Spitsbergen. Palynology, 4, pp. 57–77. https://doi.org/10.1080/01916122.1980.9989202

Bjærke, T. 1980b. Mesozoic palynology of Svalbard V. Dinoflagellates from the Agardhfjellet Member (Middle and Upper Jurassic) in Spitsbergen. Norsk Polarinstitutt, Skrifter, 172, pp.145–167.

Bjærke, T. 1993. Palynological examination of samples from Alaska. Alaska Geologic Materials Center Data Report, 210, pp. 1–18.

Bjærke, T. and Dypvik, H. 1977. Sedimentological and palynological studies of Upper Triassic–Lower Jurassic sediments in Sassenfjorden, Spitsbergen. Norsk Polarinstitutt Årbok, 1976, pp. 131–150.

Bjærke, T. and Manum, S.B. 1977. Mesozoic palynology of Svalbard I. The Rhaetian of Hopen, with a preliminary report on the Rhaetian and Jurassic of Kong Karls Land. Norsk Polarinstitutt, Skrifter, Nr. 165, 48 pp.

Bjærke, T., Edwards, M.B., and Thusu, B. 1976. Microplankton from the Janusfjellet Subgroup (Jurassic–Lower Cretaceous) at Agardhfjellet Spitsbergen. A preliminary report. Norsk Polarinstitutt Årbok, 1974, pp. 63–68.

Blakey, R. 2021. Paleotectonic and paleogeographic history of the Arctic region. Atlantic Geology, 57, pp. 7–39. https://doi.org/10.4138/atlgeol.2021.002

Brideaux, W.W. 1975. Status of Mesozoic and Tertiary dinoflagellate studies in the Canadian Arctic. American Association of Stratigraphic Palynologists Contributions Series, 4, pp. 15–28.

Brideaux, W.W. 1976. Taxonomic notes and illustrations of selected dinoflagellate cyst species from the Gulf Mobil Parsons N–10 well. Geological Survey of Canada Paper 76–1B, pp. 251–257. https://doi.org/10.4095/104107

Brideaux, W.W. and Myhr, D.W. 1976. Lithostratigraphy and dinoflagellate cyst succession in the Gulf Mobil Parsons N–10 well, District of Mackenzie. Geological Survey of Canada Paper, 76–1B, pp. 235–249. https://doi.org/10.4095/104106

Bringué, M., Fensome, R.A., Poulton, T.P., Galloway, J.M., Bujak, J.P., Golding, M.L., Orchard, M.J., and Williams, G.L. in press. The 2020 Canada datapack for TimeScale Creator: a new tool for Mesozoic–Cenozoic stratigraphy of the Canadian North. Geological Survey of Canada, Bulletin 609. https://doi.org/10.1130/abs/2020AM-353274

Bucefalo Palliani, R. and Riding, J.B. 2003. Biostratigraphy, provincialism and evolution of European early Jurassic (Pliensbachian to early Toarcian) dinoflagellate cysts. Palynology, 27, pp.179–214. https://doi.org/10.2113/27.1.179

Callomon, J.H. and Birkelund, T. 1980. The Jurassic transgression and the mid–late Jurassic succession in Milne Land, central East Greenland. Geological Magazine, 117, pp. 211–226. https://doi.org/10.1017/S0016756800030442

Cookson, I.C. and Eisenack, A. 1958. Microplankton from Australian and New Guinea Upper Mesozoic sediments. Proceedings of the Royal Society of Victoria, 70, pp. 19–79.

Correia, V.F., Riding, J.B., Duarte, L.V., Fernandes, P., and Pereira, Z. 2021. The effects of the Jenkyns Event on the radiation of Early Jurassic dinoflagellate cysts. *In* Carbon cycle and ecosystem response to the Jenkyns Event in the early Toarcian (Jurassic). *Edited by* M. Reolid, L.V. Duarte, E. Mattioli, and W Ruebsam. Geological Society, London Special Publications, 514, pp. 13–30. https://doi.org/10.1144/SP514-2020-255

Dalseg, T.S., Nakrem, H.A., and Smelror, M. 2016. Dinoflagellate biostratigraphy, palynofacies, depositional environment and sequence stratigraphy of the Agardhfjellet Formation (Upper Jurassic–Lower Cretaceous) in central Spitsbergen (Arctic Norway). Norwegian Journal of Geology, 96, pp. 119–133. https://doi.org/10.17850/njg96-2-04

Davies, E.H. 1983. The dinoflagellate Oppel zonation of the Jurassic-lower Cretaceous sequence in the Sverdrup Basin, Arctic Canada. Geological Survey of Canada, Bulletin, 359, 59 pp. https://doi.org/10.4095/119736

Davies, E.H. 1985. Dinoflagellate cyst occurrences of the Jurassic–Lower Cretaceous sequence in the Sverdrup Basin, arctic Canada. Geological Survey of Canada, Open File Report, 1153, 28 pp. https://doi.org/10.4095/129945

Drugg, W.S. 1978. Some Jurassic dinoflagellate cysts from England, France and Germany. Palaeontographica Abteilung B, 168, pp. 61–79.

Dypvik, H., Hvoslef, S., Bjærke, T., and Finnerud, E. 1985. The Wilhelmøya Formation (Upper Triassic–Lower Jurassic) at Bohemanflya, Spitsbergen. Polar Research, 3, pp. 155–165. https://doi.org/10.3402/polar.v3i2.6949

Dzyuba O.S., Pestchevitskaya E.B., Urman O.S., Shurygin B.N., Alifirov A.S., Igolnikov A.E., and Kosenko I.N. 2018. The Maurynya section, western Siberia: a key section of the Jurassic-Cretaceous boundary deposits of shallow marine origin. Russian Geology and Geophysics, 59, pp. 1072–1102. https://doi.org/10.1016/j.rgg.2018.07.010

Eisenack, A. 1972. Kritische Bemerkung zur Gattung *Pterospermopsis* (Chlorophyta, Prasinophyceae). [Critical remarks about *Pterospermopsis*]. Neues Jahrbuch für Geologie und Paläontologie, Monatshefte, 10, pp. 596–601.

Feist-Burkhardt, S. 1994. Stratigaphic compilation of Below's data (1987A, 1987B and 1990) on Early and Middle Jurassic dinoflagellate cysts. Revue de Paleobiologie, 13, pp. 313–318.

Felix, C.J. 1975. Palynological zonation of the Heiberg Formation (Triassic–Jurassic) eastern Sverdrup Basin, Arctic Canada. Bulletin of Canadian Petroleum Geology, 36, pp. 347–361.

Fensome, R.A. 1979. Dinoflagellate cysts and acritarchs from the Middle and Upper Jurassic of Jameson Land, East Greenland. Grønlands Geologiske Undersøgelse Bulletin, 132, 98 pp. https://doi.org/10.34194/bullggu.v132.6674

Fensome, R.A., Williams, G.L., and MacRae, R.A. 2019. The Lentin and Williams Index of fossil dinoflagellates 2019 edition. American Association of Stratigraphic Palynologists Contributions Series, 50, 1173 pp.

Fisher, M.J. and Riley, L.A. 1980. The stratigraphic distribution of dinoflagellate cysts at the Boreal Jurassic–Cretaceous boundary. Fourth International Palynology Conference, Lucknow, 1976–77, Proceedings, 2, pp. 313–329.

Frebold, F.H. 1964. The Jurassic faunas of the Canadian Arctic. Cadoceratinae. Geological Survey of Canada Bulletin, 119, 27 pp. https://doi.org/10.4095/100627

Frebold, H., Mountjoy, E.W., and Tempelman-Kluit, D.J. 1967. New occurrences of Jurassic rocks and fossils in central and northern Yukon Territory. Geological Survey of Canada Paper 67–12, 35 pp. https://doi.org/10.4095/100917

Galloway, J.M., Sweet, A.R., Swindles, G.T., Dewing, K., Hadlari, T., Embry, A.F., and Sanei, H. 2013. Middle Jurassic to Lower Cretaceous paleoclimate of Sverdrup Basin, Canadian Arctic Archipelago inferred from the palynostratigraphy. Marine and Petroleum Geology, 44, pp. 240–255. https://doi.org/10.1016/j.marpetgeo.2013.01.001

Goryacheva, A.A. 2017. Lower Jurassic palynostratigraphy of eastern Siberia. Stratigraphy and Geological Correlation, 25, pp. 265–295. https://doi.org/10.1134/S0869593817030042

Goryacheva, A.A. and Nikitenko, B.L. 2016. Biostratigraphy of Lower Jurassic in Borehole Middle-Nakyn 360 (East Siberia). *In* Algae in biosphere evolution. *Edited by* N.K. Lebedeva and A.A. Goryacheva. Proceedings of the Second Palaeoalgological Conference, Institute of Geology and Geophysics, Siberian Branch of the Russian Academy of Sciences, Doklady Akademii Nauk, Novosibirsk, pp. 33–35 (in Russian).

Gradstein, F.M., Ogg, J.G., Schmitz, M.D., and Ogg, G. (editors). 2021. The geologic time scale 2020. Second edition. Elsevier, The Netherlands, 1176 pp.

Gurari, F.G. and Mogucheva, N.K. (editors.). 2004. Resolution of the sixth interdepartmental stratigraphic meeting on the consideration and acceptance of refined stratigraphic charts of the Mesozoic sediments of West Siberia (Novosibirsk, 2003). SNIIGGiMS, Novosibirsk.

Håkansson, E., Birkelund, T., Piasecki, S., and Zakharov, V. 1981. Jurassic–Cretaceous boundary strata of the extreme Arctic (Peary Land, North Greenland). Bulletin of the Geological Society of Denmark, 30, pp. 11–42. https://doi.org/10.37570/bgsd-1981-30-02

Harding, I.C., Smith, G.A., Riding, J.B., and Wimbledon, W.A.P. 2011. Inter-regional correlation of Jurassic/Cretaceous boundary strata based on the Tithonian–Valanginian dinoflagellate cyst biostratigraphy of the Volga Basin, western Russia. Review of Palaeobotany and Palynology, 167, pp. 82–116. https://doi.org/10.1016/j.revpalbo.2011.07.002

Hogg, N.M. and Bailey, D.A. 1997. *Prolixosphaeridiopsis spissus* gen. et comb. nov. for the dinoflagellate cyst *Cleistosphaeridium spissum* McIntyre and Brideaux 1980. Journal of Micropalaeontology, 16, p. 50. https://doi.org/10.1144/jm.16.1.50

Ilyina, V.I. 1986. Subdivision and correlation of the marine and non-marine Jurassic sediments in Siberia based on palynological evidence. Review of Palaeobotany and Palynology, 46, 357–364. https://doi.org/10.1016/0034-6667(86)90073-4

Ilyina, V.I. 1988. Microphytoplankton of the Jurassic–Cretaceous boundary deposits of Urduk-Chaya Cape (Paksa Peninsula). *In* Palynology in the USSR. *Edited by* A.E. Khlonova. Novosibirsk: Nauka, 103–107.

Ilyina, V.I., Kulkova, I.A., and Lebedeva, N.K. 1994. Microphytofossils and detail stratigraphy of marine Mesozoic and Cenozoic of Siberia. Russian Academy of Sciences, Siberian Branch, United Institute of Geology, Geophysics and Mineralogy, Transactions, 818, 192 pp. (in Russian).

Ilyina, V.I., Nikitenko, B.L., and Glinskikh, L.A. 2005. Foraminifera and dinoflagellate cyst zonation and stratigraphy of the Callovian to Volgian reference section in the Tyumenskya superdeep well (West Siberia, Russia). *In* Recent developments in applied biostratigraphy. *Edited by* A.J. Powell and J.B. Riding. The Micropalaeontological Society, Special Publication, pp. 109–144. https://doi.org/10.1144/TMS001.8

Ingrams, S., Jolley, D.W., and Schneider, S. 2021. High latitude stratigraphical palynology of the Jurassic–Cretaceous boundary interval, Sverdrup Basin, Arctic Canada. Cretaceous Research, 126, 104922, 15 pp. https://doi.org/10.1016/j.cretres.2021.104922

Johnson, C.D. 1974. Microplankton palynostratigraphy of the Savik Formation (Jurassic), Axel Heiberg and Ellesmere Islands. Geological Association of Canada and the Canadian Society of Petroleum Geologists, Proceedings of the Canadian Arctic Geological Symposium, pp. 259–275.

Johnson, C.D. and Hills, L.V. 1973. Microplankton from the Savik Formation (Jurassic), Axel Heiberg and Ellesmere Island, District of Franklin. Bulletin of Canadian Petroleum Geology, 21, pp. 178–218.

Kelly, S.R.A., Gregory, F.J., Braham, W., Strogen, D.P., and Whitham, A.G. 2015. Towards an integrated Jurassic biostratigraphy for eastern Greenland. Volumina Jurassica, 13, pp. 43–64.

Klaus, W. 1960. Sporen der karnischen Stufe der ostalpinen Trias. Jahrbuch der Geologischen Bundesanstalt, 5, pp. 107–184.

Koevoets, M.J., Hammer, Ø., Olaussen, S., Senger, K., and Smelror, M. 2018. Integrating subsurface and outcrop

data of the Middle Jurassic to Lower Cretaceous Agardhfjellet Formation in central Spitsbergen. Norwegian Journal of Geology, 98, pp. 1–34. https://doi.org/10.17850/njg98-4-01

Koppelhus, E.B. and Dam, G. 2003. Palynostratigraphy and palaeoenvironments of the Rævekøft, Gule Horn and Ostreaelv formations (Lower–Middle Jurassic), Neill Klinter Group, Jameson Land East Greenland. *In* The Jurassic of Denmark and Greenland. *Edited by* J.R. Ineson and F. Surlyk. Geological Survey of Denmark and Greenland Bulletin, 1, pp. 723–775. https://doi.org/10.34194/geusb.v1.4688

Koppelhus, E.B. and Hansen, C.F. 2003. Palynostratigraphy and palaeoenvironment of the Middle Jurassic Sortehat Formation (Neill Klinter Group), Jameson Land East Greenland. *In* The Jurassic of Denmark and Greenland. *Edited by* J.R. Ineson and F. Surlyk. Geological Survey of Denmark and Greenland Bulletin, 1, pp. 777–811. https://doi.org/10.34194/geusb.v1.4689

Lebedeva, N.K. and Nikitenko, B.L. 1998. Microphytoplankton and microforaminifera in the Lower Cretaceous reference section in Subarctic Ural (West Siberia). Russian Geology and Geophysics, 39, pp. 810–832.

Lebedeva N.K. and Nikitenko B.L. 1999. Dinoflagellate cysts and microforaminifera of the Lower Cretaceous Yatria River section, Subarctic Ural, NW Siberia (Russia). Palaeogeographic and palaeoenvironmental discussion. Grana, 38, pp. 134–143. https://doi.org/10.1080/713786920

Lentin, J.K. and Willliams, G.L. 1981. Fossil dinoflagellates: index to genera and species, 1981 edition. Bedford Institute of Oceanography, Report Series, BI–R-81–12, 345 pp.Leschik, G. 1956. Die Keuperflora von Neuewelt bei Basel: II. Die iso-und mikrosporen. Schweiz. Paläontologisches Abhandlung, 72, pp. 1–70.

Leschik, G. 1956. Die Keuperflora yon Neuwelt bei Basel. II. Die Iso- und Mikrosporen. Schweizerische Paläontologische Abhandlungen, 71, pp. 1–70.

Lund, J.J. and Pedersen, K.R. 1985. Palynology of the marine Jurassic formations in the Vardekløft Ravine, Jameson Land, East Greenland. Bulletin of the Geological Society of Denmark, 33, pp. 371–399. https://doi.org/10.37570/bgsd-1984-33-30

Lundblad, B. 1954. Contributions to the geological history of the Hepaticae. Fossil Marchantiales from the Rhaetic-Liassic coal mines of Skrombergea (Prov. of Scania), Sweden. Svensk Botanisk Tidskrift, 48, pp. 381–417

Malyavkina, V.S. 1949. Index of spores and pollen; Jurassic-Cretaceous. Vsesoyuznyi Neftyanoi Nauchno Issledovatelskii Geologorazvedochnyi Institut, Leningrad (VNIGRI), Trudy, 33, pp.1–137, 51 pl. (in Russian).

Mangerud, G., Paterson, N.W., and Bujak, J. 2021. Triassic palynoevents in the circum-Arctic region. Atlantic Geology, 57, pp. 71–101. https://doi.org/10.4138/atlgeol.2021.005

Mantle, D.J. and Riding, J.B. 2012. Palynology of the Middle Jurassic (Bajocian–Bathonian) *Wanaea verrucosa* dinoflagellate cyst zone of the North West Shelf of Australia. Review of Palaeobotany and Palynology, 180, pp. 41–78. https://doi.org/10.1016/j.revpalbo.2012.03.005

Mantle, D.J., Riding, J.B., and Hannaford, C. 2020. Late Triassic dinoflagellate cysts from the Northern Carnarvon Basin, Western Australia. Review of Palaeobotany and Palynology, 281, 104254, 53 pp. https://doi.org/10.1016/j.revpalbo.2020.104254

McIntyre, D.J. and Brideaux, W.W. 1980. Valanginian miospore and microplankton assemblages from the northern Richardson Mountains, District of Mackenzie, Canada. Geological Survey of Canada, Bulletin, 320, 57 pp.

Meledina, S.V., Ilyina, V.I., and Nalnjaeva, T.I. 1998. Parallel biostratigraphic scales of the Boreal Bathonian and Callovian in the North Pechora region as a tool for interregional correlation. Stratigraphy and Geological Correlation, 6, pp. 29–42.

Milner, P.S. and Piasecki, S. 1996. Boreal Middle Jurassic dinoflagellate cyst stratigraphy of Jameson Land, East Greenland. Danmarks og Grønlands Geologiske Undersøgelse Rapport, 1996/30, Appendix 12, 32 pp.

Morgenroth, P. 1970. Dinoflagellate cysts from the Lias Delta of Lühnde/Germany. Neues Jahrbuch für Geologie und Paläontologie Abhandlungen, 136, pp. 345–359.

Nikitenko, B.L. 2009. Jurassic stratigraphy, palaeobiogeography and biofacies of Siberia on microfauna (foraminifers and ostracodes). Parallel, Novosibirsk (in Russian with extended English summary).

Nikitenko, B.L., Pestchevitskaya, E.B., Lebedeva, N.K., and Ilyina, V.I. 2008. Micropalaeontological and palynological analyses across the Jurassic–Cretaceous boundary on Nordvik Peninsula, northeast Siberia. Newsletters on Stratigraphy, 42, pp. 181–222. https://doi.org/10.1127/0078-0421/2008/0042-0181

Nikitenko, B.L., Lebedeva, N.K., Peshchevitskaya, E.B., Knyazev, V.G., and Kutygin, R.V. 2011. Problems of Oxfordian and Kimmeridgian stratigraphy in northern Central Siberia (Nordvik Peninsula section). Russian Geology and Geophysics, 52, pp. 963–978. https://doi.org/10.1016/j.rgg.2011.08.003

Nikitenko, B.L., Shurygin, B.N., Knyazev, V.G., Meledina, S.V., Dzyuba, O.S., Lebedeva, N.K., Peshchevitskaya, E.B., Glinskikh, L.A., Goryacheva, A.A., and Khafaeva, S.N. 2013. Jurassic and Cretaceous stratigraphy of the Anabar area (Arctic Siberia, Laptev Sea coast) and the Boreal zonal standard. Russian Geology and Geophysics, 54, pp. 808–837. https://doi.org/10.1016/j.rgg.2013.07.005

Nikitenko, B.L., Knyazev, V.G., Peshchevitskaya, E.B., Glinskikh, L.A., Kutygin, R.V., and Alifirov, A.S. 2015a. High-resolution stratigraphy of the Upper Jurassic section (Laptev Sea coast). Russian Geology and Geophysics, 56, pp. 663–685. https://doi.org/10.1016/j.rgg.2015.03.014

Nikitenko, B.L., Knyazev, V.G., Peshchevitskaya, E.B., and Glinskikh L.A. 2015b. The Upper Jurassic of the Laptev Sea: interregional correlations and paleoenvironments. Russian Geology and Geophysics, 56, pp. 1173–1193. https://doi.org/10.1016/j.rgg.2015.07.008

Nikitenko B.L., Devyatov V.PP., Lebedeva N.K., Basov V.A.,

Goryacheva A.A., Pestchevitskaya E.B., and Glinskikh L.A. 2017. Jurassic and Cretaceous stratigraphy of the New Siberian Archipelago (Laptev and East Siberian Seas): facies zoning and lithostratigraphy. Russian Geology and Geophysics, 58, pp. 1478–1493. https://doi.org/10.1016/j.rgg.2017.11.012

Nikitenko, B.L., Devyatov, V.PP., Lebedeva, N.K., Basov, V.A., Fursenko, E.A., Goryacheva, A.A., Peshchevitskaya, E.B., Glinskikh, L.A., and Khafaeva, S.N. 2018a. Jurassic and Cretaceous biostratigraphy and organic matter geochemistry of the New Siberian Islands (Russian Arctic). Russian Geology and Geophysics, 59, pp. 168–185. https://doi.org/10.1016/j.rgg.2018.01.014

Nikitenko, B.L., Pestchevitskaya, E.B., and Khafaeva, S.N. 2018b. High-resolution stratigraphy and palaeoenvironments of the Volgian–Valanginian in the Olenek section (Anabar–Lena region, Arctic Eastern Siberia). Revue de Micropalaeontology, 61, pp. 271–312. https://doi.org/10.1016/j.revmic.2018.07.001

Nilsson, T. 1958. Uber das Vorkommen eines mesozoischen Sapropelgesteins in Schonen. Lunds Universitets Arsskrift, Ny Följd, Avd. 2, 54 (10), pp. 1–112.

Olaussen, S., Larssen, G.B., Helland-Hansen, W., Johannessen, E.P., Nottvedt, A., Riis, F., Rismyhr, B., Smelror, M., and Worsley, D. 2018. Mesozoic strata of Kong Karls Land, Svalbard, Norway; a link to the northern Barents Sea basins and platforms. Norwegian Journal of Geology, 98, pp. 1–69. https://doi.org/10.17850/njg98-4-06

Paterson, N.W. and Mangerud G. 2015. Late Triassic (Carnian–Rhaetian) palynology of Hopen, Svalbard. Review of Palaeobotany and Palynology, 220, pp. 98–119. https://doi.org/10.1016/j.revpalbo.2015.05.001

Pestchevitskaya, E., Lebedeva, N., and Ryabokon, A. 2011. Uppermost Jurassic and lowermost Cretaceous dinocyst successions of Siberia, the Subarctic Urals and Russian Platform and their interregional correlation. Geologicia Carpathica, 62, pp. 189–202. https://doi.org/10.2478/v10096-011-0016-9

Piasecki, S. 1980. Mid to Late Jurassic dinoflagellate cyst stratigraphy from Milne Land (East Greenland). Ph.D. thesis, University of Copenhagen (unpublished), 167 pp. https://doi.org/10.37570/bgsd-1979-28-06

Piasecki, S. 1996. Boreal dinoflagellate cyst stratigaphy of Middle to Upper Jurassic sediments of Milne Land, East Greenland. *In* Formation of source and reservoir rocks in a sequence stratigraphic framework, Jameson Land, East Greenland. *Edited by* S. Piasecki *et al.* Energy research programme EFP-93, projects 1313/93-0010 and 0017. Danmarks og Grønlands Geologiske Undersøgelse Rapport 1996/30, v 1–2, 100 pp.

Piasecki, S. 2001. Three new Middle Jurassic dinoflagellate cysts from East Greenland. Neues Jahrbuch für Geologie und Paläontologie Abhandlungen, 219, pp. 15–31. https://doi.org/10.1127/njgpa/219/2001/15

Piasecki, S. and Stemmerik, L. 2004. Jurassic dinoflagellate cysts from Hochstetter Forland, North-East Greenland. Geological Survey of Denmark and Greenland Bulletin, 5, pp. 89–97. https://doi.org/10.34194/geusb.v5.4809

Piasecki, S., Larsen, M., Therkelsen, J., and Vosgerau, H. 2004a. Jurassic dinoflagellate cyst stratigraphy of Hold with Hope, North-East Greenland. Geological Survey of Denmark and Greenland Bulletin, 5, pp. 73–88. https://doi.org/10.34194/geusb.v5.4808

Piasecki, S., Callomon, J.H., and Stemmerik, L. 2004b. Jurassic dinoflagellate cyst stratigraphy of Store Koldewey, North-East Greenland. Geological Survey of Denmark and Greenland Bulletin, 5, pp. 99–112. https://doi.org/10.34194/geusb.v5.4810

Pimpirev, C. and Pavlishina, P. 2005a. New data on the stratigraphy and palynological asessments of the Upper Jurassic–Lower Cretaceous sediments in the area of Lake Hazen, Ellesmere Island, Canadian Arctic. Comptes rendus de l'Académie bulgare des Sciences, 58, pp. 783–788.

Pimpirev, C. and Pavlishina, P. 2005b. Stratigraphy, age constraints and paleoenvironmental interpretations of the Upper Jurassic–Lower Cretaceous sediments in the area of Lake Hazen, Ellesmere Island, Canadian Arctic. Proceedings of Anniversary International Scientific Conference, Bulgarian Geological Society 80th Anniversary, pp. 14–17.

Playford, G. 1965. Plant microfossils from Triassic sediments near Poatina, Tasmania. Journal of the Geological Society of Australia, 12, pp. 173–210. https://doi.org/10.1080/00167616508728592

Pocock, S.A.J. 1976. A preliminary dinoflagellate zonation of the uppermost Jurassic and lower part of the Cretaceous, Canadian Arctic, and possible correlation in the Western Canadian basin. Geoscience and Man, 16, pp. 101–114. https://doi.org/10.1080/00721395.1976.9989778

Pocock, S.A.J. 1980. Palynology at the Jurassic–Cretaceous boundary in North America. Proceedings of the Fourth International Palynological Conference, Lucknow (1976–1977), 2, pp. 377–385 (cover date 1978).

Pocock, S.A.J. and Sarjeant, W.A.S. 1972. Partitomorphitae, a new subgroup of Triassic and Jurassic acritarchs. Bulletin of the Geological Society of Denmark, 21, pp. 346–357.

Poulsen, N.E. 1985. Dinocystestratigrafien i den nedre del af Hareelv Formation (Øvre Jura), Jameson Land, Østgrønland. Dansk Geologisk Forening Årsskrift, 1984, pp. 133–137.

Poulsen, N.E. 1991. *Gonyaulacysta jurassica desmos*, a new subspecies of dinoflagellate cyst from the early Oxfordian (Late Jurassic) of northwestern Europe and East Greenland. Palynology, 15, pp. 211–217. https://doi.org/10.1080/01916122.1991.9989396

Poulton, T.P. 1989. Current status of Jurassic biostratigraphy and stratigraphy, northern Yukon and adjacent Mackenzie Delta. *In* Current Research, Part G. Geological Survey of Canada Paper, 89-1G, pp. 25–30. https://doi.org/10.4095/127560

Poulton, T.P., Leskiw, K., and Audretsch, A. 1982. Stratigraphy and microfossils of the Jurassic Bug Creek Group of northern Richardson Mountains, northern Yukon and

adjacent Northwest Territories. Geological Survey of Canada Bulletin, 325, 137 pp. https://doi.org/10.4095/111358

Riding, J.B. 1984. A palynological investigation of Toarcian to early Aalenian strata from the Blea Wyke area, Ravenscar, North Yorkshire. Proceedings of the Yorkshire Geological Society, 45, pp. 109–122. https://doi.org/10.1144/pygs.45.1-2.109

Riding, J.B. 2012a. The Jurassic dinoflagellate cyst *Gonyaulacysta dentata* (Raynaud 1978) Lentin and Vozzhennikova 1990 emend. nov.: an index species for the late Callovian to earliest Oxfordian of the northern hemisphere. Review of Palaeobotany and Palynology, 176–177, pp. 68–81. https://doi.org/10.1016/j.revpalbo.2012.02.008

Riding, J.B. 2012b. A compilation and review of the literature on Triassic, Jurassic, and earliest Cretaceous dinoflagellate cysts. American Association of Stratigraphic Palynologists Contributions Series, 46, 119 pp.

Riding, J.B. 2019. Vera Ivanovna Ilyina (1930–2018). Palynology, 43, pp. 349–354. https://doi.org/10.1080/01916122.2019.1586090

Riding, J.B. and Hubbard, R.N.L.B. 1999. Jurassic (Toarcian to Kimmeridgian) dinoflagellate cysts and paleoclimates. Palynology, 23, pp. 15–30. https://doi.org/10.1080/01916122.1999.9989516

Riding, J.B., and Ioannides, N.S. 1996. A review of Jurassic dinoflagellate cyst biostratigraphy and global provincialism. Bulletin de la Société Géologique de France, 167, pp. 3–14.

Riding, J.B. and Lucas-Clark, J. 2016. The life and scientific work of William R. Evitt (1923–2009). Palynology, 40, Supplement 1, 130 pp. https://doi.org/10.1080/01916122.2016.1147792

Riding, J.B. and Michoux, D. 2013. Further observations on the Jurassic dinoflagellate cyst *Gonyaulacysta dentata* (Raynaud 1978) Lentin and Vozzhennikova 1990 emended Riding 2012. Review of Palaeobotany and Palynology, 196, pp. 51–56. https://doi.org/10.1016/j.revpalbo.2013.01.010

Riding, J.B. and Thomas, J.E. 1992. Dinoflagellate cysts of the Jurassic System. *In* A stratigaphic index of dinoflagellate cysts. *Edited by* A.J. Powell. British Micropalaeontological Society Publication Series, Chapman and Hall, London, pp. 7–97. https://doi.org/10.1007/978-94-011-2386-0_2

Riding, J.B., Penn, I.E., and Woollam, R. 1985. Dinoflagellate cysts from the type area of the Bathonian Stage (Middle Jurassic; southwest England). Review of Palaeobotany and Palynology, 45, pp. 149–169. https://doi.org/10.1016/0034-6667(85)90068-5

Riding, J.B., Walton, W., and Shaw, D. 1991. Toarcian to Bathonian (Jurassic) palynology of the Inner Hebrides, northwest Scotland. Palynology, 15, pp. 115–179. https://doi.org/10.1080/01916122.1991.9989393

Riding, J.B., Fedorova, V.A., and Ilyina, V.I. 1999. Jurassic and lowermost Cretaceous dinoflagellate cyst biostratigarphy of the Russian Platform and northern Siberia. American Association of Stratigraphic Palynologists Contribution Series, 36, 179 pp.

Riding, J.B., Mantle, D.J., and Backhouse, J. 2010. A review of the chronostratigraphical ages of Middle Triassic to Late Jurassic dinoflagellate cyst biozones of the North West Shelf of Australia. Review of Palaeobotany and Palynology, 162, pp. 543–575. https://doi.org/10.1016/j.revpalbo.2010.07.008

Riding, J.B., Mariani, E., and Fensome, R.A. 2022. A review of the Jurassic dinoflagellate cyst genus *Gonyaulacysta* Deflandre 1964 emend. nov. Review of Palaeobotany and Palynology, 299, 104605. https://doi.org/10.1016/j.revpalbo.2022.104605

Rismyhr, B., Bjærke, T., Olaussen, S., Mulrooney, M.J., and Senger, K. 2019. Facies, palynostratigraphy and sequence stratigraphy of the Wilhelmøya Subgroup (Upper Triassic–Middle Jurassic) in western central Spitsbergen, Svalbard. Norwegian Journal of Geology, 99, pp. 189–218. https://doi.org/10.17850/njg001

Sarjeant, W.A.S. 1972. Dinoflagellate cysts and acritarchs from the Upper Vardekløft Formation (Jurassic) of Jameson Land, East Greenland. Medelelser Grønland, 195, pp. 1–65.

Schulz, E. 1967. Sporenpaläontologische Untersuchungen rätoliassischer Schichten im Zentralteil des Germanischen Beckens. Paläontologische Abhandlungen, Paläobotanik B2, pp. 427–633.

Shurygin, B.N., Nikitenko, B.L., Devyatov, V.PP., Ilyina, V.I., Meledina, S.V., Gaideburova, E.A., Dzyuba, O.S., Kazakov, A.M., and Mogucheva, N.K. 2000. Stratigraphy of oil and gas basins of Siberia: The Jurassic System Izd. SO RAN, Filial "Geo," Novosibirsk. (in Russian).

Smelror, M. 1988a. Bathonian to early Oxfordian dinoflagellate cysts and acritarchs from Kong Karls Land, Svalbard. Review of Palaeobotany and Palynology, 56, pp. 275–304. https://doi.org/10.1016/0034-6667(88)90061-9

Smelror, M. 1988b. Late Bathonian to early Oxfordian dinoflagellate cyst stratigraphy of Jameson Land, East Greenland. Grønlands Geologiske Undersøgelse Rapport, 137, pp. 135–159. https://doi.org/10.34194/rapggu.v137.8019

Smelror, M. 1991. Two new dinoflagellate cysts from the Middle Jurassic of the Barents Sea region. Journal of Micropalaeontology, 10, pp. 175–180. https://doi.org/10.1144/jm.10.2.175

Smelror, M. 1993. Biogeography of Bathonian to Oxfordian (Jurassic) dinoflagellates: Arctic, NW Europe and circum-Mediterranean regions. Palaeogeography, Palaeoclimatology, Palaeoecology, 102, pp. 121–160. https://doi.org/10.1016/0031-0182(93)90009-8

Smelror, M. 1994. Jurassic stratigraphy of the western Barents Sea region: a review. Geobios, 17, pp. 441–451. https://doi.org/10.1016/S0016-6995(94)80165-7

Smelror, M., and Below, R. 1992. Dinoflagellate biostratigraphy of the Toarcian to lower Oxfordian (Jurassic) of the Barents Sea region. *In* Arctic Geology and Petroleum Potential. *Edited by* T.O. Vorren, E. Bergsager, Ø.A. Dahl-Stammes, E. Holter, B. Johansen, E. Lie, and T.B. Lund. Norwegian Petroleum Society (NPF), Special Publication, 2, pp. 495–513. https://doi.org/10.1016/B978-0-444-

88943-0.50035-6

Smelror, M., and Dypvik, H. 2005. Marine microplankton biostratigraphy of the Volgian–Ryazanian boundary strata, western Barents Shelf. Norges Geologiske Undersøkelse Bulletin, 443, pp. 61–69.

Smelror, M., Mørk, A., Monteil, E., Rutledge, D., and Leereveld, H. 1998. The Klippfisk Formation — a new lithostratigraphic unit of lower Cretaceous platform carbonates on the western Barents Shelf. Polar Research, 17, pp. 181–202. https://doi.org/10.1111/j.1751-8369.1998.tb00271.x

Smelror, M., Larssen, G.B., Olaussen, S., Rømuld, A., and Williams, R. 2018. Late Triassic to Early Cretaceous palynostratigraphy of Kong Karls Land, Svalbard, Arctic Norway, with correlations to Franz Josef Land, Arctic Russia. Norwegian Journal of Geology, 98, pp. 1–31. https://doi.org/10.17850/njg004

Suneby L.B. and Hills L.V. 1988. Palynological zonation of the Heiberg Formation (Triassic–Jurassic) eastern Sverdrup Basin, Arctic Canada. Bulletin of Canadian Petroleum Geology, 36 (4), pp. 347–361.

Tan, J.T. and Hills, L.V. 1978. Oxfordian–Kimmeridgian dinoflagellate assemblage, Ringnes Formation, Arctic Canada. Current Research, Part C, Geological Survey of Canada, Paper 78-1C, pp. 63–73. https://doi.org/10.4095/104592

Thusu, B. 1978. Aptian to Toarcian dinoflagellate cysts from Arctic Norway. *In* Distribution of biostratigraphically diagnostic dinoflagellate cysts and miospores from the northwest European continental shelf and adjacent areas. *Edited by* B. Thusu. Continental Shelf Institute Publication, 100, pp. 61–95.

Tozer, E.T.1963. Mesozoic and Tertiary stratigraphy, western Ellesmere Island and Axel Heiberg Island, District of Franklin. Geological Survey of Canada, Paper 63-60, 38 pp. https://doi.org/10.4095/101061

Turner, H.E., Batenburg, S.J., Gale, A.S., and Gradstein, F.M. 2019. The Kimmeridge Clay Formation (Upper Jurassic–Lower Cretaceous) of the Norwegian Continental Shelf and Dorset, UK: a chemostratigraphic correlation. Newsletters on Stratigraphy, 52, pp. 1–32. https://doi.org/10.1127/nos/2018/0436

Valdes, P.J. and Sellwood, B.W. 1992. A palaeoclimate model for the Kimmeridgian. Palaeogeography, Palaeoclimatology, Palaeoecology, 95, pp. 47–72. https://doi.org/10.1016/0031-0182(92)90165-2

van de Schootbrugge, B., Houben, A.J.P., Ercan, F.E.Z., Verreussel, R., Kerstholt, S., Janssen, N.M.M., Nikitenko, B., and Suan, G. 2020. Enhanced Arctic–Tethys connectivity ended the Toarcian Oceanic Anoxic Event in NW Europe. Geological Magazine, 157, pp. 1593–1611. https://doi.org/10.1017/S0016756819001262

van Helden, B.G.T. 1977. Correlation of microplankton assemblages with ammonite faunas from the Jurassic Wilkie Point Formation, Prince Patrick Island, District of Franklin. Geological Survey of Canada Paper, 77–1B, pp. 163–171. https://doi.org/10.4095/102776

Vigran, J.O., Mangerud G., Mørk A., Worsley D., and Hochuli P.A. 2014. Palynology and geology of the Triassic succession of Svalbard and the Barents Sea. Geological Survey of Norway Special Publication 14, pp. 1–247.

Warrington, G. 1974. Studies in the palynological biostratigraphy of the British Trias. I. Reference sections in West Lancashire and North Somerset. Review of Palaeobotany and Palynology, 17, pp. 133–147. https://doi.org/10.1016/0034-6667(74)90095-5

Wharton, D.I. 1988. Dinoflagellates from Middle Jurassic sediments of Alaska. Palynology, 12, p. 248.

Wierzbowski, A. and Århus, N. 1990. Ammonite and dinoflagellate cyst succesion of an upper Oxfordian–Kimmeridgian black shale core from the Nordkapp Basin, southern Barents Sea. Newsletter on Stratigraphy, 22, pp. 7–19. https://doi.org/10.1127/nos/22/1990/7

Wierzbowski, A., Smelror, M., and Mørk, A. 2002. Ammonites and dinoflagellates in the upper Oxfordian and Kimmeridgian of the northeastern Norwegian Sea (Nordland VII offshore area): biostratigraphical and biogeograhical signicifance. Neues Jahrbuch für Geologie und Palaeontolgie, Abhandlungen, 226, pp. 145–164. https://doi.org/10.1127/njgpa/226/2002/145

Wiggins, V.D. 1973. The dinoflagellate family Pareodiniaceae: a discussion. Geoscience and Man, 11, pp. 95–115. https://doi.org/10.1080/00721395.1975.9989759

Witmer, R.J., Mickey, M.B., and Haga, H. 1981. Biostratigraphic correlations of selected test wells of National Petroleum Reserve in Alaska. United States Geological Survey Open-File Report, 81-1165, 89 pp. https://doi.org/10.3133/ofr811165

Wood, S.E.L., Riding, J.B., Fensome, R.A., and Williams, G.L. 2016: A review of the *Sentusidinium* complex of dinoflagellate cysts. Review of Palaeobotany and Palynology, 234, pp. 61–93. https://doi.org/10.1016/j.revpalbo.2016.08.008

Zakharov, V.A., Bogomolov, Yu.I., Ilyina, V.I., Konstantinov, A.G., Kurushin, N.I., Lebedeva, N.K., Meledina, S.V., Nikitenko, B.L., Sobolev, E.S., and Shurygin, B.N. 1997. Boreal zonal standard and biostratigraphy of the Siberian Mesozoic. Geologiya i Geofizika, 38, pp. 927–956.

Editorial responsibility: Robert A. Fensome

Supplementary data for this paper are available from the following links:
https://journals.lib.unb.ca/index.php/ag/article/view/32852/1882528176
https://journals.lib.unb.ca/index.php/ag/article/view/32852/1882528177
https://journals.lib.unb.ca/index.php/ag/article/view/32852/1882528178

APPENDIX A: TAXON NAMES WITH AUTHOR CITATIONS

Note that the references for the dinocyst author citations may be found in Fensome *et al.* (2019).

Acritarchs and Algae

Fromea tornatilis (Drugg 1978) Lentin and Williams 1981
Prolixosphaeridiopsis spissa (McIntyre and Brideaux 1980) Hogg and Bailey 1997
Pterospermopsis aureolata (Cookson and Eisenack 1958) Eisenack 1972

Dinocysts

Ambonosphaera calloviana Fensome 1979
Andreedinium arcticum Below 1987a (now *Phallocysta arctica*)
Apteodinium bucculiatum Davies 1983
Apteodinium granulatum Eisenack 1958
Apteodinium maculatum Eisenack and Cookson 1960
Arkellea teichophera (Sarjeant 1961) Below 1990
Atopodinium haromense Thomas and Cox 1988
Atopodinium prostatum Drugg 1978
Caligodinium aceras (Manum and Cookson 1964) Lentin and Williams 1973
Cassiculosphaeridia magna Davey 1974
Chlamydophorella ectotabulata Smelror 1989
Chytroeisphaeridia chytroeides (Sarjeant 1962) Downie and Sarjeant 1965
Chytroeisphaeridia? *mantellii* Gitmez and Sarjeant 1972 (now considered a taxonomic junior synonym of *Sentusidinium ringnesiorum)*
Corculodinium inaffectum (Drugg 1978) Courtinat 2000
Cribroperidinium? *ehrenbergii* (Gitmez 1970) Helenes 1984
Cribroperidinium globatum (Gitmez and Sarjeant 1972) Helenes 1984
Cribroperidinium granulatum (Klement 1960) Stover and Evitt 1978
Cribroperidinium? *longicorne* (Downie 1957) Lentin and Williams 1985
Cribroperidinium jubaris (Davies 1983) Lentin and Williams 1985
Cribroperidinium nuciforme (Deflandre 1962) Courtinat 1989
Cribroperidinium? *perforans* (Cookson and Eisenack 1958) Morgan 1980
Cribroperidinium? *perforans* subsp. *kunzeviense* (Vozzhennikova 1967) Lentin and Williams 1989
Cribroperidinium ? *perforans* subsp. *perforans (Cookson and Eisenack 1958) Morgan 1980*
Crussolia deflandrei Wolfard and Van Erve 1981 (now *Evansia deflandrei*)
Ctenidodinium combazii Dupin 1968
Ctenidodinium continuum Gocht 1970
Ctenidodinium? *schizoblatum* (Norris 1965) Lentin and Williams 1973
Dapcodinium priscum Evitt 1961
Dichadogonyaulax culmula (Norris 1965) Loeblich Jr. and Loeblich III 1968
Dichadogonyaulax sellwoodii Sarjeant 1975
Dingodinium cerviculum Cookson and Eisenack 1958
Dingodinium jurassicum Cookson and Eisenack 1958
Dingodinium minutum Dodekova 1975
Dodekovia bullula (Bjærke 1980) Below 1987a (now *Parvocysta bullula*)
Dodekovia syzygia Dörhöfer and Davies 1980
Egmontodinium? *diminutum* Davies 1983
Egmontodinium polyplacophorum Gitmez and Sarjeant 1972
Ellipsoidictyum cinctum Klement 1960
Endoscrinium galeritum (Deflandre 1939) Vozzhennikova 1967
Endoscrinium galeritum subsp. *reticulatum* (Klement 1960) Górka 1970
Endoscrinium subvallare (Sarjeant 1962) Lentin and Williams 1973
Epiplosphaera saturnalis (Brideaux and Fisher 1976) Dodekova 1994
Escharisphaeridia mantellii (Gitmez and Sarjeant 1972) Courtinat 1989 (now considered a taxonomic junior *synonym of Sentusidinium ringnesiorum)*

APPENDIX A: continued.

Escharisphaeridia pocockii (Sarjeant 1968) Erkmen and Sarjeant 1980 (now considered a taxonomic junior synonym of *Sentusidinium ringnesiorum)*
Escharisphaeridia rudis Davies 1983 (now considered a taxonomic junior synonym of *Sentusidinium ringnesiorum*)
Evansia Pocock 1972
Evansia dalei Smelror and Århus 1989
Evansia deflandrei (Wolfard and Van Erve 1981) Below 1990
Evansia evittii (Pocock 1972) Jansonius 1986
Evansia granochagrinata Below 1990
Evansia? *opeasatos* (Davies 1983) Jansonius 1986
Evansia zabra (Davies 1983) Jansonius 1986
Exochosphaeridium scitulum Singh 1971
Freboldinium arcticum Below 1990
Freboldinium regulum Below 1990
Freboldinium serrulatum (Davies 1983) Below 1990
Glossodinium dimorphum Ioannides *et al*. 1977
Gochteodinia mutabilis (Riley in Fisher and Riley 1980) Fisher and Riley 1982
Gochteodinia villosa (Vozzhennikova 1967) Norris1978
Gonyaulacysta adecta (Sarjeant 1982) Riding*et al*. 2022
Gonyaulacysta desmos (Poulsen 1991) Riding *et al*. 2022
Gonyaulacysta dualis (Brideaux and Fisher 1976) Stover and Evitt 1978
Gonyaulacysta jurassica (Deflandre 1939) Norris and Sarjeant 1965
Gonyaulacysta jurassica subsp. *adecta* var. *longicornis* (Deflandre 1938) Downie and Sarjeant 1965 *(now Gonyaulacysta longicornis)*
Gonyaulacysta jurassica subsp. *jurassica* (autonym, now redundant)
Gonyaulacysta longicornis (Deflandre 1939) Riding *et al*. 2022
Hystrichodinium? *lanceatum* Davies 1983
Imbatodinim kondratjevii Vozzhennikova 1967
Impletosphaeridium Morgenroth 1966a
Kalyptea stegasta (Sarjeant 1961a) Wiggins 1975
Komewuia glabra Cookson and Eisenack 1960
Lacrymodinium warrenii Albert *et al*. 1986
Lagenadinium callovianum Piel 1985 (now *Stephanelytron callovianum*)
Lanterna bulgarica Dodekova 1969
Lanterna? *cantrellii* (Sarjeant 1972) Williams *et al*. 1993
Leptodinium deflandrei (Riley in Fisher and Riley 1980) Lentin and Williams 1981
Leptodinium? *hyalodermopse* (Cookson and Eisenack 1958) Stover and Evitt 1978
Leptodinium mamilliferum (Deflandre 1939) Helenes 1984
Leptodinium mirabile Klement 1960
Leptodinium subtile Klement 1960
Leptodinium volgense Lentin and Williams 1981
Liesbergia liesbergensis Berger 1986 *Liesbergia scarburghensis* (Sarjeant 1964b) Berger 1986 (now *Trichodinium scarburghense*)
Limbodinium absidatum (Drugg 1978) Riding 1987
Lithodinia jurassica Eisenack 1935
Lunatadinium dissolutum Brideaux and McIntyre 1973
Mancodinium coalitum Morgenroth 1970
Mancodinium semitabulatum Morgenroth 1970
Meiourogonyaulax deflandrei Sarjeant 1968
Meiourogonyaulax planoseptata Riding 1987
Meiourogonyaulax valensii Sarjeant 1966
Mendicodinium Morgenroth 1970
Mendicodinium groenlandicum (Pocock and Sarjeant 1972) Davey 1979
Mendicodinium reticulatum Morgenroth 1970

APPENDIX A: continued.

Microdinium opacum Brideaux 1971
Mikrocysta erugata Bjærke 1980
Moesiodinium raileanui Antonesçu 1974
Muderongia simplex Alberti 1961
Nannoceratopsis deflandrei Evitt 1961b
Nannoceratopsis deflandrei subsp. *anabarensis* Ilyina in Ilyina *et al.* 1994
Nannoceratopsis deflandrei subsp. *senex* (van Helden 1977) Ilyina in Ilyina *et al.* 1994
Nannoceratopsis deflandrei subsp. *senex* var. C sensu Davies 1983
Nannoceratopsis gracilis Alberti 1961
Nannoceratopsis pellucida Deflandre 1939
Nannoceratopsis senex van Helden, 1977 (now *Nannoceratopsis deflandrei* subsp. *senex*)
Oligosphaeridium patulum Riding and Thomas 1988
Oligosphaeridium pulcherrimum (Deflandre and Cookson 1955) Davey and Williams 1966
Opaeopsomus wapellensis Pocock 1972
Ovalicysta hiata Bjærke 1980
Ovoidinium waltonii (Pocock 1972) Lentin and Williams 1976
Paragonyaulacysta Johnson and Hills 1973
Paragonyaulacysta? *borealis* (Brideaux and Fisher 1976) Stover and Evitt 1978
Paragonyaulacysta calloviensis Johnson and Hills 1973
Paragonyaulacysta capillosa (Brideaux and Fisher 1976) Stover and Evitt 1978
Paragonyaulacysta retiphragmata Dörhöfer and Davies 1980
Pareodinia asperata Riley in Fisher and Riley 1980
Pareodinia ceratophora Deflandre 1947
Pareodinia groenlandica Sarjeant 1972
Pareodinia prolongata Sarjeant 1959
Parvocysta bullula Bjærke 1980
Perisseiasphaeridium pannosum Davey and Williams 1966
Phallocysta arctica (Below 1987a) Riding 1994
Phallocysta elongata (Beju 1971) Riding 1994
Phallocysta eumekes Dörhöfer and Davies 1980
Phallocysta thomasii Smelror 1991
Pilosidinium filiatum (Davies, 1983) Courtinat 1989 (now considered a taxonomic junior synonym of *Sentusidinium capillatum*)
Prolixosphaeridium parvispinum (Deflandre 1937) Davey *et al.* 1969
Protobatioladinium elatmaense Riding and Ilyina 1996
Protobatioladinium? *elongatum* Riding and Ilyina 1998
Protobatioladinium westburiense Nøhr-Hansen 1986
Pyxidinopsis laminata (Davies 1983) Lentin and Williams 1985
Reutlingia cracens (Bjærke 1980) Prauss 1989
Rhynchodiniopsis cladophora (Deflandre 1939) Below 1981
Rhynchodiniopsis pennata (Riley in Fisher and Riley 1980) Jan du Chêne *et al.* 1985
Rigaudella aemula (Deflandre 1939) Below 1982
Rosswangia holotabulata (Davies 1983) Below 1987b
Rotosphaeropsis thule (Davey 1982) Riding and Davey 1989
Scriniocassis priscus (Gocht 1979) Below 1990
Scriniocassis weberi Gocht 1964
Scriniodinium anceps (Raynaud 1978) Jan du Chêne *et al.* 1986
Scriniodinium crystallinum (Deflandre 1939) Klement 1960
Scriniodinium dictyotum subsp. *dictyotum* Cookson and Eisenack 1960
Scriniodinium dictyotum subsp. *pyrum* Gitmez 1970
Scriniodinium inritibile Fisher and Riley 1980
Senoniasphaera jurassica (Gitmez and Sarjeant 1972) Lentin and Williams 1976

APPENDIX A: continued.

Sentusidinium capillatum (Davies 1983) Courtinat 1989
Sentusidinium ringnesiorum (Manum and Cookson 1964) Wood *et al*. 2016
Sentusidinium verrucosum (Sarjeant 1968) Sarjeant and Stover 1978
Sirmiodinium grossii Alberti 1961
Stephanelytron Sarjeant 1961a
Stephanelytron callovianum (Piel 1985) Courtinat 1999
Stephanelytron membranoideum (Vozzhennikova 1967) Courtinat 1999
Stiphrosphaeridium anthophorum (Cookson and Eisenack 1958) Lentin and Williams 1985 *Susadinium faustum* (Bjærke 1980) Lentin and Williams 1985
Susadinium scrofoides Dörhöfer and Davies 1980
Sverdrupiella Bujak and Fisher 1976
Sverdrupiella mutabilis Bujak and Fisher 1976
Systematophora? *ovata* Gitmez and Sarjeant 1972
Tanyosphaeridium isocalamum (Deflandre and Cookson 1955) Davey and Williams 1969
Trichodinium erinaceoides Davies 1983
Trichodinium scarburghense (Sarjeant 1964) Williams *et al* . 1993
Tubotuberella apatela (Cookson andEisenack 1960) Ioannides *et al* . 1977 *Tubotuberella dangeardii* (Sarjeant 1968) Stover and Evitt 1978
Tubotuberella dentata Raynaud 1978
Tubotuberella egemenii (Gitmez 1970) Stover and Evitt 1978
Tubotuberella rhombiformis Vozzhennikova 1967
Valensiella dictydia (Sarjeant 1972) Lentin and Williams 1993
Valensiella ovulum (Deflandre 1947) Eisenack 1963
Valvaeodinium aquilonium (Dörhöfer and Davies 1980) Below 1987b
Valvaeodinium cavum (Davies 1983) Below 1987b
Valvaeodinium leneae Piasecki 2001
Valvaeodinium perpunctatum (Wille and Gocht 1979) Below 1987b
Valvaeodinium punctatum (Wille and Gocht 1979) Below 1987b
Valvaeodinium spinosum (Fenton *et al*. 1980) Below 1987b
Wallodinium krutzschii (Alberti 1961) Habib 1972
Wanaea acollaris Dodekova 1975
Wanaea fimbriata Sarjeant 1961
Wanaea thysanota Woollam 1982
Wrevittia helicoidea (Eisenack andCookson 1960) Helenes and Lucas-Clark 1997

Miospores

Aratrisporites Leschik 1956
Aratrisporites laevigatus Bjærke and Manum 1977
Aratrisporites macrocavatus Bjærke and Manum 1977
Aratrisporites scabratus Klaus 1960
Aratrisporites tenuispinosus Playford 1965
Limbosporites lundbladiae Nilsson 1958
Lunatisporites rhaeticus (Schulz 1967) Warrington 1974
Quadraeculina anellaeformis Malyavkina 1949
Ricciisporites tuberculatus Lundblad 1954
Taeniasporites rhaeticus (Schulz 1967) Warrington 1974

APPENDIX B: SPREADSHEET SUMMARIZING PALYNOEVENTS

All mentions of ammonite zones refer to the Sub-Boreal ammonite zonation.

Event	Calibration
LO of *Aratrisporites*	Base of the ammonite *Psiloceras planorbis* Zone
LO of Common *Limbosporites lundbladiae*	Base of the ammonite *Psiloceras planorbis* Zone
LO of *Sverdrupiella mutabilis*	Base of the ammonite *Psiloceras planorbis* Zone
LO of Taeniate bisaccate pollen	Base of the ammonite *Psiloceras planorbis* Zone
LO of *Dapcodinium priscum*	Base of the ammonite *Arnioceras semicostatum* Zone
FO of *Mendicodinium reticulatum*	Base of the ammonite *Asteroceras obtusum* Zone
FO of *Valvaeodinium perpunctatum*	Base of the ammonite *Uptonia jamesoni* Zone
LO of *Valvaeodinium perpunctatum*	Base of the ammonite *Almaltheus margaritatus* Zone
FO of *Scriniocassis weberi*	50% up the ammonite *Amaltheus margaritatus* Zone
FO of *Freboldinium regulum*	50% up the ammonite *Pleuroceras spinatum* Zone
FO of *Susadinium scrofoides*	Base of the ammonite *Dactylioceras tenuicostatum* Zone
FO of *Phallocysta eumekes*	Base of the ammonite *Harpoceras serpentinum* Zone
FO of *Rosswangia holotabulata*	Base of the ammonite *Harpoceras serpentinum* Zone
FO of *Valvaeodinium aquilonium*	Base of the ammonite *Harpoceras serpentinum* Zone
FO of *Caligodinium aceras*	Base of the ammonite *Hildoceras bifrons* Zone
FO of *Dingodinium minutum*	Base of the ammonite *Hildoceras bifrons* Zone
FO of *Dodekovia syzygia*	Base of the ammonite *Hildoceras bifrons* Zone
FO of *Microdinium opacum*	Base of the ammonite *Hildoceras bifrons* Zone
FO of *Valvaeodinium cavum*	Base of the ammonite *Hildoceras bifrons* Zone
FO of *Nannoceratopsis gracilis*	17% up the ammonite *Hildoceras bifrons* Zone
FO of *Ovalicysta hiata*	50% up the ammonite *Hildoceras bifrons* Zone
FO of *Scriniocassis priscus*	50% up the ammonite *Hildoceras bifrons* Zone
LO of *Andreedinium arcticum*	50% up the ammonite *Hildoceras bifrons* Zone
LO of *Parvocysta bullula*	50% up the ammonite *Hildoceras bifrons* Zone
LO of *Reutlingia nasuta*	50% up the ammonite *Hildoceras bifrons* Zone
LO of *Susadinium faustum*	50% up the ammonite *Hildoceras bifrons* Zone
FO of *Opaeopsomus wapellensis*	Base of the ammonite *Haugia variabilis* Zone
FO of *Susadinium scrofoides*	Base of the ammonite *Haugia variabilis* Zone
FO of *Chytroeisphaeridia chytroeides*	Base of the ammonite *Grammoceras thouarsense* Zone
FO of *Valvaeodinium punctatum*	Base of the ammonite *Grammoceras thouarsense* Zone
LO of *Nannoceratopsis deflandrei* subsp. *senex* var C sensu Davies 1983	Base of the ammonite *Grammoceras thouarsense* Zone
LO of *Phallocysta elongata*	Base of the ammonite *Pleydellia aalensis* Zone
FO of *Phallocysta thomasii*	Base of the ammonite *Leioceras opalinum* Zone
LO of *Mikrocysta erugata*	Base of the ammonite *Leioceras opalinum* Zone
FO of *Evansia granochagrinata*	50% up the ammonite *Leioceras opalinum* Zone
LO of *Ovalicysta hiata*	50% up the ammonite *Leioceras opalinum* Zone
LO of *Freboldinium serrulatum*	Base of the ammonite *Hyperlioceras discites* Zone
LO of *Mancodinium coalitum*	Base of the ammonite *Hyperlioceras discites* Zone
LO of *Mancodinium semitabulatum*	Base of the ammonite *Hyperlioceras discites* Zone
LO of *Opaeopsomus wapellensis*	Base of the ammonite *Hyperlioceras discites* Zone
LO of *Scriniodinium dictyotum* subsp. *pyrum*	Base of the ammonite *Hyperlioceras discites* Zone
LO of *Valvaeodinium punctatum*	Base of the ammonite *Hyperlioceras discites* Zone
FO of *Freboldinium arcticum*	50% up the ammonite *Sonninia propinquans* Zone
LO of *Scriniocassis priscus*	50% up the ammonite *Sonninia propinquans* Zone
LO of *Mendicodinium reticulatum*	Base of the late Bajocian
LO of *Nannoceratopsis deflandrei* subsp. *senex*	Base of the late Bajocian
LO of *Parvocysta bullula*	Base of the late Bajocian
LO of *Phallocysta elongata*	Base of the late Bajocian
FO of *Evansia evittii*	Base of the ammonite *Zigzagiceras zigzag* Zone

APPENDIX B: Continued.

FO of *Protobatioladinium elatmaense*	Base of the ammonite *Zigzagiceras zigzag* Zone
FO of *Dichadogonyaulax sellwoodii*	75% up the ammonite *Zigzagiceras zigzag* Zone
FO of *Arkellea teichophera*	Base of the ammonite *Procerites hodsoni* Zone
FO of *Atopodinium prostatum*	Base of the ammonite *Procerites hodsoni* Zone
FO of *Paragonyaulacysta calloviensis*	Base of the ammonite *Procerites hodsoni* Zone
FO of *Paragonyaulacysta retiphragmata*	Base of the ammonite *Procerites hodsoni* Zone
FO of *Rhynchodiniopsis cladophora*	Base of the ammonite *Procerites hodsoni* Zone
FO of *Scriniodinium crystallinum*	Base of the ammonite *Procerites hodsoni* Zone
LO of *Valvaeodinium aquilonium*	Base of the ammonite *Procerites hodsoni* Zone
LO of *Wanaea acollaris*	Base of the ammonite *Procerites hodsoni* Zone
FO of *Lacrymodinium warrenii*	75% up the ammonite *Procerites hodsoni* Zone
FO of *Valensiella dictydia*	75% up the ammonite *Procerites hodsoni* Zone
LO of *Nannoceratopsis gracilis*	75% up the ammonite *Procerites hodsoni* Zone
LO of *Rosswangia holotabulata*	75% up the ammonite *Procerites hodsoni* Zone
FO of *Atopodinium haromense*	Base of the ammonite *Oxycerites orbis* Zone
FO of *Ellipsoidictyum cinctum*	Base of the ammonite *Oxycerites orbis* Zone
FO of *Evansia zabra*	Base of the ammonite *Oxycerites orbis* Zone
FO of *Evansia*? *opeasatos*	Base of the ammonite *Oxycerites orbis* Zone
FO of *Gonyaulacysta jurassica*	Base of the ammonite *Oxycerites orbis* Zone
FO of *Lithodinia jurassica*	Base of the ammonite *Oxycerites orbis* Zone
FO of *Paragonyaulacysta calloviensis*	Base of the ammonite *Oxycerites orbis* Zone
FO of *Paragonyaulacysta retiphragmata*	Base of the ammonite *Oxycerites orbis* Zone
FO of *Pareodinia ceratophora*	Base of the ammonite *Oxycerites orbis* Zone
FO of *Tubotuberella rhombiformis*	Base of the ammonite *Oxycerites orbis* Zone
LO of *Valvaeodinium leneae*	Base of the ammonite *Oxycerites orbis* Zone
LO of *Valvaeodinium spinosum*	Base of the ammonite *Oxycerites orbis* Zone
FO of *Evansia dalei*	Base of the ammonite *Macrocephalites herveyi* Zone
LO of *Protobatioladinium*? *elongatum*	Base of the ammonite *Macrocephalites herveyi* Zone
LO of *Susadinium scrofoides*	Base of the ammonite *Macrocephalites herveyi* Zone
FO of *Ambonosphaera calloviana*	Base of the ammonite *Proplanulites koenigi* Zone
FO of *Meiourogonyaulax planoseptata*	Base of the ammonite *Proplanulites koenigi* Zone
FO of *Pareodinia prolongata*	Base of the ammonite *Proplanulites koenigi* Zone
FO of *Stephanelytron callovianum*	Base of the ammonite *Proplanulites koenigi* Zone
FO of *Cribroperidinium granulatum*	Base of the ammonite *Kosmoceras jason* Zone
FO of *Cribroperidinium*? *perforans* subsp. *kunzeviense*	Base of the ammonite *Kosmoceras jason* Zone
FO of *Endoscrinium galeritum*	Base of the ammonite *Kosmoceras jason* Zone
FO of *Hystrichodinium*? *lanceatum*	Base of the ammonite *Kosmoceras jason* Zone
FO of *Komewuia glabra*	Base of the ammonite *Kosmoceras jason* Zone
FO of *Meiourogonyaulax valensii*	Base of the ammonite *Kosmoceras jason* Zone
FO of *Ovoidinium waltonii*	Base of the ammonite *Kosmoceras jason* Zone
FO of *Paragonyaulacysta*? *borealis*	Base of the ammonite *Kosmoceras jason* Zone
FO of *Rotosphaeropsis thule*	Base of the ammonite *Kosmoceras jason* Zone
FO of *Sentusidinium verrucosum*	Base of the ammonite *Kosmoceras jason* Zone
LO of *Ctenidodinium combazii*	Base of the ammonite *Kosmoceras jason* Zone
LO of *Paragonyaulacysta calloviensis*	Base of the ammonite *Kosmoceras jason* Zone
LO of *Paragonyaulacysta retiphragmata*	Base of the ammonite *Kosmoceras jason* Zone
LO of *Valensiella ovulum*	Base of the ammonite *Kosmoceras jason* Zone
LO of *Dichadogonyaulax sellwoodii*	Base of the ammonite *Erymnoceras coronatum* Zone
FO of *Evansia deflandrei*	Base of the ammonite *Peltoceras athleta* Zone
FO of *Gonyaulacysta jurassica* var. *longicornis*	Base of the ammonite *Peltoceras athleta* Zone
FO of *Wanaea thysanota*	Base of the ammonite *Peltoceras athleta* Zone

APPENDIX B: Continued.

LO of *Liesbergia liesbergensis*	Base of the ammonite *Peltoceras athleta* Zone
FO of *Trichodinium scarburghense*	Base of the ammonite *Quenstedtoceras lamberti* Zone
LO of *Pareodinia prolongata*	Base of the ammonite *Quenstedtoceras lamberti* Zone
FO of *Gonyaulacysta jurassica* subsp. *desmos*	Base of the ammonite *Quenstedtoceras mariae* Zone
FO of *Wanaea fimbriata*	Base of the ammonite *Quenstedtoceras mariae* Zone
LO of *Ambonosphaera calloviana*	Base of the ammonite *Quenstedtoceras mariae* Zone
LO of *Ctenidodinium continuum*	Base of the ammonite *Quenstedtoceras mariae* Zone
LO of *Meiourogonyaulax planoseptata*	Base of the ammonite *Quenstedtoceras mariae* Zone
LO of *Valensiella dictydia*	Base of the ammonite *Quenstedtoceras mariae* Zone
FO of *Leptodinium mirabile*	50% up the ammonite *Quenstedtoceras mariae* Zone
LO of *Gonyaulacysta dentata*	50% up the ammonite *Quenstedtoceras mariae* Zone
LO of *Limbodinium absidatum*	50% up the ammonite *Quenstedtoceras mariae* Zone
LO of *Wanaea thysanota*	50% up the ammonite *Quenstedtoceras mariae* Zone
FO of *Gonyaulacysta jurassica* subsp. *jurassica*	50% up the ammonite *Cardioceras cordatum* Zone
LO of *Gonyaulacysta jurassica* subsp. *desmos*	Base of the ammonite *Perisphinctes plicatilis* Zone
LO of *Wanaea fimbriata*	Base of the ammonite *Perisphinctes plicatilis* Zone
FO of *Gonyaulacysta dualis*	Base of the ammonite *Perisphinctes pumilus* Zone
FO of *Sentusidinium ringnesiorum*	Base of the ammonite *Perisphinctes pumilus* Zone
LO of *Trichodinium scarburghense*	Base of the ammonite *Perisphinctes pumilus* Zone
FO of *Cribroperidinium globatum*	Base of the ammonite *Perisphinctes cautisnigrae* Zone
LO of *Gonyaulacysta jurassica* var. *longicornis*	Base of the ammonite *Perisphinctes cautisnigrae* Zone
LO of *Rigaudella aemula*	Base of the ammonite *Perisphinctes cautisnigrae* Zone
FO of *Leptodinium subtile*	50% up the ammonite *Perisphinctites cautisnigrae* Zone
FO of *Apteodinium granulatum*	Base of the ammonite *Pictonia baylei* Zone
FO of *Cribroperidinium*? *ehrenbergii*	Base of the ammonite *Pictonia baylei* Zone
FO of *Cribroperidinium*? *perforans* subsp. *perforans*	Base of the ammonite *Pictonia baylei* Zone
FO of *Glossodinium dimorphum*	Base of the ammonite *Pictonia baylei* Zone
FO of *Leptodinium*? *hyalodermopse*	Base of the ammonite *Pictonia baylei* Zone
FO of *Lunatadinium dissolutum*	Base of the ammonite *Pictonia baylei* Zone
FO of *Pareodinia groenlandica*	Base of the ammonite *Pictonia baylei* Zone
FO of *Perisseiasphaeridium pannosum*	Base of the ammonite *Pictonia baylei* Zone
FO of *Pyxidinopsis laminata*	Base of the ammonite *Pictonia baylei* Zone
FO of *Scriniodinium anceps*	Base of the ammonite *Pictonia baylei* Zone
FO of *Sentusidinium capillatum*	Base of the ammonite *Pictonia baylei* Zone
FO of *Tubotuberella egemenii*	Base of the ammonite *Pictonia baylei* Zone
FO of *Wallodinium krutzschii*	Base of the ammonite *Pictonia baylei* Zone
FO of *Wrevittia helicoidea*	Base of the ammonite *Pictonia baylei* Zone
LO of *Apteodinium bucculiatum*	Base of the ammonite *Pictonia baylei* Zone
LO of *Arkellea teichophera*	Base of the ammonite *Pictonia baylei* Zone
LO of *Egmontodinium*? *diminutum*	Base of the ammonite *Pictonia baylei* Zone
LO of *Evansia deflandrei*	Base of the ammonite *Pictonia baylei* Zone
LO of *Evansia evittii*	Base of the ammonite *Pictonia baylei* Zone
LO of *Evansia zabra*	Base of the ammonite *Pictonia baylei* Zone
LO of *Evansia*? *opeasatos*	Base of the ammonite *Pictonia baylei* Zone
LO of *Komewuia glabra*	Base of the ammonite *Pictonia baylei* Zone
LO of *Meiourogonyaulax deflandrei*	Base of the ammonite *Pictonia baylei* Zone
LO of *Scriniodinium crystallinum*	Base of the ammonite *Pictonia baylei* Zone
LO of *Sentusidinium verrucosum*	Base of the ammonite *Pictonia baylei* Zone
LO of *Stephanelytron membranoideum*	Base of the ammonite *Pictonia baylei* Zone
LO of *Nannoceratopsis pellucida*	50% up the ammonite *Pictonia baylei* Zone
FO of *Apteodinium maculatum*	Base of the ammonite *Rasenia cymodoce* Zone

APPENDIX B: Continued.

FO of *Cribroperidinium jubaris*	Base of the ammonite *Aulacostephanus mutabilis* Zone
FO of *Dingodinium jurassicum*	Base of the ammonite *Aulacostephanus mutabilis* Zone
FO of *Egmontodinium polyplacophorum*	Base of the ammonite *Aulacostephanus mutabilis* Zone
FO of *Epiplosphaera saturnalis*	Base of the ammonite *Aulacostephanus mutabilis* Zone
FO of *Gochteodinia mutabilis*	Base of the ammonite *Aulacostephanus mutabilis* Zone
FO of *Paragonyaulacysta capillosa*	Base of the ammonite *Aulacostephanus mutabilis* Zone
FO of *Protobatioladinium westburiense*	Base of the ammonite *Aulacostephanus mutabilis* Zone
FO of *Scriniodinium inritibile*	Base of the ammonite *Aulacostephanus mutabilis* Zone
FO of *Stephanelytron membranoideum*	Base of the ammonite *Aulacostephanus mutabilis* Zone
LO of *Cribroperidinium*? *perforans* subsp. *kunzeviense*	Base of the ammonite *Aulacostephanus mutabilis* Zone
LO of *Endoscrinium subvallare*	Base of the ammonite *Aulacostephanus mutabilis* Zone
LO of *Lanterna*? *cantrellii*	Base of the ammonite *Aulacostephanus mutabilis* Zone
LO of *Lithodinia jurassica*	Base of the ammonite *Aulacostephanus mutabilis* Zone
FO of *Cassiculosphaeridia magna*	Base of the ammonite *Aulacostephanus eudoxus* Zone
FO of *Cribroperidinium*? *perforans*	Base of the ammonite *Aulacostephanus eudoxus* Zone
FO of *Oligosphaeridium pulcherrimum*	Base of the ammonite *Aulacostephanus eudoxus* Zone
FO of *Corculodinium inaffectum*	Base of the ammonite *Aulacostephanus autissiodorensis* Zone
FO of *Lanterna bulgarica*	Base of the ammonite *Pectinatites elegans* Zone
FO of *Leptodinium volgense*	Base of the ammonite *Pectinatites elegans* Zone
FO of *Pareodinia asperata*	Base of the ammonite *Pectinatites elegans* Zone
FO of *Dingodinium cerviculum*	Base of the ammonite *Pectinatites scitulus* Zone
FO of *Exochosphaeridium scitulum*	Base of the ammonite *Pectinatites scitulus* Zone
FO of *Leptodinium deflandrei*	Base of the ammonite *Pectinatites scitulus* Zone
FO of *Rhynchodiniopsis pennata*	Base of the ammonite *Pectinatites scitulus* Zone
FO of *Stiphrosphaeridium anthophorum*	Base of the ammonite *Pectinatites scitulus* Zone
FO of *Tanyosphaeridium isocalamum*	Base of the ammonite *Pectinatites scitulus* Zone
FO of *Tubotuberella apatela*	Base of the ammonite *Pectinatites scitulus* Zone
LO of *Pyxidinopsis laminata*	Base of the ammonite *Pectinatites scitulus* Zone
LO of *Sentusidinium ringnesiorum*	Base of the ammonite *Pectinatites scitulus* Zone
FO of *Muderongia simplex*	Base of the ammonite *Pavlovia pallasioides* Zone
LO of *Gonyaulacysta dualis*	Base of the ammonite *Pavlovia pallasioides* Zone
LO of *Pareodinia asperata*	Base of the ammonite *Pavlovia pallasioides* Zone
LO of *Rhynchodiniopsis cladophora*	Base of the ammonite *Pavlovia pallasioides* Zone
LO of *Scriniodinium dictyotum* subsp. *dictyotum*	Base of the ammonite *Pavlovia pallasioides* Zone
LO of *Senoniasphaera jurassica*	Base of the ammonite *Pavlovia pallasioides* Zone
LO of *Tubotuberella dangeardii*	Base of the ammonite *Pavlovia pallasioides* Zone
LO of *Tubotuberella egemenii*	Base of the ammonite *Pavlovia pallasioides* Zone
LO of *Cribroperidinium granulatum*	Base of the ammonite *Progalbanites albani* Zone
LO of *Cribroperidinium nuciforme*	Base of the ammonite *Progalbanites albani* Zone
LO of *Egmontodinium polyplacophorum*	Base of the ammonite *Progalbanites albani* Zone
LO of *Imbatodinim kondratjevii*	Base of the ammonite *Progalbanites albani* Zone
LO of *Leptodinium deflandrei*	Base of the ammonite *Progalbanites albani* Zone
LO of *Leptodinium volgense*	Base of the ammonite *Progalbanites albani* Zone
LO of *Scriniodinium anceps*	Base of the ammonite *Progalbanites albani* Zone
LO of *Scriniodinium inritibile*	Base of the ammonite *Progalbanites albani* Zone
LO of *Systematophora*? *ovata*	Base of the ammonite *Progalbanites albani* Zone
FO of *Prolixosphaeridiopsis spissa*	Base of the ammonite *Glaucolithites glaucolithus* Zone
LO of *Atopodinium prostatum*	Base of the ammonite *Glaucolithites glaucolithus* Zone
LO of *Cribroperidinium jubaris*	Base of the ammonite *Glaucolithites glaucolithus* Zone
LO of *Glossodinium dimorphum*	Base of the ammonite *Glaucolithites glaucolithus* Zone
LO of *Pareodinia groenlandica*	Base of the ammonite *Glaucolithites glaucolithus* Zone

APPENDIX B: Continued.

FO of *Leptodinium mamilliferum*	Base of the ammonite *Titanites anguiformis* Zone
FO of *Moesiodinium raileanui*	Base of the ammonite *Titanites anguiformis* Zone
FO of *Trichodinium erinaceoides*	Base of the ammonite *Titanites anguiformis* Zone
LO of *Oligosphaeridium patulum*	Base of the ammonite *Titanites anguiformis* Zone
LO of *Prolixosphaeridium parvispinum*	Base of the ammonite *Paracraspedites oppressus* Zone
FO of *Ctenidodinium*? *schizoblatum*	Base of the ammonite *Subcraspedites primitivus* Zone
FO of *Dichadogonyaulax culmula*	Base of the ammonite *Subcraspedites primitivus* Zone
FO of *Gochteodinia villosa*	Base of the ammonite *Subcraspedites primitivus* Zone
LO of *Cribroperidinium*? *longicorne* LO	Base of the ammonite *Subcraspedites primitivus* Zone
of *Lanterna bulgarica*	Base of the ammonite *Subcraspedites primitivus* Zone
LO of *Rhynchodiniopsis pennata*	Base of the ammonite *Subcraspedites primitivus* Zone

APPENDIX C: REFERENCE WELLS.

Charts showing palynological analyses of Beechey Point State 1 reference well (onshore northern Alaska) which provides supporting evidence for palynoevent events. The following pages includes three relevant wells that are reproduced from Mangerud *et al.* (2021) which also provide supporting evidence for palynoevent events: Fireweed 1 (offshore northern Alaska), Klondike OCS-Y-1482 (Chukchi Sea), and Romulus C-67 (Sverdrup Basin).

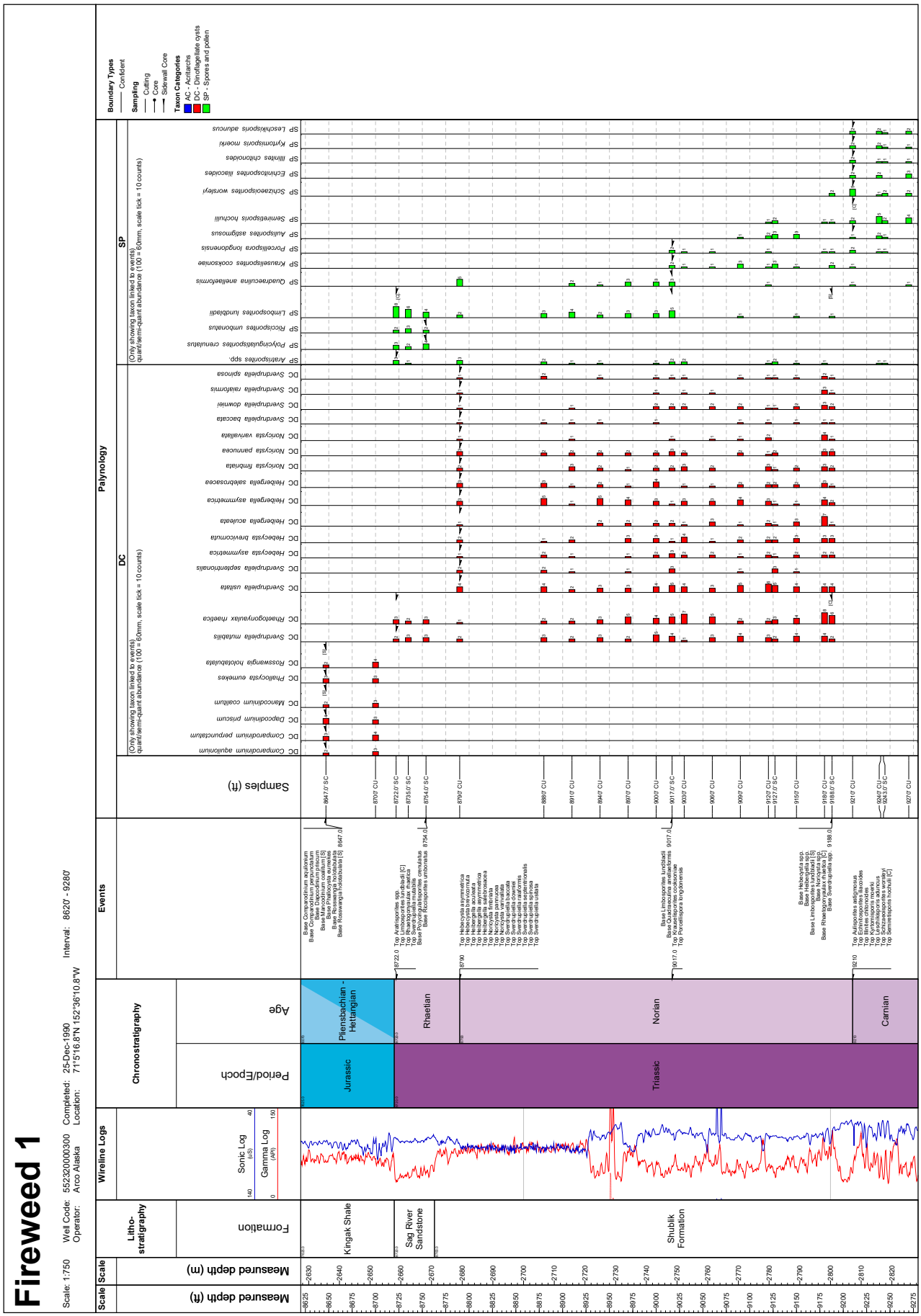

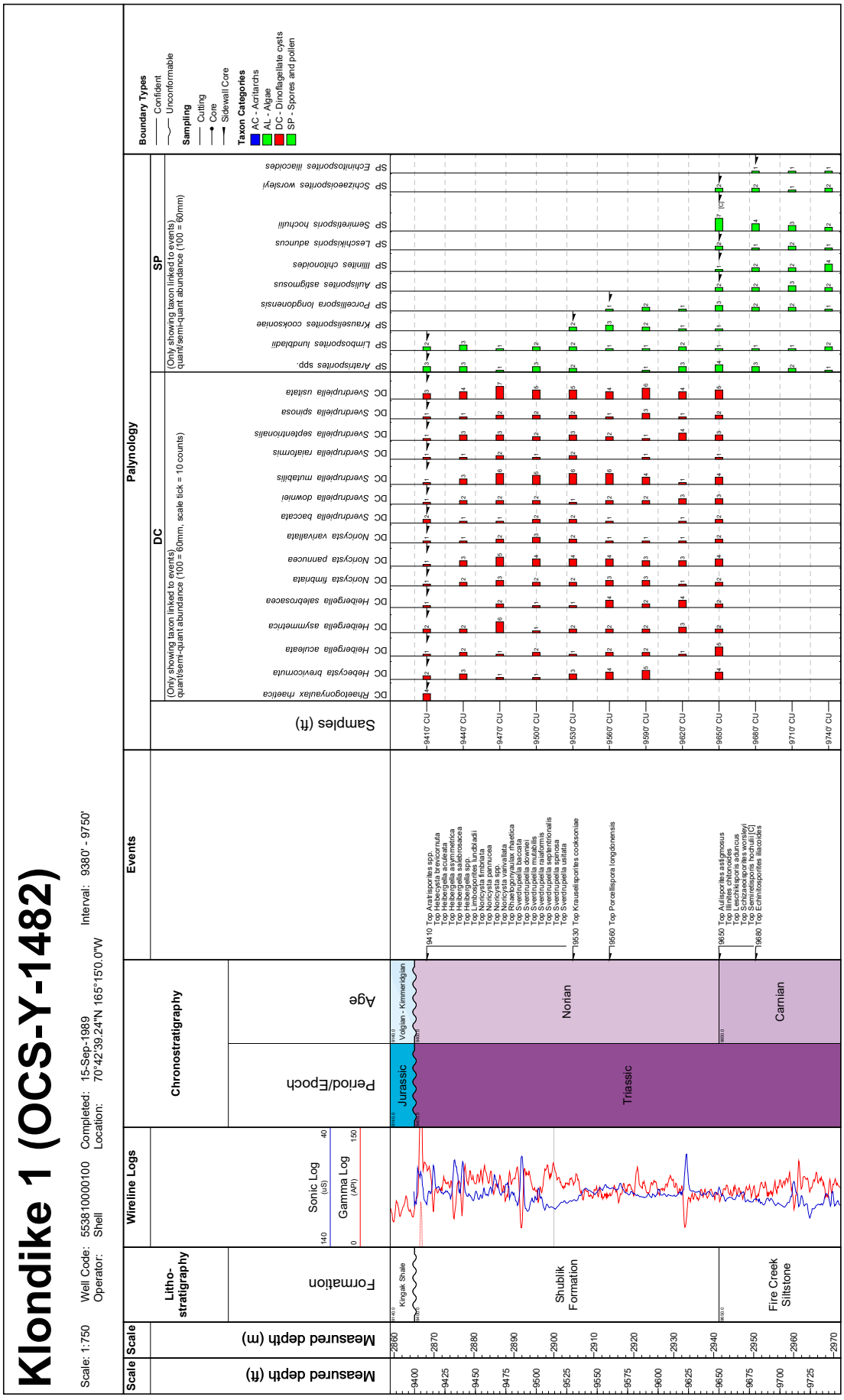

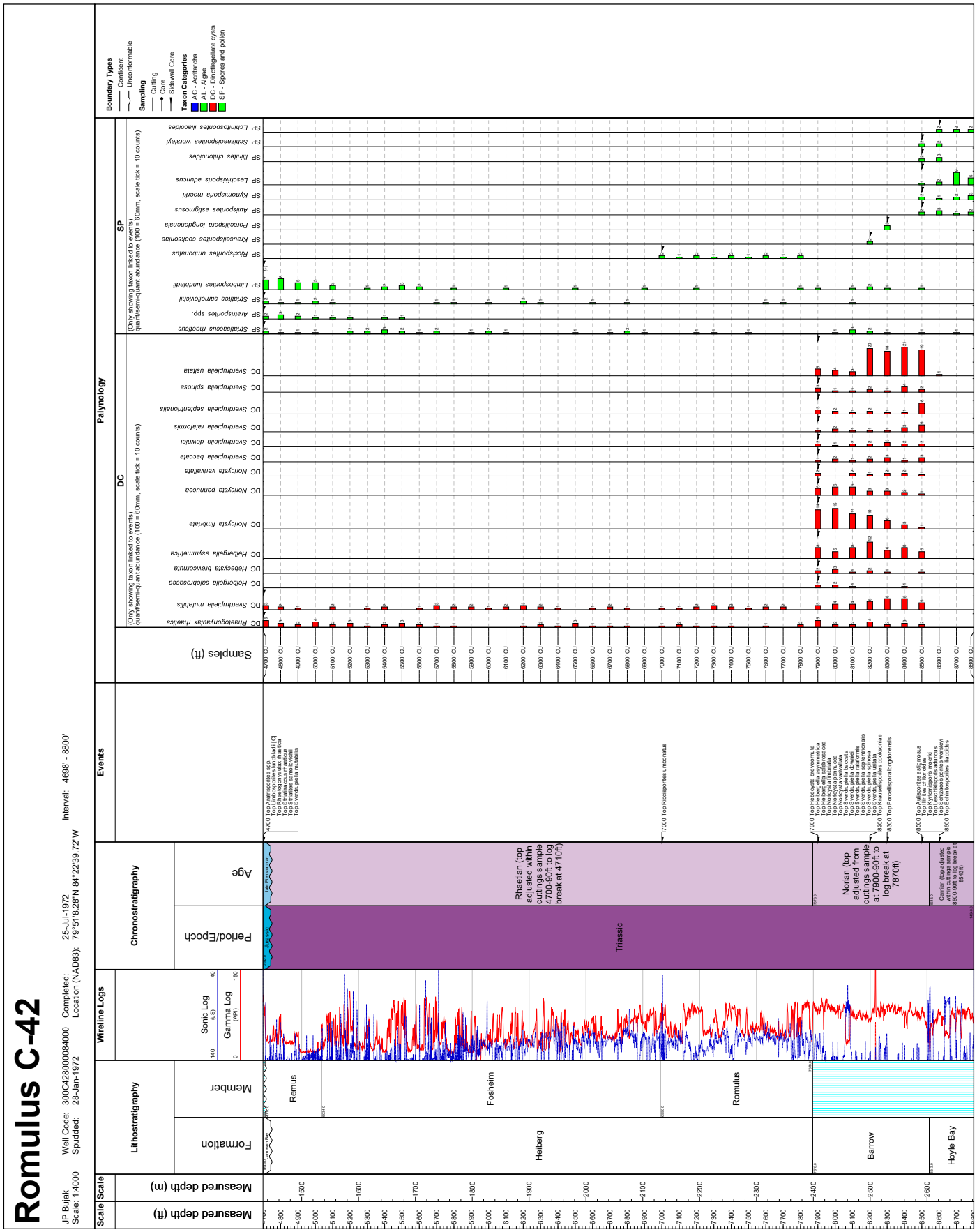

Further evidence for the East Coast fault system and faults associated with the Summerville restraining bend and their possible relationship to the 1886 Charleston earthquake, South Carolina, USA

Ronald T. Marple [1] and James D. Hurd, Jr.[2]

1. 215 Cattail Circle, Harker Heights, Texas 76548, USA
2. Department of Natural Resources and the Environment, The University of Connecticut U-87, 1376 Storrs Road, Storrs, Connecticut 06269-4087, USA
Corresponding author <ronmarple@verizon.net>

Date received: 31 January 2022 ¶ Date accepted:28 April 2022

ABSTRACT

The integration of aeromagnetic, LiDAR, and previously acquired seismic-reflection data and surficial geologic maps supports the existence of the East Coast fault system (ECFS) and faults associated with its 12° Summerville restraining bend beneath the South Carolina Coastal Plain. Aeromagnetic data revealed a 10- to 15-km-wide zone of subtle, 22- to 35-km-long linear magnetic anomalies trending ~N10°E across the southern meizoseismal area of the 1886 Charleston earthquake that we postulate are associated with Cenozoic low-displacement brittle faults in the crystalline basement west of Charleston. We hypothesize that lineaments ML4 and ML5 represent the principal displacement zone along the southern end of the ECFS because they coincide with steeply dipping, west-side-up buried faults interpreted from previously acquired seismic-reflection profiles and dextral offset of ~320 m in the Brownsville Pleistocene beach ridge deposit. The alignment of the NNE-SSW-oriented Edisto dome, uplift along releveling line 9, gently upwarped longitudinal profiles along the Caw Caw and Horse Savanna swamps, local incision along the Ashley River, and exposures of the early Oligocene Ashley Formation near the incised part of the Ashley River support Quaternary uplift along the southern ECFS. The 12° change in trend formed by lineaments ML4 and ML5 supports the existence of the Summerville restraining bend along the ECFS, east of which are numerous ENE-WSW- to NW-SE-oriented LiDAR lineaments that we postulate are surface expressions of faults that formed to compensate for the increased compression produced by dextral motion along the bend. Sinistral displacement along one of these proposed faults associated with the ~40-km-long, east-west-oriented Deer Park lineament may have produced the main shock of the 1886 Charleston earthquake.

RÉSUMÉ

L'intégration de données aéromagnétiques, de données lidar et de données de réflexion sismique récemment obtenues ainsi que de cartes géologiques de surface appuie l'existence du système de failles de la Côte est (SFCE) et des failles associées à son inflexion de restriction de 12 degrés de Summerville au-dessous de la plaine côtière de la Caroline du Sud. Les données aéromagnétiques ont révélé une zone de 10 à 15 kilomètres de largeur d'anomalies magnétiques linéaires subtiles sur une longueur de 22 à 35 kilomètres, orientées approximativement vers le nord à 10 degrés est à travers l'aire pléistoséiste méridionale du séisme de Charleston de 1886 qui, postulons-nous, sont associés à des failles cassantes de faible déplacement, cénozoïques, dans le socle cristallin à l'ouest de Charleston. Nous supposons que les linéaments ML4 et ML5 représentent la principale zone de déplacement le long de l'extrémité méridionale du SFCE parce qu'ils coïncident avec des failles enfouies dont le toit est à l'ouest et qui s'inclinent profondément, interprétées à partir de profils de réflexion sismique précédemment obtenus et du mouvement dextre d'environ 320 mètres dans le dépôt de la levée de plage du Pléistocène de Brownsville. L'alignement du dôme Edisto orienté du nord-nord-est au sud-sud-ouest, le soulèvement le long de la ligne du levé d'appoint 9, les profils longitudinaux doucement bombés le long des marécages Caw Caw et Horse Savanna, l'incision locale longeant la rivière Ashley et les affleurements de la Formation de l'Oligocène précoce d'Ashley près de la partie enfoncée de la rivière Ashley appuient l'hypothèse d'un soulèvement quaternaire le long du SFCE méridional. La variation de 12 degrés de l'orientation créée par les linéaments ML4 et ML5 appuie l'existence de l'inflexion de restriction de Summerville dans le SFCE, à l'est des nombreux linéaments lidar orientés de l'est-

doi:10.4138/atlgeo.2022.004

nord-est/ouest-sud-ouest au nord-ouest/sud-est que nous supposons des expressions en surface de failles qui se sont formées pour compenser la compression accrue produite par le mouvement dextre le long de l'inflexion. Le mouvement senestre le long des failles proposées associé au linéament d'une quarantaine de kilomètres de longueur orienté d'est en ouest de Deer Park pourrait avoir produit la principale secousse du séisme de Charleston de 1886.

[*Traduit par la redaction*]

INTRODUCTION

The main shock of the August 31, 1886 earthquake occurred northwest of Charleston, South Carolina, near Woodstock at ~9:51 PM, followed 8–10 minutes later by a smaller earthquake west of Rantowles to the south (Dutton 1889, pp. 215 and 273) (Fig. 1). Moment magnitude, M_w, estimates of the main shock range from 6.9 (Bakun and Hopper 2004) to 7.3 (Johnston 1996). Based on Wells and Coppersmith's (1994) study of earthquake magnitude versus fault rupture length, the fault rupture that produced the main shock was likely at least 25 km long.

Contemporary reports suggest that two epicenters were associated with the Charleston earthquake (Woodstock and Rantowles) (Dutton 1889) and possibly a third one near Middleton Place (McKinley 1887) (Fig. 1). The location of the Rantowles epicenter is less certain because of fewer anthropogenic structures and swampier conditions in the southern meizoseismal area (Dutton 1889). The complex shape of Earle Sloan's isoseismal contours (Dutton 1889, plate XXVII) (Fig. 1) and the 8–10 minute separation between the two earthquakes suggest that at least two faults ruptured August 31, 1886: one trending east-west north of the Ashley River and the other trending NNE-SSW in the southern meizoseismal area. The right-lateral displacement of the Charleston & Savannah Railroad near Rantowles (Dutton 1889, plate XXV) (Fig. 2) suggests that the second earthquake west of Rantowles was produced by dextral strike-slip displacement on a NNE-SSW-oriented fault.

Despite numerous investigations of the meizoseismal area (e.g., Rankin 1977; Gohn 1983), the location and orientation of the causative faults have remained elusive for several reasons. First, the modern seismicity in the area has been sparse and clustered (e.g., Chapman *et al.* 2016), rather than along well-defined trends. Furthermore, little seismicity has been recorded in the areas of greatest intensity near Woodstock and Rantowles (Fig. 2). Thus, the Middleton Place-Summerville seismic zone (MPSSZ) may not accurately reflect the locations of the faults that ruptured August 31, 1886. Second, fault plane solutions from the MPSSZ show a wide variety of fault types and orientations (Shedlock 1988; Madabhushi and Talwani 1993; Chapman *et al.* 2016) that are from displacements along several faults with different orientations. Third, faulting beneath the 700- to 1100-m-thick, southeast-dipping wedge of Cretaceous and Cenozoic unlithified sediments and weakly lithified to indurated sedimentary rocks beneath the Charleston region (Gohn 1988) would likely fold rather than fracture the overlying strata (Stein and Yeats 1989). Fourth, the swampy, densely forested area throughout much of the meizoseismal area makes it difficult to identify surface evidence of faulting. Fifth, the humid climate, easily eroded surface sediments, and the rapid urbanization of the Charleston region in modern time have erased much of the evidence of ground rupture that may have once existed. Finally, low Cenozoic fault slip rates in the eastern United States (Prowell 1988, 0.3–1.5 m/myr) result in small cumulative displacements, thus making it difficult to identify Cenozoic faults in the landscape and on regional aeromagnetic and gravity maps.

Because of these factors, numerous hypotheses have been presented to explain the 1886 Charleston earthquake and MPSSZ. Seeber and Armbruster (1981), for example, proposed that backslip on the Appalachian décollement caused the main shock. Talwani (1982) postulated that the Charleston earthquake and MPSSZ are from stresses produced by the intersection of the NNE-SSW-oriented Woodstock fault and the NW-SE-oriented Ashley River fault. Behrendt (1983) proposed that displacement on a NE-SW-oriented listric fault along the southeastern edge of the Triassic Jedburg basin near Summerville may have caused the Charleston earthquake. Using a digital elevation model and river morphology, Rhea (1989) interpreted a topographically high area in the northwestern part of the Charleston region that she postulated is from uplift, although she did not

Figure 1. (next page) Summary map showing structural domes (bold contours), buried faults interpreted from seismic-reflection profiles (solid triangles, U on upthrown side), and linear magnetic anomalies ML1–ML5 (green lines). Abbreviations of faults (black lines), LiDAR lineaments (blue lines), and scarps are shown in Tables 1 and 2. The thick red parallel lines represent the interpreted uplift along the ZRA and ECFS. Red dots are epicenters of small modern earthquakes east of Adams Run (U.S. Geological Survey 2021). The incised part of the Ashley River is highlighted with thick red contour. Red contours labeled 1–3 are LiDAR-derived elevation profiles along the Caw Caw and Horse Savanna swamps and along the Ashley River valley and Cypress Swamp (uplifted parts are dashed). Orange patterns along the lower Ashley River valley are Pleistocene fluvial terraces from Marple and Hurd (2020). Lines labeled 4–8 are elevation profiles across the Ashley River valley and Cypress Swamp. The dashed contour is the outer isoseismal contour of Sloan (Dutton 1889). Index map in the upper left shows the location of the study area with the Modified Mercalli Intensity contours of the 1886 Charleston earthquake from Bollinger (1977) overlain.

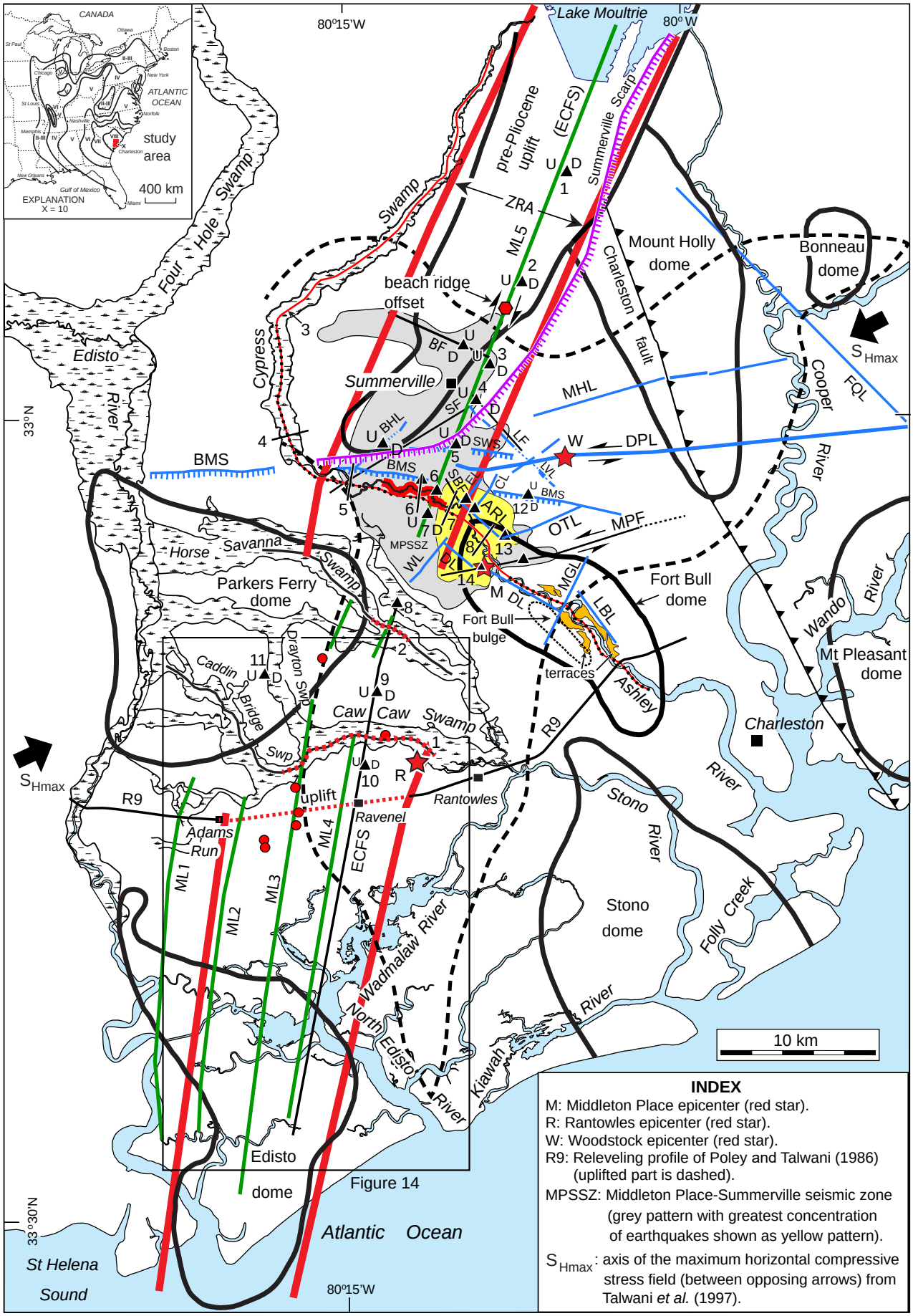

Table 1. Fault name abbreviations.

Abbreviation	Fault
ARFZ	Ashley River fault zone
BF	Berkeley fault
LF	Lincolnville fault
MPF	Middleton Place fault
SBF	Sawmill Branch fault
SF	Summerville fault

Table 2. Abbreviations for names of lineaments and scarps.

Abbreviation	Lineament or scarp
ARL	Ashley River lineament
BHL	Boone Hill lineament
CL	Coosaw Creek lineament
DL	Dawkins lineament
DPL	Deer Park lineament
EL	Eagle Creek lineament
FQL	French Quarter lineament zone
LBL	Lambs lineament
LVL	Lincolnville lineament
MS	McChune scarp
MGL	Magnolia Gardens lineament
MHL	Mount Holly lineament
OTL	Otranto lineament
SS	Summerville scarp
SWS	Summerwood scarp
WL	Waring lineament

attribute it to any known subsurface structures. Figure 2 (shaded area) shows this topographically high area interpreted from a LiDAR image of the Charleston region shown in figure 2 of Marple and Hurd (2020). Talwani (1999) modified his 1982 model in which he hypothesized that the Woodstock fault is offset 3–4 km to the southeast by the NW-SE-oriented Ashley River fault. Based on geological and geophysical data and anomalous changes in river morphology, Marple and Talwani (2000) postulated that the main shock of the Charleston earthquake occurred along the southern end of the ECFS, locally known as the Woodstock fault. Using shallow drill-hole data, Weems and Lewis (2002) hypothesized that scissors-like compression on a crustal block between a north-south-oriented Adams Run fault and the NW-SE-oriented Charleston fault causes co-seismic displacements on the Woodstock, Summerville, and Ashley River faults (Fig. 2). Marple and Miller (2006), in contrast, postulated that the 1886 Charleston earthquake was associated with a 12° restraining bend in the ECFS south of Summerville and that the MPSSZ is from displacements along the ECFS and smaller faults east of the fault bend (Fig. 1). Based on fracture data from colonial Fort Dorchester near the Ashley River, Bartholomew and Rich (2007) attributed the main shock of the Charleston earthquake to reverse displacement on a NW-SE-oriented, near-vertical Dorchester fault. Durá-Gómez and Talwani (2009) and Talwani and Durá-Gómez (2009) modified Talwani's (1999) model in which they postulated that the Woodstock fault (WF) is offset ~6 km to the southeast along the Ashley River valley and that the northern and southern segments–WF(N) and WF(S)–dip ≥ 50° to the northwest. They also postulated that the main shock of the 1886 Charleston earthquake occurred on the ~13-km-long, NW-SE-oriented, southwest-dipping Lincolnville reverse fault between WF(N) and WF(S) and that the second smaller earthquake west of Rantowles occurred on WF(S). Marple (2011) argued against an offset in the Woodstock fault based on the lack of evidence for uplift within the proposed restraining offset where a compressional pop-up between WF(N) and WF(S) would be expected. Based on seismic-reflection, seismicity, aeromagnetic, and gravity data, Chapman and Beale (2010) hypothesized that the Charleston earthquake was caused by compressional reactivation of a NE-SW-oriented early Mesozoic extensional fault. Using the results of a one-year portable seismic network that was deployed near Summerville in 2011 and 2012, Chapman *et al.* (2016) postulated that the main shock of the 1886 earthquake occurred on a ~22-km-long, N6°E-oriented reverse fault dipping ~43°W and that the MPSSZ represents aftershocks from 1886 (Fig. 2). Based on LiDAR, seismic-reflection, and surficial geologic data, Marple and Hurd (2020) postulated that the main shock in 1886 was caused by sinistral strike-slip displacement on an east-west-oriented fault associated with the ~40-km-long Deer Park lineament[1]

1 Deer Park lineament was incorrectly referred to as the Deer Creek lineament on page 86 of Marple and Hurd (2020).

Figure 2. (next page) Summary map showing seismicity recorded between 1974 and 2021 (yellow dots) (U.S. Geological Survey 2021), seismic-reflection profiles with locations of interpreted faults (black ticks, U on upthrown side), and linear magnetic anomalies ML1-ML5 (green lines). Previous interpretations of faults are grey and red lines. Light grey area in the northwest part of the area is the topographically higher area interpreted from the LiDAR data of Marple and Hurd (2020, fig. 2). The pre-Pliocene high near Summerville is shown by the thick grey contour. The incised part of the Ashley River is highlighted with thick red contour. Tables 1 and 2 show the abbreviations of faults, LiDAR lineaments (blue lines), and scarps (contours with ticks). Red dots are epicenters of small modern earthquakes east of Adams Run. Isoseismal contours of Sloan (Dutton 1889) are dashed. S1 is the location of the "ridges or permanent waves" along the Northeastern Railroad described in Dutton (1889, pp. 291). S2 is the location along the South Carolina Railroad where the direction of compressions reversed direction during the 1886 Charleston earthquake (Dutton 1889, pp. 287, 288, and 295). S3 is the location of significant S-shaped deformation of the Northeastern Railroad caused by the seismic waves during the 1886 Charleston earthquake (Dutton 1889, pp. 290).

near Woodstock (Fig. 1). They further concluded that this fault is one of several that formed to compensate for the increased compression caused by dextral displacement along a 12° restraining bend in the ECFS, referred to herein as the Summerville restraining bend (Fig. 2). Based on reprocessed seismic-reflection and aeromagnetic data and recently acquired ground penetrating radar (GPR) profiles, Pratt *et al.* (in press) interpreted several NE-SW-oriented faults deforming the Cretaceous and younger Coastal Plain strata in the epicentral area of the Charleston earthquake.

A major weakness of most of these hypotheses is that they attributed the 1886 Charleston earthquake to a single fault rupture, despite the evidence for at least two fault ruptures as previously discussed. Our goal was to reevaluate legacy aeromagnetic, LiDAR, and seismic-reflection data and surficial geologic maps to evaluate evidence for and against the existence of the ECFS and faults associated with the Summerville restraining bend.

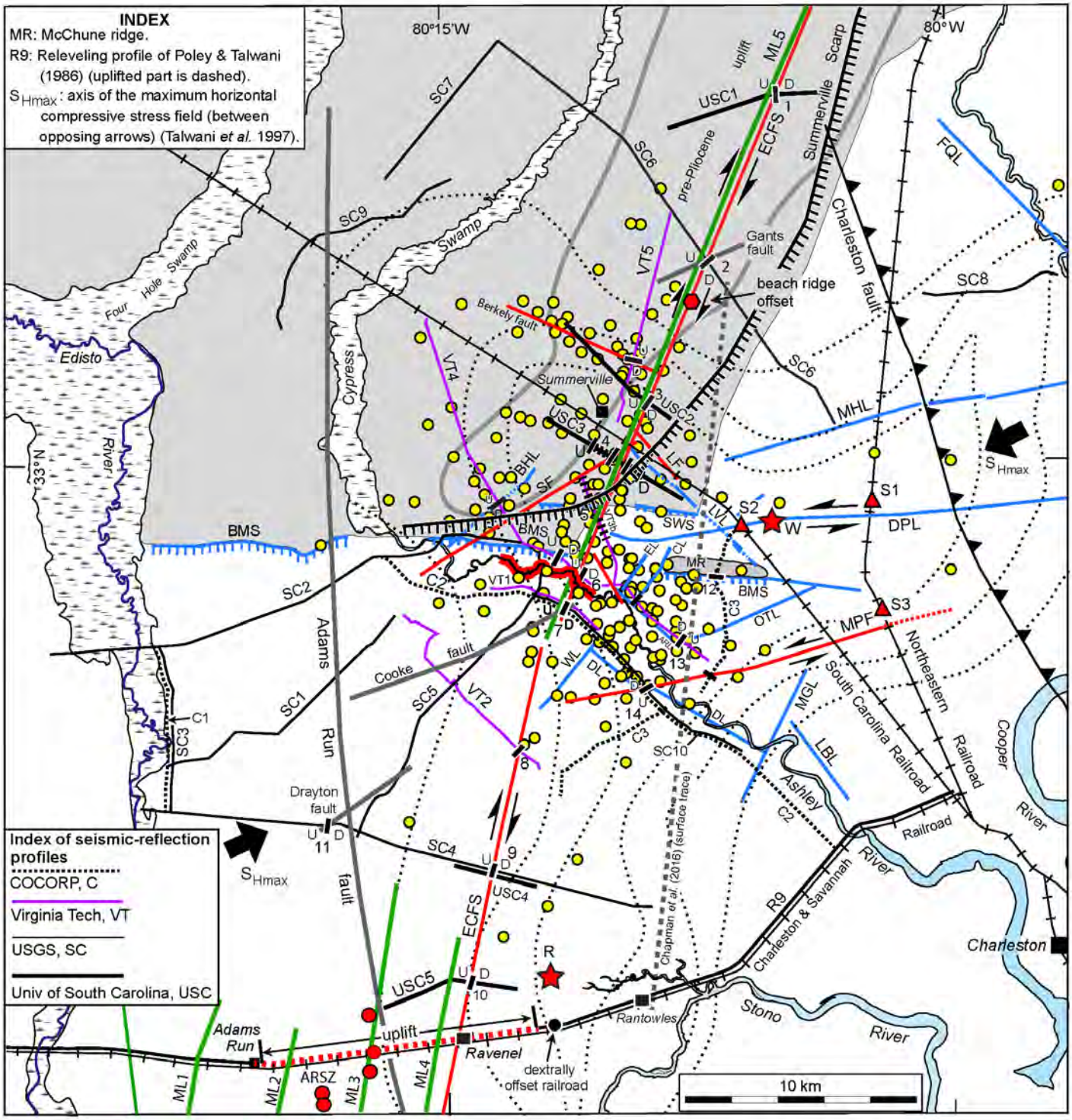

Initial aeromagnetic studies of the Charleston region

Initial aeromagnetic studies of the Charleston region (Popenoe and Zietz 1977; Phillips 1977, 1988; Daniels *et al.* 1983), combined with other geophysical and deep corehole data (Rankin 1977; Gohn 1983), revealed that the thick sedimentary wedge beneath the South Carolina Coastal Plain is underlain by the South Georgia Triassic rift basin, several early Mesozoic mafic and ultramafic plutons, and numerous N-S- and NW-SE-oriented early Mesozoic diabase dikes. Phillips (1988) used edge-enhanced grey-scale aeromagnetic images illuminated from the northwest to map buried early Mesozoic border faults and diabase intrusions. Figure 3 is a portion of his aeromagnetic image in the Charleston region that he digitally enhanced in 1988 (J.D. Phillips 2020 written communication). He interpreted a ~50-km-long, NNE-SSW-oriented aeromagnetic lineament between Summerville and the Santee River (Fig. 2, ML5) that Marple and Talwani (2000) postulated is associated with the ECFS. The aeromagnetic data of Daniels (2005) used in this study are discussed later in the Methods section.

Previously mapped faults in the Charleston region

Seismic-reflection studies of the Charleston region have revealed a number of buried faults offsetting Cretaceous and younger strata beneath the outer Coastal Plain. Using Vibroseis seismic-reflection data, Hamilton *et al.* (1983) interpreted the west-dipping Gants fault on United States Geological Survey (USGS) profile SC6 northeast of Summerville and the west-dipping Cooke and Drayton faults on profiles SC4, SC5, and SC10 southwest of Summerville (Figs. 2 and 4). Marple and Talwani (2000) later reinterpreted the Gants and Cooke faults on lines SC6 and SC10 to be associated with the ECFS. Hamilton *et al.* (1983) also interpreted a ~7-km-wide "zone of missing J" on profiles SC4 and SC10 in which the J reflection (Jurassic basalt layer) is weak or missing. Marple and Miller (2006, fig. 13) interpreted a small,~10 ms (two-way travel time, TWTT) west-side-up offset of the J horizon along the western edge of this zone at CDP 285 on seismic line USC4 and concluded that the J horizon continues ~1.5 km farther to the east than on profile SC4. Farther east, the reflector amplitudes on line USC4 are much weaker like those on profile SC4. One possible explanation for the weaker amplitudes is that a change in surficial sediments across this zone could have dampened the signal strength during data acquisition. However, surficial geologic maps of this area (e.g., Weems *et al.* 2014) do not show such a change above this zone. Alternatively, the weak reflections to the east could be from minor fracturing in this zone. Diffractions near the east end of line SC4 (Hamilton *et al.* 1983) support minor faulting within this zone. Reprocessing of seismic-reflection profile SEISDATA4, an industry line that overlaps profile SC4, also supports minor faulting of the J horizon across the zone of missing J (Buckner 2011).

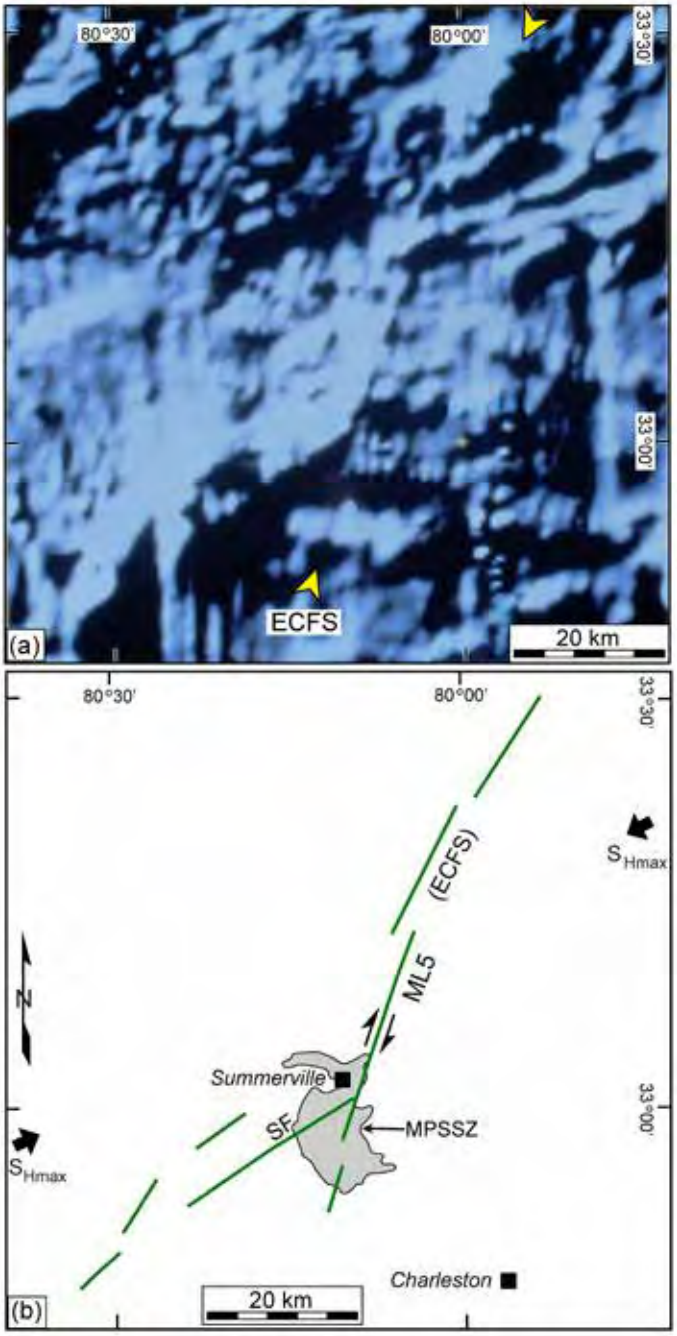

Figure 3. (a) Grey-scale aeromagnetic image of the Summerville, South Carolina, area digitally enhanced and illuminated from the northwest by J.D. Phillips (2020 written communication). Brighter areas indicate greater magnetic intensities. (b) Map for image (a). Green lines are linear aeromagnetic anomalies (e.g., ML5). SF is the Summerville fault.

The Kansas Geological Survey, in collaboration with the University of South Carolina, acquired four other seismic- reflection profiles (denoted USC) across the proposed ECFS using the Mini-Sosie and 8-gauge shotgun

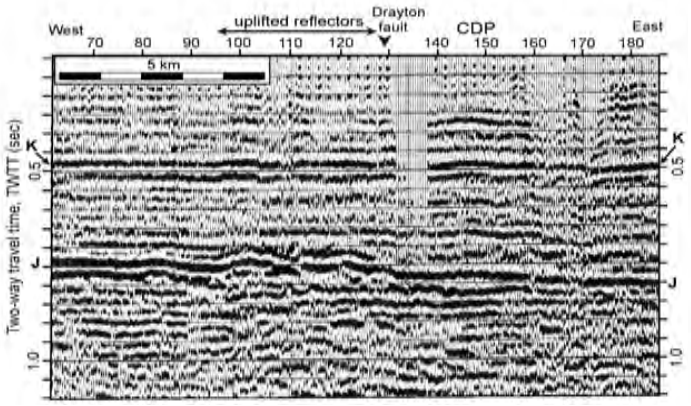

Figure 4. Part of USGS seismic-reflection profile SC4 showing the Drayton fault of Hamilton *et al.* (1983) and the uplifted J horizon. CDP is central depth point. Modified from Hamilton *et al.* (1983). Interpreted horizons: K – Upper Cretaceous, J – Jurassic basalt layer. Location of profile is shown in Figure 2.

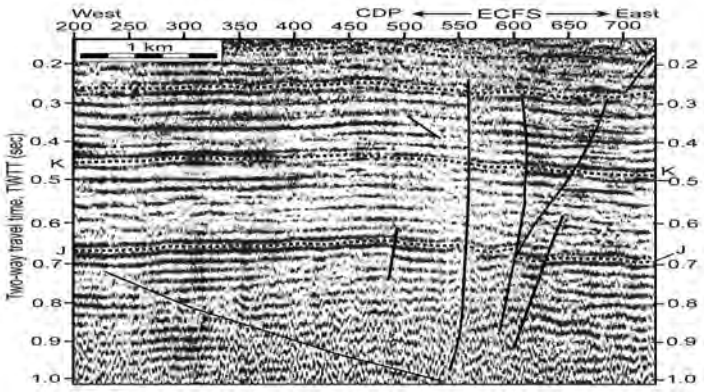

Figure 5. Interpreted seismic-reflection profile USC1 across the interpreted East Coast fault system (ECFS). CDP is the central depth point. Figure 4 caption defines J and K reflectors. Note the ~4-km-wide uplift of the horizons across the ECFS. Modified from Marple and Miller (2006). Unlabeled dashed lines are arbitrarily chosen Cenozoic horizons. Location of profile is shown in Figure 2.

methods (Marple and Miller 2006) (Figs. 1 and 2, locations 1, 3, 4, 9, and 10). Most of these profiles show buried steeply-dipping, west-side-up faults along the ECFS, commonly with folding of the overlying Cretaceous and Cenozoic strata (Figs. 5 and 6). Marple and Miller (2006) also interpreted a strike-slip fault along profile VT2 (Fig. 1, location 8, CDP 485) that was acquired by Virginia Polytechnic Institute and State University (Virginia Tech, denoted VT) where it crosses the ECFS south of the Ashley River. Although no vertical displacement was observed at this location, they interpreted a steep, west-dipping fault based on a narrow zone of low coherence that diverges upward into a positive flower structure in the overlying Cretaceous and younger strata. Two other seismic-reflection profiles in northeastern South Carolina also show buried faults where they cross the ECFS (Marple and Talwani 2000, figs. 20 and 21).

Near the northern end of COCORP (Consortium for Continental Reflection Profiling) seismic-reflection profile C3 north of the Ashley River is a buried, south-dipping, ~700-m-wide Cenozoic graben in which the horizons across the graben are offset down to the south (Schilt *et al.* 1983) (Figs. 1 and 2, location 12, and Fig. 7). This normal-style structure is anomalous in the eastern USA where reverse and transpressional strike-slip faulting have dominated the Cenozoic. The J horizon near the southwest end of profile C3 is offset up to the southwest ~100 m across a gap in this profile at the Ashley River valley (Schilt *et al.* 1983, fig. 9), which could be associated with the Ashley River fault of Talwani (1982). Vibroseis seismic-reflection profiles acquired by Virginia Tech near Summerville in the early 1980s revealed several other buried faults offsetting Cretaceous and younger strata (Costain and Glover 1983; Chapman and Beale 2008) (Fig. 2).

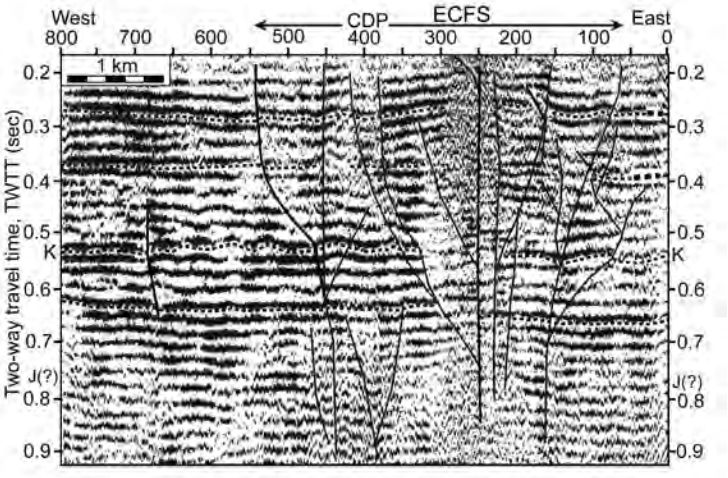

Figure 6. Interpreted seismic-reflection profile USC5 across the interpreted East Coast fault system (ECFS). CDP is the central depth point. Figure 4 caption defines J and K reflectors. Note the 3- to 4-km-wide uplift of the horizons across the ECFS. Modified from Marple and Miller (2006). Unlabeled dashed lines are arbitrarily chosen Cenozoic horizons. Location of profile is shown in Figure 2. Also note the low coherency of the reflectors approximately between CDPs 230 and 290.

Other Cenozoic faults have been mapped in the Charleston region using seismicity, aeromagnetic, shallow drill-hole, and other seismic-reflection data, including the Adams Run, Ashley River, Berkeley, Charleston, Lincolnville, Middleton Place, Sawmill Branch, and Summerville faults (Weems and Lewis 2002; Marple and Miller 2006; Talwani and Durá-Gómez 2009; Marple and Hurd 2020) (Figs. 1 and 2).

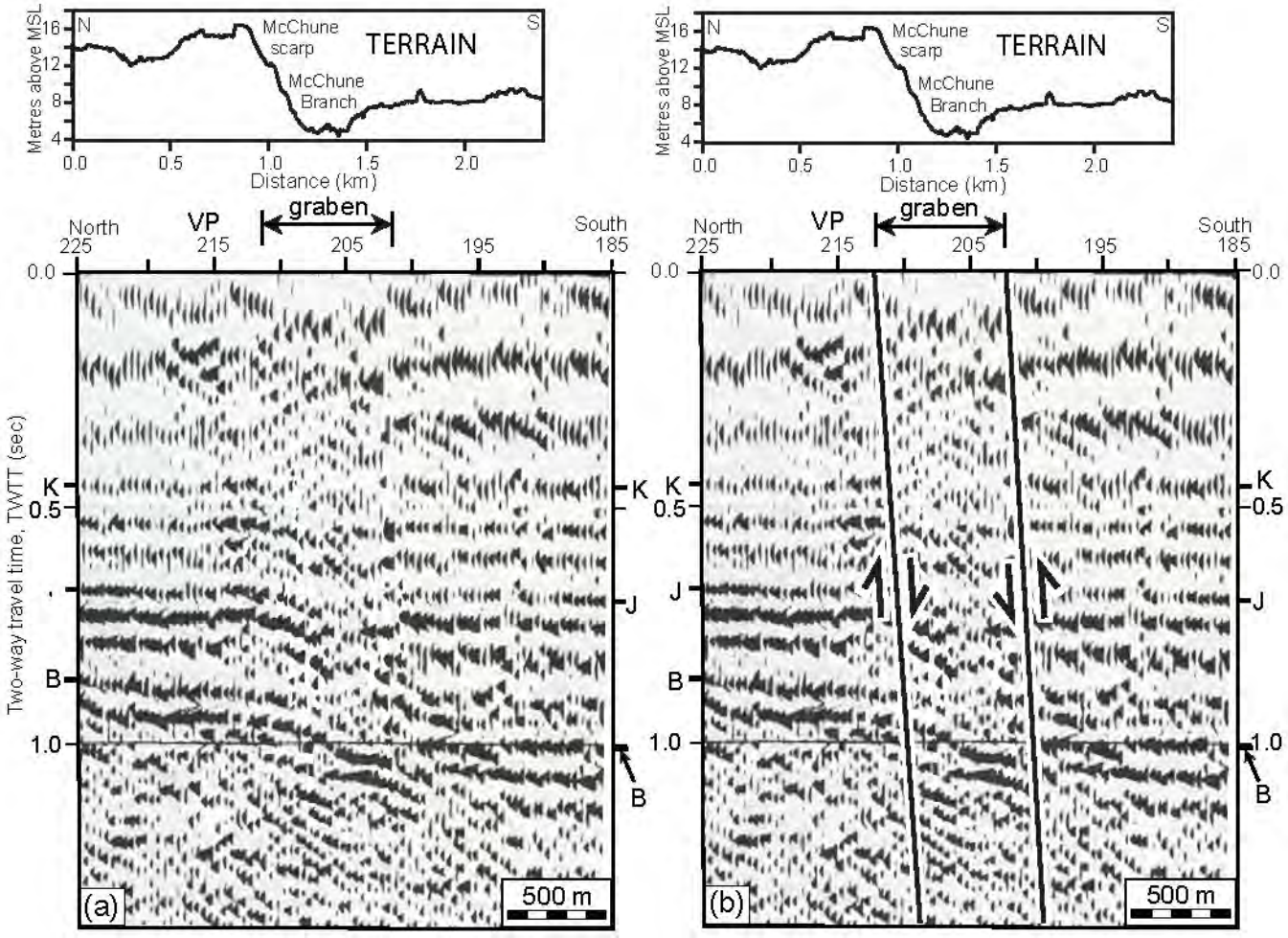

Figure 7. Part of the COCORP seismic-reflection profile C3 showing south-side-down offsets of the B (crystalline basement) and J horizons and the Cenozoic graben along the proposed McChune fault. VP is vibration point. The topographic profiles above the seismic sections are from Marple and Hurd (2020, fig. 5, profile 18). Modified from Schilt *et al.* (1983). Location of profile is shown in Figure 2.

East Coast fault system (ECFS)

Marple and Talwani (1993) interpreted a ~200-km-long buried dextral strike-slip fault system, locally known as the Woodstock fault near Summerville, in the Coastal Plain of South Carolina based on a "zone of river anomalies" (ZRA) that coincides with upwarped strata, steeply-dipping buried faults interpreted from seismic-reflection profiles, a ~50-km-long aeromagnetic lineament near Summerville (lineament ML5 in this study), and focal mechanisms of microearthquakes near Summerville that indicate dextral strike-slip motion. Marple (1994) identified a second ~200-km-long ZRA crossing the inner part of the North Carolina Coastal Plain that coincides with Cenozoic surface faults to the northeast near the Fall Line. Marple and Talwani (2000) continued this fault system into southeastern Virginia and named it the East Coast fault system (ECFS) (Fig. 1). They divided the ECFS into southern, central, and northern segments that are separated by ~10-km-wide right-step offsets. Marple and Hurd (2021) redefined the location of the central segment in southern North Carolina, thus making it continuous with the ECFS in northeastern South Carolina where it forms the 15° Cape Fear restraining bend. Uplifted Pliocene-Pleistocene fluvial terraces in the lower Cape Fear River valley in southern North Carolina (Markewich 1985; Soller 1988) and the dextral offset in the Brownsville Pleistocene beach ridge northeast of Summerville (Marple and Hurd 2020) (Fig. 8) suggest that deformation along the ECFS may have begun during the Pleistocene.

One of the most studied areas along the ECFS lies between the Ashley River and Lake Moultrie. Quaternary uplift along this part of the ECFS, combined with depositional and erosional processes associated with Pleistocene paleoshorelines, caused this area to be topographically higher than the surrounding areas (Marple and Hurd 2020) (Fig. 2). Pleistocene beach ridges that cross this area have been uplifted at least 4 m (Marple and Hurd 2020, figs. 12b and 13, profile 26) and the pre-Pliocene horizon at depth has been uplifted 10–15 m across the ZRA

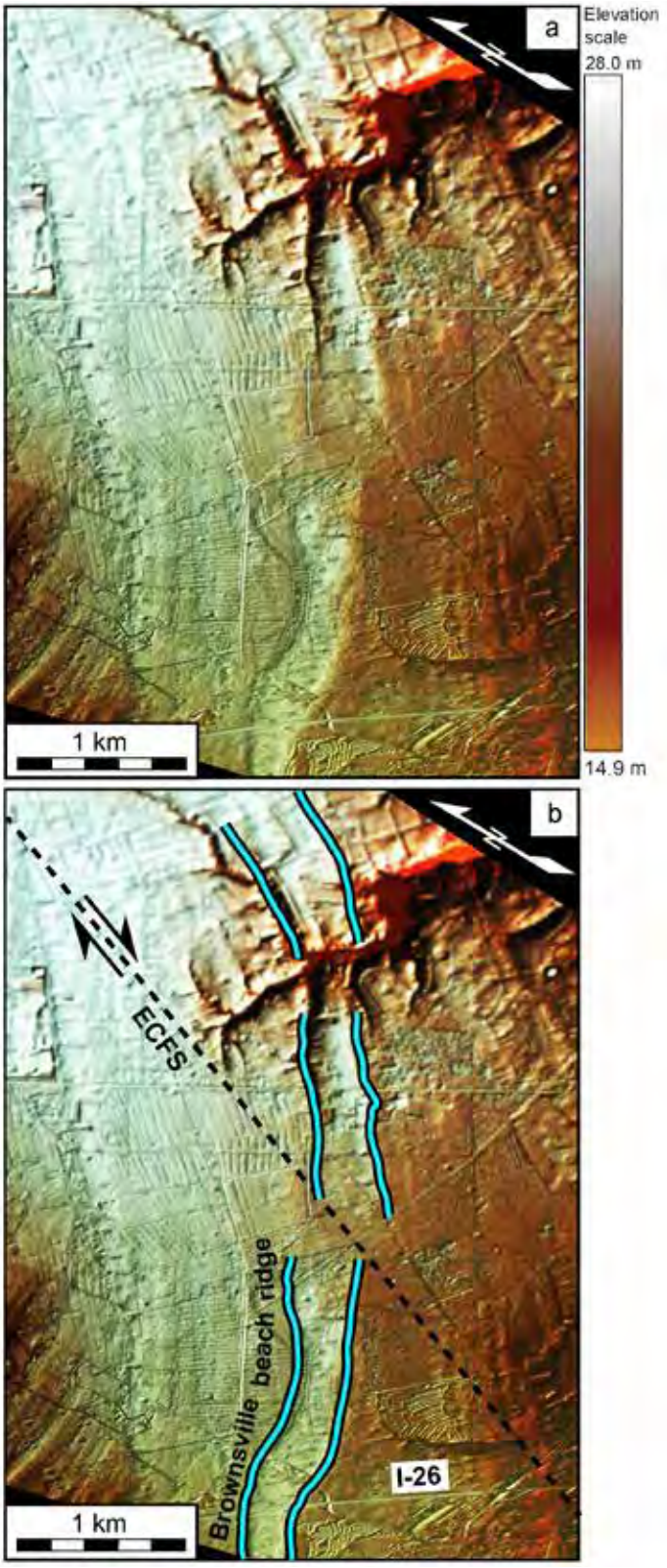

Figure 8. (a) LiDAR image of the ~320-m dextral offset in the Pleistocene Brownsville beach ridge deposit. Figure 1 shows the location of this offset. (b) Interpretation of image (a).

(McCartan *et al.* 1984, cross-section B-B'; Weems and Obermeier 1989). Changes in the age and nature of the sediments along a ~10-km-long section of the Ashley River valley floor near the southern edge of this topographic high indicate that it too has been gently uplifted during late Pleistocene or Holocene time (Marple and Talwani 1993, 2000). Here, the channel is incised 2–3 m below a late Pleistocene fluvial terrace that is underlain by sediments of the Silver Bluff and Wando formations (units *Qsbc* and *Qwc* of Weems *et al.* 2014). In contrast to this part of the river valley, the valley floor upstream is an anastomosing swamp pattern without a discrete channel and is underlain by Holocene alluvium (Cypress Swamp, unit *Qal* of Weems *et al.* 2014). Downstream from the incised part of the river the valley floor consists of Holocene tidal marsh deposits (unit *Qht* of Weems *et al.* 2014). Figure 9 is a mosaic of NAPP (National Aerial Photography Program) colour infrared photos that show this change in floodplain type along the lower Ashley River valley and Cypress Swamp. This area of interpreted uplift between Lake Moultrie and the Ashley River coincides with the ZRA (Fig. 1). Our results suggest that deformation along the ECFS and the McChune fault proposed herein may have produced this uplift.

Proposed faults associated with the Summerville 12° restraining bend

Using primarily LiDAR data, Marple and Hurd (2020) mapped a 30-km-wide area of WSW-ENE- to NW-SE-oriented lineaments and scarps east of the Summerville restraining bend (Fig. 1), which they concluded are surface expressions of faults that formed to compensate for the increased compression caused by dextral displacements along the restraining bend, including the Canter Hill, French Quarter, Mount Holly, Deer Park, Middleton Place, and Otranto lineaments. They postulated that sinistral strike-slip displacement on the ~40-km-long Deer Park lineament northeast of the bend (Fig. 1) produced the main shock of the 1886 Charleston earthquake. They based their hypothesis on the proximity of the Deer Park lineament to the Woodstock epicenter and the location along the South Carolina Railroad where compressions during the main shock reversed direction[2] (Dutton 1889, pp. 295) (Figs. 2 and 10). Marple and Hurd (2020) also noted the presence of topographic scarps that cross the ECFS just north of the restraining bend—the east-west-oriented Summerton and Bethera-McChune[3] (BMS) scarps (Fig. 2). Marple and Hurd (2020) referred to the east-west-oriented, south-facing scarp north of the incised part of the

2 The location, S2, where the direction of compressions reversed direction along the South Carolina Railroad during the main shock of 1886 was incorrectly located along the Northeastern Railroad by Weems and Lemon (1988) and Marple and Hurd (2020).

3 The Bethera-McChune scarp was previously referred to as the Summerville-McChune scarp by Marple and Hurd (2020).

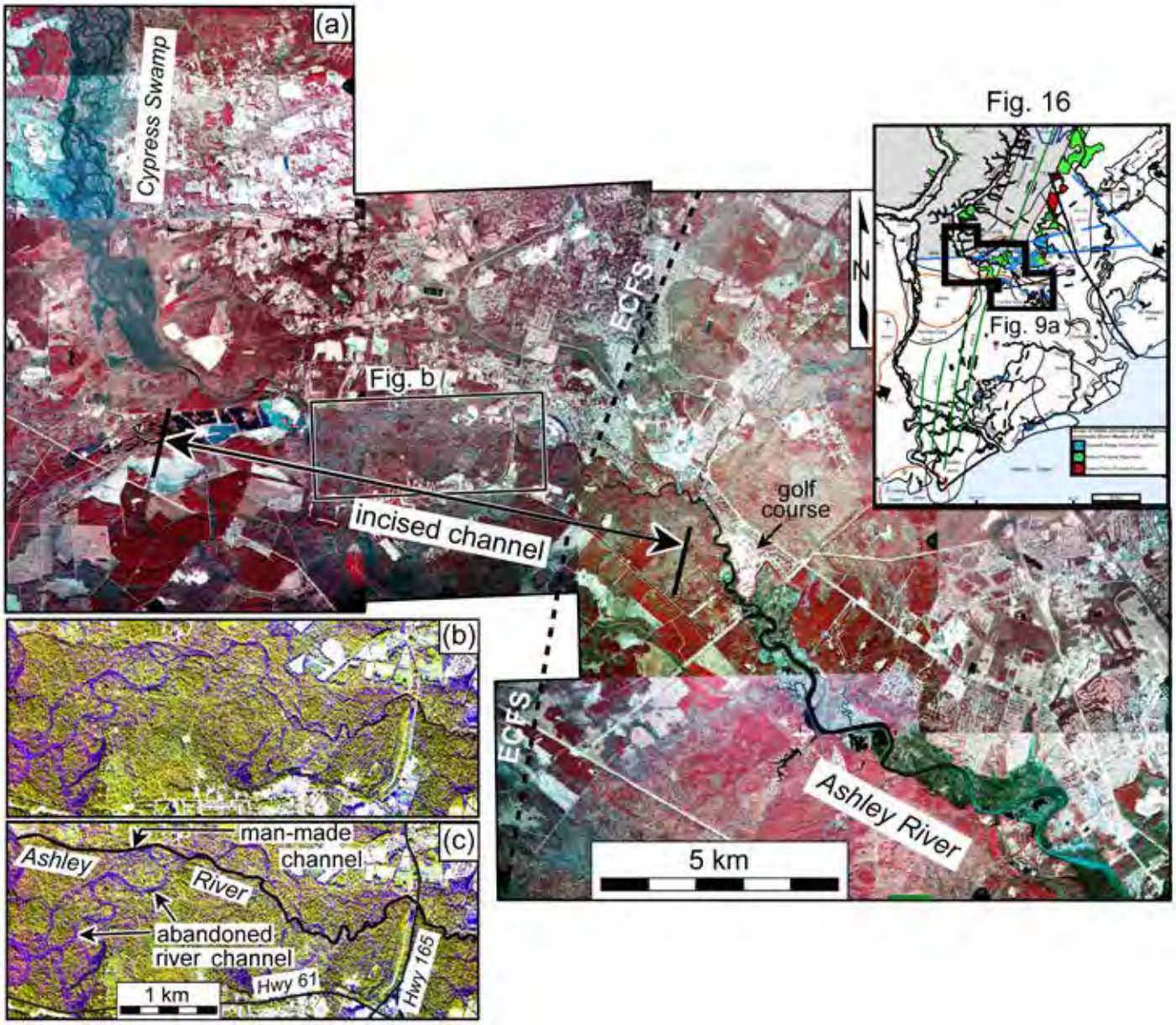

Figure 9. (a) Mosaic of NAPP colour infrared photographs acquired by the USGS in 1989 along the Ashley River valley and Cypress Swamp that shows the change in floodplain environment along the river valley where it crosses the ECFS. The Cypress Swamp upstream is dominated by an anastomosing swamp pattern whereas the floodplain to the southeast is an estuarine marsh. Between these two areas the floodplain is dominated by forested, late Pleistocene terraces. (b) IHS-enhanced subset of the mosaic along the western part of the Ashley River showing the man-made river channel and abandoned meandering channels. Location is shown in diagram (a). (c) Interpreted version of diagram (b). Location map in the upper right is from Figure 16.

Ashley River as the Summerville scarp, which is actually the Bethera scarp, whereas the Summerville scarp crosses the area 1–1.5 km to the north (Doar 2014) (Fig. 1). We, therefore, collectively refer to the two topographic scarps north of the Ashley River and McChune Branch of the Bluehouse Swamp as the Bethera-McChune scarp (BMS). Small-displacement buried faults along seismic-reflection profiles SC10 and VT3b coincide with the Middleton Place, Otranto, Eagle Creek, and Coosaw Creek lineaments (Figs. 2, 11, and 12).

GEOLOGIC AND SEISMOTECTONIC SETTING

The 1886 Charleston earthquake occurred within the swampy, heavily forested outer Coastal Plain where sea-level changes during the Pliocene and Pleistocene have produced a series of terraces underlain by emergent marine

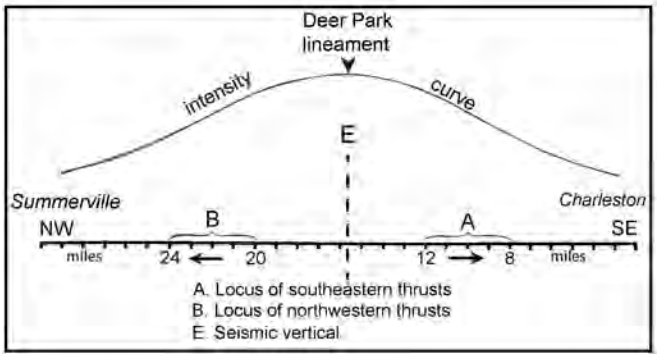

Figure 10. Location of the Deer Park lineament compared with the intensity curve of Dutton (1889) along the South Carolina Railroad that he derived for the main shock of the 1886 Charleston earthquake.

landforms, including estuarine plains, back-barrier marshes, lagoonal deposits, and sandy barrier-island ridges (Colquhoun *et al.* 1991; Weems *et al.* 2014). The terraces are bounded on the seaward (southeast) side by Pleistocene paleoshoreline scarps, including the Summerville, Macbeth, and Bethera scarps near the southern and eastern edges of the Penholoway or Wicomico terrace near Summerville (Weems *et al.* 2014; Doar 2014). Pliocene-Pleistocene uplift along the ECFS caused some of the paleoshorelines in the outer Coastal Plain to develop along and just east of the ECFS between the Ashley and Lynches rivers (Marple and Talwani 2000, fig. 12).

Nine of the near surface formations in the Charleston region are described in Table 3 because they are integrated later with some of the geomorphic observations. Exposures of the older, pre-Pleistocene sediments in fluvial valleys crossing the Charleston region could indicate Quaternary uplift. The late Eocene Parkers Ferry Formation, for example, is commonly 50–150 ft (15–50 m) beneath many areas of the Coastal Plain (e.g., Weems *et al.* 2014). Beneath the Coastal Plain sediments is a coastward-thickening, 700- to 1100-m-thick wedge of Cretaceous and Cenozoic, mostly unlithified sediments interbedded with weakly lithified to indurated sedimentary rocks that unconformably onlap and bury early Mesozoic rift basins and pre-Mesozoic terranes (Daniels *et al.* 1983; Gohn *et al.* 1983).

Modern seismicity in the Charleston region

Hypocentral depths of microearthquakes in the MPPSZ (Fig. 2) range from 1 to 12 km (Madabhushi and Talwani 1993; Chapman *et al.* 2016). Studies of focal mechanisms from the MPSSZ show a wide variety of fault types and orientations (Madabhushi and Talwani 1993; Chapman *et al.* 2016) that Marple and Hurd (2020, fig. 14) postulated is from small displacements along several faults east of the Summerville restraining bend. Chapman *et al.* (2016), in contrast, attributed the MPSSZ to aftershocks from the 1886 Charleston earthquake. However, because little modern seismicity has been recorded near the Woodstock or Rantowles epicenters, the MPSSZ may not accurately reflect the faults that ruptured in 1886.

Cenozoic structural domes in the Charleston region

Several Cenozoic structural domes have been mapped in the Charleston region using shallow drill-hole data (Fig. 1). Weems and Lewis (2002, fig. 14), for example, interpreted two such domes west of Charleston that they combined into a ~70-km-long, NNW-SSE-oriented Parkers Ferry-Edisto dome (based on structure contours of the base of the Ashley Formation) that is bounded along its eastern side by a west-dipping Adams Run fault (Figs. 1 and 2). Marple (2011) postulated that the ~20-km-long Edisto dome is a separate dome that was produced by Cenozoic uplift along the ECFS. Weems and Lewis (2002) also interpreted the Mount Holly and Mount Pleasant domes that they attributed to uplift along the upthrown (northeast) side of the Charleston fault (Colquhoun *et al.* 1983; Lennon 1985) (Fig. 1). Southeast of Summerville are the NW-SE-oriented Fort Bull bulge and dome (Weems and Lewis 2002) that are associated with uplift along the southwest-dipping, NW-SE-oriented Ashley River reverse fault (Talwani 1982; Weems and Lemon 1988) (Fig. 1). Other structural domes in the Charleston region include the Stono and Bonneau domes (Weems and Lewis 2002) (Fig. 1).

METHODS AND DATA USED

The aeromagnetic data that we used for this study were acquired from the digital aeromagnetic data of South Carolina (Daniels 2005) (Fig. 13). This map consists of eleven separate aeromagnetic surveys flown between 1958 and 1978 at 500 ft (~150 m) above ground and at a 1-mile (~1600 m) flight line separation (Daniels 2005). Flight line directions were north-south in the central part of the study area and east-west in the rest of the area. The data were reduced to the pole in order to center the anomalies over their sources (Daniels 2005). Daniels (2005) performed strike filtering in the direction of the flight lines to reduce edge effects. He then re-gridded the data to an interval of 400 m using a minimum curvature gridding algorithm and continued the data upward to 1000 feet (~305 m) above ground.

We used the Hillshade tool of ArcGIS to generate shaded relief images of Daniels' (2005) aeromagnetic data using various illumination directions, an elevation angle of 35°, and a vertical exaggeration of 30×. The data were colorized based on variations in magnetic intensities. Basic contrast enhancement routines of Adobe Photoshop were used to further enhance the aeromagnetic images, including the intensity-hue-saturation (IHS) routine. Magnetic intensity scales were not generated for the IHS-enhanced images because the IHS enhancement significantly changed their

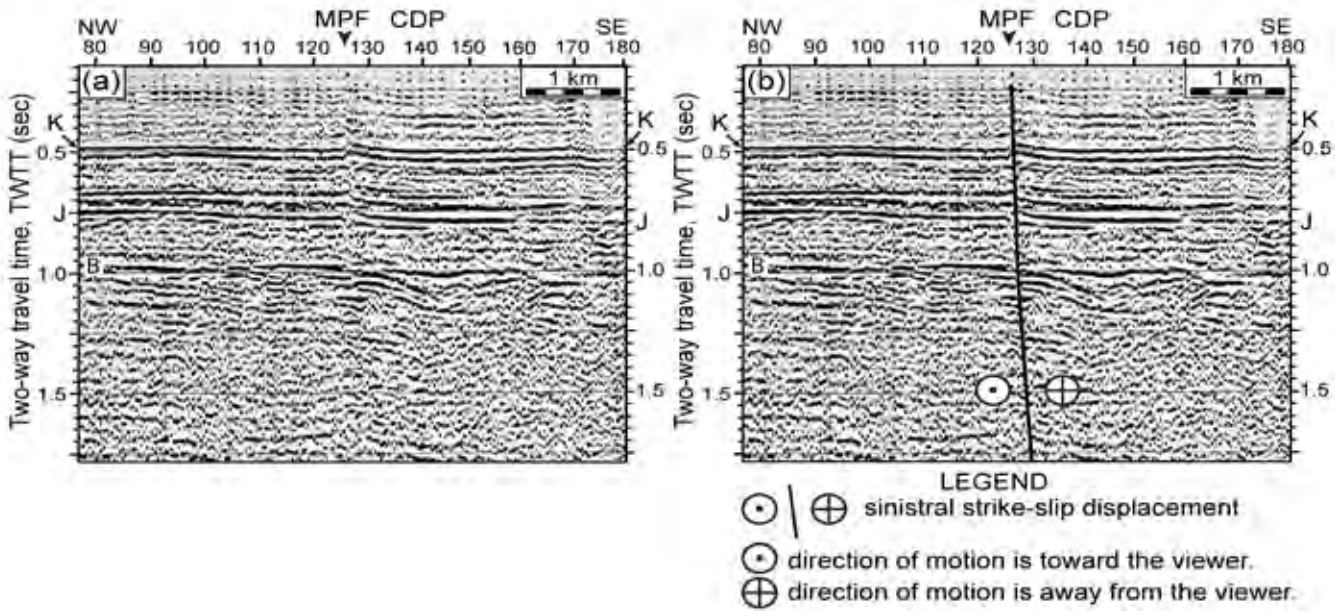

Figure 11. (a) Part of the USGS seismic-reflection profile SC10 of Hamilton *et al.* (1983) showing offsets in Cenozoic strata along the interpreted Middleton Place fault. CDP is central depth point. (b) Interpreted version of profile in diagram (a). Modified from Hamilton *et al.* (1983). Note the diffraction projecting from the fault plane just below 1.0 sec TWTT. Location of profile is shown in Figure 2.

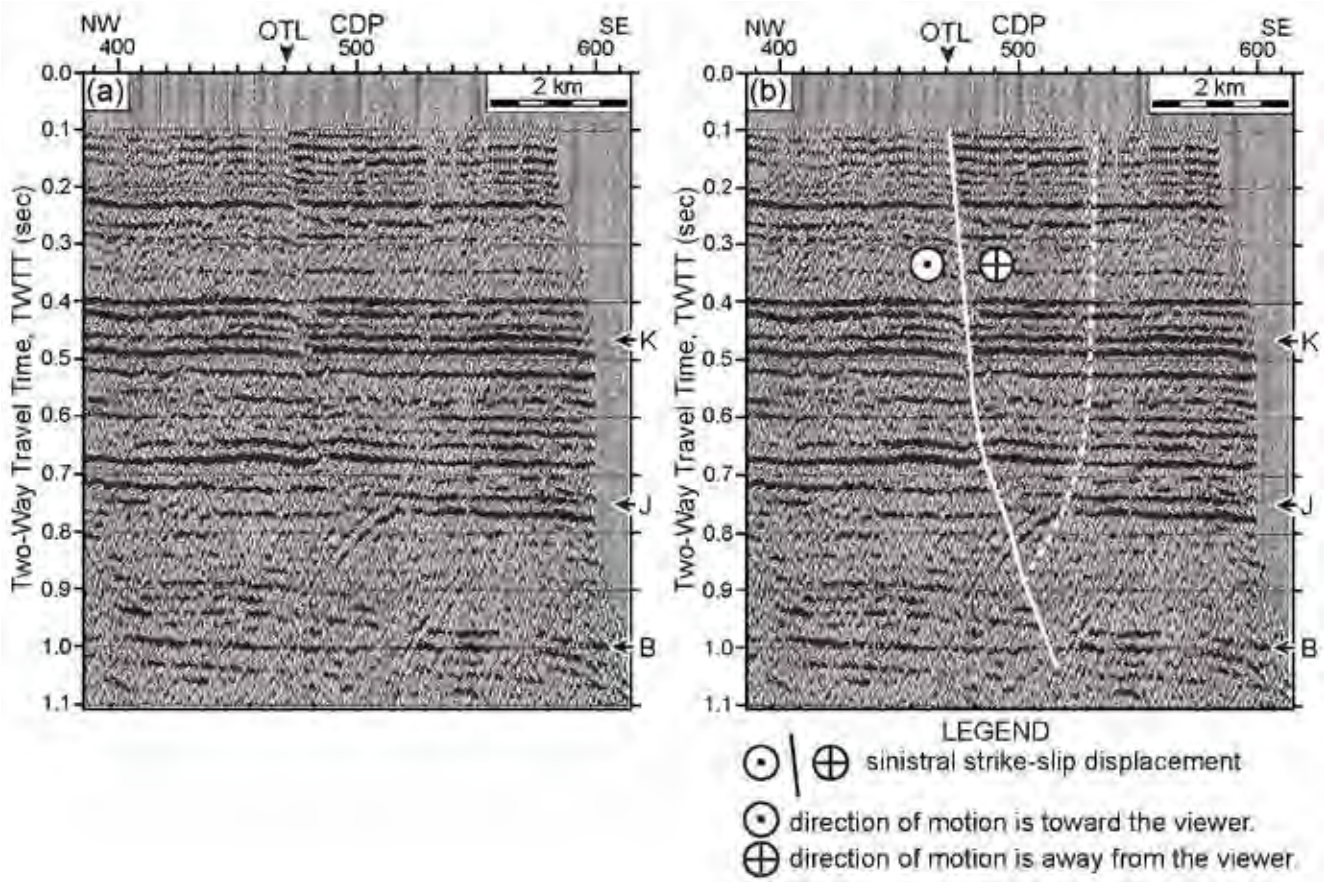

Figure 12. (a) Part of the Virginia Tech seismic-reflection profile VT3b showing offsets in the Cenozoic strata along the Otranto lineament of Marple and Hurd (2020). CDP is central depth point. (b) Interpreted version of profile in diagram (a). Modified from Chapman and Beale (2008). Location of profile is shown in Figure 2.

Table 3. Surficial deposits in the Charleston region discussed in the text.

Unit name	Unit age	Unit description and depositional environment
Parkers Ferry Formation[1,2]	Late Eocene (~36 Ma)	Stiff to plastic, dense and sticky calcilutite to fine-grained calcarenite that formed in a soft-bottomed, shallow-marine-shelf environment.
Ashley Formation[3]	Early Oligocene (~29 Ma)	Dense, erosion-resistant, weakly cemented, light-olive-brown, phosphatic and quartzose calcarenite that accumulated in an open-marine-shelf environment.
Chandler Bridge Formation[4]	Late Oligocene (~27 Ma)	Soft and easily eroded, medium-gray to dusky-green quartz phosphate sands that accumulated in a shallow-marine-shelf environment.
Raysor Formation[3]	Late Pliocene (~3.0 Ma)	Bluish-grey, shelly, clayey, and silty quartz sand that accumulated in a shallow-marine-shelf environment.
Penholoway or Wicomico Formation[2]	Early Pleistocene (Penholoway: 730–970 ka; Wicomico: 1.8–2.12 Ma)	Sand, clayey sand, and clay deposited in barrier, open lagoonal, and shallow-shelf-marine environments, especially the barrier and back-barrier complex near Summerville.
Ladson Formation[2]	Middle Pleistocene (240–730 ka)	Barrier sand and clayey sand and clay facies deposited in fluvial, estuarine, and lagoonal environments.
Ten Mile Hill beds[2]	Late Pleistocene (200–240 ka)	Poorly consolidated, easily eroded clays and clayey sands deposited in back-barrier and shallow shelf environments.
Wando Formation[2]	Late Pleistocene (70–130 ka)	Poorly consolidated, easily eroded sand, clayey sand, and clay that were deposited in fluvial, barrier, back-barrier, and estuarine marsh environments.
Silver Bluff beds[2]	Late Pleistocene (33–85 ka)	Clayey sand and clay facies that form the fluvial terrace along the incised part of the Ashley River valley.

Unit descriptions from the references: [1]Weems and Lemon (1984); [2]Weems *et al* . (2014); [3]Weems *et al* . (1997); [4]Weems and Lemon (1988).

colour schemes. Magnetic lineaments were spatially compared with previously acquired seismic-reflection profiles to determine if they spatially coincide with faults (Fig. 1).

We also examined surficial geologic maps in the Charleston region (e.g., Weems *et al.* 2014) to search for evidence of uplift along the magnetic lineaments and the LiDAR lineaments of Marple and Hurd (2020). Local exposures of older pre-Pleistocene strata, like the Parkers Ferry, Ashley, Chandler Bridge, and Raysor formations, along stream valleys could indicate areas of Quaternary uplift since they are normally buried beneath the younger Coastal Plain sediments.

Because anomalous changes in river morphology can reveal areas of Quaternary uplift (Schumm 1986), we examined topographic profiles constructed across the Ashley River valley and Cypress Swamp using LiDAR data to evaluate evidence for and against late Quaternary uplift across the ECFS in the southern meizoseismal area of the Charleston earthquake. We also sought possible evidence for late Quaternary uplift along the southern ECFS using longitudinal profiles constructed along the Horse Savanna and Caw Caw swamps and along the Ashley River valley and Cypress Swamp.

Although channel sinuosities can also be used to infer tectonic uplift (Schumm 1986), we did not construct a sinuosity profile along the Ashley River for three reasons. First, there is no consistent river channel upstream along Cypress Swamp due to its anastomosing pattern (Fig. 9). Second, the floodplain environment along the Ashley River valley changes from a dry forested terrace along the incised part of the Ashley River to a salt marsh downstream with a much larger channel affected by tides. Finally, recent field reconnaissance of the Ashley River channel near the western side of the incised part of the river revealed that the channel was straightened and deepened presumably during Colonial times to drain this part of the floodplain for rice farming. Old rice levees < 1 m high crossing this part of the floodplain are still preserved in this area and spoil from excavating the new channel is piled up along the edges of the artificial channel. The old meandering channels are easily observed south of the artificially straightened channel in Figure 9c.

OBSERVATIONS

Linear aeromagnetic anomalies southwest of the Ashley River

Illumination of Daniels' (2005) aeromagnetic data from various directions revealed a ~10-km-wide zone of several subtle 600- to 700-m-wide, 22- to 32-km-long, linear aeromagnetic anomalies trending ~N10°E west of Charleston that are formed mainly by a slight decrease in magnetization

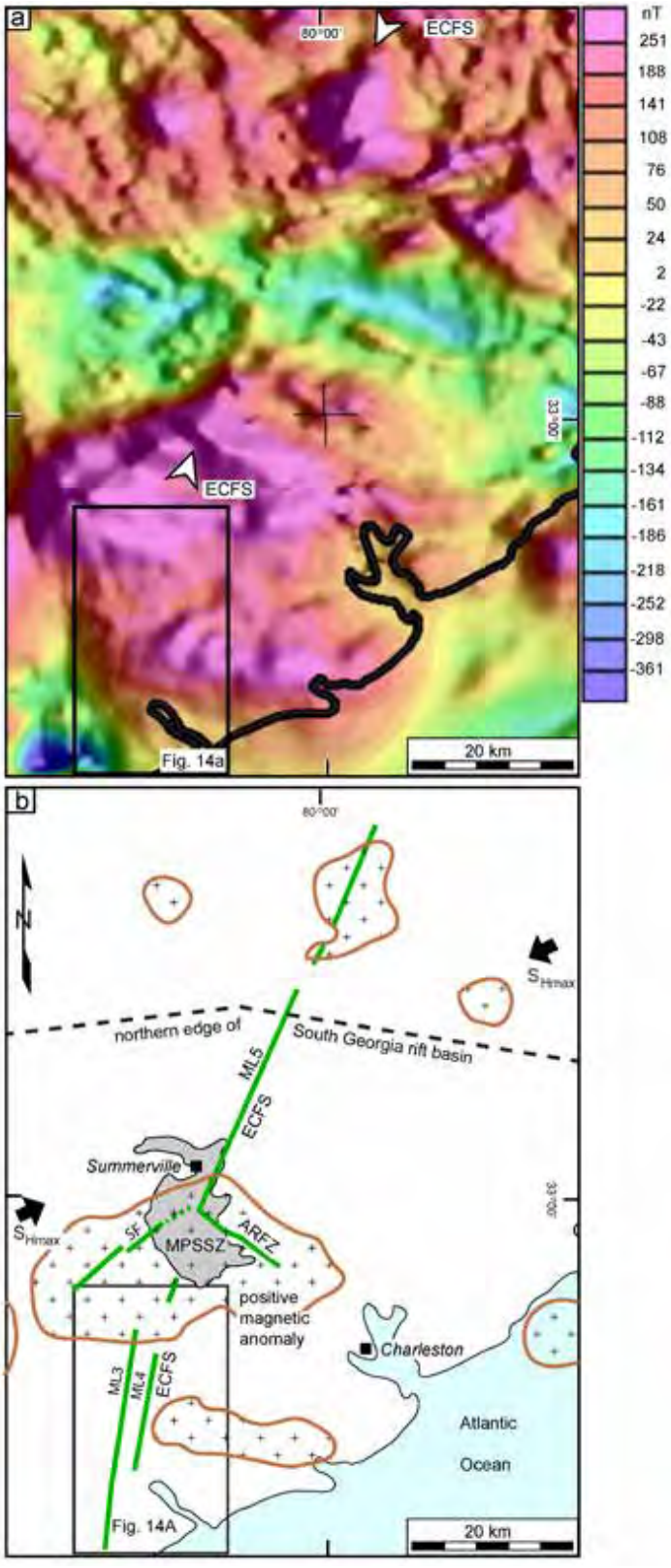

Figure 13. (a) Colour aeromagnetic image of the Charleston, South Carolina, region modified from Daniels (2005). Illumination direction is from the east. (b) Map of image (a) overlain with mafic plutons (patterned areas) in the pre-Cretaceous basement interpreted from the positive aeromagnetic anomalies in image (a).

(Figs. 1, 13, and 14, ML1-ML4). The two most prominent lineaments, ML3 and ML4, were enhanced further using the IHS enhancement and by illuminating the data from 110° (Figs. 14b–14d). The easternmost lineament, ML4, is located 1–1.5 km west of and parallels the trend formed by the buried faults along seismic-reflection profiles VT2, USC4, and USC5 (Fig. 1, locations 8–10) that define the location of the ECFS. Approximately 3 km west of ML4 is magnetic lineament ML3 that crosses the area of instrumentally-recorded earthquakes east of Adams Run (Fig. 1). Lineaments ML3 and ML4 coincide with the Edisto dome to the south and the interpreted uplifts along Caw Caw Swamp and releveling line 9 (denoted R9 in Figs. 1 and 15).

Magnetic lineaments ML1 and ML2 (Fig. 1) were optimally enhanced using the IHS enhancement and a 180° illumination azimuth. Unlike magnetic lineaments ML2-ML4, ML1 is curved (Figs. 14c and 14e). The northward projection of ML2 coincides approximately with the west-side-up Drayton fault along USGS seismic-reflection profile SC4 (Fig. 1, location 11, and Fig. 4, CDP 127). The upwarped reflectors west of this fault between CDPs 97 and 126 and at ~1 sec TWTT also coincide with the Parkers Ferry dome (Fig. 1). The northward projections of ML1 and ML3 also coincide with the east side of Parkers Ferry dome (Fig. 1).

Linear aeromagnetic anomaly ML5 along the ECFS near Summerville

Aeromagnetic lineament ML5 trends ~N22°E near Summerville (Figs. 1, 2, 3, and 13) and is located near the trend formed by several buried, steeply-dipping, west-side-up faults (Fig. 1, locations 1–7) and the ~320 m dextral offset in the Pleistocene Brownsville beach ridge deposit (Fig. 8). ML5 coincides with the ZRA (between thick red lines in Fig. 1) and crosses the MPSSZ, the incised part of the Ashley River (Fig. 9), and an area where the early Oligocene Ashley Formation is exposed beneath the middle Pleistocene Ten Mile Hill beds (next section) (Figs. 1,

Figure 14. (next page) (a) Enlarged image of magnetic lineaments (arrows) west of Charleston taken from Daniels (2005), which he illuminated from the east. Figure 13a shows the location of image (a). (b) IHS-enhanced version of image (a) illuminated from 110°. (c) IHS-enhanced version of image (a) illuminated from 180°. (d) Image (b) enhanced further with additional IHS enhancements. (e) Summary of lineaments interpreted from images (a)–(d).

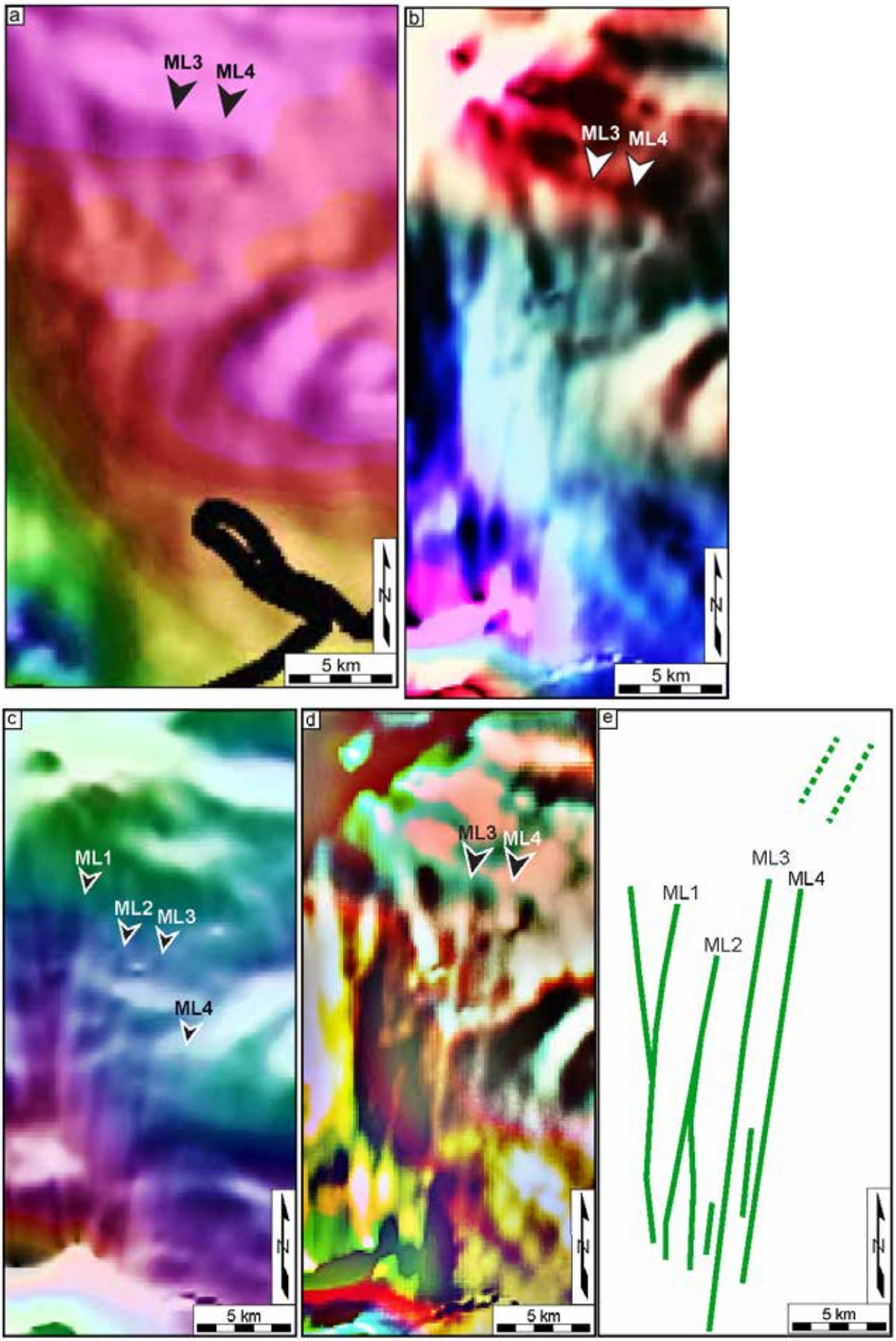

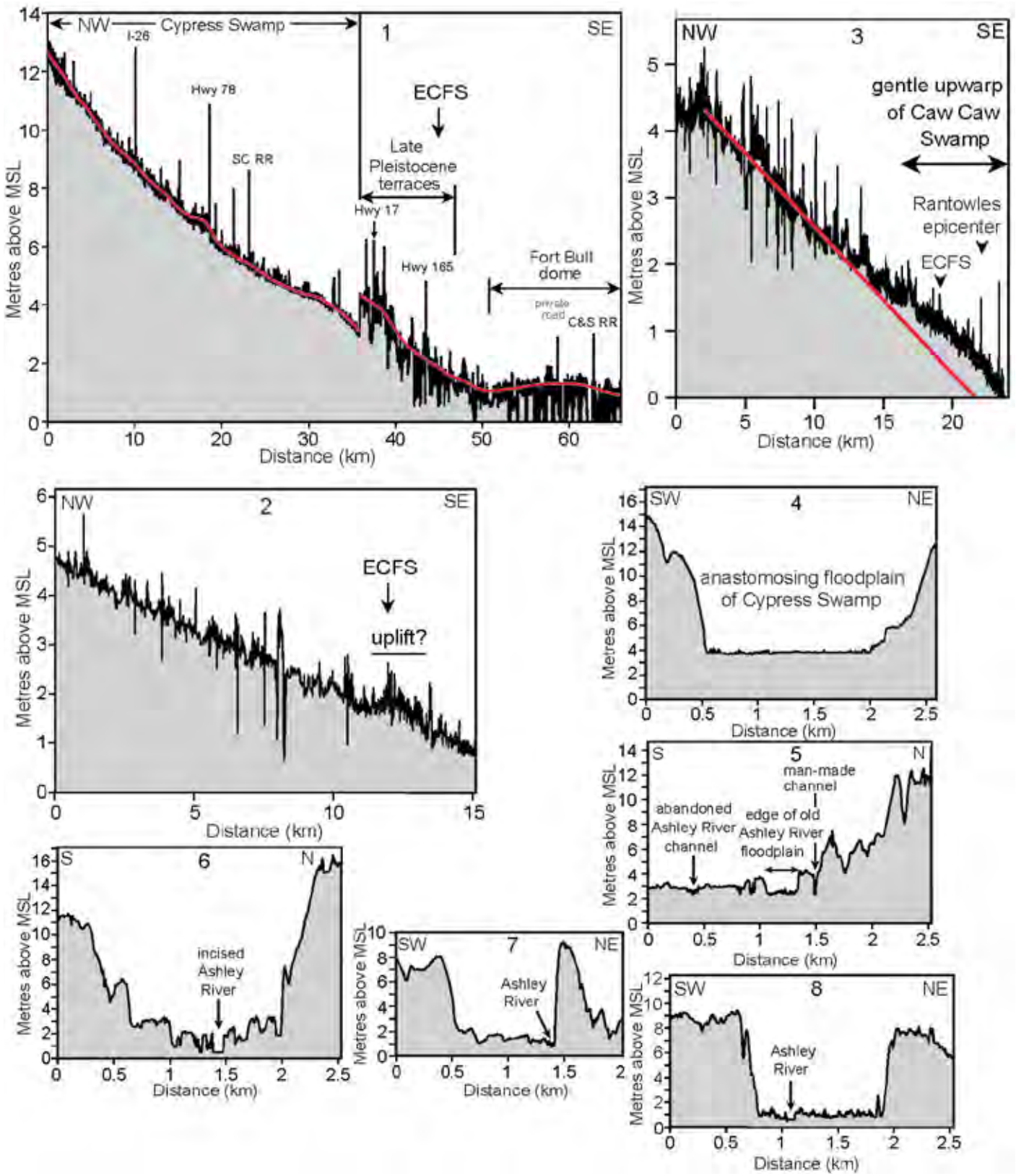

Figure 15. LiDAR-derived longitudinal profiles 1–3 along the Caw Caw and Horse Savanna swamps and the Ashley River. Red line is an arbitrary reference datum. Profiles 4–8 are LiDAR-derived profiles across the Ashley River valley and Cypress Swamp. Locations of profiles are shown in Figure 1.

16, and 17a). The trends of ML4 and ML5 intersect south of the Ashley River where they form the 12° Summerville restraining bend along the interpreted ECFS (Fig. 1).

The longitudinal profile constructed along the Ashley River valley and Cypress Swamp reveals a ~15-km-wide area that is gently upwarped upstream from the late Pleistocene terraces associated with the incised part of the Ashley River (Fig. 15, profile 1). Cross-valley elevation profiles revealed that magnetic lineament ML5 crosses the area of greatest incision, which is up to 2 m deeper than upstream or downstream (Fig. 15, profile 6). The cross-valley profile upstream across Cypress Swamp (Fig. 15, profile 4) shows that the valley floor lacks a channel, which is consistent with its anastomosing swamp pattern. Downstream, the longitudinal profile is slightly upwarped ~1 m where it crosses the Fort Bull dome (Fig. 15, profile 1).

New geomorphic and stratigraphic anomalies interpreted along the ZRA and ECFS

Investigation of LiDAR data and recently published geologic maps of the Charleston region (e.g., Weems *et al.* 2014) revealed new geomorphic and stratigraphic anomalies along the ZRA that support the existence of the ECFS. Near the coast the ZRA and ECFS coincide with the Edisto dome of Weems and Lewis (2002) (Fig. 1). North of this dome and near the Rantowles epicenter of the Charleston earthquake, the longitudinal profile along Caw Caw Swamp is gently upwarped where it crosses the ECFS and ZRA (Fig. 15b, profile 3). The valley along this part of Caw Caw Swamp is also the most deeply entrenched, up to 12 m (Marple 1994, fig. 3.4). About 6 km north of Caw Caw Swamp and near the interpreted fault along seismic-reflection profile VT2 is a ~2-km-long gently upwarped part of a longitudinal profile along Horse Savanna Swamp (Fig. 15, profile 2). Just south of the incised part of the Ashley River, the early Oligocene Ashley Formation is locally exposed beneath the middle Pleistocene Ten Mile Hill beds, yet is absent to the east and west (Weems *et al.* 2014) (Figs. 16 and 17a). The Ashley Formation is also exposed in the bed of the incised Ashley River. West of this area the LiDAR image in figure 2 of Marple and Hurd (2020) reveals that the Horse Savanna and Caddin Bridge swamps are continuous with the north-south-oriented part of the Edisto River valley to the west (Fig. 1).

New geomorphic and stratigraphic anomalies along the Bethera-McChune scarp (BMS)

The top of the early Oligocene Ashley Formation is ~14 feet (4.3 m) higher along the south-facing BMS north of the incised segment of the Ashley River than that to the south (Fig. 17a) (Weems *et al.* 2014, cross-section A-A'). Eastward, the Ashley and late Oligocene Chandler Bridge formations are exposed along the BMS along the south side of McChune ridge, yet are absent to the south (Fig. 17a). This change in elevation of the Ashley Formation also coincides with the 15- to 20-m drop in elevation south of the BMS. Beneath the McChune Branch of Bluehouse Swamp and the BMS is the ~700-m-wide, south-side-down, south-dipping Cenozoic graben on seismic-reflection profile C3 (Schilt *et al.* 1983) (Fig. 2, location 12, and Fig. 7). Between McChune Branch and Goose Creek valley to the east is a small tributary of Goose Creek that is collinear with McChune Branch. The Chandler Bridge Formation is locally exposed along this tributary (Fig. 17a). Seismic-reflection profiles VT3b and VT4 also cross the scarp trend along the 3- to 4-km-wide gap along the BMS (Fig. 1). However, profile VT3b bends ~90° to the east near the scarp and profile VT4 crosses the scarp trend at a low angle (Fig. 2) and are therefore not ideal for interpreting faults along this trend. Some fault plane solutions of microearthquakes near the BMS trend east-west where it crosses the MPSSZ (Marple and Hurd 2020, fig. 1).

Crossing the ZRA just north of the Ashley River is a discontinuous, ~20-km-long, low-lying east-west-oriented ridge, referred to herein as the Summerwood ridge, and the south-facing Summerwood scarp that cross various geologic units (Fig. 17a). They are also nearly collinear with the Deer Park lineament to the east (Fig. 17a). The western end of Summerwood ridge is capped by late Pleistocene (70–130 ka) Ladson barrier sediments (Weems *et al.* 2014) (Fig. 17a). Several horizons near the northwestern end of seismic-reflection profile VT3b are gently upwarped beneath Summerwood ridge (Chapman and Beale 2008, figs. 4 and 5, CDPs 30-150) (Fig. 2, dashed part of profile VT3b).

Anomalous outcrops of the Parkers Ferry, Ashley, Chandler Bridge, and Raysor formations in the northern Charleston region

Several of the older pre-Pleistocene formations that are normally buried beneath the younger Coastal Plain sediments are anomalously exposed in numerous fluvial valleys in the northern part of the Charleston region where the terrain is higher (Fig. 16). Between the ECFS to the west, the Canterhill lineament (surface expression of the Charleston fault) to the east, and the BMS to the south (Figs. 16 and 17b) is a NNE-oriented area where the late Eocene to Oligocene Parkers Ferry, Ashley, and Chandler Bridge formations are exposed along numerous stream valleys. This area is also 5–10 m higher than the areas to the east and south (Marple and Hurd 2020, fig. 5, profiles 1 and 2) and parallels the ECFS to the west (Fig. 16). The oldest geologic unit exposed in the Charleston region, the late Eocene Parkers Ferry Formation, outcrops along several stream valleys (Weems *et al.* 2014) where they cross the northwestern end of the Mount Holly dome and the Canterhill lineament along the Charleston fault (Figs. 16 and 17b). Near Woodstock, the Ashley Formation is locally exposed along the anomalous horse-shoe-shaped Blue-

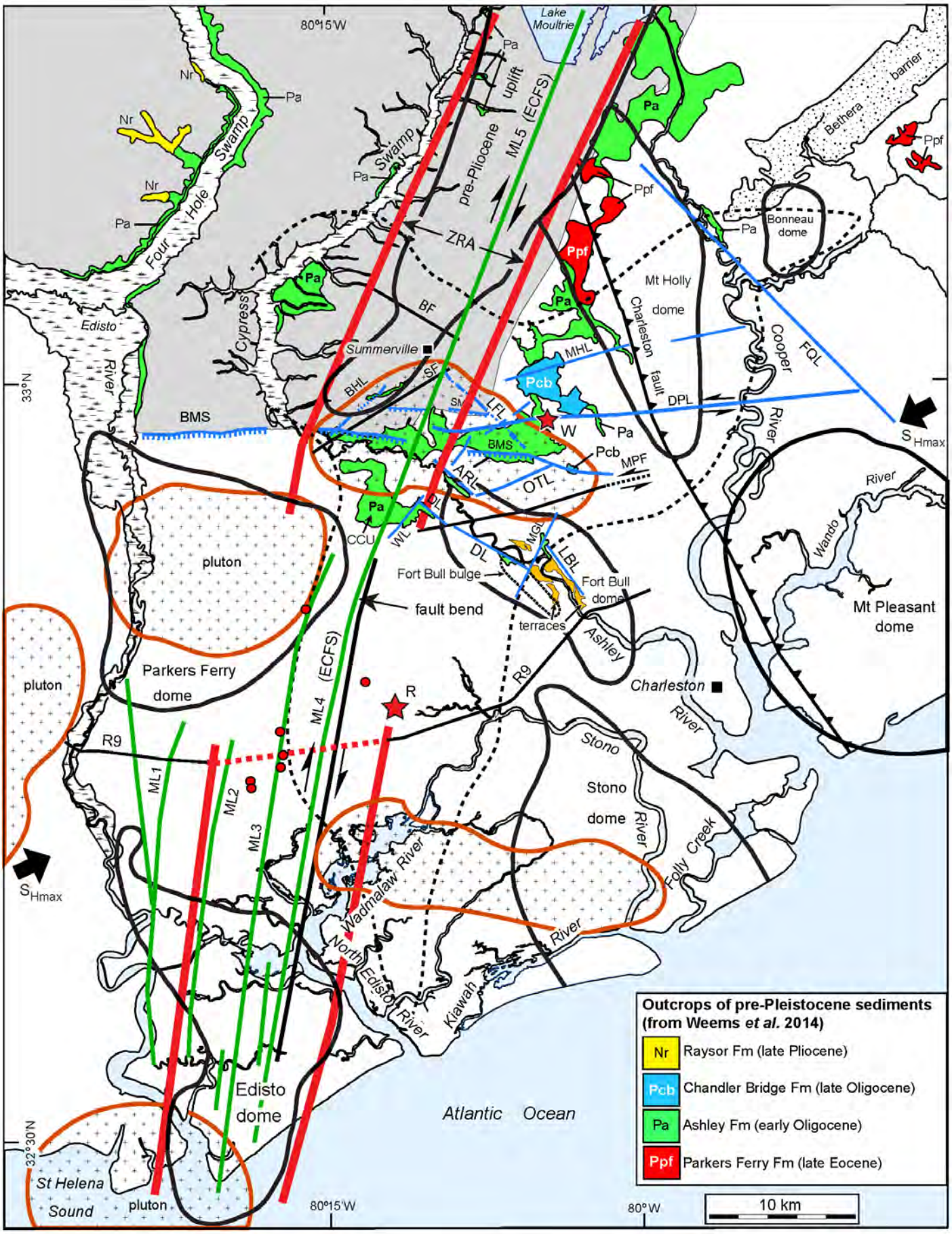

house and Goose Creek swamps where they intersect the Deer Park lineament (Fig. 17a).

Along some of the tributaries of the East Branch of the Cooper River and ~7 km northeast of Bonneau dome are other anomalous exposures of the late Eocene Parkers Ferry Formation (Fig. 16). The early Oligocene Ashley Formation is also locally exposed along an ~5 km long reach of the North Branch of the Cooper River valley where it coincides with the NW-SE-oriented French Quarter lineament (Fig. 17b). North of the BMS and west of the ZRA are exposures of the Ashley and late Pliocene Raysor formations along the Edisto River valley and the Four Hole and Cypress swamps (Figs. 16 and 17b).

Outcrops of the Ashley Formation along the Ashley River valley south of the BMS

The early Oligocene Ashley Formation outcrops along various segments of the Ashley River valley south of the BMS where they coincide with the NW-SE-oriented Ashley River, Dawkins, and Lambs lineaments of Marple and Hurd (2020, fig. 14). For example, northwest of Middleton Place and along the Ashley River lineament (ARL) of Marple and Hurd (2020) are exposures of the Ashley Formation that are absent on the opposite side of the valley (Figs. 16 and 17a). The ARL also crosses the greatest concentration of micro-seismicity in the MPSSZ (Marple and Hurd 2020, fig. 14) (Figs. 1 and 2).

The Ashley Formation also outcrops southeast of Middleton Place along the southwest side of the Ashley River valley for ~2 km (Weems *et al.* 2014) (Fig. 16). These outcrops coincide with the Dawkins lineament[4] where it crosses the Fort Bull dome (Fig. 16). The J horizon on seismic-reflection profile C3 beneath this part of the river valley is ~100 m higher to the southwest (Schilt *et al.* 1983, fig. 9).

Southeast of the NNE-SSW-oriented Magnolia Gardens lineament are exposures of the Ashley Formation along both sides of the Ashley River valley that coincide with the Pleistocene terraces of Marple and Hurd (2020, fig. 3) (Figs. 1 and 16). The outctrops along the northeast side of this part of the valley coincide with the Lambs lineament of Marple and Hurd (2020). This part of the Ashley River valley also coincides with the Fort Bull dome and is just northeast of the Fort Bull bulge (Fig. 16).

4 The Dawkins lineament was incorrectly referred to as the Dawson lineament by Marple and Hurd (2020).

DISCUSSION

Origin of the linear aeromagnetic anomalies

Although aeromagnetic lineaments ML3 and ML4 are conspicuously linear (Fig. 14b), it is unlikely that they are edge effects between flight paths because they trend N10°E whereas edge effects from the north-south flight paths would trend N0°E. Edge effects would also produce sharp linear boundaries between flight paths whereas the lineaments are 300–600 m wide (Fig. 14b). Furthermore, lineaments ML1 and ML2 are curved (Figs. 14c and 14e). It is also unlikely that the magnetic lineaments are associated with early Mesozoic dikes in the pre-Cretaceous basement because the nearest early Mesozoic dikes to the northwest are associated with NW-SE-oriented positive magnetic anomalies (Daniels 2005).

Despite the subtle nature of the magnetic lineaments, other observations suggest that they are associated with low-displacement brittle faults in the pre-Cretaceous crystalline basement. First, previous aeromagnetic studies of brittle faults elsewhere (e.g., Sims 2009; Yang *et al.* 2016) suggest that the subtle decrease in magnetization along these lineaments could be from brittle faulting in the crystalline basement beneath the 700- to 1100-m-thick sedimentary wedge in the Charleston region. Yang *et al.* (2016), for example, concluded that brittle deformation and fluid infiltration along the Yingxiu-Beichuan fault in China caused hydrothermal alteration of magnetite along the fault zone, thus decreasing the magnetization along the fault trend. Second, the proximity of ML4 to the buried faults along seismic-reflection profiles USC4 and USC5 (Fig. 1, locations 9 and 10), the parallelism of the zone of magnetic lineaments with the ZRA (Fig. 1), and the coincidence of ML3 and ML4 with the Edisto dome (Fig. 1) suggest that late Cenozoic compressional deformation and displacements along the interpreted basement faults associated with lineaments ML4 and possibly ML3 locally uplifted the overlying Coastal Plain sediments, thus producing the Edisto dome and the gentle uplifts along releveling line 9 (Fig. 1) and the Caw Caw and Horse Savanna swamps (Fig. 15, profiles 2 and 3). The parallelism between ML4 and the southern part of Sloan's isoseismals of the Charleston earthquake (Fig. 1) suggests that it may represent the fault along which the second large earthquake occurred west of Rantowles in 1886. The alignment of Drayton fault on seis-

Figure 16. (previous page) Summary map showing area of oldest outcrops of pre-Pleistocene sediments and the ECFS, LiDAR lineaments of Marple and Hurd (2020, blue lines), Cenozoic structural domes of Weems and Lewis (2002, bold contours), plutons interpreted from Figure 13 (thick orange contours surrounding patterns composed of +s), magnetic lineaments interpreted from Figure 14, and the outer contour of Sloan's isoseismals of the 1886 Charleston earthquake (Dutton 1889). Thick red parallel lines represent the area of uplift interpreted along the ZRA and ECFS. Light grey area in the northwest part of the area is the topographically higher area interpreted from the LiDAR image in figure 2 of Marple and Hurd (2020). The small red dots are small earthquakes of the Adams Run seismic zone. The orange patterns along the lower Ashley River valley are Pleistocene fluvial terraces from Marple and Hurd (2020, fig. 3b). CCU is the Clubhouse Crossroads uplift interpreted herein.

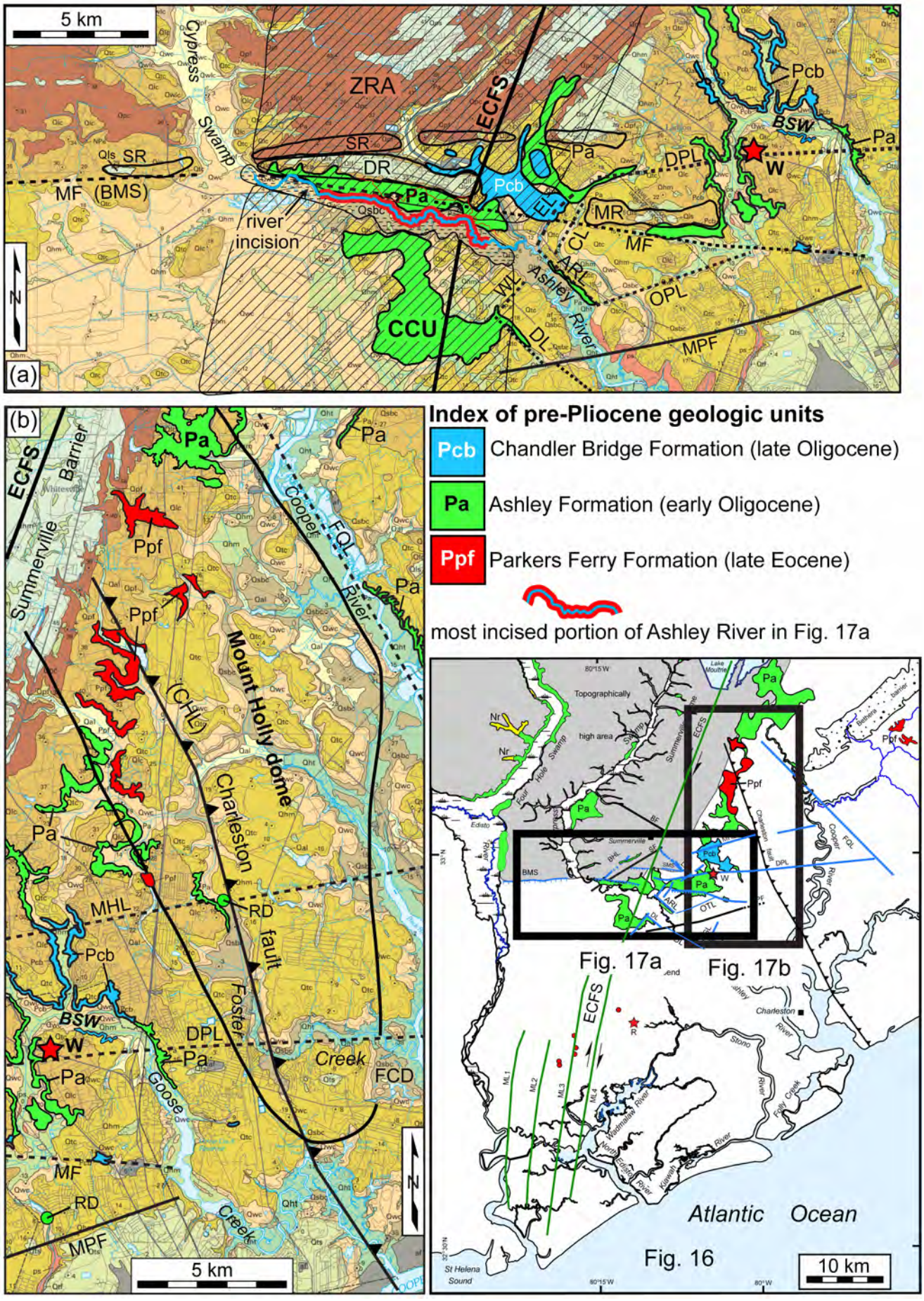

mic-reflection profile SC4 (Figs. 1 and 4) with the north-northeast projection of lineament ML2 (Fig. 1, location 11) suggests that ML2 may also be associated with a NNE-SSW-oriented fault in the pre-Cretaceous basement, uplift along which may have produced the Parkers Ferry dome (Fig. 1). The proximity of ML3 to the instrumentally recorded microearthquakes east of Adams Run (Fig. 1) suggests that it too may be a Cenozoic brittle fault in the pre-Cretaceous basement.

The continuity of magnetic lineaments ML4 and ML5 and their proximity to several buried faults interpreted from seismic-reflection profiles and the dextral offset in the Brownsville beach ridge deposit (Figs. 1 and 8) suggests that they represent the principal displacement zone along the ECFS. Because of the parallelism between lineaments ML1–ML4, we postulate that the southern end of the ECFS (Fig. 1) is associated with a broad fault zone at least 10 km wide. Thus, it is possible that the second earthquake on 31 August 1886 west of Rantowles could have been produced by dextral strike-slip displacement along the ECFS or a secondary fault east of and parallel to the ECFS.

Origin of the stratigraphic and geomorphic anomalies along the ECFS and ZRA

The anomalously thick exposures of Ashley Formation sediments along the BMS just north of the incised part of the Ashley River (Weems *et al.* 2014) (Fig. 17a) suggest that the outcrops north of the Ashley River have been exposed by late Quaternary uplift along the ECFS. The exposures of the Ashley Formation along and south of the incised part of the Ashley River valley and their absence to the east and west (Figs. 16 and 17a) suggests that this area has also been uplifted at least 3–4 m since the mid Pleistocene because of transpressional deformation along the interpreted ECFS, albeit less than that north of the river. We, therefore, refer to this area south of the Ashley River as the Clubhouse Crossroads uplift (Fig. 17a). We also considered the possibility that these outcrops are associated with buried topographic highs that were produced by differential erosion. Various observations, however, argue against this scenario. First, the incised part of the nearby Ashley River, which is interpreted to be from gentle uplift along the ECFS, crosses this area (Figs. 9, 15, profile 1, and 17a). Second, the Pleistocene fluvial deposits between the Clubhouse Crossroads area and the Edisto River (McCartan *et al.* 1984) and the continuity of the Horse Savanna Swamp with the Edisto River valley to the west (Fig. 1) suggests that the Edisto River once flowed southeastward along these swamps during the Pleistocene. Furthermore, the abrupt narrowing of the Edisto River's Holocene valley south of its intersection with the Horse Savanna Swamp (Fig. 1) and the Wando-age (70–130 ka) terraces along the edge of the lower Holocene valley (Weems *et al.* 2014) suggests that the Edisto River changed direction to the south during the late Pleistocene. We, therefore, postulate that late Pleistocene uplift across the Clubhouse Crossroads uplift and the Parkers Ferry dome (Figs. 1 and 16) diverted the Edisto River southward away from its earlier course down the Horse Savanna Swamp. Another implication of the Clubhouse Crossroads uplift is that it suggests that the ECFS continues southward beneath the Ashley River valley, rather than being offset to the southeast as previously proposed by Talwani and Durá-Gómez (2009).

The alignment of the Edisto dome, uplift along releveling line 9, and the Clubhouse Crossroads uplift (Figs. 1 and 16) with the gently upwarped longitudinal profiles along the Caw Caw and Horse Savanna swamps (Figs. 1 and 15) suggests that they are also likely from late Pleistocene to Holocene uplift along the ECFS (Figs. 1 and 16, between the red parallel lines). These upwarped profiles are not likely from differential erosion because there are no changes in the surficial geology along these swamps (Weems *et al.* 2014).

Origin of stratigraphic anomalies in the northern Charleston region

The higher terrain and anomalous exposures of the pre-Pleistocene Parkers Ferry, Ashley, Chandler Bridge, and Raysor formations in the stream valleys north of the BMS and between Four Hole Swamp to the west and the Canterhill lineament (surface expression of the Charleston fault) to the east (Figs. 16 and 17) suggest that this area has been gently uplifted during the Quaternary. Because of the more widespread pre-Pliocene outcrops along the east side of this topographically high area and because the Parkers Ferry Formation is exposed only along the east side of the ZRA (Fig. 16), we propose that the main source of this uplift is from compressional deformation along the ECFS and up-to-the-north (or down-to-the-south) displacements along the east-west-oriented McChune fault to the south (Fig. 16). The south-

Figure 17. (previous page) (a) Interpreted part of surficial geologic map of Weems *et al.* (2014) showing anomalous exposures of the pre-Pliocene Ashley and Chandler Bridge formations. Striped pattern is the ZRA. Abbreviations of faults (solid lines) and lineaments (dashed lines) are shown in Tables 1 and 2. Short-dashed pattern along the Ashley River valley shows the interpreted uplifted part of the river valley. DR, MR, and SR are the interpreted Dorchester, McChune, and Summerton ridges (thick black contours). BSW and CCU are Bluehouse Swamp and the Clubhouse Crossroads uplift. (b) Interpreted part of surficial geologic map of Weems *et al.* (2014) showing anomalous exposures of the pre-Pliocene Parkers Ferry, Ashley, and Chandler Bridge formations. Mt. Holly dome of Weems and Lewis (2002) is shown by thick black contour. The colors of the Chandler Bridge and Parkers Ferry formations were changed from Weems *et al.* (2014) to make them more visible on both maps.

dipping Cenozoic graben on seismic-reflection profile C3 (Fig. 7) suggests that the higher terrain north of this part of the BMS is from down-to-the-south displacement along the proposed McChune fault.

The alignment of the exposed Parkers Ferry sediments along tributaries of the East Branch of the Cooper River with the Bonneau dome to the southwest (Fig. 16) suggests that there may also be an area of uplift along a NE-SW-oriented buried fault. The anomalously straight Bethera paleo-barrier deposit just northwest of this trend (Fig. 16) suggests that the location of this paleo-barrier could have been influenced by uplift associated with NW-side-up displacement along this proposed buried fault.

Origin of the Cenozoic structural domes in the Charleston region

Besides uplift along Cenozoic faults, we evaluated other mechanisms to explain the interpreted Cenozoic structural domes in the Charleston region. One such mechanism is uplift along faults associated with the edges of buried Paleozoic and early Mesozoic plutons. Stevenson *et al.* (2006), for example, postulated that the edges of buried plutons in the pre-Cretaceous basement are areas of weakness where faults can form when favorably oriented relative to the direction of S_{Hmax}. However, very few of the Cenozoic domes overlie buried plutons (Fig. 16). Nor is doming of the Cenozoic strata in the Charleston region likely to fracture these uplifted strata because the deformation is too gentle. Instead, we postulate that the Cenozoic structural domes in the Charleston region are from late Cenozoic uplift along the ECFS and other buried Cenozoic faults like the Charleston fault near the southwestern edge of the Mount Holly and Mount Pleasant domes and the Ashley River fault zone beneath the Fort Bull bulge and dome (Fig. 16).

Cenozoic reactivation of a deep-seated basement fault along the ECFS

Because the ECFS crosses the Alleghanian Eastern Piedmont fault system and the early Mesozoic Florence and South Georgia rift basins, Marple and Talwani (2000) postulated that the ECFS is a Cenozoic fault system, possibly from reactivation of a pre-Alleghanian, deep-crustal fault system that was overthrust during the Alleghanian orogeny by the northwest transport of allochthonous terranes. This hypothesis is analogous to the ~1600-km-long New York-Alabama aeromagnetic lineament that is associated with a Precambrian to Cambrian right-lateral strike-slip fault system in the crystalline basement beneath the allochthonous terranes of the Allegheny Plateau and Valley and Ridge provinces (King and Zietz 1978; Steltenpohl *et al.* 2010; Powell and Thomas 2015). However, unlike the low magnetization of the terranes of the Appalachian Plateau and Valley and Ridge provinces, the higher magnetization of the allochthonous terranes beneath the thick sedimentary wedge in the Charleston region prevents detection of linear magnetic anomalies associated with pre-Mesozoic faults in the deep crust beneath the allochthonous terranes. If true, reactivation of such a deep crustal fault during Cenozoic time could have fractured through the overlying allochthonous terranes, Triassic basins, and the sedimentary wedge beneath the Coastal Plain to produce the ECFS. However, because of the low Cenozoic fault slip rate in the eastern USA (Prowell 1988, 0.3–1.5 m/myr), the accumulated strike-slip displacement along the ECFS during Cenozoic time is likely too small to be easily detected on regional gravity and aeromagnetic maps.

Summerville restraining bend

The 12° change in trend between magnetic lineaments ML5 near Summerville and ML4 to the south (Fig. 1) and their close proximity to the dextral offset in the Brownsville beach ridge deposit and buried faults along several seismic-reflection profiles (Figs. 1 and 2) support Marple and Hurd's (2020) hypothesis that the interpreted faults east of the Summerville restraining bend formed to compensate for the increased compression produced by dextral motion along the restraining bend and that displacements along the faults near the bend are responsible for the MPSSZ. Studies of fault bends have shown that secondary faults commonly develop along restraining bends in strike-slip faults (e.g., King and Nábělek 1985).

Possible relationship of the Deer Park lineament to the 1886 Charleston earthquake

The location of the Deer Park lineament in the northern meizoseismal area where the greatest intensities occurred in an east-west direction (Dutton 1889, pp. 301–302) supports our hypothesis that the main shock of the 1886 Charleston earthquake occurred along a fault associated with this lineament. The effects of the main shock in 1886 were nearly as intense near the eastern end of this area as those near Woodstock (Dutton 1889, pp. 301). Earle Sloan, for example, noted that pine trees two miles (~3.2 km) east of the Northeastern Railroad swayed violently during the main shock because dried sap had been thrown far from their trunks, the bark of which had been stripped to collect sap to make turpentine (Dutton 1889, pp. 301–302; Peters and Hermann 1986, pp. 58). Other dramatic examples of earthquake damage between Woodstock and the Cooper River are described in Dutton (1889, pp. 301–302). The Deer Park lineament also coincides approximately with the location along the old South Carolina Railroad where the direction of compressions reversed direction during the main shock in 1886 (Fig. 2, site S2, and Fig. 10), which Dutton (1889, pp. 295) emphasized in the following quote:

"Is it not a significant fact that every flexure contiguous to trestles or other points of rigid resistance, from the 15-mile post to the 27-mile post, was found to be at the south

end of such resistance; whereas preceding southerly from the 15-mile post, the flexures are found at the northerly extremities of points of resistance?"

The implication of this statement is that the main shock of the 1886 earthquake occurred on a fault that crossed the area beneath this part of the South Carolina Railroad, which we postulate is along the Deer Park lineament. The seismic waves traveling outward from the fault rupture would have produced compressional deformation in opposite directions north and south of the rupture at depth.

The alignment of the east-west-oriented part of the horseshoe-shaped Bluehouse Swamp (Fig. 17a), the "ridges or permanent waves" trending ~N80°E that Earle Sloan noted east of the old Northeastern Railroad and north of Goose Creek (Dutton 1889, pp. 291; Peters and Hermann 1986, pp. 57) (Fig. 2, site S1), the 90° eastward bend in Foster Creek (Marple and Hurd 2020, fig. 3a), and the rectangular shape of the Foster Creek depression (Marple and Hurd 2020, figs. 3a and 6a) (Fig. 17b) suggest that the proposed fault along the Deer Park lineament is associated with a broad zone of deformation and fracturing of the near surface sediments. The exposures of the Ashley Formation along the east side of the horseshoe-shaped Bluehouse and Goose Creek swamps where they cross the Deer Park lineament (Fig. 17a) suggest that uplift along the lineament exposed these older and normally buried sediments.

Possible relationship between the ECFS and Deer Park lineament and the cause of the second 1886 earthquake west of Rantowles

Studies of rupture nucleation on faults of various orientations relative to S_{Hmax} (Sibson 1990) suggest that strike-slip faults oriented 12° to 42° relative to S_{Hmax} are favorably oriented for reactivation. Thus, the 41° difference between the ~N21°E trend of the ECFS northeast of the Summerville restraining bend (ECFS(N)) and the ~N60°E orientation of S_{Hmax} (Fig. 1) favors dextral reactivation of the ECFS(N) whereas the 50° difference between this orientation of S_{Hmax} and the N10°E-oriented ECFS south of the bend (ECFS(S)) (Fig. 1) does not. However, dextral displacement along the more favorably oriented ECFS(N) would have added a south-directed horizontal stress on the crustal block east of ECFS(S) (Fig. 18). Moreover, if the direction of S_{Hmax} is closer to N50°E as proposed by Chapman *et al.* (2016), then dextral motion would also be favored on the ECFS(S).

Another mechanism that could favor dextral displacement along the ECFS(S) in 1886 is displacement on an intersecting fault, such as the interpreted fault along the Deer Park lineament. For example, the eastward motion of the crust south of the proposed Deer Park fault during the proposed sinistral-style strike-slip rupture could have decreased the normal stress on the ECFS(S) (Fig. 18), thus allowing it to slip dextrally to produce the second earthquake 8-10 minutes later west of Rantowles. An example of this mechanism is the 1987 Superstition Hills earthquake in southern California (Hudnut *et al.* 1989). During this earthquake, sinistral displacement on the NE-SW-oriented Elmore Ranch cross-fault decreased the normal stress on the NW-SE-oriented Superstitition Hills fault, thus causing it to rupture right-laterally over 11 hours later.

Conceptual model of the Summerville restraining fault bend

The interpreted deformation associated with the Summerville restraining bend is complex, as indicated by the numerous interpreted faults near the bend (Fig. 2). In general, dextral displacement across this bend would cause the area to the east to undergo compression whereas the area to the west would undergo extension (Fig. 18a). The compression to the east is accommodated by reverse and strike-slip faulting while down-to-the-south displacements along the proposed McChune fault west of the bend would accommodate extension to the west (Fig. 18a). However, this scenario changes when either the ECFS(N) or the ECFS(S) ruptures independently of the adjacent ECFS segment. For example, if only the ECFS(S) ruptures dextrally, as proposed herein in 1886, the southward movement of the crust east of ECFS(S) would favor extension, rather than compression, east of the Summerville bend (Fig. 18b), which is supported by the Cenozoic graben on seismic-reflection profile C3 that indicates normal-style faulting along the interpreted McChune fault (Fig. 7). In contrast to this scenario, the northward displacement of the crust west of the ECFS(S) would cause compression west of the Summerville bend (Fig. 18c). Other scenarios could explain the complexity of the interpreted faults associated with the Summerville bend, but are beyond the scope of this paper.

Favorable versus unfavorable orientation of faults associated with the Summerville restraining bend

Most of the interpreted faults associated with the Summerville restraining bend (Fig. 1) are favorably oriented for reactivation. The ENE-WSW orientations of the proposed faults along the Mount Holly, Middleton Place, Otranto, and Deer Park lineaments and the WNW-ESE orientation of the BMS relative to S_{Hmax} favor sinistral strike-slip displacement while the NW-SE orientations of the Charleston fault (Canterhill lineament) and the interpreted fault along the French Quarter lineament zone favor reverse-style displacement. In contrast to the ECFS and other interpreted faults east of the Summerville bend, the N57°E orientation of the Summerville fault west of the Summerville bend and other similarly oriented faults in the Charleston region are not favorably oriented for reactivation because they are nearly parallel to the N50-60°E orientation of S_{Hmax} (Fig. 1).

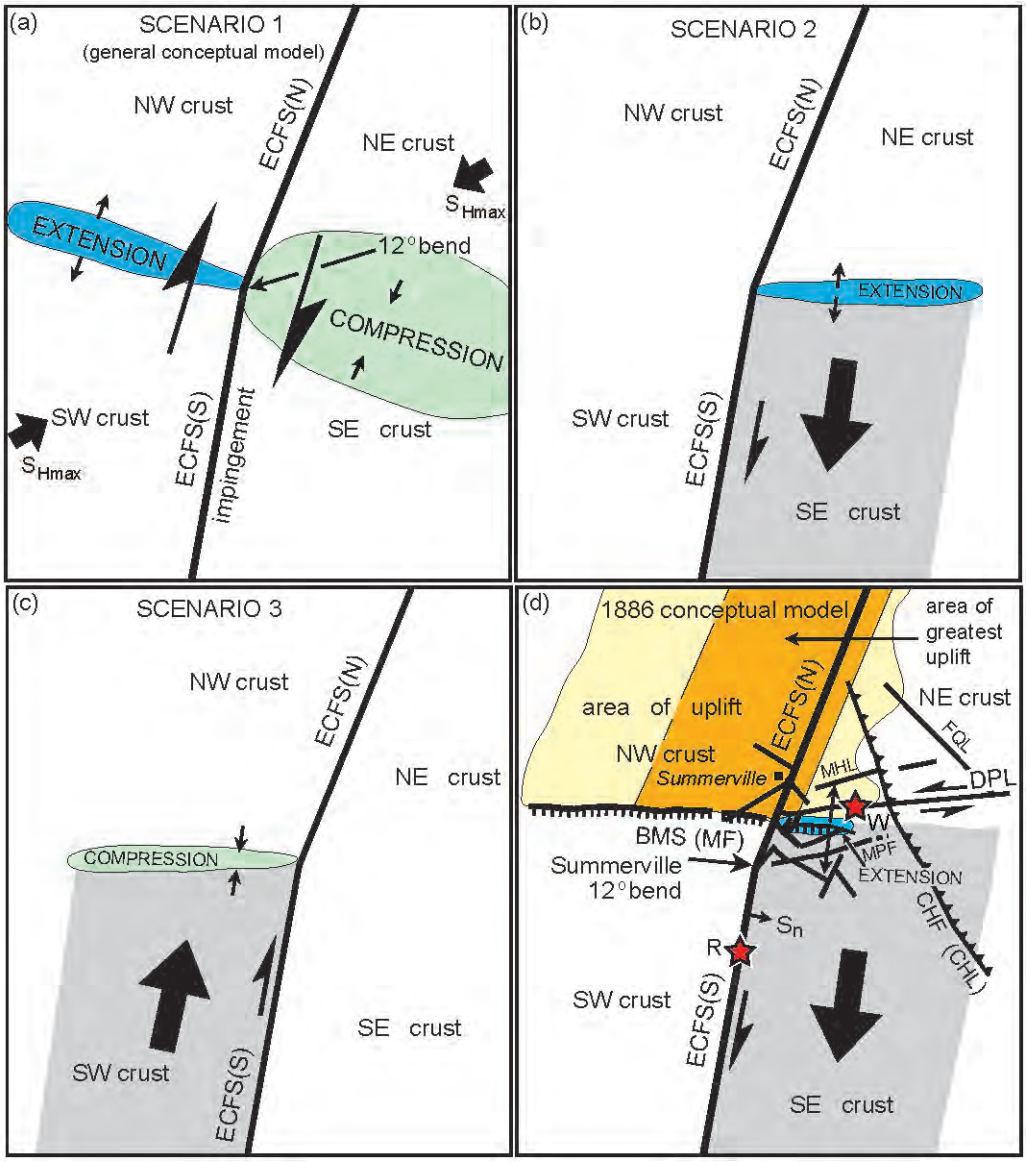

Figure 18. (a) General conceptual model showing the 12° Summerville restraining bend in the ECFS. Dextral motion along the ECFS causes compression (green pattern) east of the bend and extension (blue pattern) west of the bend. (b) Conceptual model in which the crust southeast of the restraining bend and east of the southern ECFS (ECFS(S)) moves independently of the crust east of the northern ECFS (ECFS(N)), causing extension (blue pattern) east of the Summerville bend. (c) Conceptual model in which the southwestern crust moves to the northeast, causing compression (green pattern) west of the bend. (d) Conceptual model in which sinistral motion on the Deer Park lineament (DPL) during the main shock of the 1886 Charleston earthquake decreases the normal stress (S_n) on the ECFS(S), causing it to rupture. The yellow and orange patterns to the north represent the topographically high area shown in Figures 2 and 16.

Origin and implications of the dextral offset in the Brownsville beach ridge deposit

The alignment of the dextral offset in the Pleistocene Brownsville beach ridge deposit northeast of Summerville (Fig. 8) with magnetic lineament ML5 and several buried faults interpreted from seismic-reflection profiles that cross the Summerville area (Fig. 1) strongly suggests that the beach ridge offset is from cumulative dextral strike-slip displacements along the ECFS. This offset, therefore, has several implications regarding the seismotectonics in the Charleston region. First, the ~320 m of dextral offset and the 970–730 ka age (Weems *et al.* 1997) of the Summerville barrier island complex of the Penholoway Formation yields a minimum average fault slip rate of 0.33 to 0.44 mm per year along this part of the ECFS. If, however, the Summerville barrier is part of the older Wicomico Formation (1.8–2.12 Ma, Weems *et al.* 1997) as proposed by Doar (2014), the slip rate would be smaller, 0.15–0.18 mm per year. We, therefore, postulate that the ECFS is a Cenozoic fault that has under-

gone ≤ 320 m of cumulative displacement near Summerville. Such a low amount of slip along the ECFS could explain why it is not easily identified in the landscape and on regional aeromagnetic and gravity maps of the South Carolina Coastal Plain. Another implication of the beach ridge offset relates to the orientation of S_{Hmax} in the Charleston region. Although most studies of seismicity, borehole breakouts, and GPS data suggest that the orientation of S_{Hmax} in the Charleston region is ~N50-60° E (Zoback and Zoback 1989; Madabhushi and Talwani 1993; Talwani *et al.* 1997; Chapman *et al.* 2016; Lund Snee and Zoback 2020), other recent studies (e.g., Levandowski *et al.* 2018) have suggested that S_{Hmax} is oriented nearly east-west. However, the dextral offset in the beach ridge deposit indicates that the ECFS near Summerville has undergone repeated dextral displacements since the middle Pleistocene. Thus, the direction of S_{Hmax} must be favorably oriented relative to the ~N22°E orientation of the ECFS near Summerville to cause dex-tral strike-slip displacements along the ECFS. Thus, based on Sibson's (1990) study of fault orientation relative to the horizontal compressive stress field, it is unlikely that the orientation of S_{Hmax} in the Charleston region is greater than N60°E.

The beach ridge offset also demonstrates that Cenozoic faults beneath the Coastal Plain can locally fracture the near surface sediments, albeit too minor to be easily recognized at the surface. Similarly, Marple and Hurd (2020) suggested that linear drainages along some of the LiDAR lineaments east of the Summerville restraining bend (Fig. 1) are also likely associated with minor faulting of the near surface sediments, thereby causing increased erosion and the development of linear drainages along these interpreted faults in the Charleston region.

Origin of geomorphic and stratigraphic anomalies along the Bethera-McChune scarp (BMS)

The higher elevation of the early Oligocene Ashley Formation north of the incised part of the Ashley River, the presence of the Ashley and late Oligocene Chandler Bridge formations along the south side of McChune ridge to the east (Figs. 16 and 17), and the south-dipping Cenozoic graben on seismic-reflection profile C3 (Fig. 7) suggest that the BMS is associated with north-side-up (or south-side-down) displacements along the proposed east-west-oriented Mc-Chune fault. The mid-Pleistocene Ladson barrier deposits along the tops of the Dorchester and McChune ridges (Weems *et al.* 2014, unit Qls) (Fig. 16a) suggest that north-side-up Pleistocene uplift along these ridges caused these barrier sediments to be deposited along these two ridges when sea level rose to this area 240–730 ka. Such a process was proposed by Marple *et al.* (2018) along the Merrimack ridge above the Newburyport thrust fault in northeastern Massachusetts and by Marple and Hurd (2021) along the Sloan and Jarmantown topographic highs above the interpreted Faison and Neuse faults beneath the North Carolina Coastal Plain. Thus, it is likely that the Dorchester and McChune ridges represent areas of uplift along which the Ladson barrier sediments were deposited during the mid-Pleistocene. Likewise, because the Summerwood ridge crosses various surficial sediments and because it is capped to the west by Ladson barrier sediments (Fig. 17a), it too is possibly related to Pleistocene uplift along the north side of an east-west-oriented buried fault. The alignment of the ESE-WSW-oriented tributary of Goose Creek to the southeast with the McChune Branch of Bluehouse Swamp and the anomalous exposure of late Oligocene Chandler Bridge sediments along this tributary (Fig. 17a) suggests that the proposed McChune fault continues east-southeast to the Goose Creek valley.

Origin of stratigraphic anomalies along the Ashley River fault zone

Several observations suggest that the LiDAR lineaments along the lower Ashley River represent relatively short faults of a segmented Ashley River fault zone. For example, the exposures of the Ashley Formation along the anomalously straight northeastern valley wall that defines the Ashley River lineament (ARL) and their absence along the opposite side of the valley suggests that the northeast side of this part of the valley (Fig. 17a) has been uplifted a few metres to the northeast along a fault associated with the ARL. Fracturing of the near-surface sediments near this proposed fault could have produced the fissure along the northern bank of the Ashley River valley during the 1886 earthquake shown in plate XXIII of Dutton (1889). The coincidence of the ARL with the MPSSZ suggests that this proposed fault is presently active.

Exposures of the Ashley Formation along the unnamed swamp that defines the northwestern end of the Dawkins lineament (Fig. 17a) support uplift along this lineament. Farther downstream near Middleton Gardens, the coincidence of the Dawkins lineament with outcrops of the Ashley Formation along the southwestern wall of the Ashley River valley (Fig. 16) also supports uplift along this lineament, which is consistent with the southwest-side-up fault near the southwest end of seismic-reflection profile C3 and suggests that the Dawkins lineament may be the surface expression of this fault. Exposures of the Ashley Formation and the Pleistocene terraces downstream from the Magnolia Gardens lineament (Fig. 1) and along both sides of the Ashley River valley where they cross the Fort Bull dome (Figs. 16 and 17a) suggest that this part of the valley has undergone late Quaternary uplift. The linear, northeast side of the Ashley River valley along the Lambs lineament suggests that it may be associated with uplift along a fault. Based on these observations, we postulate that Quaternary fault displacements along the Ashley River, Dawkins, Lambs, and Magnolia Gardens lineaments have produced the uplift that formed the Fort Bull dome.

Reevaluation of the ECFS

Among the most conspicuous geomorphic anomalies that define the ZRA and ECFS are the north-northeast-convex curves in the Santee, Black, and Lynches rivers in South Carolina and the Nottoway River in southeastern Virginia, which Marple and Talwani (2000) postulated were produced by a gentle, down-to-the-NNE tilt along nearby segments of the buried ECFS. Bartholomew and Rich (2012), in contrast, argued against the existence of the ECFS. Instead of a tectonic origin, they postulated that the river curves in South Carolina were produced by an early to middle Pleistocene northeastward migration of these rivers because of down-to-the-SW displacements along a NW-SE-oriented Cape Fear fault near the South Carolina/North Carolina border. Marple and Hurd (2021, pp. 317), however, argued against Bartholomew and Rich's (2012) down-to-the-NE tilt in northeastern South Carolina and the existence of the Cape Fear fault. Thus, down-to-the-NNE tilting along nearby segments of the buried ECFS remains our preferred explanation for the origin of the river curves.

Pratt *et al.* (in press) also argued against the existence of the ECFS due to the lack of conspicuous uplift along the proposed fault system. However, some seismic-reflection profiles that cross the ECFS show uplifted Cenozoic strata within a 3- to 5-km-wide zone associated with buried, up-to-the-west fault displacements (e.g., Figs. 5 and 6), although some profiles, like USC4 and USC5 (Marple and Miller 2006, figs. 12 and 13), do not show any significant vertical displacement along the trend of the ECFS. However, in these areas the predominant fault motion could be dextral strike-slip and, therefore, may not produce significant vertical offsets of the overlying strata. Moreover, the coincidence of the Edisto dome and the pre-Pliocene uplift near Summerville (Figs. 1 and 2) with the proposed ECFS shows that Oligocene strata has been gently uplifted along parts of the ECFS in the Charleston region. Pratt *et al.* (in press) also argued that the Summerville scarp (Figs. 1 and 2) should be located above the buried ECFS. This scarp, however, is a paleoshoreline scarp (e.g., Doar 2014), not a tectonic scarp. Furthermore, uplift above a steep, buried transpressional strike-slip fault like the proposed ECFS would likely produce gentle uplift of the overlying strata east and west of the fault, not just above the fault itself (e.g., Figs. 5 and 6). Lastly, several other lines of evidence support the existence of the ECFS and uplift along it, including the exposures of pre-Pleistocene strata in the northwest part of the Charleston region (Figs. 16 and 17), the uplift along releveling profile 9 (Fig. 1), the aeromagnetic lineaments presented herein (Figs. 3, 13, and 14), the dextrally offset beach ridge deposit (Fig. 8), and the local incision of the Ashley River (Figs. 1, 2, and 9).

Lack of seismicity along the ECFS

Although the orientation of the ECFS relative to the direction of S_{Hmax} favors its reactivation, recent seismicity along most of the ECFS has been low level. This observation is likely the result of the low strain rate along the Atlantic margin (10^{-9} to 10^{-10} yr^{-1}, Johnston 1989), which could cause recurrence intervals between large earthquakes along the ECFS to range from hundreds to tens of thousands of years. Numerous studies elsewhere in intraplate settings have documented evidence for Pleistocene to Holocene earthquakes along faults that currently exhibit little or no seismicity, including the Bootheel fault in southeastern Missouri (Marple and Schweig 1992; Guccione *et al.* 2005), the Saline River fault zone in southeastern Arkansas (Cox *et al.* 2012), the Newburyport fault in northeastern Massachusetts (Marple *et al.* 2018), the Faison and Neuse faults that cross the Cape Fear arch in North Carolina (Marple and Hurd 2021), the Tennant Creek earthquakes of Australia (Crone *et al.* 1997), and the proposed southwest continuation of the Norumbega fault system in southern New England where several Pleistocene drumlins are vertically offset (Marple and Hurd 2019, figs. 9 and 25).

CONCLUSIONS

In conclusion, we postulate that the NNE-SSW-oriented linear magnetic anomalies in the southern meizoseismal area of the 1886 Charleston, South Carolina, earthquake are associated with low-displacement brittle faults in the pre-Cretaceous crystalline basement and that magnetic lineaments ML4 and ML5 represent the principal displacement zone along the southern end of the ECFS. The N50-60°E orientation of S_{Hmax} relative to the ECFS in South Carolina favors its right-lateral reactivation. Evidence for Cenozoic uplift along the ECFS includes the Summerville and Clubhouse Crossroads uplifts, the zone of incision along the Ashley River, the Edisto dome near the coast, uplift along releveling profile 9, and locally upwarped longitudinal profiles along the Caw Caw and Horse Savanna swamps and along the Ashley River valley. This uplift is more pronounced north of the Ashley River.

The 12° change in trend between ML4 and ML5 supports the existence of the Summerville restraining bend along the ECFS south of the Ashley River. We postulate that the interpreted faults east of this restraining bend formed to compensate for the increased compression produced by dextral motion along the bend. We also postulate that sinistral strike-slip displacement on one of these faults associated with the ~40-km-long, east-west-oriented Deer Park lineament may have produced the main shock of the 1886 Charleston, South Carolina, earthquake. Sinistral displacement on this interpreted fault may have decreased the normal stress along the ECFS to the south, thereby causing

dextral displacement along the southern end of the ECFS and the second earthquake west of Rantowles 8–10 minutes after the main shock. Extension is generally favored west of the bend and appears to be accommodated by down-to-the-south displacements on the interpreted east-west-oriented McChune fault beneath the Bethera-McChune scarp (BMS). However, displacements along individual segments of the ECFS could have also produced local extension east of the Summerville restraining bend and compression to the west. The south-dipping Cenozoic graben east of the Summerville bend on COCORP seismic-reflection profile C3 suggests that this part of the McChune fault has undergone extension during the Cenozoic. Displacements along some of the proposed faults near the Summerville restraining bend coincide with the MPSSZ. Thus, displacements along these faults may be responsible for much of the modern seismicity between Summerville and Middleton Place. Further studies of the Summerville bend are needed, therefore, to better understand the deformation associated with this fault bend.

Exposures of the late Eocene Parkers Ferry, early Oligocene Ashley, late Oligocene Chandler Bridge, and late Pliocene Raysor formations in the stream valleys north of the proposed McChune fault and between Four Hole Swamp to the west and the Canterhill lineament (surface expression of the Charleston fault) to the east suggest that this area has been uplifted during the Quaternary with the greatest uplift between the Ashley River and Lake Moultrie. The source of this uplift is likely the result of compressional deformation along the ECFS and up-to-the-north (or down-to-the-south) displacements along the McChune fault to the south.

Several, mostly NW-SE-oriented LiDAR lineaments along the Ashley River valley south of the BMS, including the Ashley River, Dawkins, Lambs, and Magnolia Gardens lineaments, suggest that they are part of a segmented, NW-SE-oriented Ashley River fault zone. We propose that Quaternary uplift along these interpreted faults has exposed the early Oligocene Ashley Formation along various segments of the Ashley River valley and produced the Fort Bull dome and Pleistocene terraces along the lower Ashley River valley.

Further studies of the various faults interpreted herein are needed because studies of liquefaction features within the Coastal Plain of South Carolina and southeastern North Carolina have revealed several Holocene earthquakes north and south of the Charleston region (e.g., Talwani and Schaeffer 2001) where little seismicity has been recorded. These earthquakes may have occurred along the ECFS and other faults in the Coastal Plain of South Carolina and southeastern North Carolina, including the Charleston and Middleton Place faults, and the proposed McChune and Deer Park faults in the South Carolina Coastal Plain and the interpreted Neuse, Faison, and Livingston Creek faults in southeastern North Carolina (Marple andHurd 2021). Because of the rapid urbanization between Summerville and Charleston, a large earthquake today in the Charleston region would cause tremendous damage and loss of life. Therefore, further investigation of these and other potentially active faults in the Charleston region is essential to assessing seismic hazards in the southeastern United States and to better understand the evolution of Atlantic type continental margins.

ACKNOWLEDGEMENTS

We thank reviewer Ross Hartleb and Atlantic Geoscience editor Sandra Barr for their many constructive comments that helped improve our paper. This article benefited from discussions with William Doar.

REFERENCES

Bakun, W.H. and Hopper, M.G. 2004. Magnitudes and locations of the 1811–1812 New Madrid, Missouri, and the 1886 Charleston, South Carolina, earthquakes. Bulletin of the Seismological Society of America, 94, pp. 64–75. https://doi.org/10.1785/0120020122

Bartholomew, M.J. and Rich, F.J. 2007. The walls of colonial Fort Dorchester: A record of structures caused by the August 31, 1886 Charleston, South Carolina, earthquake and its subsequent earthquake history. Southeastern Geology, 44, no. 4, pp. 147–169.

Bartholomew, M.J. and Rich, F.J. 2012. Pleistocene shorelines and coastal rivers: Sensitive potential indicators of Quaternary tectonism along the Atlantic Coastal Plain of North America. *In* Recent advances in North American paleoseismology and neotectonics east of the Rockies. *Edited by* R.T. Cox, M.P. Tuttle, O.S. Boyd, and J. Locat. Geological Society of America, Special Paper 493, pp. 17–36. https://doi.org/10.1130/2012.2493(02)

Behrendt, J.C. 1983. Did movement on a northeast trending listric fault near the southeast edge of the Jedburg Triassic-Jurassic(?) basin cause the Charleston, South Carolina, 1886 earthquake? *In* A workshop on the 1886 Charleston, SC, earthquake and its implications for today. *Edited by* W.W. Hays and P.L. Gori. United States Geological Survey, Open File Report 83-843, pp. 126–131.

Bollinger, G.A. 1977. Reinterpretation of the intensity data for the 1886 Charleston, South Carolina, earthquake. *In* Studies related to the Charleston, South Carolina, earthquake of 1886: A preliminary report. *Edited by* D.W. Rankin. United States Geological Survey, Professional Paper 1028-B, pp. 17–32.

Buckner, J.C. 2011. Crustal structure in a Mesozoic extensional terrane: The South Georgia Rift and epicentral area of the 1886 Charleston, South Carolina, earthquake. Unpublished Masters thesis, Virginia Polytechnic and State University, Blacksburg, Virginia, 50 p.

Chapman, M.C. and Beale, J.N. 2008. Mesozoic and Cenozoic faulting imaged at the epicenter of the 1886 Charles-

ton, South Carolina, earthquake. Bulletin of the Seismological Society of America, 98, pp. 2533-2542. https://doi. org/10.1785/0120080923

Chapman, M.C. and Beale, J.N. 2010. On the geologic structure at the epicenter of the 1886 Charleston, South Carolina, earthquake. Bulletin of the Seismological Society of America, 100, pp. 1010–1030. https://doi.org/10.1785/0120090231

Chapman, M.C., Beale, J.N., Hardy, A.C., and Wu, Q. 2016. Modern seismicity and the fault responsible for the 1886 Charleston, South Carolina, earthquake. Bulletin of the Seismological Society of America, 106, no. 2, pp. 364–372. https://doi.org/10.1785/0120150221

Colquhoun, D.J., Woollen, I.D., Van Nieuwenhuise, D.S., Padgett, G.G., Oldham, R.W., Boylan, D.C., Howell, P.D., and Bishop, J.W. 1983. Surface and subsurface stratigraphy, structure and aquifers of the South Carolina Coastal Plain. Columbia, State of South Carolina, Office of the Governor, Ground Water Protection Division, Report for Department of Health and Environmental Control, 78 p.

Colquhoun, D.J., Johnson, G.G., Peebles, P.C., Huddlestun, P.F., and Scott, T. 1991. Quaternary geology of the Atlantic Coastal Plain. *In* Quaternary nonglacial geology: Conterminous U.S. Geology of North America. *Edited by* R.B. Morrison. Geological Society of America, K-2, Boulder, Colorado, pp. 629–650. https://doi.org/10.1130/DNAG-GNA-K2.629

Costain, J.K. and Glover, L., III. 1983. Seismicity in the eastern United States and the role of crustal reflectivity. *In* Proceedings of Conference XX: A workshop on "The 1886 Charleston, South Carolina, earthquake and its implications for today." *Edited by* W.G. Hays and P.L. Gori. United States Geological Survey, Open File Report 83-843, pp. 207–220.

Cox, R.T., Harris, J., Forman, S., Brezina, T., Gordon, J., Gardner, C., and Machin, S. 2012. Holocene faulting on the Saline River fault zone, Arkansas, along the Alabama-Oklahoma transform. *In* Recent advances in North American paleoseismology and neotectonics east of the Rockies. *Edited by* R.T. Cox, M.P. Tuttle, O.S. Boyd, and J. Locat. Geological Society of America, Special Paper 493, pp. 17–36. https://doi.org/10.1130/2012.2493(07)

Crone, A.J., Machette, M.N., and Bowman, J.R. 1997. Episodic nature of earthquake activity in stable continental regions revealed by palaeoseismicity studies of Australian and North American Quaternary faults. Australian Journal of Earth Sciences, 44, pp. 203–214. https://doi.org/10.1080/08120099708728304

Daniels, D.L. 2005. South Carolina aeromagnetic and gravity maps and data: A website for the distribution of data. United States Geological Survey, Open File Report 2005-1022. https://doi.org/10.3133/ofr20051022, accessed 1 March 2020.

Daniels, D.L., Zietz, I., and Popenoe, P. 1983. Distribution of subsurface lower Mesozoic rocks in the southeastern United States as interpreted from regional aeromagnetic and gravity maps. *In* Studies related to the Charleston, South Carolina, earthquake of 1886–Tectonics and seismicity. *Edited by* G.S. Gohn. United States Geological Survey, Professional Paper 1313-K, 24 p.

Doar, W.R., III. 2014. The geologic implications of the factors that affected relative sea-level positions in South Carolina during the Pleistocene and the associated preserved high-stand deposits. Unpublished Ph.D. thesis, University of South Carolina, Columbia, South Carolina, 172 p.

Durá-Gómez, I. and Talwani, P. 2009. Finding faults in the Charleston area, South Carolina: 1. Seismological data. Seismological Research Letters, 80, pp. 883–900. https://doi.org/10.1785/gssrl.80.5.883

Dutton, C.E. 1889. The Charleston earthquake of August 31, 1886. United States Geological Survey, U.S. Government Printing Office, Washington, D.C., pp. 203–528.

Gohn, G.S. (*Editor*). 1983. Studies related to the Charleston, South Carolina, earthquake of 1886–Tectonics and seismicity. United States Geological Survey, Professional Paper 1313, 8 plates, 467 p. https://doi.org/10.3133/ofr82134

Gohn, G.S. 1988. Late Mesozoic and early Cenozoic geology of the Atlantic Coastal Plain: North Carolina to Florida. *In* The Atlantic continental margin: Geology of North America. *Edited by* R.E. Sheridan and J.A. Grow. Boulder, Colorado, Geological Society of America, I-2, pp. 107–130. https://doi.org/10.1130/DNAG-GNA-I2.107

Gohn, G.S., Houser, B.B., and Schneider, R.R. 1983. Geology of the basement rocks near Charleston, South Carolina–Data from detrital rock fragments in lower Mesozoic(?) rocks in Clubhouse Crossroads test hole #3. *In* Studies related to the Charleston, South Carolina, earthquake of 1886–Tectonics and seismicity. *Edited by* G.S. Gohn. United States Geological Survey, Professional Paper 1313-E, 22 p. https://doi.org/10.3133/ofr82134

Guccione, M., Marple, R., and Autin, W. 2005. Evidence for Holocene displacements along the Bootheel fault (lineament) in southeastern Missouri: Seismotectonic implications for the New Madrid region. Geological Society of American Bulletin, 117, no. 3/4, pp. 319–333. https://doi.org/10.1130/B25435.1

Hamilton, R.M., Behrendt, J.C., and Ackermann, H.D. 1983. Land multichannel seismic reflection evidence for tectonic features near Charleston, South Carolina. *In* Studies related to the Charleston, South Carolina, earthquake of 1886–Tectonics and seismicity. *Edited by* G.S. Gohn. United States Geological Survey, Professional Paper 1313-I, 18 p.

Hudnut, K.W., Seeber, L., and Pacheco, J. 1989. Cross-fault triggering in the November 1987 Superstition Hills earthquake sequence, southern California. Geophysical Research Letters, 16, no. 2, pp. 199–202. https://doi.org/10.1029/GL016i002p00199

Johnston, A.C. 1989. The seismicity of "stable continental interiors." *In* Earthquakes at North Atlantic passive margins: Neotectonics and postglacial rebound. *Edited by* S. Gregersen and P.W. Basham. Kluwer Academic Publishers, Dordrecht, Netherlands, NATO ASI Series C, Math-

ematical and Physical Sciences, 266, pp. 299–327. https://idoi.org/10.1007/978-94-009-2311-9_18

Johnston, A.C. 1996. Seismic moment assessment of earthquakes in stable continental regions–III, New Madrid 1811–1812, Charleston 1886 and Lisbon 1755. Geophysical Journal International, 126, pp. 314–344. https://doi.org/10.1111/j.1365-246X.1996.tb05294.x

King, E.R. and Zietz, I. 1978. The New York-Alabama lineament: Geophysical evidence for a major crustal break in the basement beneath the Appalachian basin. Geology, 6, pp. 312–318. https://doi.org/10.1130/0091-7613(1978)6<312:TNYLGE>2.0.CO;2

King, G. and Nábělek, J. 1985. Role of fault bends in the initiation and termination of earthquake rupture. Science, 228, pp. 984–987. https://doi.org/10.1126/science.228.4702.984

Lennon, G. 1985. Identification of a northwest-trending seismogenic graben near Charleston. Unpublished Masters thesis, University of South Carolina, Columbia, South Carolina, 84 p.

Levandowski, W., Herrmann, R.B., Briggs, R., Boyd, O., and Gold R. 2018. An updated stress map of the continental United States reveals heterogeneous intraplate stress. Nature Geoscience, 11, pp. 433–437. https://doi.org/10.1038/s41561-018-0120-x

Lund Snee, J. and Zoback, M.D. 2020. Multiscale variations of the crustal stress field throughout North America. Nature Communications. pp. 1–8. https://doi.org/10.1038/s41467-020-15841-5

Madabhushi, S. and Talwani, P. 1993. Fault plane solutions and relocations of recent earthquakes in Middleton Place-Summerville seismic zone near Charleston, South Carolina. Bulletin of the Seismological Society of America, 83, no. 5, pp. 1442–1466.

Markewich, H.W. 1985. Geomorphic evidence for Pliocene-Pleistocene uplift in the area of the Cape Fear arch, North Carolina. *In* Tectonic geomorphology. *Edited by* M. Morisawa and J.T. Hack. Proceedings, 15th Annual Binghamton Geomorphology Symposium. Allen and Unwin, Boston, Massachusetts, pp. 279–297.

Marple, R.T. 1994. Discovery of a possible seismogenic fault system beneath the Coastal Plain of South and North Carolina from an integration of river morphology and geological and geophysical data. Unpublished Ph.D. thesis, University of South Carolina, Columbia, South Carolina, 354 p.

Marple, R.T. 2011. Comment on the Companion articles "Finding faults in the Charleston area, South Carolina: 1. Seismological data" by I. Durá-Gómez and P. Talwani and "Finding faults in the Charleston area, South Carolina: 2. Complementary data" by P. Talwani and I. Durá-Gómez. Seismological Research Letters, 82, no. 4, pp. 599–605. https://doi.org/10.1785/gssrl.82.4.599

Marple, R.T. and Hurd, J.D., Jr. 2019. LiDAR and other evidence for the southwest continuation of and Late Quaternary reactivation of the Norumbega fault system and a cross-cutting structure near Biddeford, Maine, USA. Atlantic Geology, 55, pp. 323–359. https://doi.org/10.4138/atlgeol.2019.011

Marple, R.T. and Hurd, J.D., Jr. 2020. Interpretation of lineaments and faults near Summerville, South Carolina, USA, using LiDAR data: Implications for the cause of the 1886 Charleston, South Carolina, earthquake. Atlantic Geology, 56, pp. 73–95. https://doi.org/10.4138/atlgeol.2020.004

Marple, R.T. and Hurd, J.D., Jr. 2021. Investigation of the Cape Fear arch and East Coast fault system (ECFS) in the Coastal Plain of North Carolina and northeastern South Carolina, USA, using LiDAR data. Atlantic Geology, 57, pp. 311–341. https://doi.org/10.4138/atlgeol.2021.015

Marple, R.T. and Miller, R. 2006. Association of the 1886 Charleston, South Carolina, earthquake and seismicity near Summerville with a 12° bend in the East Coast fault system and triple-fault junctions. Southeastern Geology, 44, no. 3, pp. 101–128.

Marple, R.T. and Schweig, E.S., III. 1992. Remote sensing of alluvial terrain in a humid, tectonically active setting: "The New Marid Seismic Zone". Photogrammetric Engineering and Remote Sensing, 58, no. 2, pp. 209–219.

Marple, R.T. and Talwani, P. 1993. Evidence of possible tectonic upwarping along the South Carolina Coastal Plain from an examination of river morphology and elevation data. Geology, 21, no. 7, pp. 651–654. https://doi.org/10.1130/0091-7613(1993)021<0651:EOPTUA>2.3.CO;2

Marple, R.T. and Talwani, P. 2000. Evidence for a buried fault system in the Coastal Plain of the Carolinas and Virginia–Implications for neotectonics in the southeastern United States. Geological Society of America Bulletin, 112, no. 2, pp. 200–220. https://doi.org/10.1130/0016-7606(2000)112<200:EFABFS>2.0.CO;2

Marple, R.T., Hurd, J.D., Jr., Liu, L., Travis, S., and Altamura, R.J. 2018. Investigation of the 1727 Newbury, Massachusetts, USA, earthquake using LiDAR imagery and P-wave velocity tomography. Atlantic Geology, 54, pp. 267–283. https://doi.org/10.4138/atlgeol.2018.009

McCartan, L., Lemon, E.M., Jr., and Weems, R.E. 1984. Geologic map of the area between Charleston and Orangeburg, South Carolina. United States Geological Survey, Miscellaneous Investigations Map I-1472, 1 sheet, scale 1:250 000.

McKinley, C. 1887. A descriptive narrative of the earthquake of August 31, 1886. *In* Appendix for the City of Charleston Year Book, 1886, Walker, Evans, and Cogswell Company, Charleston, South Carolina, pp. 345–441.

Peters, K. and Herrmann, R.B. (*Editors*). 1986. First-hand observations of the Charleston earthquake of August 31, 1886, and other earthquake materials. Reports of W.J. McGee, Earle Sloan, Gabriel E. Manigault, Simon Newcomb, and others. South Carolina Geological Survey, Bulletin 41, 116 p.

Phillips, J.D. 1977. Magnetic basement near Charleston, South Carolina–A preliminary report. *In* Studies related

to the Charleston, South Carolina, earthquake of 1886–A preliminary report. *Edited by* D.W. Rankin. United States Geological Survey, Bulletin 1028-J, 11 p.

Phillips, J.D. 1988. Buried structures at the northern end of the early Mesozoic South Georgia Basin, South Carolina, as interpreted from aeromagnetic data. *In* Studies of the early Mesozoic basins of the eastern United States. *Edited by* A.J. Froelick and G.R. Robinson. United States Geological Survey, Bulletin 1776, pp. 248–252.

Poley, C.M. and Talwani, P. 1986. Recent vertical crustal movements near Charleston, South Carolina. Journal of Geophysical Research, 91, pp. 9056–9066. https://doi.org/10.1029/JB091iB09p09056

Popenoe, P. and Zietz, I. 1977. The nature of the geophysical basement beneath the Coastal Plain of South Carolina and northeastern Georgia. *In* Studies related to the Charleston, South Carolina, earthquake of 1886–A preliminary report. *Edited by* D.W. Rankin. United States Geological Survey, Bulletin 1028-I, 19 p.

Powell, C.A. and Thomas, W.A. 2015. Grenville basement structure associated with the Eastern Tennessee seismic zone, southeastern USA. Geology, 44, no. 1, pp. 39–42. https://doi.org/10.1130/G37269.1

Pratt, T.L., Shah, A.K., Counts, R.C., Horton, J.W., Jr., and Chapman, M.C. in press. Shallow faulting and folding in the epicentral area of the 1886 Charleston, South Carolina, earthquake. Bulletin of the Seismological Society of America, 27 p. https://doi.org/10.1785/0120210329

Prowell, D.C. 1988. Cretaceous and Cenozoic tectonism on the Atlantic coastal margin. *In* The Atlantic continental margin: Geology of North America. *Edited by* R.E. Sheridan and J.A. Grow. Boulder, Colorado, Geological Society of America, I-2, pp. 557–564. https://doi.org/10.1130/DNAG-GNA-I2.557

Rankin, D.W. (*Editor*). 1977. Studies related to the Charleston, South Carolina, earthquake of 1886–A preliminary report. United States Geological Survey, Bulletin 1028, 204 p. https://doi.org/10.3133/pp1028

Rhea, S. 1989. Evidence of uplift near Charleston, South Carolina. Geology, 17, pp. 311–315. https://doi.org/10.1130/0091-7613(1989)017<0311:EOUNCS>2.3.CO;2

Schilt, F.S., Brown, L.D., Oliver, J.E., and Kaufman, S. 1983. Surface structure near Charleston, South Carolina: Results of COCORP reflection profiling in the Atlantic Coastal Plain. *In* Studies related to the Charleston, South Carolina, earthquake of 1886–Tectonics and seismicity. *Edited by* G.S. Gohn. United States Geological Survey, Professional Paper 1313-H, 19 p.

Schumm, S.A. 1986. Alluvial river response to active tectonics. *In* Studies in Geophysics: Active Tectonics. National Academy Press, Washington, D.C., pp. 80–94.

Seeber, L. and Armbruster, J.G. 1981. The 1886 Charleston, South Carolina earthquake and the Appalachian detachment. Journal of Geophysical Research, 86, no. B9, pp. 7874–7894. https://doi.org/10.1029/JB086iB09p07874

Shedlock, K.M. 1988. Seismicity in South Carolina. Seismological Research Letters, 59, pp. 165–171. https://doi.org/10.1029/JB086iB09p07874

Sibson, R.H. 1990. Rupture nucleation on unfavorably oriented faults. Bulletin of the Seismological Society of America, 80, pp. 1580–1604.

Sims, P.K. 2009. The Trans-Rocky Mountain fault system–A fundamental Precambrian strike-slip system. United States Geological Survey, Circular 1334, 13 p. https://doi.org/10.3133/cir1334

Soller, D.R. 1988. Geology and tectonic history of the lower Cape Fear River valley, southeastern North Carolina. United States Geological Survey, Professional Paper 1466-A, 60 p. https://doi.org/10.3133/pp1466A

Stein, R.S. and Yeats, R.S. 1989. Hidden earthquakes. Scientific American, 260, no. 6, pp. 48–57. https://doi.org/10.1038/scientificamerican0689-48

Steltenpohl, M.G., Zietz, I., Horton, J.W., Jr., and Daniels, D.L. 2010. New York-Alabama lineament: A right-slip fault bordering the Appalachians and mid-continent North America. Geology, 38, no. 6, pp. 571–574. https://doi.org/10.1130/G30978.1

Stevenson, D., Gangopadhyay, A., and Talwani, P. 2006. Booming plutons: Source of microearthquakes in South Carolina. Geophysical Research Letters, 33, 4 p. https://doi.org/10.1029/2005GL024679

Talwani, P. 1982. An internally consistent pattern of seismicity near Charleston, South Carolina. Geology, 10, pp. 655–658. https://doi.org/10.1130/0091-7613(1982)10%3C654:ICPOSN%3E2.0.CO;2

Talwani, P. 1999. Fault geometry and earthquakes in continental interiors. Tectonophysics, 305, pp. 371–379. https://doi.org/10.1016/S0040-1951(99)00024-4

Talwani, P. and Durá-Gómez, I. 2009. Finding faults in the Charleston area, South Carolina: 2. Complementary data. Seismological Research Letters, 80, pp. 901–919. https://doi.org/10.1785/gssrl.80.5.901

Talwani, P. and Schaeffer, W.T. 2001. Recurrence rates of large earthquakes in the South Carolina Coastal Plain based on paleoliquefaction data. Journal of Geophysical Research, 106, pp. 6621-6642. https://doi.org/10.1029/2000JB900398

Talwani, P., Kellog, J.N., and Trenkamp, R. 1997. Validation of tectonic models for an intraplate seismic zone, Charleston, South Carolina, with GPS geodetic data. United States Nuclear Regulatory Commission, Report no. NUREG CR-6529, United States Nuclear Regulatory Commission. Washington, D.C., 41 p. https://doi.org/10.2172/446309

U.S. Geological Survey. 2021. Earthquakes map. https://earthquake.usgs.gov/earthquakes/map/?extent=32.9198,-80.19642&extent=32.97044,-80.09617&range=search&baseLayer=terrain&timeZone=utc&search=%7B%22name%22:%22Search%20Results%22,%22params%22:%7B%22starttime%22:%221900-01-01%2000:00:00%22,%22maxlatitude%22:35.317,%22minlatitude%22:31.85,%22maxlongitude%22:-78.459,%22minlongitude%22:-83.513,%22minmagnitude%22:0,%22orderby%22:%22time%22%7D%7D

Weems, R.E. and Lemon, E.M., Jr. 1984. Geologic map of the Mount Holly Quadrangle, Berkeley and Charleston counties, South Carolina. United States Geological Survey, Geologic Quadrangle Map GQ-1579, 1 sheet, scale 1:24 000.

Weems, R.E. and Lemon, E.M., Jr. 1988. Geologic map of the Ladson Quadrangle, Berkeley, Charleston, and Dorchester counties, South Carolina. United States Geological Survey, Miscellaneous Investigations Map GQ-1630, 1 sheet, scale 1:24 000.

Weems, R.E. and Lewis, W.C. 2002. Structural and tectonic setting of the Charleston, South Carolina, region: Evidence from the Tertiary stratigraphic record. Geological Society of America Bulletin, 114, pp. 24–42. https://doi.org/10.1130/0016-7606(2002)114<0024:SATSOT>2.0.CO;2

Weems, R.E. and Obermeier, S.F. 1989. The 1886 Charleston earthquake–An overview of geological studies. *In* Proceedings of the United States Nuclear Regulatory Commission, Seventeenth Water Reactor Safety Information Meeting, United States Nuclear Regulatory Commission, Report no. NUREG/CP-0105, 2, Rockville, Maryland, pp. 289–313.

Weems, R.E., Lemon, E.M., Jr., and Nelson, M.S. 1997. Geology of the Pringleton, Ridgeville, Summerville, and Summerville Northwest 7.5-minute quadrangles, Berkeley, Charleston, and Dorchester counties, South Carolina. United States Geological Survey, Miscellaneous Investigations Series Map I-2502, 2 sheets, scale 1: 24 000.

Weems, R.E., Lewis, W.C., and Lemon, E.M., Jr. 2014. Surficial geologic map of the Charleston region, Berkeley, Charleston, Colleton, Dorchester, and Georgetown counties, South Carolina. United States Geological Survey, Open-File Report 2013-1030, 1 sheet, scale 1:100 000. https://doi.org/10.3133/ofr20131030

Wells, D.L. and Coppersmith, K.J. 1994. New empirical relationships among magnitude, rupture length, rupture width, rupture area, and surface displacement. Bulletin of the Seismological Society of America, 94, pp. 974–1002.

Yang, T., Yang, X., Duan, Q., Chen, J., and Dekkers, M.J. 2016. Rock magnetic expression of fluid infiltration in the Yingxiu-Beichuan fault (Longmen Shan thrust belt, China). Geochemistry, Geophysics, Geosystems, 17, pp. 1065–1085. https://doi.org/10.1002/2015GC006095

Zoback, M.D. and Zoback, M.L. 1989. Tectonic stress field of the continental United States. Geological Society of America, Memoir 172, pp. 523–540. https://doi.org/10.1130/MEM172-p523

Editorial responsibility: Sandra M. Barr

The 'lost' islands of Cardigan Bay, Wales, UK: insights into the post-glacial evolution of some Celtic coasts of northwest Europe

Simon K. Haslett[1,2*] and David Willis[1]

1. Jesus College, University of Oxford, Turl Street, Oxford OX1 3DW, United Kingdom
2. Present address: Department of Geography, Faculty of Science and Engineering, Swansea University, Singleton Park, Swansea SA2 8PP, United Kingdom.
*Corresponding author <s.k.haslett@swansea.ac.uk>

Date received: 26 December 2021 ¶ Date accepted: 2 May 2022

ABSTRACT

A 13th–14th-century map held in the Bodleian Library (the Gough Map and the oldest map of Great Britain) shows two 'lost' islands in Cardigan Bay offshore west Wales, United Kingdom. This study investigates historical sources, alongside geological and bathymetric evidence, and proposes a model of post-glacial coastal evolution that provides an explanation for the 'lost' islands and a hypothetical framework for future research: (1) during the Pleistocene, Irish Sea ice occupied the area from the north and west, and Welsh ice from the east, (2) a landscape of unconsolidated Pleistocene deposits developed seaward of a relict pre-Quaternary cliffline with a land surface up to ca. 30 m above present sea-level, (3) erosion proceeded along the lines of a template provided by a retreating shoreline affected by Holocene sea-level rise, shore-normal rivers, and surface run-off from the relict cliffline and interfluves, (4) dissection established islands occupying cores of the depositional landscape, and (5) continued down-wearing, marginal erosion and marine inundation(s) removed the two remaining islands by the 16th century. Literary evidence and folklore traditions provide support in that Cardigan Bay is associated with the 'lost' lowland of Cantre'r Gwaelod. The model offers potential for further understanding post-glacial evolution of similar lowlands along northwest European coastlines.

RÉSUMÉ

Une carte des 13e et 14e siècles que détient la bibliothèque de Bodley (carte de Gough, carte la plus ancienne de Grande-Bretagne) montre deux îles « disparues » dans la baie Cardigan au large à l'ouest du Pays de Galles, au Royaume-Uni. Cette étude examine des sources historiques, ainsi que des preuves géologiques et bathymétriques, et elle propose un modèle d'évolution côtière postglaciaire fournissant une explication de la disparition des îles et un cadre hypothétique aux fins de recherche future : (1) durant le Pléistocène, les glaces de la mer d'Irlande occupaient la région à partir du nord et de l'ouest, et les glaces galloises s'étendaient à partir de l'est; (2) un paysage de dépôts non consolidés du Pléistocène s'est formé côté mer le long de falaises préquaternaires reliques, laissant émerger une surface terrestre atteignant jusqu'à environ 30 mètres au-dessus du niveau actuel de la mer; (3) une érosion a suivi le long des lignes d'un modèle créé par un rivage en recul affecté par la hausse du niveau de la mer de l'Holocène, les rivières côtières normales et l'écoulement direct de surface des interfluves et de la ligne des falaises reliques; (4) une dissection a créé des îles occupant les coeurs du paysage de dépôt; (5) l'aplatissement continu, l'érosion marginale et les inondations marines ont fait en sorte que les deux îles qui restaient avaient disparu au 16e siècle. Des preuves littéraires et des traditions folkloriques appuient l'association de la baie Cardigan avec les basses terres « disparues » de Cantre'r Gwaelod. Le modèle pourrait permettre une compréhension plus poussée de l'évolution postglaciaire des basses terres similaires le long des littoraux du nord-ouest de l'Europe.

[Traduit par la redaction]

doi: 10.4138/atlgeo.2022.005
2564-2987|22|00131–146 $3.40|0

INTRODUCTION

Cardigan Bay (*Bae Ceredigion* in Welsh) is a large embayment in the St. George's Channel situated on the west coast of mid-Wales, United Kingdom (UK), bounded to the north by the Llŷn Peninsula and to the south by St. David's Head (Fig. 1). The geological history of Cardigan Bay and its present physical setting is provided by Tappin *et al.* (1994, and references therein) and associated geological maps (Institute of Geological Sciences 1982; British Geological Survey 1988, 1990). Only one significant island currently exists in Cardigan Bay, Bardsey Island (*Ynys Enlli*), located off the southern tip of the Llŷn Peninsula. However, the earliest map of Great Britain, known as the Gough Map, shows two additional islands in the central part of Cardigan Bay which no longer exist and have not been considered previously in terms of the post-glacial evolution of the coastline. The aim of the present study is to consider these 'lost' islands and to examine the implications for understanding post-glacial coastal evolution of Cardigan Bay and elsewhere along the Celtic seaboard of northwest Europe. In addition to the coastline of Wales, the coasts of Scotland, Ireland, the Isle of Man, Cornwall, the Isles of Scilly, and Brittany in northwest France, are included in this group of northwest European Celtic coasts. They are generally characterised by exposure to the Atlantic Ocean and hard rock Palaeozoic geology that have combined to give rise to an overall peninsula-type morphology for each region, with widespread features of Pleistocene glacial and/or periglacial origin.

SOURCES

This investigation utilises a range of historical sources, fieldwalking, and available bathymetric and topographic information, coupled with a geomythological approach to draw upon evidence from medieval literature and from folklore.

Historical sources

The two 'lost' islands of Cardigan Bay are shown on the Gough Map, which is the earliest known map of Great Britain (Pelham 1933; Parsons 1958; Skelton 1959). The historical map is held in the Bodleian Library of the University of Oxford (*ms.* Gough Gen. Top. 16) and is so named after its previous owner, Richard Gough, who donated it to the library in 1809. For many years it hung on the wall in the Map Library of the Bodleian but its significance is such that a major project undertaken by the

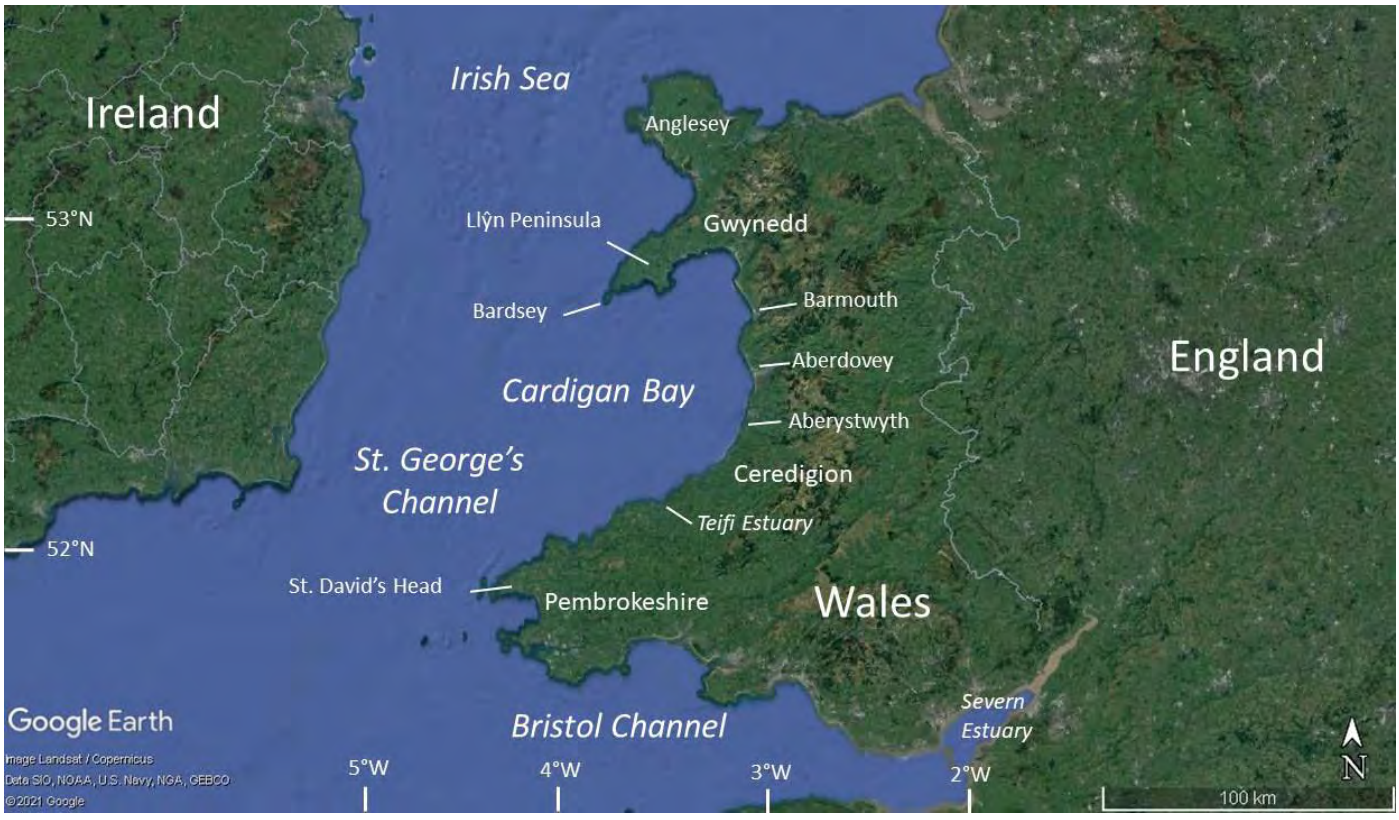

Figure 1. Location of Cardigan Bay and places mentioned in the text (reproduced under Google Earth's terms of use).

Gough Map Panel (Delano-Smith *et al.* 2017) has digitised it and made it available online for researchers to utilise (Linguistic Geographies Project 2021). The date of the map is debated with estimates ranging through the fourteenth and fifteenth centuries with ca. 1360 often cited (e.g., Parsons 1958; Lilley *et al.* 2009), but with advocates for a later date around 1400 or later (e.g., Smallwood 2009). It has also been suggested that it is based on an earlier original estimated to date from around 1280 with the surviving version being a revised copy (Birkholz 2004, 2006).

The use of historical maps in general should be made with caution; however, in this case a level of reassurance is reasonably provided by specialist opinion. For example, Lloyd and Lilley (2009) state that "one of the attributes of the Gough Map … consistently remarked on by scholars is the apparent geographical truthfulness of its content, particularly the shape of the British coastline and islands …" (p. 29). Therefore, based on such academic views and notwithstanding early survey techniques and resultant cartographic distortions, the fundamental geographical features shown on the Gough Map might be considered reasonably secure. Nevertheless, the outline of Wales is strange in shape on the Gough Map and the current embayed configuration of Cardigan Bay is absent, a fact that Bower (2015) attributes to the poor combination of separate surveys used to construct the map. Nevertheless, the lack of curvature of Cardigan Bay on the Gough Map does not cast significant doubt in itself on the distinct occurrence of the two 'lost' islands depicted on the map offshore the Cardigan Bay coast.

A second historical source is Ptolemy's *Geographia*, collated CE 120–160, and the geographical references for coastal locations in Roman Britain that it lists (Strang 1997). Ptolemy's coordinates for places listed in Cardigan Bay have been corrected by North (1957) and may be used to establish historical positions for those locations to permit comparison. Some authors have produced maps of Roman Britain based on Ptolemy's coordinates (e.g., Strang 1998) but as a few locations only are listed for Cardigan Bay, such an exercise connecting the points is of limited benefit locally.

A literature search and review for other relevant historical sources is undertaken using searchable online literature databases, such as the University of Oxford's Search Oxford Libraries Online (SOLO) service, and hard-copy sources in the collection of the Celtic Library of Jesus College, Oxford.

Physical aspects

Bathymetric information for Cardigan Bay is obtained from the Marine Themes vector data (dated March 2018) based on the UK Hydrographic Offices authorised material, and topographic information is from the Ordnance Survey, both accessed through *Digimap*. Reconnaissance fieldwalking of sections of the Cardigan Bay coastline has been undertaken to supplement the published literature on, and gain an appreciation of, the region's geology and geomorphology. The fieldwalking was conducted through the period 2016–2020 on sites of interest, principally for familiarisation and to obtain photographs. Field observation is supplemented by examination of satellite imagery using *Google Earth Pro*.

Geomythological sources

Geomythology as a sub-discipline was formally defined by Vitaliano (1968), who stated that geomythology "seeks to find the real geologic event underlying a myth or legend to which it has given rise; thus … [helping to] … convert mythology back into history" (p. 5, see also Burbery 2021). A number of geological and geographical studies have included a geomythological dimension, such as Carson and Athens (2007), Cashman and Cronin (2008), Cashman and Giordano (2008), Piccardi *et al.* (2008), Rappenglück *et al.* (2010), Nunn (2014a, b, 2016), Walsh *et al.* (2017), Helm *et al.* (2019), Liritzis *et al.* (2019), Combey *et al.* (2020), Wilkie *et al.* (2020), Stewart (2021) along with a collection of papers published in a Geological Society of London Special Publication entitled *Myth and Geology* (Piccardi and Masse 2007). The present study employs this approach to identify sources and extract coastal geomorphological information from medieval literary sources and modern folklore traditions to compare with other evidence.

RESULTS

Historical sources

The Gough Map depicts two elliptically-shaped and featureless islands lying offshore the central part of the coast of Cardigan Bay (Fig. 2). The long axes of the islands lie roughly parallel to the mainland coast. Settlements and rivers included on the map have been identified by the Linguistic Geographies Project (2021) and can be used to locate the islands more precisely. The southern island is shown to lie offshore the mainland between the river estuaries of the Afon Ystwyth in the south, close to the town of Aberystwyth, and the Afon Dyfi to the north, close to the town of Aberdovey. The northern island occurs offshore the mainland between the Dyfi and the Afon Mawddach, close to the town of Barmouth (see Fig. 3 for annotated and re-orientated version of Fig. 2).

Although no scale is given on the Gough Map, the distances between the rivers provide a guide to measurement. Using *Google Earth Pro*, the approx-imate present-day straight-line distance between the mouths of the Ystwyth and Dyfi is ca. 14.4 km, and between the Dyfi and Mawddach ca. 19.5 km. The dimensions of the offshore islands may be estimated in proportion to these respective two sets of measurements, so that the southern island measures

Figure 2. Extract of the Gough Map showing Wales and the two 'lost' islands of Cardigan Bay in the bottom-centre of the image (note the map is orientated with East at the top; reproduced with permission of the Bodleian Library, Oxford. URL <https://digital.bodleian.ox.ac.uk/objects/32638ab9-c0b2-4258-9ca7-980b4b9268f2/surfaces/72c7328e-ddb0-4a42-8e59-5f1a17add1e5/>, 21 June 2021).

approximately 6.6 × 3.8 km (ca. 19.7 km^2) and the northern island 10.7 × 5.8 km (ca. 48.7 km^2), and that the islands lie ca. 3.5–4.0 km from the mainland shore. However, these measurements must be viewed with extreme caution given the poor areal accuracy of the Gough Map.

From a review of North (1957), it appears that it is generally accepted that Ptolemy provided positions for four locations in Cardigan Bay: the Llŷn Peninsula (*Canganorum promotorium*); one of the westernmost headlands in Pembrokeshire (*Octapitarum promontorium*); and the mouths of the rivers Teifi (*Tuerobis fluvii ostia*) and Ystwyth (*Stucciae fluvii ostia*). North (1957) provides a correction to Ptolemy's coordinates, based on discrepancies between the latitude and longitude used, and concludes that the "mouth [of the Afon Teifi] … is in nearly the right position" (p. 173), being in a similar position to its present-day location, but that the mouth of the Afon Ystwyth "is about 8 miles [ca. 13 km] out in the sea" (p. 174) from its present location. Furthermore, North (1957) speculates that if "the coast lay a little farther out than it does now, a very likely possibility, the rivers Ystwyth and Rheidol would have joined before reaching the sea and Ptolemy's *Stucciae fluvii ostia* may well have been the combined estuary of those two streams" (p. 174). North (1957) advises caution but concedes in general terms that "Ptolemy's information was not so inaccurate as might first appear" (p. 173) and that Ptolemy "often came nearer to the truth than we suppose" (p. 174), which provides a degree of reassurance that the corrected positions in Cardigan Bay might be used to evaluate other information.

Relevant historical sources are the 6th-century *De Excidio*

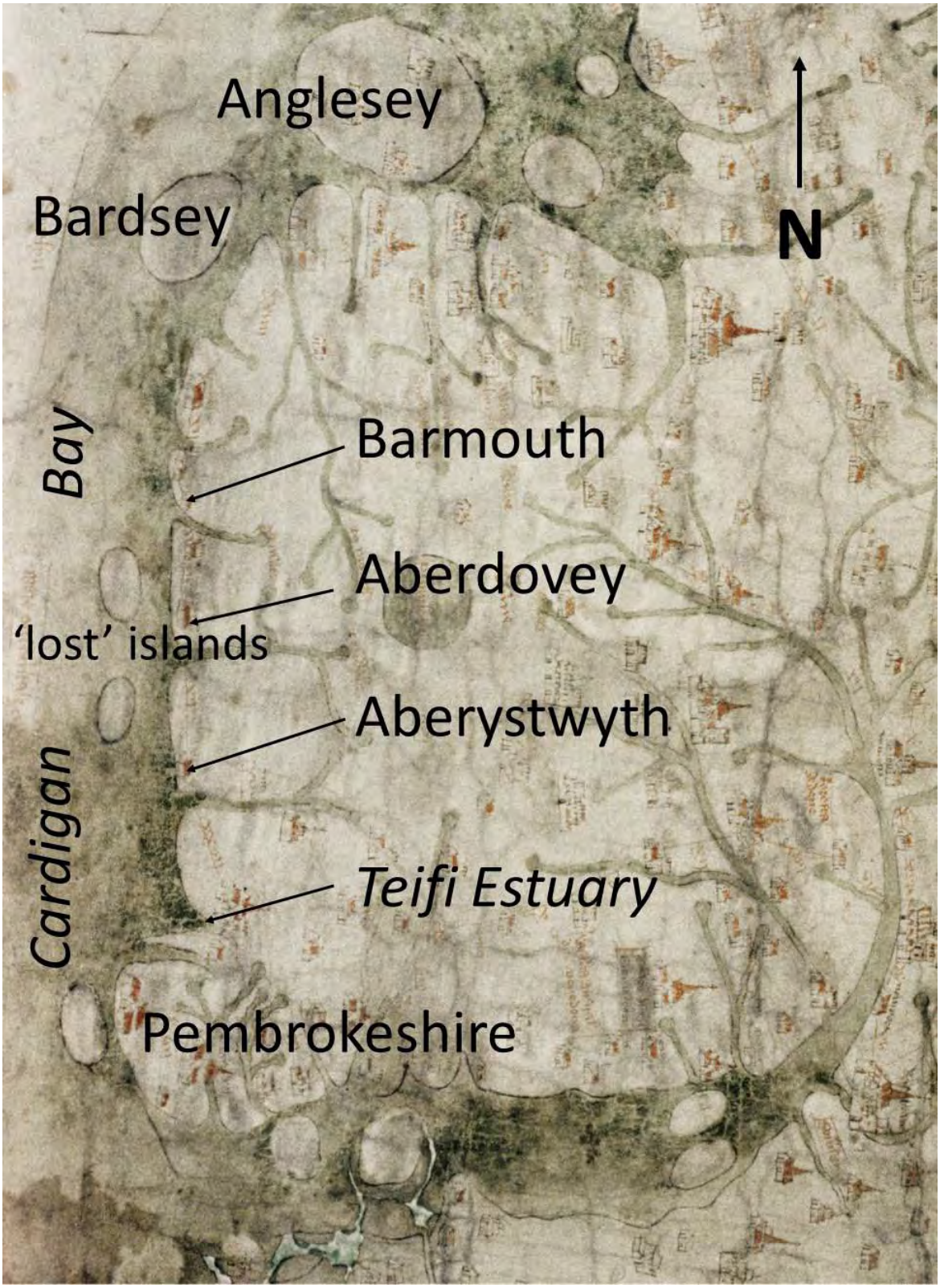

Figure 3. Re-orientated and annotated version of the Gough Map shown in Figure 2 (reproduced with permission of the Bodleian Library, Oxford).

et Conquestu Britanniae by Gildas and the 9th-century *Historia Brittonum* formerly attributed to Nennius (Giles 1841; Dumville 1975; Winterbottom 1978), Geoffrey of Monmouth's *De Gestis Britonum [Historia Regum Britanniae]* (Reeve and Wright 2007), medieval saga poetry and triads, the *Mabinogi*, and local antiquarian accounts, such as Meyrick's (1808) history of Cardiganshire. Some of these sources provide historical statements as well as reflecting literary and folkloric accounts, which nevertheless have geomythological value (see below), but caution must be exercised where the boundary between history, literature, and tradition may have become blurred. For example, the subtitle of Meyrick's (1808) history is 'collected from the few remaining documents which have escaped the destructive ravages of time, as well as from actual observation', suggesting that some of the content is based on unspecified material that, if it ever existed, may now be lost, and, therefore, not all content may be corroborated by surviving sources. Relevant details from these sources are introduced below and in the Discussion section where appropriate.

Bathymetry

The inshore bathymetry of Cardigan Bay is shown in Figure 4 and indicates water depths in excess of 30 m in the west generally shallowing eastwards towards the shore. There are four bathymetric features that are of interest. In southern Cardigan Bay a shore-parallel elongate bathymetric depression, known locally as the Trawling Grounds, extends for approximately 30 km from Aberystwyth south to New Quay and the mouth of the Teifi estuary at water depths in excess of 20 m. To the north, between Aberystwyth and the Dyfi estuary, a ridge-like submarine high (<10 m water depth) extends to approximately 12 km offshore, shallowing to less than 2 m water depth around the summit of the high. This submarine ridge is locally known as Sarn Cynfelin ('Cynfelin's Causeway') or, sometimes, Sarn Gynfelyn or Sarn Wallog. Between the Dyfi and Mawddach estuaries, a second ridge-like submarine high (<10 m water depth) extends approx-imately 8 km offshore, again shallowing to less than 2 m water depth along the crest of the submarine ridge, which is known locally as Sarn y Bwch ('The Buck's Causeway'). A third submarine high (<10 m water depth) occurs north of the Mawddach estuary, known locally as Sarn Badrig ('Patrick's Causeway'). The crest of the Sarn Badrig ridge is in water shallow enough for it to be exposed at low tide, extending over 20 km offshore.

Quaternary geology

The desk-based geological review indicates that Cardigan Bay comprises unconsolidated Quaternary deposits underlain by Palaeozoic and Mesozoic basement rocks (Tappin *et al.* 1994). The majority of the Quaternary deposits are associated with the Pleistocene glaciation of the region, including a widespread ca. 30 m-thick lodgement till assigned to the Upper Till of the Cardigan Bay Formation, and various facies assigned to the Western Irish Sea Formation, of which the Sarnau Facies characterises the geology of the Sarns. The Sarnau Facies is a diamicton that comprises gravel, cobbles, and boulders in a clay matrix and has been interpreted variously as remnants of median moraines of piedmont glaciers issuing from the Welsh mainland valleys (Garrard and Dobson 1974; Garrard 1977) or as remnants of late-glacial sandur deposits (Tappin *et al.* 1994). The facies is 50 m thick in a borehole north of the Mawddach estuary.

Subsequent to Tappin *et al.* (1994), Bowen *et al.* (1999) established the St. Asaph Formation to include the 'Irish Sea till' and the Elenid and Meirion formations to include till from glaciers sourced from upland mid- and northwest Wales respectively. North of Aberystwyth, the Welsh till extends 10–12 km seaward of the present-day coast (Garrard 1977) offshore the Ystwyth–Dyfi and Dyfi–Mawddach coastal sections, and beyond that the Irish Sea till occurs. In southern Cardigan Bay, however, the Irish Sea ice overrode the present-day coast to deposit till approximately 10 km inland and at altitudes up to approximately 250 m above present sea level (e.g., British Geological Survey 2006).

Field exposures of the Irish Sea till and associated Pleistocene deposits that remain along the present-day coast include ca. 20 m-high cliffs at New Quay and Cwm Silio, and ca. 30 m-high cliffs at Mwnt, Afon Cwinten, and south of Aberystwyth (Williams 1927; Rijsdijk and McCarroll 2001; see Fig. 5). Furthermore, Williams (1927) describes a number of coastal 'platforms' or terraces underlain by these Pleistocene deposits that extend up to ca. 1 km inland from the present-day coast, approximately to the 30 m contour, and are backed by relict cliffs representing a pre-glacial coastline (Fig. 6). Therefore, these depositional terraces occupy palaeo-embayments of a former coastline. The geomorphology of the present-day coastline in these areas typically comprises eroding cliffs of Pleistocene deposits fronted by coarse-clastic storm beaches associated seaward with sand terraces and gravel-lag deposits as may be seen along the coast south of Aberystwyth, for example (Fig. 6).

The infill of the submarine channel marked by the Trawling Grounds depression is characterised by the Mud Facies of the Western Irish Sea Formation of Tappin *et al.* (1994), which spans the end of the Pleistocene extending into the Holocene. Garrard (1977) and Haynes *et al.* (1977) report a radiocarbon date (Birm. 400) from a peat sample collected in the Trawling Grounds northeast of New Quay. The sample came from ca. 2.5 m downcore in a water depth of ca. 16 m near the base of the Mud Facies, approximately 0.5 m above the junction with underlying glacial till. The sample yielded a date of 8740 ± 110 BP [9539-10, 154 cal BP; calibrated using OxCal with IntCal20 (Reimer *et al.*

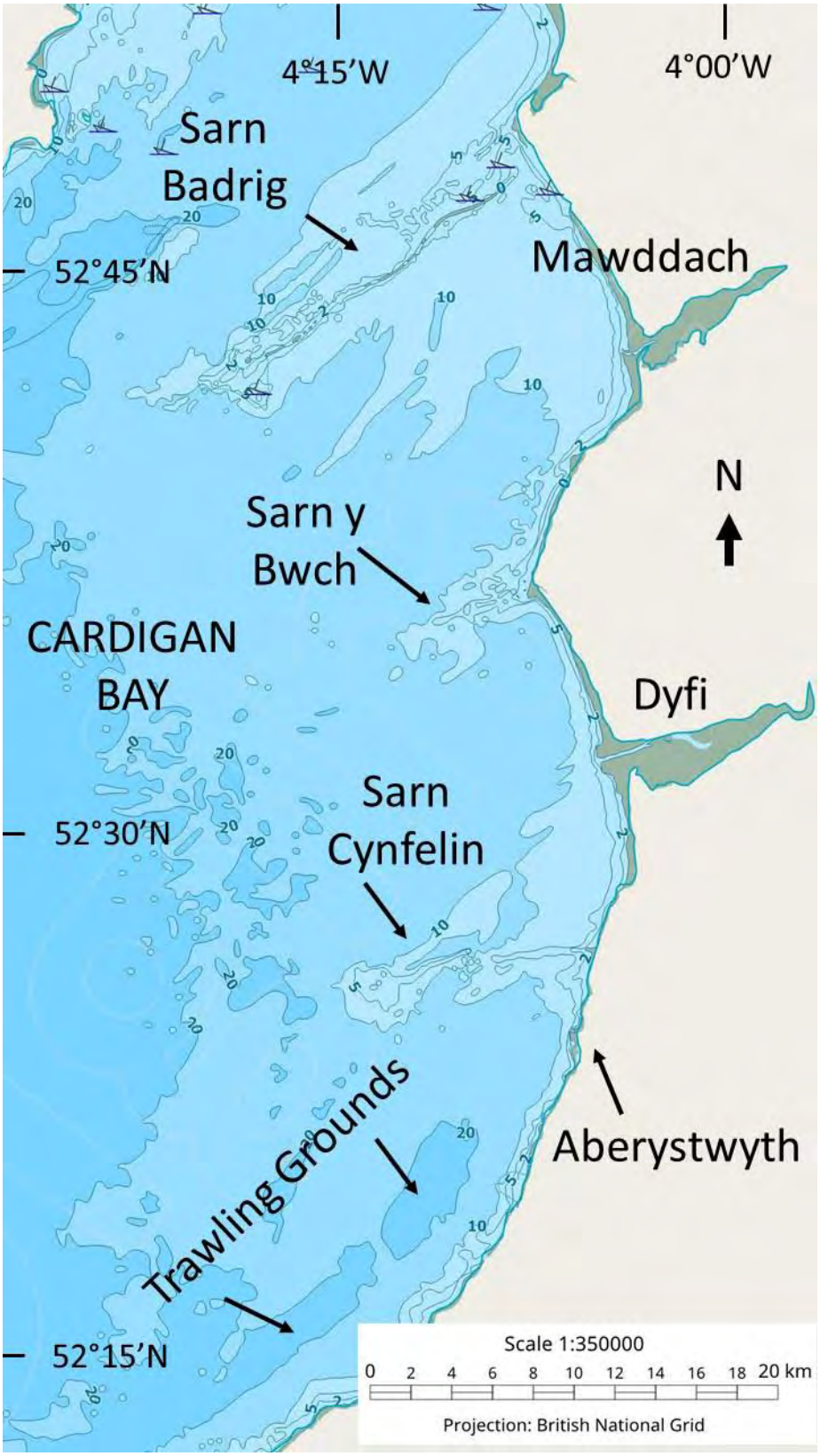

Figure 4. Bathymetry of Cardigan Bay with major submarine features and rivers marked (reproduced under Digimap's terms of use).

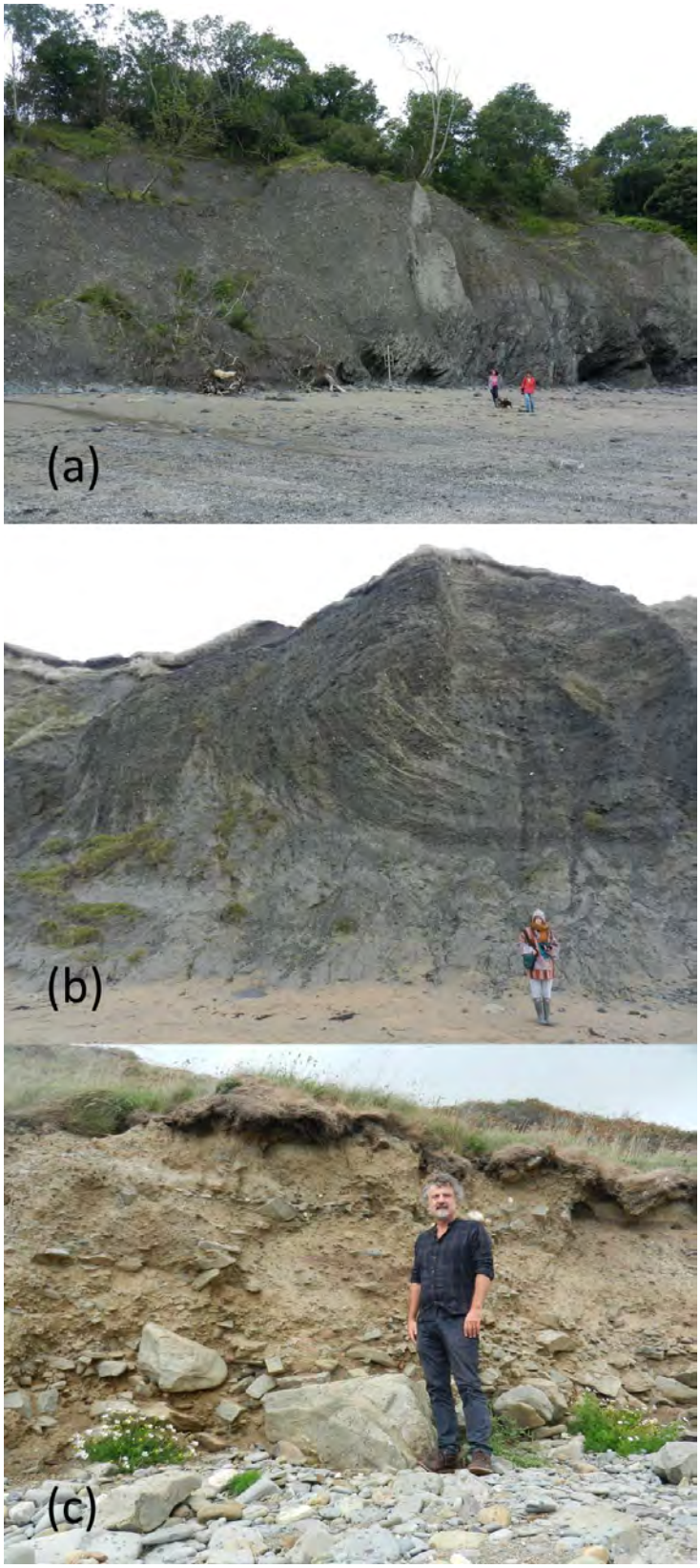

Figure 5. Field examples of coastal cliffs in unconsolidated Pleistocene deposits of Cardigan Bay, (a) New Quay (underlain to the right by Lower Palaeozoic basement), (b) Mwnt, and (c) Cwm Silio.

Figure 6. A view southward along the coast of Cardigan Bay south of Aberystwyth, between the villages of Llanrhystud and Llanon (seen in the middle distance), showing cliffs eroding into a coastal terrace comprising unconsolidated Pleistocene deposits backed landward by a pre-glacial relict cliffline; the foreshore comprises a gravel lag deposit and sand terraces with a coarse clastic storm beach fronting the eroding cliff.

2020) at 95.4% probability] and a palaeoenvironmental study of the core indicates that the Trawling Grounds channel was under estuarine conditions at this time due to postglacial sea-level rise (Haynes *et al.* 1977). Garrard (1977) interprets the Trawling Grounds channel as being initially formed by early post-glacial rivers in the southern part of Cardigan Bay being diverted to the south as the route to the west was blocked by retreating Irish Sea ice.

Estuarine deposits are also recorded from the Dyfi estuary and at Tywyn where Holocene silts and clays began to be deposited approximately 8000 yrs BP (Cave and Hains 1986; Pratt *et al.* 1995). During sea-level lowstands rivers cut channels in the underlying bedrock which became infilled and flooded during postglacial sea-level rise (e.g., Blundell *et al.* 1969). Estuarine deposition continued until the mid-Holocene when increased sedimentation and a decrease in the rate of sea-level rise resulted in the terrestrialisation of the intertidal surfaces and the growth of trees, preserved as a 'submerged forest', which by 4700 yrs BP had developed into ombrogenous mires that accumulated peat, such as Borth Bog on the southern bank of the Dyfi estuary (Cave and Hains 1986). A submerged forest also occurs between Aberystwyth and the Dyfi estuary in a valley at Clarach (Heyworth *et al.* 1985) and is dated to 5404 yrs BP (6196–6281 yrs BP). The submerged forest at Clarach occurs within a >10 m depositional sequence that remained predominantly terrestrial throughout; however, diatom evidence indicates increased marine influence at this site from 2560 ± 80 BP (2366–2783 cal BP).

Geomythology

The scholarly monograph *Celtic Folklore* (1901) by Sir John Rhŷs, former Jesus Professor of Celtic and Principal of Jesus College, Oxford, is an important early secondary source of information regarding legends and traditions in the Cardigan Bay area and elsewhere along the Celtic coastline of northwest Europe. Some of the previously mentioned historical works also present local legends and traditions (e.g., Meyrick 1808; North 1957; Reeve and Wright 2007) that make useful contributions. Of particular geomythological interest are legends regarding now 'lost' coastal lowland landscapes, not only in Cardigan Bay but also associated with Cornwall, Brittany, and elsewhere.

According to Welsh folkloric traditions (see below), a 'lost' landscape, often regarded as a submerged landscape locally, once occupied what is now Cardigan Bay and is variously referred to as Cantre'r Gwaelod (the 'Lowland Hundred' or 'Lowland of the Depth', a 'cantref' being the intermediate administrative division of medieval Wales) or Maes Gwyddno ('The Plain of Gwyddno'). In the 17th century, antiquarian Robert Vaughan, in his 'Survey of Merioneth' (National Library of Wales ms. 472B), considered Sarn Badrig to be the remains of the defensive wall of Cantre'r Gwaelod (North 1957, p. 153). J. E. Lloyd tentatively suggested that the Cantre'r Gwaelod story involves 'reminiscences handed down through many generations of the effects — at times, perhaps, startling — of this gradual subsidence [in Cardigan Bay] attested by geology' (Lloyd 1911 vol. 1, p. 5). Bromwich (1950 p. 227, 231) is more circumspect, suggesting that it is an attempt to explain the observed geological formations in Cardigan Bay, rather than a direct recollection of inundation events.

In recent folklore, Gwyddno is presented as the ruler of Cantre'r Gwaelod and the inundation is the result of the negligence of the drunken gatekeeper, Seithiennin, while, in medieval versions of the tale, Seithiennin is the focus, probably the lowland's/island's king, and Gwyddno is mentioned only indirectly in the name Maes Gwyddno. A tradition that seems to go back to triads, possibly forged by Iolo Morgannwg in the 19th century, portrays Gwyddno as King of Ceredigion in the 5th and 6th centuries (North 1957 p. 152–153). Gwyddno is also linked to the mythological figure of Taliesin in *Ystoria Taliesin*, a tale attested from the 16th century. Here, Gwyddno's castle is located specifically in Aberystwyth (in most versions of the tale) or somewhat further north, between the Ystwyth and the Dyfi (in Llywelyn Siôn's version of the same tale, Cwrtmawr ms. 20) (Ford 1975, p. 453; Wood 1980). A number of 15th-century genealogies claim descent to Gwyddno through his son Elffin.

The folkloric traditions build on earlier traditions that find literary form in a number of medieval Welsh sources (Bromwich 2014, p. 391–392). Elffin is mentioned in a number of poems of the Gogynfeirdd (Poets of the Princes). Porth Wyddno 'Gwyddno's Harbour' is mentioned in a medieval Welsh triad (Bromwich 2014, p. 246) as being in the north (of Britain); and Gwyddno is listed as one of Gwŷr y Gogledd 'the Men of the North', and a descendent of Dyfnwal Hen (Bromwich 2014, p. 256). Thus, an early tradition links him with the Old North (today's southern Scotland). Whether his name was associated with the submersion of Cantre'r Gwaelod in the Old North or only after he became known in Wales is unclear. Evidence of place names links him both to Ceredigion and the Conwy estuary: places named Cored Wyddno 'Gwyddno's weir' are found both in Aberconwy and in Ceredigion, and there is a stream called Gwenwyn meirch Gwyddno in Arfon (Williams 1957, p. 5; Bromwich 2014, p. 392).

The fate of Cantre'r Gwaelod itself is mentioned in a poem in the Black Book of Carmarthen (mid-13th century), the first stanza of which is given here in Rachel Bromwich's interpretation and translation:

Seithenhin sawde allan
ac edrychuirde varanres
mor maes guitnev ry toes.

'Stand forth, Seithenhin,
and look upon the fury of the sea;
it has covered Maes Gwyddneu.'
(Bromwich 1950, p. 217)

As noted above, Gwyddno is here not the ruler of Cantre'r Gwaelod, as in the later folkloric tradition, and appears only in the name of the land inundated. A similar presentation is found in *Bonedd y Saint*, a list of genealogies of saints first redacted in the 12th century, in which a number of saints are listed as sons of 'Seithennin Vrenhin o Vaes Gwydno a oresgynnvs mor ev tir' ('Seithennin king of Maes Gwyddno, whose land the sea overran') (Wade-Evans 1944, p. 322).

The tale of Cantre'r Gwaelod suggests the lowland was suddenly inundated and overwhelmed by a flood which Meyrick (1808) asserts occurred in CE 520, although he provides no evidence to support this date.

Similar legends also exist of other 'lost' landscapes elsewhere. In Brittany, King Gradlon (or Grallon) is said to have ruled the city of Ys, the sudden inundation of which is referred to in the Breton Life of St. Gwenôlé (Widmer and Jørgensen 2011). This report goes back to the Latin life of the saint (*Vita Sancti Winwaloei*, de Smedt 1888), believed to have been composed 860–884 (see also Bromwich 1950, pp, 232–241; Piriou 1992; Poulin 2009, p. 396–445). Taken at face value, the inundation would be contemporaneous with Gwenôlé himself, that is, in the late 5th or early 6th century. Other examples come from southwest England, where Lyonesse is claimed to have existed around the Isles of Scilly and the southern coast of Cornwall; and in north Wales, where it is also claimed that Llys Helig ('Helig's Court') suffered an inundation in the 5th or 6th century. A Latin triad interspersed among genealogical material in Exeter Cathedral Library ms. 3514 (late-13th century) lists the kingdom of Helig son of Glannog among the three realms that the sea destroyed, placing it between Ceredigion and Bardsey towards Aberdyfi (Aberdovey), in the north of Cardigan Bay (Jones 1948; Bromwich 2014, p. lxxiv–lxxv). The location of this kingdom in Cardigan Bay rather than off the north coast of Wales has been suggested to reflect the earlier tradition (North 1940), bringing it and the tale of Cantre'r Gwaelod closer together. Indeed, it has been suggested that they were originally one and the same (Bromwich 1950, p. 231).

Most famously, in *Branwen*, the second branch of the medieval Welsh *Mabinogi* tales, when Bendigeidfran, king of the Island of Britain, leads his forces across from Wales to Ireland (although not on their return), the intervening sea consists merely of two navigable rivers, called Lli and Archan: "Bendigeiduran, a'r yniuer a dywedyssam ni, a hwylyssant parth ac Iwerdon, ac nyt oed uawr y weilgi yna: y ueis yd aeth ef. Nyt oed namyn dwy auon: Lli ac Archan y gelwit. A guedy hynny yd amlawys y weilgi, pan oreskynwys y weilgi y tyrnassoed" (*Branwen*, ed. Thomson 1986 lines 252–256) ('Bendigeidfran and the army we mentioned sailed towards Ireland, and the sea was not wide then; Bendigeidfran waded across. There were only two rivers, called the Lli and the Archan. Later the sea spread out when it flooded the kingdoms', trans. Davies 2007, p.28; see also Rhŷs 1901, p. 386; Sims-Williams 2010, p. 192–196).

DISCUSSION

The 13th–14th-century Gough Map provides cartographic evidence for the existence of two 'lost' offshore islands located in Cardigan Bay. Considering the geological setting, any such islands are likely to have comprised unconsolidated Pleistocene deposits that were susceptible to lateral erosion. It is also likely that the geomorphology of island coasts, at least on the exposed seaward sides, would be analogous to present-day coastal settings in Cardigan Bay with eroding cliffs of unconsolidated deposits fronted by coarse-clastic storm beaches, sand terraces and gravel-lag deposits. The recession of the cliffs would have resulted in the areal reduction of the islands with marine action in the surf zone further eroding the exposed surface of the Pleistocene deposits. Indeed, Garrard (1977) recognised that such erosion across the region resulted in "a thin but extensive cover of lag gravel, resting on a distinct plane of marine erosion" (p. 91). The more sheltered, landward-facing, leeside, island coasts may have been different in character and supported depositional landforms comprising more fine-grained sediments.

Bathymetrically, the two islands depicted on the Gough Map appear to be located approximately coincident with Sarn Cynfelin, between the Ystwyth and Dyfi estuaries, and Sarn y Bwch, between the Dyfi and Mawddach estuaries, suggesting that the coarse clasts of these sarns may have 'anchored' the islands resulting in significant gravel lag accumulations following erosion of the diamicton's finer-grained matrix. Furthermore, the height of the land surface of the islands may be estimated if the altitude of the 20–30 m-high cliffs of Pleistocene deposits that remain along the Cardigan Bay coast is extrapolated westward. This approach suggests the land surface height of the islands in the areas of the two sarns might have been up to 15–25 m above sea-level in areas enclosed by the present-day 5 m isobath or 10–20 m in waters enclosed by the 10 m isobath. However, due to surface lowering, through simultaneous weathering and erosion of the unconsolidated sediments, it is likely that the altitude was lower than these maximum estimates.

It appears that the erosion of the two islands was completed by the mid-16th century, as the islands do not appear on later maps, such as Thomas Butler's *Mape off Ynglonnd* dated to 1547–1554 (Birkholz 2006). Therefore, the disappearance of the two 'lost' islands may represent a stage in the gradual planation and removal from Cardigan Bay of the top decametres of unconsolidated Quaternary deposits due to marine action operating on the Holocene sea-level high-stand, a process that has not yet been fully completed, as substantial areas of Quaternary deposits remain as terraces and exposed in cliffs along the Cardigan Bay coast as observed in the field seaward of the relict pre-glacial coastline (e.g., Fig. 6).

Historical, literary and geomythological evidence might suggest that the two 'lost' islands were remnants of a larger area of lowland formerly occupying Cardigan Bay. Ptolemy's coordinates place the mouth of the Afon Ystwyth in the 2nd century CE ca. 10–15 km to the west of its present position (North 1957), approximately coincident with the 10 m isobath, and south of Sarn Cynfelin roughly along the line of longitude of its westernmost tip. This suggests that the coastline at this time was seaward of the western shores of the 'lost' islands. Furthermore, the tale of Cantre'r Gwaelod might suggest that the lowland, or at least part of it, continued to be inhabited up until the 5th–6th centuries.

A number of authors have considered the legend of Cantre'r Gwaelod to represent a folk memory of gradual landscape submergence through rising sea levels during the Holocene marine transgression (e.g., Matthews 1993; Nunn *et al.* 2021; see also Kavanagh and Bates 2019). However, the association of this memory with a sudden inundation tends to contradict this view. Elsewhere, coastal submergence due to gradual post-glacial sea-level rise is represented in traditions, such as in Australian Aboriginal myths, that either recall "how two landmasses, now separated by a water gap, were once joined" or "how people once crossed a water gap (by wading or swimming) from one landmass to another, a feat that would be impossible today" (Nunn 2016, p. 397). In Wales, the *Mabinogi* description of Bendigeidfran's crossing to Ireland, with only two navigable rivers lying in between, aligns well with the second of these tradition types involving gradual sea-level rise, but the sudden inundation of Cantre'r Gwaelod does not align with a sea-level rise explanation for its demise and instead evokes a more rapid event or series of events.

In support of a sudden inundation event or events, the only 6th-century historical source, that of the British monk Gildas, in his *De excidio et conquestu Britanniae*, records the pleas of the Britons in the face of barbarian invaders in the following way: "repellunt barbari ad mare, repellit mare ad

barbaros; inter haec duo genera funerum aut iugulamur aut mergimur" ("the barbarians push us back to the sea, the sea pushes us back to the barbarians; between these two kinds of death, we are either drowned or slaughtered" (Winterbottom 1978. p. 23–24); "the barbarians drive us to the sea; the sea throws us back on the barbarians: thus two modes of death await us, we are either slain or drowned" (Giles 1841, p. 32)). While this may simply mean that the Britons were caught between the sea and the attackers, it might also imply that both were seen as equally hostile as a result of a significant marine event or events at this period causing loss of life. This event is usually dated to CE 446 (Thompson 1979, p. 214; see also Sims-Williams 1983, p. 5–15).

Whether such an inundation(s) was due to storm surge or tsunami is not possible to discern but an interesting account (the legend of Aber Llyn Lliwan) included in the 9th-century *Historia Brittonum*, and repeated by Geoffrey of Monmouth (Reeve and Wright 2007), recounts a marine phenomenon linked to the 5th or 6th century that describes unusual tidal conditions and a mountainous wave in the Severn Estuary along the south Wales coast (Rhŷs 1901). Evans *et al.* (2008) have suggested that this refers to a specific site where whirlpools occur near the coast; however, it may also be describing a tsunami event and, moreover, Bryant and Haslett (2007) and Haslett and Bryant (2007) present historic and physical evidence suggestive of historic tsunami events in south and north Wales respectively. It is clear that this question requires further investigation in the future.

Taken together, the cartographic, historical, physical and geomythological evidence conspire to provide a preliminary framework for the post-glacial evolution of Cardigan Bay, developing a hypothesis that may be tested through future research:

1. During the late Glacial, Cardigan Bay was occupied from the north and west by Irish Sea ice and Welsh ice from the east. In southern Cardigan Bay, the Irish Sea ice deposited glacial till approximately 10 km inland of the present-day coastline up to 250 m above present sea-level. In the northern part of Cardigan Bay Welsh ice extended ca. 10–12 km west of the present coastline. The Welsh ice deposited significant accumulations of coarse clasts, including those that comprise the present-day sarns of Cardigan Bay.

2. Unconsolidated Pleistocene deposits, including glacial till, were deposited across Cardigan Bay seaward of a relict pre-glacial coastline producing a depositional subglacial landscape. Remaining cliffs of unconsolidated deposits that occur along the modern coastline suggest a surface altitude of up to 30 m above present sea-level for these unconsolidated deposits.

3. The post-glacial erosion of the unconsolidated Pleistocene deposits may have followed a template provided by land drainage and Holocene sea-level rise. initial retreat of the Irish Sea ice, from the present shoreline of southern Cardigan Bay, forced emerging rivers, such as the Afon Teifi and Aeron, to flow southwards excavating the Trawling Grounds channel. More northerly rivers, such as the Afon Ystwyth, Dyfi, and Mawddach flowed westward as the Welsh ice retreated eastwards from its confluence with Irish Sea ice. Once Irish Sea ice had fully retreated to the west and north, the Holocene transgression would begin to act on the western margin of the deposits and establish estuarine conditions in the coastal river valleys. Run-off from upland bedrock areas between the rivers is likely, in places, to have removed material fronting the relict pre-glacial cliffline.

4. As erosion progressed, the landscape would become dissected by westward flowing rivers eroding laterally to widen their valleys, coastal erosion and eastward retreat of the western margin, and erosion and north-south removal of materials from the foot of the inter-river upland bedrock areas, perhaps eventually connecting southwards with the Trawling Grounds channel. This process might have resulted in the formation of islands in the cores of these dissected areas, such as the two 'lost' islands depicted on the Gough Map positioned between the lines of rivers.

5. Marine inundation(s) and continued down-wearing of the interfluves and marginal erosion removed the two remaining islands by the 16th century and the process continues in eroding and removing areas along the present-day coast underlain by unconsolidated Pleistocene deposits.

Through this process, the river valleys, including the Trawling Grounds channel, became submerged landscapes, preserving post-glacial deposits in palaeochannel infills. However, islands of unconsolidated Pleistocene deposits forming the inter-river areas were not submerged but removed through lateral erosion to produce a plane of combined fluvial and marine erosion constituting a stratigraphic unconformity between underlying Pleistocene deposits and overlying modern seabed sediments.

The mean rate of removal of the depositional landscape in the period between the recording of Ptolemy's coordinates and the drafting of the Gough Map is estimated to be ca. 10 m/yr if marine erosion only of the coastline was responsible for retreat of the shore back to the approximate position of the present-day coast. However, a dissection model with combined marine and fluvial erosion would require a lower mean removal rate of ca. 5 m/yr to erode towards the core of remnant islands within a dissected landscape, a rate that might be accelerated due to gradually deepening water adjacent to the coast bringing higher energy waves to the shore and occasional high-magnitude marine inundation(s). Although the current rate of erosion along the Cardigan Bay coast is estimated to be up to ca. 1 m/yr (West Wales Shoreline Management Plan Consultation 2011), coastlines on the more protected coast of eastern England, with cliffs comprising similarly unconsolidated Pleistocene sediments, have retreated ca. 5.5 km since Roman times (ca. 2.75 m/yr) along the Yorkshire coast (Sistermans and Nieuwenhuis

2013) and rapid cliff erosion of up to ca. 6 m/yr in Suffolk (May 2003).

Across the North Sea in the German Bight, historical cartographic evidence indicates that the island of Heligoland has experienced a major reduction in size (Hebbeln *et al.* 2003) from 60 km in length in CE 800 to 25 km in 1300 and 1.5 km in the 20th century (Bryant 2005). Presently, the island's shoreline has retreated to a resistant core of Mesozoic rocks (Kelletat 1992) but is surrounded on the seafloor by a basement of Pleistocene sediments (Wunderlich 1980) indicating that the material removed through historic coastal erosion comprised unconsolidated deposits. Indeed, Hebbeln *et al.* (2003) attribute very high historic sedimentation rates in the nearby Helgoland mud area to the disintegration of the island.

Elsewhere in the North Atlantic, the exposed shore of Nova Scotia in Canada has experienced rapid erosion of cliffs in unconsolidated Pleistocene deposits, such as drumlins, with recent measured rates of 5.4 m/yr, and perhaps up to 7.6 m/yr, on the western inlet of Chezzettcook Inlet (Shaw *et al.* 1993), and ca. 8.33 m/yr through a six-year period at Cap la Ronde on Isle Madame (Force 2013). Furthermore, an island mapped offshore Nova Scotia in the eighteenth century, Fish Isle, has subsequently been removed though erosion and is "now represented only by intertidal boulder shoals" (Force 2013, p. 37), which shows a similarity to the 'lost' islands of Cardigan Bay where the Sarns, and/or associated gravel lag deposits, may be considered to be analogous to the 'boulder shoals'.

Taken together, the rates of historical erosion proposed for the 'lost' islands of Cardigan Bay are entirely plausible within the context of other coasts where unconsolidated Pleistocene deposits are exposed in coastal cliffs and occur within a high-energy wave environment. Moreover, the geological and geomorphological similarity between Cardigan Bay and other areas along the northwest European coast, such as the Celtic coasts of Brittany and Cornwall, along with similar geomythological evidence, might suggest marine and fluvial dissection and erosion of 'lost' landscapes underlain by unconsolidated Pleistocene deposits provides a credible model to further investigate coastal evolution in these regions.

CONCLUSION

This study has investigated the significance of two 'lost' islands located in Cardigan Bay as shown on the 13th–14th-century Gough Map. Drawing upon historical, literary and folklore sources, and geological and bathymetric evidence, the existence of the 'lost' islands is considered plausible and offers a possible insight into the post-glacial coastal evolution of Cardigan Bay. A preliminary post-glacial coastal evolution model is presented that provides an integrated hypothetical framework upon which further research may be undertaken to test its validity and to offer refinements with the potential to offer new insights into the post-glacial evolution of lowland areas of the northwest European coastline. The model is also consistent with traditions that associate lost landscapes with these coastal areas, such as Cantre'r Gwaelod supposedly situated in Cardigan Bay.

ACKNOWLEDGEMENTS

This study is a contribution to UNESCO's International Geoscience Program (IGCP) Project 639 *Sea Level Change from Minutes to Millennia*, and the Celtic Coasts Project. The authors are extremely grateful to Tim Burbery and three anonymous reviewers for their helpful comments and guidance on improving the manuscript. The writing of this paper was undertaken whilst SKH was in receipt of a Short-Term Visiting Fellowship at Jesus College, University of Oxford. Thanks are extended to Owen McKnight of Jesus College Library and the staff of Bodleian Library, Oxford, for their assistance, and to Oxford colleagues Andrew Dunning, Nick Millea and Jenyth Evans for initial discussions and guidance on historic sources. This research did not receive any specific grant from funding agencies in the public, commercial, or not-for-profit sectors.

REFERENCES

Birkholz, D. 2004. The King's two maps: cartography and culture in thirteenth-century England. Routledge, New York, 254 p. https://doi.org/10.4324/9780203505427

Birkholz, D. 2006. The Gough Map revisited: Thomas Butler's *The Mape off Ynglonnd*, c. 1547-1554. Imago Mundi, 53, pp. 23–47. https://doi.org/10.1080/03085690500362298

Blundell, D.J., Griffiths, D.H., and King, R.F. 1969. Geophysical investigations of buried river valleys around Cardigan Bay. Geological Journal, 6, pp. 161–181. https://doi.org/10.1002/gj.3350060203

Bowen, D.Q., Aldhouse-Green, S., and Thomas, G.S.P. 1999. Wales. *In* A revised correlation of Quaternary deposits in the British Isles. *Edited by* D.Q. Bowen. The Geological Society Special Report, No. 23, pp. 79–90.

Bower, D.L. 2015. The Medieval Gough Map, Its Settlement Geography and the Inaccurate Representation of Wales. Imago Mundi, 67, pp. 145–167. https://doi.org/10.1080/03085694.2015.1027548

British Geological Survey 1988. Cardigan Bay Sheet 52N 06W Seabed sediments map, scale 1:250 000.

British Geological Survey 1990. Cardigan Bay Sheet 52N 06W Quaternary map, scale 1:250 000.

British Geological Survey 2006. Llangranog. England and Wales Sheet 194. Bedrock and Superficial Deposits map,

scale 1:50 000.
Bromwich, R. (*Editor*). 2014. Trioedd Ynys Prydein: The Triads of the Island of Britain, 4th edition. University of Wales Press, Cardiff, 559 p.
Bromwich, R. 1950. Cantre'r Gwaelod and Ker-Is. *In* The early cultures of north-west Europe. *Edited by* C. Fox and B. Dickins. Cambridge University Press, Cambridge, pp. 217–241.
Bryant, E. A. 2005. Natural Hazards. 2nd edition. Cambridge University Press, Cambridge, 312 p. https://doi.org/10.1086/430540
Bryant, E.A. and Haslett, S.K. 2007. Catastrophic wave erosion, Bristol Channel, United Kingdom: impact of tsunami? Journal of Geology, 115, pp. 253–269. https://doi.org/10.1086/512750
Burbery, T. J. 2021. Geomythology: how common stories reflect earth events. Routledge, New York, 118 p. https://doi.org/10.4324/9781003149323
Carson, M.T. and Athens, J.S. 2007. Integration of coastal geomorphology, mythology, and archaeological evidence at Kualoa Beach, Windward O 'ahu, Hawaiian Islands. Journal of Island and Coastal Archaeology, 2, pp. 24–43. https://doi.org/10.1080/15564890701219693
Cashman, K.V. and Cronin, S.J. 2008. Welcoming a monster to the world: Myths, oral tradition, and modern societal response to volcanic disasters. Journal of Volcanology and Geothermal Research, 176, pp. 407–418. https://doi.org/10.1016/j.jvolgeores.2008.01.040
Cashman, K.V. and Giordano, G. 2008. Volcanoes and human history. Journal of Volcanology and Geothermal Research, 176, pp. 325–329. https://doi.org/10.1016/j.jvolgeores.2008.01.036
Cave, R. and Hains, B.A. 1986. Geology of the country between Aberystwyth and Machynlleth. Memoir of the 1:50 000 geological sheet 163 (England and Wales). British Geological Survey, HMSO, 148 p.
Combey, A., Audin, L., Benavente, C., Bouysse-Cassagne, T., Marconato, L., and Rosell, L. 2020. Evidence of a large "prehistorical" earthquake during Inca times? New insights from an indigenous chronicle (Cusco, Peru). Journal of Archaeological Science: Reports, 34, pp. 102659. https://doi.org/10.1016/j.jasrep.2020.102659
Davies, S. (*Translator*). 2007. The Mabinogion. Oxford University Press, Oxford, 336 p.
de Smedt, C. 1888. Vita S. Winwaloei primi abbatis Landevenecensis auctore Wurdestino. Analecta Bollandiana, 7, pp. 168–264.
Delano-Smith, C., Barber, P., Bove, D., Clarkson, C., Harvey,P.D.A., Millea, N., Saul, N., Shannon, W., Whittick, C., and Willoughby, J. 2017. New Light on the Medieval Gough Map of Britain, Imago Mundi, 69, pp. 1–36. https://doi.org/10.1080/03085694.2017.1242838
Dumville, D. 1975. "Nennius" and the Historia Brittonum. Studia Celtica, 10, pp. 78–95.
Evans, A.J., Nettleship, J., and Perry, S. 2008. *Linn Liuan/Llynn Llyw*: the wondrous lake of the *Historia Brittonum's de Mirabilibus Britanniae* and *Culhwch ac Olwen*. Folklore, 119, pp. 295–318. https://doi.org/10.1080/00155870802352236
Force, E. R. 2013. Sea-cliff erosion with rising sea-level along shores exposing glacial material in Atlantic Canada: the effect of bedrock slope and an example from Isle Madame, Nova Scotia. Geoscience Canada, 40, pp. 32–39. https://doi.org/10.12789/geocanj.2013.40.004
Ford, P.K. 1975. A fragment of the Hanes Taliesin by Llywelyn Siôn. Études Celtiques, 14, pp. 451–460. https://doi.org/10.3406/ecelt.1975.1548
Garrard, R.A. 1977. The sediments of the South Irish Sea and Nymphe Bank area of the Celtic Sea. *In* The Quaternary of the Irish Sea. *Edited by* C. Kidson and M.J., Tooley. Geological Journal Special Issue No. 7, Seel House Press, Liverpool, pp. 69–92.
Garrard, R.A. and Dobson, M.R. 1974. The nature and maximum extent of glacial sediments off the west coast of Wales. Marine Geology, 16, pp. 31–44. https://doi.org/10.1016/0025-3227(74)90024-3
Giles, J.A. (*Translator*). 1841. Early Welsh histories: Gildas and Nennius. James Bohn, London [2020 edition by Cockatrice Books, 112 p.
Haslett, S.K. and Bryant, E.A. 2007. Evidence for historic coastal high-energy wave impact (tsunami?) in North Wales, United Kingdom. Atlantic Geology, 43, pp. 137–147. https://doi.org/10.4138/4215
Haynes, J.R., Kiteley, R.J., Whatley, R.C., and Wilks, P.J. 1977. Microfaunas, microfloras and the environmental stratigraphy of the Late Glacial and Holocene in Cardigan Bay. Geological Journal, 12, pp. 129–158. https://doi.org/10.1002/gj.3350120203
Hebbeln, D., Scheurle, C., and Lamy, F. 2003. Depositional history of the Helgoland mud area, German Bight, North Sea. Geo-Marine Letters, 23, pp. 81–90. https://doi.org/10.1007/s00367-003-0127-0
Helm, C.W., Benoit, J., Mayor, A., Cawthra, H.C., Penn-Clarke, C.R., and Rust, R. 2019. Interest in geological and palaeontological curiosities by southern African non-western societies: A review and perspectives for future study. Proceedings of the Geologists' Association, 130, p. 541-558. https://doi.org/10.1016/j.pgeola.2019.01.001
Heyworth, A., Kidson, C., and Wilks, P. 1985. Late-Glacial and Holocene sediments at Clarach Bay, near Aberystwyth. Journal of Ecology, 73, pp. 459–480. https://doi.org/10.2307/2260487
Institute of Geological Sciences 1982. Cardigan Bay Sheet 52N 06W Solid Geology Map, scale 1:250 000.
Jones, T. 1948. Triawd Lladin ar y gorlifiadau ['A Latin triad on the inundations']. Bulletin of the Board of Celtic Studies, 12, pp. 79–83.
Kavanagh, K.E. and Bates, M.R. 2019. Semantics of the sea

— stories and science along the Celtic seaboard. Internet Archaeology, 53, unpaginated. https://doi.org/10.11141/ia.53.8

Kelletat. D. 1992. Coastal erosion and protection measures at the German North Sea coast. Journal of Coastal Research, 8, pp. 699–711.

Lilley, K.D., Lloyd, C.D., and Campbell, B.M.S. 2009. Mapping the realm: a new look at the Gough Map of Britain (c.1360). Imago Mundi, 61, pp. 1–28. https://doi.org/10.1080/03085690802456228

Linguistic Geographies Project, 2021. Linguistic geographies: the Gough Map of Great Britain. URL <http://www.goughmap.org/>, 2 February 2021.

Liritzis, I., Westra, A., and Miao, C. 2019. Disaster geoarchaeology and natural cataclysms in World cultural evolution: an overview. Journal of Coastal Research, 35, pp. 1307–1330. https://doi.org/10.2112/JCOASTRES-D-19-00035.1

Lloyd, C.D. and Lilley, K.D. 2009. Cartographic veracity in medieval mapping: analyzing geographical variation in the Gough Map of Great Britain. Annals of the Association of American Geographers, 99, pp. 27–48. https://doi.org/10.1080/00045600802224638

Lloyd, J.E. 1911. A history of Wales. Longmans, Green, and Co, London, 816 p.

Matthews, J.P. 1993. Sarn Badrig, Cantre'r Gwaelod a dinasoedd coll Bae Ceredigion: Golwg o'r gofod ['Sarn Badrig, Cantre'r Gwaelod and the lost cities of Cardigan Bay: A view from space']. Y Gwyddonydd, 30, pp. 71–76.

May, V. J. 2003. Benacre Ness, Suffolk (TM 532 824-TM 535 831). *In* Coastal Geomorphology of Great Britain. *Edited by* V.J. May and J.D. Hansom. Geological Conservation Review Series, No. 28. Joint Nature Conservation Committee, Peterborough, pp. 301–304.

Meyrick, S.R. 1808. The history and antiquities of the County of Cardiganshire. T. Bensley, London, 380 p.

North, F.J. 1940. The legend of Llys Helig - its origin and its significance. Llandudno, Colwyn Bay and District Field Club (a Supplement to the Proceedings), pp. 1–67.

North, F.J. 1957. Sunken cities: some legends of the coast and lakes of Wales. University of Wales Press, Cardiff, 256 p.

Nunn, P.D. 2014a. Geohazards and myths: ancient memories of rapid coastal change in the Asia-Pacific region and their value to future adaptation. Geoscience Letters, 1, pp. 1–11. https://doi.org/10.1186/2196-4092-1-3

Nunn, P.D. 2014b. Lashed by sharks, pelted by demons, drowned for apostasy: the value of myths that explain geohazards in the Asia-Pacific region. Asian Geographer, 31, pp. 59–82. https://doi.org/10.1080/10225706.2013.870080

Nunn, P.D. 2016. Australian Aboriginal traditions about coastal change reconciled with postglacial sea-level history: a first synthesis. Environment and History, 22, pp. 393–420. https://doi.org/10.3197/096734016X14661540219311

Nunn, P.D., Creach, A., Gehrels, W.R., Bradley, S.L., Armit, I., Stéphan, P., Sturt, F., and Baltzer, A. 2021. Observations of postglacial sea-level rise in northwest European traditions. Geoarchaeology, pp. 1–17. https://doi.org/10.1002/gea.21898

Parsons, E.J.S. 1958. The map of Great Britain circa AD 1360 known as the Gough Map. Bodleian Library, Oxford, 38 p.

Pelham, R.A. 1933. Early maps of Great Britain, II: the Gough Map. Geographical Journal, 81, pp. 34–39. https://doi.org/10.2307/1783891

Piccardi, L. and Masse, W.B. (*Editors*). 2007. Myth and geology. Geological Society of London Special Publication, No. 273, 360 p. https://doi.org/10.1144/GSL.SP.2007.273.01.08

Piccardi, L., Monti, C., Vaselli, O., Tassi, F., Gaki-Papanastassiou, K., and Papanastassiou, D. 2008. Scent of a myth: tectonics, geochemistry and geomythology at Delphi (Greece). Journal of the Geological Society, 165, pp. 5–18. https://doi.org/10.1144/0016-76492007-055

Piriou, Y.B. 1992. Quelques remarques à propos de l'ancien mystère de Saint Gwénolé. *In* Bretagne et pays celtiques: Langues, histoire, civilisation. *Edited by* G. Le Menn and J.Y. Le Moing. Rennes/Saint Brieuc: Presses Universitaires Rennes/Skol, pp. 193–211.

Poulin, J.C. 2009. L'hagiographie bretonne du haut moyen âge. Jan Thorbecke Verlag, Ostfildern, 493 p.

Pratt, W.T., Woodhall, D.G., and Howells, M.F. 1995. Geology of the country around Cadair Idris. Memoir for the 1:50 000 geological sheet 149 (England and Wales). British Geological Survey, HMSO, 111 p.

Rappenglück, B., Rappenglück, M.A., Ernstson, K., Mayer, W., Neumair, A., Sudhaus, D., and Liritzis, I. 2010. The fall of Phaethon: a Greco-Roman geomyth preserves the memory of a meteorite impact in Bavaria (south-east Germany). Antiquity, 84, pp. 428–439. https://doi.org/10.1017/S0003598X00066680

Reeve, M.D. and Wright, N. 2007. Geoffrey of Monmouth: the History of the Kings of Britain (an edition and translation of De gestis Britonum [Historia Regum Britaniae]). Boydell Press, Woodbridge, 307 p.

Reimer, P.J., Austin, W.E., Bard, E., Bayliss, A., Blackwell, P.G., Ramsey, C.B., Butzin, M., Cheng, H., Edwards, R.L., Friedrich, M., and Grootes, P.M. 2020. The IntCal20 Northern Hemisphere radiocarbon age calibration curve (0-55 cal kBP). Radiocarbon, 62, pp. 725–757. https://doi.org/10.1017/RDC.2020.41

Rhŷs, J. 1901. Celtic Folklore: Welsh and Manx. Clarendon Press, Oxford, 718 p.

Rijsdijl, K. and McCarroll, D. 2001. Traeth y Mwnt. *In* The Quaternary of West Wales: Field Guide. *Edited by* M.J.C. Walker and D. McCarroll. Quaternary Research Association, London, pp. 57–60.

Shaw, J., Taylor, R. B., and Forbes, D. L. 1993. Impact of the Holocene transgression on the Atlantic Coastline of Nova Scotia. Géographie physique et Quaternaire, 47, pp. 221–238. https://doi.org/10.7202/032950ar

Sims-Williams, P. 1983. The settlement of England in Bede and the Chronicle. Anglo-Saxon England, 12, pp. 1–41. https://doi.org/10.1017/S0263675100003331

Sims-Williams, P. 2010. Irish influence on medieval Welsh literature. Oxford University Press, Oxford, 425 p.

Sistermans, P. and Nieuwnhuis, O. 2013. Holderness Coast (United Kingdom). Case Study. Amerstfoort: DHV Group, 22 p.

Skelton, R.A. 1959. A medieval map of Britain. Geographical Journal, 125, pp. 237–239. https://doi.org/10.2307/1790508

Smallwood, T.M. 2009. The date of the Gough Map. Imago Mundi, 62, pp. 3–29. https://doi.org/10.1080/03085690903407997

Stewart, I. 2021. Archaeological and cultural records of active tectonics. Reference Module in Earth Systems and Environmental Sciences, Elsevier, 21 p.

Strang, A. 1997. Explaining Ptolemy's Roman Britain. Britannia, 28, pp. 1–30. https://doi.org/10.2307/526763

Strang, A. 1998. Recreating a possible Flavian map of Roman Britain with a detailed map for Scotland. Proceedings of the Society of Antiquaries of. Scotland, 128, pp. 425–440.

Tappin, D.R., Chadwick, R.A., Jackson, A.A., Wingfield, R.T R., and Smith, N.J.P. 1994. United Kingdom offshore regional report: the geology of Cardigan Bay and the Bristol Channel. British Geological Survey, HMSO, London, 107 p.

Thompson, E.A. 1979. Gildas and the history of Britain. Britannia, 10, pp. 203–226. https://doi.org/10.2307/526057

Thomson, D.S. (*Editor*). 1986. Branwen uerch Lyr. Dublin Institute for Advanced Studies, Dublin, 7 pp.

Vitaliano, D.B. 1968. Geomythology: the impact of geologic events on history and legend with special reference to Atlantis. Journal of the Folklore Institute, 5, pp. 5–30. https://doi.org/10.2307/3813842

Wade-Evans, A.W. 1944. Vitae sanctorum Britanniae et genealogiae. University of Wales Press, Cardiff, 387 p.

Walsh, K., Brown, A.G., Gourley, B., and Scaife, R. 2017. Archaeology, hydrogeology and geomythology in the Stymphalos valley. Journal of Archaeological Science: Reports, 15, pp. 446–458. https://doi.org/10.1016/j.jvolgeores.2020.106999

West of Wales Shoreline Management Plan Consultation 2011. Policy Development Coastal Area C. 9T9001/RSection4Cav4/303908/PBor, 134 p.

Widmer, P., and Jørgensen, A.R. 2011. An Buhez Sant Gwenôlé. Edition Praesens, Vienna, 171 p.

Wilkie, B., Cahir, F., and Clark, I.D. 2020. Volcanism in aboriginal Australian oral traditions: Ethnographic evidence from the Newer Volcanics Province. Journal of Volcanology and Geothermal Research, 403, unpaginated, https://doi.org/10.1016/j.jvolgeores.2020.106999

Williams, I. 1957. Chwedl Taliesin. University of Wales Press, Cardiff, 24 p.

Williams, K.E. 1927. The glacial drifts of western Cardiganshire. Geological Magazine, 64, pp. 205–227. https://doi.org/10.1017/S0016756800103279

Winterbottom, M. (*Translator*). 1978. Gildas: The ruin of Britain and other works. Phillimore, London, 16 pp.

Wood, J. 1980. The mid-Wales context of *Hanes Taliesin:* local place-names in the manuscript tales. Journal of the Cardiganshire Antiquarian Society, 9, pp. 53–57.

Wunderlich, F. 1980. Transgression und Umlagerung im Gebiet des Helgoland-Riffs. Eiszeitalter und Gegenwart, 30, pp. 213–220. https://doi.org/10.3285/eg.30.1.17

Editorial responsibility: Denise Brushett

Note on the discovery of Carboniferous amber associated with the seed fern *Linopteris obliqua*, Sydney Coalfield, Nova Scotia, Canada

Maria Mastalerz[1*] and Erwin L. Zodrow[2]

1. Indiana Geological and Water Survey, Indiana University, Bloomington, Indiana 47405, USA
2. 503 Coxheath Road, Sydney, Nova Scotia B1R 1S1, Canada
* corresponding author: mmastale@indiana.edu

Date received:15 February 2022 ¶ Date accepted 10 May 2022

ABSTRACT

We report on a discovery of amber from the Carboniferous sedimentary rocks of the Sydney Coalfield, Nova Scotia, Canada. The amber occurs in the form of droplets and as a linear feature and ranges in colour from light brown to dark purple. The amber was found in situ in siltstone above the Middle Pennsylvanian Hub coal seam, where it was associated with abundantly abscised pinnules of the seed fern *Linopteris obliqua*. The amber specimens were analyzed by infrared spectrometry and their spectrochemical characteristics were compared with those of other fossil ambers. This discovery not only expands the inventory of amber to as old as ~300 million years, but also documents that Carboniferous seed ferns were able to utilize biosynthetic mechanisms to produce resinous exudates.

RÉSUMÉ

Nous rapportons une découverte d'ambre dans les roches sédimentaires Carbonifères du terrain houiller de Sydney, en Nouvelle-Écosse, Canada. L'ambre se manifeste sous forme de gouttelettes ainsi que de figures linéaires, et il a une teinte variant du brun pâle au mauve foncé. L'ambre a été découvert in situ dans de la siltite au-dessus du filon de charbon du Pennsylvanien moyen Hub, où il est associé à des pinnules abondamment falsifiées de la fougère à graines *Linopteris obliqua*. Les spécimens d'ambre ont été analysés par spectrométrie infrarouge et leurs caractéristiques spectrochimiques ont été comparées à celles d'autres ambres fossiles. Cette découverte élargit non seulement l'inventaire de l'ambre à une période remontant à environ 300 millions d'années, mais documente également la capacité des fougères à graines Carbonifères d'utiliser des mécanismes biosynthétiques pour produire des exsudats résineux.

[*Traduit par la redaction*]

INTRODUCTION

Fossil resin, or amber, has been known since prehistoric times and used in a variety of applications, such as varnish, paint binder, adhesive, and jewelry (Lucas and Harris 1962). Resins can be defined as lipid soluble mixtures of volatile and non-volatile terpenoid and/or phenolic secondary compounds that are secreted either within or on the surface of plants (Langenheim 2003). Fossilization of resins and their preservation in the fossil record as amber provide important sources of information in relation to chemotaxonomy, geochemical processes, and provenance studies (e.g., Anderson *et al*. 1992; Broughton 1972; Lyons *et al.* 2009). Most fossil resins come from Cretaceous to Neogene sediments, and they are mostly products of conifers and angiosperms (Langenheim 2003).

Amber in Canada is known mainly from the western provinces, notably from Alberta, where it occurs in Late Cretaceous and, to a lesser extent, in Paleocene formations. In these rocks it was dominantly sourced from conifers, likely from members of the family Cupressaceae (McKellar and Wolfe 2010). Although mostly recovered from bituminous coal seams, amber is also found in organic-rich shale beds overlying those coals in Alberta.

In this paper we report the discovery of amber from Carboniferous (Middle Pennsylvanian) sedimentary rock from the Sydney Coalfield, Nova Scotia, Canada (Fig. 1). To our knowledge, it is the first discovery of amber in association with a seed fern. We compare the spectrochemical characteristics of the amber with other selected fossil ambers.

doi:10.4138/atlgeo.2022.006

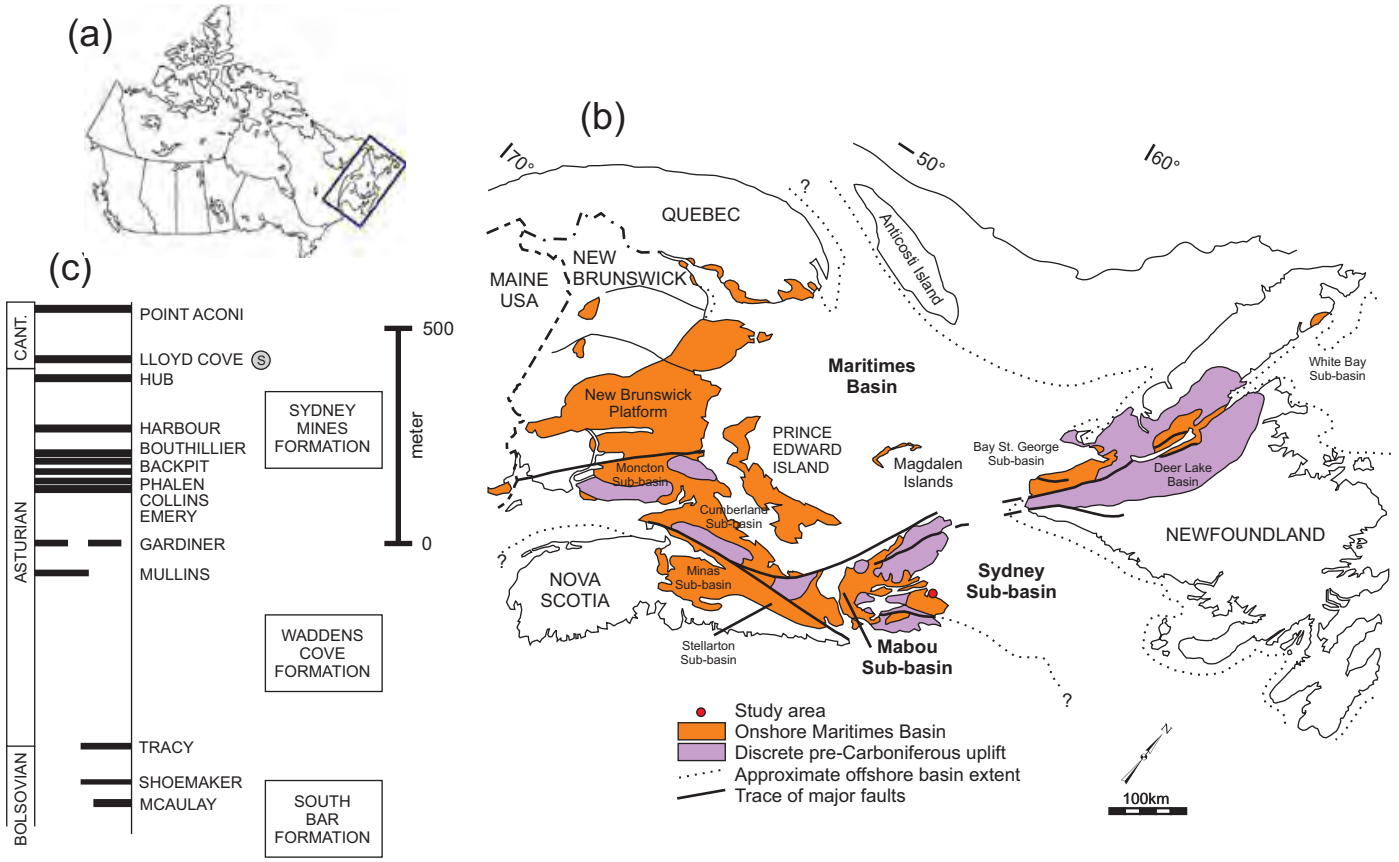

Figure 1. Location map and coal stratigraphy. (a) Regional. (b) Carboniferous basins and sub-basins in Atlantic Canada. (c) Coal stratigraphy. Amber samples (S) described in this study occurred approximately 5 m above the Upper Asturian Hub coal seam of the Sydney Sub-basin. Cant. = Cantabrian age.

MATERIAL AND METHODS

Material

In 2008, a fossiliferous in-situ siltstone block was recovered above the upper Asturian Hub coal seam, Sydney Coalfield, in a developing open pit. The block measures 30 × 40 × 7 cm (Fig. 2a) and weighs 22 kg. Its accession number in the Palaeontological Collection of Cape Breton University, Sydney, Nova Scotia, Canada is 08-10/15-9. The block was systematically deconstructed, and a careful record of the process was kept. The megascopic analysis showed that abscised foliage of the tree fern *Linopteris obliqua* (Bunbury 1847) Zeiller 1899 (Zodrow and McCandlish 1978; Zodrow *et al.* 2007) was the overwhelmingly dominant compression fossil present, numbering in the thousands. Interestingly, Bunbury (1847, p. 427) commented on the abundance of this species in the Sydney Coalfield and its absence in American and European collections.

Two fragmentary amber samples were found. Sample 8-10/15-9 13 is a droplet 3 mm across and weighing ca. 5 mg (Fig. 2b, arrow). Enlarged 30 times (Fig. 2c), it shows micrometre-scale brownish-red grains under reflected light and no inclusions. The droplet is encased in a dark-coloured rim, ca. 130 μm wide, that appears to have a different composition than the surrounding shaly matrix. The other amber sample is a composite specimen, 08-10/15-9 2, consisting of three fragments, each 3–4 mm in size (Fig. 2d). In contrast with the previous sample, these fragments are translucent, darkish in colour, and inclusion-free. The spatial relationship on these fragments in the block is unknown.

Methods

After megascopic observations and careful isolation of the amber, the samples were analyzed by the Fourier transform infrared spectroscopy (FTIR) technique. This technique has long been proven helpful in investigating the source of amber, especially of Cretaceous and younger age (Langenheim and Beck 1965). For FTIR analysis, both amber samples (8-10/15-9 13 and 08-10/15-9 2) were analyzed on a Nicolet 6700 instrument equipped with a DTGS detector. Three FTIR spectra were obtained from the lighter coloured amber droplet (8-10/15-9 13), and three spectra from the darker coloured fragments (08-10/15-9 2, one spectrum from each fragment). For these analyses, a small amount of amber was mixed with finely ground KBr (the resin accounting for ca. 2 wt.% of the mixture) to form

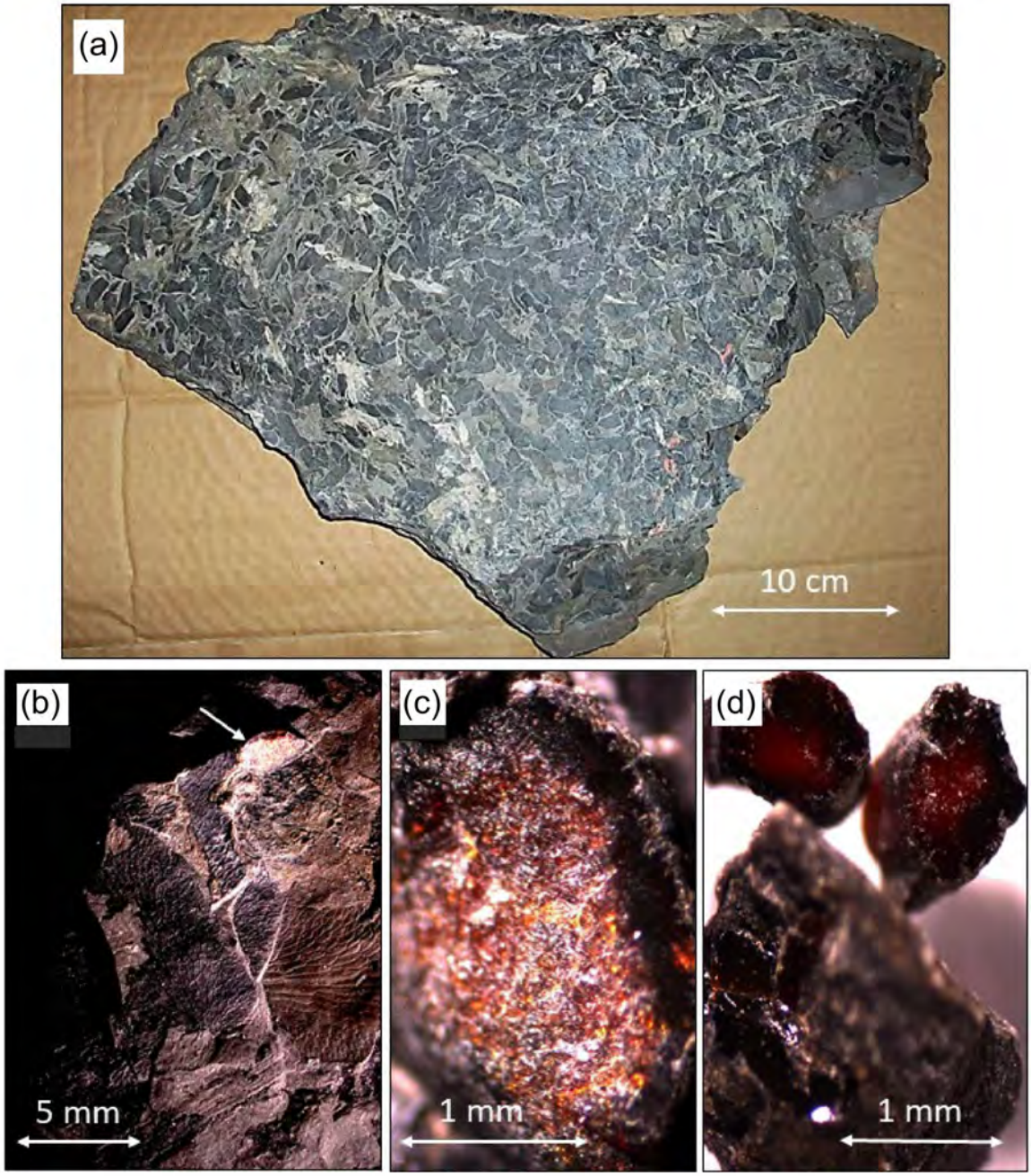

Figure 2. Documentation of amber in the Carboniferous, Sydney Coalfield, Nova Scotia, Canada. (a) amber-bearing block showing abundant compression pinnules of *Linopteris obliqua* (Bunbury 1847) Zeiller 1899 (accession number 08-10/15-9 13). (b) Bright in situ droplet, arrowed, in association with compression pinnules (sample 8-10/15-9 13. (c) The bright granular amber droplet itself. (d) The dark, dense, and transparent amber pieces (sample 08-10/15-9 2).

a KBr pellet. Spectra were obtained in reflectance mode at a resolution of 4 cm^{-1} and 400 scans were collected per analysis. The IR signal was recorded in the region of 400 to 4000 cm^{-1} wavenumber. IR bands were identified by comparison with published assignments (e.g., Painter *et al.* 1981; Wang and Griffith 1985; Goodarzi and McFarlane 1991; McFarlane *et al.* 1993). The following three ratios of the integration-band areas (Table 1) were calculated: CH_2/CH_3, Ox_1, and Al/1035. The CH_2/CH_3 ratio was calculated in the 2800–3000 cm^{-1} aliphatic stretching region after band deconvolution, and two bands (CH_2 at 2925 and CH_3 at 2960 cm^{-1}) were used in calculation, following our previous procedures (e.g., Lis *et al.* 2005). Ox_1 is a ratio of the C=O + C=C bands in the 1500–1800 cm^{-1} region to the bands in the aliphatic stretching region (2800–3000 cm^{-1}), and Al/1035 is a ratio of the bands in the aliphatic stretching region (2800–3000 cm^{-1}) to the band with the peak at 1035 cm^{-1}.

Table 1. FTIR derived ratios of the amber samples.

Analysis	CH_2/CH_3	Ox_1	AI/1035
8-10/15-9-13 analysis 1	1.36	0.18	0.40
8-10/15-9-13 analysis 2	1.18	1.09	3.12
8-10/15-9-13 analysis 3	1.50	0.39	1.60
Average	1.35	0.56	1.71
08-10/15 9 2 - fragment 1	1.27	0.54	0.38
08-10/15 9 2 - fragment 2	1.32	0.53	0.07
08-10/15 9 2 - fragment 3	1.42	0.77	0.88
Average	1.34	0.61	0.44

CH_2/CH_3 was calculated after band deconvolution in the 2800–3000 cm^{-1} region; Ox_1 is a ratio of the bands in 1500–1800/2800–3000 cm^{-1} and AI/1035 uses intergration areas of 2800–3000 cm^{-1} bands.

RESULTS

The FTIR spectra of both amber samples are dominated by aliphatic hydrogen bands in the stretching 2800–3000 cm^{-1} region and the 1300–1500 cm^{-1} aliphatic bending region, and have a broad band with the peak at ~1035 cm^{-1} (Figs. 3–4). The latter band could come from v(SO) undissociated sulphonate groups that were detected in some resins (Edwards *et al.* 2000); but more likely it represents C-O stretching bands (like those in lignin). Oxygenated groups and aromatic carbon bands in the 1500–1800 cm^{-1} region are distinct, but their intensity is not large relative to aliphatic hydrogen bands. Small bands in the 700–900 cm^{-1} region also occur, as do two prominent bands at 537 and 470 cm^{-1} of an unassigned nature. It is interesting that bands representing exomethylene (CH_2) groups in diterpenoid form with peaks at ~3082, 1644, and 887 cm^{-1}, characteristic of many fossilized resins (Streibl *et al.* 1976; Poinar and Mastalerz 2000) were not recorded in the amber studied here (Figs. 3–4).

Qualitative comparison between spectra of the two amber samples (8-10/15-9 13 and 08-10/15-9 2) reveal close similarities between the functional-group distribution and their relative proportions (Figs. 3–4), and the difference between the two samples are not more distinct than within-sample differences. While three splits of sample 8-10/15-9 13 are very similar (Fig. 3), in sample 08-10/15-9 2 composed of three fragments (Fig. 4), one fragment has very reduced aliphatic bands (both in 2800–3000 and 1300–1500 cm^{-1}) and the band with the peak at ~1037 cm^{-1} was dominant; it is likely that this fragment has significant lignin content.

This functional-group similarity between the two amber samples is also supported by semiquantitative ratios (Table 1). CH_2/CH_3 ratios range from 1.18 to 1.50 between individual analyses, with a very similar average values of 1.34 and 1.35 for the two samples, suggest similarity in the length and branching of aliphatic chains (e.g., Lin and Ritz

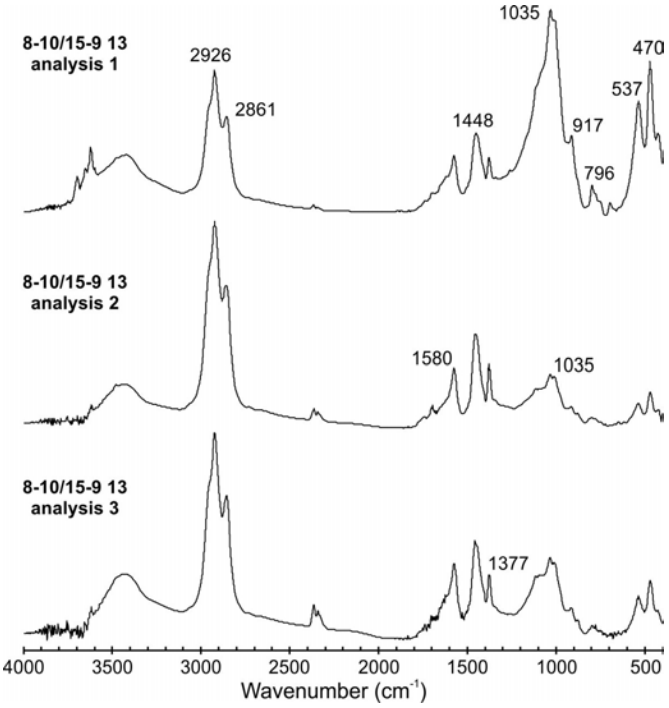

Figure 3. FTIR spectra of the amber droplet shown in Figure 2c. The three spectra represent three splits of sample 8-10/15-9 13.

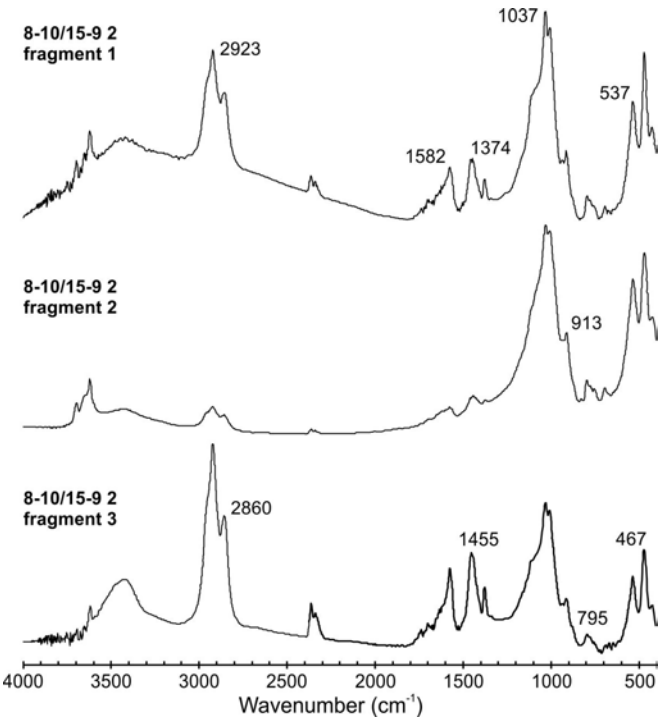

Figure 4. FTIR spectra of three fragments of sample 08-10/15-9 2 (Fig. 2d).

1993). Ratio Ox_1 is dependent on the relationship between the oxygenated plus aromatic carbon groups and aliphatic-hydrogen bands and usually reflects the oxidation level of the organic matter: CH_2 and CH_3 are known to be consumed during oxidation, with C=O groups being formed (Kister *et al.* 1988; Vasallo *et al.* 1991; Pradier *et al.* 1992). Following this interpretation, darker amber 08-10/15 9 2 would be on average slightly more oxidized compared to amber 8-10/15-9 13, as reflected by a higher Ox^1 value of 0.61 compared to 0.56 in the latter (Table 1). In their study of the amber from Dominican Republic, Poinar and Mastalerz (2000) noted that the increase in oxidation/weathering was associated with a change from lighter to darker colour, an observation that seems to be supported in the present study. The main difference between the two amber samples is in the Al/1035 ratio, which is greater for the 8-10/15-9 13 sample, mainly because of significantly smaller absorbance of the bands with the peak at ~1035–1037 cm^{-1} (likely coming from lignin) relative to the aliphatic stretching bands in this sample.

DISCUSSION AND CONCLUSIONS

Our discovery of Carboniferous amber expands the inventory of amber to as old as ~ 300 million years, and thus beyond that documented from Desmoinesian coal seams in Illinois (Bray and Anderson 2009). As those authors concluded, such early occurrences of amber demonstrate that pre-conifer gymnosperms were able to utilize the biosynthetic mechanisms to produce resins well before the onset of angiosperms, which are considered to be one of the main group of resin producers (Langenheim 2003). In fact, the development and utilization of these mechanisms by Carboniferous plants is indicated by the occurrence of maceral resinite (fossil resin) in Carboniferous coals, and by the presence of medullosalean seed-fern resin in Pennsylvanian coal balls (C. Eble, written communication 2022). Crelling and Kruge (1998) separated resinite from the Pennsylvanian Herrin Coal in Illinois and argued that its properties differed from those of Cretaceous and younger resins. The petrographic properties of Carboniferous resinites (Crelling 1995) are, however, similar to those of younger resins, and older resins likely served similar botanical functions to those of younger plants for example, sealing and protecting wounds and repelling insects (Langenheim 2003). In the Carboniferous sedimentarty rocks, however, the resins are of small, typically microscopic size and, unlike the younger resins, megascopic "amber-size" occurrences are extremely rare (e.g., Grimaldi 2009). The very rare and small occurrences of amber and resinite in Carboniferous sedimentary rocks suggest that only limited types of plants then had the ability to utilize biosynthetic mechanisms to produce resins.

Identification of the parent plants of ambers is often impossible because ambers often occur isolated and in dissociation from the source plant (Langenheim 2003). Therefore, documenting the association of the studied amber with an arborescent seed fern is an important aspect of this study. It is well known that resins are produced by almost all modern conifers and many angiosperms. So far, the earliest evidence of fossil resin comes from the Late Carboniferous with arborescent cordaitaleans (early relatives of conifers) or from seed ferns suggested as source plants (Langenheim 2003). In this study, the occurrence of the amber in association with huge quantities of abscised medullosalean seed-fern foliage *Linopteris obliqua* indicates that seed ferns were also able to utilize the biosynthetic mechanisms to produce resin exudates.

In their py-GC/MS study of Carboniferous amber from an Illinois Basin coal seam ~320 million years old, Bray and Anderson (2009) suggested that the amber had Class I (polylabdanoid) characteristics, similar to that produced by a wide variety of modern species. In contrast, Crelling and Kruge (1998), in their study of resinite from a different Illinois Basin coal seam revealed predominantly aliphatic character (straight chain hydrocarbons), with only minor alkylbenzenes and phenols, characteristic of a cross-linked aliphatic biogeopolymer. They further concluded that these Carboniferous resinites differed from typical Cretaceous or younger resinites in their chemistry: the Cretaceous resinites were composed mainly of aromatized and unsaturated cadinanes, small aromatic molecules and isoprenoid hydrocarbons, characteristic of polycadinane structure. In the present study, we analyzed the chemistry of functional groups and it is therefore difficult to make direct comparison with the py-GC-MS compound data of Bray and Anderson (2009) or Crelling and Kruge (1998). However, the comparison of functional-group distribution of the studied amber to the younger ambers and modern resin from the other areas (Fig. 5) reveal two main differences: (1) the absence of oxygenated group bands around 1700 cm^{-1} in the Carboniferous amber studied; this band is very prominent in Miocene ambers and in modern *Agathis* resin (Fig. 5), as well as in Cretaceous ambers from Canada (McKellar and Wolfe 2010); and (2) the presence of a distinct 1580 cm^{-1} band in the Carboniferous amber; this band, likely represents aromatic carbon and does not occur in the spectra of other ambers. Van Bergen *et al.* (1995) also mentioned the unusual chemistry of Carboniferous resin rodlets, dominated by (alkyl)naphtalenes, alkylbenzenes, and phenols.

For now it is difficult to conclude whether these differences are related to the original chemistry of the resin or are the result of more a advanced maturation processes for the Carboniferous resin. Clifford and Hatcher (1995a, b) found that, with increased maturation from lignite to subbituminous coal, fossil resins showed depletion in exomethylene groups and increase in alkylnaphtalenes. The coals associated with the amber studied are of high volatile bituminous rank (R_o % 0.64–0.66 %), and the reduction in oxygenated groups and the absence of exomethylene groups, at least to some extent, may be related to their more advanced maturation.

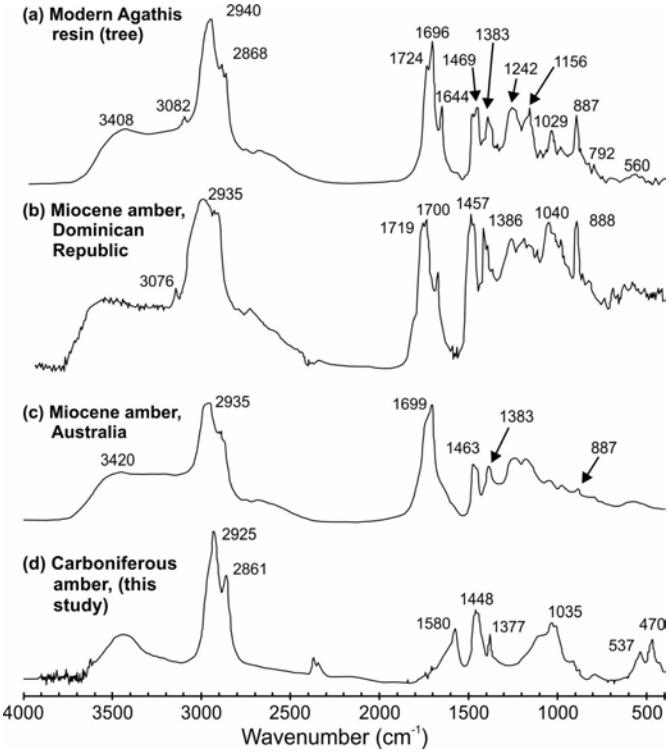

Figure 5. Comparison of FTIR spectra of the amber studied here with selected younger resins.

ACKNOWLEGEMENTS

We appreciate with thanks the technical corrections made by the journal reviewers J.A. D'Angelo (Universidad Nacional de Cuyo, Mendoza, Argentina) and C. Eble (Kentucky Geological Survey, Lexington, USA). This paper also benefited from valuable comments by the Editor, R. Fensome.

REFERENCES

Anderson, K.B., Winans, R.E., and Botto, R.E. 1992. The nature and fate of natural resins in the geosphere, II. Identification, classification, and nomenclature of resinite. Organic Geochemistry, 18, pp. 829–841. https://doi.org/10.1126/science.1177539

Bray, P.S. and Anderson, K.B. 2009. Identification of Carboniferous (320 million years old) class Ic amber. Science, 326,pp. 132–134. https://doi.org/10.1126/science.1177539

Broughton, P.L. 1972. Conceptual framework for geographical-botanical affinities of fossil resins. Canadian Journal of Earth Sciences, 11, pp. 583–594. https://doi.org/ 10.1139/e74-053

Bunbury, C.J.F. 1847. On fossil plants from the Coal Formation of Cape Breton. Quarterly Journal of the Geological Society of London, 3, pp. 423–438. https://doi.org/10.1144/GSL.JGS.1847.003.01-02.44

Clifford, D.J. and Hatcher, P.G. 1995a. Maturation of Class 1b (polylabdanoid) resinites. *In* Amber, resinite, and fossil resins. *Edited by* K.B. Anderson and J.C. Crelling. American Chemical Society Symposium Series 617. American Chemical Society, Washington DC, pp. 92–104. https://doi.org/10.1021/bk-1995-0617.ch005

Clifford, D.J. and Hatcher, P.G. 1995b. Structural transformation of polylabdanoid resinites during maturation. Organic Geochemistry, 23, pp. 407–418. https://doi.org/10.1016/0146-6380(95)00022-7

Crelling, J.C. 1995. The petrology of resinite in American coals. *In* Amber, resinite, and fossil resins. *Edited by* K.B. Anderson and J.C. Crelling. American Chemical Society Symposium Series 617. American Chemical Society, Washington DC, pp. 218–233. https://doi.org/10.1021/bk-1995-0617.ch012

Crelling, J.C. and Kruge, M. 1998. Petrographic and chemical properties of Carboniferous resinite from the Herrin #6 coal seam. International Journal of Coal Geology, 37, pp. 55–71. https://doi.org/10.1016/S0166-5162(98)00021-4

Edwards, H.G.M., Brown, D.R., Dale, J.A., and Plant, S. 2000. Raman spectroscopy of sulfonated polystyrene resins. Vibrational Spectroscopy, 24, 213–224. https://doi.org/10.1016/S0924-2031(00)00070-9

Goodarzi, F. and McFarlane, R.A. 1991. Chemistry of fresh and weathered resinites - an infrared photoacoustic spectroscopic study. International Journal of Coal Geology, 19, pp. 283–301. https://doi.org/10.1016/0166-5162(91)90024-D

Grimaldi, D. 2009. Pushing back amber production. Science, 326, pp. 51–52. https://doi.org/10.1126/science.1179328

Kister, J., Guiliano, M., Mille, G., and Dou, H. 1988. Changes in the chemical structure of low rank coal after low temperature oxidation or demineralization by acid treatment. Fuel, 67, pp. 1076–1082. https://doi.org/10.1016/0016-2361(88)90373-0

Langenheim, J.H. 2003. Plant resins. chemistry, evolution, ecology, ethnobotany. Timber Press, Portland, USA and Cambridge, UK, 586 p.

Langenheim, J.H. and Beck, C.W. 1965. Infrared spectra as a means of determining botanical sources of amber. Science, New Series, 149, pp. 52–55. https://doi.org/10.1126/science.149.3679.52

Lin, R. and Ritz, G.P. 1993. Studying individual macerals using IR microspectroscopy, and implications on oil versus gas/condensate proneness and "low-rank" generation. Organic Geochemistry, 20, pp. 695–706. https://doi.org/10.1016/0146-6380(93)90055-G

Lis, G.P., Mastalerz, M., Schimmelmann, A., Lewan, M.D., and Stankiewicz, B.A. 2005. FTIR absorption indices for thermal maturity in comparison with vitrinite reflectance R_0 in type-II kerogens from Devonian black shales. Organic Geochemistry, 36, pp. 1533–1552. https://doi.org/10.1016/j.orggeochem.2005.07.001

Lucas, A. and Harris, J.R. 1962. Ancient Egyptian materials

and industries. 4th Edition, Edward Arnold, London, 523 p.

Lyons, P.C., Mastalerz, M., and Orem, W.H. 2009. Organic geochemistry of resins from modern *Agathis australis* and Eocene resins from New Zealand: diagenetic and taxonomic implications. International Journal of Coal Geology, 80, pp. 61–62. https://doi.org/10.1016/j.coal.2009.07.015

McFarlane, R.A., Gentzis, T., Goodarzi, F., Hanna, J.V., and Vassallo, A.M. 1993. Evolution of the chemical structure of Hat Creek resinite during oxidation: a combined FT-IR photoacoustic, NMR and optical microscopic study. International Journal of Coal Geology, 22, pp. 119–149. https://doi.org/10.1016/0166-5162(93)90021-2

McKellar, R.C. and Wolfe, A.P. 2010. Canadian amber. *In* Biodiversity of fossils in amber from the major world deposits. *Edited by* D. Penney. Siri Scientific Press, pp. 96–113 (includes Appendix: arthropod families recorded from Canadian amber).

Painter, P.C., Snyder, R.W., Starsinic, M., Coleman, M.M., Kuehn, D.W., and Davis, A. 1981. Concerning the application of FTIR to the study of coal: a critical assessment of band assignments and the application of spectral analysis programs. Applied Spectroscopy, 35, pp. 475–485. https://doi.org/10.1366/0003702814732256

Poinar, G.O. and Mastalerz, M. 2000. Taphonomy of fossilized resins: determining the biostratinomy of amber. Acta Geologica Hispanica, 35, pp. 171–182.

Pradier, B., Landis, P., Rochdi, A., and Davis, A. 1992. Chemical basis of fluorescence alteration of crude oils and kerogens - II. Fluorescence and infrared microspectrometric analyses of vitrinite and liptinite. Organic Geochemistry, 18, pp. 241–249. https://doi.org/10.1016/0146-6380(92)90065-6

Streibl, V., Vasickova, S., Herout, V., and Bouska, V. 1976. Chemical composition of Cenomanian fossil resins from Moravia. Collection of Czechoslovak Chemical Communications., 41, pp. 3138–3145. https://doi.org/10.1135/cccc19763138

Van Bergen, P.F., Collinson, M.E., Scott, A.C., and Leeuw de, J.W. 1995. Unusual resin chemistry from Upper Carboniferous pteridosperm resin rodlets. *In* Amber, resinite, and fossil resins. *Edited by* K.B. Anderson and J.C. Crelling. American Chemical Society Symposium Series 617. American Chemical Society, Washington DC, pp. 149–169. https://doi.org/10.1021/bk-1995-0617.ch008

Vasallo, A.M., Lui, Y.L., Pang, L.S.K., and Wilson, M.A. 1991. Infrared spectroscopy of coal maceral concentrates at elevated temperatures. Fuel, 70, pp. 635–639. https://doi.org/10.1016/0016-2361(91)90178-D

Wang, S.H. and Griffith, P.R. 1985. Resolution enhancement of reflectance IR spectra of coals by Fourier self-deconvolution, 1. C-H stretching and bending modes. Fuel, 64, pp. 229–236. https://doi.org/10.1016/0016-2361(85)90223-6

Zeiller, R. 1899. Étude sur le flore fossile du Bassin houiller d'Héraclée. Memoires de la Societé Géologique de la France. Paléontologie, 21, pp. 1–91. https://doi.org/10.5962/bhl.title.110944

Zodrow, E.L. and McCandlish, K. 1978. Distribution of *Linopteris obliqua* in the Sydney Coalfield of Cape Breton, Nova Scotia. Palaeontographica B, 168, pp. 1–16.

Zodrow, E.L., Tenchov, Y.G., and Cleal, C.J. 2007. The arborescent *Linopteris obliqua* plant (Medullosales, Pennsylvanian). Bulletin of Geosciences, 82, pp. 51–84. https://doi.org/10.3140/bull.geosci.2007.01.51

Editorial responsibility: Robert A. Fensome

Potential for critical mineral deposits in Maine, USA

John F. Slack[1, 2*], Frederick M. Beck[3], Dwight C. Bradley[4],
Myles M. Felch[5], Robert G. Marvinney[6, †], and Amber T.H. Whittaker[6]

1. U.S. Geological Survey (Emeritus), National Center, Reston, Virginia 20192, USA
2. Department of Earth Sciences, Memorial University of Newfoundland,
St. John's, Newfoundland and Labrador A1B 3X5, Canada
3. Maine Environmental Laboratory, Yarmouth, Maine 04096, USA
4. U.S. Geological Survey (Emeritus), Randolph, New Hampshire 03593, USA
5. Maine Mineral & Gem Museum, Bethel, Maine 04217, USA
6. Maine Geological Survey, Augusta, Maine 04333, USA
† Present address: P.O. Box 615, Readfield, Maine 04355, USA
*Corresponding author <jfslack@usgs.gov>

Date received:1 March 2022 ¶ Date accepted 17 July 2022

ABSTRACT

An analysis of the potential for deposits of critical minerals and elements in Maine presented here includes data and discussions for antimony, beryllium, cesium, chromium, cobalt, graphite, lithium, manganese, niobium, platinum group elements, rhenium, rare earth elements, tin, tantalum, tellurium, titanium, uranium, vanadium, tungsten, and zirconium. Deposits are divided into two groups based on geological settings and common ore-deposit terminology. One group consists of known deposits (sediment-hosted manganese, volcanogenic massive sulphide, porphyry copper-molybdenum, mafic- and ultramafic-hosted nickel-copper [-cobalt-platinum group elements], pegmatitic lithium-cesium-tantalum) that are in most cases relatively large, well-documented, and have been explored extensively in the past. The second, and much larger group of different minerals and elements, comprises small deposits, prospects, and occurrences that are minimally explored or unexplored. The qualitative assessment used in this study relies on three key criteria: (1) the presence of known deposits, prospects, or mineral occurrences; (2) favourable geologic settings for having certain deposit types based on current ore deposit models; and (3) geochemical anomalies in rocks or stream sediments, including panned concentrates. Among 20 different deposit types considered herein, a high resource potential is assigned only to three: (1) sediment-hosted manganese, (2) mafic- and ultramafic-hosted nickel-copper(-cobalt-platinum group elements), and (3) pegmatitic lithium-cesium-tantalum. Moderate potential is assigned to 11 other deposit types, including: (1) porphyry copper-molybdenum (-rhenium, selenium, tellurium, bismuth, platinum group elements); (2) chromium in ophiolites; (3) platinum group elements in ophiolitic ultramafic rocks; (4) granite-hosted uranium-thorium; (5) tin in granitic plutons and veins; (6) niobium, tantalum, and rare earth elements in alkaline intrusions; (7) tungsten and bismuth in polymetallic veins; (8) vanadium in black shales; (9) antimony in orogenic veins and replacements; (10) tellurium in epithermal deposits; and (11) uranium in peat.

RÉSUMÉ

L'analyse du potentiel de gîtes de minéraux et d'éléments critiques au Maine exposée aux présentes comporte des données et des examens concernant l'antimoine, le béryllium, le césium, le chrome, le cobalt, le graphite, le lithium, le manganèse, le niobium, les éléments du groupe du platine, le rhénium, les éléments des terres rares, l'étain, le tantale, le tellure, le titane, l'uranium, le vanadium, le tungstène et le zirconium. Les gîtes sont répartis en deux groupes selon les cadres géologiques et la terminologie des minéraux métallifères communs. Un groupe est constitué de gîtes connus [manganèse dans des roches sédimentaires, sulfures massifs volcanogènes, gîtes porphyriques de cuivre-molybdène nickel-cuivre (-cobalt-éléments du groupe du platine) dans des roches mafiques et ultramafiques ainsi que gisements pegmatitiques de lithium-césium-tantale] qui sont dans la majorité des cas relativement vastes, qui sont bien documentés et qui ont fait l'objet d'une exploration poussée par le passé. Le second groupe, beaucoup plus nombreux, de minéraux et d'éléments différents, est composé de petits gîtes, de zones prometteuses et de venues ayant été peu explorées ou inexplorées. L'évaluation qualitative utilisée dans le cadre de l'étude repose sur trois critères clés : 1) la présence de gîtes, de zones prometteuses ou de venues minérales connus; 2) les cadres géologiques favorables en raison de la présence de certains types de gîtes basés sur les modèles de dépôts de minerai courants; et 3) les anomalies géochimiques dans les roches ou les

doi:10.4138/atlgeo.2022.007

sédiments fluviatiles, notamment les concentrés lavés à la batée. Parmi les 20 différents types de gîtes considérés aux présentes, seuls trois se voient conférer un potentiel de ressources élevé : 1) les gîtes de manganèse dans des roches sédimentaires, 2) le nickel-cuivre (-cobalt-éléments du groupe du platine) dans des roches mafiques et ultramafiques, et 3) les gîtes pegmatitiques de lithium-césium-tantale. Un potentiel moyen est attribué à 11 autres types de gîtes, notamment : les gîtes porphyriques de cuivre-molybdène (-rhénium, sélénium, tellure, bismuth, éléments du groupe du platine); 2) le chrome dans des ophiolites; 3) les éléments du groupe du platine dans des roches ultramafiques ophiolitiques; 4) l'uranium-thorium dans du granite; 5) l'étain dans des plutons et filons granitiques; 6) le niobium, le tantale et les éléments des terres rares dans des intrusions alcalines; 7) le tungstène et le bismuth dans des filons polymétalliques; 8) le vanadium dans des schistes noirs; 9) des filons orogéniques et des substitutions; 10) le tellure dans des gîtes épithermaux et 11) l'uranium dans la tourbe.

[*Traduit par la redaction*]

INTRODUCTION

Certain minerals have long been recognized as being critical for industrial, military, medical, and recently low-carbon technologies (e.g., Price 2013; Fortier *et al.* 2017; Sovacool *et al.* 2020; Simandl *et al.* 2021). Most countries prioritize critical minerals differently owing to individual national parameters such as local resources and economies. In the United States, a critical mineral is defined by federal statute as (1) a nonfuel material that is essential to the economic and national security of the USA, (2) part of a supply chain that is vulnerable to disruption, or (3) serving an essential function in the manufacturing of a product, the absence of which would have significant consequences for the U.S. economy or national security (Presidential Executive Order No. 13817 2017). The USA currently relies on imports for 50 to 100% of 50 different critical minerals (U.S. Geological Survey 2021b). As of 2018, the U.S. Geological Survey (USGS) listed 35 critical minerals (and elements), specifically Al, Sb, As, barite, Be, Bi, Cs, Cr, Co, fluorspar, Ga, Ge, graphite, Hf, He, In, Li, Mg, Mn, Nb, platinum-group elements (PGEs), potash, rare earth elements (REE), Re, Rb, Sc, Sr, Ta, Te, Sn, Ti, W, U, V, and Zr (Fortier *et al.* 2018).

In this study, we report on the potential in Maine for resources of 20 critical minerals and elements including Be, Co, Cr, Cs, graphite, Li, Mn, Nb, PGEs, Re, REE, Sb, Sn, Ta, Te, Ti, U, V, W, and Zr. This group was selected because it focuses on metals that are known to occur in previously mined deposits, in documented (but unmined) deposits, and that may exist within minimally explored or undiscovered deposits. The last types include not only known mineral occurrences and small mines (typically without recorded production), but also areas lacking deposits that nonetheless have a speculative potential based on favourable geological, geochemical, and/or geophysical signatures. Not discussed in this report are critical minerals and elements such as arsenic, barite, and fluorspar that occur in a few deposit types in Maine but without sufficiently large tonnages or high grades to be economically viable now and in the near future, or alternatively reside in the crystal lattice of other minerals for which economic recovery is not commercially feasible.

Lacking detailed data on tonnages and grades for most of the deposits and prospects considered herein, we cannot provide a quantitative mineral resource assessment for critical minerals and elements in Maine (e.g., Singer and Menzie 2010). Such quantitative assessments also require estimates by an expert panel of economic and exploration geologists on the number of undiscovered deposits, which are currently not possible for Maine, and on the density distributions of different deposit types occurring elsewhere, which are unavailable for nearly all major metal deposits known in the state. As a result, our study is necessarily a qualitative assessment using high, moderate, and low designations, as has been done elsewhere in New England by the USGS for the Glens Falls and Sherbrooke-Lewiston 1° × 2° quadrangles (Slack 1990; Moench *et al.* 1999). In this present study, we distinguish between ore reserves (proven, indicated, and inferred) for deposits that could be mined economically under current market and technological conditions, and mineral resources that are concentrations of materials for which economic extraction of a commodity is potentially feasible, either currently or at some future time. Note that except as indicated in the cited references, data for reserves and resources are not compliant with modern exploration practices and related guidelines (e.g., NI 43-101 and JORC). Also, the resource evaluations presented herein do not consider state restrictions that may exist on exploration or mining, regardless of land status or commodity.

Throughout this paper all measurements originally reported in the Imperial system have been changed to the metric system. These changes include surface and underground dimensions as well as depths in mines and drill cores.

KNOWN DEPOSIT TYPES

Sediment-hosted manganese

Manganese is one of the most critical elements used in modern society. Its principal use is in the manufacture of steel as a purifying agent and an alloy that converts iron into steel (Cannon *et al.* 2017). Based on recent research, manganese may also serve an important role as a replacement for cobalt in rechargeable Li-ion batteries (Liu *et al.* 2021). The United States and Canada are totally dependent on foreign sources of manganese, which is imported chiefly from Gabon, Australia, South Africa, and Brazil. There are no defined U.S. domestic reserves, but some significant low-

grade resources exist of which the largest known is in Maine (Cannon *et al.* 2017).

Sediment-hosted manganese deposits typically occur within marine black shales. Such deposits are abundant in weakly metamorphosed (prehnite-pumpellyite facies) Silurian shale and locally in limestone of eastern Aroostook County (Fig. 1). These deposits were first described in the early 19th Century by Jackson (1838), but little interest was shown until the late 1930s (Pavlides 1962). Due to the critical importance of manganese in steel making, and the fact that at that time the United States imported all of its manganese, in 1941 the USGS and the State of Maine began an intensive study of the deposits (White 1943). From 1942 through 1944, the Manganese Ore Company sampled by trenching many of the deposits in both the northern (Presque Isle) and southern (Houlton) areas, as well as in the central (Maple Mountain and Hovey Mountain) area, including diamond drilling of two of the deposits in the northern area. The northern, central, and southern areas are considered separate districts for descriptive purposes. There are 19 known deposits in the northern district, one in the central district, and 15 in the southern district. Dimensions of the various deposits are poorly constrained in general, owing to limited drilling and scarcity of outcrops, among other factors. Moreover, as a result of current field work in the manganese districts, lithologic settings and correlation of map units are problematic and stratigraphic revisions are thus likely. The following descriptions of the three districts are taken mainly from the older literature, with formational assignments provisionally revised on the basis of recent studies by Prof. Chunzeng Wang of the University of Maine at Presque Isle (C. Wang, written communication 2022).

The iron-manganese deposits in the northern district occur as three sedimentary lenses within and just above a limestone (White 1943) assigned herein to the Silurian New Sweden Formation. Below the surficial oxidized zone, principal manganese minerals are the Mn-carbonate rhodochrosite ($MnCO_3$) and the Mn-silicates braunite [$(Mn^{2+}Mn^{3+})_6(SiO_4)O_8$] and bementite [$Mn_7Si_6O_{15}(OH)_8$]. In places, up to 20 wt% Fe is present in hematite, magnetite, and limonite (Pavlides 1962).

The central manganese district is represented solely by the large Maple Mountain-Hovey Mountain deposits. These lenticular Mn-Fe deposits (Pavlides 1962) are contained within grey and grey-green slate of the Silurian Maple Mountain Formation. Metavolcanic rocks are closely associated with the Mn- and Fe-bearing units, but are probably older (Pavlides 1962). The deposits of the Maple and Hovey Mountains area consist mainly of Mn-silicates such as braunite, with minor Fe-rich rhodochrosite, hosted within hematitic ironstone.

The southern manganese district differs from the central and northern districts in complexity of geology, absence of igneous rocks, likelihood of numerous faults, higher degree of metamorphism, and paucity of outcrops (White 1943; Miller 1947; Pavlides 1962). Manganiferous rocks there occur in slate and locally in siliceous limestone of the Silurian Smyrna Mills Formation. The principal manganese mineral is rhodochrosite, accompanied by minor Mn-siderite, chlorite, and magnetite (Earl and Eilertsen 1962). Early studies concluded that the magnetite in these southern deposits formed during metamorphism, but a primary sedimentary or early diagenetic origin cannot be ruled out for some occurrences.

In 1949, the U.S. Bureau of Mines (USBM) became involved in studies of the Aroostook County deposits. These studies included trenching, drilling, and airborne magnetic surveys. In 1951 and 1952, the USBM conducted numerous metallurgical tests on ores from the Maple Mountain and Hovey Mountains deposits (MacMillan and Turner 1954). The ores proved to be highly refractive and not amenable to conventional ore dressing techniques such as flotation, or magnetic or gravity separation. However, the ores were amenable to leaching using a variety of acids.

An early USBM estimate of the crude ore reserves in the region amounted to 232 Mt grading 8.9 wt% Mn and 20.7 wt% Fe (Eilertsen 1952). A later USBM evaluation by Kilgore and Thomas (1982), which is the most recent, determined a resource of 260.0 Mt @ 8.87 wt% Mn for the central district (Maple Mountain and Hovey Mountain deposits), and a resource of 63.1 Mt @ 9.54 wt% Mn for the north Aroostook district (e.g., Dudley and Gelot Hill deposits). However, this total excludes much smaller deposits in the southern district (e.g., Littleton Ridge, Henderson Hill), for which estimated reserves amount to 3.7 Mt at an average grade of 7.5 wt% Mn (Miller 1947). Based on these values, a combined resource (including reserves designated in early studies) for the Aroostook County deposits is calculated here to be ~327 Mt @ 9.0 wt% Mn.

Future exploration in the Aroostook County districts would benefit by considering the two main genetic models proposed for sedimentary manganese deposits. One model, developed by Cannon and Force (1983) and Force and Cannon (1988), involves syngenetic manganese concentration along the margins of anoxic marine basins, at the redoxcline between deep anoxic to sulphidic waters and variably oxidized surface waters. A modern example may be formation of the Mn-rich sediments in Gotland Deep of the Baltic Sea (Huckriede and Meischner 1996). In this model, dissolved manganese at high concentrations in oxygen-deficient deep seawater is transported by upwelling currents to the redoxcline, where Mn-carbonates precipitate on the seafloor. Mn-silicates are also deposited below this redox interface, similarly on the seafloor, whereas Mn-oxides form above, within oxidized surface waters. The second model is based on a wholly diagenetic process, from the studies of Okita (1992) and Okita and Shanks (1992) of the giant Molango manganese deposit in southern Mexico. This deposit is the largest known in North America, containing 1.52 Gt of ore at an average grade of about 10% Mn. The ore occurs within Upper Jurassic limestone and in part of the district directly overlies black pyritic shale. The high-grade ore zone contains 30% Mn but only 3% Fe, unlike the Fe-rich manganese deposits in Aroostook County. Carbon and sulphur

Figure 1. (next page) Simplified geologic map of Maine showing regional metamorphic zones and locations of mines and other significant mineral deposits having known concentrations of critical minerals or elements. Cambrian–Devonian plutons consist mainly of granite with subordinate gabbro; Carboniferous–Mesozoic plutons are mostly granitic or alkalic. Sedimentary (and metasedimentary) rocks are chiefly Cambrian to Devonian; not shown are small areas of Mesoproterozoic metasedimentary rocks in the western Penobscot Bay area. Volcanic (and metavolcanic) rocks are both mafic and felsic, and are dominantly Ordovician but include some Cambrian, Silurian, and Early Devonian strata together with minor sedimentary (and metasedimentary) rocks. Geology and metamorphic zones (coloured dashed lines) modified from Osberg *et al.* (1985). Faults are not shown. Abbreviations for cities and towns: A, Augusta; B, Bangor; BH, Blue Hill; F, Farmington; H, Houlton; L, Lewiston; M, Madrid; Pa, Paris; PI, Presque Isle; Po, Portland. Abbreviations for igneous plutons (some are grouped) and other igneous bodies: ad, Adamstown; ag, Agamenticus; am, Abbott Mountain; at, Attean; bl, Bottle Lake Complex; cm, Cadillac Mountain; db, Deboullie; dl, Deblois; kd, Katahdin; le, Leeds; lu, Lucerne; mb, Meddybemps; mo, Mooselookmeguntic; mw, Mount Waldo; mx, Moxie; ph, Phillips; pl, Priestly Lake; ps, Pocomoonshine; rb, Red Beach; rd, Redington; rm, Rattlesnake Mountain; sb, Sebago; tl, Tunk Lake (Catherine); ub, Umbagog; um, ultramafic rocks. Abbreviations for coastal bays: CB, Casco Bay; MB, Machias Bay; OB, Oak Bay; PB, Penobscot Bay; SB, Saco Bay. Distribution of migmatite-granite terrane, and of Sebago pluton, from Solar and Tomascak (2016). Abbreviations for mines, prospects, and important (key) occurrences, grouped by deposit type, are (1) Volcanogenic massive sulphide: BM, Bald Mountain; PM, Pickett Mountain; AP, Alder Pond; LR, Ledge Ridge; BH, Black Hawk; HS, Harborside; (2) Sediment-hosted Mn districts: MH, Maple Mountain-Hovey Mountain; NA, North Aroostook; SA, South Aroostook; (3) Porphyry Cu-Mo: CM, Catheart Mountain; SM, Sally Mountain; DB, Deboullie; PL, Priestly Lake; CO, Cooper; CD, Cadillac Mountain; (4) Mafic- and ultramafic-hosted Ni-Cu(-Co-PGE): AL, Alexander (includes Frost); KD, Katahdin; MO, Moxie; UN, Union (Warren); and (5) Pegmatitic Li-Cs-Ta: PN, Plumbago North.

isotope data for the Molango deposit, and for other large stratiform sediment-hosted manganese deposits in China and Hungary, also point to deposition in an anoxic marine basin, analogous to the model of Cannon and Force (1983), but with manganese mineralization occurring during early diagenesis in the shallow subsurface (Okita *et al.* 1988; Polgári *et al.* 1991; Okita and Shanks 1992). The carbon isotope values, in particular, indicate that rhodochrosite deposition was linked to the oxidation of organic matter.

The pyritic black shale directly below the high-grade Mn-carbonate ore zone at Molango may have played an important role in this diagenetic process, by providing dissolved organic matter (OM) for the oxidation process, when pore waters contained high concentrations of OM prior to lithification. More recent studies of the Úrkút deposit in Hungary also suggest that manganese mineralization there involved microbes (Polgári *et al.* 2012). Application of the organic matter oxidation model to the Aroostook County manganese districts is problematic, however, because of the apparent scarcity of black shale within the host sedimentary sequence (e.g., Pavlides 1962), but outcrops and drill core are very limited in the northern and southern districts, where a siliceous limestone unit directly underlies the manganese deposits. However, if the microbial model is correct, then black shale within the manganese ore sequence is not required, hence only a limestone host is needed. Regardless of the applicable ore-forming model, these two districts have a high potential for the discovery of additional manganese deposits, including low-Fe deposits similar to Molango occurring within one or more limestones of the district. Also possible, although less likely from our perspective, are Mn-carbonate or Mn-oxide deposits occurring in the Smyrna Mills Formation. Potential also exists for more manganese deposits in hematitic ironstone of the central district (Maple and Hovey Mountains area) but the economic viability of such Fe-rich deposits is uncertain. Sediment-hosted manganese deposits in Silurian strata of the Woodstock area of New Brunswick ca. 19 km east of Houlton were mined for iron in the 19th Century (Miller 1947). This area is currently being explored by a Canadian company, Manganese X Energy Corporation, which has announced measured and indicated reserves for the Battery Hill deposit of 34.9 Mt grading 6.42 wt% Mn and 10.7 wt% Fe, and an additional inferred reserve of 25.9 Mt grading 6.66 wt% Mn (Ténière *et al.* 2021). Incorporating these reserves with the resources compiled by Way (2014) for the Woodstock area (six deposits) yields a total of 212 Mt @ ~8 wt% Mn. Metallurgical testing of manganese in the Battery Hill deposit, using a novel leaching process to produce ultrapure $MnSO_4$, is reportedly encouraging with manganese recoveries of greater than 85% being achieved (Manganese X Energy Corporation 2021). It is unclear whether this metallurgical technology could be applied successfully to the manganese deposits of Aroostook County.

Volcanogenic massive sulphide

Maine has a lengthy history of mining volcanogenic massive sulphide (VMS) deposits (e.g., Lepage *et al.* 1991; Beck 2012; Marvinney 2015; Marvinney and Berry 2015; Slack 2019; Fig. 1). These deposits are well known in terms of geological setting and modes of formation, based on extensive studies of ancient and modern examples (Shanks and Thurston 2012, and references therein). In addition to common base (Cu, Zn, Pb) and precious (Ag, Au) metals, VMS deposits may contain appreciable amounts (tens to thousands of ppm) of numerous critical elements including As, Bi, Cd, Co, Ga, Ge, In, Mo, Sb, Se, Sn, Te, and PGEs (e.g., Monecke

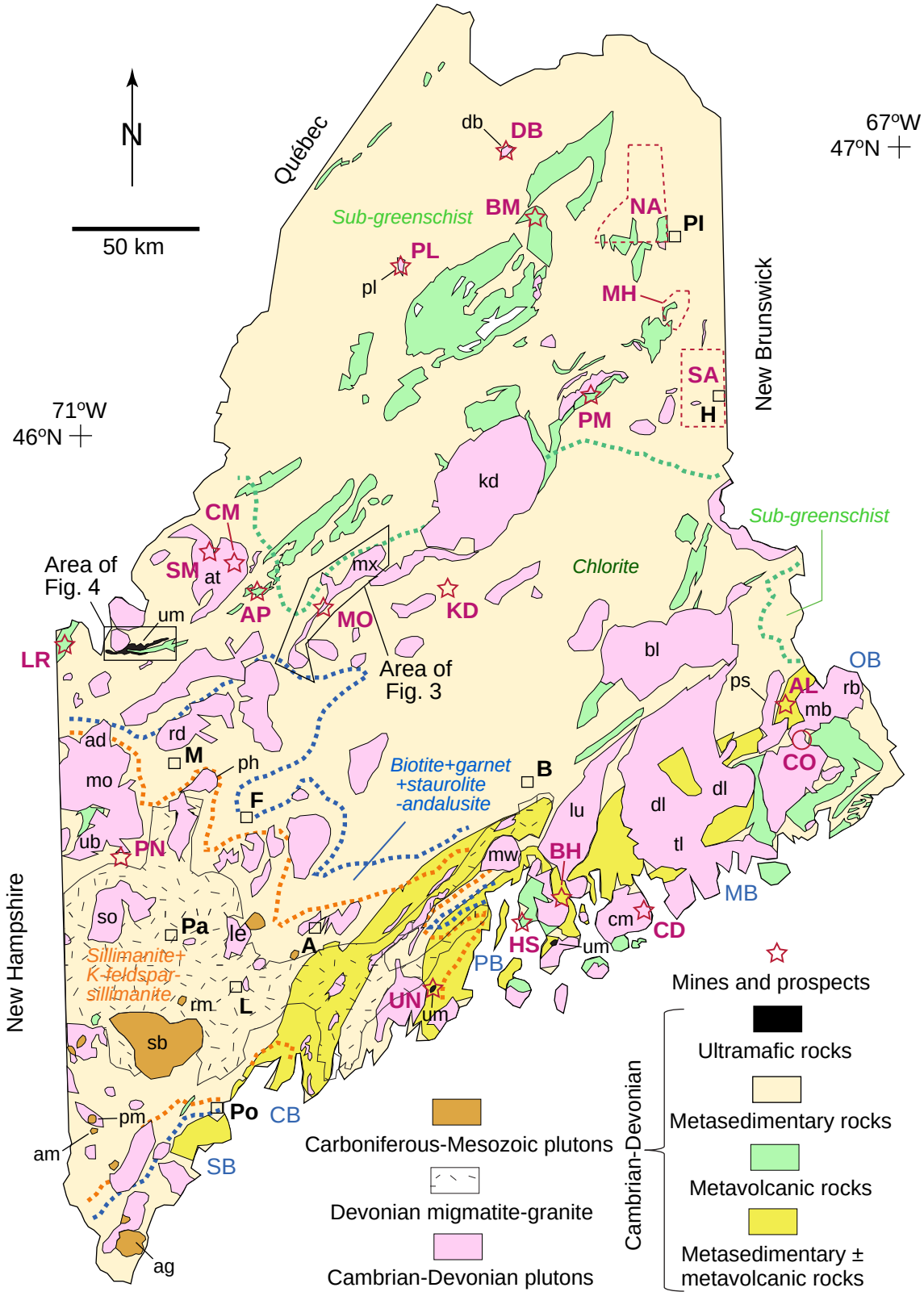

et al. 2016). Early mining of VMS deposits in Maine took place chiefly from 1878 to 1882 at very small deposits hosted within Cambrian volcanic and volcaniclastic rocks on or near the coast (Emmons 1910; Hussey *et al.* 1958; Lepage *et al.* 1991). During the period 1968 to 1972, much larger deposits were mined in the same Cambrian volcanic belt at the Black Hawk (Second Pond) Zn-Cu-Pb-Ag deposit that prior to production contained 0.9 Mt @ 7.4% Zn, 0.9% Cu, and 0.4% Pb, and at the Harborside (Callahan) Zn-Pb-Ag-Au deposit that had 0.7 Mt @ 5.5% Zn, 1.3% Cu, 0.5%

Pb, and 14 g/t Ag (Beck 2012; Marvinney and Berry 2015). From the mid-1970s to the mid-1980s, four other significant VMS deposits were discovered in Ordovician volcanic rocks of western and northern Maine (Beck 2012), including Bald Mountain (30.0 Mt @ 1.0 wt% Cu, 1.0 wt% Zn, 14 g/t Ag, 0.5 g/t Au; Slack *et al.* 2003), Ledge Ridge (4.0 Mt @ 2.0 wt% Zn, 1.0 wt% Cu, 1.0 wt% Pb, 17 g/t Ag, 0.6 g/t Au), Alder Pond (3.4 Mt @ 9.0 wt% Zn, 2.2 wt% Cu, 0.5 wt% Pb, 84 g/t Ag), and Pickett Mountain (measured + inferred resources of 6.3 Mt @ 9.1 wt% Zn, 3.8 wt% Pb, 1.1 wt% Cu, 102 g/t Ag, 0.7 g/t Au; Wolfden Resources Corporation 2021). The last deposit, previously named Mount Chase, has been studied recently by McCormick (2021) and is the subject of ongoing exploration and economic evaluation by Wolfden Resources Corporation. Early exploration in the 1960s in western Maine for VMS-type mineralization identified additional areas of interest, such as the Squirtgun prospect where one drill hole intersected felsic tuffs with 3.3 wt% Cu and 31.8 g/t Ag, together with appreciable Zn, over an interval of 4.9 m (Young 1968).

Economically recoverable critical metals in VMS deposits are limited. Importantly, on a global scale few of these metals are recovered from VMS deposits by current mining and processing methods, except as byproducts. With respect to cobalt, VMS deposits constitute less than 1% of global production, and each typically contains at most 0.3 wt% Co (Slack *et al.* 2017). A very large North American example is the Triassic Windy Craggy VMS deposit in British Columbia (297 Mt @ 1.38 wt% Cu) that has an average of 820 ppm Co (Peter and Scott 1999). Importantly, at Windy Craggy discrete Co-bearing minerals like cobaltite are rare, suggesting that the majority of the cobalt there resides in abundant pyrite and lesser pyrrhotite (Peter and Scott 1999), neither of which would likely be recovered and processed for cobalt during potential mining of copper, although recent technology may make this feasible in some cases (Luganov *et al.* 2020). The same interpretation can be applied to the Bald Mountain deposit in Maine, which lacks cobaltite or other Co-rich minerals but has up to 1400 ppm Co in bulk massive sulphide (pyrite ± pyrrhotite ± chalcopyrite ± sphalerite ± arsenopyrite ± galena) and as much as 0.25 wt% Co in pyrite, as determined by electron microprobe analysis (Slack *et al.* 2003). Also present at Bald Mountain are elevated bulk values for other critical metals including arsenic and antimony (up to 1.52 wt% and 1670 ppm, respectively); maximum values of others in massive sulphide facies of the deposit are relatively low (Bi, 26.3 ppm; In, 6.8 ppm; Sn, 58 ppm; Te, 64 ppm)(Slack *et al.* 2003). The mineralogical residence of arsenic and antimony is complex, and includes not only separate grains of arsenopyrite and tetrahedrite but also probable crystallographic substitutions of arsenic and antimony in pyrite and sphalerite, and locally in pyrrhotite (Slack *et al.* 2003). Bulk analysis of a representative composite sample of high-grade sulphide-rich rock from the Pickett Mountain deposit (A-Z Mining Professionals Limited 2020) shows relatively high average contents of As (953 ppm), Cd (246 ppm), Bi (81 ppm), and W (518 ppm); the cadmium and tungsten, and possibly bismuth, probably do not reside in pyrite, hence these critical elements could be recovered as byproducts during mining. Excluding Bald Mountain and Pickett Mountain, no published data are available on the contents of critical metals in the other VMS deposits of Maine.

Porphyry copper-molybdenum

Porphyry-type Cu-Mo deposits are major global sources of Co, Mo, Re, Se, and Te and locally contain trace to minor amounts of other critical metals and minerals including As, Bi, fluorite, PGEs, and W (John *et al.* 2010; John and Taylor 2016). Rhenium concentrations in such deposits and in granite-related Mo-rich veins are important because this metal is fundamental in the manufacture of high-temperature superalloys for jet aircraft engines and of Pt-Re catalysts for the petroleum industry (John *et al.* 2017). Numerous porphyry-type deposits and prospects are documented in Maine (Hollister *et al.* 1974; Ayuso 1989; Fig. 1). The best known and most explored is at Catheart Mountain, a Cu-Mo deposit hosted in a Devonian quartz-porphyry pluton that intrudes a larger Ordovician body of the Attean Quartz Monzonite (Ayuso 1989). This deposit has not been delineated fully in terms of tonnage and grade, but an early estimate suggested an endowment of 20 to 25 Mt @ 0.25 wt% Cu and 0.04 wt% Mo (F.C. Canney *in* Nowlan 1989). Sulphide mineralization at Catheart Mountain comprises disseminations and fracture-fillings of pyrite, chalcopyrite, molybdenite, and rare bornite and stannite in a gangue of quartz, sericite, K-feldspar, and local albite and carbonate (Atkinson 1977; Ayuso 1989). Typical whole-rock metal concentrations for entire drill cores, averaged over hundreds of metres, are 1000 to 2500 ppm Cu and 100 to 500 ppm Mo; the highest values for individual (separate) drill cores are 3600 ppm Cu over 240.5 m and 1100 ppm Mo over 135.6 m (Atkinson 1977). Wall-rock alteration of the host porphyry is characterized by an inner potassic zone and outer phyllic, argillic, and propylitic zones (Schmidt 1974; Atkinson 1977). Reconnaissance data for rhenium in molybdenite separates from Catheart Mountain (n = 9) show concentrations of 80 to 280 ppm with an average of 146 ppm (Atkinson 1977); this range and average are low relative to those of many porphyry Cu-Mo deposits worldwide (John and Taylor 2016) based on existing data that indicate, on a global scale, that molybdenite in porphyry molybdenum deposits and molybdenite-rich quartz veins have low contents of rhenium (typically <200 ppm) compared to the those in porphyry copper deposits that typically contain 1000 to 3000 ppm Re (John *et al.* 2017). In addition to rhenium, analysis of eight pyrite separates from the Catheart Mountain deposit indicates the presence of elevated bismuth and tungsten, up to 394 and 182 ppm, respectively (Atkinson 1977).

The other porphyry-type deposits in the state have not been described in detail. The Sally Mountain Cu-Mo deposit, ca. 10 km west of the Catheart deposit, has a similar style of mineralization dominated by disseminated and

veinlet-hosted chalcopyrite and lesser molybdenite within a Devonian quartz-porphyry pluton (Ayuso 1989). A regional geochemical survey of stream sediment by Nowlan (1989) shows areas of anomalously high copper and molybdenum that extend beyond the known bedrock sites of porphyry-type Cu-Mo mineralization, suggesting that the potential for this deposit type is spatially larger than was recognized previously.

In northern Maine, the Devonian syenite pluton at Deboullie contains weakly developed Cu-Mo mineralization within pyrite-bearing quartz-porphyry dikes (Ayuso and Loferski 1992; Loferski and Ayuso 1995). To the south, the Priestly Lake granodiorite pluton, of Devonian age, locally has quartz-molybdenite veins up to 15 cm wide and fracture-controlled molybdenite in granodiorite (Ayuso and Shank 1983). A different type of molybdenum occurrence is found in northeastern Maine, consisting of molybdenite with pyrite and minor chalcopyrite and arsenopyrite in a calc-silicate rock near a small granitic pluton (Canney *et al.* 1961; Burbank and Miller 1965). On and near the coast, minor disseminated and vein-hosted molybdenite occurrences are known within the Cooper, Cadillac Mountain, and Catherine (Tunk Lake) plutons (Burbank 1965; Young 1968; Hollister *et al.* 1974), in parts of the Bottle Lake Complex (Post *et al.* 1967; Nowlan and Hessin 1972), and elsewhere in the state (Hess 1908). Other areas in Maine that may have porphyry Cu-Mo potential are described by Schmidt (1978).

Mafic- and ultramafic-hosted nickel-copper (-cobalt-platinum group elements)

Mafic and ultramafic igneous intrusions that contain significant deposits of nickel and copper may have elevated concentrations of cobalt and/or PGEs that can be recovered as byproducts during mining and processing (Slack *et al.* 2017; Zientek *et al.* 2017). In the United States, cobalt and PGEs are defined as critical elements because of use in rechargeable lithium batteries and catalytic converters, respectively, and minimal domestic production. Three mafic- and ultramafic-hosted Ni-Cu(-Co-PGEs) deposits in Maine, known for many decades, have been moderately explored by several mining companies. Except for iron production in the 19th Century from the large Katahdin deposit east of Greenville (Fig. 1), no other deposits of this type in Maine have been mined for other metals such as nickel, copper, cobalt, or PGEs.

The Katahdin (also known as Ore Mountain) deposit was reportedly used by the native population since 4000 B.C. as a source of red pigment used for decorative purposes. The gossan of this deposit was mined intermittently from 1848 to 1890 and smelted on site at the nearby community of Katahdin Iron Works; the underlying hypogene pyrrhotite body, estimated to total more than 200 Mt @ ~45 wt% Fe (Slack 2019), was not mined. In 1976, the Superior Mining Company did deep drilling and conducted metallurgical testing to develop a method to separate the cobalt from the nickel and copper. As a result of this work, a resource of 60 Mt with a grade of 0.10 wt% Co, 0.13 wt% Ni, and 0.07 wt% Cu was defined, with reported metallurgical recoveries of 65% for Co and Ni, and 80% for Cu (Beck, review of landowner files, 1980–2000). The Katahdin deposit, ca. 600 m long and 120 m wide on average, consists of massive (>75 vol%) to disseminated or interstitial pyrrhotite with minor (<2 vol%) chalcopyrite in a syntectonic, Acadian norite intrusion, the 405.6 ± 3.3 Ma Ore Mountain pluton (Miller 1945; Houston 1956; Bradley and Tucker 2002).

The Union-Warren deposits near the coast (Fig. 1) form two main mineralized bodies within a ~13-km-long, northeast-striking zone of Devonian basic rocks that includes peridotite in the northeast and gabbro and diorite in the southwest. Host strata are chiefly sulphidic black shale of the Ordovician Penobscot Formation. Sulphide minerals are dominantly Ni-rich pentlandite, chalcopyrite, and pyrrhotite, together with minor niccolite and cobaltite; magnetite is a common accessory (Young 1968; Rainville and Park 1976). In 1965, the No. 5 deposit was discovered in Warren using a variety of geophysical techniques. In 1980, the Boliden Company conducted geochemical and additional geophysical surveys (F.M. Beck files, 1980-2000). In 1989, Black Hawk Mining Company did additional drilling and mine planning. A stringent mining ordinance that was adopted by the Town of Warren in 1992 apparently led Black Hawk to give up its leases in the mid-1990s. No work has been done on the properties since then. At the time of Boliden's work, proven and probable open-pit reserves were reported to be 13.6 Mt grading 0.925 wt% Ni, 0.423 wt% Cu, and 0.08 wt% Co (Boliden reports in F.M. Beck files).

The Black Narrows deposit in west-central Maine (Fig. 2) is within the southern part of the elongate Moxie mafic-ultramafic pluton of Early Devonian age (406.3 ± 3.8 Ma; Bradley *et al.* 2000). Early exploration in the area, carried out by several companies from 1948 to 1961, included airborne and ground geophysical surveys, and diamond drilling of six holes by Beers and three by Freeport Sulfur Company, none of which intersected significant nickel, cobalt, or copper mineralization (Beers *et al.* 1962; Beck, purchased Knox files, 1980–2000). Reconnaissance data for a limited number of rock samples from the Moxie pluton show relatively low total PGE concentrations of ca. 250 ppb (Paktunc 1990). The dominant igneous rocks are troctolite and olivine gabbro, with local peridotite, dunite, norite, and gabbro (Visher 1960; Espenshade 1972; Thompson 1984). Sulphide mineralization consists of pyrrhotite with minor pentlandite and chalcopyrite hosted within an altered peridotite. Other Ni-Cu sulphide prospects at Big Indian Pond and Burnt Nubble, in the northern part of the pluton, occur in troctolite and olivine gabbro (Fig. 2).

The Alexander and nearby Frost Ni-Cu-Co prospects in eastern Maine (Fig. 1) comprise massive and disseminated pyrrhotite with minor chalcopyrite in a small gabbroic body east of the large Pocomoonshine Gabbro that intrudes sulphidic metasedimentary rocks of the early Paleozoic Cooksson Formation (Young 1963; Thompson 1984; U.S. Geological Survey 2021a). The gabbro-hosted St. Stephen Ni-Cu

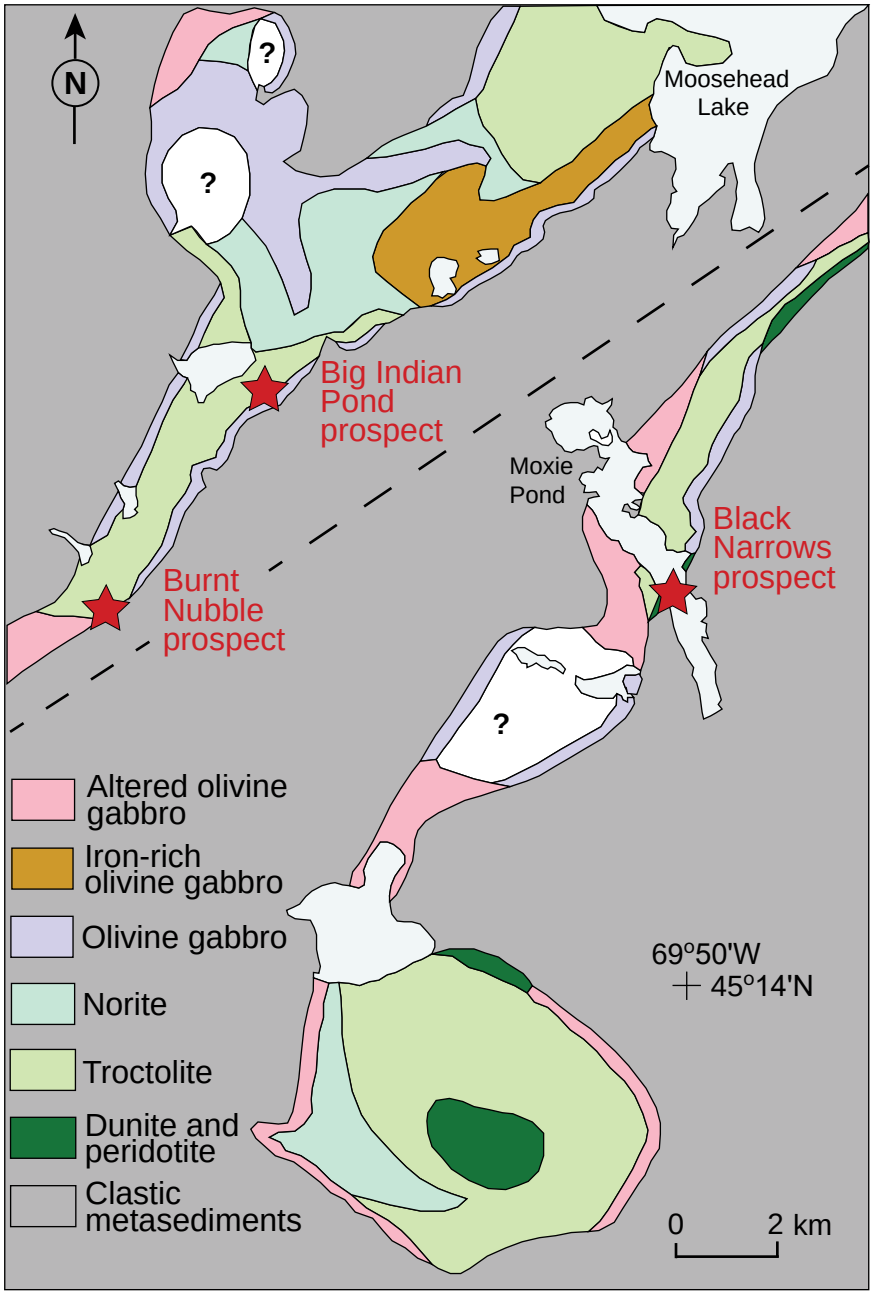

Figure 2. Geologic map of Moxie pluton and surrounding area showing locations of Cu ± Ni deposits and prospects. Regional geology modified from Osberg *et al.* (1985); detailed pluton geology from Thompson (1984).

deposit in southwestern New Brunswick, ca. 50 km to the northeast, contains reserves of 1.0 Mt @ 1.05 wt% Ni and 0.53 wt% Cu (Paktunc 1986, 1987), and in places as much as 0.24 wt% Co with up to 863 ppb Pd and 270 ppb Pt (Continental Nickel Ltd. 2012).

A high potential is proposed here for Ni-Cu(-Co-PGE) deposits in mafic/ultramafic dike-sill complexes. The model of Schulz et al. (2014) suggests that this deposit type, which is widespread worldwide and includes giant orebodies such as those in Noril'sk in Russia, Voisey's Bay in Labrador, and Jinchuan in North China, forms preferentially in mafic dikes or sills that served as conduits to overlying large intrusions. The very elongate nature of the Moxie pluton is similar to that of the pluton hosting the Jinchuan deposit, which contains 515 Mt of ore at an average grade of 1.06% Ni and 0.67% Cu, with byproduct Co and PGEs (Chai and Naldrett 1992; Song *et al.* 2009), and thus strongly suggests formation as a dike complex and a favourable setting for Ni-Cu-(Co-PGE) mineralization. Moreover, low nickel contents in olivine (<0.1 wt % NiO) for all but the most forsterite-rich compositions ($\leq Fo_{80}$) in the Moxie deposits (Thompson 1984) are consistent with early removal of nickel in sulphides, by which interaction of the igneous melt with sulphide-rich country rocks (e.g., black shale) results in sulphur saturation

of the magma followed by segregation of sulphides into basal zones or conduits (Naldrett 1989, 1992). Because of high metal grades, conduit-type deposits are now recognized as having greater economic potential than basal deposits like those in the Duluth Complex of Minnesota (e.g., Schulz *et al.* 2014). In a reconnaissance study of peridotite in northern Michigan, electron-microprobe analysis documented low-Ni olivine in this peridotite that suggested early sulphur saturation of the magma and hence a potential for Ni-Cu mineralization at depth (Klasner *et al.* 1979). This report led, in part, to the 2002 discovery within this peridotite of the high-grade Eagle Ni-Cu-Co orebody in the Upper Peninsula of Michigan (Ding *et al.* 2010, 2012). At the end of 2016, Eagle operations had produced 1.67 Mt of ore @ 3.97 wt% Ni and 3.19 wt% Cu, with then-unmined reserves (including for the East Eagle deposit) of 4.82 Mt @ 2.8 wt% Ni, 2.4 wt% Cu, 0.1 wt% Co, 0.3 g/t Au, 3.4 g/t Ag, 0.7 g/t Pt, and 0.5 g/t Pd (Clow *et al.* 2017). The Eagle mine is the largest producer of nickel in the United States.

Pegmatitic lithium-cesium-tantalum

The critical elements lithium, cesium, and tantalum have diverse uses including for rechargeable batteries, ceramics, and glass; for high-pressure and high-temperature well drilling in oil and gas production and photoelectric cells; and for gas turbines, mobile phones, and personal computers (Bradley *et al.* 2017a; Jaskula 2021; Tuck 2021; Callaghan 2021). Lithium-cesium-tantalum (LCT) pegmatites, one of three compositionally defined categories of granitic pegmatite, account for about one-fourth of the world's lithium production and nearly all of the cesium and tantalum production (Bradley *et al.* 2017b). In addition to enrichments in lithium, cesium, and tantalum (whence the acronym), LCT pegmatites are also typically enriched in rubidium, beryllium, and tin. Lithium enrichment is generally indicated by the presence of spodumene [$LiAlSi_2O_6$], petalite [$LiAlSi_4O_{10}$], lepidolite [$(K,Rb)(Li,Al)_2(Al,Si)_4O_{10}(OH,F)_2$], montebrasite [$LiAl(PO_4)(OH,F)$], and/or elbaite [$Na(Li_{1.5}Al_{1.5})Al_6Si_6O_{18}(BO_3)_3(OH)_4$]; cesium by pollucite [$(Cs,Na)_2(Al_2Si_4O_{12})\cdot 2H_2O$]; and tantalum, most commonly, by minerals of the columbite-tantalite group [$(Fe,Mn)(Nb,Ta)_2O_6$].

Maine's many LCT pegmatites have been mined for gemstones, mineral specimens, feldspar, muscovite, quartz, and beryl, with minor spodumene and pollucite produced as co-products in a few cases (Cameron *et al.* 1954; King and Foord 1994; King 2000). As of October 2021, the database of Mindat.org listed 48 pegmatites in Maine with spodumene, 17 with tantalite, and 23 with pollucite. Maine's LCT pegmatites occur in six clusters, which Wise and Francis (1992) termed "series" (Fig. 3). Available geochronology (Bradley *et al.* 2016; D.C. Bradley, unpublished data) shows that the six series formed during at least four, and probably as many as six, middle- to late Paleozoic episodes: the Waldoboro series before 356 Ma, the Phillips series before 324 Ma, the Rumford series before 295 Ma, the Topsham series at 273 Ma, the Oxford series at 264 Ma, and the undated Georgetown series. Pegmatites of the Waldoboro series were described by Sundelius (1963). The Oxford, Rumford, and Topsham series have been the most thoroughly investigated (e.g., Tomascak *et al.* 1998; Brown and Wise 2001; Roda-Robles *et al.* 2015; Simmons *et al.* 2016, 2020). Pegmatites of all these series are late orogenic bodies that were emplaced during the staged assembly of Pangea (Bradley *et al.* 2016).

Until a few years ago, the potential for significant lithium resources in Maine appeared to be low. Spodumene occurs in various pegmatites of the Rumford series in the Newry area, one being the Spodumene Brook locality on Plumbago Mountain. Now known as Plumbago North, this pegmatite contains spodumene crystals up to 11.5 m in length (Simmons *et al.* 2020). Also present are montebrasite, beryl, cassiterite, pollucite, almandine-spessartine garnet, fluorapatite, and columbite-group mineral species. Exploratory drilling has outlined a preliminary lithium resource of 10 Mt with an average Li_2O content of 4.68 wt% (Simmons *et al.* 2020). This is undoubtedly the most important critical mineral resource yet discovered in Maine, and if confirmed by more detailed exploration (including compliance with NI 43-101 guidelines), it may be the 10th-largest resource of pegmatite-hosted lithium in the world. Importantly, the Newry area shows promise for additional lithium discoveries; it is well mapped and hosts a number of LCT pegmatites. Giant spodumene crystals, reminiscent of those at Plumbago North, have also been reported from the Martin (6.3 m long), Kinglet (3 m), and Main (3 m) pegmatites, all in the Newry area (Shainin and Dellwig 1955; Barton and Goldsmith 1968; King and Foord 2000). None of Maine's other five LCT pegmatite series has yet shown comparable evidence of world-class lithium resources.

Known cesium resources in Maine are insignificant. In the 1800s and 1900s, pollucite was mined at times from three pegmatites of the Oxford series (e.g., Bennett), and from the Dunton pegmatite of the Rumford series. Total production of cesium, however, was only about 15 t (King and Foord 2000). For comparison, the original cesium reserve at the giant Tanco LCT pegmatite in Manitoba was over 350 000 t at an average grade of 23.3 wt% Cs_2O (Černý and Simpson 1978). Despite the presence of Ta-bearing minerals in a number of Maine pegmatites (e.g., tantalite-Mn [$MnTa_2O_6$] and tantalowodginite [$Mn(Ta,Sn)Ta_2O_8$]; King and Foord 2000), these minerals commonly occur as relatively small (<6 cm), isolated crystals (authors' observations). There appears to be no significant past production or resource potential for tantalum in the state.

Additional research will be needed to better evaluate Maine's pegmatites, with special attention to undiscovered lithium endowment. Important issues include evaluating known pegmatites, finding new pegmatites in areas where others are known, and elucidating the origins of each of the pegmatite fields. The last issue can be framed this way: why did the LCT pegmatites form in six geographically distinct clusters during an approximately 100 m.y. interval? Although the Rumford pegmatite series has the greatest potential for lithium, most past research on the mineralogy

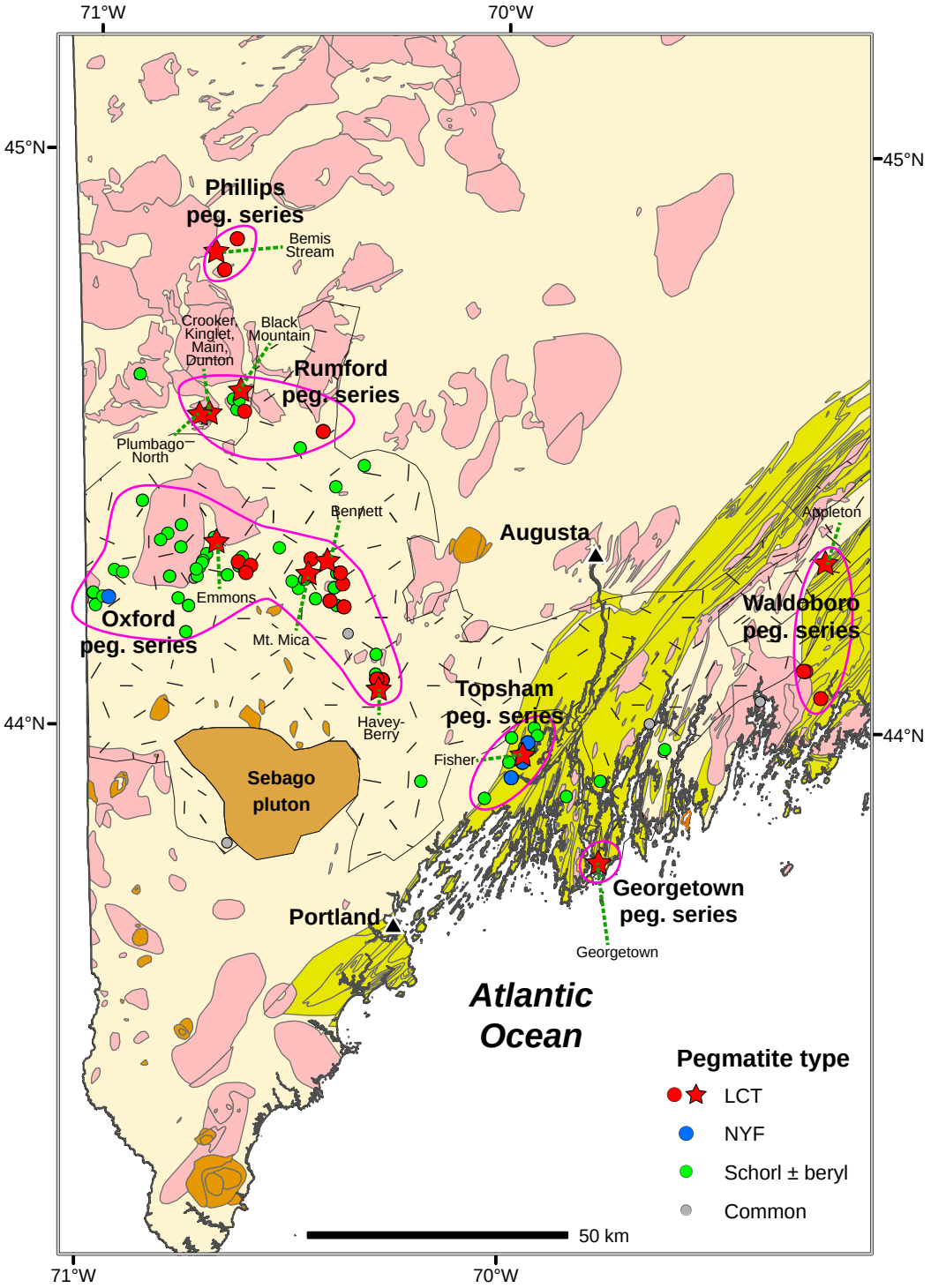

Figure 3. Geologic map of western Maine showing distribution of LCT and other granitic pegmatites. Abbreviations: peg., pegmatites; LCT, lithium-cesium-tantalum; NYF, niobium-yttrium-fluorine. Various pegmatite series typically include more than one type of pegmatite. Geology from Figure 1; note hachured area that represents Devonian granite-migmatite terrane. Pegmatite locations modified from MRDS mineral deposit database of the U.S. Geological Survey.

and origins of Maine pegmatites has focused on the substantially younger Oxford series. Three hypotheses have been proposed that bear on the genesis of the Oxford pegmatites. In the "parental granite" model, LCT pegmatites are highly fractionated offshoots from a granite pluton (Trueman and Černý 1982). The problem with this model, as applied to western Maine, is that there are no identified plutons with ages close to the 264 Ma zircon age of the Mt. Mica pegmatite (Bradley *et al.* 2016). The same problem also applies to the other five LCT pegmatite series in Maine: a lack of age

matches between the numerous, tightly dated plutons and the few tightly dated pegmatites. An alternative, the "direct anatexis" model, interprets LCT pegmatites as the products of low-degree partial melting during anatexis (Webber *et al.* 2019). In this scenario, the Oxford pegmatites formed as a result of decompression melting of previously formed migmatites, the melting being triggered by post-collisional unroofing, with additional heat supplied from below during initial rifting at the onset of Pangea's breakup (Webber *et al.* 2019). However, these special circumstances cannot account for any of Maine's five older LCT pegmatite series. A third hypothesis follows a very different thread. As proposed by Bradley (2019) and amplified by Hillenbrand *et al.* (2021), this model postulates that LCT pegmatites form below salars in active orogenic belts, where downward-circulating brines enriched in lithium, boron, and other fluxing elements interact with orogenic magmas. This process is consistent with the reconstructed paleolatitude of Maine at 264 Ma, which puts Mt. Mica in arid latitudes where salars exist today. Therefore, much depends on reconstructing the paleolatitudes of what is now western Maine during the interval of LCT pegmatite formation. Continued research on these genetic models is needed, integrating constraints from all six of Maine's LCT pegmatite series.

MINIMALLY EXPLORED AND UNEXPLORED DEPOSIT TYPES

Chromium and platinum-group elements in ophiolites

Maine is unique among New England states in having a nearly complete ophiolite sequence. The Boil Mountain ophiolite in western Maine (Fig. 4), the largest such body known in the eastern U.S., is ca. 1500 m thick and has a spatial extent of up to 30 km. Boudette (1982, 1991) distinguished three main intrusive facies of the ophiolite: (1) a lower serpentinite composed of variably altered harzburgite, dunite, and websterite; (2) a middle and upper sequence of gabbro, epidiorite, and pyroxenite; and (3) semi-concordant bodies of tonalite. The ophiolite apparently lacks a sheeted dike complex. Overlying the ophiolite are abundant felsic metavolcanic rocks, in addition to mafic metavolcanic rocks, which together constitute the Jim Pond Formation. The lower contact with the Chain Lakes Massif is tectonic, whereas the upper contact with the Jim Pond Formation is conformable (Boudette 1982, 1991). U–Pb zircon geochronology indicates that the ophiolite was emplaced in the Early Ordovician at 477 ± 6 Ma (Gerbi *et al.* 2006). The ophiolite is cut both by thrust faults and high-angle faults (Osberg *et al.* 1985; Moench *et al.* 1995). Geochemical data suggest formation in a supra-subduction zone (SSZ) setting related to a backarc environment, and not in a mid-ocean ridge setting (Coish and Rogers 1987; Gerbi *et al.* 2006). Widespread serpentinized ultramafic rocks have lherzolite, websterite, and harzburgite protoliths; dunite protoliths are inferred locally.

Chromium

Numerous industries rely on chromium for diverse uses that chiefly involve stainless steel and superalloys. As of 2020, the United States was totally dependent on foreign sources of this critical metal (U.S. Geological Survey 2021b). In the Boil Mountain ophiolite, layered chromite-rich rock (chromitite) occurs within ultramafic rocks at the base of the ophiolite in the Blanchard Pond area (Moench *et al.* 1999), but with an unknown thickness and extent. Concentrations of chromite are also present, together with magnetite, in amphibolite in the Arnold Pond area to the northeast (Harwood 1973). This latter occurrence was interpreted by Moench *et al.* (1999) as a tectonic block of the ophiolite encased in mélange of the Hurricane Mountain Formation; other chromitite occurrences in this general area may be large xenoliths within younger granite. Nowlan *et al.* (1987, 1990a) reported high chromium contents of up to 7000 ppm in stream sediments in the Boil Mountain region, but these high values reflect in part glacial dispersion from ophiolite up to 160 km to the northwest in the Thetford mines area of southeastern Québec.

Importantly, the SSZ setting of the Boil Mountain ophiolite is considered more favourable than mid-ocean ridge ophiolites for containing economic deposits of chromium and PGEs, as discussed by Yumul and Balce (1994) and Prichard and Brough (2009). Deposits of chromium and PGEs in ophiolites are generally very small and thus not commercially viable (Foose 1991; Mosier *et al.* 2012; Zientek *et al.* 2017). However, some ultramafic bodies in this setting may have significant amounts of ore, such as within the Zambales ophiolite in the Philippines (Zhou *et al.* 2000; Yumul 2001; Zhang *et al.* 2020) that in total contain 27.0 Mt of high-grade chromite (Mosier *et al.* 2012). Another example is a chromitite orebody at the base of the Oman ophiolite that is several hundred metres in diameter and ca. 50 m thick (Rospabé *et al.* 2019).

Processes that post-date the crystallization of ophiolitic ultramafic rocks are also important to consider in evaluating potential for chromium resources. Tectonic overprints such as faults and shear zones, which are reported in the Boil Mountain Complex (Moench *et al.* 1995), can localize and concentrate chromite into large bodies. One example is from the Vourinos ophiolite in Greece where the richest chromite ores, exploited at the Xeerolivado mine, occur in schlieren zones that represent the highest degree of deformation within the ophiolite complex (Rassios *et al.* 2020).

Platinum-group elements

Platinum-group elements have diverse uses including in the manufacture of catalytic converters, fertilizers, chemicals, fiberglass, jewelry, and computers, and in the refining of crude oil (Zientek *et al.* 2017). As of 2020, the U.S. had a 79% net reliance on foreign sources of PGEs; sole domestic production is from the layered mafic-ultramafic Stillwater Complex in Montana. Platinum and palladium contents of

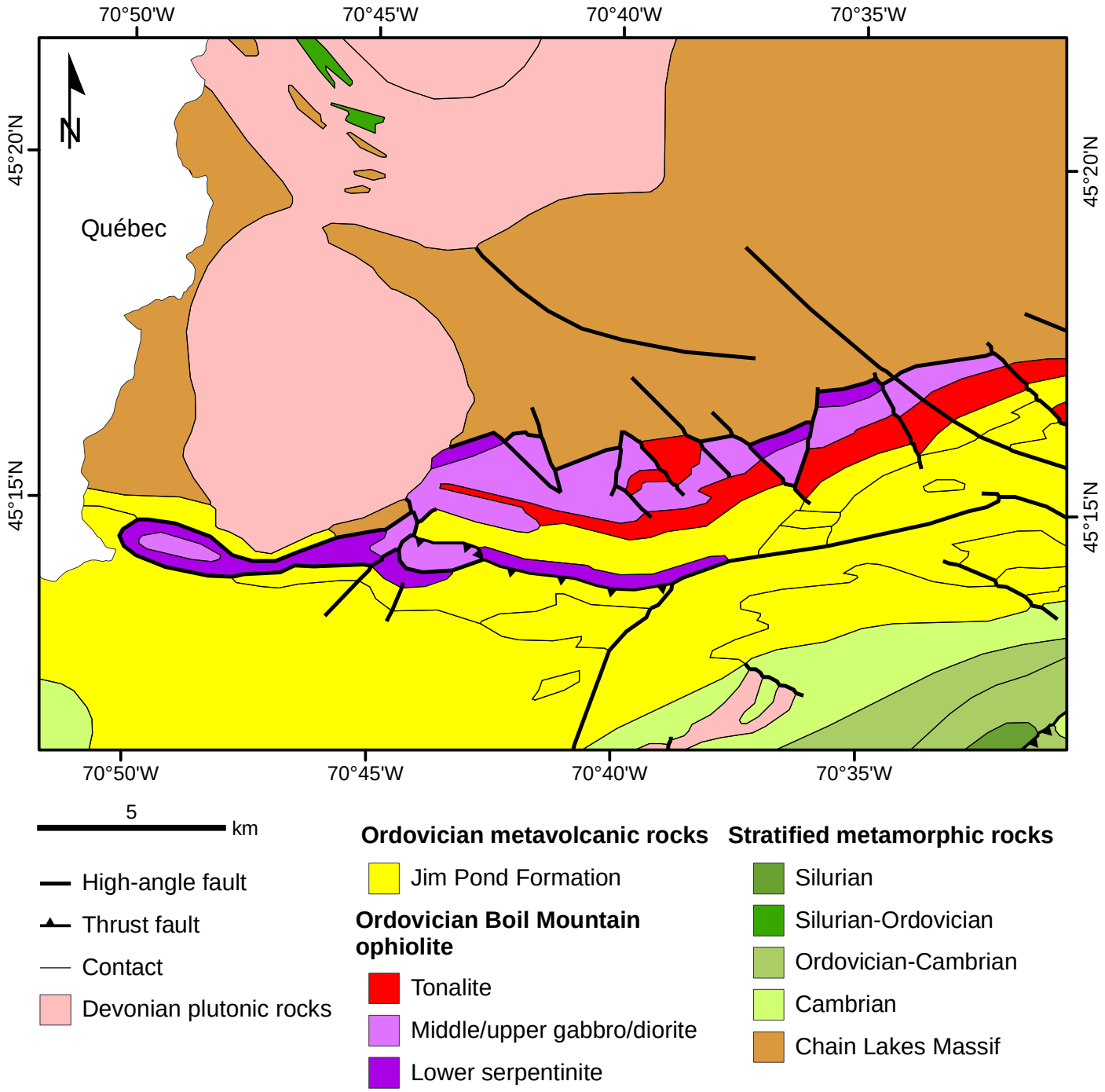

Figure 4. Simplified geologic map of Boil Mountain ophiolite and surrounding region, modified from Boudette (1982) and Osberg *et al.* (1985). Internal contacts shown within plutonic bodies and groups of stratified rocks separate different units as identified in Osberg *et al.* (1985).

ophiolite-hosted chromitites are typically very low (<40 ppb Pt and <18 ppb Pd, respectively), whereas Ir and Ru can be relatively high (up to ca. 350 ppb each) (Mosier *et al.* 2012). Importantly, sulphide-rich chromitites—which are uncommon globally—may have very high platinum and palladium concentrations, in some cases totaling more than 20 ppm (Economou-Eliopoulos 1996; Tsoupas and Economou-Eliopoulos 2008; Prichard and Brough 2009). In the Zambales ophiolite, Philippines, ore-grade values of PGEs in chromite bodies hosted within cumulate peridotites and dunite pods contain up to 550 ppb Ir, 1100 ppb Ru, 760 ppb Rh, 5960 ppb Pt, and 8350 ppb Pd (Bacuta *et al.* 1990). In the central Advocate ophiolite, Newfoundland, total PGE values in chromitite and dunite are up to 1028 and 216 ppb, respectively (Escayola *et al.* 2011).

A detailed study of the Leka ophiolite in Norway by Ped-

ersen *et al.* (1993) identified high PGEs both in chromitites and enclosing ultramafic rocks. Chromitites within orthopyroxenite veins average 4.77 ppm PGEs + Au (Pt>Pd), with maximum values of 4.6 ppm Pt and 2.7 ppm Pd; separate sulphide-bearing layers within olivine cumulate zones have up to 4 ppm total PGEs (Pd>Pt). Based on these data and local geological relationships, Pedersen *et al.* (1993) suggested that exploration for PGE deposits in ophiolites (1) should not focus solely on chromitites but also on ultramafic rocks just above the chromitites; (2) that if chromitites are absent, then sampling should be done close to the base of macrorhythmic cumulate units; and (3) that Pt may be preferentially enriched within or near the central parts of the magma chambers. Serpentinized ophiolitic dunites, such as those in the Zambales ophiolite, contain up to 3.7 ppm Pt + Pd that likely reflect remobilization and concentration during the serpentinization process (Yumul 2001). Importantly, these PGE-rich serpentinized dunites typically are volumetrically much larger than tectonically emplaced podiform chromitites, and hence have greater economic potential for exploitable PGEs.

Reconnaissance sampling of serpentinized ultramafic rocks from the base of the Boil Mountain ophiolite in the Blanchard Pond area (n = 45) revealed up to 150 ppb Pt and 350 ppb Pd from a zone ~1 km long and 50 m thick (Foose 1998). Importantly, however, samples of chromitite that occur in the Blanchard Pond and Arnold Pond areas (Harwood 1973; Moench *et al.* 1999) were not collected for analysis. Nonetheless, these locally elevated values for Pt and Pd suggest a high potential for PGE concentrations within the Boil Mountain ophiolite.

Potential for PGEs may also exist in the ultramafic body on the north end of Deer Isle ca. 18 km south of Blue Hill (Stewart 1998). This oblate body, 1.5 km in diameter, consists of variably serpentinized harzburgite and minor dunite (Reusch 2002). Although no PGE data are available for this body, it may have potential for ultramafic-hosted concentrations of these metals and hence warrants consideration for geochemical sampling.

In addition to remobilization and concentration of PGEs that can occur during serpentinization (Bussolesi *et al.* 2020), gold may be concentrated in carbonate-altered ultramafic rocks, termed listwanite or listvenite, which typically are localized along faults (e.g., Buisson and Leblanc 1986; Belogub *et al.* 2017). Based on analogy with these occurrences, ultramafic rocks of the Boil Mountain Complex could have potential for gold deposits within serpentinized zones. To our knowledge, none of these zones has been sampled geochemically for gold or other metals.

Granite-hosted uranium-thorium

Uranium and thorium are critical to the United States economy. Uranium is used for fuel in nuclear reactors and in the production of isotopes for industrial, medical, and defense purposes. On a global scale, most production comes from unconformity-type deposits within sedimentary rocks and from concentrations in evolved granites. Thorium, used chiefly for metal alloys and radiation shields, occurs economically in placers, veins, and carbonatites (U.S. Geological Survey 2021b). More than 95% of the uranium and all of the thorium consumed in the U.S. is imported. Although neither uranium nor thorium has been mined in Maine, many occurrences are known in the state, mostly within granitic pegmatites. Grauch and Zarinski (1976) list 43 such occurrences in non-sedimentary rocks of Maine.

Some evolved granites are well known for having uranium and/or thorium resources (e.g., Cuney 2014). Examples are the granite-hosted uranium deposits in the Liueryilin district of southeast China where major orebodies formed in two-mica granites with low U (<14 ppm) by multistage hydrothermal processes that increased uranium contents up to 3000 ppm, concentrating uraninite ± coffinite in faults and shear zones (Min *et al.* 2005). Two-mica granites are evolved felsic igneous bodies that contain both muscovite and biotite as primary magmatic phases. In New England, the Conway Granite in northern New Hampshire has been known for many years as one of the world's largest, low-grade resources of uranium and thorium, estimated to contain on average 11 ppm U and 53 ppm Th (Adams *et al.* 1962; Page 1980). Other coeval intrusions of the White Mountain Magma Series in New Hampshire have up to 25.5 ppm U and 77.0 ppm Th (Butler 1975). In Maine, among more than a dozen two-mica granites, one of the largest is the Permian Sebago pluton (Tomascak *et al.* 1996; Fig. 1), which in places has uranium contents up to 17.5 ppm (Dorais and Paige 2000). Prospects within this intrusion were drilled in the 1970s by Kerr-McGee and Exxon Corporation (W.A. Anderson, oral communication 2018), but no results are available. Other granitic bodies in eastern Maine locally have elevated uranium and/or thorium contents, including the Meddybemps Granite that in one sample has 25.6 ppm U and 46.8 ppm Th (Ludman and Hill 1990). These and other granites in the southern part of the state, such as the Lucerne, Mount Waldo, and Red Beach intrusions contain high radon values in associated groundwaters (Norton *et al.* 1989). Based on analogy with the large granite-hosted uranium deposits of southeast China, faults and shear zones that cut these uraniferous granites may be favourable sites for hosting potentially economic deposits.

The National Uranium Resource Evaluation (NURE) program was initiated by the U.S. Atomic Energy Commission (AEC) in 1973 with the goal of identifying uranium resources in the United States. Many surveys were conducted throughout the nation including in Maine. Of particular interest were the results of two projects, including reconnaissance hydrogeochemical and stream sediment surveys (Smith 1997) and aeromagnetic and aeroradiometric surveys (Hill *et al.* 2009). Aerial gamma-ray data obtained for the southern part of the state (Figs. 5 and 6) show regional anomalous highs on and surrounding the Permian Sebago pluton, the Devonian Lucerne and Tunk Lake plutons, and the western part of the Devonian Deblois pluton; high gamma-ray values occur mostly within the Devonian granite-

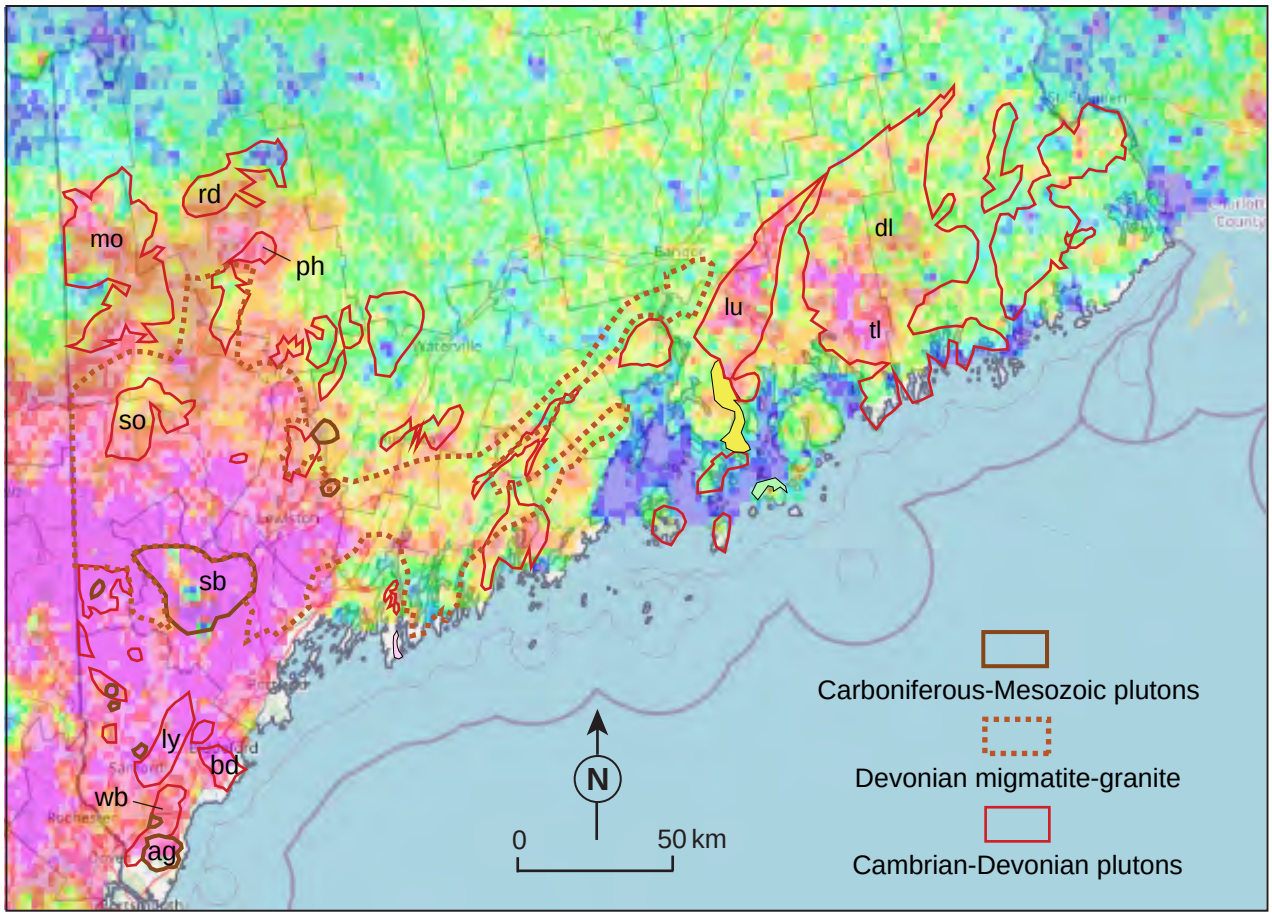

Figure 5. Map of southern Maine showing uranium anomalies determined by aerial gamma-ray spectrometer surveys conducted by NURE (Hill *et al.* 2009). Note general correspondence between highest values (hot colours) and selected igneous plutons. Abbreviations for labelled plutons: ag, Agamenticus; bd, Biddeford; dl, Deblois; lu, Lucerne; ly, Lyman; mo, Mooselookmeguntic; ph, Phillips; rd, Reddington; sb, Sebago; so, Songo; tl, Tunk Lake (Catherine); wb, Webhannet.

migmatite terrane of Solar and Tomascak (2016), except for the two elongate eastern lobes. Other anomalous areas in western Maine coincide with various Devonian granitic intrusions such as the Phillips, Adamstown, and Mooselookmeguntic plutons.

Many contractors were involved in the collection of both the geochemical and airborne data. Unfortunately, these data were reported in a variety of formats. There was a concerted effort by the USGS to reformat all the data, but according to Smith (1997) many problems remain. To our knowledge, there has been no follow-up by the USGS or others to do additional exploration work on the geochemical or airborne anomalies identified during the NURE program, nor has there been any systematic sampling of the two-mica granites for uranium or thorium potential. In 1989, the Maine government enacted legislation prohibiting the mining of uranium and thorium in the state (MRS Title 38, Section 489-B).

Tin in granitic plutons and veins

Tin has not been mined in the United States since 1993 (Kamilli *et al.* 2017). Seventy-five percent of the U.S. tin supply was imported in 2020, mostly from Peru, Indonesia, Malaysia, and Bolivia (Merrill 2021b). The balance came from recycling. Tin is used principally as solder, but also as tinplate and in alloys. The United States has no tin reserves, and hence this metal is considered critical and strategic for national security (McGroarty and Wirtz 2012). Approximately 70% of the world's tin output is from cassiterite in placer deposits, the remainder being derived from granitic plutons, greisens (mica-rich altered granites), and granite-related veins. Tin-bearing veins and greisens characteristically occur within the upper portions of shallowly emplaced, felsic and highly fractionated granites and in overlying country rocks. Such granites are typically silica rich, and peraluminous, metaluminous, or less commonly alkaline (Černý *et al.* 2005). For example, many granite plutons in southern and west-central New Brunswick are enriched in tin (Wilson and Kamo 2016; Mohammadi *et al.* 2020) including economic concentrations of this and other metals at the large Mount Pleasant Sn-Zn-In-W-Mo-Bi deposit (Kooiman *et al.* 1986; Yang *et al.* 2003). Maine has many tin occurrences, but with few exceptions these are small concentrations in

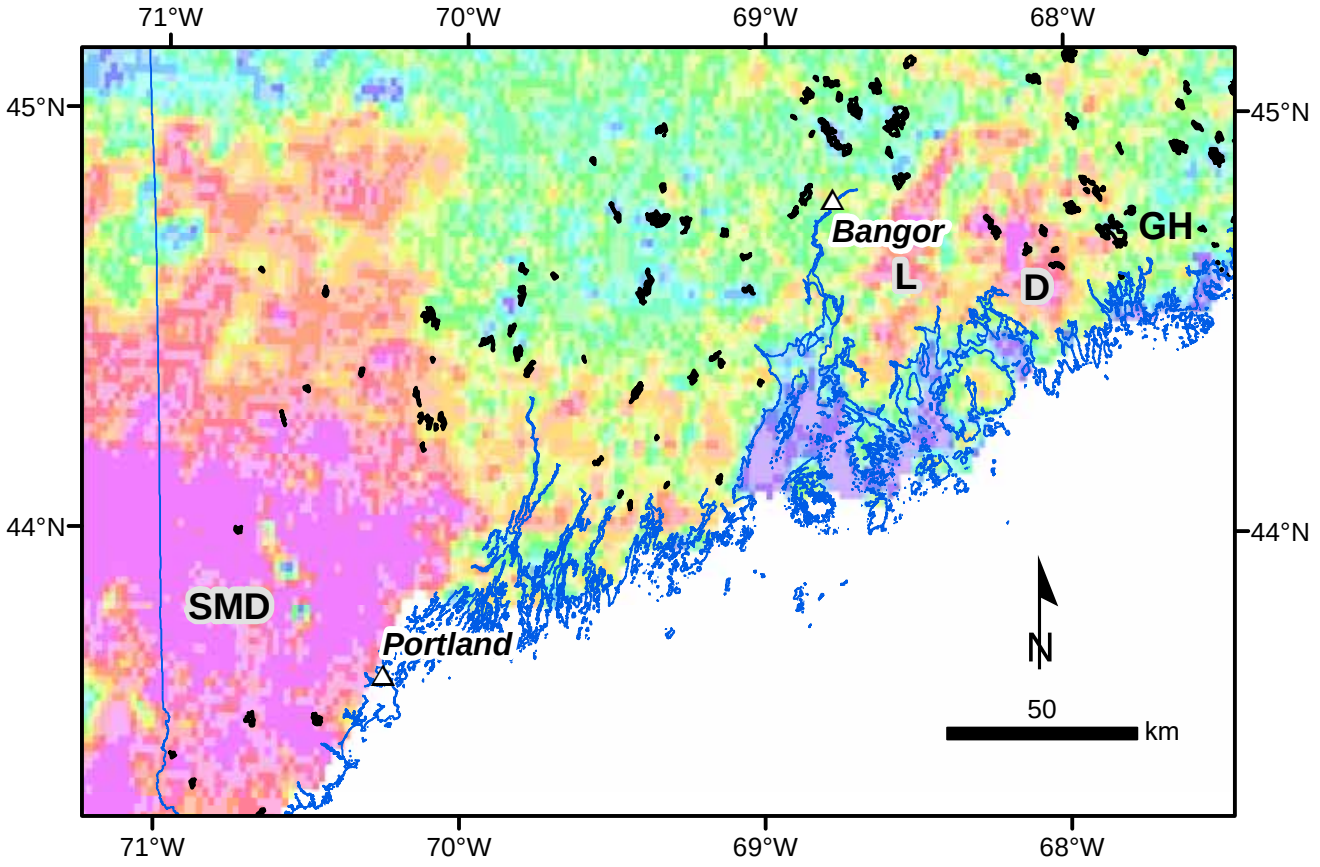

Figure 6. Map of southern Maine showing peat deposits (black) and uranium anomalies determined by aerial gamma-ray spectrometry (Hill *et al.* 2009). Distribution of peat deposits from Cameron *et al.* (1984a, b, c, d, e). Note location of Great Heath (GH) peat deposit (Cameron and Anderson 1980a).

granite pegmatites that lack resource potential.

Only one non-pegmatitic deposit in Maine has been mined and produced tin. The Winslow tin mine, located just south of Waterville, was operated in 1880 and 1881. A shaft reportedly 29 m deep with one or more crosscuts was described in the Maine Mining Journal in 1881 (King 2000). An unknown number of ingots of tin were smelted from the ore. The ore forms a series of veins up to ca. 50 cm in diameter that define a zone ca. 4.5 m wide and at least 67 m long; cassiterite is the sole tin mineral accompanied by minor galena, with a gangue composed of quartz, fluorite, calcite, and muscovite, all hosted in calcareous slate of the Silurian Waterville Formation (King 2000). The nearest exposed pluton is a granite body ca. 10 km to the west. Billiton Exploration, USA, Inc., undertook a regional and detailed survey in the vicinity of the Winslow tin mine in the early 1980s (Lippitt 1984). This survey included geologic mapping, regional and local gravity surveys, soil geochemical surveys, and diamond core drilling. The targets were suspected buried granitic cupolas within highly evolved granites that might have economic concentrations of tin in greisen veins associated with the cupolas. Owing to extreme deflection of the drill pipes, the targeted cupolas were not reached at depth. Drilling of the down-dip extension of the near-surface vein lacked promising results according to Lippitt (1984).

Tin exploration programs elsewhere in Maine included reconnaissance surveys in the coastal belt between Ellsworth and the New Brunswick border. Of particular interest in the coastal belt was the discovery in the 1970s of a large boulder containing abundant cassiterite (F.M. Beck files, 1980–2000). Stream-sediment heavy mineral, rock-chip, and stream-water surveys were conducted on drainages surrounding many of the granite bodies. Anomalous tin and tungsten contents were evident in the vicinity of the biotite granites, but no obvious source for the "tin boulder" was discovered during this survey.

One other small non-pegmatitic tin occurrence warrants mention. The Piper Hill (Bergensdahl) prospect, in York County, is a vein that contains molybdenite, pyrite, pyrrhotite, chalcopyrite, orpiment, galena, sphalerite, and argentite (Morrill 1958). Cassiterite is likely present, although stannite or a different Sn-sulphosalt may occur; no tin mineral has been identified. The host lithology is a calc-silicate rock near the Mesozoic Pickett Mountain syenite pluton (U.S. Geological Survey 2021a).

Niobium, tantalum, and rare earth elements in alkaline intrusions

Niobium, tantalum, and REE are critical minerals in the United States because of supply risk and minimal or no domestic production. Chief uses of these metals are in high-strength steel alloys; cell phones, computer drives, and implanted medical devices such as pacemakers; and in glass, magnets, and catalysts in petroleum refining, catalytic converters, and for making phosphors in cathode ray tubes and flat panel display screens, respectively (Schulz *et al.* 2017; Van Gosen *et al.* 2017). Many alkaline igneous rocks globally contain significant concentrations of these metals (e.g., Dostal 2016). Based on current knowledge, this is the only type of REE occurrence reported in Maine, although the economic potential is tenuous. Two Paleozoic ultrapotassic syenite intrusions in the eastern part of the state (Turner Mountain syenite; Wang *et al.* 2014) and in central-coastal Maine (Lincoln syenite; West *et al.* 2007) have somewhat elevated concentrations of light rare earth elements (LREE). Maximum LREE values are higher for the Lincoln syenite, including 96.3 ppm La, 210 ppm Ce, and 100 ppm Nd (West *et al.* 2007).

One of the most promising intrusions from a resource standpoint is the Carboniferous Litchfield pluton in south-central Maine (West *et al.* 2016). This alkaline syenite complex, ca. 16 km southwest of Augusta (Fig. 7), is the type locality for litchfieldite that is a coarse-grained nepheline syenite containing albite, microcline, nepheline, sodalite, cancrinite, and calcite, with local magnetite, Fe-rich biotite, and in places zircon crystals up to 4 cm in length. Barker (1965) also reported the presence of the Nb-rich mineral pyrochlore [$(Na,Ca)_2Nb_2O_6(OH,F)$]. Susceptibility to weathering has limited the exposure of this intrusion. The composite pluton is a geographic depression with its extent and compositional heterogeneity inferred by surface boulders (West and Ellenberger 2010). Lithologically, the pluton can be divided into several units based on mineralogy, although scarce exposures make this division somewhat conjectural. Whole-rock geochemical data for six samples (West *et al.* 2016) lack enrichment in Y (<15 ppm) and REE (e.g., La <28 ppm), but show locally high Zr and Nb (up to 1809 and 68.0 ppm, respectively). Other reported occurrences of nepheline ± cancrinite such as at the South Cochnewagon Pond locality ca. 25 km southwest of Augusta, apparently are in glacial boulders (King and Foord 1994) and are unlikely to have been transported ca. 15 km west from the Litchfield pluton, thus suggesting the presence of additional bedrock sources of these mineralogically distinctive boulders from other (one or more) unmapped alkaline igneous intrusions in the area.

Nearly a dozen alkaline igneous complexes and stocks, some including peralkaline units, are reported from southwestern Maine. These intrusions occur in a south-southeast-trending belt and are inferred to be part of the Mesozoic White Mountain Magma Series based on spatial, compositional, and geochronological similarities. The Osceola Granite, one phase of this magma series in northern New Hampshire, contains up to 158 ppm Nb, 12.1 Ta, 289 ppm La, 566 ppm Ce, and 270 ppm Nd (Eby *et al.* 1992). In Maine, whole-rock analyses by Gilman (1989, 1991) of samples from small Mesozoic intrusions included results for two samples from the Triassic Abbott Mountain pluton (Fig. 1) that separately contain 140 ppm Nb and 1010 ppm Zr; no REE data were reported for this pluton or others analyzed in these studies. The Jurassic Rattlesnake Mountain pluton locally has higher contents of Nb (up to 203.9 ppm) and Zr (up to 1136.0 ppm), within nepheline syenite and trachyte, but has relatively low REE, e.g., maximum of 105 ppm La (Creasey 1989). The anomalous values for niobium and zirconium warrant additional analyses of these plutons, and of other alkaline intrusions in the region, for proper evaluation of potential economic resources of these metals, and possibly also for REE.

A small area in northern Maine may also have resource potential for this deposit type. Results of a 2021 airborne radiometric survey by the U.S. Geological Survey identified a high-Th zone ca. 800 m long and 300 m wide within altered trachyte tuff (Duff *et al.* 2022). The trachyte host rock in this area, within the Ordovician Winterville Formation, locally contains very high concentrations of REE, Zr, Nb, Ta, Th, and Ba (C. Wang, written communication 2022). More work will be required to evaluate this occurrence and determine whether it is an economically viable Nb-Ta-REE deposit.

Tungsten in skarn and replacement deposits

Tungsten is a critical metal used mainly in the manufacture of steel and other alloys, for cemented carbide parts in hardening tools, and in light bulbs, X-ray tubes, radiation shields, and industrial catalysts (U.S. Geological Survey 2021b). Tungsten occurs in several types of mineral deposits, but on a global basis the most important economically are granite-related skarn deposits. Scheelite is the main host mineral; wolframite is subordinate. Historically, these skarn deposits, together with local granite-hosted greisens and veins, have provided the vast majority of tungsten production and resources (Green *et al.* 2020). Important examples in North America include the Pine Creek deposit in eastern California (Newberry 1982) and the high-grade Cantung and Mactung deposits in Northwest Territories and Yukon Territory, respectively (Elongo *et al.* 2020). The last mine production of tungsten concentrates in the United States was in 2015; currently, the U.S. is wholly dependent on imports of this metal.

A different type of tungsten deposit consists of stratabound concentrations of scheelite in regionally metamorphosed rocks lacking a clear relationship to granites or other felsic intrusions (e.g., Cheilletz 1988). These deposits, typically within calc-silicate rocks, consist of scheelite together with quartz, sericite, garnet, pyroxene, plagioclase, clinozoisite, and local vesuvianite, fluorite, apatite, scapolite, and molybdenite (Gibert *et al.* 1992; Höll and Eichhorn 2000; Guo *et al.* 2016); tourmaline is abundant locally (Raith 1988). The

garnet in stratabound scheelite deposits typically has a major component of grossular [$Ca_3Al_2(SiO_4)_3$] (Gibert *et al.* 1992; Guo *et al.* 2016), whereas in granite-related scheelite skarns the garnets can be compositionally diverse, with major proportions of grossular, almandine [$Fe^{2+}{}_2Al_2(SiO_4)_3$], andradite [$Ca_3Fe^{3+}{}_2(SiO_4)_3$], or spessartine [$Mn_3Al_2(SiO_4)_3$] (Meinert 2000). Limited published data for stratabound scheelite deposits suggest that associated pyroxenes contain a large component of hedenbergite [$(Fe,Ca)Si_2O_6$], in contrast to scheelite skarn pyroxenes that have compositions dominated by diopside [$(Mg,Ca)Si_2O_6$] and/or hedenbergite (Meinert 2000). Long-standing controversy surrounds the origin of the stratabound deposit type, specifically as to whether the tungsten mineralization formed during emplacement of a hidden granite or instead by metamorphic fluids that were focused along chemically reactive carbonate layers (Raith and Prochaska 1995). An older model involving syngenetic-exhalative processes on the seafloor (e.g., Boyer and Routhier 1974) is not considered viable by most workers. The economically most important stratabound deposit is Mittersill (Felbertal) in Austria, which is the largest scheelite mine in Europe, having a production of 7.0 Mt @ 0.5% W and unmined resources of 6.1 Mt @ 0.5% W (Bureau de Recherches Géologiques et Minières 2002); the total amount of contained tungsten at Mittersill (>65 500 t) ranks high in comparison to all large tungsten skarns of the world (cf. Green *et al.* 2020). The genesis of the Mittersill deposit is still debated, but the weight of evidence suggests formation by metamorphic fluids and not magmatic-hydrothermal fluids derived from a hidden granite (Raith and Stein 2006). Geologically and mineralogically similar stratabound scheelite deposits in other metamorphic terranes, such as those in France (Gibert *et al.* 1992), Norway (Larsen 1991), Australia (Barnes 1983), Pakistan (Leake *et al.* 1989), and Myanmar (Guo *et al.* 2016), are probably metamorphogenic in origin.

In Maine, several small prospects of granite-related scheelite or wolframite are known along the coast (U.S. Geological Survey 2021a) but likely have limited resource potential, although new exploration efforts could change this outlook. A more promising region in our estimation is the western part of the state, where widespread tungsten anomalies occur in stream sediments and panned concentrates (Nowlan *et al.* 1987, 1990b). Most of the high concentrations, in the range of 60 to 3000 ppm W, are within or near Devonian granite plutons (Fig. 7) that intrude early Paleozoic metasedimentary rocks including local carbonate strata that would be favourable for development of skarns via replacement by magmatic-hydrothermal fluids. Importantly, however, other high values in sediment and concentrate samples—above 120 ppm W—were collected 3 to as much as 15 km from known granite contacts, e.g., south of Madrid, west of Farmington, and within the Farmington area. Some of these anomalies likely reflect glacial transport from granite plutons to the north or northwest, but others instead may be derived from local bedrock. The latter possibility is supported by the presence in this region of numerous outcrops containing scheelite in quartz ± calcite veins and quartz-garnet lenses within metasedimentary rocks, such as several occurrences in the Farmington area (Trefethen *et al.* 1955; Moench *et al.* 1999). It is unclear, without more detailed field investigations, whether these bedrock scheelite occurrences as well as the many tungsten anomalies in panned concentrates are linked to stratabound deposits or granitic skarns. No examples of the former type are known in New England and vicinity, but a small scheelite skarn is present at Lac Lyster, just north of the Vermont-Québec border within the contact aureole of a Devonian granite pluton (Gauthier *et al.* 1994). Most of the bedrock scheelite occurrences and panned concentrate anomalies in western Maine are likely very small and lack economic significance, but some may have resource potential (cf. Case *et al.* 2022). One candidate is on the south border of the Umbagog pluton where locally abundant scheelite (0.7 wt% W) occurs in the lower part of the Ordovician Quimby Formation, within a calc-silicate unit 9 m thick that extends along strike for at least 11 km (Moench *et al.* 1999). Other scheelite occurrences and prospects are known within calc-silicate layers of several other metasedimentary rock units in this region, including Silurian strata of the Rangeley, Greenvale Cove, and Smalls Falls formations (Moench *et al.* 1999). In the southern part of the state, excluding pegmatites, scheelite has been found in metasedimentary rocks in skarn-type assemblages with quartz, calcite, garnet, diopside, molybdenite, vesuvianite, epidote, scapolite, wollastonite, apatite, pyrite, and/or axinite near the towns of Sanford and Cornish (Morrill 1958) and Phippsburg (Mindat.org 2021).

Tungsten and bismuth in polymetallic veins

Some polymetallic Mo-rich veins in Maine contain critical elements such as tungsten and bismuth. Bismuth is included in this category owing to total dependence of the United States on foreign sources and the importance of this metal in cosmetic, industrial, laboratory, and pharmaceutical industries, and in the foundry industry as an additive to improve metallurgical quality (Merrill 2021a). Polymetallic Mo-rich veins are typically associated closely with granitic plutons, including at the giant Sisson Brook W-Mo-Cu deposit in central New Brunswick (Fyffe and Thorne 2010; Zhang 2015) that has proven and probable ore reserves of 334.4 Mt @ 0.066% W and 0.021% Mo (Northcliff Resources Ltd. 2022). In eastern Maine, two Mo-rich prospects with minor tungsten and bismuth are known at the Catherine Hill and Cooper prospects. Mineralization at the Catherine Hill prospect, in the western lobe of the Devonian Deblois Granite, consists of disseminations and fracture-fillings of molybdenite and pyrite with lesser scheelite and wolframite in a gangue of quartz and minor fluorite (Emmons 1910; Morrill and Hinckley 1959; Young 1963). The Cooper prospect, containing molybdenite, scheelite, chalcopyrite, quartz, and fluorite, is similarly hosted in a Devonian granite but with associated pegmatite (Emmons 1910; Young 1963; Burbank 1965). The minimal amount of data available on these two

Figure 7. (next page) Simplified geologic map of Maine showing regional metamorphic zones and locations of mines, prospects, and important (key) occurrences (including areas with geochemical anomalies) of critical minerals or elements. Geology and abbreviations for cities and towns, coastal bays, and igneous plutons and other igneous bodies after Fig. 1. Abbreviations for mines, prospects, and key occurrences (including for areas of geochemical anomalies): (1) Ophiolite-hosted Cr: AP, Arnold Pond; BP, Blanchard Pond; (2) Sn in granitic plutons and veins: PH, Piper Hill (Bergensdahl); WL, Winslow; (3) Nb, Ta, and REE in alkaline intrusions: LF, Litchfield; SC, South Cochnewagon Pond; TH, thorium anomaly; (4) W in skarn and replacement deposits: CN, Cornish; PB, Phippsburg; SF, Sanford; UP, Umbagog pluton contact; green dotted lines outline western Maine geochemical anomalies (120-3000 ppm W) in nonmagnetic heavy-mineral panned concentrates; (5) W and Bi in polymetallic veins: CH, Catherine Hill; CO, Cooper; CP, Crocker Pond area; GC, Golden Circle; (6) V in black shales: BM, Bowers Mountain Formation; PF, Penobscot Formation; (7) Sb in granite-related settings: DH, Drew Hill; GB, Gouldsboro; HT, Hector; WS, West and Soule; (8) Sb in orogenic veins and replacements: CM, Carmel; LR, Lawrence; LV, Levant; SR, Shorey; (9) Te in epithermal deposits: BB, Big Hill and Barrett; (10) Be in evolved and altered felsic tuffs: CI, Cranberry Islands; (11) Graphite in high-grade metamorphic rocks: MV, Milletville; PL, Phillips; (12) Ti, Zr, and REE in heavy-mineral sands: HB, Hunnewell barrier; (13) U in peat: GH, Great Heath.

prospects limits an understanding of the deposit type (e.g., alternatively porphyry Cu-Mo) and an assessment of potential resources of tungsten and bismuth. The Golden Circle prospect near the mid-coast consists of one or more Au-Ag-Bi-Te veins containing sylvanite [(Ag,Au)Te_2] and native bismuth (U.S. Geological Survey 2021a) along the projected trend of a nearby Devonian granite. This assemblage suggests an epithermal metallogenic association, but more work will be required to evaluate this model. Importantly, however, the presence of large ore reserves of tungsten in the granite-related Sisson Brook deposit in New Brunswick suggests a moderate potential for this deposit type within or near Devonian granites of eastern and coastal Maine.

Relevant to western Maine is the St-Robert W-Pb-Zn-Ag-Bi-Au vein deposit in southeastern Québec 10 km northwest of the border (Cattalani 1987; Gauthier *et al.* 1994; Athurion 2013). Production from the central zone of this deposit in 1958 was 1000 t @ 6.28 wt% Pb, 0.91 wt% Zn, 0.64 wt% Bi, 0.06 wt% Cu, and 381 g/t Ag. Reserves in this zone are reported to be 129 000 t @ 0.6 wt% WO_3 and 6000 t @ 1.36 wt% Pb, 0.5 wt% Bi, and 105 g/t Ag; an additional 250 000 t @ 11.3 g/t Au has also been identified (Gauthier *et al.* 1994). The St-Robert vein system forms a northeast-trending mineralized zone dominated by quartz veins containing pyrite, sphalerite, Ag-rich galena, scheelite, cosalite [$Pb_2Bi_2S_5$], chalcopyrite, bismuthinite [Bi_2S_3], and pyrrhotite. The host rock is a metasedimentary hornfels of the Devonian Frontenac Formation; presence of this hornfels and proximity of the veins to quartz-feldspar porphyry dikes suggest a genetic link to an unexposed felsic intrusion at shallow depth (Moench *et al.* 1999). Importantly, however, the St-Robert vein system parallels a major pre-ore regional fault and hence may be controlled by it. Based on the presence in westernmost Maine of similar northeast-trending regional faults, such as the Woburn and Thrasher Peak faults in the Crawford Pond area (Moench *et al.* 1999), a resource potential may exist there for polymetallic vein deposits containing tungsten and bismuth, in addition to other metals such as lead and zinc.

Vanadium in black shales

Vanadium is used in a variety of industrial applications including steel alloys, ceramics, glasses, pigments, chemical catalysts, and redox-flow batteries (Kelley *et al.* 2017). The majority of the world's vanadium is mined from vanadiferous titanomagnetite concentrations in mafic plutons, with minor production coming from sandstone-hosted deposits and some other sources. Although not mined in the past, black shales have recently been identified as potentially containing important vanadium resources. For example, in eastern Nevada, detailed exploration of Devonian black shales has identified two deposits with economic potential, at the Carlin and Gibellini prospects that have measured + indicated reserves of 24.6 Mt at an average grade of 3440 ppm V and 23.0 Mt @ 1625 ppm V, respectively (Phenom Resources Corp. 2021; Nevada Vanadium Mining Corp. 2022). Much larger resources occur in Cretaceous oil shale at Julia Creek in Queensland, Australia (220 Mt @ 1680 ppm V; QEM Limited 2021) and in Neoproterozoic black shale at Häggån in Sweden (90.0 Mt @ 2350 ppm V; Mining Technology 2018). Black-shale hosted vanadium deposits are also known in South China, Madagascar, and other countries (Kelley *et al.* 2017). To date, none of these shale-hosted vanadium deposits has been mined on a large scale but several, including those in Nevada, are currently being evaluated for development and mining; at the Gibellini deposit, mine construction is scheduled to begin in 2022. The primary concentration of vanadium in black shales is generally attributed to a specific redox facies that reflects deposition within bottom waters or pore fluids that were suboxic with very low dis-solved oxygen contents, at the redox couple where V^{4+} is re-duced to V^{2+} (e.g., Algeo and Li 2020).

Black shales and metamorphic equivalents (graphitic schists) occur in many parts of Maine. These strata, in early Paleozoic formations, are exposed chiefly in central and eastern Maine, with some known along or near the coast. Despite extensive geological mapping, however, few of these formations have been studied by whole-rock geochemistry. One of the best known is the Smalls Falls Formation, of Silurian age, but reconnaissance data indicate that this

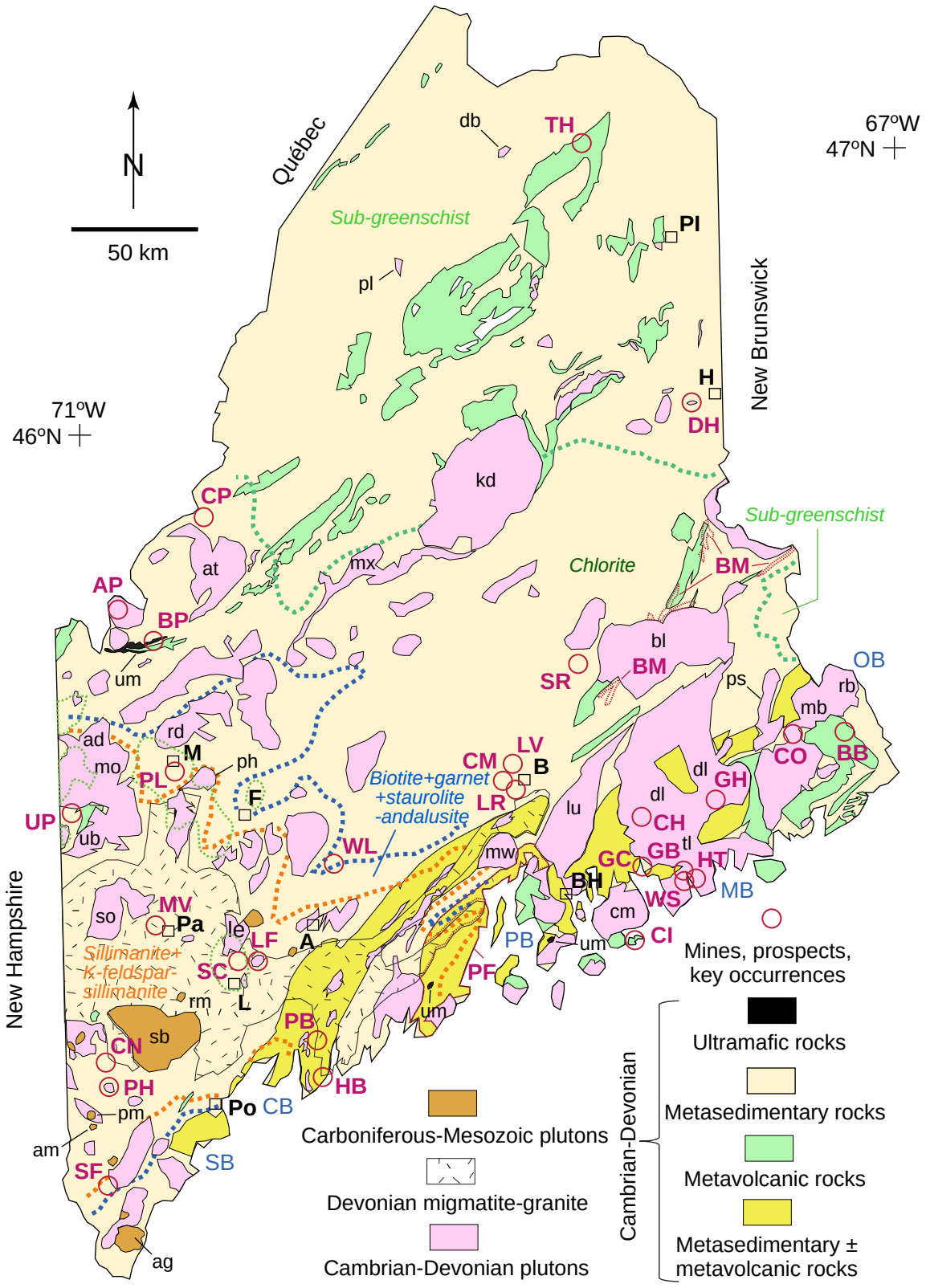

widespread stratigraphic unit lacks elevated vanadium contents (<220 ppm; Slack *et al.* 2020). Black shale and schist of the Ordovician Penobscot Formation, on the west side of Penobscot Bay (Fig. 7), has up to 1600 ppm V (Foley *et al.* 2001), but importantly only a few samples from this unit have been analyzed. The Penobscot Formation thus could have potential for vanadium resources. Potential also may exist in Early Ordovician black shales of the Miramichi belt in eastern Maine, including within the Bowers Mountain Formation (Fig. 7; see Ludman *et al.* 2018), based on mostly

high vanadium contents of 723 to 3016 ppm (avg 1917 ± 778 ppm; n = 7) reported for approximately coeval black shale of the Bright Eye Brook Formation in southwestern New Brunswick (Hennessy and Mossman 1996). A previous study by Fyffe and Pickerill (1993) reported comparable values for this formation, with average concentrations for three samples at two sites of 2429 and 1617 ppm V. The Greenfield Formation in eastern Maine, correlated by Ludman *et al.* (2018) with the Bowers Mountain Formation to the northeast, is lithologically similar in containing black shale but also has Mn-rich mudstone and iron formation, suggesting a more oxidizing depositional environment above the V^{4+}/V^{2+} redox couple that consequently would have prevented high vanadium concentrations during sedimentation (see Algeo and Li 2020), hence the Greenfield Formation probably lacks a potential resource of this metal.

Antimony in granite-related settings

Antimony has diverse uses including in batteries, chemicals, ceramics, glass, flame-retardant materials, heat stabilizers, and plastics (Seal *et al.* 2017). Concentrations of stibnite, the predominant economic antimony mineral, are mined mainly from orogenic deposits without a link to granitic intrusions. Granite-related stibnite veins and breccias are also economically important in some countries. In western New Brunswick, the Lake George antimony deposit (~2 Mt @ 3.0–4.2 wt % Sb), which at one time was the largest antimony producer in North America, forms quartz + stibnite ± arsenopyrite veins in Silurian greywacke and slate within the contact aureole of an Early Devonian granodiorite pluton (Scratch *et al.* 1984; Seal *et al.* 1988). The antimony ores there formed paragenetically late, following earlier stages of W-Mo quartz and Au-bearing quartz-carbonate vein mineralization (Lentz *et al.* 2020).

Several granite-related antimony deposits are known in Maine. One is at the Drew Hill (Eben Lake) prospect west of Houlton. This deposit, in early Paleozoic metasedimentary rocks within the contact aureole of a Devonian granite accompanied by felsic and local mafic dikes, consists of stibnite-rich quartz veins in metasedimentary hornfels. Other mineralized zones occur in this area, including (1) pyrite and pyrrhotite in massive replacements of marble; (2) pyrite, chalcopyrite, and arsenopyrite in phyllite-hosted veins; and (3) pyrite, galena, and chalcopyrite in quartz veins within hornfels and phyllite (Houston 1956; Pavlides and Canney 1964).

Several polymetallic Sb-bearing vein deposits related to igneous plutons occur in coastal Maine. The largest of these was exploited at the Gouldsboro Pb-Cu-Zn-Ag-Au-Sb mine, which produced a minor amount of lead and copper ore from 1878 to 1928. This deposit consists of thin fissure veins of sulphides and sulphosalts (tetrahedrite, stephanite) in a gangue of quartz and orthoclase, hosted within a quartz diorite cut by granitic and pegmatitic dikes (Emmons 1910; Li 1942; Young 1962). Other small Sb-bearing deposits in the area were exploited at the Hector and West and Soule Sb-Cu-Au-Pb-Ag mines (Morrill and Hinckley 1959; Young 1962; U.S. Geological Survey 2021a).

Antimony in orogenic veins and replacements

A major source of global antimony production is from the giant Xikuangshan deposit in China. This deposit, the largest in the world, contains ca. 50 Mt of ore at an average grade of 4.0 wt% Sb (Yang *et al.* 2006). Xikuangshan and other geologically similar deposits in South China are characterized by Sb, Sb-Au, Sb-Hg, and Au veins and siliceous replacements in deformed Devonian and Cretaceous carbonate and minor clastic sedimentary rocks, with the orebodies being controlled by fault intersections and anticlinal structures (Hu and Peng 2018; Zhang *et al.* 2019; Yan *et al.* 2022).

Small antimony prospects and occurrences are known within deformed early Paleozoic metasedimentary rocks in the Bangor area of Maine (Fig. 7) in a geological setting broadly similar to that in parts of South China. Examples are the Carmel and Levant Sb prospects, the Shorey Sb-Au-Ag prospect, and the Lawrence Sb-Cu-Au-Pb-Ag prospect (Morrill and Hinckley 1959; U.S. Geological Survey 2021a). No granitic or igneous bodies are known in this area, and hence are classified here as having formed by orogenic Sb-rich hydrothermal systems. Although the host rocks to these prospects are predominantly clastic, limestone has been mapped locally as in the Stetson quadrangle northwest of Bangor (Griffin 1971) and hence is likely a favourable lithology for hydrothermal replacement mineralization, as documented at the Xikuangshan deposit (Hu and Peng 2018). To our knowledge, none of the antimony prospects or occurrences in the Bangor area has been studied or explored using modern concepts and methods, or application of current ore deposit models (Slack 2022).

Tellurium in epithermal deposits

Tellurium is a critical element because of its use in photovoltaic solar cells (Goldfarb *et al.* 2017). Some epithermal mineral deposits have elevated contents of tellurium including up to hundreds of ppm in local ore zones. Such deposits typically contain appreciable amounts of silver and gold together with variable amounts of zinc, lead, and copper (John *et al.* 2018). Host rocks are chiefly subaerial volcanic rocks, both felsic and mafic; less common are submarine volcanics that formed in relatively shallow seawater, a setting termed hybrid epithermal-VMS by many workers. In addition to precious and base metals, and tellurium, some epithermal deposits contain trace quantities of a variety of critical metals including As, Bi, Sb, Se, Sn, and W, some of which can be recovered economically (Goldfarb *et al.* 2016, 2017; John *et al.* 2018).

Maine has two important epithermal-type deposits located in the Eastport-Machias area near the New Brunswick border. These are the Big Hill and Barrett deposits, both of which are hosted by shallow-marine felsic and mafic

volcanic rocks of the Silurian Leighton Formation (Gates and Moench 1981; Piñán Llamas and Hepburn 2013). The only mining in this area was for lead in the early 1900s at Big Hill; no production figures are recorded. Exploration and drilling in the area took place intermittently in the 1960s until the early 1980s (Young 1968; Lepage *et al.* 1991).

The Big Hill deposit has proven (drilled) reserves of 4.44 Mt @ 1.58 wt% Zn + Pb, 0.15 wt% Cu, 63.5g/t Ag, and 0.28 g/t Au, and indicated reserves of 20.0 Mt @ 1.75 wt% Zn + Pb and 17.0 g/t Ag (Schaaf 1985). Mineralization there comprises irregular veins and disseminations of quartz, galena, and sphalerite with minor pyrite, chalcopyrite, pyrrhotite, and silver sulphides hosted mainly in basalt of the Leighton Formation (Li 1942; Young 1968). Wolfden Resources Corporation (2022) is currently involved in exploration of the Bill Hill (Big Silver) deposit.

The smaller Barrett deposit contains 0.35 Mt @ 1.75 wt% Cu, 20.6 g/t Ag, and 7.9 g/t Au. Major mineralized zones consist of chalcopyrite and sphalerite, with local gold, all occurring as amygdules, replacements, and breccia fillings within basalt of the Leighton Formation (Emmons 1910; Li 1942; Gates and Moench 1981).

Deposits of the Eastport-Machias area are best classified as hybrid epithermal-volcanogenic (e.g., Hronsky *et al.* 2012). This classification is based on the high concentrations of precious metals and on evidence of predominantly shallow-water deposition of the host Leighton Formation (Gates and Moench 1981; Piñán Llamas and Hepburn 2013). We emphasize that elsewhere, hybrid epithermal-volcanogenic sulphide deposits may have high concentrations of tellurium and other critical elements that can be recovered as byproducts during mining. For example, the Eskay Creek deposit in western British Columbia, mined from 1995 to 2008, produced 2.1 Mt of ore averaging 2221 g/t Ag and 48.4 g/t Au with appreciable Cu and Zn, plus locally elevated Ba, Cd, As, Sb, Pb, Te, and Hg; these critical elements occur locally in the Eskay Creek deposit and also in geologically and mineralogically similar deposits elsewhere in the district (Lindsay *et al.* 2021). Note, however, that no analytical data are available for critical elements that may be present in the polymetallic deposits of the Eastport-Machias area.

Beryllium in evolved and altered felsic tuffs

The light element beryllium is widely used in many industries including medical, defense, computer, aerospace, and telecommunications, among others (Foley *et al.* 2017). The United States is self-sufficient in beryllium based on production from the giant volcanogenic Spor Mountain deposit in western Utah that is the largest in the world, containing 9.6 Mt of ore at an average grade of 0.25 wt% Be (Foley *et al.* 2012; Ayuso *et al.* 2020). However, beryllium nevertheless is listed as a critical element because the U.S. Department of Defense requires a long-term domestic supply given that U.S. production has diminished in the past decade. Other countries rely on beryllium contained in pegmatite-hosted beryl. The beryllium in the Spor Mountain deposit is concentrated in the mineral bertrandite, a hydrous Be-rich silicate mineral [$Be_4Si_2O_7(OH)_2$] that occurs in limestone clasts within alkaline lithic-rich rhyolite tuffs of Tertiary age. Abundant fluorite and high uranium contents (up to 2000 ppm U) are also characteristic of the ores (Lindsey *et al.* 1973). An integrated model for the formation of this deposit involves low-temperature (<200°C) hydrothermal alteration of calcite in the clasts by a Be-F aqueous complex, which together with water and dissolved silica yield products of bertrandite plus fluorite and CO_2 (Foley *et al.* 2012). Three important components of the model are (1) occurrence of lithic-rich alkaline rhyolite tuff; (2) presence of carbonate rocks stratigraphically below the tuffs to provide a source for the calcite-rich clasts, and (3) post-depositional hydrothermal alteration by F- and Be-rich fluids that are concentrated via dissolution of these elements in the host alkaline tuff.

A major limitation to applying the Spor Mountain model to Maine is the apparent lack of alkaline rhyolite tuffs in Maine. Some large-volume rhyolite tuffs are known in the state (Seaman *et al.* 2019) including the thick ignimbrites of the Devonian Traveler Rhyolite that contains groundmass fluorite, but limited whole-rock geochemical data for major, trace, and rare earth elements suggest that both members of this tuff are calc-alkaline and not alkaline (Hon 1976). Widespread rhyolites also occur in the coastal volcanic belt of the Penobscot Bay area (Pinette and Osberg 1989; Schulz *et al.* 2008) and the Machias-Eastport area (Gates and Moench 1981; Piñán Llamas and Hepburn 2013), all of which are compositionally calc-alkaline or tholeiitic and not alkaline.

One possible candidate for undiscovered beryllium mineralization in Maine is in lithic-rich rhyolite tuffs of the Late Silurian Cranberry Island series (Fig. 7). Described by Seaman *et al.* (1999), these volcanic rocks are mainly tholeiitic although one sample of dacite has a high Na_2O + K_2O content that plots compositionally in the alkaline field; several samples of rhyolite ignimbrite contain elevated La (up to 47.6 ppm), Y (up to 280 ppm), and Zr (up to 384 ppm), but uranium concentrations are uniformly low (<3.2 ppm). No whole-rock data are available for beryllium or fluorine. Importantly, the lithic clasts are rhyolite, granite, basalt, or siltstone, without reported carbonate. Basement to the Cranberry Islands volcanic rocks is not exposed in the area, but likely is dominated by siliciclastic metasedimentary rocks (e.g., Cambrian Ellsworth Schist), although limestones of this approximate age are known elsewhere in the coastal region, such as on the west side of Penobscot Bay (i.e., Coombs Limestone), and potentially could underlie the Cranberry Islands at depth. On balance, the possibility for Spor Mountain-type beryllium mineralization in the Cranberry Islands volcanic rocks is considered to be low, but we nonetheless suggest a speculative potential based on several favourable criteria. More focused mineralogical studies and whole-rock geochemical analyses (i.e., for Be and F) are recommended, in order to better evaluate this volcanic series for cryptic beryllium mineralization.

Graphite in high-grade metamorphic rocks

Graphite is a critical component used in many industries including for electronics, lubricants, metallurgy, steelmaking, and recently for batteries in electric vehicles (Simandl *et al.* 2015; Robinson *et al.* 2017). Since the 1990 closure of the last graphite mine in the U.S., in Montana, the nation has been totally dependent on foreign sources of this mineral. The economically most important deposit type contains flake graphite, which commonly occurs in high-grade metamorphic terranes dominated by metasedimentary rocks. Major deposits that contain large reserves and/or resources of abundant flake graphite include Zavalyevskiy in Ukraine (100.0 Mt @ 5.5% graphitic C; Robinson *et al.* 2017) and Graphite Creek in northwestern Alaska (102.8 Mt @ 8.0% graphitic C; King *et al.* 2019).

The setting and origin of the Graphite Creek deposit can be used as a template for evaluating the potential of other regions with similar geology. At the Graphite Creek deposit, flake graphite is concentrated in veins and massive lenses up to 0.5 m thick within upper amphibolite- to granulite-facies, quartz-plagioclase-biotite paragneiss of late Paleozoic age, and near Late Cretaceous granitic intrusions (Case *et al.* 2020). In Maine, many granitic pegmatites contain small amounts of flake graphite (Smith 1906), but these are not commercially viable. Importantly, however, three small graphite mines and prospects in the western part of the state are within highly metamorphosed sedimentary rocks like those that host the Graphite Creek deposit. The graphite mine on Plumbago Mountain southwest of Farmington, the Milletville prospect west of Paris, and the Phillips mine in Madrid, are all in amphibolite- to granulite-facies metasedimentary rocks, and most have spatially associated granitic intrusions (Fig. 7). More work will be required to evaluate the potential of these small mines and prospects for containing significant undiscovered resources of flake graphite.

Titanium, zirconium, and rare earth elements in heavy-mineral sands

Heavy-mineral sands are important sources of critical minerals worldwide (Van Gosen *et al.* 2014). Such sands may contain economic concentrations of resistant minerals like rutile, ilmenite, zircon, and monazite that can be mined for titanium, zirconium, and REE. These metals are of critical importance to the U.S. economy because of minimal domestic production and importance in the manufacturing of paint, paper, and metal alloys; in the chemical and nuclear-reactor industries; and in glass, magnets, and catalysts in petroleum refining, catalytic converters; and for making phosphors in cathode ray tubes and flat panel display screens (Woodruff *et al.* 2017; Jones *et al.* 2017; Van Gosen *et al.* 2017). Heavy-mineral sands have been mined on the U.S. Atlantic Coastal Plain since 1949 (Van Gosen *et al.* 2014); current mining of ilmenite and rutile in these types of sands is ongoing in Florida, Georgia, and South Carolina (Gambogi 2021). Several publications have suggested a potential exists for important accumulations of heavy-mineral sands both onshore and nearshore coastal Maine (Kelley *et al.* 1997; Buynevich and FitzGerald 2001), but to date there has not been a comprehensive analysis for such deposits in the state.

Most sand deposits onshore in Maine are products of erosion of the landscape by Pleistocene glaciation and subsequent fluvial processes that redistributed meltwater sediments. The majority of these deposits are in southern and coastal Maine (Thompson and Borns 1985), occurring as outwash plains, deltas, esker ridges, beaches, and ice-contact deposits. Many of these readily accessible deposits have been exploited for aggregate resources. Most of the glacial sand deposits were reworked by marine processes as sea-level fell to a low of -60 m below current sea level, and then rose again in response to long-term isostatic adjustment coupled with eustatic sea-level rise during the late Pleistocene and early Holocene (Barnhardt *et al.* 1995).

The work summarized in Kelley *et al.* (1998), based on maps created during a decade-long research program, is the most comprehensive presentation of the geologic environments of the inner continental shelf of Maine. Results of this mapping generally extend offshore to Maine's territorial limit of three nautical miles, and mostly extends to depths beyond the -60 m post-glacial lowstand. About 8% of the ocean bottom materials in the entire region surveyed is sand. Kelley *et al.* (1998) provided statistical summaries of the ocean bottom types, divided into key physiographic zones. The nearshore ramp zone, a region that slopes gently seaward with widely spaced, shore-parallel bathymetric contours, contains the majority of sand resources and represents nearly 350 km^2 of ocean bottom and 66% of this zone. Other physiographic zones have considerably less sand, but the shelf valley zone may have locally abundant sand bodies.

The most detailed analysis of heavy minerals in onshore deposits was done by Buynevich and FitzGerald (2001) in their study of progradation in coastal barrier beach systems. Among the studied field localities were three paraglacial barrier beach systems near the mouth of the Kennebec River in mid-coastal Maine. Their analysis of progradation included the collection of ground penetrating radar data and coring. One core taken at the Hunnewell barrier (Fig. 7) through reflectors recognized in ground-penetrating radar (GPR) data revealed medium- to fine-grained sands with a significant content of heavy minerals (>30 vol% magnetite + ilmenite + garnet) at a depth of between 2 and 3 m. These heavy-mineral sands are interpreted as lag deposits produced by erosion during significant storms. Unfortunately, Buynevich and FitzGerald (2001) did not analyze for monazite, zircon, or other critical minerals (I.V. Buynevich, oral communication 2021) that are likely present in trace amounts, at least. Similar erosional lag deposits probably exist in other onshore deposits of Maine, but additional work has not been done to assess their resource potential.

Several researchers have analyzed offshore deposits for heavy mineral content. Luepke and Grosz (1986) collected

and analyzed 12 vibracore samples from Saco Bay in southern Maine, one of the nearshore ramps that contains abundant sand as noted by Kelley *et al.* (1998). Heavy minerals of economic interest—ilmenite, leucoxene, rutile, zircon, and aluminosilicates (sillimanite and andalusite)—constitute an average of about 14 wt% of the heavy minerals in the analyzed sediments, and an average of about 0.1 wt% of the bulk samples. Monazite was not detected in any of their samples. Grosz (1987) summarized what was then known of heavy mineral deposits along the Atlantic continental shelf. This study noted several areas in the Gulf of Maine where heavy minerals in surficial materials of the ocean bottom contain at least 4 wt% heavy minerals, including one offshore Saco.

As part of the inner continental shelf mapping effort, Kelley *et al.* (1997) collected 1303 grab samples of all bottom types. For 31 sand-rich samples collected in bays spanning the coast (Saco Bay, Casco Bay, Penobscot Bay, Machias Bay, Oak Bay in New Brunswick; Fig. 1), heavy minerals were separated using standard techniques. The highest concentration in a single sample, 6% of the dry sample weight, was found in Casco Bay, where the bay-wide average was higher than elsewhere, 2.6%. Although each of the areas studied was variable, Oak Bay contained the lowest concentrations with a mean of 0.21%. Mineral species were identified via microscopy, X-ray diffraction, or both techniques. The highest average concentration of ilmenite was in Oak Bay (6.19%), followed by Casco Bay (3.89%), and Saco Bay (3.66%). The highest concentrations of zircon were in Saco Bay (1.70%) and Machias Bay (1.15%); all other areas averaging less than 1% zircon. Rutile averaged less than 0.50% in all samples. Kelley *et al.* (1997) did not report REE mineral species, presumably because they were not present or occurred only in trace amounts.

Although some work has been done on heavy-mineral sands both onshore and nearshore Maine, these efforts were not comprehensive. Importantly, the tantalizing data of Buynevich and FitzGerald (2001) do indicate a potential for onshore concentrations of heavy minerals. However, many readily accessible sand deposits onshore have already been mined for aggregate. The results of Kelley *et al.* (1997) suggest the potential for undiscovered heavy-mineral concentrations in the sand-dominated nearshore ramp environment offshore (e.g., Kelley *et al.* 2003), with areas in southern and central Maine having the highest potential, particularly for titanium and zircon resources. High-resolution aeroradiometric surveys like those described by Shah *et al.* (2021) could reveal Th-rich sands that may have economic potential for REE present in monazite and other minerals.

Uranium in peat

Uranium in peat was mined during the 1980s in Washington State at the Flodelle Creek deposit (Johnson *et al.* 1987). A geological reserve of uranium in this deposit has been estimated at 200 t (J.K. Otton *in* Zielinski and Burruss 1991). The local bedrock source of the uranium is a Cretaceous two-mica granite that contains 9 to 16 ppm U (Zielinski and Burruss 1991).

The studies of Cameron *et al.* (1986, 1990) on trace elements in thirty-eight Holocene peat deposits of New Hampshire and Vermont highlight their potential as uranium resources. Uranium concentrations in these samples range from 1.0 to 467.0 ppm, with a mean of 48.3 ppm. The highest values, in western Vermont, occur in peat underlain by a Cambrian dolostone, which is ca. 4 km from Proterozoic granitic gneiss in the Green Mountains massif. In the New Hampshire occurrences, the ultimate source of uranium is the two-mica Sunapee granite of Late Devonian to Early Mississippian age. Results of these studies suggest that uranium-rich rocks beneath or near peat deposits leach uranium into shallow groundwater (Cameron *et al.* 1986, 1990). As groundwater flows, uranium is fixed in peat-hosted organic matter largely by processes of adsorption and ion exchange.

Two-mica granite is recognized for its metallogenic specialization in concentrating tin, tungsten, beryllium, lithium, fluorine, and uranium (Boudette 1977; Cuney 2014). Two-mica granites in New England are the products of tectonic interactions of ancestral North America with island arcs, microplates, and continents that thickened the crust through Ordovician-Devonian time. Metasedimentary rocks near the base of the thickened crust melted partially to form felsic magma that migrated upward through the crust to crystallize as two-mica granite.

Most two-mica granites in Maine occur in the western and coastal regions of the state. Geochemical data collected through the North American soil geochemical landscapes project (Smith *et al.* 2014) and airborne radiometric data collected through the National Uranium Resource Evaluation (NURE) program (Hill *et al.* 2009; Kucks 2005) show anomalously high concentrations of uranium in the Sebago migmatite domain area of western Maine (Figs. 5 and 6). The Sebago granite proper occupies only the southernmost part of this area, the remainder being underlain by a complex association of high-grade metamorphic rocks, migmatite, granitic dikes, and pegmatite (Solar and Tomascak 2016). The uranium anomaly in the NURE data for the Sebago area is similar to that in central New Hampshire studied by Cameron *et al.* (1986, 1990). Additionally, water from private wells in this area of southern Maine have some of the highest uranium concentrations found anywhere in the state. According to data compiled by the Maine Department of Health and Human Services (MEDHHS 2021), up to 58% of tested wells in some area towns exceed the state guideline for uranium of 30 μg/l.

In addition to the two-mica granites, the alkali-calcic Lucerne and Deblois plutons (Ayuso and Arth 1991) in eastern coastal Maine may also provide uranium to peat deposits in the manner described by Cameron *et al.* (1986). The NURE airborne radiometric data (Kucks 2005; Hill *et al.* 2009) show anomalously high uranium concentrations in close geographic association with these two plutons (Fig. 5). Similarly, private well waters in this region of eastern Maine underlain by the Lucerne and Deblois plutons have high

uranium concentrations (MEDHHS 2021).

Cameron and Mullen (1982) summarized the peat resources of southern and coastal Maine as part of a comprehensive effort led by Cameron to investigate peat resources statewide (Cameron 1975; Cameron and Massey 1978; Cameron and Anderson 1979, 1980a, 1980b). The deposits characterized by these studies contain air-dried peat amounts ranging from 34,300 t to nearly 9.1 Mt, with a total in the studied deposits of ca. 36 Mt. Although many peat deposits occur in the area underlain by the Sebago Migmatite Domain, these tend to be small in area and of low total tonnage. The largest peat deposit characterized by Cameron and Mullen (1982) of just over 1.8 Mt falls within the area underlain by the Deblois granite pluton. In a focused study of the Great Heath, Cameron and Anderson (1980a) identified nearly 9.1 Mt of air-dried peat that is also underlain by the Deblois pluton. Norton (1990) investigated the geochemistry of the Great Heath and three other large peat deposits in Maine, but this study did not analyze for uranium. Although no studies have been done to assess the uranium content of peat in eastern Maine, given the high uranium concentrations there as suggested by the NURE data, and by elevated concentrations of uranium in groundwater, we conclude that a considerable potential exists for uranium resources in peat underlain by the Lucerne and Deblois plutons.

DISCUSSION

Our qualitative assessment of potential for the occurrence of critical mineral deposits in Maine is based on several factors. Following the approach used elsewhere in New England by the USGS for the Glens Falls and Sherbrooke-Lewiston 1° × 2° quadrangles (Slack 1990; Moench *et al.* 1999), this assessment ranks the potential into high, medium, and low categories. A quantitative mineral resource assessment (Singer and Menzie 2010), like those described for some major deposit types worldwide (e.g., Zientek *et al.* 2010), cannot be done for Maine owing to a lack of adequate data on tonnages and grades for most of the mines and deposits in the state. Key consideration in the qualitative assessment is given to (1) the presence of known deposits, prospects, or occurrences; (2) geological settings that are favourable for the formation of certain deposit types; and (3) geochemical data including those obtained on stream sediments and panned concentrates in regional surveys, and on rocks whether visibly mineralized or not. Descriptive and genetic geologic models for the origin of the mineralization are also used (e.g., Pirajno 1999; Hagemann *et al.* 2016), where applicable to Maine (Slack 2019, 2021, 2022). Importantly, data on small mines or prospects unworked for a century or more can nevertheless be valuable if the nature of the mineralization and geological setting are comparable to those of major orebodies elsewhere in the world. Geophysical data may be helpful for some cases, but in Maine few areas have modern coverage by high-resolution aerial magnetic and radiometric surveys.

Table 1 summarizes the potential in Maine for occurrence of 20 different deposit types and possible contained resources of critical minerals (and elements). A high resource potential is assigned only to three deposit types: (1) sediment-hosted manganese, (2) mafic- and ultramafic-hosted Ni-Cu(-Co-PGE), and (3) pegmatitic lithium-cesium-tantalum. In all designated areas, large deposits are either known or considered likely to exist based on various criteria including the presence of documented prospects that contain critical minerals and that can be evaluated using modern ore deposit models. Also important is the fact that the specified critical minerals within these three deposit types are potentially recoverable during mining and processing, assuming economic viability of the deposit.

Moderate potential is suggested for 11 other deposit types. These include: (1) porphyry Cu-Mo (Re, Se, Te, Bi, PGE); (2) chromium in ophiolites; (3) PGE in ophiolitic ultramafic rocks; (4) granite-hosted uranium-thorium; (5) tin in granitic plutons and veins; (6) niobium, tantalum, and REE in alkaline intrusions; (7) tungsten and bismuth in polymetallic veins; (8) vanadium in black shales; (9) antimony in orogenic veins and replacements; (10) tellurium in epithermal deposits; and (11) uranium in peat. Deposit types such as VMS that are known in some cases to have elevated concentrations of critical elements are nonetheless designated as having low resource potential because the contained critical elements are typically present in solid solution within other minerals (e.g., pyrite) that would likely not be recovered economically during mine beneficiation. Other small deposits such as Pb-Zn, Cu, and Mo veins (U.S. Geological Survey, 2021a) that apparently lack elevated concentrations of critical elements are not discussed.

Only the sediment-hosted manganese deposits in northeastern Maine and the pegmatitic lithium (spodumene) deposit at Plumbago Mountain in the western part of the state have reported mineral resources. However, in both areas, more exploration work such as extensive drilling and sampling will be required in order to accurately define mineral reserves that are compliant with internationally recognized codes such as NI 43-101 and JORC. The other deposit types for which we assign a moderate or low potential for critical minerals (Table 1) need significant field-based efforts to better characterize local geological settings and the nature and extent of mineralization, plus detailed laboratory studies to accurately define the mineralogical siting of the critical elements and whether these can be extracted during milling and beneficiation of the ores.

After this manuscript was completed the USGS released a new list of critical minerals for the United States (U.S. Geological Survey 2022). With respect to minerals and elements considered in this report, deletions include rhenium and uranium, with additions of nickel and zinc. Nickel is already discussed, but zinc is not. Potential for new zinc resources in Maine will likely be restricted to VMS deposits within pre-Devonian volcanic belts that occur throughout the state (Fig. 1).

Table 1. Qualitative ranking of potential for resources of critical minerals in different deposit types in Maine, USA.

Deposit type	Critical minerals	Occurrence potential	Resource potential
Sediment-hosted Mn	Mn	High	High
Volcanogenic massive sulphide Cu-Zn(-Pb-Ag-Au)	Co, As, Sb, Te	High	Low
Porphyry Cu-Mo	Re, Se, Te, Bi, PGE	High	Moderate
Mafic- and ultramafic-hosted Ni-Cu(-Co-PGE)	Co, PGE	High	High
Pegmatitic Li-Cs-Ta	Li, Cs, Ta	High	High
Cr in ophiolites	Cr, PGE	High	Moderate
PGE in ophiolitic ultramafic rocks	PGE	Moderate	Moderate
Granite-hosted U-Th	U, Th	Moderate	Moderate
Sn in granitic plutons and veins	Sn	Moderate	Moderate
Nb, Ta, and REE in alkaline intrusions	Nb, Ta, REE	Moderate	Moderate
W in skarn and replacement deposits	W	Moderate	Low
W and Bi in polymetallic veins	W, Bi	Moderate	Moderate
V in black shales	V	Moderate	Moderate
Sb in granite-related settings	Sb	Moderate	Moderate
Sb in orogenic veins and replacements	Sb	Moderate	Low
Te in epithermal deposits	Te	Moderate	Moderate
Be in evolved and altered felsic tuffs	Be	Low	Low
Graphite in high-grade metamorphic rocks	Graphite	Low	Low
Ti, Zr, and REE in heavy-mineral sands	Ti, Zr, REE	Moderate	Low
U in peat	U	High	Moderate

ACKNOWLEDGMENTS

Funding for this study came in part from the Maine Geological Survey through a grant from the USGS Earth MRI project. Any use of trade, product, or firm names is for descriptive purposes only and does not imply endorsement by the U.S. Government.

We thank Bill Cannon for discussions on sediment-hosted manganese deposits, and Chunzeng Wang and Allan Ludman for advice on the Silurian stratigraphy of eastern Aroostook County. Reviews by Dave Lentz, Ryan Taylor, and an anonymous referee helped clarify aspects of the manuscript and are appreciated.

REFERENCES

Adams, J.A.S., Kline, M.-C., Richardson, K.A., and Rogers, J.J.W. 1962. The Conway Granite of New Hampshire as a major low-grade thorium resource. Proceedings of the National Academy of Sciences, 48, pp. 1898–1905. https://doi.org/10.1073/pnas.48.11.1898

Algeo, T.J. and Li, C. 2020. Redox classification and calibration of redox thresholds in sedimentary systems. Geochimica et Cosmochimica Acta, 287, pp. 8–26. https://doi.org/10.1016/j.gca.2020.01.055

Athurion, C. 2013. Réévaluation du potentiel minéral de la propriété de l'ancienne mine de St-Robert, Beauce, Québec. Unpublished M.Sc. thesis, Université du Québec à Montréal, Montréal, Québec, 288 p.

Atkinson, D. 1977. Catheart Mountain, an Ordovician porphyry copper molybdenum occurrence in northern Appalachia. Unpublished Ph.D. thesis, University of Western Ontario, London, Ontario, 191 p.

Ayuso, R.A. 1989. Geochemistry of the Catheart Mountain porphyry copper deposit, Maine. *In* Studies in Maine geology: Volume 4 – Igneous and metamorphic geology. *Edited by* R.D. Tucker and R.G. Marvinney. Augusta, Maine, Maine Geological Survey, 4, pp. 139–162.

Ayuso, R.A. and Arth, J.G. 1991. Geochemistry and metallogeny of granitic rocks from the Appalachian Mountains—examples from the Northeast Kingdom batholith, Vermont, and the Lucerne and Deblois batholiths, Maine. U. S. Geological Survey Circular 1062, 3 p.

Ayuso, R.A. and Loferski, P.J. 1992. Trace element geochemistry of syenite and granodiorite in the Deboullie pluton, northern Maine. Geological Association of Canada/Mineralogical Association of Canada, Abstracts, 17, p. A5.

Ayuso, R.A. and Shank, S.G. 1983. Quartz-molybdenite veins in the Priestly Lake granodiorite, north-central Maine. U.S. Geological Survey Open-File Report 83–800, 12 p. https://doi.org/10.3133/ofr83800

Ayuso, R.A., Foley, N.K., Vazquez, J.A., and Jackson, J.C. 2020. SHRIMP U–Pb zircon geochronology of volcanic rocks hosting world class Be-U mineralization at Spor Mountain, Utah, U.S.A. Journal of Geochemical Explo-

ration, 209, pp. 106401. https://doi.org/10.1016/j.gexplo.2019.106401.

A-Z Mining Professionals Limited. 2020. Preliminary economic assessment, Pickett Mountain project. Prepared for Wolfden Resources Corporation. URL <https://www.wolfdenresources.com/projects/pickett-mountain-maine/technical-reports/,> 17 June 2022.

Bacuta, G.C. Jr., Kay, R.W., Gibbs, A.K., and Lipin, B.R. 1990. Platinum-group element abundance and distribution in chromite deposits of the Acoje block, Zambales ophiolite complex, Philippines. Journal of Geochemical Exploration, 37, pp. 113–145. https://doi.org/10.1016/0375-6742(90)90086-P

Barker, D.S. 1965. Alkalic rocks at Litchfield, Maine. Journal of Petrology, 6, pp. 1–27. https://doi.org/10.1093/petrology/6.1.1-a

Barnes, R.G. 1983. Stratiform and stratabound tungsten mineralization in the Broken Hill Block, N.S.W. Journal of the Geological Society of Australia, 30, pp. 225–239. https://doi.org/10.1080/00167618308729250

Barnhardt, W.A., Gehrels, W.R., Belknap, D.F., and Kelley, J.T. 1995. Late Quaternary relative sea-level change in the western Gulf of Maine: evidence for a migrating glacial fore bulge. Geology, 23, pp. 317–320. https://doi.org/10.1130/0091-7613(1995)023<0317:LQRSLC>2.3.CO;2

Barton, W.R. and Goldsmith, C.E. 1968. New England beryllium investigations. U.S. Bureau of Mines Report of Investigations 7070, 177 p.

Beck, F.M. 2012. A history of non-ferrous metal mining and exploration in Maine. Geological Society of Maine, Annual Meeting, Bangor, Maine, PowerPoint presentation. URL <https://docplayer.net/21096234-A-history-of-non-ferrous-metal-mining-and-exploration-in-maine-by-frederick-m-beck-f-m-beck-inc-yarmouth-maine.html> 12 June 2020.

Beers, R.F., Casey, C.F., Wyke, D.E., and Young, R.S. 1962. Exploration of the Crawford Pond nickel deposit: a case study. Society of Mining Engineers, Preprint 62L90, 7 p., 13 plates.

Belogub, E.V., Melekestseva, I.Yu., Novoselov, K.A., Zabotina, M.V., Tret'yakov, G.A., Zaykov, V.V., and Yuminov, A.M. 2017. Listvenite-related gold deposits of the South Urals (Russia): a review. Ore Geology Reviews, 85, pp. 247–270. https://doi.org/10.1016/j.oregeorev.2016.11.008

Boudette, E.L. 1977. Two-mica granite and uranium potential in the northern Appalachian orogen of New England. U.S. Geological Survey Circular 753, pp. 23–24.

Boudette, E.L. 1982. Ophiolite assemblage of early Paleozoic age in central western Maine. *In* Major structural zones and faults of the northern Appalachians. *Edited by* P. St-Julien, and J. Beland. Geological Association of Canada Special Paper 24, pp. 209–230.

Boudette, E.L. 1991. Geologic map of the Kennebago Lake quadrangle, Franklin County, Maine. U.S. Geological Survey Miscellaneous Investigations Series Map 1–2058, 12 p., scale 1:62 500.

Boyer, F. and Routhier, P. 1974. Extension régionale de couches à scheelite dans la couverture métamorphique de la zone axiale en Montagne Noire (Hérault, France). Comptes rendus de l'Académie des Sciences Paris, Serie D, 279, pp. 1829–1832.

Bradley, D.C. 2019. Tectonic and paleoclimatic controls of lithium-cesium-tantalum (LCT) pegmatite genesis, exhumation, and preservation in the Appalachians. The Canadian Mineralogist, 57, pp. 715–717. https://doi.org/10.3749/canmin.AB00002

Bradley, D.C. and Tucker, R.D. 2002. Emsian synorogenic paleogeography of the Maine Appalachians. The Journal of Geology, 110, pp. 483–492. https://doi.org/10.1086/340634

Bradley, D., Tucker, R., Lux, D., Harris, A., and McGregor, D. 2000. Migration of the Acadian orogen and foreland basin across the northern Appalachians of Maine and adjacent areas. U.S. Geological Survey Professional Paper 1624, 51 p. https://doi.org/10.3133/pp1624

Bradley, D.C., Shea, E., Buchwaldt, R., Bowring, S., Benowitz, J., O'Sullivan, P., and McCauley, A. 2016. Geochronology and tectonic context of lithium-cesium-tantalum pegmatites in the Appalachians. The Canadian Mineralogist, 54, pp. 1–25. https://doi.org/10.1130/abs/2016NE-271707

Bradley, D.C., McCauley, A.D., and Stillings, L.M. 2017a. Mineral-deposit model for lithium-cesium-tantalum pegmatites. U.S. Geological Survey Scientific Investigations Report 2010–5070–O, 65 p. https://doi.org/10.3133/sir20105070O

Bradley, D.C., Stillings, L.L. Jaskula, B.W., Munk, L.A., and McCauley, A.D. 2017b. Lithium. *In* Critical mineral resources of the United States—economic and environmental geology and prospects for future supply. *Edited by* K.J. Schulz, J.H. DeYoung Jr., R.R. Seal II, and D.C. Bradley. U.S. Geological Survey Professional Paper 1802–K, 21 p.

Brown, C.D. and Wise, M.A. 2001. Internal zonation and chemical evolution of the Black Mountain granitic pegmatite, Maine. The Canadian Mineralogist, 39, pp. 45–55. https://doi.org/10.2113/gscanmin.39.1.45

Buisson, G. and Leblanc, M. 1986. Gold-bearing listwaenites (carbonatized ultramafic rocks) from ophiolite complexes. *In* Metallogeny of basic and ultrabasic rocks. *Edited by* M.J. Gallagher, R.A. Ixer, C.R. Neary, and H.M. Prichard. Institution of Mining and Metallurgy, London, pp. 121–131.

Burbank, W.S. 1965. Cooper mine. U.S. Geological Survey Bulletin 1182–E, pp. E61–E62.

Burbank, W.S. and Miller, R.L. 1965. Henderson Farm prospect. U.S. Geological Survey Bulletin 1182–E, pp. E59–E60.

Bureau de Recherches Géologiques et Minières. 2002. Mittersill, Austria. URL https://web.archive.org/web/20110815202458/http://eswww.rhul.ac.uk/geode/ABCD/Mittersill.html> 15 June 2011.

Bussolesi, M., Grieco, G., Zaccarini, F., Tzamos, E., and Eslami, A. 2020. Platinum group element (PGE) distribution and mobility during post magmatic processes in ophiolite chromitites. Goldschmidt2020 Conference, Honolulu,

Hawaii, 21–26 June 2020, Abstracts Volume. https://doi.org/10.46427/gold2020.290

Butler, A.P. Jr. 1975. Uranium and thorium in samples of rocks of the White Mountain plutonic series, New Hampshire, and whole rock chemical and spectrographic analyses of selected samples. U.S. Geological Survey Open-File Report 75–59, 17 p. https://doi.org/10.3133/ofr7559

Buynevich, I.V. and FitzGerald, D.M. 2001. Styles of coastal progradation revealed in subsurface records of paraglacial barriers: Duxbury, Massachusetts, USA. Journal of Coastal Research, 34, pp. 194–208.

Callaghan, R.M. 2021. Tantalum. U.S. Geological Survey mineral commodity summaries 2021, pp. 164–165. URL <https://pubs.usgs.gov/periodicals/mcs2021/mcs2021.pdf.>

Cameron, C.C. 1975. Some peat deposits in Washington and southeastern Aroostook Counties, Maine. U.S. Geological Survey Bulletin 1317–C, 40 p. https://doi.org/10.3133/ofr74189

Cameron, C.C. and Anderson, W.A. 1979. Some peat deposits in Penobscot County, Maine. U.S. Geological Survey Open-File Report 79–1096, 31 p. https://doi.org/10.3133/ofr791096

Cameron, C.C. and Anderson, W.A. 1980a. Peat resources of the Great Heath, Washington County, Maine. U.S. Geological Survey Open-File Report 80–379, 31 p. https://doi.org/10.3133/ofr80379

Cameron, C.C. and Anderson, W.A. 1980b. Some peat deposits in northern Penobscot, eastern Piscataquis, and eastern Aroostook Counties, Maine. U.S. Geological Survey Open-File Report 80–718, 47 p. https://doi.org/10.3133/ofr80718

Cameron, C.C. and Massey, W. D. 1978. Some peat deposits in northern Hancock County, Maine. U.S. Geological Survey Open-File Report 78–210, 19 p. https://doi.org/10.3133/ofr78210

Cameron, C.C. and Mullen, M.K. 1982. Sketch maps showing areal extent, thickness and amount of commercial-quality peat in deposits of southern and western Maine. U.S. Geological Survey, Open File Report 82–0184, 77 p. https://doi.org/10.3133/ofr82184

Cameron, C.C., Mullen, M.K., Lepage, C.A., and Anderson, W.A. 1984a. Peat resources of Maine; Volume 1, Aroostook County. Maine Geological Survey Bulletin 28, 107 p.

Cameron, C.C., Mullen, M.K., Lepage, C.A., and Anderson, W.A. 1984b. Peat resources of Maine; Volume 2, Penobscot County. Maine Geological Survey Bulletin 29, 124 p.

Cameron, C.C., Mullen, M.K., Lepage, C.A., and Anderson, W.A. 1984c. Peat resources of Maine; Volume 3, Piscataquis and Somerset Counties. Maine Geological Survey Bulletin 30, 127 p.

Cameron, C.C., Mullen, M.K., Lepage, C.A., and Anderson, W.A. 1984d. Peat resources of Maine; Volume 4, Southern and western Maine. Maine Geological Survey Bulletin 31, 123 p.

Cameron, C.C., Mullen, M.K., Lepage, C.A., and Anderson, W.A. 1984e. Peat resources of Maine; Volume 5, Washington County. Maine Geological Survey Bulletin 32, 143 p.

Cameron, C.C, Schruben, P.G., and Boudette, E.L. 1986. Some controls on trace-element concentrations, especially uranium, in selected peat deposits of Vermont and New Hampshire. U.S. Geological Survey Open-File Report 86-361, 32 p. https://doi.org/10.3133/ofr86361

Cameron, C.C., Schruben, P.G., and Boudette, E.L. 1990. Some controls on trace-element concentrations, especially uranium, in selected peat deposits in Vermont and New Hampshire. U.S. Geological Survey Bulletin 1887–M, 10 p.

Cameron, E.N., Larrabee, D.M., McNair, A.H., Page, J.J., Stewart, G.W., and Shainin, V.E. 1954. Pegmatite investigations, 1942–45, in New England. U.S. Geological Survey Professional Paper 255, 352 p., 48 plates.

Canney, F.C., Ward, F.N., and Bright, M.J., Jr. 1961. Molybdenum content of glacial drift related to molybdenite-bearing bedrock, Aroostook County, Maine. U.S. Geological Survey Professional Paper 424–B, pp. 276–278.

Cannon, W.F. and Force, E.R. 1983. Potential for high-grade shallow-marine manganese deposits in North America. *In* Cameron volume on unconventional mineral deposits. *Edited by* W.C. Shanks. American Institute of Mining, Metallurgical, and Petroleum Engineers, New York, pp. 175–189.

Cannon, W.F., Kimball, B.E., and Corathers, L.A. 2017. Manganese. *In* Critical mineral resources of the United States—economic and environmental geology and prospects for future supply. *Edited by* K.J. Schulz, J.H. DeYoung Jr., R.R. Seal II, and D.C. Bradley. U.S. Geological Survey Professional Paper 1802–L, 28 p.

Case, G., Karl, S.M., Regan, S.P., O'Sullivan, P., Holm-Denoma, C.S., Pianowski, L.S., and Jones, J.V. III, 2020. U–Pb age constraints on host rock deposition and high-T metamorphism at the Graphite Creek flake graphite deposit, Seward Peninsula, Alaska. Geological Society of America Abstracts with Programs 52(6). https://doi.org/10.1130/abs/2020AM-358275

Case, G.N.D., Graham, G.E., Marsh, E.E., Taylor, R.G., Green, C.J., Brown, P.J., and Labay, K.A. 2022. Tungsten skarn potential of the Yukon-Tanana upland, eastern Alaska, USA—a mineral resource assessment. Journal of Geochemical Exploration, 232, pp 106700. https://doi.org/10.1016/j.gexplo.2020.106700.

Cattalani, S. 1987. A fluid inclusion and stable isotope study of the St. Robert, W-Ag-Bi vein deposit, Eastern Townships, Quebec. Unpublished M.Sc. thesis, McGill University, Montréal, Québec, 112 p.

Černý, P. and Simpson, F.M. 1978. The Tanco pegmatite at Bernic Lake, Manitoba. X. Pollucite. The Canadian Mineralogist, 16, pp. 325–333.

Černý, P., Masau, M., Goad, B.E., and Ferreira, K. 2005. The Greer Lake leucogranite, Manitoba, and the origin of lepidolite-subtype granitic pegmatites. Lithos, 80, pp. 305–321. https://doi.org/10.1016/j.lithos.2003.11.003

Chai, G. and Naldrett, A.J. 1992. Characteristics of Ni-Cu-PGE mineralization and genesis of the Jinchuan deposit,

northwest China. Economic Geology, 87, pp. 1475–1495. https://doi.org/10.2113/gsecongeo.87.6.1475

Cheilletz, A. 1988. Stratiform tungsten deposits: a review. Geologie en Mijnbouw, 67, pp. 293–311.

Clow, G.G., Lecuyer, N.L., Rennie, D.W., and Scholey, B.J.Y. 2017. Technical report on the Eagle mine, Michigan, U.S.A. Report for Lundin Mining Corporation. URL <https://www.lundinmining.com/site/assets/files/3640/2017-04-26-eagle-ni-43-101.pdf> 17 June 2022

Coish, R.A. and Rogers, N.W. 1987. Geochemistry of the Boil Mountain ophiolitic complex, northwest Maine, and tectonic implications. Contributions to Mineralogy and Petrology, 97, pp. 51–65. https://doi.org/10.1007/BF00375214

Continental Nickel Limited. 2012. Press release: Continental Nickel reports new assays including 3.02% nickel and 0.56% copper over 3.65 metres at the St. Stephen nickel-copper sulphide project, New Brunswick. URL <https://www.kitco.com/pr/1267/article_05032012081321.pdf> 17 June 2022

Creasey, J.W. 1989. Geology and geochemistry of the Rattlesnake Mountain igneous complex, Raymond and Casco, Maine. *In* Studies in Maine geology; Volume 4 – Igneous and metamorphic geology. *Edited by* R.D. Tucker and R.G. Marvinney. Maine Geological Survey, Augusta, Maine, 4, pp. 63–78.

Cuney M. 2014. Felsic magmatism and uranium deposits. Bulletin de la Société Géologique de France, 185, pp. 75–92. https://doi.org/10.2113/gssgfbull.185.2.75

Ding, X., Li, C., Ripley, E.M., Rossell, D., and Kamo, S. 2010. The Eagle and East Eagle sulfide ore-bearing mafic-ultramafic intrusions in the Midcontinent Rift System, Upper Michigan: geochronology and petrologic evolution. Geochemistry, Geophysics, Geosystems, 11. https://doi.org/10.1029/2009GC002546

Ding, X., Ripley, E.M., and Li, C. 2012. PGE geochemistry of the Eagle Ni-Cu-(PGE) deposit, Upper Michigan: constraints on ore genesis in a dynamic magma conduit. Mineralium Deposita, 47, pp. 89–104. https://doi.org/10.1007/s00126-011-0350-y

Dorais, M.J. and Paige, M.L. 2000. Regional geochemical and isotopic variations of northern New England plutons: implications for magma sources and for Grenville and Avalon basement-terrane boundaries. Geological Society of America Bulletin, 112, pp. 900–914. https://doi.org/10.1130/0016-7606(2000)112<900:RGAIVO>2.0.CO;2

Dostal, J. 2016. Rare metal deposits associated with alkaline/peralkaline igneous rocks. Reviews in Economic Geology, 18, pp. 33–54. https://doi.org/10.5382/Rev.18.02

Duff, P.D., Shah, A., Wang, C., Whittaker, A.H., Slack, J.F., Marvinney, R., and Dickson, S. 2022. New airborne geophysical data illuminate Ordovician volcanic arc systems of northern Maine. Geological Society of America, Abstracts with Programs, 54(3). https://doi.org/10.1130/abs/2022NE-374972

Earl, K.M. and Eilertsen, N.A. 1962. Investigation of manganese deposits, Hodgdon and Linneus townships, southern district, Aroostook County, Maine. U.S. Bureau of Mines Report of Investigations 6119, 47 p.

Eby, G.N., Krueger, H.W., and Creasy, J.W. 1992. Geology, geochronology, and geochemistry of the White Mountain batholith, New Hampshire. *In* Eastern North America Mesozoic magmatism. *Edited by* J.H. Puffer and P.C. Ragland. Geological Society of America Special Paper 268, pp. 379–397. https://doi.org/10.1130/SPE268-p379

Economou-Eliopoulos, M. 1996. Platinum-group element distribution in chromite ores from ophiolite complexes: implications for their exploration. Ore Geology Reviews, 11, pp. 363–381. https://doi.org/10.1016/S0169-1368(96)00008-X

Eilertsen, N.A. 1952. Maple Mountain-Hovey Mountain manganese project, central district, Aroostook County, Maine. U.S. Bureau of Mines Report of Investigations 4921, 118 p., 5 plates.

Elongo, V., Lecumberri-Sanchez, P., Legros, H., Falck, H., Adlakha, E., and Roy-Garand, A. 2020. Paragenetic constraints on the Cantung, Mactung and Lened tungsten skarn deposits, Canada: implications for grade distribution. Ore Geology Reviews, 125, pp. 103677. https://doi.org/10.1016/j.oregeorev.2020.103677.

Emmons, W.H. 1910. Some ore deposits in Maine and the Milan mine in New Hampshire. U.S. Geological Survey Bulletin 432, 62 p. https://doi.org/10.5962/bhl.title.46275

Escayola, M., Garuti, G., Zaccarini, F., Proenza, J.A., Bédard, J.H., and van Staal, C. 2011. Chromitite and platinum-group element mineralization at Middle Arm Brook, central Advocate ophiolite complex, Baie Verte Peninsula, Newfoundland, Canada. The Canadian Mineralogist, 49, pp. 1523–1547. https://doi.org/10.3749/canmin.49.6.1523

Espenshade, G.H. 1972. Geology of the Moxie pluton in the Moosehead Lake–Jo-Mary Mountain area, Piscataquis County, Maine. U.S. Geological Survey Bulletin 1340, 40 p.

Foley, N., Southworth, S., Schultz, A.P., Ayuso, R.A., Robinson, G.R., and Seal, R.R. 2001. Geochemical, mineralogical, and environmental characteristics of metamorphosed black shales of the central Appalachians, with comparisons to metalliferous shales of the northern Appalachians. U.S. Geological Survey Open-File Report 01–406, pp. 111–114.

Foley, N.K., Hofstra, A.H., Lindsey, D.A., Seal, R.R. II, Jaskula, B., and Piatak, N.M. 2012. Occurrence model for volcanogenic beryllium. U.S. Geological Survey Scientific Investigations Report 2010–5070–F, 43 p. https://doi.org/10.3133/sir20105070F

Foley, N.K, Jaskula, B.W., Piatak, N.M., and Schulte, R.F. 2017. Beryllium. *In* Critical mineral resources of the United States—economic and environmental geology and prospects for future supply. *Edited by* K.J. Schulz, J.H. DeYoung Jr., R.R. Seal II, and D.C. Bradley. U.S. Geological Survey Professional Paper 1802–F, 39 p.

Foose, M.P. 1991. Deposits containing nickel, cobalt, chromium, and platinum-group elements in the United States.

In Economic geology, U.S. *Edited by* H.J. Gluskoter, D.D. Rice, and R.B. Taylor. Boulder, Colo., Geological Society of America, The Geology of North America, P–2, pp. 87–102. https://doi.org/10.1130/DNAG-GNA-P2.87

Foose, M.P. 1998. Platinum group element occurrence associated with the Boil Mountain ophiolite, west central Maine: a reconnaissance study. Geological Society of America Abstracts with Programs, 30(1), p. 19.

Force, E.R. and Cannon, W.F. 1988. Depositional model for shallow-marine manganese deposits around black shale basins. Economic Geology, 83, pp. 93–117. https://doi.org/10.2113/gsecongeo.83.1.93

Fortier, S.M., Thomas, C.L., McCullough, E.A., and Tolcin, A.C. 2017. Global trends in mineral commodities for advanced technologies. Natural Resources Research, 27, pp. 191–200. https://doi.org/10.1007/s11053-017-9340-9

Fortier, S.M., Nassar, N.T., Lederer, G.W., Brainard, J., Gambogi, J., and McCullough, E.A. 2018. Draft critical mineral list—summary of methodology and background information—U.S. Geological Survey technical input document in response to Secretarial Order No. 3359. U.S. Geological Survey Open-File Report 2018–1021, 15 p. https://doi.org/10.3133/ofr20181021

Fyffe, L.R. and Pickerill, R.K. 1993. Geochemistry of Upper Cambrian-Lower Ordovician black shale along a northeastern Appalachian transect. Geological Society of America Bulletin, 105, pp. 897–910. https://doi.org/10.1130/0016-7606(1993)105<0897:GOUCLO>2.3.CO;2

Fyffe, L.R. and Thorne, K.G. 2010. Polymetallic deposits of Sisson Brook and Mount Pleasant, New Brunswick, Canada. New Brunswick Department of Natural Resources, Field Guide No. 3, pp. 37–68.

Gambogi, J. 2021. Titanium mineral concentrates. U.S. Geological Survey mineral commodity summaries 2021, pp. 176–177.

Gates, O. and Moench, R.H. 1981. Bimodal Silurian and Lower Devonian volcanic rock assemblages in the Machias-Eastport area, Maine. U.S. Geological Survey Profession Paper 1184, 32 p. https://doi.org/10.3133/pp1184

Gauthier, M., Chartrand, F., and Trottier, J. 1994. Metallogenic epochs and metallogenic provinces of the Estrie-Beauce region, southern Quebec Appalachians. Economic Geology, 89, pp. 1322–1360. https://doi.org/10.2113/gsecongeo.89.6.1322

Gerbi, C.C., Johnson, S.E., Aleinikoff, J.N., Bédard, J.H., Dunning, G.R., and Fanning, C.M. 2006. Early Paleozoic development of the Maine-Quebec Boundary Mountains region. Canadian Journal of Earth Sciences, 43, pp. 367–389. https://doi.org/10.1139/e05-113

Gibert, F., Moine, B., Schott, J., and Dandurand, J.-L. 1992. Modeling of the transport and deposition of tungsten in the scheelite-bearing calc-silicate gneisses of the Montagne Noire, France. Contributions to Mineralogy and Petrology, 112, pp. 317–384. https://doi.org/10.1007/BF00310467

Gilman, R.A. 1989. Preliminary studies of five Mesozoic stocks in the Newfield 15′ quadrangle, Maine. *In* Studies in Maine geology; Volume 4 – Igneous and metamorphic geology. *Edited by* R.D. Tucker and R.G. Marvinney. Maine Geological Survey, Augusta, Maine, 4, pp. 79–86.

Gilman, R.A. 1991. Bedrock geology of the Newfield 15' quadrangle, Maine - New Hampshire. Maine Geological Survey, Augusta, Maine, Open-File Report 91–2, scale 1:62 500, 10 p.

Goldfarb, R.J., Hofstra, A.H., and Simmons, S.F. 2016. Critical elements in Carlin, epithermal, and orogenic gold deposits. Reviews in Economic Geology, 18, pp. 217–244. https://doi.org/10.5382/Rev.18.10

Goldfarb, R.J., Berger, B.R., George, M.W., and Seal, R.R. II. 2017. Tellurium. *In* Critical mineral resources of the United States—economic and environmental geology and prospects for future supply. *Edited by* K.J. Schulz, J.H. DeYoung Jr., R.R. Seal II, and D.C. Bradley. U.S. Geological Survey Professional Paper 1802–R, 27 p.

Grauch, R.I. and Zarinski, K. 1976. Generalized descriptions of uranium-bearing veins, pegmatites, and disseminations in non-sedimentary rocks, eastern United States. U.S. Geological Survey Open-File Report 76–582, 114 p. https://doi.org/10.3133/ofr76582

Green, C.J., Lederer, G.W., Parks, H.L., and Zientek, M.L. 2020. Grade and tonnage model for tungsten skarn deposits—2020 update. U.S. Geological Survey Scientific Investigations Report 2020–5085, 23 p. https://doi.org/10.3133/sir20205085

Griffin, J.R. 1971. Reconnaissance bedrock geology of the Stetson quadrangle, Maine. Maine Geological Survey Open-File Map 71–1, scale 1:62 500.

Grosz, A.E. 1987. Nature and distribution of potential heavy-mineral resources offshore of the Atlantic coast of the United States. Marine Mining, 6, pp. 339–357.

Guo, S., Chen, Y., Liu, C.-Z., Wang, J.-G., Su, B., Gao, Y.-J., Wu, F.-Y., Sein, K., Yang, Y.-H., and Mao, Q. 2016. Scheelite and coexisting F-rich zoned garnet, vesuvianite, fluorite, and apatite in calc-silicate rocks from the Mogok metamorphic belt, Myanmar: implications for metasomatism in marble and the role of halogens in W mobilization and mineralization. Journal of Asian Earth Sciences, 117, pp. 82–106. https://doi.org/10.1016/j.jseaes.2015.12.004

Hagemann, S.G., Lisitsin, V.A., and Huston, D.L. 2016. Mineral system analysis: quo vadis. Ore Geology Reviews, 76, pp. 504–522. https://doi.org/10.1016/j.oregeorev.2015.12.012

Harwood, D.S. 1973. Bedrock geology of the Cupsuptic and Arnold Pond quadrangles, west-central Maine. U.S. Geological Survey Bulletin 1346, 90 p., scale 1:62 500, 2 plates.

Hennessy, J.F. and Mossman, D.J. 1996. Geochemistry of Ordovician black shales at Meductic, southern Miramichi highlands, New Brunswick. Atlantic Geology, 32, pp. 233–245. https://doi.org/10.4138/2089

Hess, F.L. 1908. Molybdenum deposits of Maine. U.S. Geological Survey Bulletin 340–D, pp. 231–240.

Hill, P.L., Kucks, R.P., and Ravat, D. 2009. Aeromagnetic and aeroradiometric data for the conterminous United States and Alaska from the National Uranium Resource Evalu-

ation (NURE) program of the U.S. Department of Energy. U.S. Geological Survey Open-File Report 2009–1129: Connecticut, Maine, Massachusetts, New Hampshire, Rhode Island, and Vermont NURE aeromagnetic and aeroradiometric data. https://doi.org/10.3133/ofr20091129

Hillenbrand, I.W., Williams, M.L., Li, C., and Gao, H. 2021. Rise and fall of the Acadian altiplano: evidence for a Paleozoic orogenic plateau in New England. Earth and Planetary Science Letters, 560, pp. 116797. https://doi.org/10.1016/j.epsl.2021.116797.

Höll, R. and Eichhorn, R. 2000. Tungsten mineralization and metamorphic remobilization in the Felbertal scheelite deposit, Central Alps, Austria. Reviews in Economic Geology, 11, pp. 233–264.

Hollister, V.F., Potter, R.R., and Barker, A.L. 1974. Porphyry-type deposits of the Appalachian orogen. Economic Geology, 69, pp. 618–630. https://doi.org/10.2113/gsecongeo.69.5.618

Hon, R. 1976. Geology, petrology and geochemistry of Traveler Rhyolite and Katahdin pluton (northcentral Maine). Unpublished Ph.D. thesis, Massachusetts Institute of Technology, Cambridge, Massachusetts, 239 p.

Houston, R.S. 1956. Genetic study of some pyrrhotite deposits of Maine and New Brunswick. Maine Geological Survey Bulletin 7, 117 pp.

Hronsky, J.M.A., Groves, D.I., Loucks, R.R., Begg, G.C. 2012. A unified model for gold mineralisation in accretionary orogens and implications for regional-scale exploration targeting methods. Mineralium Deposita, 47, pp. 339–358. https://doi.org/10.1007/s00126-012-0402-y

Hu, A. and Peng, J. 2018. Fluid inclusions and ore precipitation mechanism in the giant Xikuangshan mesothermal antimony deposit, South China: conventional and infrared microthermometric constraints. Ore Geology Reviews, 95, pp. 49–64. https://doi.org/10.1016/j.oregeorev.2018.02.005

Huckriede, H. and Meischner, D. 1996. Origin and environment of manganese-rich sediments within black-shale basins. Geochimica et Cosmochimica Acta, 60, pp. 1399–1413. https://doi.org/10.1016/0016-7037(96)00008-7

Hussey, A.M. II, Rand, J.R., and Austin, M.B. (*Compilers*). 1958. Maine Geological Survey, Augusta, Maine, Minerals Resources Index No. 3, 53 p.

Jackson, C.T. 1838. Second annual report on the geology of the public lands, belonging to the two states of Maine and Massachusetts. Luther Severance, Augusta, Maine, 166 p.

Jaskula, B.W. 2021. Lithium. U.S. Geological Survey mineral commodity summaries 2021, pp. 98–99. https://pubs.usgs.gov/periodicals/mcs2021/mcs2021.pdf.

John, D.A. and Taylor, R.D. 2016. By-products of porphyry copper and molybdenum deposits. Reviews in Economic Geology, 18, pp. 137–164. https://doi.org/10.5382/Rev.18.07

John, D.A., Ayuso, R.A., Barton, M.D., Blakely, R.J., Bodnar, R.J., Dilles, J.H., Gray, Floyd, Graybeal, F.T., Mars, J.C., McPhee, D.K., Seal, R.R., Taylor, R.D., and Vikre, P.G. 2010. Porphyry copper deposit model. U.S. Geological Survey Scientific Investigations Report 2010–5070–B, 169 p.

John, D.A., Seal, R.R. II, and Polyak, D.E. 2017. Rhenium. *In* Critical mineral resources of the United States—economic and environmental geology and prospects for future supply. *Edited by* K.J. Schulz, J.H. DeYoung Jr., R.R. Seal II, and D.C. Bradley. U.S. Geological Survey Professional Paper 1802–P, 49 p.

John, D.A., Vikre, P.G., du Bray, E.A., Blakely, R.J., Fey, D.L., Rockwell, B.W., Mauk, J.L., Anderson, E.D., and Graybeal, F.T. 2018. Descriptive models for epithermal gold-silver deposits. U.S. Geological Survey Scientific Investigations Report 2010–5070–Q, 247 p. https://doi.org/10.3133/sir20105070Q

Johnson, S.Y., Otton, J.K., and Macke, D.L. 1987. Geology of the surficial uranium deposit of the north fork of Flodelle Creek, northeastern Washington. Geological Society of America Bulletin, 98, pp. 77–85. https://doi.org/10.1130/0016-7606(1987)98<77:GOTHSU>2.0.CO;2

Jones, J.V. III, Piatak, N.M., and Bedinger, G.M. 2017. Zirconium and hafnium. *In* Critical mineral resources of the United States—economic and environmental geology and prospects for future supply. *Edited by* K.J. Schulz, J.H. DeYoung, Jr., R.R. Seal II, and D.C. Bradley. U.S. Geological Survey Professional Paper 1802–V, 26 p.

Kamilli, R.J., Kimball, B.E., and Carlin, J.F. Jr. 2017. Tin. *In* Critical mineral resources of the United States—economic and environmental geology and prospects for future supply. *Edited by* K.J. Schulz, J.H. DeYoung Jr., R.R. Seal II, and D.C. Bradley. U.S. Geological Survey Professional Paper 1802–S, 53 p.

Kelley, J.T., Dickson, S.M., Lehmann, C., and Barnhardt, W.A. 1997. Sedimentary framework of the inner continental shelf of Maine with special emphasis on commercial quality sand and gravel deposits and potentially economic heavy mineral placers. Maine Geological Survey, Open-File Report 97–4, 31 p.

Kelley, J.T., Barnhardt, W.A., Belknap, D.F., Dickson, S.M., and Kelley, A.R. 1998. The seafloor revealed: the geology of the northwestern Gulf of Maine inner continental shelf. Maine Geological Survey, Open-File Report 96–6, 55 p.

Kelley, J.T., Dickson, S.M., Belknap, D.F., Barnhardt, W.A., and Barber, D.C. 2003. Sand volume and distribution on the paraglacial inner continental shelf of the northwestern Gulf of Maine. Journal of Coastal Research, 19, pp. 41–56.

Kelley, K.D., Scott, C.T., Polyak, D.E., and Kimball, B.E. 2017. Vanadium. *In* Critical mineral resources of the United States—economic and environmental geology and prospects for future supply. *Edited by* K.J. Schulz, J.H. DeYoung Jr., R.R. Seal II, and D.C. Bradley. U.S. Geological Survey Professional Paper 1802–U, 36 p.

Kilgore, C.C. and Thomas, P.R. 1982. Manganese availability—domestic. U.S. Bureau of Mines Information Circular 8889, 14 p.

King, N., Valorose, C., and Ellis, W., 2019. 2019 NI 43-101

mineral resource update for Graphite Creek, Seward Peninsula, Alaska, USA. Alaska Earth Sciences report, 258 p. Prepared for Graphite One Inc.

King, V.T. 2000. The Winslow tin mine. *In* Mineralogy of Maine. *Edited by* V.T. King. Maine Geological Survey, Augusta, Maine, 2, pp. 106–110.

King, V.T. and Foord, E.E. (*Editors*). 1994. Mineralogy of Maine. Volume 1. Descriptive mineralogy. Maine Geological Survey, Augusta, Maine, 418 p.

King, V.T. and Foord, E.E. 2000. Mineralogy of Maine—addenda to Volume 1. *In* Mineralogy of Maine. *Edited by* V.T. King. Maine Geological Survey, Augusta, Maine, 2, pp. 427–432.

Klasner, J.S., Snider, D.W., Cannon, W.F., and Slack, J.F. 1979. The Yellow Dog peridotite and a possible buried igneous complex of Lower Keweenawan age in the northern peninsula of Michigan. Michigan Department of Natural Resources, Report of Investigations 24, 31 p.

Kooiman, G.J.A., McLeod, M.J., and Sinclair, W.D. 1986. Porphyry tungsten-molybdenum orebodies, polymetallic veins and replacement bodies, and tin-bearing greisen zones in the Fire Tower zone, Mount Pleasant, New Brunswick. Economic Geology, 81, pp. 1356–1373. https://doi.org/10.2113/gsecongeo.81.6.1356

Kucks, R.P. 2005. Terrestrial radioactivity and gamma-ray exposure in the United States and Canada: gridded geographic images. URL <https://mrdata.usgs.gov/radiometric/> 20 October 2021.

Larsen, R.B. 1991. Tungsten skarn mineralizations in a regional metamorphic terrain in northern Norway: a possible metamorphic ore deposit. Mineralium Deposita, 26, pp. 281–289. https://doi.org/10.1007/BF00191075

Leake, R.C., Fletcher, C.J.N, Haslam, H.W., Khan, B., and Shakirullah. 1989. Origin and tectonic setting of stratabound tungsten mineralizations within the Hindu Kush of Pakistan. Journal of the Geological Society, 146, pp. 1003–1016. https://doi.org/10.1144/gsjgs.146.6.1003

Lentz, C., Thorne, K., McFarlane, C.R.M., and Archibald, D.A. 2020. U–Pb, Ar/Ar, and Re–Os geochronological constraints on multiple magmatic-hydrothermal episodes at the Lake George mine, central New Brunswick. Minerals, 10, pp. 566. https://doi.org/10.3390/min10060566

Lepage, C.A., Foley, M.E., and Thompson, W.B. 1991. Mining in Maine: past, present, and future. Maine Geological Survey, Augusta, Maine, Open-File 91–7, 9 p.

Li, C.-Y. 1942. Genesis of some ore deposits of southeastern Maine. Geological Society of America Bulletin, 53, pp. 15–52. https://doi.org/10.1130/GSAB-53-15

Lindsay, D., Prowse, N.D., DeDecker, J., Mitchell, A.J., and Kim, R.S.Y. 2021. NI 43-101 technical report on the Sib-Corey-North Mitchell property for Eskay Mining. URL <https://eskaymining.com/site/assets/files/3904/eskay_mining_corp_ni_43-101_final-compressed.pdf>

Lindsey, D.A., Ganow, H., and Mountjoy, W. 1973. Hydrothermal alteration associated with beryllium deposits at Spor Mountain, Utah. U.S. Geological Survey Professional Paper 818–A, 20 p. https://doi.org/10.3133/pp818A

Lippitt, C.R. 1984. Appalachian tin project, final report, Winslow/Cook Hill. Maine Geological Survey critical minerals database, ID # 132, 215 p.

Liu, T., Yu, L., Liu, J., Lu, J., Bi, X., Dai, A., Li, M., Li, M., Hu, Z., Ma, L., Luo, D., Zheng, J., Wu, T., Ren, Y., Wen, J., Pan, F., and Amine, K. 2021. Understanding Co roles towards developing Co-free Ni-rich cathodes for rechargeable batteries. Nature Energy, 6, pp. 277–286. https://doi.org/10.1038/s41560-021-00776-y

Loferski, P.J. and Ayuso, R.A. 1995. Petrography and mineral chemistry of the composite Deboullie pluton, northern Maine, U.S.A.: implications for the genesis of Cu-Mo mineralization. Chemical Geology, 123, pp. 89–105. https://doi.org/10.1016/0009-2541(95)00040-S

Ludman, A. and Hill, M. 1990. Bedrock geology of the Calais 15′ quadrangle, eastern Maine. Maine Geological Survey, Open-File No. 90–27, 32 p.

Ludman, A., Aleinikoff, J., Berry, H.N. IV, and Hopeck, J.T. 2018. SHRIMP U–Pb zircon evidence for age, provenance, and tectonic history of early Paleozoic Ganderian rocks, east-central Maine, USA. Atlantic Geology, 54, pp. 335–387. https://doi.org/10.4138/atlgeol.2018.012

Luepke, G. and Grosz, A.E. 1986. Distribution of economic heavy minerals in sediments of Saco Bay, Maine. U.S. Geological Survey Bulletin 1681, 12 p.

Luganov, V.A., Chepushtanova, T.A., Guseynova, G.D., Merkibayev, Y.S., Mamyrbaeva, K.K., and Mishra, B. 2020. Processing of pyrite concentrates with the extraction of non-ferrous metals: nickel and cobalt technology elaboration. Sustainable Extraction and Processing of Raw Materials Journal, 1, pp. 53–58.

MacMillan, R.T. and Turner, T.L. 1954. Recovery of manganese from ores of Aroostook County, Maine. U.S. Bureau of Mines Report of Investigations 5082, 24 p.

Manganese X Energy Corporation. 2021. Press release, 10 March 2021. URL <https://www.manganesexenergycorp.com> 12 March 2021.

Marvinney, R.G. 2015. Overview of Maine metallic mineral deposits and mining. Maine Geological Survey Circular 15–9, 13 p. including state map.

Marvinney, R.G. and Berry, H.N. IV. 2015. Legacy mines in Maine. Maine Geological Survey, Circular 15–10, 9 p.

McCormick, M. 2021. Geology and lithogeochemistry of the Pickett Mountain volcanogenic massive sulfide deposit, northern Maine. Unpublished M.S. thesis, University of Maine, Orono, Maine, 205 p.

McGroarty, D. and Wirtz, S. 2012. Reviewing risk: critical minerals & national security. American Resources Policy Network, 34 p. URL <https://www.americanresources.org/wp-content/uploads/2012/06/ARPN_Quarterly_Report_WEB.pdf> 20 March 2022.

MEDHHS. 2021. Maine tracking network private well water data. URL <https://data.mainepublichealth.gov/tracking/data-topics/privatewells> 26 October 2021.

Meinert, L.D. 2000. Skarns and skarn deposits. Geoscience Canada, 19, pp. 145–162.

Merrill, A. 2021a. Bismuth. U.S. Geological Survey mineral

commodity summaries 2021, pp. 34–35.
Merrill, A. 2021b. Tin. U.S. Geological Survey Mineral Commodity Summaries 2021, pp. 172–173.
Miller, R.L. 1945. Geology of the Katahdin pyrrhotite deposit and vicinity, Piscataquis County, Maine. Maine Geological Survey Bulletin 2, 21 p., 5 plates. https://doi.org/10.3133/ofr4461
Miller, R.L. 1947. Manganese deposits of Aroostook County, Maine. Maine Geological Survey Bulletin 4, 77 p.
Min, M., Fang, C., and Fayek, M. 2005. Petrography and genetic history of coffinite and uraninite from the Liueryiqi granite-hosted uranium deposit, SE China. Ore Geology Reviews, 26, pp. 187–197. https://doi.org/10.1016/j.oregeorev.2004.10.006
Mindat.org. 2021. Basin locality, Phippsburg, Sagadahoc Co., Maine, USA. URL <https://www.mindat.org/loc-3807.html> 17 June 2022.
Mining Technology. 2018. Aura Energy confirms new vanadium zone at Häggån project. URL <https://www.mining-technology.com/news/aura-energy-confirms-new-vanadium-zone-at-haggan-project/> 17 June 2022.
Moench, R.H., Boone, G.M., Bothner, W.A., Boudette, E.L., Hatch, N.L., Jr., Hussey, A.M., II, Marvinney, R.G., and Aleinikoff, J.N. 1995. Geologic map of the Sherbrooke-Lewiston area, Maine, New Hampshire, and Vermont, United States, and Quebec, Canada. U.S. Geological Survey Miscellaneous Investigations Series Map I–1898–D, scale 1:250 000.
Moench, R.H., Boudette, E.L., and Bothner, W.A. 1999. Tectonic lithofacies, geophysical, and mineral-resource appraisal maps of the Sherbrooke-Lewiston area, Maine, New Hampshire, and Vermont, United States, and Quebec, Canada. U.S. Geological Survey Miscellaneous Investigations Series Map I–1898–E, pamphlet, 107 p.
Mohammadi, N., Lentz, D.R., McFarlane, C.R.M., and Cousens, B. 2020. Geochemistry of the highly evolved Sn-W-Mo-bearing Mount Douglas granite, New Brunswick, Canada: implications for origin and mineralization. Ore Geology Reviews, 117. https://doi.org/10.1016/j.oregeorev.2019.103266.
Monecke, T., Petersen, S., Hannington, M.D., Grant, H., and Samson, I.M. 2016. The minor element endowment of modern sea-floor massive sulfides and comparison with deposits hosted in ancient volcanic successions. Reviews in Economic Geology, 18, pp. 245–306. https://doi.org/10.5382/Rev.18.11
Morrill, P. 1958. Maine mines and minerals; Volume 1, western Maine. Winthrop Minerals Shop, Winthrop, Maine, 81 p.
Morrill, P. and Hinckley, W.P. 1959. Maine mines and minerals; Volume 2, eastern Maine. Winthrop Minerals Shop, Winthrop, Maine, 80 p.
Mosier, D.L., Singer, D.A., Moring, B.C., and Galloway, J.P. 2012. Podiform chromite deposits—database and grade and tonnage models. U.S. Geological Survey Scientific Investigations Report 2012–5157, 45 p. https://doi.org/10.3133/sir20125157
Naldrett, A.J. 1989. Magmatic sulfide deposits. Oxford University Press, Oxford, U.K., 186 p.
Naldrett, A.J. 1992. A model for the Ni-Cu-PGE ores of the Noril'sk region and its application to other areas of flood basalt. Economic Geology, 87, pp. 1945–1962. https://doi.org/10.2113/gsecongeo.87.8.1945
Nevada Vanadium Mining Corp. 2022. Gibellini (vanadium). URL <https://www.nevadavanadium.com/> 17 June 2022.
Newberry, R.J. 1982. Tungsten-bearing skarns of the Sierra Nevada. I. The Pine Creek mine, California. Economic Geology, 77, pp. 823–844. https://doi.org/10.2113/gsecongeo.77.4.823
Northcliff Resources Ltd. 2022. Sisson tungsten-molybdenum project, New Brunswick, Canada. Includes data from NI 43-101 report of 29 January 2013. URL <https://northcliffresources.com/s/Development.asp.html> 17 June 2022.
Norton, S.A. 1990. Geochemistry of selected Maine peat deposits. Maine Geological Survey Bulletin 34, 39 p.
Norton, S.A., Hess, C.T., and Brutsaert, W.F. 1989. Radon, geology, and human health in Maine. *In* Studies in Maine geology; Volume 5 – Quaternary geology. *Edited by* R.D. Tucker and R.G. Marvinney. Maine Geological Survey, Augusta, Maine, 5, pp. 169–176.
Nowlan, G.A. 1989. Stream-sediment geochemistry of the Attean quartz monzonite and nearby rocks, Somerset and Franklin Counties, Maine. *In* Studies in Maine geology; Volume 3 – Igneous and metamorphic geology. *Edited by* R.D. Tucker and R.G. Marvinney. Maine Geological Survey, Augusta, Maine, 3, pp. 111–130.
Nowlan, G.A. and Hessin, T.D. 1972. Molybdenum, arsenic, and other elements in stream sediments, Tomah Mountain, Topsfield, Maine. U.S. Geological Survey Open-File Report 1766, 18 p. https://doi.org/10.3133/ofr72273
Nowlan, G.A., Canney, F.C., Howd, F.H., and Domenico, J.A. 1987. Regional geochemical studies in parts of Maine, New Hampshire and Vermont, U.S.A. Journal of Geochemical Exploration, 29, pp. 129–150. https://doi.org/10.1016/0375-6742(87)90074-4
Nowlan, G.A., Canney, F.C., Howd, F.H., and Domenico, J.A. 1990a. Maps showing the distribution of chromium, molybdenum, and uranium in stream sediments, Sherbrooke and Lewiston 1° × 2° quadrangles, Maine, New Hampshire, and Vermont. U.S. Geological Survey Miscellaneous Investigations Series Map I–1898–A, 2 sheets, scale 1:250 000.
Nowlan, G.A., Howd, F.A., Canney, F.C., and Domenico, J.A. 1990b. Maps showing the distribution of tin, tungsten, arsenic, gold, and silver in non-magnetic concentrates derived from stream sediments, Sherbrooke and Lewiston 1° × 2° quadrangles, Maine, New Hampshire, and Vermont. U.S. Geological Survey Miscellaneous Investigations Series Map I–1898–C, 2 sheets, scale 1:250 000.
Okita, P.M. 1992. Manganese carbonate mineralization in

the Molango district, Mexico. Economic Geology, 87, pp. 1345–1366. https://doi.org/10.2113/gsecongeo.87.5.1345

Okita, P.M. and Shanks, W.C. III. 1992. Origin of stratiform sediment-hosted manganese carbonate ore deposits: examples from Molango, Mexico, and TaoJiang, China. Chemical Geology, 99, pp. 139–164. https://doi.org/10.1016/0009-2541(92)90036-5

Okita, P.M., Maynard, J.D., Spiker, E.C. and Force, E.R. 1988. Isotopic evidence for organic matter oxidation by manganese reduction in the formation of stratiform manganese carbonate ore. Geochimica et Cosmochimica Acta, 52, pp. 2679–2685. https://doi.org/10.1016/0016-7037(88)90036-1

Osberg, P.H., Hussey, A.M. II, and Boone, G.M. 1985. Bedrock geologic map of Maine. Maine Geological Survey, Augusta, Maine, scale 1:500 000.

Page, L.R. 1980. Guides to prospecting for uranium and thorium in New Hampshire and adjacent areas. U.S. Geological Survey Open-File Report 80–657, 23 p. https://doi.org/10.3133/ofr80657

Paktunc, A.D. 1986. St. Stephen mafic-ultramafic intrusion and related nickel-copper deposits, New Brunswick. Geological Survey of Canada, Current Research Paper 86–1A, pp. 327–331. https://doi.org/10.4095/120381

Paktunc, A.D. 1987. Nickel, copper, platinum and palladium relations in Ni-Cu deposits of the St. Stephen intrusion, New Brunswick. Geological Survey of Canada, Current Research Paper 87–1A, pp. 543–553. https://doi.org/10.4095/122475

Paktunc, A.D. 1990. Comparative geochemistry of platinum-group elements of nickel-copper sulfide occurrences associated with mafic-ultramafic intrusions in the Appalachian orogen. Journal of Geochemical Exploration, 37, pp. 101–111. https://doi.org/10.1016/0375-6742(90)90085-O

Pavlides, L. 1962. Geology and manganese deposits of the Maple and Hovey Mountains area, Aroostook County, Maine. U.S. Geological Survey Professional Paper 362, 116 p. https://doi.org/10.3133/pp362

Pavlides, L. and Canney, F.C. 1964. Geological and geochemical reconnaissance, southern part of the Smyrna Mills quadrangle, Aroostook County, Maine. U.S. Geological Survey 475–D, pp. D96–D99.

Pedersen, R.-B., Johannesen, G.M., and Boyd, R. 1993. Stratiform platinum-group element mineralizations in the ultramafic cumulates of the Leka ophiolite complex, central Norway. Economic Geology, 88, pp. 782–803. https://doi.org/10.2113/gsecongeo.88.4.782

Peter, J.M. and Scott, S.D. 1999. Windy Craggy, northwestern British Columbia—the world's largest Besshi-type deposit. Reviews in Economic Geology, 8, pp. 261–295.

Phenom Resources Corp. 2021. Carlin gold-vanadium. URL <https://phenomresources.com/index.php/projects/carlin-gold-vanadium> 17 June 2022.

Piñán Llamas, A. and Hepburn, C. 2013. Geochemistry of Silurian-Devonian volcanic rocks in the Coastal volcanic belt, Machias-Eastport area, Maine: evidence for a pre-Acadian arc. Geological Society of America Bulletin, 125, pp. 1930–1942. https://doi.org/10.1130/B30776.1

Pinette, S.R. and Osberg, P.H. 1989. Geochemical aspects of volcanic rocks on islands in east Penobscot Bay, Maine. *In* Studies in Maine geology; Volume 3 – Igneous and metamorphic geology. *Edited by* R.D. Tucker and R.G. Marvinney. Maine Geological Survey, Augusta, Maine, 3, pp. 91–110.

Pirajno, F. 1999. Past achievements and future challenges in the use of mineral deposit models, regional tectonics, and metallogeny in mineral exploration. South African Journal of Geology, 102, pp. 123–138.

Polgári, M., Okita, P.M., and Hein, J.R. 1991. Stable isotope evidence for the origin of the Úrkút manganese ore deposit, Hungary. Journal of Sedimentary Petrology, 61, pp. 384–393. https://doi.org/10.1306/D426771C-2B26-11D7-8648000102C1865D

Polgári, M., Hein, J.R., Vigh, T., Szabó-Drubina, M., Fórizs, I., Bíró, L, Müller, A., and Tóth, A.L. 2012. Microbial processes and the origin of the Úrkút manganese deposit, Hungary. Ore Geology Reviews, 47, pp. 87–109. https://doi.org/10.1016/j.oregeorev.2011.10.001

Post, E.V., Lehmbeck, W.L., Dennen, W.H., and Nowlan, G.A. 1967. Map of southeastern Maine showing heavy metals in stream sediments. U.S. Geological Survey Mineral Investigations Field Studies Map MF–301, scale 1:250 000.

Presidential Executive Order No. 13817. 2017. A federal strategy to ensure secure and reliable supplies of critical minerals. U.S. Federal Register, 82 (246), 3 pp. URL <https://www.govinfo.gov/content/pkg/FR-2017-12-26/pdf/2017-27899.pdf>

Price, J.G. 2013. The challenges of mineral resources for society. *In* The impact of the geological sciences on society. *Edited by* M.E. Bickford. Geological Society of America Special Paper 501, pp. 1–19. https://doi.org/10.1130/2013.2501(01)

Prichard, H.M. and Brough, C. 2009. Potential of ophiolite complexes to host PGE deposits. *In* New developments in magmatic Ni-Cu and PGE deposits. *Edited by* C. Li and E.M. Ripley. Geological Publishing House, Beijing, pp. 277–290.

QEM Limited. 2021. The Julia Creek vanadium/oil shale project. URL <https://www.qldem.com.au/project/> 17 June 2022.

Rainville, G.D. and Park, W.C. 1976. Nickeliferous pyrrhotite deposits, Knox County, southeastern Maine. *In* Studies in New England geology. *Edited by* P.C. Lyons and A.H. Brownlow. Geological Society of America Memoir 146, pp. 319–347. https://doi.org/10.1130/MEM146-p319

Raith, J.G. 1988. Tourmaline rocks associated with stratabound scheelite mineralization in the Austroalpine crystalline complex, Austria. Mineralogy and Petrology, 39, pp. 265–288. https://doi.org/10.1007/BF01163040

Raith, J.G. and Prochaska, W. 1995. Tungsten deposits in the Wolfram Schist, Namaqualand, South Africa: strata-bound versus granite-related genetic concepts.

Economic Geology, 90, pp. 1934–1954. https://doi.org/10.2113/gsecongeo.90.7.1934

Raith, J.G. and Stein, H.J. 2006. Variscan ore formation and metamorphism at the Felbertal scheelite deposit (Austria): constraining tungsten mineralisation from Re–Os dating of molybdenite. Contributions to Mineralogy and Petrology, 152, pp. 505–521. https://doi.org/10.1007/s00410-006-0118-z

Rassios, A., Tzamos, E., Dilek, Y., Bussolesi, M., Grieco, G., Batsi, A., and Gamaletsos, P.N. 2020. A structural approach to the genesis of chrome ores within the Vourinos ophiolite (Greece): significance of ductile and brittle deformation processes in the formation of economic ore bodies in oceanic upper mantle peridotites. Ore Geology Reviews, 125, pp. 103684 https://doi.org/10.1016/j.oregeorev.2020.103684

Reusch, D.N. 2002. Tectonic evolution of the Ellsworth terrane. Unpublished field guide for Geological Society of Maine Summer Field Trip, August 2-4, 2002, 13 figures, 16 p.

Robinson, G.R., Hammarstrom, J.M., and Olson, D.W. 2017. Graphite. *In* Critical mineral resources of the United States—economic and environmental geology and prospects for future supply. *Edited by* K.J. Schulz, J.H. DeYoung Jr., R.R. Seal II, and D.C. Bradley. U.S. Geological Survey Professional Paper 1802–J, 24 p.

Roda-Robles, E., Simmons, W., Pesquera, A., Gil-Crespo, P. P., Nizamoff, J., Torres-Ruiz, J. 2015. Tourmaline as a petrogenetic monitor of the origin and evolution of the Berry-Havey pegmatite (Maine, USA). American Mineralogist, 100, pp. 95–109. https://doi.org/10.2138/am-2015-4829

Rospabé, M., Ceuleneer, G., Granier, N., Arai, S., and Borisova, A.Y. 2019. Multi-scale development of a stratiform chromite ore body at the base of the dunitic mantle-crust transition zone (Maqsad diapir, Oman ophiolite): the role of repeated melt and fluid influxes. Lithos, pp. 350–351, https://doi.org/10.1016/j.lithos.2019.105235.

Schaaf, R.E. 1985. Big Hill deposit Pembroke, Maine, U.S.A., summary evaluation. Unpublished report for Scintilore Explorations Ltd.

Schmidt, R.G. 1974, Preliminary study of rock alteration in the Catheart Mountain molybdenum-copper deposit, Maine. U.S. Geological Survey Journal of Research, 2, pp. 189–194.

Schmidt, R.G. 1978. The potential for porphyry copper-molybdenum deposits in the eastern United States. U.S. Geological Survey Professional Paper 907–E, 31 p. https://doi.org/10.3133/pp907E

Schulz, K.J., Stewart, D.B., Tucker, R.D., Pollock, J.C., and Ayuso, R.A. 2008. The Ellsworth terrane, coastal Maine: geochronology, geochemistry, and Nd-Pb isotopic composition—implications for the rifting of Ganderia. Geological Society of America Bulletin, 120, pp. 1134–1158. https://doi.org/10.1130/B26336.1

Schulz, K.J., Woodruff, L.G., Nicholson, S.W., Seal, R.R. II, Piatak, N.M., Chandler, V.W., and Mars, J.L. 2014. Occurrence model for magmatic sulfide-rich nickel-copper-(platinum-group element) deposits related to mafic and ultramafic dike-sill complexes. U.S. Geological Survey Scientific Investigations Report 2010–5070–I, 80 p. https://doi.org/10.3133/sir20105070I

Schulz, K.J., Piatak, N.M., and Papp, J.F. 2017. Niobium and tantalum. *In* Critical mineral resources of the United States—economic and environmental geology and prospects for future supply. *Edited by* K.J. Schulz, J.H. DeYoung Jr., R.R. Seal II, and D.C. Bradley. U.S. Geological Survey Professional Paper 1802–M, 34 p. https://doi.org/10.3133/pp1802

Scratch, R.B., Watson, G.P., Kerrich, R., and Hutchinson, R.W. 1984. Fracture-controlled antimony-quartz mineralization, Lake George deposit, New Brunswick: mineralogy, geochemistry, alteration, and hydrothermal regimes. Economic Geology, 79, pp. 1159–1186. https://doi.org/10.2113/gsecongeo.79.5.1159

Seal, R.R. II, Clark, A.H., and Morrissy, C.J. 1988. Lake George, southwestern New Brunswick––a Silurian, multi-stage, polymetallic (Sb-W-Mo-Au-base metal) hydrothermal centre. *In* Recent advances in the geology of granite-related mineral deposits. *Edited by* R.P. Taylor and D.F. Strong. Canadian Institute of Mining and Metallurgy, Special Volume 39, pp. 252–264.

Seal, R.R. II, Schulz, K.J., and DeYoung, J.H. Jr. 2017. Antimony. *In* Critical mineral resources of the United States—economic and environmental geology and prospects for future supply. *Edited by* K.J. Schulz, J.H. DeYoung Jr., R.R. Seal II, and D.C. Bradley. U.S. Geological Survey Professional Paper 1802–C, 17 p.

Seaman, S.J., Scherer, E.E., Wobus, R.A., Zimmer, J.H., and Sales, J.G. 1999. Late Silurian volcanism in coastal Maine: the Cranberry Island Series. Geological Society of America Bulletin, 111, pp. 686–708. https://doi.org/10.1130/0016-7606(1999)111<0686:LSVICM>2.3.CO;2

Seaman, S.J., Hon, R., Whitman, M., Wobus, R.A., Hogan, J.P., Chapman, M., Koteas, G.C., Rankin, D., Piñán-Llamas, A., and Hepburn, J.C. 2019. Late Paleozoic supervolcano-scale eruptions in Maine, USA. Geological Society of America Bulletin, 131, pp. 1995–2010. https://doi.org/10.1130/B32058.1

Shah, A.K., Morrow, R.H. IV, Pace, M.D., Harris, M.S., and Doar, W.R. III. 2021. Mapping critical minerals from the sky. GSA Today, 31, pp. 4–10. https://doi.org/10.1130/GSATG512A.1

Shainin, V. and Dellwig, L.F. 1955. Pegmatites and associated rocks in the Newry Hill area, Oxford County, Maine. Maine Geological Survey Bulletin 6, 58 p.

Shanks, W.C. III and Thurston, R., eds. 2012. Volcanogenic massive sulfide occurrence model. U.S. Geological Survey Scientific Investigations Report 2010–5070–C, 345 p.

Simandl, L., Simandl, G.J., and Paradis, S. 2021. Economic geology models 5. Specialty, critical, battery, magnet and photovoltaic materials: market facts, projections and implications for exploration and development. Geoscience Canada, 48, pp. 73–91. https://doi.org/10.12789/geo-

canj.2021.48.174

Simandl, G.J., Paradis, S., and Akam, C. 2015. Graphite deposit types, their origin, and economic significance. *In* Symposium on strategic and critical minerals proceedings. *Edited by* G.J. Simandl and M. Neetz. British Columbia Geological Survey Paper 2015–3, pp. 163–171.

Simmons, W.B., Falster, A.U., Webber, K., Roda-Robles, E., Boudreaux, A.P., Grassi, L.R., and Freeman, G. 2016. Bulk composition of Mt. Mica pegmatite, Maine, USA: implications for the origin of an LCT type pegmatite by anatexis. The Canadian Mineralogist, 54, pp. 1053–1070. https://doi.org/10.3749/canmin.1600017

Simmons, W.B., Falster, A.U., and Freeman, G. 2020. The Plumbago North pegmatite, Maine, USA: a new potential lithium resource. Mineralium Deposita, 55, pp. 1505–1510. https://doi.org/10.1007/s00126-020-00956-y

Singer, D. and Menzie, D.W. 2010. Quantitative mineral resource assessments: an integrated approach. Oxford University Press, Oxford, U.K., 232 p. https://doi.org/10.1093/oso/9780195399592.001.0001

Slack, J.F. 1990. Preliminary assessment of metallic mineral resources in the Glens Falls 1° x 2° quadrangle, New York, Vermont, and New Hampshire. U.S. Geological Survey Bulletin 1887–R, pp. R1–R26.

Slack, J.F. 2019. Metallic mineral deposits of New England: historical overview, known deposits, and potential undiscovered resources. Geological Society of America Abstracts with Programs 51(1). https://doi.org/10.1130/abs/2019NE-327914

Slack, J.F. 2021. Potential for critical mineral deposits in Maine with applications to the Maritimes. Atlantic Geoscience Society, 47th Colloquium and Annual Meeting, Atlantic Geoscience, 57, p 132. https://doi.org/10.4138/atlgeol.2021.006

Slack, J.F. 2022. Application of ore deposit models for critical mineral assessments: examples from Maine, USA. Atlantic Geoscience Society, 48th Colloquium and Annual Meeting, Fredericton, New Brunswick. Atlantic Geoscience, 58, p 30. https://doi.org/10.4138/atlgeo.2022.001

Slack, J.F., Foose, M.P., Flohr, M.J.K., Scully, M.V., and Belkin, H.E. 2003. Exhalative and subseafloor replacement processes in the formation of the Bald Mountain massive sulfide deposit, northern Maine. *In* Volcanogenic massive sulfide deposits of the Bathurst district, New Brunswick, and northern Maine. *Edited by* W.D. Goodfellow, S.R. McCutcheon, and J.M. Peter. Economic Geology Monograph 11, pp. 513–548. https://doi.org/10.5382/Mono.11.23

Slack, J.F., Kimball, B.E., and Shedd, K.B. 2017. Cobalt. *In* Critical mineral resources of the United States—economic and environmental geology and prospects for future supply. *Edited by* K.J. Schulz, J.H. DeYoung, Jr., R.R. Seal II, and D.C. Bradley. U.S. Geological Survey Professional Paper 1802–E, 32 p.

Slack, J.F., Van Baalen, M., and Reusch, D.R. 2020. Regional geochemical variations in a metamorphosed black shale: a reconnaissance study of the Silurian Smalls Falls Formation, Maine, USA. Atlantic Geology, 56, pp. 231–255. https://doi.org/10.4138/atlgeol.2020.010

Smith, D.B., Cannon, W.F., Woodruff, L.G., Solano, F. and Ellefsen, K.J. 2014. Geochemical and mineralogical maps for soils of the conterminous United States. U.S. Geological Survey Open-File Report 2014–1082, 386 p. https://doi.org/10.3133/ofr20141082

Smith, G.O. 1906. Graphite in Maine. U.S. Geological Survey Bulletin 285, pp. 480–483.

Smith, S.M. 1997. Brief history and description of Portland quadrangle data, NURE HSSR program. U.S. Geological Survey Open-File Report 97–492. https://pubs.usgs.gov/of/1997/ofr-97-0492/quad/q_portln.htm.

Solar, G.S. and Tomascak, P.B. 2016. The migmatite-granite complex of southern Maine: its structure, petrology, geochemistry, geochronology, and relation to the Sebago pluton. *In*: Guidebook for field trips along the Maine coast from Maquoit Bay to Muscongus Bay. *Edited by* HN Berry, IV and DP West, Jr. New England Intercollegiate Geological Conference, 108th Annual Meeting, pp. 19–42.

Song, X.-Y., Keays, R.R., Zhou, M.-F., Qi, L., Ihlenfeld, C., and Xiao, J.-F. 2009. Siderophile and chalcophile elemental constraints on the origin of the Jinchuan Ni-Cu-(PGE) sulfide deposit, NW China. Geochimica et Cosmochimica Acta, 73, pp. 404–424. https://doi.org/10.1016/j.gca.2008.10.029

Sovacool, B.K., Ali, S.H., Bazilian M., Radley, B., Nemery, B., Okatz, J., and Mulvaney, D. 2020. Sustainable minerals and metals for a low-carbon future. Science, 367, pp. 30–33. https://doi.org/10.1126/science.aaz6003

Stewart, D.B., 1998, Geology of northern Penobscot Bay, Maine. U.S. Geological Survey Miscellaneous Investigations Series Map I-2551, scale 1:62 500.

Sundelius, H.W. 1963. The Peg Claims spodumene pegmatites, Maine. Economic Geology, 58, pp. 84–106. https://doi.org/10.2113/gsecongeo.58.1.84

Ténière, P., Harrington, M., Warkentin, D., and Elgert, L. 2021. Battery Hill project mineral resource estimate, Woodstock area, New Brunswick, Canada. Mercātor Geological Services, NI 43-101 technical report for Manganese X Energy Corporation, 133 p.

Thompson, J.F.H. 1984. Acadian synorogenic mafic intrusions in the Maine Appalachians. American Journal of Science, 284, pp. 463–483. https://doi.org/10.2475/ajs.284.4-5.462

Thompson, W.B. and Borns, H.W., Jr. (*Editors*). 1985. Surficial geologic map of Maine. Maine Geological Survey, scale 1:500 000.

Tomascak, P.B., Krogstad, E.J., and Walker, R.J. 1996. Nature of the crust in Maine, USA: evidence from the Sebago batholith. Contributions to Mineralogy and Petrology, 125, pp. 45–59. https://doi.org/10.1007/s004100050205

Tomascak, P.B., Krogstad, E.J., Walker, R.J. 1998. Sm–Nd isotope systematics and the derivation of granitic pegmatites in southwestern Maine. The Canadian Mineralogist, 36, pp. 327–337.

Trefethen, J.M., Allen, H., and Forsyth, W. 1955. Scheelite occurrences in Maine. Maine Development Commission,

Report of the State Geologist, 1953–1954, pp. 63–69.
Trueman, D.L. and Černý, P. 1982. Exploration for rare-element granitic pegmatites. Mineralogical Association of Canada, Short Course Handbook, 8, pp. 463–493.
Tsoupas, G. and Economou-Eliopoulos, M. 2008. High PGE contents and extremely abundant PGE-minerals hosted in chromitites from the Veria ophiolite complex, northern Greece. Ore Geology Reviews, 33, pp. 3–19. https://doi.org/10.1016/j.oregeorev.2006.10.008
Tuck, C. 2021. Cesium. U.S. Geological Survey mineral commodity summaries 2021, pp. 44–45. URL <https://pubs.usgs.gov/periodicals/mcs2021/mcs2021.pdf>
U.S. Geological Survey. 2021a. Mineral resources data system. URL <https://mrdata.usgs.gov/mrds/>
U.S. Geological Survey. 2021b. U.S. Geological Survey mineral commodity summaries 2021. URL <https://pubs.usgs.gov/periodicals/mcs2021/mcs2021.pdf>
U.S. Geological Survey. 2022. List of critical minerals. URL <https://www.usgs.gov/news/national-news-release/us-geological-survey-releases-2022-list-critical-minerals> 17 June 2022.
Van Gosen, B.S., Fey, D.L., Shah, A.K., Verplanck, P.L., and Hoefen, T.M. 2014. Deposit model for heavy-mineral sands in coastal environments. U.S. Geological Survey Scientific Investigations Report 2010–5070–L, 51 p. https://doi.org/10.3133/sir20105070L
Van Gosen, B.S., Verplanck, P.L., Seal, R.R. II, Long, K.R., and Gambogi, J. 2017. Rare-earth elements. *In* Critical mineral resources of the United States—economic and environmental geology and prospects for future supply. *Edited by* K.J. Schulz, J.H. DeYoung, Jr., R.R. Seal II, and D.C. Bradley. U.S. Geological Survey Professional Paper 1802–O, 31 p. https://doi.org/10.3133/pp1802O
Visher, G.S. 1960. The geology of the Moxie pluton, west-central Maine. Unpublished Ph.D. thesis, Northwestern University, Evanston, Illinois, 137 p.
Wang, C., Ludman, A., and Wiao, L.X. 2014. The Turner Mountain syenite, Maine, USA: geology, geochemistry, geochronology, petrogenesis, and post-orogenic exhumation. Atlantic Geology, 50, pp. 233–248. https://doi.org/10.4138/atlgeol.2014.012
Way, B. 2014. Stratigraphic and paleoenvironmental setting of the Woodstock Fe-Mn deposits in west-central New Brunswick. Geological Association of Canada/Mineralogical Association of Canada, Joint Annual Meeting, Field Trip Guidebook, Trip B10, 37 p.
Webber, K.L., Simmons, W.B., Falster, A.U., and Hanson, S.L. 2019. Anatectic pegmatites of the Oxford County pegmatite field, Maine, USA. The Canadian Mineralogist, 57, pp. 811–815. https://doi.org/10.3749/canmin.AB00028
West, D.P., Jr. and Ellenberger, E.D. 2010. Bedrock geology of the Purgatory 7.5′ quadrangle, Maine. Maine Geological Survey Open File Map 10–21, scale 1:24 000.
West, D.P. Jr., Tomascak, P.B., Coish, R.A., Yates, M.G., and Reilly, M.J. 2007. Petrogenesis of the ultrapotassic Lincoln Syenite, Maine: Late Silurian-Early Devonian melting of a source region modified by subduction driving metasomatism. American Journal of Science, 307, pp. 265–310. https://doi.org/10.2475/01.2007.08
West, D.P. Jr., Bradley, D.C., and Coish, R.A. 2016. The Litchfield pluton in south-central Maine: Carboniferous alkalic magmatism in northern New England. Atlantic Geology, 52, pp. 169–187. https://doi.org/10.4138/atlgeol.2016.008
White, W.S. 1943. Occurrence of manganese in eastern Aroostook County, Maine. U.S. Geological Survey Bulletin 940–E, pp. 125–161. https://doi.org/10.3133/ofr4347
Wilson, R.A. and Kamo, S.L. 2016. Geochronology and lithogeochemistry of granitoid rocks from the central part of the central plutonic belt, New Brunswick, Canada: implications for Sn-W-Mo exploration. Atlantic Geology, 52, pp. 125–167. https://doi.org/10.4138/atlgeol.2016.007
Wise, M.A. and Francis, C.A. 1992. Distribution, classification, and geological setting of granitic pegmatites in Maine. Northeastern Geology, 14, pp. 82–93.
Wolfden Resources Corporation. 2021. Pickett Mountain property. Includes NI 43-101 report of 14 September 2020. URL <https://www.wolfdenresources.com/projects/pickett-mountain-maine/>
Wolfden Resources Corporation. 2022. Wolfden announces exploration results for Big Silver project in Maine, 21 March 2022. URL https://www.wolfdenresources.com/news/ 17 June 2022.
Woodruff, L.G., Bedinger, G.M., and Piatak, N.M. 2017. Titanium. *In* Critical mineral resources of the United States—economic and environmental geology and prospects for future supply. *Edited by* K.J. Schulz, J.H. DeYoung, Jr., R.R. Seal II, and D.C. Bradley. U.S. Geological Survey Professional Paper 1802–T, 23 p.
Yan, J., Fu, S., Liu, S., Wei, L., and Wang, T. 2022. Giant Sb metallogenic belt in South China: a product of late Mesozoic flat-slab subduction of paleo-Pacific plate. Ore Geology Reviews, 142, pp. 104697. https://doi.org/10.1016/j.oregeorev.2022.104697
Yang, D.-S., Shimizu, M., Shimazaki, H., Li, X.-H., and Xie, Q.-L. 2006. Sulfur isotope geochemistry of the supergiant Xikuangshan Sb deposit, central Hunan, China––constraints on sources of ore constituents. Resource Geology, 56, pp. 385–396. https://doi.org/10.1111/j.1751-3928.2006.tb00291.x
Yang, X.-M., Lentz, D.R., and McCutcheon, S.R. 2003. Petrochemical evolution of subvolcanic granitoid intrusions within the Late Devonian Mount Pleasant caldera, southwestern New Brunswick, Canada: comparison of Au versus Sn-W-Mo-polymetallic mineralization systems. Atlantic Geology, 39, pp. 97–122. https://doi.org/10.4138/1175
Young, R.S. 1962. Prospect evaluations, Hancock County, Maine. Maine Geological Survey Special Economic Studies Series 2, 113 p.
Young, R.S. 1963. Prospect evaluations, Washington County, Maine. Maine Geological Survey Special Economic Studies Series 3, 86 p.
Young, R.S. 1968. Mineral exploration and development in

Maine. *In* Graton-Sales volume: Ore Deposits of the United States, 1933–1967. *Edited by* J.D. Ridge. The American Institute of Mining, Metallurgical, and Petroleum Engineers, Inc., New York, 1, pp. 125–139.

Yumul, G.P. Jr. 2001. The Acoje block platiniferous dunite horizon, Zambales ophiolite complex, Philippines: melt type and associated geochemical controls. Resource Geology, 51, pp. 165–174. https://doi.org/10.1111/j.1751-3928.2001.tb00089.x

Yumul, G.P. Jr. and Balce, G.R. 1994. Supra-subduction zone ophiolites as favorable hosts for chromite, platinum and massive sulfide deposits. Journal of Southeast Asian Earth Sciences, 10, pp. 65–79. https://doi.org/10.1016/0743-9547(94)90009-4

Zhang, L., Yang, L.-Q., Groves, D.I., Sun, S.-C., Liu, Y., Wang, J.-Y., Li, R.-H., Wu, S.-G., Gao, L., Guo, J.-L., Chen, X.-G., and Chen, J.-H. 2019. An overview of timing and structural geometry of gold, gold-antimony and antimony mineralization in the Jiangnan orogen, southern China. Ore Geology Reviews, 115, pp. 103173. https://doi.org/10.1016/j.oregeorev.2019.103173

Zhang, P.-F., Zhou, M.-F., Malpas, J., and Robinson, P.T. 2020. Origin of high-Cr chromite deposits in nascent mantle wedges: petrological and geochemical constraints from the Neo-Tethyan Luobusa ophiolite, Tibet. Ore Geology Reviews, 123, pp. 103581. https://doi.org/10.1016/j.oregeorev.2020.103581

Zhang, W. 2015. Petrological and metallogenic studies of the Nashwaak granite and felsic dykes associated with the Sisson Brook W-Mo-(Cu) deposit, west-central New Brunswick. Unpublished Ph.D. thesis, University of New Brunswick, Fredericton, 281 p. https://doi.org/10.4095/296484

Zhou, M.-F., Yumul, G.P., Malpas, J., and Sun, M. 2000. Comparative study of platinum-group elements in the Coto and Acoje blocks of the Zambales ophiolite complex, Philippines. The Island Arc, 9, pp. 556–564. https://doi.org/10.1046/j.1440-1738.2000.00301.x

Zielinski, R.A. and Burruss, R.C. 1991. Petrogenesis and geological history of a uranium source rock: a case study in northeastern Washington, U.S.A. Applied Geochemistry, 6, pp. 597–612. https://doi.org/10.1016/0883-2927(91)90072-W

Zientek, M.L., Hammarstrom, J.M., Johnson, K.M., and Pierce, F.W. 2010. Global mineral resource assessment. U.S. Geological Survey Scientific Investigations Report 2010–5090, 24 chapters. https://doi.org/10.3133/sir20105090

Zientek, M.L., Loferski, P.J., Parks, H.L., Schulte, R.F., and Seal, R.R. II. 2017. Platinum-group elements. *In* Critical mineral resources of the United States—economic and environmental geology and prospects for future supply. *Edited by* K.J. Schulz, J.H. DeYoung Jr., R.R. Seal II, and D.C. Bradley. U.S. Geological Survey Professional Paper 1802–N, 91 p. https://doi.org/10.3133/pp1802N

Editorial responsibility: Aaron Bustard

Revised stratigraphy in the eastern Meguma terrane, Nova Scotia, Canada, and variations in whole-rock chemical and Sm–Nd isotopic compositions of the Goldenville and Halifax groups

Sandra M. Barr[1], Chris E. White[2], and Christian Pin[3]

1. Department of Earth and Environmental Science, Acadia University, Wolfville, Nova Scotia B4P 2R6 Canada
2. Department of Natural Resources and Renewables, Halifax, Nova Scotia, B3J 2T9 Canada
3. Département de Géologie, UMR 6524 CNRS, Université Blaise Pascal, 5 rue Kessler 63 038 Clermont-Ferrand Cedex, France (retired)
*Corresponding author: sandra.barr@acadiau.ca

Date received: 22 February 2022 ¶ Date accepted 05 June 2022

ABSTRACT

As a result of new geological mapping, the Goldenville and Halifax groups in the eastern Meguma terrane have been divided into formations. They have a total stratigraphic thickness of about 7750 m and correspond to only the upper half of the Goldenville Group and lower half of the Halifax Group in the northwestern and southeastern areas of the terrane. The revised stratigraphy combined with compiled and new whole-rock major and trace element and Sm–Nd isotopic analyses enable more detailed documentation of the chemical changes with stratigraphy that were demonstrated in previous studies. Based on chemical compositions, the protolith compositions of the analysed samples range from lithic arenite to wacke to shale. Major and trace element characteristics are consistent with deposition in an active continental margin, basins associated with island arcs, or most likely at a passive continental margin with volcanic rocks in the source area. Chemical compositions show a scattered but overall increasing abundance of lithophile elements such as La and Th with stratigraphic position. Epsilon $_{Nd(t)}$ values become increasingly negative up-section, and depleted mantle model ages become increasingly older. The data are consistent with increased mixing between sediments derived from Mesoproterozoic upper crustal sources and sediments derived from a magmatic arc. These data are consistent with published detrital zircon patterns which show increasing amounts of ca. 2 Ga zircon with decreasing age, and with a source area comprising a Pan-African (800–540 Ma) volcanic arc and/or active margin magmatism and mainly Eburnean crust, most likely in the West African craton.

RÉSUMÉ

À la suite de nouveaux travaux de cartographie géologique, les groupes de Goldenville et d'Halifax dans l'est du terrane de Meguma ont été subdivisés en formations. Ils ont une épaisseur stratigraphique totale d'environ 7 750 mètres et correspondent à seulement la moitié supérieure du groupe de Goldenville et à la moitié inférieure du groupe d'Halifax dans les secteurs nord-ouest et sud-est du terrane. La stratigraphie révisée combinée à des données compilées et à de nouvelles analyses des compositions isotopiques en Sm–Nd et en éléments majeurs et traces de roche totale permet une documentation plus détaillée des changements chimiques de la stratigraphie ayant été révélés dans des études antérieures. D'après les compositions chimiques, les compositions protolithiques des échantillons analysés varient de l'arénite lithique au wacke et au schiste. les caractéristiques des éléments majeurs et traces correspondent à une sédimentation dans une marge continentale

doi: 10.4138/atlgeo.2022.008

active, à des bassins associés à des arcs insulaires ou très probablement à une marge continentale passive comportant des roches volcaniques dans la région d'origine. Les compositions chimiques affichent une abondance sporadique, mais généralement grandissante des éléments lithophiles comme le La et le Th selon la position stratigraphique. Les valeurs epsilon $_{Nd(t)}$ deviennent de plus en plus négatives en allant vers le haut de la section et les âges du modèle mantellique épuisé deviennent de plus en plus avancés. Les données sont conformes à un mélange accru entre des sédiments en provenance de sources crustales supérieures du Mésoprotérozoïque et des sédiments provenant d'un arc magmatique. De telles données correspondent aux configurations du zircon détritique publiées faisant état de quantités croissantes de zircon d'environ 2 Ga ainsi qu'avec une région d'origine comprenant un arc volcanique panafricain (800 à 540 Ma) ou un magmatisme de marge active et une croûte principalement éburnéenne, très probablement dans le craton d'Afrique occidentale.

[Traduit par la redaction]

INTRODUCTION

Meguma is the most outboard terrane in the northern Appalachian orogen, exposed on land only in Nova Scotia south of the Cobequid–Chedabucto fault zone (Fig. 1, inset). It is characterized by a thick succession of Cambrian to lower Ordovician metasedimentary rocks (Goldenville and Halifax groups), overlain along the northwestern margin by localized areas of Silurian to lower Devonian metavolcanic and metasedimentary rocks of the Rockville Notch Group (e.g., Waldron *et al.* 2009; White *et al.* 2018 and references therein). These stratified units are intruded by voluminous mainly Middle to Late Devonian granitoid rocks dominated by the South Mountain Batholith, and overlain unconformably by upper Paleozoic and lower Mesozoic sedimentary and volcanic rocks (Fig. 1).

White (2010, 2013) divided the Goldenville and Halifax formations in the southwestern part of the Meguma terrane

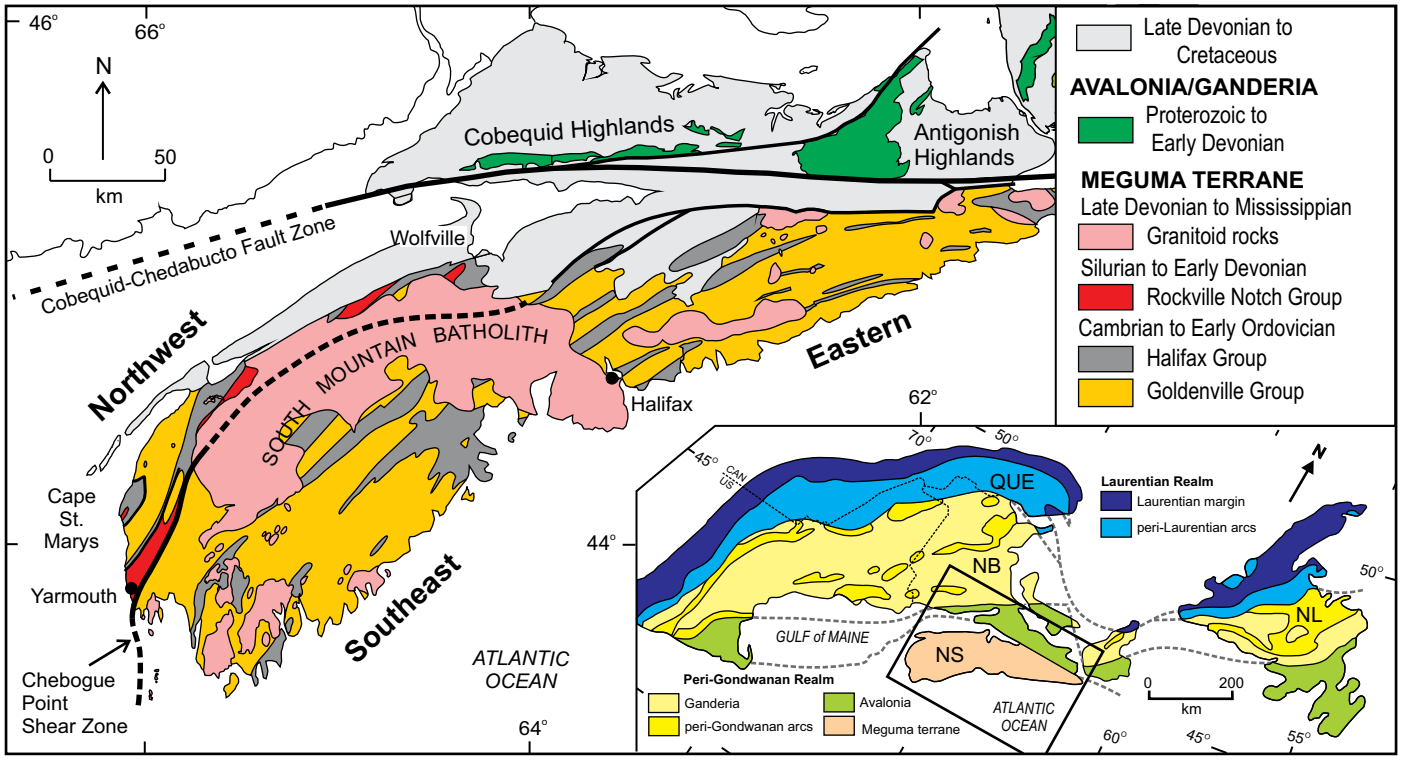

Figure 1. Simplified geological map of the Meguma terrane after White (2010) with inset map showing its location in the northern Appalachian orogen after Hibbard *et al.* (2006). Abbreviations: NB, New Brunswick; NL, Newfoundland; NS, Nova Scotia; QUE, Quebec.

into mappable formations (Fig. 2), thus elevating the former formations to Goldenville and Halifax groups and the former Meguma Group to Supergroup. Because of the possibility of confusion where the word Meguma has two meanings, in this paper we use the term Meguma only to refer to the terrane, and do not refer to the supergroup. In combination with the mapping and definition of formations, age constraints were provided by studies of trace and microfossils (White *et al.* 2012; Gingras *et al.* 2011), $^{40}Ar/^{39}Ar$ dating of detrital and metamorphic muscovite (Reynolds *et al.* 2012), and U–Pb dating of detrital zircon (Waldron *et al.* 2009, 2011; Pothier *et al.* 2015; Henderson 2016). The new stratigraphic framework also facilitated investigation of variations with time in characteristics such as sedimentary geochemistry, isotopic composition, and detrital zircon provenance (Waldron *et al.* 2009; White and Barr 2010), and interpretation of possible stratigraphic constraints on gold mineralization (White and Barr 2012a, b).

Those studies focused on the southwestern part of the Meguma terrane and included few data from the eastern half of the terrane because of lack in that area of systematic regional mapping and stratigraphic information, except in localized areas (Henderson 1986; Hill 1991; Ryan *et al.* 1996; Horne and Pelley 2007; White and Scallion 2011). However, recent mapping in the eastern Meguma terrane has resulted in a new bedrock geology map (Fig. 3) and revised stratigraphy (White and Vaccaro 2019, 2020; White and Nickerson 2021). Hence, the purpose of this paper is to present a revised assessment of variations in whole-rock chemistry, Sm–Nd isotopic composition, and detrital zircon signatures in the Meguma terrane that incorporates the new understanding of stratigraphy in the eastern part of the terrane. We present whole-rock chemical and Sm–Nd isotopic analyses for 22 samples from both the southwestern and eastern parts of the Meguma terrane which, in combination with previous data, provide better constraints on chemical variations with stratigraphy.

GEOLOGICAL SETTING

The Meguma terrane is generally inferred to have originated as a lower Paleozoic continental margin of Gondwana, although its original position and underlying basement remain uncertain. It has been interpreted to have been adjacent to the West African craton during the Cambrian (e.g., Schenk 1971, 1981, 1991, 1995, 1997; Waldron *et al.* 2009; van Staal and Hatcher 2010; Letsch *et al.* 2018; van Staal *et al.* 2021a, b), although other workers have included the Meguma terrane in Avalonia and/or interpreted it to have formed as a continental margin succession on Avalonia (e.g., Murphy *et al.* 2004; Romer *et al.* 2011). During opening of the Rheic Ocean, Meguma was one of several terranes or terrane assemblages that separated from Gondwana and eventually accreted to composite Laurentia, although the details of its journey remain unclear (e.g., Nance *et al.* 2010; Murphy *et al.* 2011; van Staal and Barr 2012; van Staal *et al.* 2021a, b; Warsame *et al.* 2021).

The Goldenville and Halifax groups have been interpreted as turbiditic continental rise and/or slope deposits (Schenk 1971, 1981, 1991, 1995, 1997; Waldron and Jensen 1985; Waldron 1992). They are unconformably overlain by a thinner sequence of early Silurian to Early Devonian slate, quartzite, and metavolcanic rocks of the Rockville Notch Group (White 2010, 2019; White and Barr 2012a, b, 2017; White *et al.* 2018). All these rocks were deformed into regional-scale upright shallow north- and south-plunging folds with well-developed north-striking steep axial-planar foliation (e.g., Culshaw and Lee 2006) and regionally metamorphosed at grades varying from lower greenschist- to upper amphibolite-facies between 406 and 388 Ma (Muecke *et al.* 1988; Raeside and Jamieson 1992; Hicks *et al.* 1999; Reynolds *et al.* 2012; White and Barr 2012a, b). They were also intruded by numerous, late syn- to post-tectonic, mainly Middle to Late Devonian, peraluminous granitic plutons (e.g., Clarke *et al.* 1997, 2000; Bickerton *et al.* 2022). Deformation, regional metamorphism, and plutonism were associated with a Middle to Late Devonian orogenic event that has been traditionally called the Acadian orogeny. However, the main events of the Acadian orogeny are interpreted to have been associated with late Silurian-Early Devonian accretion of Avalonia to the composite margin of Ganderia and Laurentia (Hibbard *et al.* 2007; van Staal and Barr 2012, van Staal *et al.* 2021a, b), a model which does not readily accommodate younger events in the Meguma terrane outboard of Avalonia. Alternatively, in recognition of its younger age, the orogenic event in Meguma also has been termed Neoacadian, but that term is also inappropriate because it refers to a Late Devonian to Early Carboniferous event in New England (Robinson *et al.* 1998), also far inboard of the Meguma terrane. Hence, to emphasize its unique character and timing, we here introduce the term Kejimkujik orogeny for the Middle Devonian orogenic event in Meguma to distinguish it from the more inboard older Acadian and younger Neoacadian events. Subsequent Carboniferous motion on the Cobequid–Chedabucto fault zone and renewed transpression throughout the Meguma terrane (e.g., Culshaw and Leisa 1997; Culshaw and Reynolds 1997) was likely related to docking of Gondwana (Africa) outboard of the Meguma terrane before and during the Alleghanian orogeny (Murphy *et al.* 2011; van Staal and Barr 2012; White and Barr 2012a, b).

Waldron *et al.* (2011) noted similarities in the Cambrian to Tremadocian lithological successions of the Meguma terrane and the Harlech Dome of North Wales, including the presence of Cambrian Series 3 (Miaolingian) manganese-rich sedimentary rocks. They proposed that both Meguma and North Wales were part of the Megumia

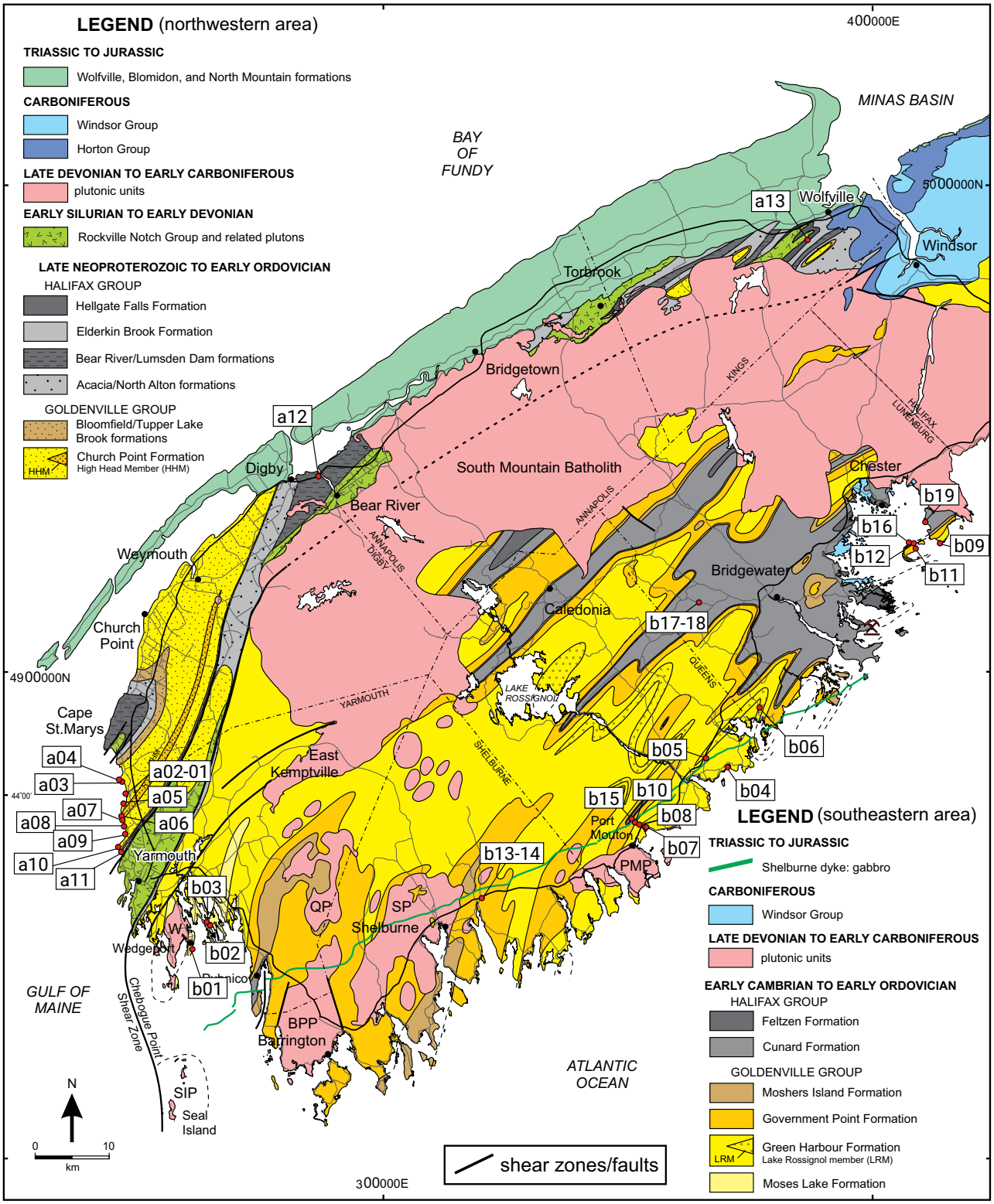

Figure 2. Geological map of the northwestern and southeastern parts of the Meguma terrane after White (2013) and White and Barr (2012b). Locations of samples a01 to a13 and b01 to b19 are shown; UTM for sample locations are listed in Table A1. Pluton abbreviations: BPP, Barrington Passage, PMP, Port Mouton; QP, Quinan; SP, Shelburne; SIP, Seal Island; W, Wedgeport.

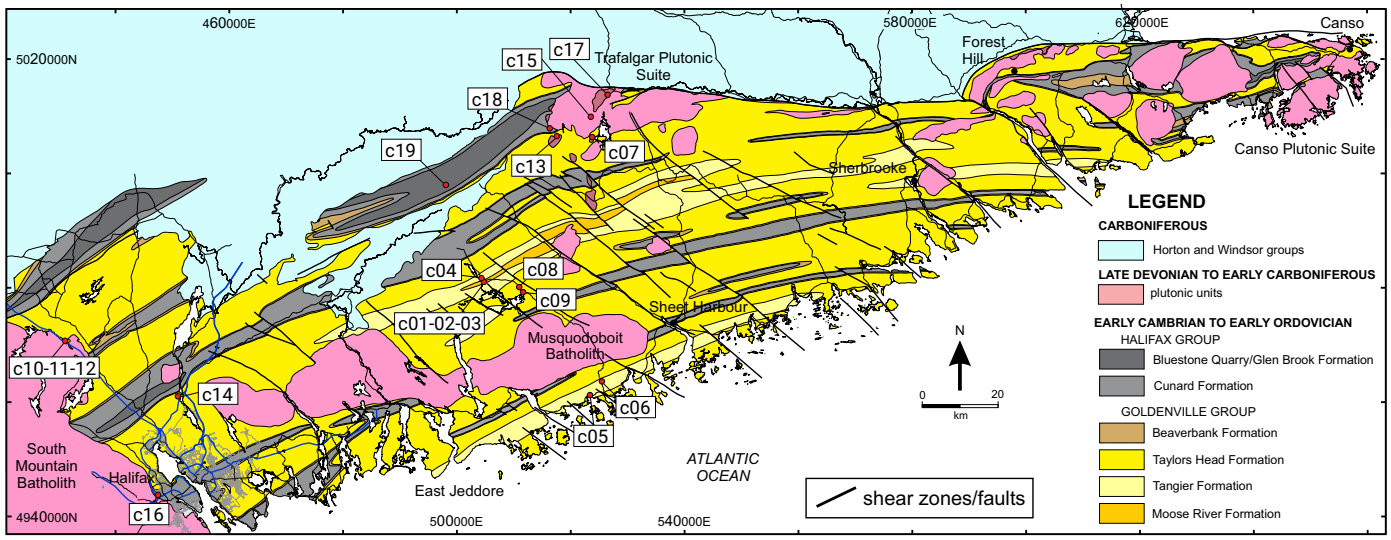

Figure 3. New geological map of the eastern Meguma terrane after White and Nickerson (2021) and unpublished data. Locations of samples c01 to c13 are shown; UTM for sample locations are listed in Table A1.

domain that occupied a rift at the margin of Gondwana in the early Paleozoic. Acritarch data (White *et al.* 2012) suggest that deposition continued in the Halifax Group at a time when rocks of the Harlech Dome were being uplifted and eroded and the Meguma terrane lacks evidence for the Ordovician volcanism present in North Wales, so if these areas were contiguous in the Cambrian, their histories diverged in the Ordovician (Pothier *et al.* 2015).

STRATIGRAPHY OF THE GOLDENVILLE AND HALIFAX GROUPS

The Chebogue Point shear zone and South Mountain Batholith are used to divide the Meguma terrane into three areas here termed northwestern (NW), southeastern (SE), and eastern (E) (Fig. 1). The lithologically distinctive and typically manganiferous beds of the correlative Bloomfield, Tupper Lake Brook, Moshers Island, and Beaver Bank formations provide a marker horizon at ca. 500 Ma throughout the terrane and were assigned to the uppermost Goldenville Group by White (2010). The underlying units have broad similarities but differ in detail among the NW, SE, and E areas of the terrane (Fig. 4). The thickest unit is the Church Point Formation in the NW area, with an estimated stratigraphic thickness of about 7.8 km, although the base is not exposed (Fig. 4). The oldest rocks of the formation occur in the core of an anticline on the coast between Yarmouth and Cape St. Mary (Fig. 2), from which U–Pb detrital zircon data suggest a maximum depositional age of about 540 Ma with large errors (Waldron *et al.* 2009; Henderson 2016). In the area southeast of the Cheborgue Point shear zone, the rocks that appear to be laterally age-equivalent to the Church Point Formation are subdivided into three formations (Moses Lake, Green Harbour, and Government Point).

In the eastern area of the terrane, the most extensive unit is the Taylors Head Formation (Fig. 3), with lithological similarities and similar stratigraphic thickness to the Government Point Formation (Fig. 4). Based on this correlation, the underlying Tangier and Moose River formations are interpreted to be laterally equivalent to the upper part of the Green Harbour Formation (Fig. 4).

The manganiferous Bloomfield, Tupper Lake Brook, Moshers Island, and Beaver Bank formations are overlain by sulphidic slate, metasiltstone, and metasandstone of the lowermost formation of the Halifax Group, named Acacia Brook and North Alton formations in the NW area and Cunard Formation in the SE and E (Fig. 4). The overlying Bear River, Lumsden Dam, Feltzen, and Glen Brook/Bluestone Quarry formations are interpreted to be age equivalent because of lithological similarity and the presence in most of Lower Ordovician fossils (White *et al.* 2012). The youngest units of the Halifax Group (Elderkin Brook and Hells Gate Falls) outcrop only in the Wolfville area (Fig. 2) where fossils indicate a minimum age of late Floian (ca. 470 Ma).

SAMPLE DISTRIBUTION AND ANALYTICAL METHODS

For this study, twenty-two samples were collected for Sm–Nd isotopic analysis to provide increased coverage throughout the terrane when combined with data from 13 samples reported by Waldron *et al.* (2009) and 16 samples compiled from Clarke and Halliday (1985), Clarke *et al.* (1988, 1993), and Currie *et al.* (1998). The stratigraphic

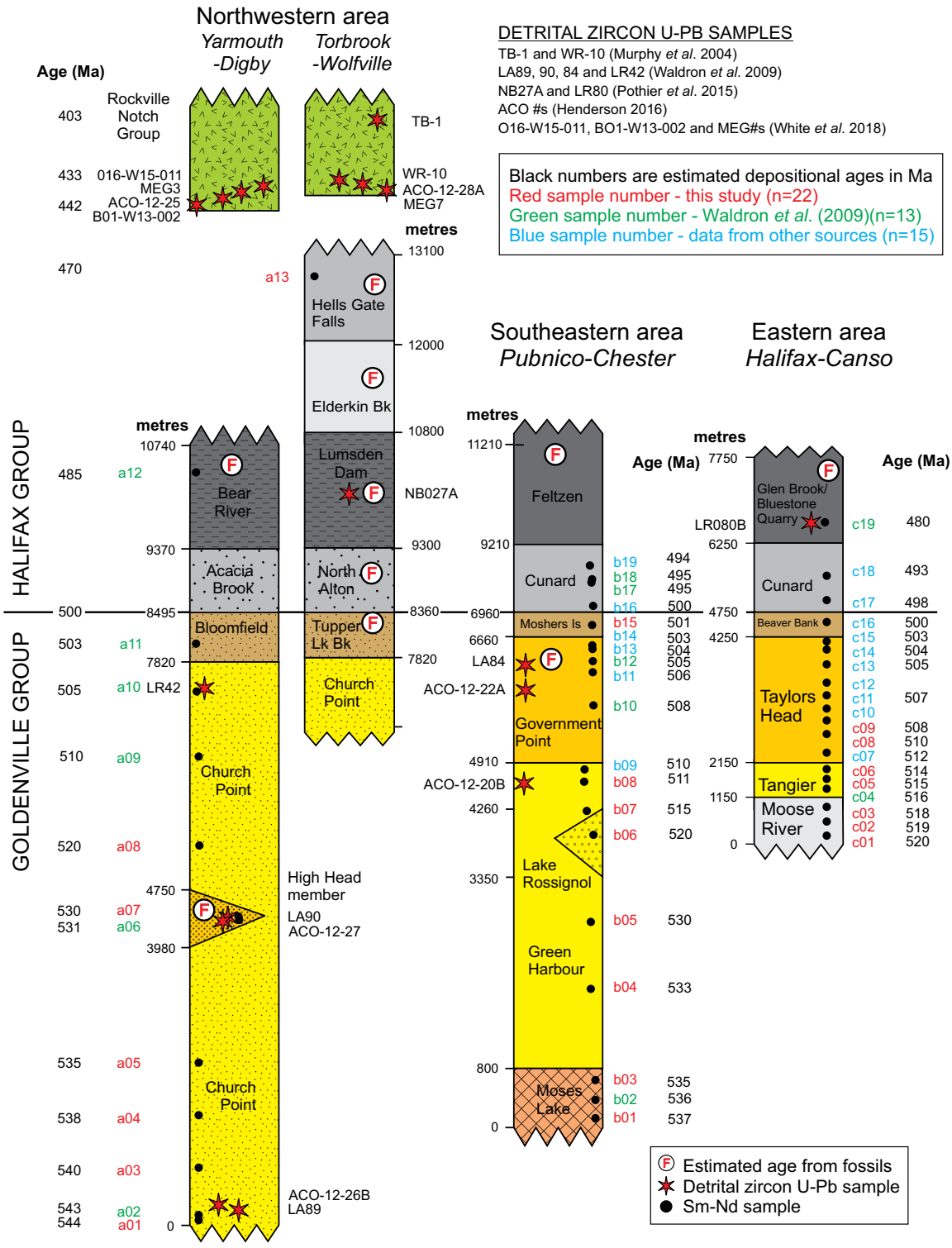

Figure 4. Simplified stratigraphic columns for the northwestern, southeastern, and eastern areas of the Meguma terrane showing sample positions (black circles). Stratigraphic units are from White (2010), Pothier *et al.* (2015), and C. White (unpublished) are labelled and coloured similar to Figures 2 and 3. Stratigraphic thickness estimates and sample depositional ages are based on maps in Figures 2 and 3 and cited U–Pb data. Fossil occurrences are from White *et al.* (2012), Pratt and Waldron (1991), and Cumming (1985). Sm–Nd data sources are from this study and Waldron *et al.* (2009), Clarke and Halliday (1985), Clarke *et al.* (1988, 1993), and Currie *et al.* (1998), as tabulated in Table A1.

positions and ages of the samples (Fig. 4) were estimated from field relations and locations on the new maps of the Meguma terrane (Figs. 2, 3). Locations for the published samples are constrained as much as possible based on information provided in the original papers. In addition to the isotopic data, whole-rock chemical data are available for most of the samples, as well as petrographic information for samples from the present study and Waldron *et al.* (2009). Whole-rock chemical analyses for samples from this study were done by Bureau Veritas Laboratory, Vancouver, BC. Major elements were analyzed by X-ray fluorescence after $LiBO_2$ fusion and rare earth and refractory elements by Inductively Coupled Plasma - Mass Spectrometry (ICP-MS) following lithium metaborate/tetraborate fusion and nitric acid digestion or Aqua Regia digestion. The data are listed in Supplementary data Table S1 (see footnote 1), in combination with chemical data compiled from the sources of the isotopic data where available. The new Sm–Nd isotopic analyses were done at the Université Blaise Pascal, Clermont-Ferrand, France, following techniques adapted from those described by Pin and Santos (1997) and LeFèvre and Pin (2002). The samples were decomposed by fusion with a $LiBO_2$ flux at ca. 1150°C in an induction furnace and the resulting melt was quenched in 1.25M HCl, after addition of a mixed ^{149}Sm–^{150}Nd-enriched tracer. Then, a fraction containing the LREE was separated from most other elements by cation exchange chromatography. This LREE fraction was further purified by extraction chromatography on a micro-column filled with TRU resin (Eichrom). Then, Nd and Sm suitable for mass spectrometry were isolated from lighter lanthanides and from each other by using another extraction chromatography column filled with Ln resin (Eichrom) and operated on-line downstream of the TRU micro-column. The Sm concentrations were determined by isotope dilution thermal ionization mass spectrometry (ID-TIMS) with an upgraded, fully automated VG54E instrument, with sample loaded in a drop of phosphoric acid on a single tantalum filament. The $^{143}Nd/^{144}Nd$ isotope ratios (and $^{150}Nd/^{144}Nd$ ratios allowing determination of the Nd concentrations by isotope dilution) were measured with a Triton mass spectrometer operated in static multicollection mode at Laboratoire GIS, Université de Nîmes, with Nd loaded on a double rhenium filament assembly. The $^{143}Nd/^{144}Nd$ ratios are given relative to a value of 0.512110 for the JNdi-1 isotopic standard (Tanaka *et al.* 2000), and the precision of $^{147}Sm/^{144}Nd$ ratios is ± 0.2%. The new isotopic data are listed in Appendix Table A1, together with a compilation of other published data, listed in inferred stratigraphic order with estimated age in each of the NW, SE, and E areas.

[1]Supplemental Data. Table S1. Please visit https://journals.lib.unb.ca/index.php/ag/article/view/32794/1882528212 to access the supplementary material

PETROGRAPHY

Metamorphic grade varies widely over the Meguma terrane as a result of both regional and contact metamorphism (e.g., Raeside and Jamieson 1992; Mahoney 1996; White and Barr 2012a, b). Samples analyzed in this study are in the greenschist facies (chlorite and biotite zones), although some data compiled from previous work are from higher grade samples. Based mainly on grain size and abundance of quartz relative to other minerals, the samples range from pelitic to psammitic. Overall, the proportion of finer (pelitic and semi-pelitic) material increases up-section in the Goldenville and Halifax groups and, overall, the Halifax Group is finer grained and more pelitic than the Goldenville Group. Our study focussed on the coarser-grained semi-pelitic and psammitic samples in both groups, and hence pelitic rocks are less well represented in the dataset. Petrographic features show little variation throughout the stratigraphy in all three areas, except that the three lowermost psammitic samples in the Church Point Formation in the northwestern area (Fig. 2) lack detrital muscovite.

In general, psammitic samples retain more clastic-looking textures and are less recrystallized than the pelitic and semi-pelitic samples, but all samples are metamorphosed and original sedimentary features such as laminae which are readily visible in hand sample are obscured by new mineral growth when viewed in thin section. In the psammitic samples, the original clay matrix has been recrystallized to sericite, chlorite, and epidote, but sand-sized detrital grains appear little affected. Such grains include quartz, Na-rich plagioclase, muscovite, zircon, tourmaline, and opaque grains. Most psammitic samples have more than 5% matrix and are classified as feldspathic wacke to quartz wacke (classification of Boggs 2001).

Detrital muscovite is a prominent component of psammitic samples throughout the Goldenville and Halifax groups, except near the base of the section in the NW area, but no biotite of detrital origin was observed. Single-grain $^{40}Ar/^{39}Ar$ dating of detrital muscovite in the Meguma terrane by Reynolds *et al.* (2012) showed evidence for a Mesoproterozoic source, interpreted to be the Amazonian craton, but the nature of the source — metamorphic or igneous — was not indicated by the chemical characteristics of the muscovite. Most of the analyzed muscovite grains show evidence of late Neoproterozoic to early Cambrian resetting just prior to sediment deposition, interpreted by Reynolds *et al.* (2012) to be consistent with rapid uplift associated with a rifting environment.

WHOLE-ROCK CHEMISTRY

White and Barr (2010) presented a detailed assessment of the whole-rock chemical variations in the NW and SE

areas of the Meguma terrane; here we restrict our discussion to data from 43 samples from which we also have Sm–Nd isotopic data; the remaining 8 samples with Sm–Nd data lack whole-rock chemical data. Samples with chemical data include 18 from the eastern area of the terrane that was not covered in the study by White and Barr (2010), and a subset of about 30 samples from throughout the terrane which includes trace elements such as La and Sc that were not available in the dataset utilized by White and Barr (2010).

Overall, the samples display an increase in SiO_2 content from ~44% in pelitic samples to close to 80% in the most quartz-rich psammitic samples (Fig. 5a). None of the analyzed samples from the SE area has SiO_2 content less than 55%, but otherwise all 3 areas contain similar ranges of sample compositions. Loss-on-ignition varies from less than 1% in high SiO_2 samples to more than 6% in some lower SiO_2 samples (Fig. 5a). Hence, to facilitate comparisons, the analyses were recalculated to total 100% excluding loss-on-ignition before plotting on Figures 5b, c, d and 6a.

On a chemical classification diagram using ratios of Fe_2O_3/K_2O and SiO_2/Al_2O_3 (Fig. 5b), the samples lie mainly in the shale, wacke, and lithic arenite fields, with a few plotting in the high-iron shale/sandstone fields. None of the samples are close to the quartz arenite field, consistent with maximum SiO_2 contents of ~80% and the results of White and Barr (2010) from a much larger data set (~600 samples) from the NW and SE areas. On the plot of molar $Al_2O_3/Al_2O_3+ CaO+Na_2O+ K_2O$ (Chemical Index of Alteration or CIA; Nesbitt and Young 1982) against SiO_2 (Fig. 5c) the lower SiO_2 samples generally display higher CIA than the higher SiO_2 samples. In the CIA calculation for Figure 5c, corrections were made for CaO included in apatite and carbonate minerals, following McLennan (1993) so that the CIA reflects mainly weathering of silicate minerals. According to McLennan (1993), CIA values of about 45 to 55 indicate virtually no weathering, whereas values close to 100 indicate intense weathering with complete removal of alkali and alkaline earth elements. In general, samples from the Goldenville and Halifax groups with higher SiO_2 (more quartz) have lower CIA than the lower SiO_2 samples. Most of the pelitic and semi-pelitic samples fall in the intermediate stage of silicate weathering (CIA 60–80), close to the mean CIA value of 72 for suspended (fine-grained) sediment in 44 modern rivers reported by Li and Yang (2010). These data are interpreted to indicate that the sediments that formed the Goldenville and Halifax groups were moderately weathered or reworked sediments.

On the tectonic setting discrimination diagram using K_2O/Na_2O ratio and SiO_2 (Fig. 6a), most samples plot in the active continental margin field, consistent with the results from the larger dataset of White and Barr (2010). However, on a Th-La diagram, the majority of samples plot in the field for island arcs with continental crust, rather than in the combined active and passive continental

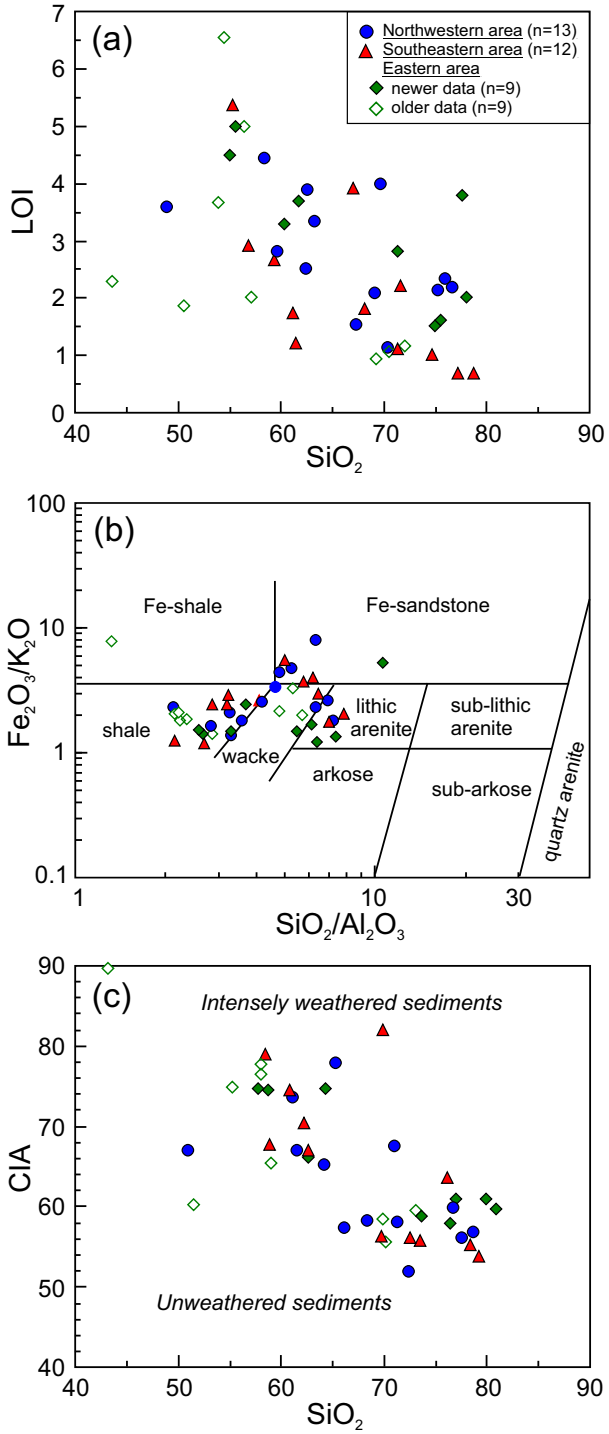

Figure 5. Diagrams illustrating whole-rock chemical characteristics using data from Supplementary Data Table S1. (a) Loss-on-ignition (LOI) plotted against SiO_2. (b) Fe_2O_3/K_2O vs SiO_2/Al_2O_3 with fields from Herron (1988). (c) Chemical Index of Alteration (CIA) of Nesbitt and Young (1982) against SiO_2. CIA is molar $Al_2O_3/(Al_2O_3+CaO+Na_2O+K_2O)$, with CaO corrected for P_2O_5 and carbonate minerals following McLennan (1993).

margin field (Fig. 6b). Scatter to higher La values outside the defined continental island arc field is common in samples from the NW and SE areas, whereas the samples from the eastern area plot mainly in the that field. A similar result is shown by a diagram using ratios of Ti/Zr and La/Sc, with samples from the NW and SE areas showing wider range in La/Sc ratios at high Ti/Zr and plotting outside the defined field (Fig. 6c). Less scatter is displayed in the Th-Sc-Zr ternary diagram and almost all samples plot in the continental island arc field (Fig. 6d). Hence, overall, these data support the conclusion of White and Barr (2010) that the chemical characteristics of the Goldenville and Halifax groups are not consistent with a source that provided compositionally mature sediments but were more likely derived from a source area that included volcanic material.

In their study of mainly major element chemical data for samples from the NW and SE parts of the Meguma terrane, White and Barr (2010) did not detect systematic changes in composition with stratigraphic position through the Goldenville and Halifax groups, suggesting that provenance did not change significantly over time. However, results from this study suggest that some trace elements and trace element ratios do show such variations. For example, using estimated age as an approximate measure of stratigraphic position, plots of age against La, Th, and La/Sc and Th/Sc, although scattered, all tend to increase up section (Fig. 7a–d).

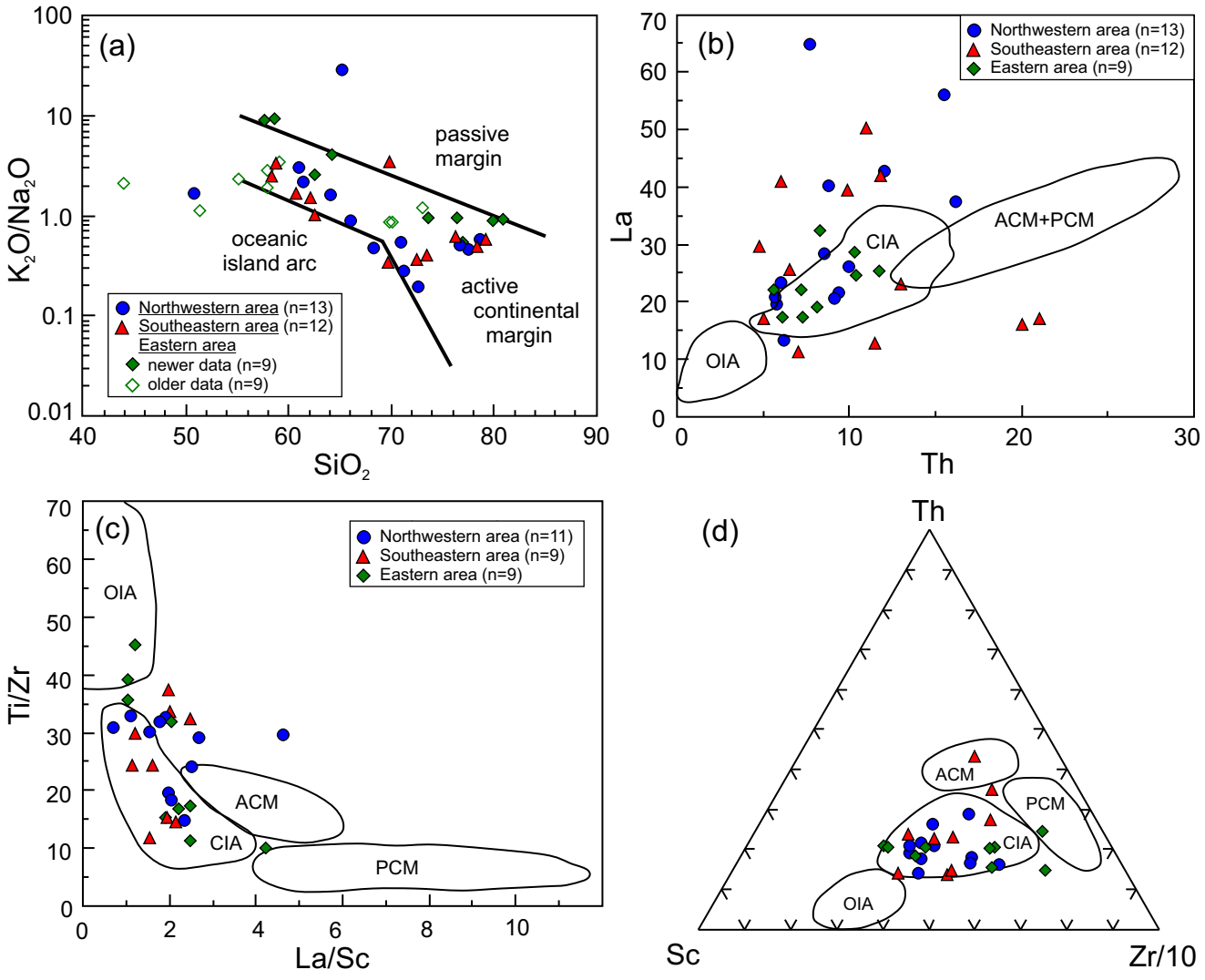

Figure 6. Tectonic setting discrimination diagrams for sedimentary rocks. (a) K_2O/Na_2O against SiO_2 with fields from Roser and Korsch (1986). (b) La against Th. (c) Ti/Zr against La/Sc. (d) Ternary Th-Sc-Zr/10 diagram. Fields in (b), (c), and (d) are from Bhatia and Crook (1986) for greywacke samples deposited in various tectonic settings: ACM, active continental margin; CIA, continental island arc; OIA, oceanic island arc; PCM, passive continental margin.

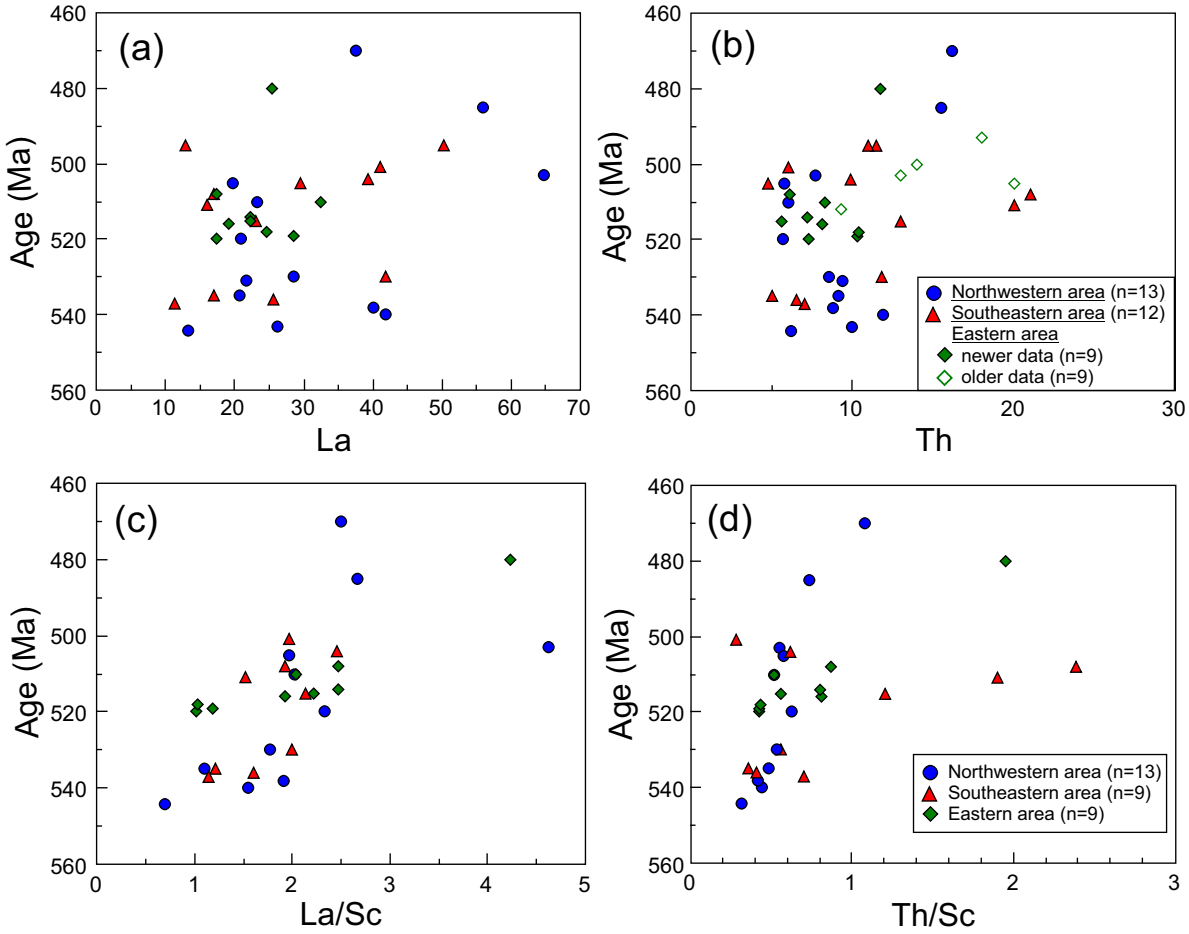

Figure 7. Plots of estimated sample age against (a) La, (b) Th, (c) La/Sc, and Th/Sc. Legend in (a) is the same as in (b) except no La data are available for older samples from the Eastern area. Legend in (c) is the same as in (d).

Sm-Nd ISOTOPIC COMPOSITIONS

Samples with estimated depositional ages between about 530 Ma and 544 Ma occur only in the NW and SE areas (Fig. 4). The $\varepsilon_{Nd(t)}$ numbers for those samples show a wide range from +0.89 to –6.67 (Fig. 8a). Although the overall pattern is obscured by three outlying samples b02, b03, and a06 which have positive $\varepsilon_{Nd(t)}$, the remaining samples older than ~530 Ma, although scattered, display a trend of increasingly negative $\varepsilon_{Nd(t)}$ with decreasing age. Among the younger samples (<530 Ma), including those from the eastern area where the stratigraphically lowest samples are estimated to have an age of ~520 Ma (Fig. 4), the $\varepsilon_{Nd(t)}$ ranges from -3 to -9.96, and a scattered trend of increasingly negative numbers with decreasing age is similarly present (Fig. 8a).

The corresponding plot of depleted mantle model ages against age also shows wide range, especially in the samples estimated to have an age of ~530 Ma or older, where T_{DM} varies 1.20 Ga to 1.86 (Fig. 8b). Among the younger samples (<530 Ma), the range in T_{DM} is similar (1.63 to 2.22 Ga). Depleted-mantle model ages in sedimentary rock have no geological significance and represent an average of all the components in the source (e.g., Arndt and Goldstein 1987). However, the data indicate that the sedimentary rocks contain increasing amounts of older, more evolved components with decreasing age, as also noted by Waldron *et al.* (2009) in a smaller subset of these data. The trend is also apparent on an expanded-scale plot of $\varepsilon_{Nd(t)}$ against age showing the Meguma terrane data in comparison with isotopic evolution of depleted mantle (DePaolo 1981) and various crustal units through time (Fig. 9a). Fields are shown for evolution of Neoproterozoic Pan-African granite and metamorphic rocks and Eburnean metamorphic rocks in Cameroon from Toteu *et al.* (2001), and for Amazonian Mesoproterozoic crust from Santos *et al.* (2008). Meguma terrane samples become increasingly negative with decreasing age, as is apparent in the curve in the sample data (Fig. 9a) that is consistent with an

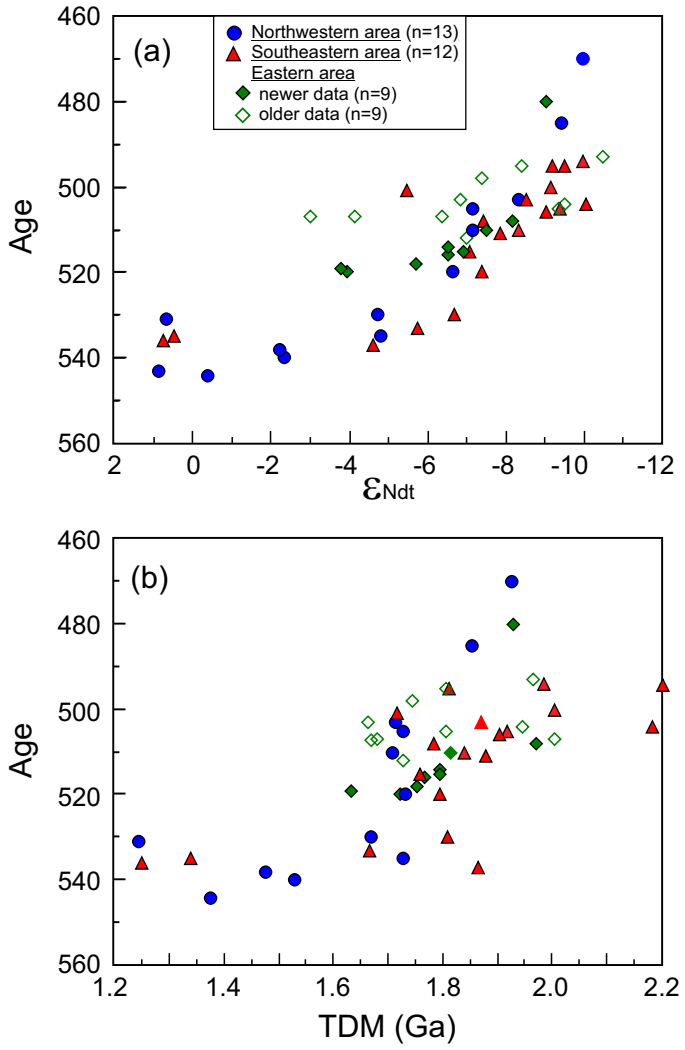

Figure 8. Plots of (a) $\varepsilon_{Nd(t)}$ against estimated depositional age and (b) depleted mantle model age against estimated depositional age from Figure 4. Isotopic data for the Goldenville and Halifax groups are from Table A1.

increasing proportion of older (Mesoproterozoic) sediment. The pattern in the Meguma terrane samples is similar to that in the Cameroon Pan-African samples. The Pan-African field is similarly interpreted to be a result of mixing between relatively juvenile and older, more evolved sources (Toteu *et al.* 2001). However, unlike the Cameroon Pan-African samples, the sources for the Meguma terrane samples do not extend to ages as old as the Paleoproterozoic (Eburnean) sources for the Pan-African field (Fig. 9a). The mixing model is supported further by a plot of $\varepsilon_{Nd(t)}$ against Th/Sc ratio on which the samples fall on the mixing line between average island-arc andesite and average upper continental crust (Fig. 9b). They also plot in the field for deep-sea turbidites of both quartzose and non-quartzose composition deposited at active continental margins from McLennan *et al.* (1990). McLennan *et al.* (1990) interpreted these samples to reflect variable mixtures of younger arc-derived detritus and older upper continental crust sources. Unlike the deep-sea turbidite samples, the Meguma terrane samples do not show evidence for the involvement of older (Paleoproterozoic) crust, consistent with the data shown in Figure 9a.

DETRITAL ZIRCON AGES

As shown by earlier work (e.g., Waldron *et al.* 2009; Pothier *et al.* 2015) additional evidence for increasing contribution of older crust with time in the sediment sources for the Goldenville and Halifax groups is provided by the detrital zircon age spectra (Fig. 10). Although no new detrital zircon data were obtained in this study, additional data from Henderson (2016) and White *et al.* (2018) have been added which were not available for the compilations by Waldron *et al.* (2009) and Pothier *et al.* (2015). Two additional spectra from the NW area from Henderson (2016), one from the lowermost part of the Church Point Formation (Fig. 10a) and one from the High Head member (Fig. 10c), confirm the results from those areas reported by Waldron *et al.* (2009). The samples contain almost entirely Neoproterozoic zircon grains with peaks in the Cryogenian and Ediacaran. Taking errors into account, the maximum depositional ages of 579 ± 7 Ma and 551 ± 8 Ma interpreted by Henderson (2016) are similar to those of Waldron *et al.* (2009) at 544 ± 18 Ma and 529 ± 19 Ma, respectively.

The spectrum obtained by Henderson (2016) for a sample from the Green Harbour Formation (Fig. 10e) is especially significant because it is the stratigraphically lowermost detrital zircon sample available from the SE area (Fig. 4). The spectrum includes the abundant Cryogenian and Ediacaran peaks seen in the older samples from the Church Point Formation but also includes a Tonian peak at 860 Ma and a Paleoproterozoic peak at ~2080 Ma (Fig. 10e). A similar Paleoproterozoic peak is seen in the sample from the upper part of the Church Point Formation in the NW area (Fig. 10f).

Henderson (2016) also reported an age spectrum from a sample from the Government Point Formation in the SE area (Fig. 10g), with results similar to those in a somewhat younger sample (Fig. 10h) reported by Waldron *et al.* (2009) but with more resolution of Paleoproterozoic (2075 Ma) and Tonian (881 Ma) and Cryogenian-Ediacaran peaks. She interpreted a maximum depositional age of 535 ± 5 Ma. Two samples from the overlying Halifax Group have similar signatures with more numerous Paleoproterozoic and Mesoproterozoic peaks (Fig. 10i, j).

The increased proportion of Paleoproterozoic and Mesoproterozoic zircon grains in these samples is consistent with the increasingly negative $\varepsilon_{Nd(t)}$ and older depleted mantle model ages (Fig. 8a, b) which

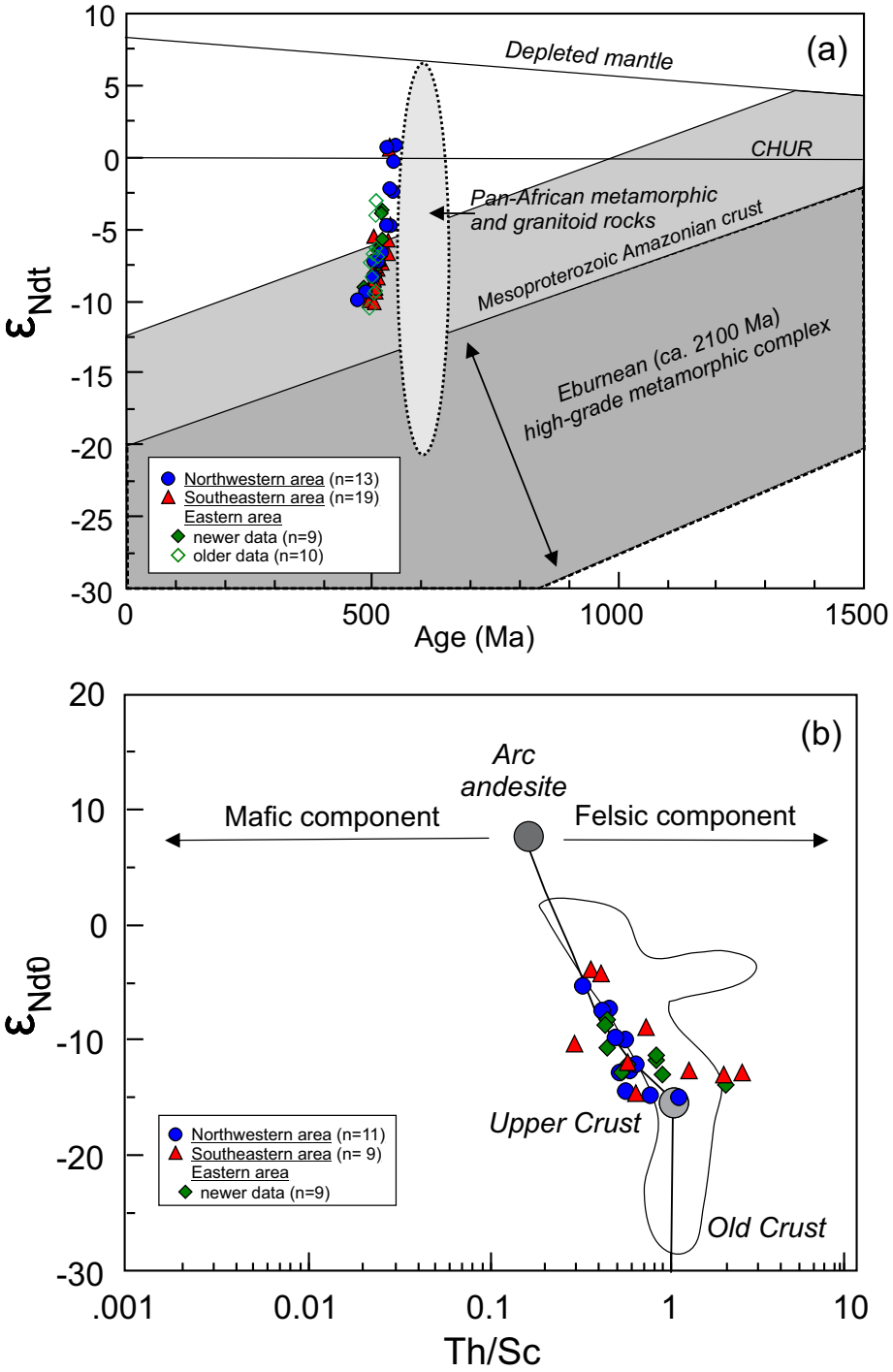

Figure 9. Plots of (a) $\varepsilon_{Nd(t)}$ against estimated depositional age and (b)$\varepsilon_{Nd(0)}$ against Th/Sc ratio. In (a) fields for Nd isotopic evolution are shown from Toteu *et al.* (2001) for Pan-African granite and metamorphic rocks and Eburnean high-grade metamorphic rocks from Cameroon. Mesoproterozoic Amazonian crust is from Santos *et al.* (2008). The depleted-mantle evolution curve is from the model of DePaolo *et al.* (1991). CHUR is chondrite uniform reservoir. Diagram (b) is after McLennan *et al.* (1990) and shows the field for deep-sea turbidites (both quartzose and non-quartzose) deposited at active continental margins and derived from variable mixtures of younger arc-derived detritus and older upper continental crust sources. Curved line shows mixing relationship between average island-arc andesite (dark grey circle) and upper continental crust (light grey circle). Meguma terrane samples follow that curve but do not show evidence for involvement of older crust, consistent with (a).

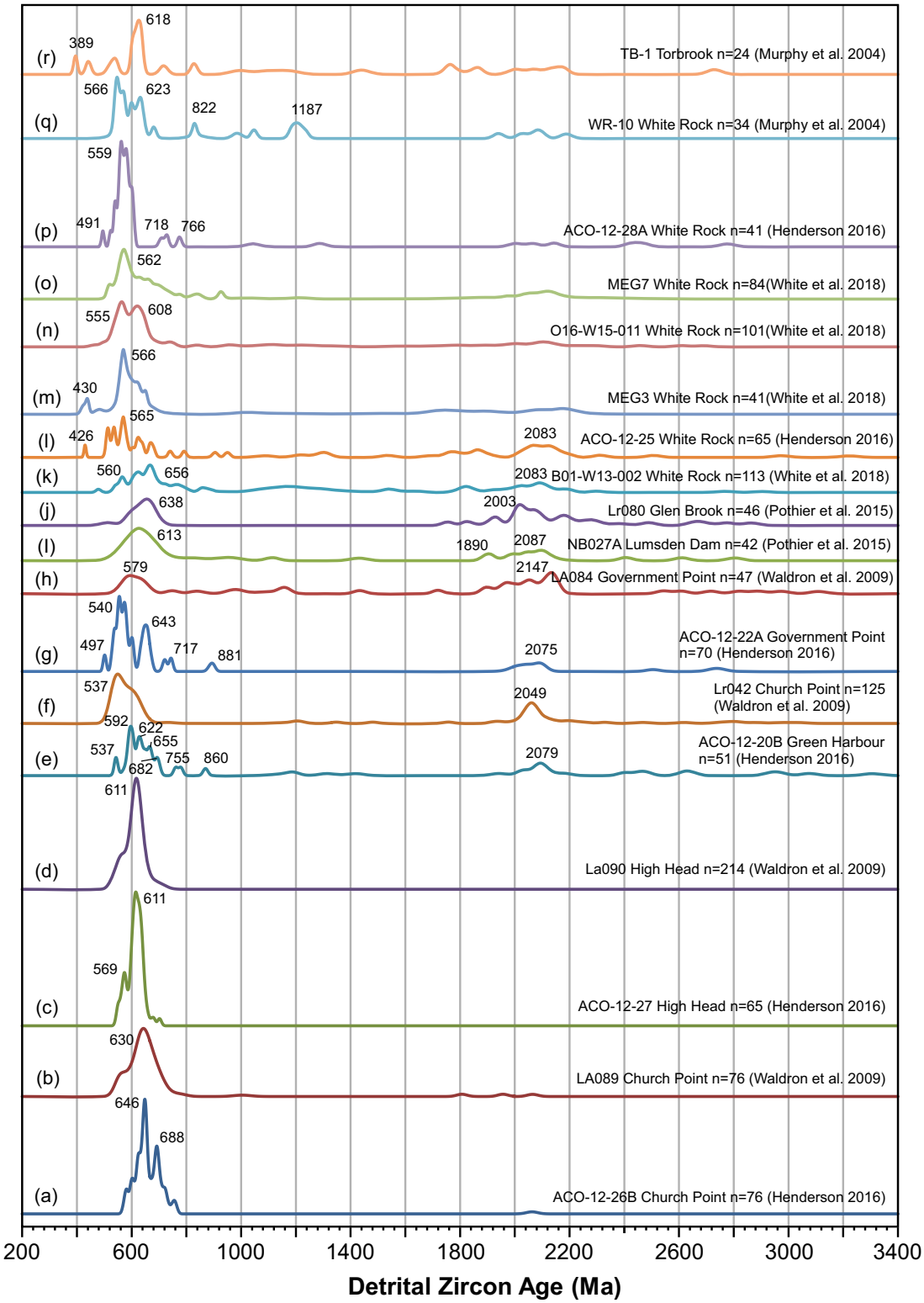

Figure 10. Compilation of normalized detrital zircon age probability plots for samples from the Goldenville and Halifax groups and overlying Rockville Notch Group arranged from oldest (a) to youngest (r). Stratigraphic positions and approximate inferred depositional ages of samples are shown on Figure 4. Reference to data source is indicated on each profile. Normalized age probability plots were constructed using the downloadable Excel file from Arizona Laser Chroncenter (2010). Data are normalized by the number of analyses used so that each curve contains the same area.

suggest increased contributions of older material during sediment deposition. These results corroborate the trends reported by Waldron *et al.* (2009) based on fewer detrital zircon spectra and on Sm–Nd data. Eight detrital zircon spectra from the overlying Rockville Notch Group are also shown in Figure 4 and show patterns similar to those in the underlying Halifax and upper Goldenville groups, with mainly Cryogenian and Ediacaran peaks and scattered older peaks (Fig. 10k–r). The "Eburnian" peak at 2000–2200 Ma in these profiles is generally interpreted to be consistent with West African provenance for Cambrian-Devonian sediments deposited in the Meguma terrane (e.g., Krogh and Keppie 1990; Waldron *et al.* 2009; White *et al.* 2018). That peak persists to the exposed base of the Goldenville Group in the NW area, but it is weak (Fig. 10a).

DISCUSSION

Deposition of the Goldenville and Halifax groups at an active continental margin, in basins within a Japan-type island arc with continental crust, or in a passive margin with volcanic rocks in the source area is suggested by the whole-rock and trace-element chemical data presented here. These environments differ from the classical view of deposition of the Goldenville and Halifax groups at a continental passive margin of sediment derived from a quartz-rich continental source (e.g., Schenk 1971, 1981, 1991, 1995, 1997; Keppie and Krogh 1990; Romer *et al.* 2011). However, it is consistent with the conclusion of White and Barr (2010) that the petrographic and chemical characteristics of the sediments are the result of derivation from Pan-African orogenic belts containing recycled sediments from older cratons as well as juvenile material from igneous units in those belts.

The increasingly evolved $\varepsilon_{Nd(t)}$ isotopic signatures recorded in the samples are consistent with the continued addition of sediment derived from older, more evolved crust, or less addition of juvenile material from Pan African magmatism. However, the detrital zircon populations show that Neoproterozoic sources were dominant throughout deposition of the Goldenville and Halifax groups and Rockville Notch Group. The abundance of Eburnean zircon reaches a maximum in the upper Goldenville and Halifax groups, and then diminishes through the deposition of the Rockville Notch Group. This change is consistent with a model proposed by MacDonald *et al.* (2002) that bimodal magmatism in the Rockville Notch Group is indicative of rifting of the Meguma terrane from Gondwana, the likely source of Eburnean zircon. The almost complete absence of Mesoproterozoic zircon in most age spectra suggests that Amazonia was not the source area and external detritus was derived from the West African craton. Although the most negative $\varepsilon_{Nd(t)}$ values and depleted mantle model ages suggest that sediment was derived from Mesoproterozoic crust, that interpretation is not supported by the detrital zircon spectra. Instead, the data suggest that the Mesoproterozoic model ages result from mixing of Paleoproterozoic and Neoproterozoic sources.

The evolutionary pattern could have resulted from erosion of a given crustal segment that progressively unroofed deeper and older levels, thereby generating an inverted stratigraphy in the resulting sedimentary basin (e.g., Ugidos *et al.* 2003). However, instead of vertical change, a lateral change of source is also likely to occur during the opening and evolution of a rift basin or rifted margin. The rift shoulders would be the major, relatively proximal contributors in the early stages, until removed by erosion and subsidence, thus allowing sediment transport from more distant and much more widespread sources located in the plate interior, through potentially extremely long river systems (e.g., Uguidos *et al.* 2003; Thomas *et al.* 2017).

Potential sources of sediment are numerous among the terranes that occurred at the periphery of the West African craton of Gondwana near Neoproterozoic-Cambrian transition. For example, Cadomia (e.g., Linnemann *et al.* 2014) contains ca. 2.0 Ga Icartian basement and exposes a tectonic collage of units recording a complex, protracted igneous evolution from early ensimatic arc remnants at ca. 750–630 Ma to continental arc magmatism at ca. 580 Ma and a crustal melting event and abundant granites at ca. 540 Ma interpreted to reflect the final pulse of the Cadomian orogeny. Hence Cadomia as well as other Pan-African belts such as that in Cameroon (Fig. 9a) could have been the source of the lower Paleozoic sediments with an active margin or volcanic arc signature deposited on the Meguma terrane.

A similar pattern of Neoproterozoic-dominated detrital zircon populations and increasingly negative $\varepsilon_{Nd(t)}$ has also been documented in Avalonia in New Brunswick and Nova Scotia (Satkoski *et al.* 2010; Barr *et al.* 2012). However, Cambrian to early Ordovician sediments deposited in those areas contain a higher proportion of Mesoproterozoic zircon than the Goldenville and Halifax groups, and a less prominent Eburnean peak. Furthermore, Avalonia is generally viewed as an oceanic ribbon continent and unlikely to have provided the more than 13 km-thick (after lithification and metamorphism) pile of relatively uniform sediment that is represented by the exposed rocks of the Goldenville and Halifax groups. Hence Avalonia is a less likely contributor to the Goldenville and Halifax groups than Cadomia or other Pan-African belts combined with the landmass of the West African craton.

CONCLUSIONS

Combined with improved understanding of stratigraphy in the eastern part of the Meguma terrane, the additional

isotopic data and detrital zircon compilation presented here provide increased support for the evolutionary pattern during deposition of the Goldenville and Halifax groups as described in the model of Waldron *et al.* (2009). In this model, deposition of this thick (>13 km) pile of sediment initiated in a rifted margin, with increasing sediment up-section from the West African craton. Hence, through the Cambrian and early Ordovician, sediments were derived from increasingly older and more age-diverse sources, while retaining a consistently strong component of Cryogenian and Ediacaran (Cadomian or "Pan-African") zircon ages. Petrographic characteristics and major- and trace-element chemical compositions are consistent with the detrital zircon and isotopic data by indicating the same depositional environment throughout deposition of the Goldenville and Halifax groups. However, the trace-element database is sparse considering the thickness of these sedimentary deposits, especially in the Halifax Group, and more data are needed to better constrain the timing of changes in sediment sources. More detrital zircon data are necessary, especially from the lower part of the Green Harbour Formation in the southeastern area of the Meguma terrane, and from the eastern area where the only detrital zircon spectrum is from the Halifax Group near the top of the stratigraphic section.

ACKNOWLEDGEMENTS

We thank Jon Uttley for providing samples from Moose River mine core. The Southwest Nova Scotia and on-going Eastern Shore mapping projects are supported by the Nova Scotia Department of Natural Resources and Renewables, Geoscience and Mines Branch. Sandra Barr's involvement in this work was supported by Discovery Grants from the Natural Sciences and Engineering Research Council of Canada. We thank Kevin Neyedley for his helpful comments on an earlier draft of the manuscript. We also thank journal reviewers Brendan Murphy and John Waldron whose insightful reviews resulted in changes that improved the clarity of the manuscript and figures.

REFERENCES

Arizona Laser Chroncenter 2010. Excel based tools: normalized age probability plots (2010). URL <https://sites.google.com/laserchron.org/arizonalaserchroncenter/home>, 20 February 2022.

Arndt, N.T. and Goldstein, S.L. 1987. Use and abuse of crust-formation ages. Geology 15, pp. 893–895. https://doi.org/10.1130/0091-7613(1987)15<893:UAAOCA>2.0.CO;2

Barr, S.M., Hamilton, M.A., Samson, S.D., Satkoski, A., and White, C.E. 2012. Provenance variations in northern Appalachian Avalonia based on detrital zircon age patterns in Ediacaran and Cambrian sedimentary rocks, New Brunswick and Nova Scotia, Canada. Canadian Journal of Earth Sciences, 49, pp. 533–546. https://doi.org/10.1139/e11-070

Bhatia, M.R. and Crook, K.A.W. 1986. Trace element characteristics of graywackes and tectonic setting discrimination of sedimentary basins. Contributions to Mineralogy and Petrology, 92, pp. 181–193. https://doi.org/10.1007/BF00375292

Bickerton, L., Kontak, D.J., Murphy, J.B., Kellett, D.A., Samson, I.M., Marsh, J.H., Dunning, G., and Stern, R. 2022. Petrochronology constrains the generation and assembly of the South Mountain Batholith, Nova Scotia, Canada: Implications for metallogenic inheritance. Canadian Journal of Earth Sciences. Preprint. https://doi.org/10.1139/cjes-2021-0097

Boggs, S., Jr., 2001, Principles of Sedimentology and Stratigraphy (3rd edition): Upper Saddle River, New Jersey, Prentice Hall, 726p.

Clarke, D.B. and Halliday, A.N. 1985. Sm/Nd isotopic investigation of the age and origin of the Meguma Zone metasedimentary rocks. Canadian Journal of Earth Sciences, 22, pp.102–107. https://doi.org/10.1139/e85-008

Clarke, D.B., Halliday, A.N., and Hamilton, P.J. 1988. Neodymium and strontium isotopic constraints on the origin of the peraluminous granitoids of the South Mountain Batholith, Nova Scotia, Canada. Chemical Geology. Isotope Geoscience Section, 73, pp.15–24. https://doi.org/10.1016/0168-9622(88)90018-8

Clarke, D. B., Chatterjee, A. K., and Giles, P. S. 1993. Petrochemistry, tectonic history, and Sr-Nd systematics of the Liscomb Complex, Meguma Lithotectonic Zone, Nova Scotia. Canadian Journal of Earth Sciences, 30, pp. 449–464. https://doi.org/10.1139/e93-033

Clarke, D.B., MacDonald, M.A., and Tate, M.C. 1997. Late Devonian mafic-felsic magmatism in the Meguma Zone, Nova Scotia. *In* The nature of magmatism in the Appalachian orogen. *Edited by* A.K. Sinha, J.F. Whalen, and J.P. Hogan. Geological Society of America Memoir, 191, pp. 107–127. https://doi.org/10.1130/0-8137-1191-6.107

Clarke, D.B., Fallon, R., and Heaman, L.M. 2000. Interaction among upper crustal, lower crustal, and mantle materials in the Port Mouton pluton, Meguma Lithotectonic Zone, southwest Nova Scotia. Canadian Journal of Earth Sciences, 37, pp. 579–600. https://doi.org/10.1139/e99-124

Culshaw, N.G. and Lee, S.K.Y. 2006. The Acadian Fold Belt in the Meguma Terrane, Nova Scotia: Cross sections, fold mechanisms and tectonic implications. Tectonics, 25. https://doi.org/10.1029/2004TC001752

Culshaw, N. and Liesa, M. 1997. Alleghanian reactivation

of the Acadian fold belt, Meguma Zone, southwest Nova Scotia. Canadian Journal of Earth Sciences, 34, pp. 833–847. https://doi.org/10.1139/e17-068

Culshaw, N. and Reynolds, P. 1997. $^{40}Ar/^{39}Ar$ age of shear zones in the southwest Meguma Zone between Yarmouth and Meteghan, Nova Scotia. Canadian Journal of Earth Sciences, 34, 848–853. https://doi.org/10.1139/e17-069

Cumming, L.M. 1985. A Halifax slate graptolite locality, Nova Scotia. Geological Survey of Canada, Current Research, part A., Paper 85-1A, pp. 215–221. https://doi.org/10.4095/120057

Currie, K.L., Whalen, J.B., Davis, W.J., Longstaffe, F.J., and Cousens, B.L. 1998. Geochemical evolution of peraluminous plutons in southern Nova Scotia, Canada – a pegmatite-poor suite; Lithos, 44, pp. 117–140. https://doi.org/10.1016/S0024-4937(98)00051-6

DePaolo, D. J. 1981. Neodymium isotopes in the Colorado Front Range and crust-mantle evolution in the Proterozoic. Nature, 291, pp. 193–196. https://doi.org/10.1038/291193a0

DePaolo, D. J., Linn, A. M., and Schubert, G. 1991. The continental crustal age distribution: Methods of determining mantle separation ages from Sm–Nd isotopic data and application to the southwestern United States: Journal of Geophysical Research, 96, pp. 2071–2088. https://doi.org/10.1029/90JB02219

Gingras, M.K., Waldron, J.W.F., White, C.E., and Barr, S.M. 2011. The evolutionary significance of a lower Cambrian trace fossil assemblage from the Meguma terrane, Nova Scotia. Canadian Journal of Earth Sciences, 48, pp. 71–85. https://doi.org/10.1139/E10-086

Henderson, B.J. 2016. What do epsilon hafnium isotopic arrays tell us about Wilson cycle tectonics? Implications for the type area in the Appalachian-Variscan Orogen. Unpublished Ph.D. thesis, Geology and Geophysics, School of Physical Sciences, University of Adelaide, Australia, 332p.

Henderson, J. R. 1986. Geology, Ecum Secum area, Nova Scotia; Geological Survey of Canada, "A" Series Map 1648A, scale 1:50 000. https://doi.org/10.4095/120535

Herron, M.M. 1988, Geochemical classification of terrigenous sands from core or log data. Journal of Sedimentary Petrology, 58, pp. 820–829. https://doi.org/10.1306/212F8E77-2B24-11D7-8648000102C1865D

Hibbard, J.P., van Staal, C.R., Rankin, D., and Williams H. 2006. Lithotectonic map of the Appalachian orogen (north), Canada-United States of America. Geological Survey of Canada Map 02041A, 1 sheet, scale 1:1 500 000. https://doi.org/10.4095/221912

Hibbard, J.P., van Staal, C.R., and Miller, B.V. 2007. Links between Carolinia, Avalonia and Ganderia in the Appalachian peri-Gondwanan realm. *In* Whence the Mountains? Inquiries into the Evolution of Orogenic Systems: A Volume in Honor of Raymond A. Price. *Edited by* J.W. Sears, T.A. Harms, C.A. and Evenchick. Geological Society of America Special Paper 433, pp. 291–311. https://doi.org/10.1130/2007.2433(14)

Hicks, R.J., Jamieson, R.A., and Reynolds, P.H. 1999. Detrital and metamorphic $^{40}Ar/^{39}Ar$ ages from muscovite and whole-rock samples, Meguma Supergroup, southern Nova Scotia. Canadian Journal of Earth Sciences, 36, pp. 23–32. https://doi.org/10.1139/e98-081

Hill, J.D. 1991. Geology of the Forest Hill area; in Petrology, tectonic setting, and economic potential of peraluminous granitoid plutons in the Canso and Forest Hill areas, eastern Meguma Terrane, Nova Scotia. Geological Survey of Canada, Bulletin 383, 96p (includes 2 1:50 000-scale maps). https://doi.org/10.4095/131924

Horne, R.J. and Pelley, D. 2007. Geological transect of the Meguma terrane from Centre Musquodoboit to Tangier. *In* Mineral Resources Branch, Report of Activities 2006. *Edited by* D.R. MacDonald. Nova Scotia Department of Natural Resources, Report ME 2007-1, pp. 71–89.

Krogh, T.E. and Keppie, J.D. 1990. Age of detrital zircon and titanite in the Meguma Group, southern Nova Scotia, Canada: Clues to the origin of the Meguma Terrane. Tectonophysics, 177, pp. 307–323. https://doi.org/10.1016/0040-1951(90)90287-I

Le Fèvre, B. and Pin, C. 2002. Determination of Zr, Hf, Th and U by isotope dilution and inductively coupled plasmaquadrupole mass spectrometry after concomitant separation using extraction chromatography. Geostandards and Geoanalytical Research, 26, pp. 161–70. https://doi.org/10.1111/j.1751-908X.2002.tb00884.x

Letsch, D., El Houicha, M., von Quadt, A., and Winkler, W. 2018. A missing link in the peri-Gondwanan terrane collage: the Precambrian basement of the Moroccan Meseta and its lower Paleozoic cover. Canadian Journal of Earth Sciences, 55, pp. 33–51. https://doi.org/10.1139/cjes-2017-0086

Li, C. and Yang, S. 2010. Is Chemical Index of Alteration (CIA) a reliable proxy for chemical weathering in global drainage basins? American Journal of Science, 310, pp. 111–127. https://doi.org/10.2475/02.2010.03

Linnemann, U., Gerdes, A., Hofmann, M., and Marko, L. 2014. The Cadomian orogen: Neoproterozoic to Early Cambrian crustal growth and orogenic zoning along the periphery of the West African Craton—constraints from U–Pb zircon ages and Hf isotopes (Schwarzburg Antiform, Germany). Precambrian Research, 244, pp. 236–278. https://doi.org/10.1016/j.precamres.2013.08.007

MacDonald, L.A., Barr, S.M., White, C.E., and Ketchum, J.W.F. 2002. Petrology, age, and tectonic setting of the White Rock Formation, Meguma terrane, Nova Scotia: evidence for Silurian continental rifting. Canadian Journal of Earth Sciences, 39, pp. 259–277. https://doi.org/10.1139/e01-074

Mahoney, K.L. 1996. The contact metamorphic aureole of

the South Mountain Batholith, Nova Scotia. Unpublished M.Sc. thesis, Acadia University, Wolfville, Nova Scotia, 153 p.

McLennan, S. M. 1993, Weathering and global denudation: The Journal of Geology, 101, pp. 295–303. https://doi.org/10.1086/648222

McLennan, S.M., Taylor, S.R., McCulloch, M.T., and Maynard, J.B. 1990. Geochemical and Nd-Sr isotopic composition of deep-sea turbidites: Crustal evolution and plate tectonic associations. Geochimica et Cosmochimica Acta, 54, pp. 2015–2050. https://doi.org/10.1016/0016-7037(90)90269-Q

Muecke, G.K., Elias, P., and Reynolds, P.H. 1988. Hercynian/Alleghanian overprinting of an Acadian Terrane: $^{40}Ar/^{39}Ar$ studies in the Meguma Zone, Nova Scotia, Canada. Chemical Geology, 73, pp. 153–167. https://doi.org/10.1016/0168-9622(88)90013-9

Murphy, J.B., Fernández-Suárez, J., Keppie, J.D., and Jeffries, T.E. 2004. Contiguous rather than discrete Paleozoic histories for the Avalon and Meguma Terranes based on detrital zircon data: Geology, 32, pp. 585–588. https://doi.org/10.1130/G20351.1

Murphy, J. B., Waldron, J. W. F., Kontak, D. J., Pe-Piper, G., and Piper, D. J. W. 2011. Minas fault zone: Late Paleozoic history of an intra-continental orogenic transform fault in the Canadian Appalachians. Journal of Structural Geology, 33, pp. 312–328. https://doi.org/10.1016/j.jsg.2010.11.012

Nance R.D., Gutiérrez-Alonso G., Keppie J.D., Linnemann U., Murphy J.B., Quesada C., Strachan R.A., and Woodcock N.H. 2010. Evolution of the Rheic Ocean. Gondwana Research, 17, pp. 194–222. https://doi.org/10.1016/j.gr.2009.08.001

Nesbitt, H.W. and Young, G.M. 1982. Early Proterozoic climates and plate motions inferred from major element chemistry of lutites. Nature, 299, pp. 715–717. https://doi.org/10.1038/299715a0

Pin C. and Santos J. F. 1997. Sequential separation of light rare-earth elements, thorium and uranium by miniaturized extraction chromatography: application to isotopic analyses of silicate rocks. Analytica Chimica Acta, 339, pp. 79–89. https://doi.org/10.1016/S0003-2670(96)00499-0

Pothier, H.D., Waldron, J.W.F., White, C.E., Dufrane, A.S., and Jamieson, R.A. 2015. Stratigraphy, provenance and tectonic setting of the Lumsden Dam and Bluestone Quarry formations (Lower Ordovician), Halifax Group, Nova Scotia, Canada. Atlantic Geology, 51, pp. 51–83. https://doi.org/10.4138/atlgeol.2015.003

Pratt, B.R. and Waldron, J.W.F. 1991. A Middle Cambrian trilobite faunule from the Meguma Group of Nova Scotia. Canadian Journal of Earth Sciences, 28, pp. 1843–1853. https://doi.org/10.1139/e91-164

Raeside, R.P. and Jamieson, R.A. 1992. Low-pressure metamorphism of the Meguma terrane, Nova Scotia. Field excursion C-5, GAC-MAC field trip guide, 25 p.

Reynolds, P.H., White, C.E., Barr, S.M., and Muir, C.M. 2012. $^{40}Ar/^{39}Ar$ ages for detrital white mica in Meguma terrane, Nova Scotia, Canada: implications for provenance of the Goldenville and Halifax groups. Canadian Journal of Earth Sciences, 49, pp. 781–795. https://doi.org/10.1139/e2012-022

Robinson, P., Tucker, R.D., Bradley, D., Berry IV, H.N., and Osberg, P.H. 1998. Paleozoic orogens in New England, USA. GFF, 120, pp. 119–148. https://doi.org/10.1080/11035899801202119

Romer, R.L., Kirsch, M., and Kroner, U. 2011. Geochemical signature of Ordovician Mn-rich sedimentary rocks on the Avalonian shelf: Canadian Journal of Earth Sciences, 48, pp. 703–718. https://doi.org/10.1139/e10-092

Roser, B.P. and Korsch, R.J. 1986. Determination of tectonic setting of sandstone-mudstone suites using SiO_2 content and K_2O/Na_2O ratio. Journal of Geology, 94, pp. 635–650. https://doi.org/10.1086/629071

Ryan, R.J., Fox, D., Horne, R.J., Corey, M.C., and Smith, P.K. 1996. Preliminary stratigraphy of the Meguma Group in central Nova Scotia. *In* Minerals and Energy Branch Report of Activities 1995. *Edited by* D.R. MacDonald. Nova Scotia Department of Natural Resources Report ME 1996-001, pp. 27–34.

Santos, J.O.S., Rizzotto, G.J., Potter, P.E., McNaughton, N.J., Matos, R.S., Hartmann, L.A., Chemale, F., Jr.; and Quadros, M.E.S. 2008. Age and autochthonous evolution of the Sunsas Orogen in West Amazon Craton based on mapping and U–Pb geochronology. Precambrian Research, 165, pp. 120–152. https://doi.org/10.1016/j.precamres.2008.06.009

Satkoski, A.M., Barr, S.M., and Samson, S.D. 2010. Provenance of late Neoproterozoic and Cambrian sediments in Avalonia: Constraints from detrital zircon ages and Sm–Nd isotopic compositions in southern New Brunswick, Canada. Journal of Geology, 118, pp. 187–200. https://doi.org/10.1086/649818

Schenk, P.E. 1971. Southern Atlantic Canada, northwestern Africa and continental drift. Canadian Journal of Earth Sciences, 8, pp. 1218–1251. https://doi.org/10.1139/e71-113

Schenk, P.E. 1981. The Meguma Zone of Nova Scotia – a remnant of Western Europe, South America, or Africa? *In* Geology of North Atlantic borderlands. *Edited by* J.M. Kerr, A.J. Ferguson, and L.C. Machan. Canadian Society of Petroleum Geologists Memoir, 7, pp.119–148.

Schenk, P.E. 1991. Events and sea level changes on Gondwana's margin: the Meguma Zone (Cambrian to Devonian) of Nova Scotia, Canada. Geological Society of America Bulletin, 103, pp. 512–521. https://doi.org/10.1130/0016-7606(1991)103<0512:EASLCO>2.3.CO;2

Schenk, P.E. 1995. Meguma Zone. *In* Geology of the

Appalachian-Caledonian Orogen in Canada and Greenland. *Edited by* H. Williams. Geological Survey of Canada, Geology of Canada, 6, pp. 261–277.

Schenk, P.E. 1997. Sequence stratigraphy and provenance on Gondwana's margin: the Meguma Zone (Cambrian to Devonian) of Nova Scotia, Canada: Geological Society of America Bulletin, 109, pp. 395–409. https://doi.org/10.1130/0016-7606(1997)109<0395:SSAPOG>2.3.CO;2

Tanaka, T., Togashi, S., Kamioka, H., Amakawa, H., Kagami, H., Hamamoto, T., Yuhara, M., Orihashi, Y.,Yoneda, S., Shimizu, H.,Kunimaru, T., Takahashi, K.,Yanagi, T.,Nakano, T., Fujimaki, H., Shinjo, R., Asahara, Y., Tanimizu, M. and Dragusanu, C. 2000. JNdi-1: a neodymium isotopic reference in consistency with LaJolla neodymium. Chemical Geology, 168, pp. 279–281. https://doi.org/10.1016/S0009-2541(00)00198-4

Thomas, W.A., Gehrels, G.E., Greb, S.F., Nadon, G.C., Satkoski, A.M., and Romero, M.C. 2017. Detrital zircons and sediment dispersal in the Appalachian foreland: Geosphere, 13, pp. 2206–2230. https://doi.org/10.1130/GES01525.1

Toteu, S. F., Van Schmus, W. R., Penaye, J., and Michard, A. 2001. New U–Pb and Sm–Nd data from northcentral Cameroon and its bearing on the pre-Pan African history of central Africa. Precambrian Research, 108, pp. 45–73. https://doi.org/10.1016/S0301-9268(00)00149-2

Ugidos, J.M., Valladares, M.I., Barba P., and Ellam R.M. 2003. The Upper Neoproterozoic-Lower Cambrian of the Central Iberian Zone, Spain: chemical and isotopic (Sm–Nd) evidence that the sedimentary succession records an inverted stratigraphy of its source. Geochimica et Cosmochimica Acta, 67, pp. 2615–2629. https://doi.org/10.1016/S0016-7037(03)00027-9

van Staal, C.R. and Hatcher, R.D. Jr. 2010. Global setting of Ordovician orogenesis. *In* The Ordovician Earth System. *Edited by* S.C. Finney and W.B.N. Berry. Geological Society of America, Special Paper 466, pp. 1–11. https://doi.org/10.1130/2010.2466(01)

van Staal, C.R. and Barr, S.M. 2012. Lithospheric architecture and tectonic evolution of the Canadian Appalachians. *In* Tectonic Styles in Canada Revisited: the LITHOPROBE perspective. *Edited by* J.A. Percival, F.A. Cook, and R.M. Clowes. Geological Association of Canada Special Paper 49, pp. 41–95.

van Staal, C.R., Barr, S.M., McCausland, P.J.A., Thompson, M.D., and White, C.E., 2021a, Tonian-Ediacaran tectonomagmatic evolution of West Avalonia and its Ediacaran-Early Cambrian interactions with Ganderia: An example of complex terrane transfer due to arc-arc collision? Geological Society of London Special Publication 503, pp. 143–167. https://doi.org/10.1144/SP503-2020-23

van Staal, C.R., Barr, S.M., Waldron, J.W.F., Schofield, D.I., Zagorevski, A., and White, C.E. 2021b. Provenance and Paleozoic tectonic evolution of Ganderia and its relationships with Avalonia and Megumia in the Appalachian-Caledonide orogen. Gondwana Research, 98, pp. 212–243. https://doi.org/10.1016/j.gr.2021.05.025

Waldron, J.W.F. 1992. The Goldenville–Halifax transition, Mahone Bay, Nova Scotia: relative sea-level change in the Meguma source terrane. Canadian Journal of Earth Sciences, 29, pp. 1091–1105. https://doi.org/10.1139/e92-087

Waldron, J.W.F. and Jensen, L.R. 1985. Sedimentology of the Goldenville Formation, Eastern Shore, Nova Scotia. Geological Survey of Canada Paper 85-15, 31 p. https://doi.org/10.4095/120314

Waldron, J.W.F., White, C.E., Barr, S.M., Simonetti, A., and Heaman, L.M. 2009. Provenance of the Meguma terrane, Nova Scotia: rifted margin of early Paleozoic Gondwana. Canadian Journal of Earth Sciences, 46, pp. 1–8. https://doi.org/10.1139/E09-004

Waldron, J.W.F., Schofield, D.I., White, C.E., and Barr, S.M., 2011. Cambrian successions of the Meguma Terrane, Nova Scotia, and Harlech Dome, North Wales: dispersed fragments of a peri-Gondwanan basin? Journal of the Geological Society, London, 168, pp. 83–98. https://doi.org/10.1144/0016-76492010-068

Warsame, H, McCausland, P, White, C.E., Barr, S.M., Dunning, G.R., and Waldron, J. 2021. Meguma terrane orocline: U–Pb age and paleomagnetism of the Silurian Mavillette gabbro, Nova Scotia, Canada. Canadian Journal of Earth Sciences, 58, pp. 315–331. https://doi.org/10.1139/cjes-2020-0089

White, C.E. 2010. Stratigraphy of the Lower Paleozoic Goldenville and Halifax groups in southwestern Nova Scotia. Atlantic Geology, 46, pp. 136–154. https://doi.org/10.4138/atlgeol.2010.008

White, C.E., 2013. Overview geological map of southwestern Nova Scotia. Nova Scotia. Department of Natural Resources, Mineral Resources Branch, Open File Map ME2012-1, scale 1:100 000.

White, C.E. 2019. Bedrock geology map of the central Annapolis Valley area, Nova Scotia. Nova Scotia Department of Energy and Mines, Geoscience and Mines Branch, Open File Map ME 2019-006, scale 1:50 000.

White, C.E. and Barr, S.M. 2010. Lithochemistry of the Lower Paleozoic Goldenville and Halifax groups, southwestern Nova Scotia, Canada: Implications for stratigraphy, provenance, and tectonic setting of Meguma. *In* From Rodinia to Pangea: The Lithotectonic Record of the Appalachian Region. *Edited by* R.P. Tollo, M.J. Bartholomew, M.J., J.P. Hibbard, and P.M. Karabinos. Geological Society of America Memoir, 206, pp. 347–366. https://doi.org/10.1130/2010.1206(15)

White, C.E. and Barr, S.M. 2012a. Meguma terrane revisited: stratigraphy, metamorphism, paleontology, and provenance: GAC-MAC 2012 St. John's post meeting field

guide summary. Geoscience Canada 39, pp. 8–12.

White, C.E. and Barr, S.M. 2012b. The new Meguma: stratigraphy, metamorphism, paleontology, and provenance. Field Trip Guidebook B5, prepared for St. John's 2012 GAC-MAC Joint Annual Meeting, 68 p.

White, C.E. and Barr, S.M. 2017. Stratigraphy and depositional setting of the Silurian–Devonian Rockville Notch Group, Meguma terrane, Nova Scotia, Canada. Atlantic Geology, 53, pp. 337–365. https://doi.org/10.4138/atlgeol.2017.015

White, C. E. and Nickerson, S. J. 2021. Working towards a new bedrock geology map of the Meguma terrane, eastern shore of Nova Scotia: Building a stratigraphy. *In* Geoscience and Mines Branch, Report of Activities 2020-2021. *Edited by* E.W. MacDonald and D.R. MacDonald. Nova Scotia Department of Natural Resources and Renewables, Report ME 2021-002, pp. 73–78.

White, C.E. and Scallion, K-L.2011. Bedrock geology map of the Governor Lake area, part of NTS sheets 21E/01, 02, 07, and 08, Colchester, Guysborough, Halifax, and Pictou counties, Nova Scotia. Nova Scotia Department of Natural Resources, Mineral Resources Branch, Open File Map ME 2011-013, scale 1:50 000.

White, C.E. and Vaccaro, M. 2019. Bedrock mapping in the Meguma terrane: a long-awaited return to the Eastern Shore of Nova Scotia. *In* Geoscience and Mines Branch, Report of Activities 2018-2019. *Edited by* E.W. MacDonald and D.R. MacDonald. Nova Scotia Department of Energy and Mines, Report ME 2019-002, pp. 77–79.

White, C.E. and Vaccaro, M. 2020. Meguma terrane bedrock mapping project, Eastern Shore of Nova Scotia: a progress report. *In* Geoscience and Mines Branch, Report of Activities 2019-2020. *Edited by* D.R. MacDonald and E.W. MacDonald. Nova Scotia Department of Energy and Mines, Report ME 2020-002, pp. 137-140.

White, C.E., Palacios, T., Jensen, S, and Barr, S.M. 2012. Cambrian–Ordovician acritarchs in the Meguma terrane, Nova Scotia, Canada: resolution of Early Paleozoic stratigraphy and implications for paleogeography. Geological Society of America Bulletin, 124, pp. 1773–1792. https://doi.org/10.1130/B30638.1

White, C.E., Barr, S.M., and Linnemann, U. 2018. U–Pb (zircon) ages and provenance of the White Rock Formation of the Rockville Notch Group, Meguma terrane, Nova Scotia, Canada: Evidence for the "Sardian gap" and West African origin. Canadian Journal of Earth Sciences, 55:(6), pp. 589–603. https://doi.org/10.1139/cjes-2017-0196

Editorial responsibility: David P. West, Jr.

APPENDIX

Table A1. Compilation of new and previously published Sm-Nd isotopic data* from the Goldenville and Halifax groups, Meguma terrane, Nova Scotia.

Map #	Sample #	Ch	GZ	Easting	Northing	Rock type	Group	Formation/ Member	Age (Ma)	Nd (ppm)	Sm (ppm)	$^{147}Sm/^{144}Nd$	$^{143}Nd/^{144}Nd$	εNd (t)	εNd (0)	εNd (370)	TDM2	Data source
a13	H01-W09-136	y	20T	389034	4988767	metasiltstone	Halifax	Hells Gate Falls	470	34.30	6.39	0.1126	0.511869	-9.96	-15.0	-11.1	1927	This study
a12	A12-RT05-004	y	20T	286945	4943686	metasiltstone	Halifax	Bear River	485	51.27	9.28	0.1094	0.511879	-9.41	-14.8	-10.7	1854	Waldron *et al* . 2009
a11	O16-RT05-010	y	19T	727447	4864299	metasiltstone	Goldenville	Bloomfield	503	60.80	10.40	0.1031	0.511904	-8.31	-14.4	-9.9	1715	This study
a10	O16-RT05-011(LR042A)	y	19T	727368	4864751	metasandstone	Goldenville	Church Pt	505	20.81	3.85	0.1117	0.511991	-7.14	-12.6	-8.7	1729	Waldron *et al* . 2009
a09	O16-RT-05-013	y	19T	728656	4867810	metasandstone	Goldenville	Church Pt	510	21.45	3.89	0.1096	0.511981	-7.15	-12.9	-8.8	1709	Waldron *et al* . 2009
a08	O16-RT-05-014	y	19T	728321	4869531	metasandstone	Goldenville	Church Pt	520	20.35	3.83	0.1136	0.512015	-6.64	-12.2	-8.3	1726	Waldron *et al* . 2009
a07	O16-RT05-015	y	19T	727738	4870922	metasiltstone	Goldenville	High Head	530	28.40	5.68	0.1209	0.512132	-4.74	-9.9	-6.3	1670	This study
a06	LA-090	y	19T	727630	4870991	metasandstone	Goldenville	High Head	531	20.59	4.24	0.1244	0.512422	0.69	-4.3	-0.8	1243	Waldron *et al* . 2009
a05	O16-RT05-017	y	19T	727582	4873886	metasiltstone	Goldenville	Church Pt	535	21.10	4.34	0.1245	0.512138	-4.82	-9.8	-6.4	1727	This study
a04	B01-W13-002B	y	19T	726585	4878837	metasiltstone	Goldenville	Church Pt	538	37.10	7.50	0.1222	0.512263	-2.20	-7.4	-3.8	1477	This study
a03	B01-W13-001A	y	19T	726797	4878710	metamudstone	Goldenville	Church Pt	540	42.20	8.78	0.1258	0.512268	-2.33	-7.3	-3.9	1528	This study
a02	LA-089	y	19T	727834	4877396	metasandstone	Goldenville	Church Pt	543	17.52	3.45	0.1190	0.512407	0.89	-4.5	-0.9	1196	Waldron *et al* . 2009
a01	B01-RT05-18A	y	19T	727833	4877395	metasandstone	Goldenville	Church Pt	544	15.60	3.28	0.1275	0.512372	-0.38	-5.2	-2.0	1375	This study
b19	76-20		20T	410424	4928978	slate	Halifax	Cunard	494	65.35	12.46	0.1152	0.511864	-9.97	-15.1	-11.3	1985	Clarke and Halliday 1985
b18	A07-W06-086A	y	20T	365065	4913939	metasiltstone	Halifax	Cunard	495	10.82	2.34	0.1306	0.511937	-9.51	-13.7	-10.6	2218	Waldron *et al* . 2009
b17	A07-W06-086B	y	20T	365065	4913939	slate	Halifax	Cunard	495	41.08	7.27	0.1069	0.511877	-9.18	-14.9	-10.7	1813	Waldron *et al* . 2009
b16	76-18		20T	407867	4924763	slate	Halifax	Cunard	500	26.65	5.31	0.1205	0.511921	-9.13	-14.0	-10.4	2005	Clarke and Halliday 1985
b15	P15-RT05-027A	y	20T	350491	4870120	metasiltstone	Goldenville	Moshers Island	501	37.30	7.52	0.1218	0.512113	-5.45	-10.3	-6.8	1718	This study
b14	WXNS-17b	y	20T	320800	4853750	hornfels - metasiltstone	Goldenville	Government Pt	503	35.10	6.65	0.1146	0.511931	-8.53	-13.8	-10.0	1871	Currie *et al* . 1998
b13	WXNS-17a		20T	320800	4853750	hornfels - metasiltstone	Goldenville	Government Pt	504	11.73	2.45	0.1261	0.511891	-10.04	-14.6	-11.3	2184	Currie *et al* . 1998
b12	LA-084	y	20T	408396	4924408	metasandstone	Goldenville	Government Pt	505	22.08	4.16	0.1140	0.511902	-9.02	-14.4	-10.5	1904	Waldron *et al* . 2009
b11	76-13		20T	408640	4923762	metasandstone	Goldenville	Government Pt	506	23.95	4.48	0.1130	0.511881	-9.38	-14.8	-10.9	1917	Clarke and Halliday 1985
b10	P15-RT05-025A	y	20T	351142	4869124	metasandstone	Goldenville	Government Pt	508	20.09	3.80	0.1142	0.511983	-7.43	-12.8	-8.9	1785	Waldron *et al* . 2009
b09	76-22		20T	413439	4924618	metasandstone	Goldenville	Green Hbr	510	25.14	4.70	0.1130	0.511933	-8.31	-13.8	-9.9	1839	Clarke and Halliday 1985
b08	P15-RT05-023A	y	20T	352300	4868824	metasandstone	Goldenville	Green Hbr	511	17.70	3.47	0.1185	0.511975	-7.84	-13.0	-9.3	1878	This study
b07	P15-RT05-029	y	20T	353380	4868477	metasandstone	Goldenville	Green Hbr	515	23.20	4.36	0.1137	0.511995	-7.09	-12.6	-8.7	1758	This study
b06	A02-W05-153A		20T	375773	4894501	metasandstone	Goldenville	Lake Rossignol	520	24.50	4.64	0.1145	0.511980	-7.38	-12.9	-9.0	1795	This study
b05	A02-W13-003	y	20T	365707	4883099	metasiltstone	Goldenville	Green Hbr	530	37.80	7.46	0.1193	0.512028	-6.67	-11.9	-8.3	1809	This study
b04	A02-W05-027		20T	370201	4881098	metasandstone	Goldenville	Green Hbr	533	19.70	3.70	0.1136	0.512054	-5.74	-11.4	-7.5	1667	This study
b03	P13-W02-028	y	20T	263670	4849771	metasandstone	Goldenville	Moses Lk	535	17.50	3.85	0.1327	0.512439	0.49	-3.9	-0.9	1338	This study
b02	P13-WO2-085	y	20T	264760	4849158	metasandstone	Goldenville	Moses Lk	536	22.79	4.73	0.1255	0.512427	0.76	-4.2	-0.8	1250	Waldron *et al* . 2009
b01	P12-W02-002	y	20T	260746	4844529	metasandstone	Goldenville	Moses Lk	537	11.20	2.51	0.1350	0.512186	-4.59	-8.9	-6.0	1864	This study
c19	LR080B	y	20T	498149	4997829	metasandstone	Halifax	Glen Brook	480	16.18	3.14	0.1173	0.511927	-9.01	-13.9	-10.2	1930	Waldron *et al* . 2009
c18	LG064a	y	20T	516193	5007794	hornfels - metasiltstone	Halifax	Cunard	493	46.64	8.60	0.1113	0.511827	-10.46	-15.9	-11.8	1966	Clarke et al. 1993
c17	76-12	y	20T	447834	4943756	hornfels - slate	Halifax	Cunard	498	47.81	8.86	0.1120	0.511984	-7.38	-12.8	-8.8	1745	Clarke and Halliday 1985
c16	LG120-2	y	20T	526341	5013572	hornfels - metamudstone	Halifax	Cunard	500	32.45	5.96	0.1108	0.511930	-8.39	-13.8	-9.8	1805	Clarke et al. 1993
c15	LG094		20T	523777	5010568	xenolith in Porcupine Lk pluton	Goldenville	Taylors Hd	503	33.26	5.96	0.1082	0.511997	-6.82	-12.5	-8.4	1663	Clarke et al. 1993
c14	76-07	y	20T	451638	4961254	metasandstone	Goldenville	Taylors Hd	504	43.98	8.32	0.1143	0.511879	-9.51	-14.8	-11.0	1945	Clarke and Halliday 1985
c13	LG171-2	y	20T	517570	5006253	hornfels - metasiltstone	Goldenville	Taylors Hd	505	69.95	12.13	0.1047	0.511856	-9.33	-15.3	-11.0	1806	Clarke et al. 1993
c12	NS2/3	y	20T	431285	4970561	metasandstone xeno	Goldenville	Taylors Hd	507	43.53	8.06	0.1119	0.512031	-6.35	-11.9	-7.9	1673	Clarke *et al* . 1988
c11	NS2/4	y	20T	431285	4970561	metasandstone xeno	Goldenville	Taylors Hd	507	31.52	7.62	0.1461	0.512259	-4.12	-7.4	-5.1	2005	Clarke *et al* . 1988
c10	NS2/5b		20T	431285	4970561	metasandstone xeno	Goldenville	Taylors Hd	507	68.66	15.31	0.1348	0.512279	-3.00	-7.0	-4.1	1681	Clarke *et al* . 1988

APPENDIX

Table A1. Continued.

Map #	Sample #	Ch	GZ	Easting	Northing	Rock type	Group	Formation/ Member	Age (Ma)	Nd (ppm)	Sm (ppm)	$^{147}Sm/^{144}Nd$	$^{143}Nd/^{144}Nd$	εNd (t)	εNd (0)	εNd (370)	TDM2	Data source
c09	SMB13-185	y	20T	511582	4979268	metasandstone	Goldenville	Taylors Hd	508	16.30	3.33	0.1230	0.511975	-8.16	-13.0	-9.5	1970	This study
c08	SMB13-186	y	20T	511127	4979788	metasiltstone	Goldenville	Taylors Hd	510	29.70	5.70	0.1159	0.511984	-7.50	-12.8	-9.0	1814	This study
c07	LG068	y	20T	523685	5006145	metasandstone	Goldenville	Taylors Hd	512	32.78	6.09	0.1121	0.511997	-6.98	-12.5	-8.6	1728	Clarke *et al*. 1993
c06	SMB13-183	y	20T	525299	4963752	metasandstone	Goldenville	Tangier	514	20.70	4.11	0.1202	0.512047	-6.51	-11.6	-8.0	1795	This study
c05	SMB13-184	y	20T	523336	4961278	metasandstone	Goldenville	Tangier	515	20.00	3.90	0.1177	0.512017	-6.92	-12.2	-8.4	1796	This study
c04	LR083A	y	20T	504308	4981611	metasandstone	Goldenville	Tangier	516	17.35	3.38	0.1179	0.512037	-6.54	-11.8	-8.1	1768	Waldron *et al*. 2009
c03	MR05-097-2	y	20T	504750	4980977	metasiltstone	Goldenville	Moose River	520	16.90	3.65	0.1306	0.512210	-3.96	-8.4	-5.3	1722	This study
c02	MR05-097-8	y	20T	504750	4980977	metasiltstone	Goldenville	Moose River	519	26.60	5.52	0.1253	0.512202	-3.77	-8.5	-5.2	1633	This study
c01	MR05-097-9	y	20T	504750	4980977	metasiltstone	Goldenville	Moose River	518	23.90	4.82	0.1219	0.512092	-5.71	-10.7	-7.2	1754	This study

*Analytical methods for this study are described in the manuscript text.
Abbreviations: Ch, whole-rock chemistry; y, yes (data available in Table S1); xeno, xenolith; Hd, Head; Lk, Lake; Hbr, Harbour

U–Pb geochronology of Late Silurian (Wenlock to Pridoli) volcanic and sedimentary rocks, central Newfoundland Appalachians: targeting the timing of transient extension as a prelude to Devonian orogenic gold mineralization

Ian W. Honsberger[1*], Wouter Bleeker[1], Sandra L. Kamo[2], Chelsea N. Sutcliffe[2], and Hamish A.I. Sandeman[3]

1. Geological Survey of Canada, Ottawa, Ontario K1A 0E8, Canada
2. Jack Satterly Geochronology Laboratory, Department of Earth Sciences, University of Toronto, Toronto, Ontario M5S 3B1, Canada
3. Geological Survey Division, Department of Industry, Energy and Technology, Government of Newfoundland and Labrador, St. John's, Newfoundland A1B 4J6, Canada
*Corresponding author: ian.honsberger@nrcan-rncan.gc.ca

Date received:14 March 2022 ¶ Date accepted 10 June 2022

ABSTRACT

Bimodal igneous suites and associated immature clastic sedimentary rocks are characteristic of many orogenic gold-mineralized, crustal-scale fault zones globally. In the central Newfoundland Appalachian orogen, the Rogerson Lake Conglomerate belt and Botwood basin are Late Silurian (Wenlock to Pridoli), fault-controlled sedimentary rock sequences and magmatic suites closely associated with orogenic gold mineralization; however, the spatio-temporal evolution of faulting and associated sedimentation and magmatism are not fully resolved.

U–Pb zircon geochronological results were obtained by using an integrated approach employing LA-ICPMS (laser ablation-inductively coupled plasma mass spectrometry) followed by CA-ID-TIMS (chemical abrasion-isotope dilution-thermal ionization mass spectrometry) on the same detrital samples. Using this approach, a maximum depositional age for sedimentary rocks of the Rogerson Lake Conglomerate sequence is 421.9 ± 1.0 Ma (Pridoli), which confirms that they are younger than, and stratigraphically overlie, ca. 422–420 Ma igneous rocks exposed along the central Newfoundland gold belt. Towards the stratigraphic middle of the Botwood basin in north-central Newfoundland, a tuffite layer intercalated with graded siltstone produced a maximum depositional age of 427.9 ± 3.1 Ma (Wenlock; Homerian). The age of emplacement of an autobrecciated, flow-banded rhyolite dome of the Charles Lake volcanic belt along the northwestern Botwood basin is 429.3 ± 0.7 Ma (Wenlock; Homerian). The high-precision CA-ID-TIMS zircon data establish a clear link between Wenlock to Pridoli magmatism and sedimentation throughout central Newfoundland. Furthermore, these geochronological results are consistent with a structural model involving the southeastward (present-day coordinates) advancement of a transient extensional fault system across strike of the Exploits Subzone between ca. 429 and 418 Ma, with propagation along strike to the southwest (Rogerson Lake Conglomerate belt) between ca. 422 and 418 Ma. Extensional faulting may have contributed to basin formation, subsidence, and exhumation of pre-Late Silurian rocks of the Exploits Subzone.

Time-transgressive, extension-related magmatism and clastic sedimentation appear to mark the transition between the Salinic and Acadian orogenic cycles along the central Newfoundland gold belt. Transient Wenlock to Pridoli lithospheric extension may have been important for increasing heat and fluid flow in the crust as a prelude to Devonian crustal thickening, fluid focussing, and orogenic gold mineralization.

RÉSUMÉ

Les suites ignées bimodales et les roches sédimentaires clastiques immatures connexes sont caractéristiques de nombreuses zones faillées d'échelle crustale à minéralisation aurifère orogénique à l'échelle planétaire. Dans l'orogenèse appalachienne du centre de Terre-Neuve, la ceinture du conglomérat du lac Rogerson et le bassin de Botwood sont des suites magmatiques contrôlées par des failles et des séquences de roches sédimentaires du Silurien tardif (du Wenlock au Pridoli), étroitement associées à une minéralisation aurifère orogénique; l'évolution spatio-temporelle de la déformation par failles et le magmatisme ainsi que la sédimentation connexe n'ont toutefois pas été tout à fait résolus.

doi:10.4138/atlgeo.2022.009

On a obtenu des résultats géochronologiques U–Pb sur zircon au moyen d'une approche intégrée employant l'ablation par laser et la spectrométrie de masse avec plasma à couplage inductif (LA-ICPMS), suivies d'une analyse par abrasion chimique, par dilution isotopique et par spectrométrie de masse à thermoionisation (CA-ID-TIMS) des mêmes échantillons détritiques. Selon cette approche, l'âge maximal de sédimentation de la séquence de conglomérat du lac Rogerson est de 421,9 ± 1,0 Ma (Pridoli), ce qui confirme qu'elle est plus récente et qu'elle recouvre stratigraphiquement les roches ignées d'environ 422 à 420 Ma affleurant le long de la ceinture aurifère du centre de Terre-Neuve. Vers le milieu stratigraphique du bassin de Botwood dans le centre-nord de Terre-Neuve, une couche de tuffite interlitée de siltite granoclassée a produit un âge de sédimentation maximal de 427,9 ± 3,1 Ma (Wenlock, Homérien). L'âge de mise en place d'un dôme de rhyolite à rubanement de coulée, autobréchifié, de la ceinture volcanique du lac Charles le long du nord-ouest du bassin de Botwood est de 429,3 ± 0,7 Ma (Wenlock, Homérien). Les données de datation sur zircon par CA-ID-TIMS haute précision établissent un lien clair entre le magmatisme du Wenlock au Pridoli et la sédimentation partout dans le centre de Terre-Neuve. De plus, ces résultats chronologiques correspondent à un modèle structural présumant un avancement vers le sud-est (coordonnées actuelles) d'un système de failles d'extension transitoire en travers de l'orientation longitudinale de la sous-zone Exploits entre environ 429 et 418 Ma, avec une propagation le long de l'axe longitudinal vers le sud-ouest (ceinture du conglomérat du lac Rogerson) entre 422 et 418 Ma. La déformation par failles d'extension pourrait avoir contribué à la formation du bassin, à l'affaissement et à l'exhumation des roches préalables au Silurien tardif de la sous-zone Exploits.

Le magmatisme apparenté à l'extension, transgressif au fil du temps, et la sédimentation clastique semblent marquer la transition entre les cycles orogénique, salinique et acadien le long de la ceinture aurifère du centre de Terre-Neuve. L'extension lithosphérique transitoire du Wenlock au Pridoli pourrait s'être avérée importante pour accroître la chaleur et la circulation des fluides dans la croûte en guise de prélude à l'épaississement de la croûte, à la concentration des fluides et à la minéralisation aurifère orogénique du Dévonien.

[*Traduit par la redaction*]

INTRODUCTION

Fault-controlled magmatic suites and upper-crustal, immature clastic sedimentary rock sequences containing panels of polymict conglomerate are characteristic of many orogenic gold-mineralized fault systems globally (e.g., Hodgson 1993; Evans 1996; Poulsen *et al.* 2000; Bleeker 2002). Such rock sequences are not only key targets for gold exploration, but also provide records of fault zone dynamics that drive gold mineralization events (e.g., Bleeker 2012, 2015). Accordingly, constraining the setting, age, and process evolution of igneous and clastic sedimentary rocks associated with orogenic gold mineralization is essential for understanding the controls on mineralization.

In the central Newfoundland Appalachians, an approximately 400 km-long system of crustal-scale, northeast-southwest trending fault zones of the Exploits Subzone (Dunnage Zone) are delineated by post-Ordovician magmatic suites and immature clastic sedimentary rock sequences and closely associated orogenic gold mineralization (Figs. 1 and 2; Tuach *et al.* 1988; Tuach 1992; Evans 1996; Wardle 2005). The setting, timing, and associated faulting processes in this mineralized terrane are not fully understood because outcrop is sparse and gold-focussed exploration in areas of little outcrop has a relatively short history (~35 years, see Sandeman *et al.* this volume). The processes of polyphase fault reactivation that control orogenic gold mineralization, for example, are only beginning to be constrained (Figs. 1 and 2; Willner *et al.* 2018, 2022; Honsberger *et al.* 2022). Additionally, the occurrence of extension-related Silurian basins in central and western Newfoundland with strongly bimodal magmatic suites and clastic sedimentary rock sequences (Fig. 1; Colman-Sadd *et al.* 1990; Kusky and Kidd 1996; O'Brien 2003; Whalen *et al.* 2006) is in contrast to compressional deformational structures documented throughout the Dunnage Zone (e.g., Karlstrom *et al.* 1982; Valverde-Vaquero *et al.* 2006; van Staal and Barr 2012). Accordingly, some workers have interpreted these Silurian basin rocks to have formed during thrusting (e.g., Karlstrom *et al.* 1982; van Staal *et al.* 2014), whereas others considered such sequences to represent pull-apart basins related to protracted strike-slip motion (Kusky *et al.* 1987; Buchan and Hodych 1992; Kusky and Kidd 1996; O'Brien 2003). To resolve such discrepancies related to the Silurian tectonic evolution of central Newfoundland, stratigraphic, structural, geochemical, and geochronological data must be integrated. High-precision geochronological data are particularly useful in the Exploits Subzone because of rapid transitions (<5 million years) between deformational events and tectonic environments spanning the Salinic (Late Silurian) and Acadian (Early Devonian) orogenic cycles (e.g., van Staal *et al.* 2014).

In the present investigation, regional field observations, targeted geochronology sampling, and integrated LA-ICPMS and CA-ID-TIMS U–Pb zircon geochronological analyses of volcanic and sedimentary rocks establish the spatiotemporal dynamics of Wenlock to Pridoli extensional faulting in central Newfoundland, which may have been the operative process marking the transition between the Salinic and Acadian orogenic cycles. Silurian clastic sedimentary rocks in central Newfoundland were the subjects of a previous U–Pb LA-ICPMS geochronological study (Pollock *et al.* 2007) and, as well, one sample of these rocks was analyzed as part of a combined U–Pb-Hf isotopic study (Henderson *et al.* 2018). These previous investigations focussed on detrital zircon provenance but maximum depositional and

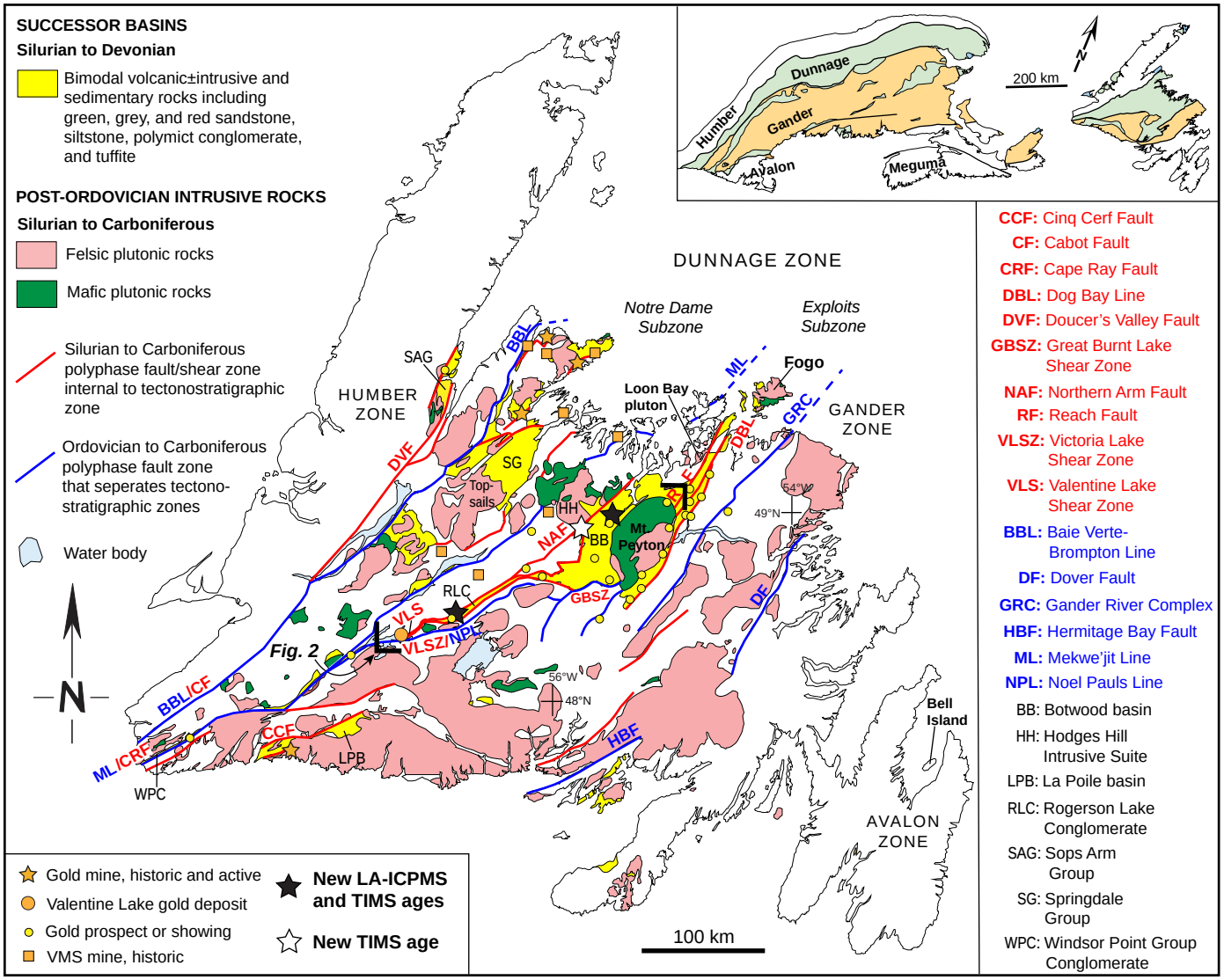

Figure 1. Simplified geologic map of the island of Newfoundland showing major fault zones, post-Ordovician magmatic and sedimentary rocks, and select gold-mineralized zones and historic volcanogenic massive sulfide (VMS) mines (modified from Colman-Sadd *et al.* 1990). Blue lines delineate polyphase fault zones that separate the tectonostratigraphic zones defined by Williams (1978), Williams *et al.* (1988), and Hibbard *et al.* (2006). The names of the boundary fault zones (blue lines) are labelled with blue text. The red lines with red text are fault/shear zones that occur internal to the tectonostratigraphic zones. Red text along blue lines is the name of the fault/shear zone that reactivates and overprints the boundary fault zone. The black text is used for notable geological units. Two bold, black, L-shaped lines mark the southwest and northeast corners of the rectangular area enlarged in Figure 2. Geochronology sample locations are marked by black (LA-ICPMS and TIMS) and white (TIMS) stars. Gold occurrences are from the Geological Survey of Newfoundland and Labrador, Department of Industry, Energy and Technology's Mineral Occurrence Database. Inset is a simplified tectonic lithofacies map of the northern Appalachian orogen based on Williams (1978) and Hibbard *et al.* (2006).

crystallization ages for the sedimentary and igneous rocks were not determined more precisely by CA-ID-TIMS. Absolute minimum ages of deposition for clastic sedimentary rocks in central Newfoundland have been estimated from U–Pb rutile and $^{40}Ar/^{39}Ar$ white mica ages of ca. 410 Ma (Honsberger *et al.* 2022) and ca. 390 Ma (Willner *et al.* 2018), respectively, in quartz veins that cut polymict conglomerate (Rogerson Lake Conglomerate).

GEOLOGICAL SETTING

The island of Newfoundland exposes Mesoproterozoic to Ordovician accretionary terranes from four fault-bounded tectonostratigraphic zones of the northern Appalachian orogen: Humber, Dunnage (Notre Dame and Exploits subzones), Gander, and Avalon zones (Fig. 1; Williams 1978; Williams *et al.* 1988). Orogenic gold mineralization in central Newfoundland, however, is not structurally controlled

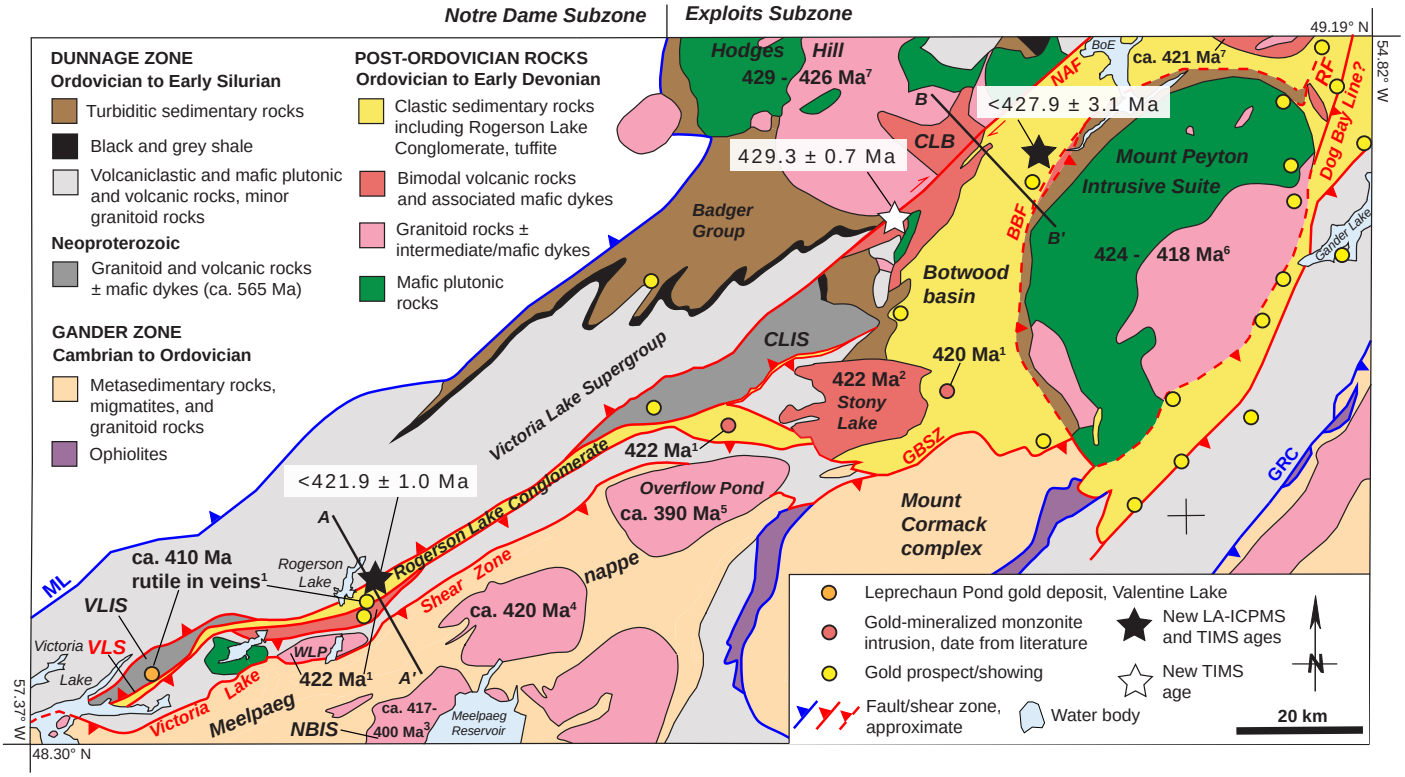

Figure 2. Simplified geologic map of the central Newfoundland orogenic gold belt (modified from Colman-Sadd et al. 1990; O'Brien 2003; Rogers and van Staal 2005; Rogers *et al.* 2005; van Staal *et al.* 2005). Red lines and text mark major Early Devonian fault/shear zones related to emplacement of orogenic gold-bearing veins (Honsberger et al. 2022). A local boundary between the Dunnage and Gander zones in this area has been referred to as Noel Paul's Line (Fig. 1; Williams *et al.* 1988), which is the same age as the regionally extensive Early Devonian Victoria Lake Shear Zone that overprints and imbricates the Dunnage-Gander boundary across central Newfoundland (Valverde-Vaquero and van Staal 2002). Accordingly, the Victoria Lake Shear Zone is coloured red, unlike in Figure 1, to demonstrate that it does not represent sensu stricto the original boundary between the Dunnage and Gander zones. Blue lines and text are fault zones that separate the tectonostratigraphic zones. Faults within the Victoria Lake Supergroup are not illustrated. Geochronology sample locations are marked by black (LA-ICPMS and TIMS) and white (TIMS) stars, with absolute ages indicated. References to ages from the literature are as follows: 1, Honsberger *et al.* (2022); 2, Dunning *et al.* (1990) and McNicoll *et al.* (2006); 3, Kerr (1997); 4, Valverde-Vaquero *et al.* (2006); 5, Dallmeyer *et al.* (1983); 6, Sandeman *et al.* (2017); 7, Dickson (2000), van Staal et al. (2014), and G. Dunning, personal communication 2021. Cross-section lines A-A′ and B-B′ are illustrated in Figures 3 and 4, respectively. Gold occurrences are from the Geological Survey of Newfoundland and Labrador, Department of Industry, Energy and Technology's Mineral Occurrence Database. Abbreviations: BBF – Botwood Basin Fault Zone; BoE – Bay of Exploits; CLB – Charles Lake volcanic belt; CLIS – Crippleback Lake Intrusive Suite; GBSZ – Great Burnt Lake Shear Zone; GRC – Gander River Complex; ML – Mekwe'jit Line; NAF – Northern Arm Fault; NBIS – North Bay Intrusive Suite; RF – Reach Fault; VLIS – Valentine Lake Intrusive Suite; VLS – Valentine Lake Shear Zone; WLP – Wilding Lake pluton.

sensu stricto by the fault zones that separate the tectonostratigraphic zones. Instead, gold mineralization is hosted along younger fault/shear zones that overprint, reactivate, and crosscut older stratigraphy and tectonostratigraphic zone boundaries (Figs. 1 and 2; e.g., Honsberger *et al.* 2022). In the Exploits Subzone (Fig. 2), for example, gold mineralization occurs along a Devonian crustal-scale thrust fault system that imbricates Gander Zone basement of the Meelpaeg Subzone and Ordovician Exploits Subzone rocks (Kean and Jayasinghe 1980; Colman-Sadd *et al.* 1990; Honsberger *et al.* 2022). This fault system corresponds to the Acadian deformation front and includes the regionally extensive, southeast-dipping Victoria Lake Shear Zone (Valverde-Vaquero *et al.* 2006), which correlates with Noel Paul's Line (Williams *et al.* 1988; Valverde-Vaquero and van Staal 2002), a local boundary in central Newfoundland that separates rocks of the Dunnage and Gander zones. Accordingly, a northwest-dipping Salinic suture zone representing the Dunnage-Gander boundary (e.g., van Staal *et al.* 2014) is not preserved in central Newfoundland because it was overprinted by Devonian thrusts during far-field compression associated with the Acadian orogenic cycle (e.g., Valverde-Vaquero *et al.* 2006). Northwest-dipping structures along the central Newfoundland gold belt are associated with

Devonian deformation and include the Valentine Lake Shear Zone, which hosts an approximately five-million-ounce orogenic gold deposit at Valentine Lake (Dunsworth and Walford 2018; Lincoln *et al.* 2018; Figs. 1 and 2).

The pre-Silurian terranes of the Exploits Subzone (Fig. 2) consist of Neoproterozoic magmatic suites (ca. 565 Ma Valentine Lake and Crippleback Lake intrusive suites) and overlying Cambrian to Ordovician, volcano-sedimentary assemblages of the Penobscot and Popelogan-Victoria arc and backarc systems including the Victoria Lake Supergroup and correlatives (Kean and Evans 1988; Evans *et al.* 1990; O'Brien 2003; Rogers *et al.* 2006). Accretion of pre-Silurian rocks in the Exploits Subzone to composite Laurentia along the Laurentia-Gondwana suture zone or "Mekwe'jit Line" (see White and Waldron 2022; Sandeman *et al.* this volume) began in the Late Ordovician during the third and final phase of the Taconic orogenic cycle (Zagorevski *et al.* 2007; van Staal and Barr 2012). The subsequent initiation of subduction of the Tetagouche-Exploits backarc basin beneath composite Laurentia (Salinic orogenic cycle) was then accompanied by deposition of overlying Late Ordovician—Early Silurian black and grey shale and turbiditic forearc sequences of the Badger Group (Fig. 2; Colman-Sadd *et al.* 1990; O'Brien 2003; van Staal and Barr 2012; Waldron *et al.* 2012). The terminal Salinic suture zone (ca. 435 Ma, van Staal *et al.* 2014) is interpreted to correspond to the Dog Bay Line in north-central Newfoundland (Figs. 1 and 2; Williams 1993; Williams *et al.* 1993; Pollock *et al.* 2007). However, detailed local and regional field-based observations indicate that the Dog Bay Line sensu stricto is a post-Salinic, southeast-dipping zone of strong deformation associated with the Acadian orogenic cycle (Dickson 2006; Dickson *et al.* 2007; Sandeman 2021). This implies that the precise trace of the northwest-dipping Salinic suture is not well defined in the field because it was overprinted by Devonian deformation along the southeast-dipping Dog Bay Line (i.e., Dog Bay fault, Sandeman 2021), which is the preferred interpretation herein.

In central Newfoundland, Wenlock to Pridoli bimodal igneous rocks and associated polymict conglomerate and arenitic sandstone of the Rogerson Lake Conglomerate sequence (Kean and Jayasinghe 1980) are juxtaposed against, and nonconformably overlie, Neoproterozoic tonalite, trondhjemite, and granodiorite basement (±mafic dykes) of the Valentine Lake and Crippleback Lake intrusive suites (Colman-Sadd *et al.* 1990; van Staal *et al.* 2005; Figs. 2–4). The gold-mineralized Rogerson Lake Conglomerate is the diagnostic immature clastic sedimentary rock that delineates the structurally controlled central Newfoundland gold belt (Fig. 2; Evans 1996; Wardle 2005). This polymict conglomerate (±intercalated grey to pinkish sandstone) ranges from unmetamorphosed to lower greenschist facies and is purplish-grey to grey, poorly sorted and clast supported, and contains locally-sourced, deformed to undeformed, pebble to cobble-sized clasts of felsic and mafic igneous rocks, sandstone, siltstone, shale, and jasper, within a matrix of sand, silt, and clay (Kean and Jayasinghe 1980; Valverde-Vaquero and van Staal 2002; Rogers *et al.* 2005; Pollock *et al.* 2007; Honsberger *et al.* 2019). The purplish-red jasper clasts are distinctive and suggestive of an Early Ordovician ironstone source similar to that now exposed on Bell Island offshore the Avalon Peninsula (Fig. 1; Todd *et al.* 2018). The Rogerson Lake Conglomerate is imbricated with ca. 422 Ma felsic volcanic and volcaniclastic rocks, granitoid and gabbro bodies, and is locally cut by lower greenschist facies mafic dykes (Honsberger *et al.* 2019, 2020). The Neoproterozoic to Late Silurian rocks in central Newfoundland are cut by orogenic gold-bearing quartz vein systems that define the main mineral resource of the central Newfoundland gold belt (Evans 1996; Honsberger *et al.* 2022).

Northeast along strike of the Rogerson Lake Conglomerate belt, related clastic sedimentary rocks of the Botwood Group (Williams 1962) occur in the Botwood basin (Figs. 1 and 2; Kusky *et al.* 1987; O'Brien 2003). Sedimentary rocks of the Botwood Group include gold-mineralized, grey, green, and red sandstone and siltstone intercalated with felsic tuff (Wigwam Formation; O'Brien 1993; Colman-Sadd 1994; Williams *et al.* 1995; Dickson *et al.* 2000). Magmatic rocks associated with the Botwood Group include: the ca. 424–418 Ma bimodal Mount Peyton Intrusive Suite (Strong 1979; Blackwood 1982; Strong and Dupuy 1982; Dickson 1993; Sandeman *et al.* 2017); the ca. 422 Ma Laurenceton and Stony Lake volcanic rocks and equivalents (Williams 1972; Colman-Sadd *et al.* 1990; Dunning *et al.* 1990; McNicoll *et al.* 2006; van Staal *et al.* 2014; Honsberger *et al.* 2022); the ca. 422 volcanic rocks and dykes of the composite Fogo Island Intrusive Suite (Elliot *et al.* 1991; Sandeman and Malpas 1995; Kerr 2013; Donaldson *et al.* 2015), and ca. 420 monzonite intrusions (Fig. 2; Honsberger *et al.* 2020). Carbonate-bearing and fossiliferous sandstone and siltstone sequences of the Indian Islands Group (Boyce and Dickson 2006; Dickson 2006; Dickson *et al.* 2007) comprise the rocks of the easternmost Botwood basin. Some workers interpret these sedimentary rocks to represent peri-Gondwanan detrital sediments deposited exclusively on the Ganderian side of the Salinic suture zone (Williams 1993; Williams *et al.* 1993; Currie 1995; Pollock *et al.* 2007), whereas others have questioned their lithologic distinction from similar but fossil-poor clastic sedimentary rocks of the adjacent Botwood Group (Dickson 2006; Dickson *et al.* 2007).

Northwest of the Botwood Group, the Hodges Hill Intrusive Suite, which represents a slightly older pulse of Late Silurian magmatism (ca. 429 to 426 Ma; Whalen *et al.* 1997, 2006; Dickson 1999, 2000; van Staal *et al.* 2014; G. Dunning, personal communication 2021), crosscuts the Mekwe'jit Line (Figs. 1 and 2; Colman-Sadd *et al.* 1990). The Hodges Hill Intrusive Suite comprises granitic to gabbroic units that are cut by intermediate and mafic dykes and intrudes, in the east, contemporaneous bimodal volcanic rocks of the Charles Lake volcanic belt (Figs. 1 and 2; Dickson 1999, 2000). Slightly older, Late Silurian (ca. 429–426 Ma) magmatic and clastic sedimentary rocks of the Topsails Intrusive Suite and Springdale Group (Chandler *et al.* 1987; Whalen *et al.* 1997, 2006), respectively, occur farther northwest and are

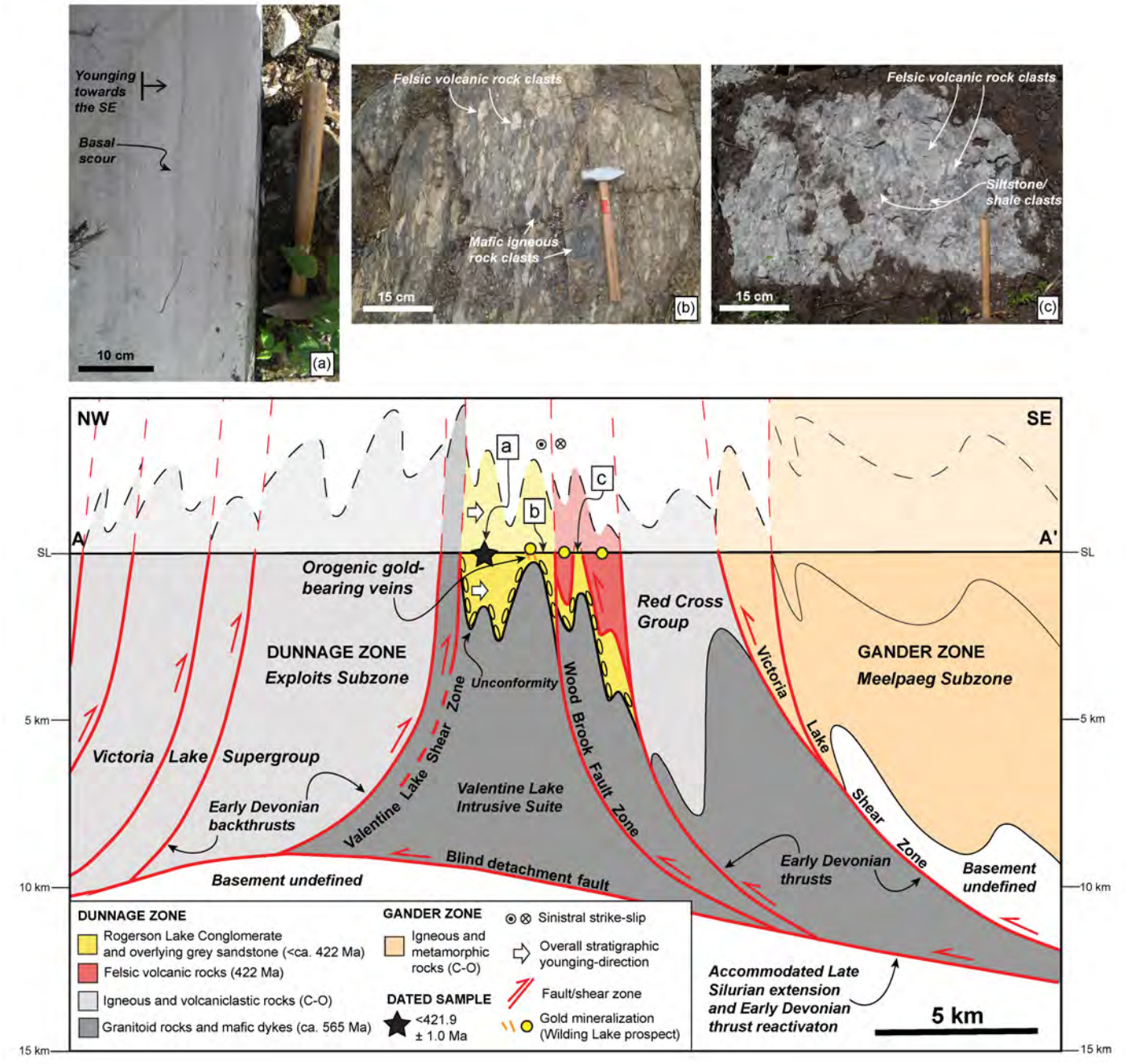

Figure 3. Cross-section interpretation along A-A′ (see Fig. 2). The black star marks the location of the Rogerson Lake Conglomerate sandstone (BNB18-IHNL-072) that was sampled for LA-ICPMS and CA-ID-TIMS U–Pb detrital zircon geochronology. Gold mineralization (yellow circles and orange lines on section) represent the Wilding Lake prospect. Pictures are as follows: A) Rogerson Lake Conglomerate sandstone geochronology sample BNB18-IHNL-072; B) Strongly deformed and gold-mineralized Rogerson Lake Conglomerate; C) Relatively undeformed Rogerson Lake Conglomerate.

associated with Latest Silurian to Devonian gold mineralization along fault splays of the Baie Verte – Brompton Line (Fig. 1; Evans 2004). Southeast of the central Newfoundland gold belt, Cambrian to Ordovician metamorphic terranes of the Gander Zone are uplifted along Early Devonian, Acadian thrust faults and intruded by Early to Middle Devonian granitoid rocks (Fig. 2; Colman-Sadd *et al.* 1990; Kerr 1997; Valverde-Vaquero *et al.* 2006).

STRUCTURAL CONTEXT

The central Newfoundland gold belt is hosted within a cross-sectional triangle zone-like structural domain that is bounded by southeast- and northwest-dipping imbricated fault/shear zones and an inferred, relatively flat-lying, blind detachment fault at depth (Figs. 2–4; van der Velden *et al.* 2004; van Staal and Barr 2012; Honsberger *et al.* 2020, 2022;

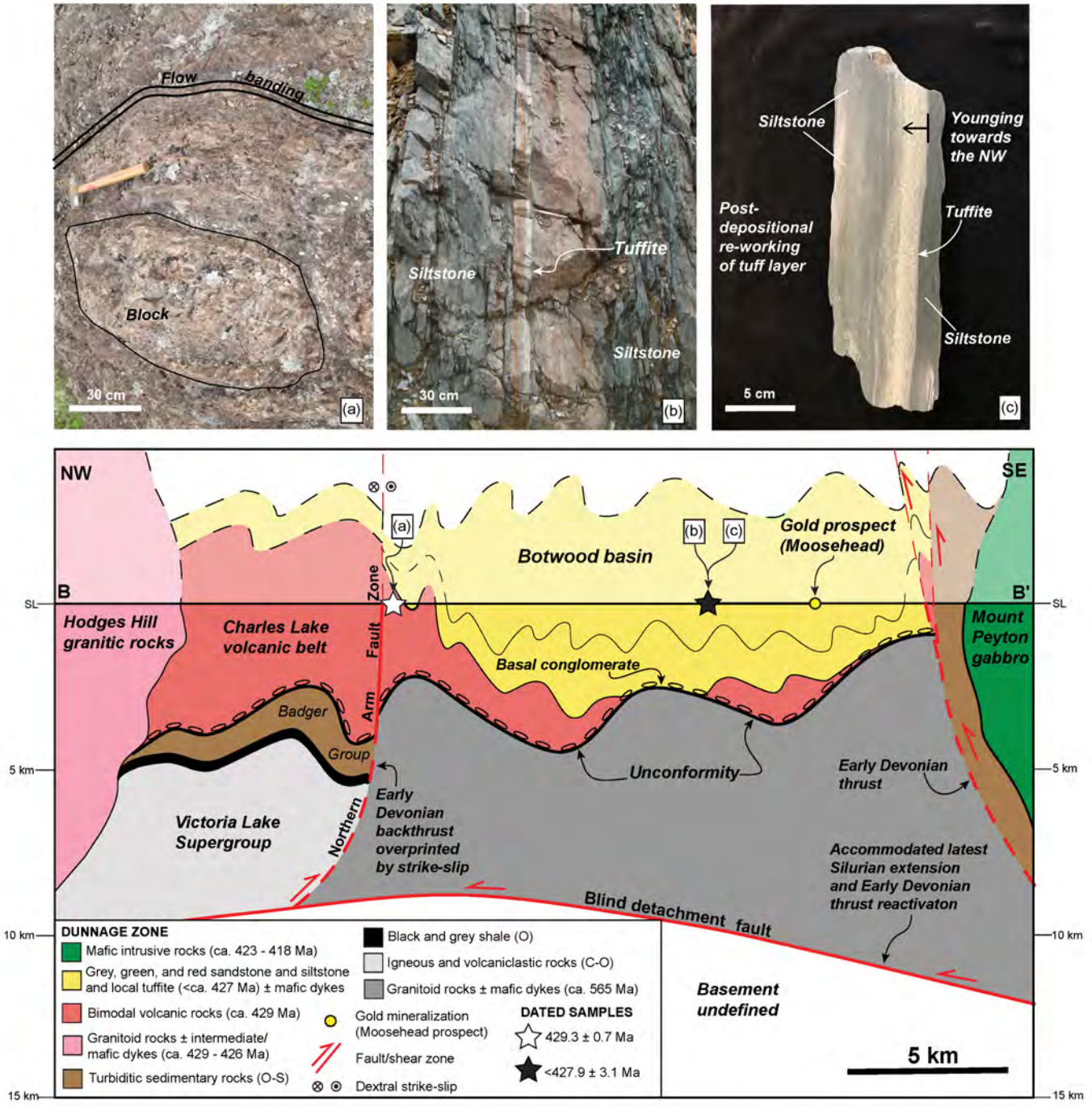

Figure 4. Cross-section interpretation along B-B′ (see Fig. 2). Geochronology sample locations are projected horizontally onto the line of section and are marked by black and white stars. The black star marks the location of the felsic tuffite sample (BNB19-IHNL-291) analyzed by both LA-ICPMS and CA-ID-TIMS U–Pb zircon geochronology, whereas the white star marks the location of the flow-banded rhyolite sample (BNB18-IHNL-092) analyzed only for CA-ID-TIMS U–Pb geochronology. Gold mineralization (yellow circle on section) represents the Moosehead prospect. Pictures are as follows: A) Flow-banded rhyolite geochronology sample BNB18-IHNL-092; B) Felsic tuffite outcrop sampled for geochronology; C) Felsic tuffite geochronology sample BNB19-IHNL-291.

Bleeker and Honsberger 2022). The southeast-dipping fault/shear zones include the Victoria Lake Shear Zone and Wood Brook Fault Zone (Valverde-Vaquero *et al.* 2006), whereas the northwest-dipping structures include the orogenic gold -mineralized Valentine Lake Shear Zone (Figs. 2 and 3; Dunsworth and Walford 2018; Lincoln *et al.* 2018). These fault/shear zones were active from at least the Late Silurian to the Early Devonian as the Meelpaeg nappe (Ganderian

deformation front) advanced to the northwest as a result of far-field collision of Avalonia with composite Laurentia during the Acadian orogenic cycle (Valverde-Vaquero *et al.* 2006; van Staal and Barr 2012).

At Valentine Lake, the Valentine Lake Shear Zone crosscuts, uplifts, and juxtaposes the Valentine Lake Intrusive Suite against the Rogerson Lake Conglomerate in the overall footwall of the Victoria Lake Shear Zone (Figs. 2 and 3; Honsberger *et al.* 2020). The Valentine Lake gold deposit is hosted within structurally controlled, fault-fill and extensional quartz vein systems that emanate from the Valentine Lake Shear Zone and crosscut the Valentine Lake Intrusive Suite (Lincoln *et al.* 2018). Approximately 30 km northeast of the Valentine Lake deposit, gold-mineralized quartz veins of the Wilding Lake gold prospect form offshoots of the Wood Brook Fault Zone and cut southeast-younging stratigraphy of the Rogerson Lake Conglomerate sequence (Fig. 3; Honsberger *et al.* 2019). The Valentine Lake Shear Zone structure extends farther to the northeast along the northwestern boundary of the Crippleback Lake Intrusive Suite before merging with the Northern Arm Fault (Figs. 1 and 2), a zone of protracted, oblique dextral strike-slip faulting that marks the northwestern margin of the Botwood basin (Kusky *et al.* 1987; Colman-Sadd *et al.* 1990; O'Brien 2003).

The northeastern extension of the Victoria Lake Shear Zone system is the Great Burnt Lake Shear Zone, which uplifts Ganderian rocks of the Mount Cormack Complex and buries sandstone-siltstone sequences and monzonite intrusions of the southern Botwood basin (Fig. 2; Colman-Sadd 1980, 1985; Dec and Colman-Sadd 1990; Valverde-Vaquero *et al.* 2006; Honsberger *et al.* 2020, 2022). Farther northeast in the Botwood basin, the gold-mineralized Mount Peyton Intrusive Suite is bounded by southeast-dipping fault zones; a thrust fault system to the northwest, which we hereby name the "Botwood Basin Fault Zone", and a thrust structure to the southeast that may correlate with the Dog Bay Line in north-central Newfoundland (Figs. 2 and 4; Dickson *et al.* 2000; O'Brien 2003). In the overall footwall of the "Botwood Basin Fault Zone", orogenic gold mineralization of the Moosehead prospect is hosted within sandstones and siltstones (±mafic dykes) of the Wigwam Formation (Fig. 4; Froude 2021; Sandeman *et al.* this volume). A southeast-dipping fault zone bounds the southeastern-most contact of the Botwood Group, in contrast to the presumably northwest- to west-dipping fault trace of the Gander River Complex (Blackwood 1982; Miller 1988; O'Neill and Blackwood 1989), which delineates a peri-Ganderian, Cambro-Ordovician ophiolite tract that separates rocks of the Dunnage and Gander zones (Figs. 1–4; Colman-Sadd *et al.* 1990; van Staal and Barr 2012).

U–PB GEOCHRONOLOGY SAMPLING

In order to constrain the spatio-temporal history of faulting, magmatism, and sedimentation along the central Newfoundland gold belt, sampling for geochronological analysis was undertaken in the Rogerson Lake Conglomerate belt and Botwood basin (Figs. 1–4). In the Rogerson Lake Conglomerate belt, a sample of fresh, pink-grey, medium-grained, muscovitic sandstone containing local heavy mineral laminae and conformably overlying polymict conglomerate was processed for detrital zircon to be analyzed by LA-ICPMS and follow-up CA-ID-TIMS U–Pb dating methods. The same analytical approach was applied to a reworked felsic tuff (i.e., tuffite) intercalated with graded, muscovitic siltstone beds of the Wigwam Formation along the limb of a local anticline in the Botwood basin. The tuffite is a distinctive ~5 to 10 cm, yellowish-beige coloured layer in the field that contains medium-grained and angular epiclastic quartz and feldspar fragments (Fig. 4). An autobrecciated, flow-banded rhyolite dome of the Charles Lake volcanic belt adjacent to the Northern Arm Fault near Grand Falls, and along the northwestern margin of the Botwood basin, was sampled for direct CA-ID-TIMS dating of zircon to examine magmatic linkages with the felsic tuffite sample. UTM coordinates for geochronology samples are given in Supplementary data Tables S1 and S2 (see footnote 1).

ANALYTICAL METHODS

Laser ablation-inductively coupled plasma mass spectrometry

Following crushing and pulverization, initial separation of heavy minerals occurred on a Wilfley table, with subsequent paramagnetic and density separations performed, respectively, with a Frantz isodynamic separator and using methylene iodide. The freshest, least cracked zircon grains were hand picked under a binocular microscope with incident light (Fig. 5). Zircon grains from the sandstone sample (BNB18-IHNL-072) were annealed prior to analysis (Mattinson 2005), whereas zircon grains from the tuffite sample (BNB19-IHNL-291) were not pre-treated.

Grains were mounted on sticky tape and partially ablated using a 193 nm New Wave excimer laser and an Agilent 7900 inductively coupled plasma mass spectrometer. Depending on the sample, the laser generally operated at 5 Hz and about 5 J/cm^2 fluence with typical beam diame-ter of 20–30 microns. Data were collected on ^{88}Sr (10 ms) ^{206}Pb (30 ms) 207Pb (70 ms) 232Th (10 ms) and 238U (20 ms). Prior to analysis, spots were pre-ablated with a larger beam diameter for 2 s (10 pulses) to clean the surface. Following a 10 s period of baseline accumulation, the laser sampling beam was turned on and data were collected for 25 s before a washout period that preceded the next spot analysis. About 150 measurement cycles per sample were accumulated and resulting ablation pits are about 15 microns deep.

[1]Supplemental Data. Table S1 and S2. Please visit https://journals.lib.unb.ca/index.php/ag/article/view/32815/1882528251 and https://journals.lib.unb.ca/index.php/ag/article/view/32815/1882528252 to access the supplementary material

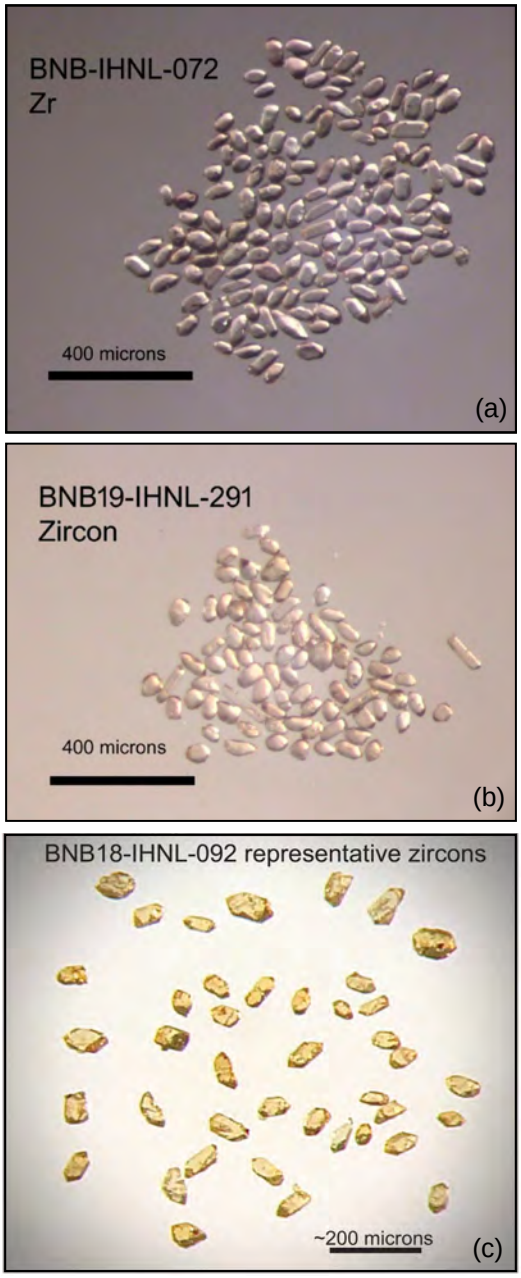

Figure 5. Images of representative zircon crystals analyzed for LA-ICPMS and CA-ID-TIMS U–Pb geochronology. (a) BNB18-IHNL-072, whole grains; (b) BNB19-IHNL-291, whole grains; (c) BNB18-IHNL-092, polished grains (CA-ID-TIMS only). Images were taken with a binocular microscope with incident light.

Data were edited and reduced using custom VBA software (UtilLAZ program) written by D. W. Davis, University of Toronto. $^{206}Pb/^{238}U$ ratios showed increasing fractionation throughout zircon runs caused by loss of refractory U with increasing penetration depth. No corrections were made for common Pb because the ^{204}Pb peak is too small to be measured precisely. If present, common Pb would have the effect of pushing data to the right of the concordia curve along a shallow mixing line with the slope determined by the isotopic composition of the common Pb contaminant. ^{88}Sr in zircon was monitored in order to detect intersection of the beam with zones of alteration or inclusions, and data showing high Sr or irregular time resolved profiles were either averaged over restricted Sr-free time windows or rejected. The Th/U ratio of zircon was calculated using the $^{208}Pb/^{206}Pb$ ratio and the $^{207}Pb/^{206}Pb$ age. This is more accuate than measuring the Th/U ratio directly because Th^{+} yield is strongly biased by oxidation in the plasma and, as well, the Th/U ratio in the standard available to correct the bias is not constant. Low Th/U (<0.1) is characteristic of metamorphic and hydrothermal zircon, whereas most zircon crystallized from felsic melts has Th/U in the range 0.1–1.0.

Two zircon standards were analysed: one from a quartz diorite from the Marmion batholith in northwest Ontario (DD85-17), which is dated at 3002 ± 2 Ma by ID-TIMS (Tomlinson *et al.* 2003); and one from a monzodiorite from the Pontiac province of Quebec (DD91-1) dated at 2682 ± 1 Ma (Davis 2002). Sets of four sample measurements are bracketed by measurements of DD85-17. DD91-1 was used as a secondary standard. Differences between standards were time interpolated when correcting sample measurements. Average age errors noted in the text, and error ellipses in Figures 6 and 7, are expressed at 2σ (twice the 1σ errors in Supplementary data Table S1 (see footnote 1). Ages and errors were calculated and plotted using the Isoplot program of Ludwig (1998, 2003). MSWD (mean square of weighted deviations) are expected to be around 1 or slightly higher with correctly chosen analytical errors for $^{207}Pb/^{206}Pb$ ages if the age population is unimodal. Pb/U errors do not include possible biases from compositional differences between samples and standard, therefore scatter above and below concordia may be pronounced. Uranium decay constants are taken from Jaffey *et al.* (1971).

Chemical abrasion-isotope dilution-thermal ionization mass spectrometry

Prior to analyses, zircon crystals were thermally annealed and chemically etched ('chemically abraded'), which provides penetrative removal of alteration zones where Pb loss has occurred and generally improves concordance (Mattinson 2005). These zones correlate with high U zones that have suffered radiation damage prior to alteration. The pre-treatment involved placing zircon grains in a muffle furnace at ~900°C for ~24–60 hours to repair radiation damage and anneal the crystal lattice, followed by a modified single-step partial dissolution procedure in ~0.10 ml of ~50% HF and 0.020 ml 7N HNO_3 in Teflon dissolution vessels at 200°C for 3–8 hours. Zircon grains were rinsed with 8N HNO_3 at room temperature prior to dissolution. A ^{205}Pb-$^{233–235}U$ spike or $^{202–205}Pb$-$^{233–235}U$ spike (EARTHTIME community tracers) was added to the Teflon dissolution capsules during sample loading. The zircon grains were dissolved using ~0.10 ml of concentrated HF acid and ~0.02 ml of 7N HNO_3 at 200°C for 3–5 days, then dried to a precipitate and re-dissolved in ~0.15 ml of 3N HCl overnight

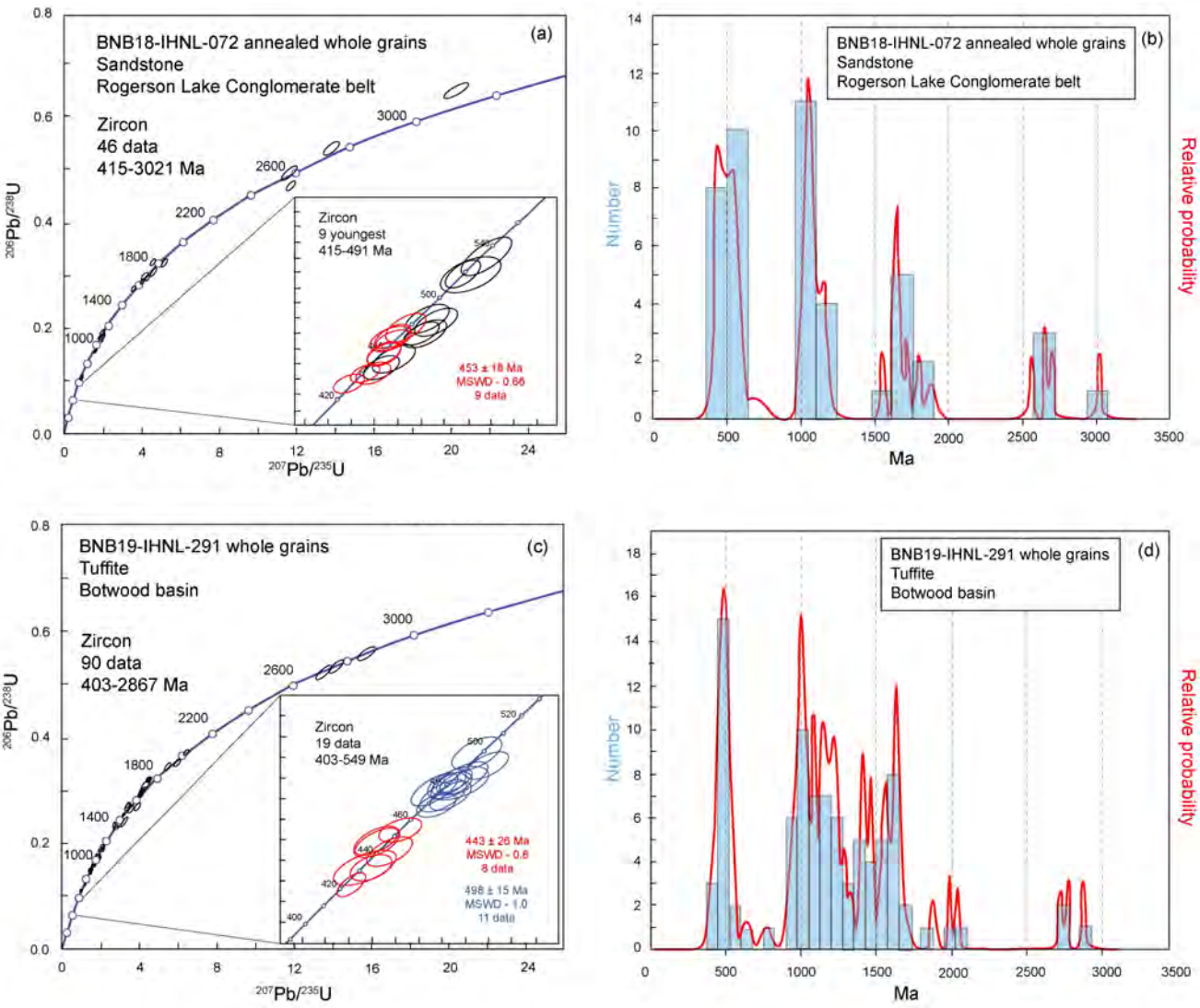

Figure 6. U–Pb LA-ICPMS geochronological results for zircon. (a) Concordia plot showing U–Pb LA-ICPMS isotopic data on annealed whole-grain zircon (N=46) from Rogerson Lake Conglomerate sandstone sample BNB18-IHNL-072. The inset shows the youngest grains (red ellipses) that give a mean $^{207}Pb/^{206}Pb$ age of 453 ± 18 (MSWD=0.66, N=9). Black ellipses represent data that are not included in the age estimates; (b) Relative probability density plot of $^{207}Pb/^{208}Pb$ ages on annealed whole-grain zircon from Rogerson Lake Conglomerate sandstone sample BNB18-IHNL-072; (c) Concordia plot showing all U–Pb LA-ICPMS isotopic data (N=90) and, as well, data for the 19 youngest whole-grain zircons (inset) from felsic tuffite sample BNB19-IHNL-291. The red ellipses represent data for the younger population and give a mean $^{207}Pb/^{206}Pb$ age of 443 ± 26 (MSWD=0.8, N=6). The blue ellipses represent data for the older population and give a mean $^{207}Pb/^{206}Pb$ age of 499 ± 15 (MSWD=1.0, N=14). The black ellipses represent data that are not included in the age estimates; (d) Relative probability density plot of $^{207}Pb/^{206}Pb$ ages on whole-grain zircons from felsic tuffite BNB19-IHNL-291. Note: all error ellipses are 2σ.

(Krogh 1973). U and Pb were isolated from zircon using 50 µl anion exchange columns with HCl, dried to a small droplet in H_3PO_4, deposited onto outgassed rhenium filaments with silica gel (Gerstenberger and Haase 1997), and analyzed with a VG354 mass spectrometer at the University of Toronto (Jack Satterly Geochronology Laboratory) using a Daly detector in pulse counting mode. Corrections to the ^{206}Pb-^{238}U ages for initial ^{203}Th disequilibrium in the zircon have been made assuming a Th/U ratio in the magma of 4.2. All common Pb was assigned to procedural Pb blank. Overall dead time of the measuring system for Pb and U was 16 and 14 ns, respectively. The mass discrimination correction for the Daly detector is constant at 0.05% per atomic mass unit. Amplifier gains and Daly characteristics were moni-tored using the SRM 982 Pb standard. Thermal mass discrimination corrections are 0.10% per atomic mass unit. Decay constants are those of Jaffey *et al.* (1971). All age errors quoted in the text and table, and error ellipses in the concordia diagrams, are expressed at the 95% confidence interval. Plotting and age calculations used Isoplot 3.00 (Ludwig 2003).

GEOCHRONOLOGICAL DATA

U–Pb LA-ICPMS isotopic data for zircon are given in Supplementary data Table S1 (see footnote 1) and geochronological results are plotted in Figure 6. In order to more closely constrain the precise time of deposition of the Rogerson Lake Conglomerate sequence and Botwood basin, the youngest, freshest zircon grains detected by LA-ICPMS in the sandstone (BNB18-IHNL-072) and tuffite (BNB19-IHNL-291) samples were removed from the sticky tape mounts and analyzed by CA-ID-TIMS (Supplementary data Table S2 - see footnote 1) (Fig. 7). The pre-screening of detrital zircon grains by LA-ICPMS helps minimize the number of analyses required by TIMS. The flow-banded rhyolite sample was analyzed by CA-ID-TIMS only (Fig. 7e).

BNB18-IHNL-072: Sandstone, Rogerson Lake Conglomerate sequence

Abundant zircon crystals consist of mixed populations of fresh and rounded, clear to beige grains (Fig. 5a), with some larger, cracked grains displaying visible reddish alteration. Fifty-two annealed whole grains were analyzed, six of which were discarded due to alteration and discordance over 15% (Supplementary data Table S1 - see footnote 1). The LA-ICPMS $^{207}Pb/^{206}Pb$ ages range from 415 to 3021 Ma (Supplementary data Table S1 - see footnote 1) (Figs. 6a and b). The nine youngest grains have a mean $^{207}Pb/^{206}Pb$ age of 453 ± 18 Ma (MSWD=0.66, N=9) and a mean $^{206}Pb/^{238}U$ age of 455 ± 12 Ma (MSWD=16, N=9; Supplementary data Table S1 - see footnote 1) (Fig. 6a). The LA-ICPMS U–Pb anal-yses show two additional age peaks of detrital grains at ca. 1100 and 1660 Ma, and scattered ages from 1886 to 3021 Ma (Figs. 6a and b).

Four of the youngest, least altered zircon grains dated by LA-ICPMS were removed from the sticky tape mount and individually chemically abraded. Grains numbered 43, 45, 48, and 51 yield concordant CA-ID-TIMS $^{206}Pb/^{238}U$ dates of 435.8 ± 0.8 Ma (grain 43), 435.2 ± 0.5 Ma (grain 51), 431.1 ± 0.8 Ma (grain 48), and 421.9 ± 1.0 Ma (grain 45) (Supplementary data Table S2 - see footnote 1) (Figs. 7a and b). The youngest grain at 421.9 ± 1.0 Ma provides a maximum age for the time of deposition of the sandstone sample.

BNB19-IHNL-291: Felsic tuffite, Botwood basin

Zircon crystals consist of small rounded subhedral grains and euhedral laths yellow to clear in color (Fig. 5b). Grains are fresh with few inclusions and cracks. Of one-hundred and twelve whole-grain analyses, twenty-two were discarded due to alteration and discordance over 15% (Supplementary data Table S1 - see footnote 1). The LA-ICPMS $^{207}Pb/^{206}Pb$ dates range in age from 403 to 2867 Ma and show a complicated age profile with a significant detrital component (Supplementary data Table S1 - see footnote 1) (Figs. 6c and d)). The analyses peak at ca. 480 Ma and the majority of grains form a continuous age distribution from 820 to 1695 Ma (Figs. 6c and d). The six oldest detrital zircon grains range from 1873 to 2867 Ma. The nineteen youngest grains show a bimodal age distribution (Supplementary data Table S1 - see footnote 1) (Figs. 6c and d). Applying the Unmix Ages utility in Isoplot (Sambridge and Compston 1994), gives LA-ICPMS $^{207}Pb/^{206}Pb$ age estimates of 443 ± 26 Ma (30%) and 498 ± 15 Ma (70%) under the assumption that there are just two age populations, whereas the $^{206}Pb/^{238}U$ ages of the nineteen youngest grains range from 422 to 498 Ma and correspond to Unmix ages of 439 ± 3 Ma (37%) and 480 ± 2 Ma (63%) (Supplementary data Table S1 - see footnote 1) (Fig. 6c).

Four of the youngest, fresh zircon grains numbered 22, 46, 71, and 72 give concordant CA-ID-TIMS $^{206}Pb/^{238}U$ dates of 470.8 ± 1.7 Ma (grain 46), 443.7 ± 6.0 Ma (grain 72), 438.0 ± 0.9 Ma (grain 22), and 427.9 ± 3.1 Ma (grain 71) (Supplementary data Table S2 - see footnote 1) (Figs. 7c and d). The youngest grain at 427.9 ± 3.1 Ma provides a maximum age for the time of deposition of the felsic tuff, with minor physical reworking (and mixing) into tuffite soon thereafter.

BNB18-IHNL-092: Rhyolite dome, Charles Lake volcanic belt

A range in concordant $^{206}Pb–^{238}U$ dates from 458 Ma to 429 Ma was determined from ten CA-ID-TIMS zircon grain analyses (Supplementary data Table S2 - see footnote 1) (Fig. 7e). A single result is 458.2 ± 2.7 Ma (Z1), data for three zircon analyses cluster at 438–437 Ma (Z2-4), three cluster at 434–433 Ma (Z5-7), and the youngest three data overlap with a weighted mean age of 429.3 ± 0.7 Ma (Z8-10). This latter date is interpreted as a maximum age for emplacement of the rhyolite. It is apparent from the results that there was a significant xenocrystic and/or antecrystic zircon component acquired at the magma source or during emplacement.

DISCUSSION

One of the biggest challenges to interpreting Silurian fault zone histories in central Newfoundland is that compression and strike-slip associated with Devonian to Carboniferous orogenesis overprint Silurian structures (e.g., van Staal and Barr 2012; Willner *et al.* 2018). Integrated LA-ICPMS and CA-ID-TIMS geochronology of sandstone of the Rogerson Lake Conglomerate sequence (BNB18-IHNL-072), felsic tuffite intercalated with graded siltstone of the Botwood basin (BNB19-IHNL-291), and a flow-banded rhyolite dome of the Charles Lake volcanic belt (BNB18-IHNL-092) provides new insights into the precise timing of Wenlock to Pridoli tectonics leading to Devonian orogenic gold mineralization in central Newfoundland. In order to place constraints on the time of deposition of the Rogerson Lake Conglomerate and Botwood basin sequences, the youngest detrital zircon grains were identified first by LA-ICPMS and then subjected to high-precision CA-ID-TIMS dating. For such samples,

Figure 7. (next page) U–Pb CA-ID-TIMS geochronological results for youngest zircon grains, as well as images taken with a binocular microscope with incident light. (a) Images of the youngest and best preserved detrital zircon grains identi-fied by LA-ICPMS and dated with follow-up CA-ID-TIMS for BNB18-IHNL-072; (b) U–Pb concordia diagram displaying the CA-ID-TIMS dates of the youngest detrital zircon grains from BNB18-IHNL-072 (youngest grain, 421.9 ± 1.0 Ma); (c) Images of the youngest and best preserved detrital zircon grains identified by LA-ICPMS and dated by follow-up CA-ID-TIMS for BNB19-IHNL-291; (d) U–Pb concordia diagram displaying the CA-ID-TIMS dates of the youngest detrital zircon grains from BNB19-IHNL-291 (youngest grain, 427.9 ± 3.1 Ma); (e) U–Pb concordia diagram displaying the CA-ID-TIMS date for zircon from the flow-banded rhyolite sample BNB18-IHNL-092 (429.29 ± 0.7 Ma). Note: all error ellipses are 2σ.

the mean U–Pb ages determined by LA-ICPMS range from Late Cambrian to latest Ordovician and have large statistical errors (Supplementary data Table S1 - see footnote 1) (Fig. 6); therefore, they are not sufficient alone to resolve depositional ages.

LA-ICPMS detrital zircon age distributions for the sandstone and felsic tuffite are very similar (Fig. 6), suggesting that the felsic tuffite sample includes detrital zircon grains from the intercalated sedimentary (siltstone) fraction. Although analysis of provenance is limited by the relatively small numbers of individual LA-ICPMS zircon analyses, both the sandstone and tuffite-siltstone samples display Neoproterozoic to Cambrian peaks, compatible with detrital zircon grains sourced from the underlying Victoria Lake Supergroup and its Ganderian basement (Evans *et al.* 1990, Rogers *et al.* 2006). The ca. 1000 to 1300 Ma zircon grains in both samples correspond with typical Mesoproterozoic ages for metamorphic rocks of the eastern Laurentian margin in western Newfoundland and southern Labrador (e.g., Connelly and Heaman 1993; Tucker and Gower 1994; Gower and Krogh 2002; Heaman *et al.* 2002; Kuiper and Hepburn 2021). Furthermore, the 1600–1700 Ma grains overlap in age with the oldest dated rocks of the Long Range Inlier in western Newfoundland (ca. 1631 Ma, Heaman *et al.* op. cit.) and, as well, with Trans-Labrador and Pre-Labradorian orogenic events documented in Laurentian basement of southern Labrador (Gower and Krogh 2002). The ages of the few Archean zircon grains are similar to Meso- to Neoarchean rocks of Laurentia that occur in the Makkovik and Nain provinces of central and northern Labrador (e.g., James *et al.* 2002; Ketchum *et al.* 2002; Hinchey *et al.* 2020).

Overall, the U–Pb LA-ICPMS zircon age spectra corroborate the provenance study of Pollock *et al.* (2007) in that strong Paleoproterozoic and Mesoproterozoic Laurentian detrital zircon signatures are represented (e.g., Waldron *et al.* 2012; Fig. 6). However, the geochronological results herein for the sandstone and tuffite-siltstone samples also establish a Neoproterozoic to Cambrian detrital zircon source typical of the peri-Ganderian Valentine Lake and Crippleback Lake intrusive suites (ca. 565 Ma, Evans *et al.* 1990; Rogers *et al.* 2006; Fig. 6). A mixed Laurentian-Gondwanan provenance for rocks of the Rogerson Lake Conglomerate sequence and Botwood basin, combined with the occurrence of Wenlock to Pridoli zircon grains (Figs. 6 and 7), is consistent with local depositional sources.

U–Pb CA-ID-TIMS dating of four of the youngest, best preserved zircon grains from each of the Rogerson Lake Conglomerate sandstone and Botwood basin tuffite-siltstone produced maximum $^{206}Pb/^{238}U$ depositional ages of 421.9 ± 1.0 Ma (Pridoli) and 427.9 ± 3.1 Ma (Wenlock; Homerian), respectively (Supplementary data Table S2 - see footnote 1) (Fig. 7). The ages are considered maxima because it cannot be discounted that younger detrital and/or igneous zircon grains are present in portions of the rock units that were not processed for geochronology. Absolute minimum depositional age constraints for the basal Rogerson Lake Conglomerate are ca. 410 Ma (Honsberger *et al.* 2022) and ca. 390 Ma (Willner *et al.* 2018), which are, respectively, for rutile and white mica in quartz veins that crosscut the Rogerson Lake Conglomerate. U–Pb CA-ID-TIMS zircon geochronology produced an igneous crystallization age of 429.29 ± 0.70 Ma (Wenlock; Homerian) for the autobrecciated, flow-banded rhyolite dome of the Charles Lake volcanic belt along the western margin of the Botwood basin (Fig. 7e); therefore, these volcanic rocks appear to be genetically related to the felsic tuffite.

The maximum depositional ages for the rhyolite dome and tuffite are interpreted to represent the time of Homerian (ca. 430–427 Ma) volcanism and associated volcanogenic sedimentation in the western Botwood basin. In this interpretation, felsic volcanism was active between at least ca. 429 and 428 Ma, with deposition of felsic tuff and siltstone of the Wigwam Formation at ca. 428 Ma, accompanied by minor physical reworking of the tuffaceous material. The Pridoli maximum age for deposition of the Rogerson Lake Conglomerate sandstone suggests that sedimentation may have been initiated later along this belt than to the northwest and northeast in the Botwood basin. Furthermore, the maximum ca. 422 Ma detrital zircon age for the Rogerson Lake Conglomerate sandstone sample confirms that ca. 422–420 Ma igneous rocks in central Newfoundland are included as clasts and grains within the Rogerson Lake Con-glomerate sequence, again, consistent with locally derived sediment sources. The new U–Pb CA-ID-TIMS zircon ages establish that Wenlock to Pridoli magmatism preceded sedimentation in both the Botwood basin and along the Rogerson Lake Conglomerate belt (Fig. 8).

The ca. 429 (rhyolite dome) age and ca. 428 Ma (tuffite) maximum age for felsic volcanism and volcanogenic sedimentation are consistent with available age determinations for the bimodal Hodges Hill Intrusive Suite (ca. 429–426 Ma, Dickson 2000; G. Dunning, personal communication 2021), thus, the rhyolite dome and other volcanic rocks of the Charles Lake belt are confirmed as contemporaneous

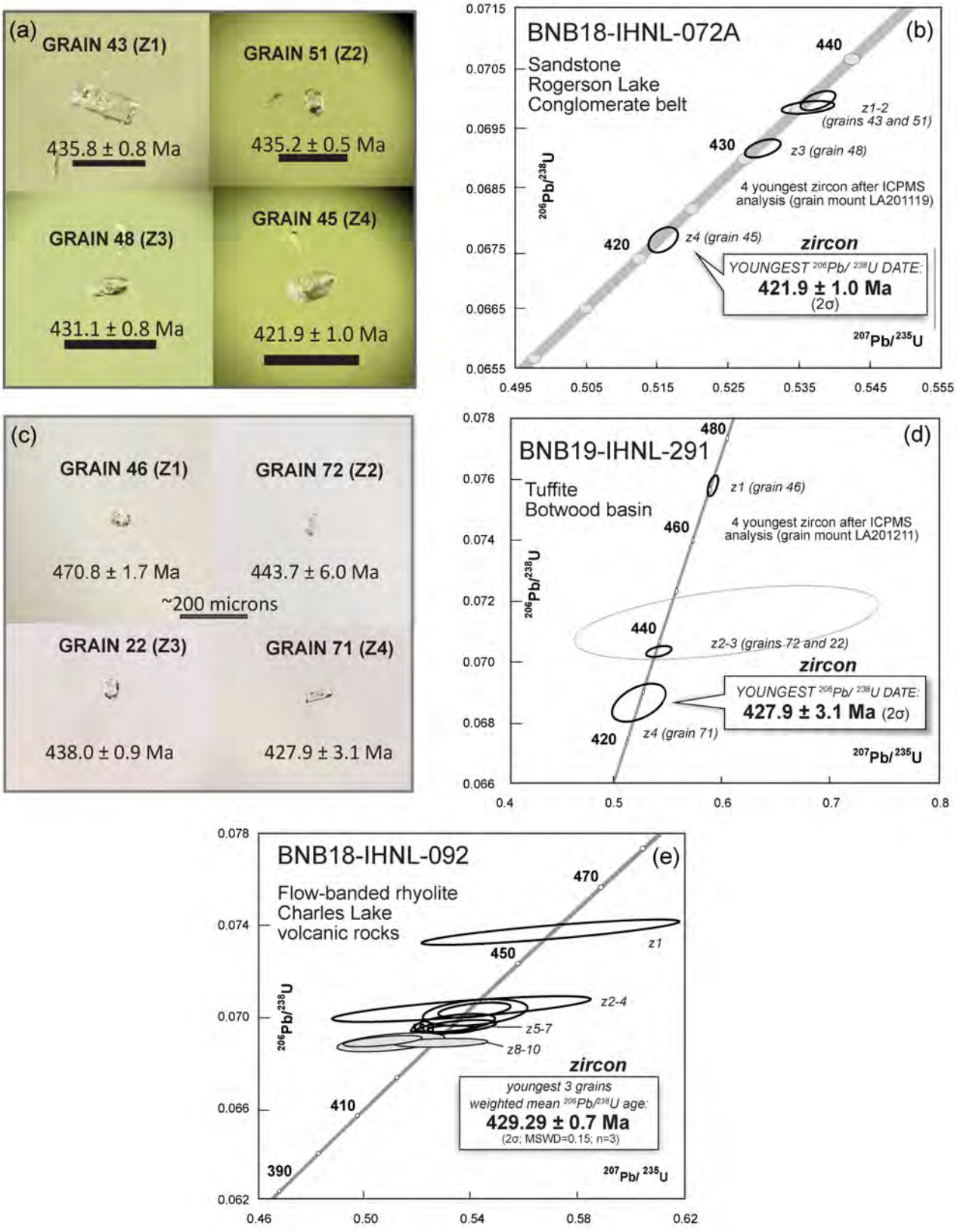

with Hodges Hill plutonism. The ca. 429 and 428 Ma dates also fall within the age range of the Topsails Intrusive Suite and Springdale Group in the Notre Dame Subzone (ca. 429–426 Ma, Chandler *et al.* 1987; Whalen *et al.* 1997, 2006). Further, the ca. 422 Ma youngest zircon date from the Rogerson Lake Conglomerate sandstone sample falls within the age range of the Mount Peyton Intrusive Suite (ca. 424–418 Ma, Sandeman *et al.* 2017), and is also similar to age constraints for some rocks of the composite Fogo Island Intrusive Suite (e.g., ca. 422 Ma, Elliot *et al.* 1991; Aydin 1995).

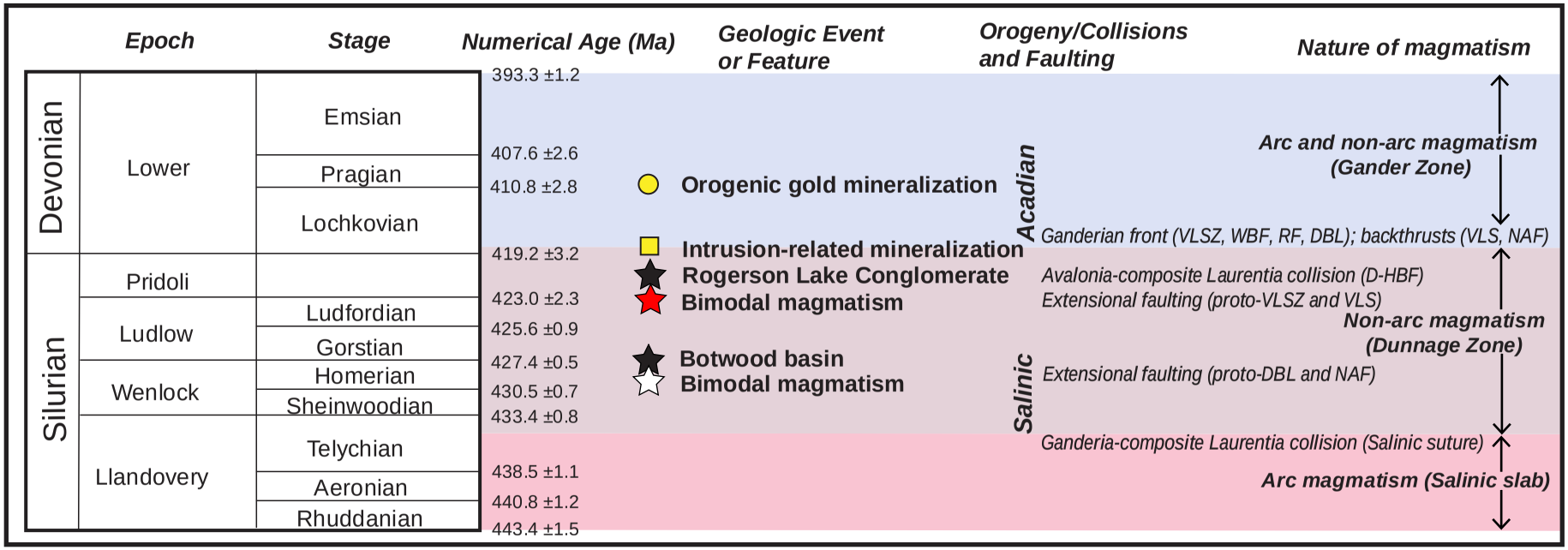

Figure 8. Silurian–Devonian geochronological summary of new U–Pb data (white and black stars) and previously published constraints on orogenesis and fault zone development in central Newfoundland (van Staal and Barr 2012; this study). Magmatic intervals are colour-coded as defined by Whalen *et al.* (2006) and van Staal *et al.* (2014). Additional age references are as follows: red star (Dunning *et al.* 1990; McNicoll *et al.* 2006; Sandeman *et al.* 2017; Honsberger *et al.* 2022); yellow square (Sandeman *et al.* 2017); and yellow circle (Honsberger *et al.* 2022). Time-scale from the International Commission on Stratigraphy (Cohen *et al.* 2013: updated 2021). Abbreviations: DBL – Dog Bay Line; D-HBF – Dover – Hermitage Bay Fault; NAF – Northern Arm Fault; RF – Reach Fault; VLS – Valentine Lake Shear Zone; VLSZ – Victoria Lake Shear Zone; WBF – Wood Brook Fault.

Additionally, the ca. 422 Ma date is consistent with ages reported for felsic volcanic rocks of the Laurenceton Formation (ca. 421 Ma, van Staal *et al.* 2014), as well as for felsic igneous rocks along the Rogerson Lake Conglomerate belt and within the southern Botwood basin (ca. 422–420 Ma, Honsberger *et al.* 2022; Figs. 1 and 2). In sum, the new geochronological data from this study, in combination with these previously published ages, indicate that volcanism and sedimentation along the western Botwood basin were active between ca. 429 and 428 Ma, whereas plutonism, volcanism, and sedimentation in the southeastern and eastern Botwood basin were active between ca. 424 and 418 Ma, with a strong pulse of felsic magmatism and associated sedimentation along the Rogerson Lake Conglomerate belt at ca. 422 Ma (Figs. 8 and 9; see Honsberger *et al.* 2022).

Transient lithospheric extension is inferred to have controlled the formation of bimodal magmatic suites and associated sedimentary rocks in the Botwood basin and Rogerson Lake Conglomerate belt of central Newfoundland (Fig. 9). Lithospheric extension provides a mechanism to explain mixing and emplacement of mantle-derived mafic magmas with their felsic anatectic products, such as the Mount Peyton Intrusive Suite (Strong 1979; Strong and Dupuy 1982) and the Fogo Island Intrusive Suite (Aydin 1995; Sandeman and Malpas 1995). Furthermore, Wenlock to Pridoli magmatism and associated clastic sedimentation corresponds to a time-period between the largely compressive stress regimes associated with the Salinic and Acadian orogenic cycles in central Newfoundland (Fig. 8), when orogenic collapse and extension would have been expected (e.g., Barbarin 1999). The occurrence of mature sandstones and siltstones in the Botwood basin is consistent with longer-lived, more-evolved extension in north-central Newfoundland compared to along the structurally thinner Rogerson Lake Conglomerate belt to the south and southwest. As such, extension, clastic sedimentation, and magmatism were time-transgressive both across- and along-strike of the Exploits Subzone, with resultant along-strike variations in the volume of sedimentary input (Fig. 9). Therefore, the Rogerson Lake Conglomerate belt is not correlative temporally with the stratigraphic base of the Botwood basin, even though the polymict conglomerate is a basal unit.

In our model, predominantly southeast-dipping (present-day coordinates) extensional fault systems were active along the western Botwood basin at ca. 429 Ma, and propagated southeastward (across-strike) and to the southwest and northeast (along-strike) between ca. 424 and 418 Ma (Fig. 9). The Wenlock to Pridoli spatio-temporal development of this extensional fault network is consistent with the findings of van Staal *et al.* (2014), who noted that Silurian magmatism gets progressively younger west-to-east across the Dunnage Zone. Such extensional fault systems may have formed during thinning associated with asthenospheric and lithospheric decompression melting and upwelling related to slab rollback and break-off, and potentially lithospheric delamination, following the terminal Salinic collision of Ganderia with composite Laurentia (Pitcher 1983, 1993; Barbarin 1990, 1999; Whalen *et al.* 1997, 2006; van Staal and Barr 2012; van Staal *et al.* 2014; Whalen and Hildebrand 2019). In this context, listric normal faults facilitated exhumation of the middle and lower crust of the Exploits Subzone (Victoria Lake Supergroup and correlatives), and erosion and deposition of such rocks contributed to the formation of clastic sedimentary cover sequences of the Botwood basin and Rogerson Lake Conglomerate belt (Fig. 9). Wenlock to Pridoli lithospheric thinning may have been an important primer for orogenic gold mineralization (e.g., Bleeker 2015) because it increased heat and fluid flow in the crust prior to Early Devonian compression, metamorphism, and magmatism.

Considering that latest Silurian extensional faulting in central Newfoundland overlaps in time with far-field collision of Avalonia and composite Laurentia (Fig. 8), extension may have involved some components of strike-slip and transtension (Dewey *et al.* 1998) because sinuous collisional boundaries would have produced oblique deformation zones (e.g., O'Brien *et al.* 1993; Dubé *et al.* 1996; O'Brien 2003; Hibbard *et al.* 2006; van Staal and Barr 2012). The relative influence of extension compared to transtension in central Newfoundland, however, remains ambiguous because of fault reactivation and deformational overprint. Thrust fault reactivation appears to have occurred throughout the Devonian to accommodate Acadian, intra-terrane, thick-skinned thrusting and shortening associated with the emplacement of structurally controlled, gold-bearing quartz veins (e.g., O'Brien *et al.* 1993; O'Brien 2003; van Staal and Barr 2012; Willner *et al.* 2018; Honsberger *et al.* 2022). Such Devonian thrust fault systems then may have been reactivated as later oblique, dextral strike-slip, transpressional deformation zones (e.g., Lafrance 1989; O'Brien *et al.* 1993; de Roo and van Staal 1994; O'Brien 2003), which we interpret to have produced the "lazy Z"-shape (Mann *et al.* 1983) of the Botwood basin and its southwesterly (Rogerson Lake Conglomerate belt) and north-easterly extensions (Figs. 1 and 2). This interpretation is consistent with the occurrence of post-Silurian, dextral strike-slip faults (e.g., Northern Arm Fault-Reach Fault) along the margins of the Botwood basin, implying that a Wenlock to Pridoli extensional fault system in central Newfoundland may have been more linear than the present map pattern suggests (Fig. 9; cf. Kusky *et al.* 1987; Kusky and Kidd 1996). The occurrence of orogenic gold-mineralized, Wenlock to Pridoli igneous and sedimentary rocks in the overall footwall of the Victoria Lake Shear Zone (Figs. 1–4) indicates that thrust burial played an essential role in the preservation of syn-extensional rocks along the central Newfoundland gold belt, opposed to uplifting these rocks and exposing them to erosion (e.g., Bleeker 2015).

In the Chaleur Bay synclinorium of northern New Brunswick, latest Silurian, extension-related magmatic suites and clastic sedimentary rock sequences of the Dickie Cove Group are associated with orogenic gold-mineralized fault splays of the Early Devonian, or younger, Rocky Brook–Millstream Fault Zone (Tremblay and Dubé 1991; Tremblay

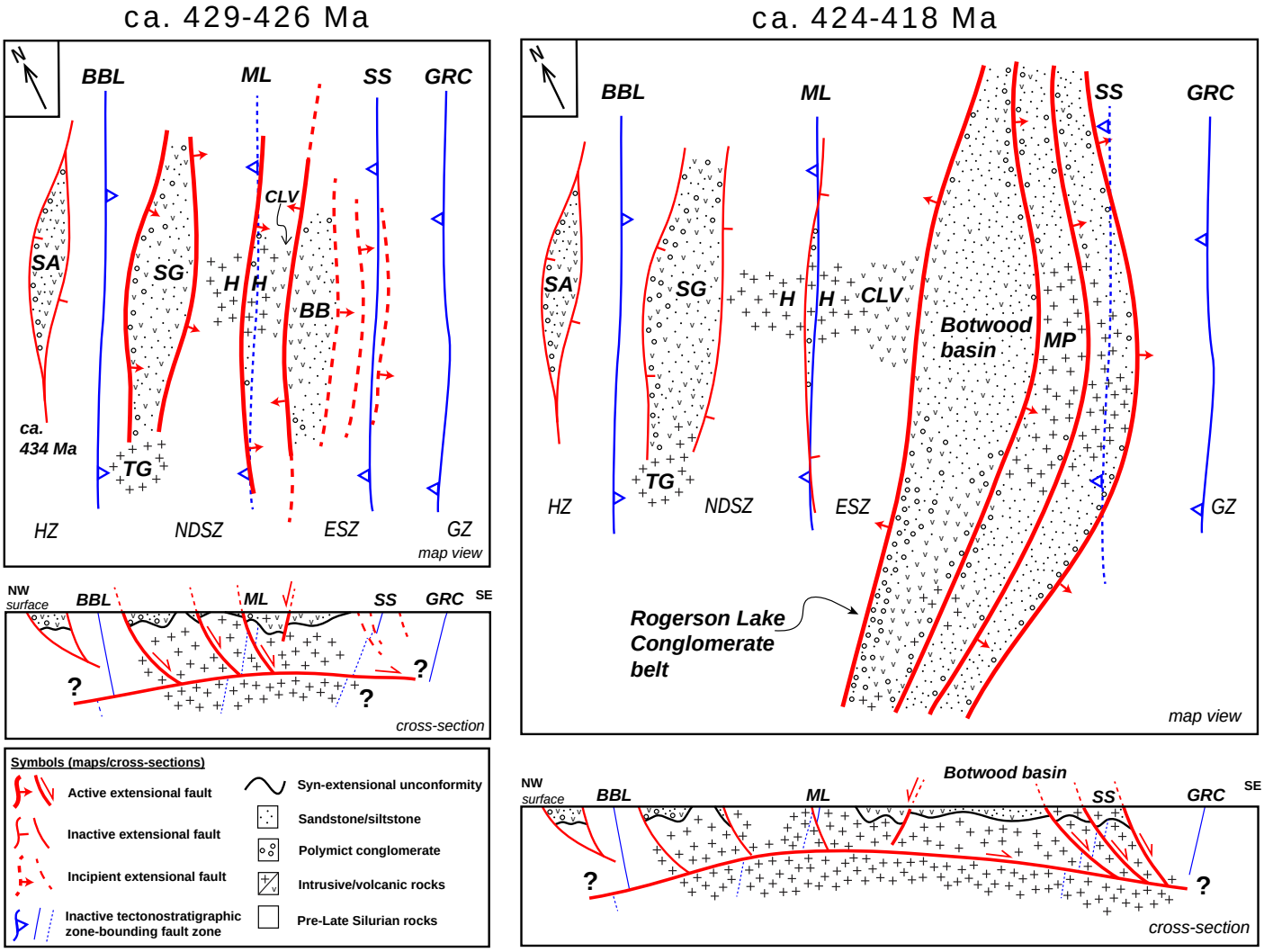

Figure 9. Structural synthesis illustrating the Late Silurian (Wenlock to Pridoli) evolution of transient extensional faults across the Dunnage Zone as a prelude to Devonian orogenic gold mineralization. Not drawn to scale. Extension in the western Botwood basin, and farther northwest in the Dunnage Zone, is inferred between ca. 429 and 426 Ma (left side), whereas extension in the southeastern and eastern Botwood basin and along the Rogerson Lake Conglomerate belt is inferred between ca. 424 and 418 Ma (right side). Cross-section interpretations are given below each map view. In this model, exhumation and erosion of pre-Late Silurian rocks (Victoria Lake Supergroup and correlatives) contributed to the formation of syn-extensional igneous and clastic sedimentary rocks along the central Newfoundland orogenic gold belt. Tectonostratigraphic zone-bounding fault zones are blue lines (dotted lines where approximate) and younger, cross-cutting extensional faults are red lines, which are interpreted to have been reactivated subsequently as thick-skinned thrusts in the Devonian. As per our interpretation of the Dog Bay Line, "Salinic suture" is used to denote the Dunnage-Gander accretionary boundary, which may not be traceable at the present erosional surface. Abbreviations: BB – Botwood basin; BBL – Baie Verte – Brompton Line; ESZ – Exploits Subzone; GRC – Gander River Complex; GZ – Gander Zone; HH/CLB – Hodges Hill Intrusive Suite and Charles Lake volcanic belt; HZ – Humber Zone; MP – Mount Peyton Intrusive Suite; ML – Mekwe'jit Line; NDSZ – Notre Dame Subzone; SA – Sops Arm Group; SG – Springdale Group; SS – Salinic suture; TG – Topsails Group/Intrusive Suite.

et al. 1993; Wilson 2007; Wilson *et al.* 2017; Dostal *et al.* 2020; Bustard *et al.* 2021). This fault zone appears to correlate with the Cape Ray–Victoria Lake–Valentine Lake fault corridor in southwestern and central Newfoundland, strongly suggesting that the orogenic gold system of central Newfoundland is continuous along-strike in the northern Appalachians.

CONCLUSIONS

Late Silurian (Wenlock to Pridoli), extension-related, bimodal magmatic suites and clastic sedimentary rocks of the Rogerson Lake Conglomerate belt and Botwood basin sequence delineate the central Newfoundland gold belt. Integrated LA-ICPMS and CA-ID-TIMS U–Pb zircon tech-

niques produced a maximum date for deposition of the Rogerson Lake Conglomerate sequence at 421.9 ± 1.0 Ma (Pridoli); therefore, it is younger than, and stratigraphically overlies, ca. 422 Ma igneous rocks that occur along the gold belt. The same analytical approach applied to a tuffite layer toward the stratigraphic middle of the Wigwam Formation in the Botwood basin produced a maximum eruption age of 427.9 ± 3.1 Ma (Wenlock; Homerian), which is interpreted to be contemporaneous and cogenetic with the Hodges Hill Intrusive Suite, the Charles Lake volcanic belt, and associated volcanogenic sedimentation in the western Botwood basin. Although provenance interpretations are limited by the relatively small numbers of individual zircon analyses, LA-ICPMS detrital zircon age distributions are consistent with a mixed Laurentian-Gondwanan provenance for sedimentary rocks of the Rogerson Lake Conglomerate sequence and Botwood basin. An autobrecciated, flow-banded rhyolite of the Charles Lake volcanic belt from the northwestern Botwood basin has a U–Pb zircon CA-ID-TIMS age of 429.3 ± 0.7 Ma (Wenlock; Homerian), which we interpret as the eruptive age. Collectively, the new U–Pb zircon geochronological data confirm a clear spatio-temporal link between syn-extensional, Wenlock to Pridoli magmatism and sedimentation both along and across strike of the central Newfoundland gold belt (Figs. 8 and 9).

Wenlock to Pridoli magmatic and depositional ages are consistent with a structural model involving the overall southeastward (present day coordinates) propagation of a transient, time-transgressive, extensional fault system across the Exploits Subzone between ca. 429 and 418 Ma. Extensional faulting may have contributed to basin formation, subsidence, and exhumation of pre-Silurian rocks of the Exploits Subzone during that time-period. The earlier part of the history is marked by ca. 429–426 Ma syn-extensional magmatism (Hodges Hill Intrusive Suite and Charles Lake volcanic belt) and sedimentation along the northwestern margin of the Botwood basin and farther west in the Dunnage Zone (Topsails Intrusive Suite and Springdale Group). The later part is preserved as ca. 424–418 Ma syn-extensional magmatic suites and clastic sedimentary rocks along the Rogerson Lake Conglomerate belt and its extensions to the northeast along and within the Botwood basin (e.g., Mount Peyton Intrusive Suite and associated rocks). Transient lithospheric extension appears to mark the transition between the Salinic and Acadian orogenic cycles (e.g., Sandeman *et al.* this volume) and may have been important for increasing heat and fluid flow in the lithospheric mantle and crust leading to Devonian fault reactivation, crustal thickening, fluid focussing, and orogenic gold mineralization.

ACKNOWLEDGEMENTS

This research constitutes part of Natural Resources Canada's Targeted Geoscience Initiative. Thanks to Dave Evans, Cees van Staal, and Tyler Nickson for assistance with fieldwork. Appreciation is extended to the staff of the Jack Satterly Geochronology Laboratory at the University of Toronto for their on-going support and dedication. Hamish Sandeman acknowledges colleagues and staff of the Geological Survey of Newfoundland and Labrador. Internal review by Jean-Luc Pilote and external reviews by Graham Layne and David West improved the manuscript. NRCan Contribution 20220005.

REFERENCES

Aydin, N.S. 1995. Petrology of the composite mafic-felsic rocks of the Fogo Island batholith: a window to mafic magma chamber processes and the role of mantle in the petrogenesis of granitoid rocks. Unpublished Ph.D. Thesis, Department of Earth Sciences, Memorial University of Newfoundland, St. John's, Newfoundland and Labrador, 307 p.

Barbarin, B. 1990. Granitoids: main petrogenetic classification in relation to origin and tectonic setting. Geological Journal 25, pp. 227–238. https://doi.org/10.1002/gj.3350250306

Barbarin, B. 1999. A review of the relationships between granitoid types, their origins and their geodynamic environments. Lithos, 46, pp. 605–626. https://doi.org/10.1016/S0024-4937(98)00085-1

Blackwood, R.F. 1982. Gander (Mount Peyton E.), Newfoundland. Map 80-198, scale 1:50 000. Geology of the Gander Lake (2D/15) and Gander River (2E/2) Area. Government of Newfoundland and Labrador, Department of Mines and Energy, Mineral Development Division, Report 82-04, 63 p.

Bleeker, W. 2002 "Timiskaming-type" conglomerate-sandstone sequences: indicators of the buoyant ascent and unroofing of composite Archean granitoid-gneiss domes. *In* Geological Association of Canada-Mineralogical Association of Canada, Program with Abstracts 27. Joint annual meeting, Saskatoon, May 27–29, 2002, p. 11.

Bleeker, W. 2012. Lode gold deposits in ancient deformed and metamorphosed terranes: the role of extension in the formation of Timiskaming basins and large gold deposits, Abitibi greenstone belt—a discussion. *In* Targeted Geoscience Initiative (TGI-4), Summary of Field Work and Other Activities 2012. Ontario Geological Survey, Open File Report 6280, pp. 47-1–47-12.

Bleeker, W. 2015. Synorogenic gold mineralization in granite-greenstone terranes: the deep connection between extension, major faults, synorogenic clastic basins, magmatism, thrust inversion, and long-term preservation. *In* Targeted Geoscience Initiative (TGI-4), Contributions to the Understanding of Precambrian Lode Gold Deposits and Implications for Exploration. *Edited by* B. Dubé and P. Mercier-Langevin. Geological Survey of Canada, Open File 7852, pp. 25–47. https://doi.org/10.4095/296626

Bleeker, W. and Honsberger, I.W. 2022. Triangle zone thrust geometry as a natural focusing mechanism in orogenic gold systems. Geological Association of Canada, Miner-

alogical Association of Canada, International Association of Hydrogeologists/Canadian National Committee, and the Canadian Society of Petroleum Geologists May 15–18, 2022. (Halifax2022-Abstract 1), p. 57. https://halifax2022.atlanticgeosciencesociety.ca/technical-program/

Boyce, W.D. and Dickson, W.L. 2006. Recent fossil finds in the Indian Islands Group, central Newfoundland. *In* Current Research. Government of Newfoundland and Labrador, Department of Natural Resources, Geological Survey, Report 6-1, pages 221–231.

Buchan K.L. and Hodych J.P. 1992. Early Silurian paleolatitude for central Newfoundland from paleomagnetism of the Wigwam Formation. Canadian Journal of Earth Sciences, 29, pp. 1652–1661. https://doi.org/10.1139/e92-130

Bustard, A.L. Lentz, D.R., and Walker, J.A. 2021. Geochemical evaluation of mineralization and igneous activity in the vicinity of the Elmtree deposit, northeastern New Brunswick, Canada. Atlantic Geoscience Society Abstracts. Atlantic Geology, 57, p. 107.https://doi.org/10.4138/atlgeol.2021.001

Chandler, F., Sullivan, R., and Currie, K. 1987. The age of the Springdale Group, western Newfoundland, and correlative rocks–evidence for a Llandovery overlap assemblage in the Canadian Appalachians. Transactions of the Royal Society of Edinburgh, Earth Sciences, 78, pp. 41–49. https://doi.org/10.1017/S0263593300010944

Cohen, K.M., Finney, S.C., Gibbard, P.L., and Fan, J.X. 2013. Updated 2021. The ICS International Chronostratigraphic Chart. Episodes, 36, pp. 199–204. https://doi.org/10.18814/epiiugs/2013/v36i3/002

Colman-Sadd, S.P. 1980. Geology of south–central Newfoundland and evolution of the eastern margin of Iapetus. American Journal of Science 280, pp. 991–1017. https://doi.org/10.2475/ajs.280.10.991

Colman-Sadd, S.P. 1985. Geology of the Burnt Hill map area (NTS 2D/5), Newfoundland. Newfoundland Department of Mines and Energy, Mineral Development Division, Report 85-3, 108 p. includes map 85-001 Burnt Hill, scale 1:50 000.

Colman-Sadd, S.P. 1994. Silurian subaerial rocks near Lewisporte, central Newfoundland. *In* Current Research, Newfoundland Department of Mines and Energy, Geological Survey Branch, Report 94-1, pp. 65–76.

Colman-Sadd, S., Hayes, J., and Knight, I. 1990. The geology of the Island of Newfoundland. Government of Newfoundland and Labrador, Department of Mines and Energy, Geological Survey Branch, Map 90-01, GS# NFLD/2192, scale 1:1 000 000.

Connelly, J.N. and Heaman, L.M. 1993. U–Pb geochronological constraints on the tectonic evolution of the Grenville Province, western Labrador. Precambrian Research, 63, pp. 123–142. https://doi.org/10.1016/0301-9268(93)90008-P

Currie, K. L. 1995. The northeastern end of the Dunnage Zone in Newfoundland. Atlantic Geology, 31, pp. 25–38. https://doi.org/10.4138/2096

Dallmeyer, R.D., Kean, B.F., Odom, A.L., and Jayasinghe, N.R. 1983. Age and contact-metamorphic effects of the Overflow Pond granite: an undeformed pluton in the Dunnage Zone of the Newfoundland Appalachians. Canadian Journal of Earth Sciences, 20, pp. 1639–1645. https://doi.org/10.1139/e83-155

Davis, D.W. 2002. U–Pb geochronology of Archean metasediments in the Pontiac and Abitibi subprovinces, Quebec, constraints on timing, provenance and regional tectonics. Precambrian Research, 115, pp. 97–117. https://doi.org/10.1016/S0301-9268(02)00007-4

de Roo, J.A. and van Staal, C.R. 1994. Transpression and extensional collapse: steep belts and flat belts in the Appalachian Central Mobile Belt, northern New Brunswick, Canada. Geological Society of America Bulletin, 106, pp. 541–552. https://doi.org/10.1130/0016-7606(1994)106<0541:-TAECSB>2.3.CO;2

Dec, T. and Colman-Sadd, S.P. 1990. Timing of ophiolite emplacement onto the Gander Zone: evidence from providence studies in the Mount Cormack Subzone. *In* Current Research, Newfoundland Department of Mines and Energy, Geological Survey Branch, Report 90-1, pp. 289–303.

Dewey, J.F., Holdsworth, R.E., and Strachan, R.A. 1998. Transpression and transtension zones. *In* Continental transpressional and transtensional tectonics. *Edited by* R.E. Holdsworth, R.A. Strachan, and J.F. Dewey. Geological Society, London, Special Publications, 135, pp. 1–14. https://doi.org/10.1144/GSL.SP.1998.135.01.01

Dickson, W.L. 1993. Geology of the Mount Peyton map area (NTS 2D/14), central Newfoundland. *In* Current Research, Government of Newfoundland and Labrador, Department of Mines and Energy, Geological Survey Branch, Report 93-1, pp. 209–220.

Dickson, W.L. 1999. Geology of the Hodges Hill (NTS 2E/04) map area, north-central Newfoundland. *In* Current Research, Newfoundland Department of Mines and Energy, Geological Survey, Report 99-1, pp. 317–342.

Dickson, W.L. 2000. Geology of the Hodges Hill (NTS 2E/04) map area, central Newfoundland. Newfoundland Department of Mines and Energy, Geological Survey, Map 2000-23, Open File 002E/04/1082, scale 1:50 000.

Dickson, W.L. 2006. The Silurian Indian Islands Group and its relationships to adjacent units. *In* Current Research, Newfoundland and Labrador Department of Natural Resources, Geological Survey, Report 06-1, pp. 1–24.

Dickson, W.L., O'Brien, B.H., and Colman-Sadd, S.P. 2000. Geology of the Botwood map area [NTS 2E/3], central Newfoundland. Government of Newfoundland and Labrador, Department of Mines and Energy, Geological Survey, Open File 2E/03/1067 Version 2.0, Map 2000-11, scale 1:50 000.

Dickson, W.L., McNicoll, V.J., Nowlan, G.S., and Dunning, G.R. 2007. The Indian Islands Group and its relationships to adjacent units: recent Data. *In* Current Research, Newfoundland and Labrador Department of Natural Resources, Geological Survey, Report 07-1, pp. 1–9.

Donaldson, C., Sood, R., Barth, A., Christie, H., and Kerr, A. 2015. Geological relationships in northwestern Fogo Island and their implications for the timing of orogenic events. Newfoundland and Labrador Department of Natural Resources, Geological Survey, Report 15-1, pp. 27–42.

Dostal, J., Wilson, R.A., and Jutras, P. 2020. Petrogenesis of Siluro-Devonian rhyolite of the Tobique Group in the northwestern Appalachians (northern New Brunswick, Canada): tectonic implications for the accretion history of peri-Gondwanan terranes along the Laurentian margin. *In* Pannotia to Pangea: Neoproterozoic and Paleozoic orogenic cycles in the Circum-Atlantic region. *Edited by* J.B. Murphy, R.A. Strachan, and C. Quesada. Geological Society of London Special Publications, 503, pp. 391–407. https://doi.org/10.1144/SP503-2019-229.

Dubé, B., Dunning, G.R., Lauzière, K., and Roddick, J.C. 1996. New insights into the Appalachian Orogen from geology and geochronology along the Cape Ray fault zone, southwest Newfoundland. Geological Society of America Bulletin, 108, pp. 101–116. https://doi.org/10.1130/0016-7606(1996)108<0101:NIITAO>2.3.CO;2

Dunning, G.R., O'Brien, S.J., Colman-Sadd, S.P., Blackwood, R.F., Dickson, W.L., O'Neill, P.P., and Krogh, T.E. 1990. Silurian Orogeny in the Newfoundland Appalachians. Journal of Geology, 98, pp. 895–913. https://doi.org/10.1086/629460

Dunsworth, S. and Walford, P. 2018. Marathon's Valentine Lake Property – A developing multi-million-ounce gold camp in central Newfoundland, Canada. Geological Association of Canada-Newfoundland and Labrador section abstracts. Atlantic Geology, 54, 136–137 p. https://doi.org/10.4138/atlgeol.2018.003

Elliot, C.G., Dunning, G.R., and Williams, P.F. 1991. New U–Pb zircon age constraints on the timing of deformation in north-central Newfoundland and implications for early Paleozoic Appalachian orogenesis. Geological Society of America Bulletin, 103, pp. 125–135. https://doi.org/10.1130/0016-7606(1991)103<0125:NUPZAC>2.3.CO;2

Evans, D.T.W. 1996. Epigenetic gold occurrences, eastern and central Dunnage Zone, Newfoundland. Government of Newfoundland and Labrador, Department of Mines and Energy, Geological Survey, Mineral Resources Report 9, 135 p.

Evans, D.T.W. 2004. Epigenetic gold occurrences, Baie Verte Peninsula, (NTS 12H/09,16 and 12I/01) Newfoundland. Newfoundland and Labrador Department of Natural Resources, Geological Survey, Mineral Resource Report 11, 159 p.

Evans, D.T.W., Kean, B.F., and Dunning, G.R. 1990. Geological studies, Victoria Lake Group, central Newfoundland. *In* Current Research, Government of Newfoundland and Labrador, Department of Mines and Energy, Geological Survey Branch, Report 90-1, p. 135–144.

Froude, T. 2021. Sokoman reports first barge-based drill results Moosehead Gold Project, Central Newfoundland; Phase 6 drill Program doubled to 100 000 m. Sokoman Minerals Corp. press release, November 10, 2021. URL https://sokomanmineralscorp.com/2021/11/10/sokoman-reports-first-barge-based-drill-results-moosehead-gold-project-central-newfoundland/ 10 December 2021.

Gerstenberger, H. and Haase, G. 1997. A highly effective emitter substance for mass spectrometric Pb isotope ratio determinations. Chemical Geology, 136, pp. 309–312. https://doi.org/10.1016/S0009-2541(96)00033-2

Gower, C.F. and Krogh, T.E. 2002. A U–Pb geochronological review of the Proterozoic history of the eastern Grenville Province. Canadian Journal of Earth Sciences, 39, pp. 795–829. https://doi.org/10.1139/e01-090

Heaman, L.M., Erdmer, P., and Owen, J.V. 2002. U–Pb geochronologic constraints on the crustal evolution of the Long Range Inlier, Newfoundland. Canadian Journal of Earth Sciences, 39, pp. 845–865. https://doi.org/10.1139/e02-015

Henderson, B.J., Collins, W.J., Murphy, J.B., and Hand, M. 2018. A hafnium isotopic record of magmatic arcs and continental growth in the Iapetus Ocean: the contrasting evolution of Ganderia and the peri-Laurentian margin. Gondwana Research, 58, pp. 141–160. https://doi.org/10.1016/j.gr.2018.02.015

Hibbard, J.P., van Staal, C.R. Rankin, D.W., and Williams, H. 2006. Lithotectonic map of the Appalachian Orogen, Canada-United States of America. Geological Survey of Canada Map 2096A, scale 1:1 500 000. https://doi.org/10.4095/221912

Hinchey, A.M., Rayner, N., and Davis, W.J. 2020. Episodic Paleoproterozoic crustal growth preserved in the Aillik Domain, Makkovik Province, Labrador. Precambrian Research, 337, 105526. https://doi.org/10.1016/j.precamres.2019.105526

Hodgson, C.J. 1993. Mesothermal lode-gold deposits. *In* Mineral Deposit Modelling. *Edited by* R.V. Kirkham, W.D. Sinclair, R.I. Thorpe, and J.M. Duke. Geological Association of Canada, Special Paper 40, pp. 635–678.

Honsberger, I.W., Bleeker, W., Sandeman, H.A.I., and Evans, D.T.W. 2019. Lithological and structural setting of structurally controlled gold mineralization in the Wilding Lake region, central Newfoundland. *In* Targeted Geoscience Initiative 2018 report of activities. *Edited by* N. Rogers. Geological Survey of Canada, Open File 8549, pp. 59–69. https://doi.org/10.4095/313640

Honsberger, I.W., Bleeker, W., Kamo, S.L., Sandeman, H.A.I., and Evans, D.T.W. 2020. The emerging Paleozoic gold district of central Newfoundland: new insights on structural controls and tectonic drivers of gold mineralization and preservation. *In* Targeted Geoscience Initiative 5: Contributions to the Understanding of Gold Deposits. *Edited by* P. Mercier-Langevin, C.J.M. Lawley, and S. Castonguay. Geological Survey of Canada, Open File 8712, pp. 193–210. https://doi.org/10.4095/326024

Honsberger, I.W., Bleeker, W., Kamo, S.L., Sandeman, H.A.I., Evans, D.T.W., van Staal, C.R., Rogers, N., and Dunning, G.R. 2022. Latest Silurian syntectonic sedimentation and

magmatism and Early Devonian orogenic gold mineralization, central Newfoundland Appalachians, Canada: setting, structure, lithogeochemistry, and high-precision U–Pb geochronology. Geological Society of America Bulletin 133, Published on-line March 3, 2022. https://doi.org/10.1130/B36083.1

Jaffey, A.H., Flynn, K.F., Glendenin, L.E., Bentley, W.C., and Essling, A.M. 1971. Precision measurement of half-lives and specific activities of ^{235}U and ^{238}U. Physical Review C 4, pp. 1889–1906. https://doi.org/10.1103/PhysRevC.4.1889

James, D.T., Kamo, S., and Krogh, T. 2002. Evolution of 3.1 and 3.0 Ga volcanic belts and a new thermotectonic model for the Hopedale Block, North Atlantic craton, Canada. Canadian Journal of Earth Sciences, 39, pp. 687–710. https://doi.org/10.1139/e01-092

Karlstrom K. E., van der Pluijm B. A., and Williams P. F. 1982. Structural interpretation of the eastern Notre Dame Bay area, Newfoundland: regional post-Middle Silurian thrusting and asymmetrical folding. Canadian Journal of Earth Sciences, 19, pp. 2325–2341. https://doi.org/10.1139/e82-204

Kean, B.F. and Evans, D.T.W. 1988. Regional metallogeny of the Victoria Lake Group. *In* Current Research, Newfoundland Department of Mines, Mineral Developments Division, Report 88-1, pp. 319–330.

Kean, B.F. and Jayasinghe, N.R. 1980. Geology of the Lake Ambrose (12A/10) and Noel Paul's Brook (12A/9) map areas, Newfoundland. Newfoundland Department of Mines and Energy Report 88-1, 29 p.

Kerr, A. 1997. Space-time composition relationships among Appalachian plutonic suites in Newfoundland. *In* The Nature of Magmatism in the Appalachian orogen. *Edited by* A.K. Sinha, J.B. Whalen, and J.P. Hogan. Geological Society of America Memoirs, 191. pp. 193–220. https://doi.org/10.1130/0-8137-1191-6.193

Kerr, A. 2013. The Fogo Process from a geologist's perspective: a discussion of models and research problems. *In* Current Research, Newfoundland and Labrador Department of Natural Resources, Geological Survey, Report 13-1, pp. 233–265.

Ketchum, J.W.F., Culshaw, N.G., and Barr, S.M. 2002. Anatomy and orogenic history of a Paleoproterozoic accretionary belt: the Makkovik Province, Labrador, Canada. Canadian Journal of Earth Sciences, 39, pp. 711–730. https://doi.org/10.1139/e01-099

Krogh, T.E. 1973. A low-contamination method for hydrothermal decomposition of zircon and extraction of U and Pb for isotopic age determinations. Geochimica et Cosmochimica Acta, 37, pp. 485–494. https://doi.org/10.1016/0016-7037(73)90213-5

Kuiper, Y.D. and Hepburn, J.C. 2021. Detrital zircon populations of the eastern Laurentian margin in the Appalachians. Geology, 49, pp. 233–237. https://doi.org/10.1130/G48012.1

Kusky, T.M. and Kidd, W.S.F. 1996. Tectonic implication of early Silurian thrust imbrication of the northern Exploits Subzone, central Newfoundland. Journal of Geodynamics 22, pp. 229–265. https://doi.org/10.1016/0264-3707(96)00011-7

Kusky T.M., Kidd W.S.F., and Bradley D.C. 1987. Displacement history of the Northern Arm Fault, and its bearing on the post-Taconic evolution of North-central Newfoundland. Journal of Geodynamics, 7, pp. 105–133. https://doi.org/10.1016/0264-3707(87)90067-6

Lafrance, B. 1989. Structural evolution of a transpression zone in north central Newfoundland. Journal of Structural Geology, 11, pp. 705–716. https://doi.org/10.1016/0191-8141(89)90006-0

Lincoln, N., Farmer, R., Eccles, R., and Deering, P.D. 2018. Preliminary economic assessment of the Valentine Lake gold project Newfoundland, NL, Canada. Lycopodium Minerals Canada Ltd. for Marathon Gold. <www.marathongold.com/site/assets/files/5047/2018-10-pea.pdf> December 2, 2018.

Ludwig, K.R. 1998. On the treatment of concordant uranium-lead ages. Geochimica et Cosmochimica Acta, 62, pp. 665–676. https://doi.org/10.1016/S0016-7037(98)00059-3

Ludwig, K.R. 2003. User's manual for Isoplot 3.00 a geochronological toolkit for Excel. Berkeley Geochronological Center Special Publication 4, 71 p.

Mann, W.P., Hempton, M., Bradley, D., and Burke, K. 1983. Development of pull-apart basins. Journal of Geology, 91, pp. 529–554. https://doi.org/10.1086/628803

Mattinson, J.M. 2005. Zircon U–Pb chemical abrasion ("CA-TIMS") method: combined annealing and multi-step partial dissolution analysis for improved precision and accuracy of zircon ages. Chemical Geology 220, pp. 47–66. https://doi.org/10.1016/j.chemgeo.2005.03.011

McNicoll, V.J., Squires, G.C., Wardle, R.J., Dunning, G.R., and O'Brien, B.H. 2006. U–Pb geochronological evidence for Devonian deformation and gold mineralization in the eastern Dunnage Zone, Newfoundland. *In* Current Research, Report 06-1, pp. 45–60.

Miller, H.G. 1988. Geophysical interpretation of the geology of the northeast Gander Terrane, Newfoundland. Canadian Journal of Earth Sciences 25, pp. 1161–1174. https://doi.org/10.1139/e88-114

O'Brien, B.H. 1993. Geology of the region around Botwood (parts of 2E/3,4,6), north-central Newfoundland. Newfoundland Department of Mines and Energy, Geological Survey, Map 93-168, Open File 002E/0869, scale 1:50 000

O'Brien, B.H. 2003. Geology of the central Notre Dame Bay region (Parts of NTS areas 2E/3,6,11) northeastern Newfoundland. Newfoundland and Labrador Department of Mines and Energy, Geological Survey Report 03-03, 147 p.

O'Brien, B.H., O'Brien, S.J., Dunning, G.R., and Tucker, R.D. 1993. Episodic reactivation of a Late Precambrian mylonite zone on the Gondwana margin of the Appalachians, southern Newfoundland. Tectonics, 12, pp. 1043–1055. https://doi.org/10.1029/93TC00110

O'Neill, P. and Blackwood, F. 1989. A proposal for revised stratigraphic nomenclature of the Gander and Davidsville Groups and the Gander River Ultrabasic belt of northeastern Newfound-

land Department of Mines, Geological Survey of Newfoundland, Report 89-1, pp. 127–130.

Pitcher, W.S. 1983. Granite type and tectonic environment. *In* Mountain Building Processes. *Edited by* K.J. Hsü. London, Academic Press, pp. 19–40.

Pitcher, W.S. 1993. The Nature and Origin of Granite. London, Blackie, 321 p. https://doi.org/10.1007/978-94-017-3393-9

Pollock, J.C., Wilton, D.H.C., van Staal, C.R., and Morrissey, K.D. 2007. U–Pb detrital zircon geochronological constraints on the Early Silurian collision of Ganderia and Laurentia along the Dog Bay Line: the terminal Iapetan suture in the Newfoundland Appalachians. American Journal of Science, 307, pp. 399–433. https://doi.org/10.2475/02.2007.04

Poulsen, K.H., Robert, F., and Dubé, B. 2000. Geological classification of Canadian gold deposits. Geological Survey of Canada, Bulletin 540, 106 p. https://doi.org/10.4095/211094

Rogers, N. and van Staal, C.R. 2005. Geology, Grand Falls, Newfoundland and Labrador. Geological Survey of Canada, Open File 4545, scale 1: 50 000. https://doi.org/10.4095/221290

Rogers, N., van Staal, C.R., McNicoll, V.J., Squires, G.C., Pollock, J., and Zagorevski, A. 2005. Geology, Lake Ambrose and part of Buchans, Newfoundland and Labrador. Geological Survey of Canada, Open File 4544, scale 1:50 000. https://doi.org/10.4095/221289

Rogers, N., van Staal, C.R., McNicoll, V.J., Pollock, J., Zagorevski, A., and Whalen, J. 2006. Neoproterozoic and Cambrian arc magmatism along the eastern margin of the Victoria Lake Supergroup: a remnant of Ganderian basement in central Newfoundland? Precambrian Research, 147, pp. 320–341. https://doi.org/10.1016/j.precamres.2006.01.025

Sambridge, M.S. and Compston, W. 1994. Mixture modeling of multi-component data sets with application to ion-probe zircon ages. Earth Planetary Science Letters, 128, p. 373–390. https://doi.org/10.1016/0012-821X(94)90157-0

Sandeman, H.A.I. 2021. The Dog Bay Line in northeast Newfoundland, Canada: an overview of the current state of knowledge. Geological Association of Canada-Newfoundland and Labrador section abstracts. Atlantic Geology, 57, p. 144. https://doi.org/10.4138/atlgeol.2021.001

Sandeman, H.A.I. and Malpas, J.G. 1995. Epizonal I- and A-type granites and associated ash-flow tuffs, Fogo Island, northeast Newfoundland. Canadian Journal of Earth Sciences, 32, pp. 1835–1844. https://doi.org/10.1139/e95-141

Sandeman, H.A.I., Dunning, G.R., McCullough, C.K., and Peddle, C. 2017. U–Pb geochronology, petrogenetic relationships and intrusion-related precious-metal mineralization in the northern Mount Peyton Intrusive Suite: implications for the origin of the Mount Peyton trend, central Newfoundland (NTS 2D/04). *In* Current Research. Government of Newfoundland and Labrador, Department of Natural Resources, Geological Survey, Report 17-1, pp 189–217.

Sandeman, H.A.I., Honsberger, I.W., and Camacho, A. 2022 (this volume). Overview of age constraints for gold mineralization in central and western Newfoundland and new $^{40}Ar/^{39}Ar$ ages for white mica from selected auriferous zones. Atlantic Geoscience, 58,. https://doi.org/10.4138/atlgeo.2022.010.

Stacey, J.S. and Kramers, J.D. 1975. Approximation of terrestrial lead isotope evolution by a two-stage model. Earth and Planetary Science Letters 26, pp. 207–221. https://doi.org/10.1016/0012-821X(75)90088-6

Strong, D.F. 1979. The Mount Peyton batholith, central Newfoundland: a bimodal calc-alkaline suite. Journal of Petrology 20, pp. 119–138. https://doi.org/10.1093/petrology/20.1.119

Strong, D.F. and Dupuy, C. 1982. Rare earth elements in the bimodal Mount Peyton batholith: evidence of the crustal anataxis by mantle-derived magma. Canadian Journal of Earth Sciences, 19, pp. 308–315. https://doi.org/10.1139/e82-022

Todd, S.E., Pufahl, P.K., Murphy, J.B., and Taylor, K.G. 2018. Sedimentology and oceanography of Early Ordovician ironstone, Bell Island, Newfoundland: ferruginous seawater and upwelling in the Rheic Ocean. Sedimentary Geology, 379, pp. 1–15. https://doi.org/10.1016/j.sedgeo.2018.10.007

Tomlinson, K.Y., Davis, D.W., Stone, D., and Hart, T.R. 2003. U–Pb age and Nd isotopic evidence for crustal recycling and Archean terrane development in the south-central Wabigoon subprovince, Canada. Contributions to Mineralogy and Petrology, 144, pp. 684–702. https://doi.org/10.1007/s00410-002-0423-0

Tremblay, A. and Dubé, B.1991. Structural relationships between some gold occurrences and fault zones in the Bathurst area, northern New Brunswick. *In* Current Research, Part D. Geological Survey of Canada, Paper 91-1D, pp. 89–99. https://doi.org/10.4095/132590

Tremblay, A., Faure, S., and Dubé, B. 1993. Gold occurrences of the Rocky Brook–Millstream Fault, northern Appalachians, New Brunswick. *In* Current Research, Part E. Geological Survey of Canada, Paper 93-1E, pp. 337–346. https://doi.org/10.4095/184129

Tuach, J. 1992. List of gold occurrences and deposits on the Island of Newfoundland. Newfoundland Department of Mines and Energy, Geological Survey Branch, Open File 2188, 107 p.

Tuach, J., Dean, P.L., Swinden, H.S., O'Driscoll, C., Kean, B.F., and Evans, D.T.W. 1988. Gold mineralization in Newfoundland: a 1988 review. Newfoundland Department of Mines, Mineral Development Division, Report 88-1, p. 279–306.

Tucker, R.D. and Gower, C.F. 1994. A U–Pb geochronological framework for the Pinware Terrane, Grenville Province, Southeast Labrador. Journal of Geology, 102, pp. 67–78. https://doi.org/10.1086/629648

Valverde-Vaquero, P. and van Staal, C.R. 2002. Geology and magnetic anomalies of the Exploits-Meelpaeg boundary

zone in the Victoria Lake area (central Newfoundland): regional implications. *In* Current Research, Newfoundland Department of Mines and Energy, Geological Survey, Report 02-1, p. 197–209.

Valverde-Vaquero, P., van Staal, C.R., McNicoll, V., and Dunning, G.R. 2006. Mid-Late Ordovician magmatism and metamorphism along the Gander margin in central Newfoundland. Journal of the Geological Society of London, 163, pp. 347–362. https://doi.org/10.1144/0016-764904-130

van der Velden, A.J., van Staal, C.R., and Cook, F.A. 2004. Crustal structure, fossil subduction, and the tectonic evolution of the Newfoundland Appalachians: evidence from a reprocessed seismic reflection survey. Geological Society of America Bulletin, 116, pp. 1485–1498, https://doi.org/10.1130/B25518.1

van Staal, C.R. and Barr, S.M. 2012. Lithospheric architecture and tectonic evolution of the Canadian Appalachians and associated Atlantic margin. *In* Tectonic Styles in Canada Revisited: the LITHOPROBE Perspective. *Edited by* J.A. Percival, F.A. Cook, and R.M. Clowes. Geological Association of Canada Special Paper 49, pp. 41–95.

van Staal, C.R., Valverde-Vaquero, P., Zagorevski, A., Rogers, N., Lissenberg, C.J., and McNicoll, V.J. 2005. Geology, Victoria Lake, Newfoundland and Labrador. Geological Survey of Canada, Open File 1667, scale 1:50 000. https://doi.org/10.4095/221287

van Staal, C.R., Zagorevski, A., McNicoll, V.J., and Rogers, N. 2014. Time-transgressive Salinic and Acadian orogenesis, magmatism, and Old Red Sandstone sedimentation in Newfoundland. Geoscience Canada, 41, pp. 138–164. https://doi.org/10.12789/geocanj.2014.41.031

Waldron, J.W.F., McNicoll, V.J., and van Staal, C.R. 2012. Laurentia-derived detritus in the Badger Group of central Newfoundland: deposition during closing of the Iapetus Ocean. Canadian Journal of Earth Sciences, 49, pp. 207–221. https://doi.org/10.1139/e11-030

Wardle, R.J. 2005. Gold. Newfoundland and Labrador Department of Natural Resources, Geological Survey, Commodity Series Report 4, 12 p.

Whalen, J.B. and Hildebrand, R. S. 2019. Trace element discrimination of arc, slab failure, and A-type granitic rocks. Lithos, 348-349, 105179. https://doi.org/10.1016/j.lithos.2019.105179

Whalen, J.B., Jenner, G.A., Longstaffe, F.J., Gariepy, C., and Fryer, B. 1997. Implications of granitoid geochemical and isotopic (Nd, O, Pb) data from the Cambro–Ordovician Notre Dame arc for the evolution of the Central Mobile Belt, Newfoundland Appalachians. *In* The Nature of Magmatism in the Appalachian Orogen. *Edited by* A.K. Sinha, J.B. Whalen, and J.P. Hogan. Geological Society America Memoir, 191, pp. 367–395. https://doi.org/10.1130/0-8137-1191-6.367

Whalen, J.B., McNicoll, V.J., van Staal, C.R., Lissenberg, C.J., Longstaffe, F.J., Jenner, G.A., and van Breemen, O. 2006. Spatial, temporal and geochemical characteristics of Silurian collision zone magmatism, Newfoundland Appalachians: an example of a rapidly evolving magmatic system related to slab break-off. Lithos, 89, pp. 377–404. https://doi.org/10.1016/j.lithos.2005.12.011

White, S.E. and Waldron, J.W.F. 2022. Along-strike variations in the deformed Laurentian margin in the Northern Appalachians: role of inherited margin geometry and colliding arcs. Earth Science Reviews 226, 103931. https://doi.org/10.1016/j.earscirev.2022.103931

Willner, A.P., van Staal, C.R., Zagorevski, A., Glodnye, J., Romere, R.L., and Sudof, M. 2018. Tectonometamorphic evolution along the Iapetus suture zone in Newfoundland: evidence for polyphase Salinic, Acadian and Neoacadian very low- to medium-grade metamorphism and deformation. Tectonophysics, 742–743, pp. 137–167. https://doi.org/10.1016/j.tecto.2018.05.023

Willner, A.P., van staal, C.R., Glodny, J., Sudo, M., Zagorevski, A. 2022. Conditions and timing of metamorphism near the Baie Verte Line (Baie Verte Peninsula, NW Newfoundland, Canada): multiple reactivations within the suture zone of an arc-continent collision. *In* New Developments in the Appalachian-Caledonian-Variscan Orogen. *Edited by* Y.D. Kuiper, J.B. Murphy, R.D. Nance, R.A. Strachan, and M.D. Thompson. Geological Society of America Special Paper 554. https://doi.org/10.1130/2022.2554(09)

Williams, H. 1962. Botwood (West Half) Map-area, Newfoundland. Geological Survey of Canada Paper 62-9, 16 p. https://doi.org/10.4095/123914

Williams, H. 1972. Stratigraphy of Botwood map-area, northeastern Newfoundland. Geological Survey of Canada, Open File Report 113, 98 p.

Williams, H. 1978. Tectonic lithofacies map of the Appalachian Orogen. Memorial University of Newfoundland, St John's, Newfoundland and Labrador, scale 1:1 000 000.

Williams, H. 1993. Stratigraphy and structure of the Botwood Belt and definition of the Dog Bay Line in northeastern Newfoundland. *In* Current Research, Part D, Geological Survey of Canada, Paper 93-1D, pp. 19–27. https://doi.org/10.4095/134267

Williams, H., Colman-Sadd, S.P., and Swinden, H.S. 1988. Tectonic-stratigraphic subdivisions of central Newfoundland. Geological Survey of Canada Paper 88-1B, pp. 91–98. https://doi.org/10.4095/122425

Williams, H., Currie, K.L., and Piasecki, M.A.J. 1993. The Dog Bay Line: a major Silurian tectonic boundary in northeast Newfoundland. Canadian Journal of Earth Sciences, 30, pp. 2481–2494. https://doi.org/10.1139/e93-215

Williams, H., Dean, P.L., and Pickering, K.T. 1995. Botwood Belt. *In* Geology of the Appalachian–Caledonian Orogen in Greenland. *Edited by* H. Williams. Geological Survey of Canada, Geology of Canada, 6, pp. 413–420. https://doi.org/10.4095/205242

Wilson, R. 2007. Silurian–Devonian stratigraphy and structure in the Arleau Brook region, northern margin of the Miramichi Highlands, New Brunswick. *In* Abstracts 2007, Exploration and Mining New Brunswick. *Edited by* S.A.A Merlini. New Brunswick Department of Natural Resourc-

es; Minerals, Policy and Planning Division Information Circular 2007-1, pp. 53-56.

Wilson, R.A., van Staal, C.R., and Kamo, S.L. 2017. Rapid transition from the Salinic to Acadian orogenic cycles in the northern Appalachian orogen: evidence from northern New Brunswick, Canada. American Journal of Science, 317, pp. 449–482. https://doi.org/10.2475/04.2017.02

Zagorevski, A., van Staal, C.R., McNicoll, V., and Rogers, N. 2007. Tectonic architecture of an arc-arc collision zone, Newfoundland Appalachians. *In* Formation and Applications of the Sedimentary Record in Arc Collision Zones. *Edited by* A. Draut, P.D. Clift, and D.W. Scholl. Geological Society of America Special Paper 436, pp. 1–26. https://doi.org/10.1130/2008.2436(14)

Editorial responsibility: Mitchell Kerr

A *Batrachichnus salamandroides* trackway from the Minto Formation of central New Brunswick, Canada: implications for alternative tracemaker interpretations

Luke F. Allen[1,2,3*], Matthew R. Stimson[3,4], Olivia A. King[3,4], Rowan E. Norrad[1,5], Spencer G. Lucas[6], Arjan Mann[7], Steven J. Hinds[8], Adrian F. Park[8], John H. Calder[4], Hillary Maddin[9], and Martin Montplaisir[10]

1. Citadel High School, Halifax, Nova Scotia B3H 0A4, Canada
2. Department of Earth Sciences, University of New Brunswick, Fredericton, New Brunswick B3H 0A4, Canada
3. Steinhammer Paleontological Laboratories, Geology/Paleontology section, Natural History Department, New Brunswick Museum, Saint John New Brunswick E2K 1E5, Canada
4. Department of Geology, Saint Mary's University, Halifax Nova Scotia B3H 3C3, Canada
5. Departmentof Earth and Environmental Science, Acadia University, Wolfville, Nova Scotia B4P 2R6, Canada
6. NewMexico Museum of Natural History, Albuquerque, New Mexico 87104, USA
7. Smithsonian Museum of Natural History, Department of Paleobiology, Washington DC, 20560, USA
8. New Brunswick Department of Natural Resources and Energy Development, Fredericton, New Brunswick E3B 5H1, Canada
9. Department of Earth Sciences, Carleton University, Ottawa, Ontario K1S 5B6,Canada
10. Visual Q Technologies, Moncton, New Brunswick E1E 2K2, Canada
*Corresponding author: luke.allen@unb.ca

Date received: 18 April 2022 ¶ Date accepted: 22 July 2022

ABSTRACT

A new specimen of *Batrachichnus salamandroides* was recovered from a recently discovered fossil-bearing site situated along the southern shore of Grand Lake, New Brunswick, among a diverse ichnofaunal assemblage from the Middle Pennsylvanian (upper Bolsovian; lower Moscovian), upper Minto Formation. The identity of the tracemaker of this ichnogenus is reinterpreted as a composite of various late Paleozoic tetrapod taxa, based on similarities of the postcranial skeletons, notably that of the manus and pes, of both temnospondyls and some "microsaurs". These results indicate that the tracemaker of the monospecific ichnogenus *Batrachnichus* is not limited solely to a temnospondyl tracemaker, as previously interpreted, and that some "microsaurs" should also be considered among tracemaker candidates for this ichnotaxon.

RÉSUMÉ

Un nouveau spécimen de *Batrachichnus salamandroides* a été récupéré d'un emplacement fossilifère récemment découvert le long de la rive méridionale du Grand Lac, Nouveau-Brunswick, parmi un assemblage ichnofaunique diversifié remontant au Pennsylvanien moyen (Bolsovien supérieur, Moscovien inférieur) de la partie supérieure de la Formation de Minto. On a réinterprété l'identité de l'auteur des traces de cet ichnogenre y voyant un composite de divers taxons tétrapodes du Paléozoïque tardif d'après des similarités des squelettes postcrâniens, notamment ceux des paumes et des pieds, des deux temnospondyles et de certains « microsauriens ». Ces résultats révèlent que l'auteur des traces de l'ichnogène monospécifique *Batrachnichus* ne se limite pas seulement à un producteur de traces temnospondyle, comme l'avaient supposé des interprétations antérieures, et que certains « microsauriens » devraient également être considérés parmi les producteurs de traces possibles de cet ichnotaxon.

[*Traduit par la redaction*]

INTRODUCTION

The Maritimes Basin of Atlantic Canada has yielded the most complete record of Carboniferous fossil tetrapod footprints in the world (Lucas *et al.* 2005, 2022), spanning the interval from the earliest Mississippian (Tournaisian) of Nova Scotia and New Brunswick to the early Permian (Artinskian) strata of Prince Edward Island (Lucas *et al.* 2022; Figs. 1 and 2). However, the occurrence of "middle" Carboniferous (late Bashkirian to early Moscovian) terrestrial

doi:10.4138/atlgeo.2022.010

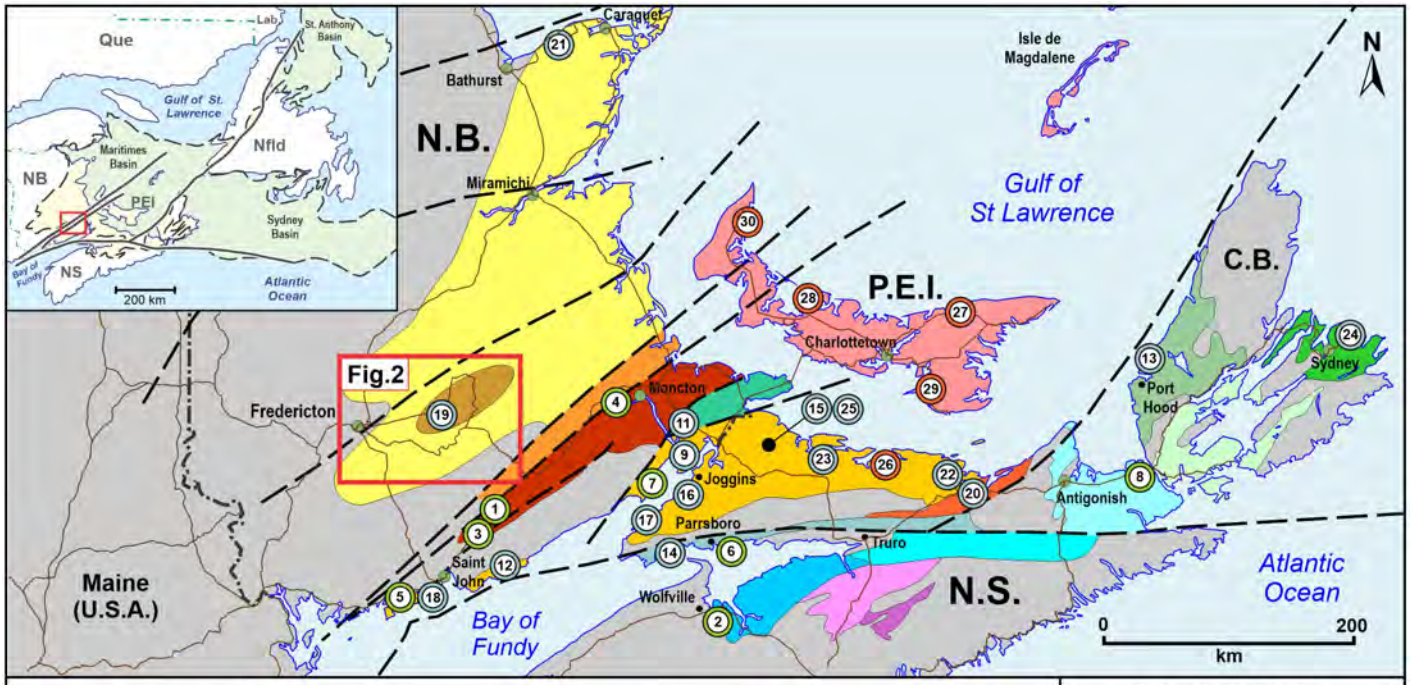

Map #	Location	Province	Age	Subbasin
Mississippian				
10	Heron Island	NB	Visean to Serpukhovian	Restigouch Area
9	Marigouin Peninsula	NB	Serpukhovian	Cumberland
8	Riley's Beach	NS	Serpukhovian	Antigonish
7	Munson Pond	NB	Visean	Cumberland
6	West Bay	NS	Visean	Debert-Kempton
5	Lepreau Falls	NB	Visean	West Cumberland
4	Stileville	NB	Tournaisian	Moncton
3	Bloomfield	NB	Tournaisian	Moncton
2	Horton Bluff	NS	Tournaisian	Windsor-Kennetcook
1	Norton	NB	Tournaisian	Moncton

Map #	Location	Province	Age	Subbasin
Pennsylvanian				
20	Stellarton	NS	Westphalian C	Stellarton
19	Grand Lake	NB	Westphalian C	Marysville
18	Fern Ledges	NB	Westphalian A-B	West Cumberland
17	Spicer's Cove	NS	Westphalian A-B	Cumberland
16	Springhill Mines	NS	Westphalian A	Cumberland
15	Wentworth Station	NS	Westphalian A	Cumberland
14	Parrsboro	NS	Westphalian A	Debert-Kempton
13	Port Hood	NS	Westphalian A	Western Cape Breton
12	Tynemouth Creek	NB	Westphalian A	West Cumberland
11	Johnson's Mills	NB	Westphalian A	Cumberland

Map #	Location	Province	Age	Subbasin
Permian				
30	Cavendish	PEI	Artinskian	PEI
29	Point Prim	PEI	Sakmarian	PEI
28	Malpeque	PEI	Asselian	PEI
27	Egmont Bay	PEI	Kasimovian-Gzhelian	PEI
26	Brule	NS	Gzelian	Cumberland
25	Wentworth Station	NS	Westphalian D	Cumberland
24	Sydney Mines	NS	Westphalian D	Sydney
23	River Philip	NS	Westphalian C-D	Cumberland
22	Aber-crombie	NS	Westphalian C	Cumberland
21	Clifton	NB	Westphalian C-D	New Brunswick

Figure 1. Map of the Atlantic Provinces of Canada and adjacent areas showing the extent of the latest Devonian to earliest Permian Maritimes Basin (after St. Peter and Johnson 2009; Gibling *et al.* 2019; and Bethoux *et al.* 2021). Subbasins are colour-coded as indicated in the upper legend. Fossil sites are numbered as indicated in the lower legend. In the lower legend, blue = Mississippian (1–10), green = Pennsylvanian (11–26), and pink = Permian (27–30); NB = New Brunswick, NS = Nova Scotia, and PEI = Prince Edward Island. Inset map shows broader geographic context.

ichnofossil localities in Atlantic Canada was unknown prior to the present study. Previously documented records of tetrapod tracks from the Bashkirian of the Maritimes Basin are from: the Joggins Formation in Nova Scotia (Dawson 1863; Matthew 1903, 1904; Sternberg 1933; Sarjeant and Mossman 1978; Lucas *et al.* 2005; Cotton *et al.* 1995; Stimson *et al.* 2012; Stimson *et al.* 2015; Prescott *et al.* 2014); the Tynemouth Creek Formation of New Brunswick (Falcon-Lang *et al.* 2010); the Lancaster Formation at Fern Ledges, Saint John, New Brunswick (Matthew 1910; Falcon-Lang and Miller 2007; Stimson *et al.* 2016a); and the Grand Anse Formation at Johnstons Mills, New Brunswick (Falcon-Lang *et*

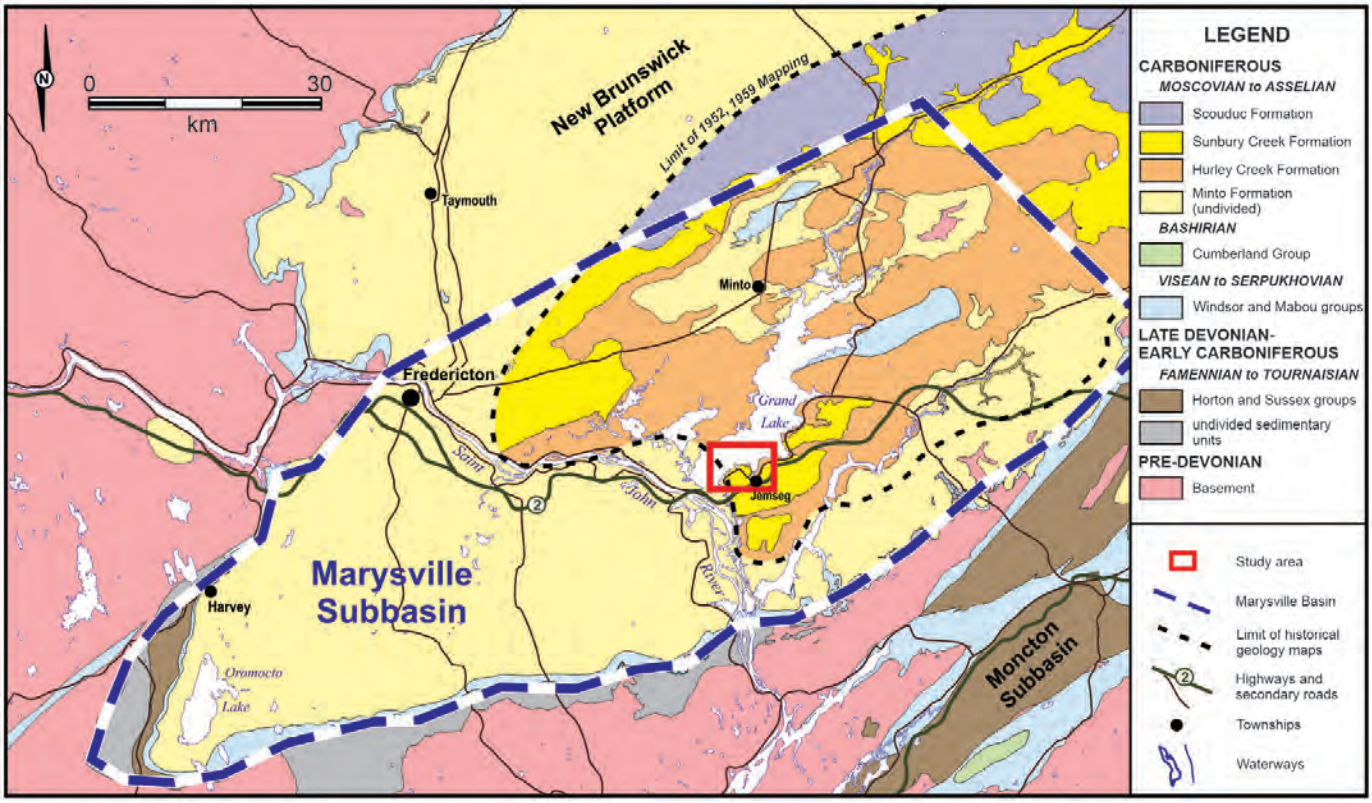

Figure 2. Geological map of part of the Maritimes Basin known as the Marysville Subbasin. (after Dyer 1926; Muller 1951, Hamilton 1960, 1962a, b, c; van de Poll *et al.* 1995). Study area outlined with a red box.

al. 2007). Tracks from Moscovian–Kasimovian strata have been found in the Clifton Formation of New Brunswick (Keough *et al.* 2020) and the Sydney Mines Formation of Cape Breton Island, Nova Scotia (Matthew 1903; Fig. 3).

Previous paleontological work on the Minto Formation is restricted to paleofloral assemblages documented by Bell (1962). A single trigonotarbid invertebrate body fossil (Miller and Forbes 2001) and a diverse faunal assemblage of aquatic vertebrates, which included undescribed tetrapod skeletal remains (Ó Gogáin *et al.* 2016), represent the only known evidence of terrestrial biota from the Minto Formation of central New Brunswick. Prior to the present study, ichnofossils had not been documented from the Minto Formation.

The absence of upper Bashkirian to lower Moscovian terrestrial tetrapod material represents an apparent gap in the fossil record of Atlantic Canada as, in contrast to other regions in North America (i.e., Mazon Creek, Illinois, and Five Points and Linton, Ohio; Fig. 3). This gap is due to poor surface exposure of strata from that time interval available for study. In addition, a major turnover in ecological conditions has been postulated during the Kasimovian, when the classic tropical ecosystems that made up the iconic image of "Coal-Age" ecosystems collapsed as a result of the formation of Pangea (Sahney *et al.* 2010; Pardo *et al.* 2019). Dunne *et al.* (2018) also suggested that the "Coal Age" collapse was likely more of a gradual transition. Taking into consideration the extensive Mississippian to Pennsylvanian rocks throughout New Brunswick, the lack of fossil tetrapod localities is surprising when comparison to the situation in neighbouring Nova Scotia. However, a newly discovered fossil tetrapod footprint assemblage from the Minto Formation represents a high-diversity population comprising several ichnotaxa interpreted to be of both reptilian and amphibian affinity. This material occurs alongside various invertebrate ichnotaxa and a classic Pennsylvanian flora, and can be used as a proxy for biodiversity. The Minto assemblage is preserved within a mudstone interval on the flanks of an incised channel body backfilled with sandstone and conglomerate, and is interpreted as the floodplain interdistributary deposits of the broader New Brunswick Platform fluvial sedimentary depositional setting (Kalkreuth *et al.* 2000; St. Peter and Johnston 2009). Furthermore, this site offers a hitherto unavailable window into Middle Pennsylvanian paleoecology and aids in providing a more comprehensive understanding of the Carboniferous evolution of Atlantic Canada. However, we plan to discuss the full extent of this assemblage in future work. Here, we present and evaluate a tetrapod trackway of the ichnospecies *Batrachichnus salamandroides* (collected by RN and LA). This discovery offers new insights into tracemaker candidates for the ichnotaxon, expanding the traditional interpretation of a temnospondyl tracemaker to encompass particular "microsaur" tetrapod genera. ("Microsaurs" are further discussed below.)

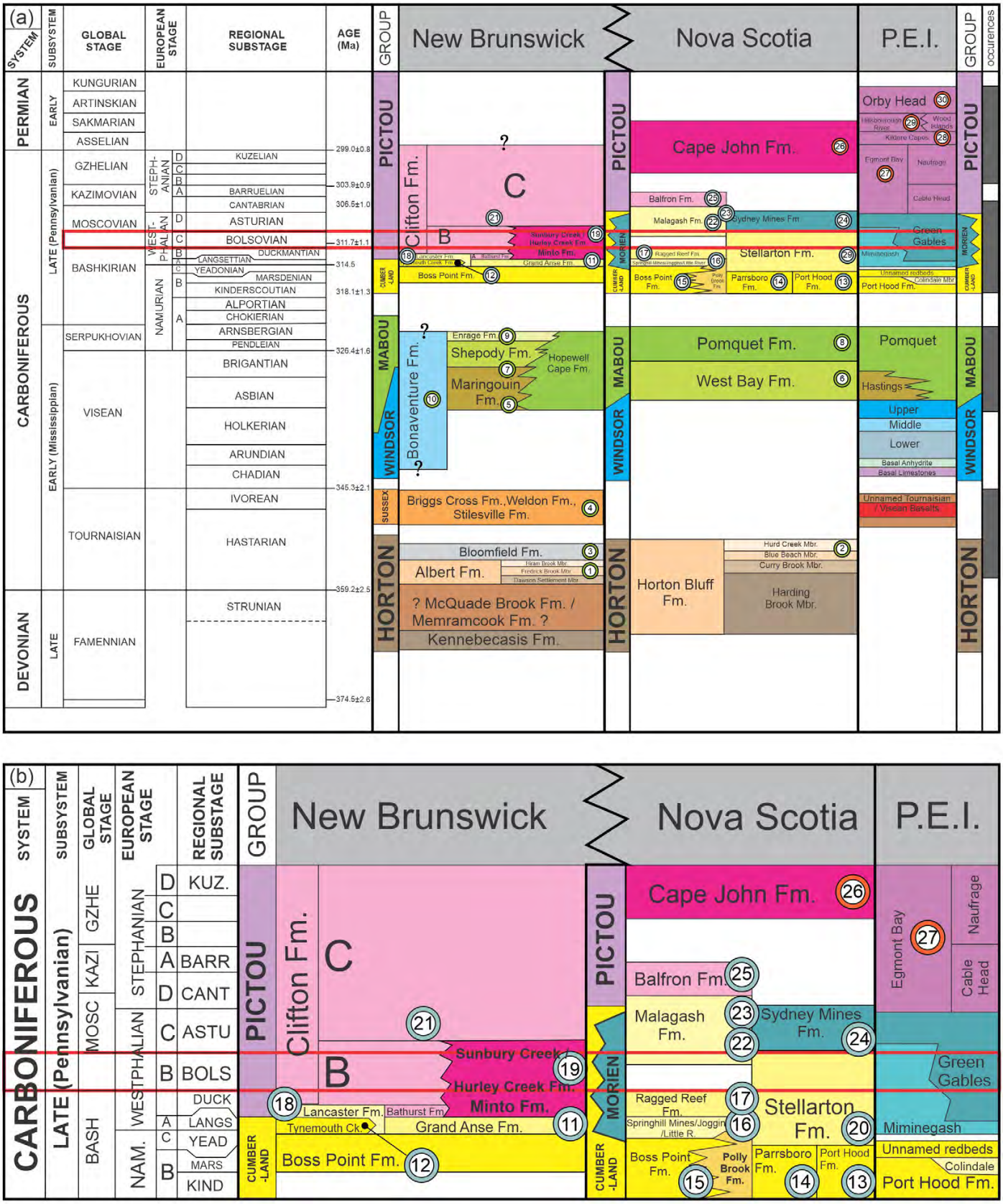

Figure 3. (a) Maritimes Basin stratigraphy for New Brunswick, Nova Scotia, and Prince Edward Island with the known Carboniferous-Permian tetrapod tracks plotted; for key to numbers see Fig. 1. Red box indicates the approximate stratigraphic horizon of the Minto Formation tetrapod tracks (NBMG 21591). After Lucas *et al.* (2022). (b) Detail of Cumberland and Pictou Group stratigraphy.

GEOLOGICAL BACKGROUND

In New Brunswick, Devonian–Carboniferous strata are deposited within a triangular region that covers roughly 25 900 km^2 within the approximate 250 000 km^2 area of the Maritimes Basin (Ball *et al.* 1981; St. Peter and Johnston 2009; Lavoie *et al.* 2009; Williams 1974; Dietrich *et al.* 2011; Gibling *et al.* 2019; Fig. 1). Of the seven lithostratigraphic groups within the New Brunswick portion of the Maritimes Basin, only the Pictou Group (Middle Pennsylvanian to early Permian strata) will be discussed (Fig. 3). Traditionally in New Brunswick the Pictou Group has included strata as old as the Pennsylvanian Bolsovian (early Moscovian) stage, which sit conformably above the underlying Cumberland Group, or unconformably on crystalline basement rocks or older Mississippian sedimentary rocks. More recently, Jutras *et al.* (2007) reassigned the formations of the Pictou Group in central New Brunswick to the Cumberland Group. Bethoux *et al.* (2021) used the traditional stratigraphic classification — i.e., the Pictou Group (Bell 1944; Dyer 1926; Muller 1951; St. Peter 2000) — an approach we follow here pending further study. The Minto Formation sits at the base of the Pictou Group within the New Brunswick Platform (Dyer 1926; Muller 1951). Muller (1951) reassigned the Grand Lake Formation of Dyer (1926) to the Pictou Group of Bell (1944) and upgraded the Minto, Hurley Creek and Sunbury Creek members to formation status (Fig. 3).

Using the traditional stratigraphic nomenclature, the Minto Formation is defined as a 200–230-m-thick section of grey to reddish-brown and locally maroon strata exposed in central New Brunswick (Dyer 1926; Muller 1951). Conformably above the Minto Formation is the Hurley Creek Formation, defined as a 45–60-m-thick stratigraphic package containing abundant redbeds that coarsen upwards as a whole. Lithologies consist dominantly of red and grey mudstones with fine-grained sandstones in the lower strata and red (locally green–grey), coarse feldspathic and lithic sandstones with polymictic conglomerates in the upper strata (Muller 1951). Muller (1951) estimated the overlying Sunbury Creek Formation to have a maximum thickness of approximately 90 m and is lithologically similar to the basal Minto Formation, but is stratigraphically younger than the Minto and the Hurley Creek formations. The interpreted similarity of the Minto and Sunbury formations led St. Peter (1997a, b) to informally incorporate the Sunbury Creek into the Minto Formation and downgrade the Hurley Creek Formation to member status. The member status of the three subdivisions of the Minto Formation is currently being revised and will be the subject of a future publication by some of the present authors. The stratigraphic descriptions of Muller (1951) were recently used by Bethoux *et al.* (2021), and will be followed here as the fossil reported in this study was discovered from the same fossil locality.

Robertson Point locality

The footprint locality discussed here is situated at Robertson Point along the southern shoreline of Grand Lake, Queens County, central New Brunswick (~45°52′11.64″ N, ~66°05′37.40″ W; Figs. 1 and 2, 4a–c). The outcrop extends 860 m along the southern shore of Grand Lake (between 45°52′7.77″ N, 66° 5′46.03″ W and 45°52′12.88″ N, 66° 5′7.65″ W), where a total of 18 m of strata are exposed. These strata have a strike of 150° and a shallow dip of 5° to the southwest. They are subdivided into two distinct sedimentary units: a lower 6.5-m-thick redbed unit interpreted below as belonging to the Hurley Creek Formation and an upper 11.5-m-thick unit composed dominantly of grey to red shales and buff-coloured sandstones that are interpreted below as belonging to the basal Sunbury Creek Formation. The contact between these two formations at this locality is erosive, with the basal deposits of the Sunbury Creek Formation (exposed along the shoreline for roughly 500 m) filling eroded hollows cut in the underlying Hurley Creek Formation. The basal Sunbury Creek Formation at the fossil locality is composed of coarse pebble conglomerates that form a wave-cut platform and, locally, raised sandstone platforms (Figs. 4 and 5, unit 2).

The fossil locality is thus in a shoreline section composed of resistant sandstone headlands and actively eroding embayments of mudstone and shale. Recent erosion of the shale units within coves adjacent to the sandstone headlands has exposed the three-dimensional nature of the channel body and the paleo-erosional cut banks at the channel margin. The outcrop exhibits the channel incision into the shales completely, demonstrating that the shales and resistant sandstone that comprise the headlands are lateral equivalents (Fig. 4c). This observation suggests that the shales represent the interdistributary zone of a fluvial channel system, whereas the incised sandstones and conglomerates may be interpreted as the backfilled channel thalweg of the distributary system. The *Batrachichnus* trackway (NBMG 21591) described below is preserved in the interdistributary shales.

Sedimentology

The sedimentology of the Robertson Point site was first described by Bethoux *et al.* (2021). The lower redbed unit, which they assigned to the Hurley Creek Formation, consists of ~6.5 m of maroon to buff-coloured, fine-grained sandstones; the sediments were deposited in backfilled channel thalwegs locally incised by, or lateral to, red to maroon mudstones and siltstones that represent interdistributary floodplain deposits with localized paleosols. Macrofloral elements of *Cordaites principalis, Calamites* sp. and cf. *Pecopteris* suggest a Pennsylvanian age, which is consistent with determinations from the Hurley Creek Formation fossils (Muller 1951).

Bethoux *et al.* (2021) assigned the overlying 11.5 m of grey to buff-coloured strata to the Sunbury Creek Formation of Muller (1951). This formation includes a basal ~6 m thick extraformational polymictic conglomeratic unit has localized coarse sandstone lenses at the base (Figs. 4 and 5, unit 1). The conglomerates locally incise up to 2 m into

the underlying redbeds of the Hurley Creek Formation. The basal conglomerates of the Sunbury Creek Formation are overlain by 2.5 m of buff-coloured, coarse to very fine-grained sandstones that locally exhibit trough cross-beds and form sheet sandstone beds (Figs. 4 and 5, unit 2). This sandstone, the basal portion of which locally contains reworked pebbles derived from the conglomerate underneath, locally incises the underlying conglomerate unit a depth of to 2.5 m. A specimen of a new genus of odonate wing (Bethoux *et al.* 2021) was described from the upper part (~9 m above the base of the measured section) of these incising sandstone strata; it occurred with transported plant stems and constituted the first fossils documented from the Sunbury Creek Formation. The top of unit 2 is 13.5 m above the base of the measured section at Robertson Point. The upper 2 m of unit 2 (Fig. 4) comprise heterolithic strata that locally incise the strata below. These heterolithic sedimentary beds are composed of thinly bedded siltstone and mudstones and very-fine trough cross-bedded sandstones.

A fossil-rich unit is located between 12.0 and 15.0 m above the base of the measured section (at 45°52′11.68″N, 66° 5′37.45″W; Figs. 4 and 5, unit 3). This unit is a 3 m thick section of light to medium grey fine-grained siltstone that laterally grades to a maroon colour. This unit contains abundant well-preserved plant fossils (i.e., transported and in situ *Calamites*, cf. *Sphenopteris*, and *Cordaites principalis*); abundant vertebrate and invertebrate ichnofossils; and a yet-undescribed forewing of a stem-relative of cockroaches and mantids (family Archimylacridae according to J. Schneider, personal communication to MS 2021). The unit varies locally from coarser siltstones at the base to claystone with centimetre scale bedding in the middle; both variations contain tetrapod and invertebrate ichnofossils, including the trackway described in this paper.

The fossil-bearing shales (Figs. 4 and 5, unit 3) are incised 2 m by a 6.5 m thick channel body composed of buff to grey extraformational polymictic conglomerates and coarse-grained sandstones (Figs. 4 and 5, unit 4). These channel bodies preserve abundant carbonized plant axes, likely of pteridosperm and cordaitalean affinities (Figs. 4 and 5, unit 4). The uppermost sandstone strata of unit 4 is locally incised by a 1.5-m-thick, mud-filled channel that is backfilled with maroon-coloured mudstone with very fine sandstone lenses 5–10 cm thick (Figs. 4 and 5, unit 5).

Age

The Minto Formation (lower Minto Formation of St. Peter 2000) is assigned a latest Bashkirian age, whereas the overlying Hurley Creek Formation (middle Minto Formation of St. Peter 2000) straddles the Bashkirian–Moscovian boundary. The overlying Sunbury Creek Formation (upper Minto Formation of St. Peter 2000) has been considered Bolsovian (late Bashkirian to early Moscovian; St. Peter and Johnson 2009). With the lack of volcanic rocks or ash beds throughout these formations, ages were determined through palynological analysis. Palynomorph assemblages were analyzed by Hacquebard (1972) and Hacquebard and Barss (1970), who determined that the Minto Formation is within the *Vestispora* Palynomorph Zone — of Bolsovian age (late Bashkirian to early Moscovian). This assignment corroborated the paleobotanical age assignment of Bell (1962), whose work was focused on the coal resources of the lower Minto Formation, stratigraphically below the Hurley Creek and Sunbury Creek formations as used in this study.

More recently, samples of grey shale from the present study site (13.5 m above the base of the measured section) were processed for palynology. The results, as reported in Bethoux *et al.* (2021), showed that the palynomorph assemblage at Roberson Point belonged to the *Torispora* Biozone (Bethoux *et al.* 2021). The Bolsovian stage of the Pennsylvanian (latest Bashkirian and early Moscovian) is divided into two palynomorph biozones: the older (late Bashkiriane) *Vestispora* Biozone and the younger (early Moscovian) *Torispora* Biozone. The miospore assemblage is dominated by *Calamospora* spp. with subdominant *Florinites pumicosus* and *Punctatisporites* spp. This age determination is based on the presence of the palynomorphs *Vestispora fenestrata* and ? *Thymospora pseudothiessenii*. The Robertson Point outcrop is thus considered to be of earliest Moscovian age (i.e., early Westphalian C), which conforms with the youngest determination of Hacquebard (1972) and Hacquebard and Barss (1970), agreeing with the relative stratigraphic position of the Sunbury Creek Formation of Muller (1951).

METHODS

The Robertson Point fossil site was documented using both standard digital photography and drone imaging. Three drones with 40 megapixel cameras were used to document the fossil site from high altitudes and beyond the water's edge, locations that would otherwise be inaccessible. The cliffs were photographed at various elevations to capture the 3D details of the broader shoreline as well as close-up images of the fossil site using a 48 megapixel camera mounted on a Mavic Air 2 Drone (Fig. 4a). The local stratigraphy was logged by hand at centimetre scale using metre sticks and later drafted digitally using CorelDraw 2019.

The trackway specimen (NBMG 21591) under discussion was coated in ammonium chloride at Saint Mary's University, Halifax, to accentuate the vertical relief of the footprints during specimen photography. Low-angled illumination from 6000 lumen work lamps were used to cast shadows and

Figure 4. (next page) Fossil site on Grand Lake, NB. (a) Aerial drone images of the fossil site. (b) Geological map plotted against LIDAR images for Robertson Point. (c) Aerial Drone images of the fossil site, where numbers correspond to the different sedimentary units plotted on Figure 5.

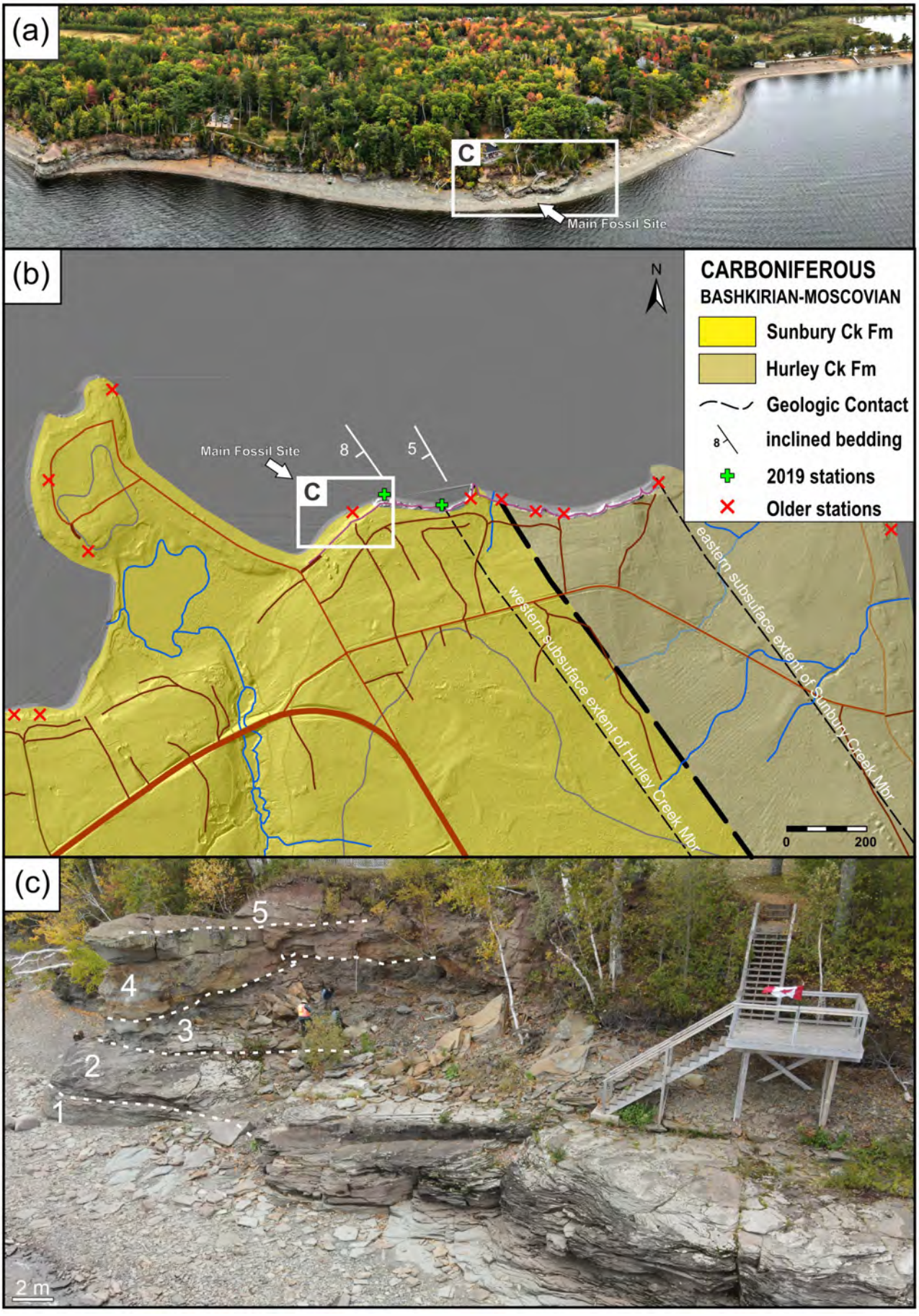

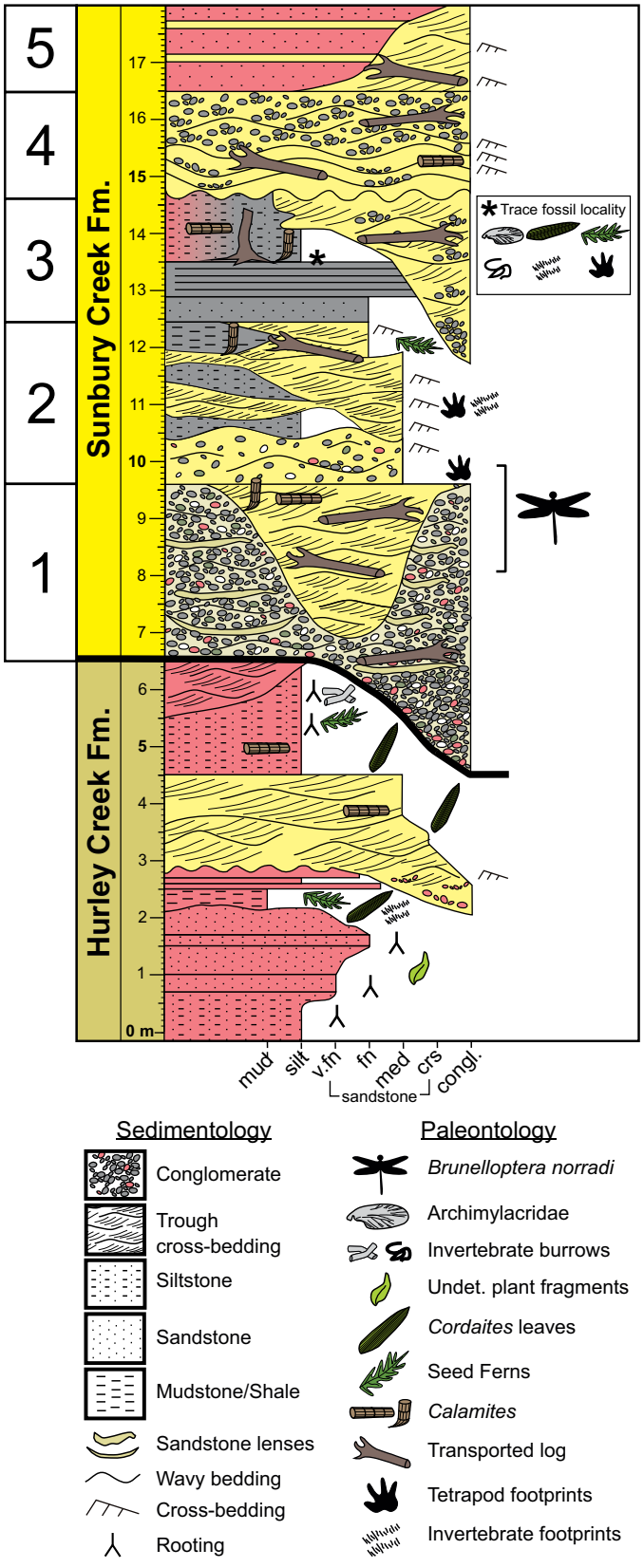

Figure 5. Stratigraphic log of the Hurley Creek and Sunbury Creek formations exposed at Robertson Point, New Brunswick.

highlight the footprint morphology (Teichert 1948; Grabau and Shimer 1910; Ulrich and Bassler 1923; Stimson *et al.* 2012; Stimson *et al.* 2016a, b). False colour topographic relief maps of the trackway were generated by photographing the specimen in a tiled pattern with the same zoom factor and 50–80% overlap. Images were then rendered as a 3D photogrammetry model using the digital software Agisoft Photoscan. The digital model was subsequently modified into a false colour relief map using the digital software packages of Metlab, Cloud Compare, and Paraview. The digital software program ImageJ was used to record morphometric data of the footprints, which were then verified using digital vernier calipers. Standard vertebrate ichnotaxonomy measurements were collected following the work of Leonardi (1987), Stimson *et al.* (2012), and Marchetti *et al.* (2020). The footprint impressions are considered underprints, yet they express the most distal impressions of the digits and sole impressions. The morphological quality of the footprints was evaluated based on Marchetti *et al.*'s (2019) numerical preservation scale. Measurements were taken using the most distal and proximal expressions of the tracks, eliminating extramorphological distortion where appropriate.

Figures were drafted using digital drafting and photo editing software (e.g., CorelDRAW). This specimen of *Batrachichnus salamandroides* has been accessioned into the New Brunswick Museum Geology/Paleontology Collection under the specimen number NBMG 21591.

Previous published literature was extensively consulted for vertebrate comparative anatomy. Manus and pes reconstructions, as well as skeletal reconstructions (Carroll 1967, 1968; Holmes *et al.* 1998; Carroll and Gaskill 1978; Mann *et al.* 2020), were used to obtain glenoacetabular distance measurements; published images of fossil specimens were also used where available. Following the work of Stimson *et al.* (2012, 2016b), skeletal reconstructions of temnospondyl and "microsaur" candidates were used as models to estimate the length of the potential cranial and postcranial skeletons of the tracemaker of NBMG 21591. Measurements of the skull (tip of the premaxilla to the base of the skull), presacral vertebral series (the cervical vertebrae to the base of the pelvic girdle), and caudal vertebral series of each tetrapod were recorded and calculated as percentages of the respective glenoacetabular distance (GAD). To maintain consistency, the caudal vertebral series is inferred to be roughly equal in length to the GAD.

SYSTEMATIC ICHNOLOGY

Ichnogenus ***Batrachichnus*** (Woodworth 1900)

Ichnospecies ***Batrachichnus salamandroides***
(Geinitz 1861)
(Figs. 6–7, 8a)

Referred Materials. NBMG 21591a and b.

Description. Specimen NBMG 21591 consists of a single tetrapod trackway associated with a single *Undichna* trail, and is preserved as part and counterpart on a dark grey, ~1 cm thick siltstone slab that measures 15 by 27 cm (concave epirelief) and 30 by 12 cm (convex hyporelief). The trackway consists of 13 shallow underprints preserved in concave epirelief with the counterpart preserving 12 prints in corresponding convex hyporelief. Manus and pes imprints are paired, resulting in an approximately evenly spaced trackway pattern. Minimal extramorphological distortion is present in the trackway with the exception of faint, shallow digit drags. Manus and pes sets are positioned approximately 2.65 cm apart, with the manus and pes oriented parallel to the midline, and the manus situated much more medially in relation to the trackway midline.

Manus prints are slightly wider than long with average measurements of 1.07 by 0.83 cm, width and length, respectively. Footprints are preserved as semi-digitigrade tracks with faint diminutive sole pads. The manus is tetradactyl. Digits increase in length from I–III with digit IV being subequal in length to digit II. The relative digits lengths of the manus are thus 1-2-3-2. Digits are evenly and well-spaced with digit I and IV diverging laterally in relation to the trackway midline. Digits I and IV exhibit greater curvature in their distal portions. Digits II and III display arcuate curvature in opposite directions to form a "pincer-like" morphology and are oriented approximately parallel to each other. Digits are long and appear elongated, with more deeply impressed rounded digit terminations likely associated with toe pads.

Pes imprints are wider than long, measuring 1.31 by 0.92 cm, length and width, respectively. Footprints are preserved as digitigrade tracks likely associated with undertrack preservation. Pes is pentadactyl with only the digit tips impressed. Digits increase in length from I–IV with digit V being subequal to digit II. The relative digit lengths of the pes are thus 1-2-3-4-2. Digits I–IV are evenly and closely spaced, and digit V is somewhat divergently spaced. Digit terminations appear rounded/blunt, with deeply impressed digits III and IV exhibiting terminal curvature.

The trackway extends in a semi-straight path until the part of the slab where a change in direction occurs, veering to the left on the original concave epirelief surface. Measurements taken from this section of trackway were not incorporated into the averages due to the alteration of the following values. The average external trackway width is 5.5 cm, decreasing to 4.7 cm during the turn. The average internal trackway width is 1.83 cm, decreasing to 1.29 cm on the turn. The average manus pace is 3.8 cm. The manus pace angulation averages 74.3°, increasing during the change in direction to 98.91°. The average pace for the pes measures 5.2 cm. Average pes pace angulation is 66.5°, increasing to 78.5° during the turn. The manus stride measures approximately 4.65 cm and increases to 5.98 cm during the change in direction. The average stride for the pes is 5.22 cm and increases during the change in direction to 6.45 cm.

Following the model of Baird (1952) and Stimson *et al.* (2012, 2016b), the glenoacetabular distance (GAD) was measured to be 5.4 cm (Figs. 9a, b); however, given the spacing between the manus and pes impressions, this GAD measurement is equivocal. A second GAD interpretation is also possible if an elongated body form is considered, following Haubold (1971; fig. 4D). This longer body form would result in a longer GAD, which can be measured as 9.9 cm in length (Fig. 9c).

Remarks. The ichnotaxonomy of the ichnogenera *Batrachichnus* and *Anthichnium* was studied in detail by Voigt (2005). Voigt agreed with the observations made by Haubold *et al* (1995) that the multiple ichnospecies of *Batrachichnus* and *Anthichnium* were morphologically similar, and that these ichnotaxa encompassed a wide range of morphological variability. Voigt (2005) synonymized several ichnotaxa under the new combination *Batrachichnus salamandroides*. *Batrachichnus* is common in the Pennsylvanian strata of Atlantic Canada (Stimson *et al.* 2012; Lucas *et al.* 2005; Lucas *et al.* 2022) and elsewhere (Lucas *et al.* 2022 and references therein). In Atlantic Canada, the stratigraphic range of *Batrachichnus* extends from the lowest Mississippian (lower Tournaisian age) strata of the Albert Formation in New Brunswick (Stimson *et al.* 2018; Stimson *et al.* 2019) and the Horton Bluff Formation in Nova Scotia (Mansky and Lucas 2013) to the lower Permian Cape John Formation at Brule, Nova Scotia.

Baird (1952) and Tucker and Smith (2004) recognized the morphological similarities and size continuum between *Batrachichnus* and *Limnopus*, the only difference being the size of the footprints. Tucker and Smith (2004) thus recognized the *Limnopus–Batrachichnus* spectrum with an ~2.1 cm pes length boundary to distinguish the two ichnogenera on dimensions (i.e., *Batrachichnus* pes length less than 2.1 cm, *Limnopus* greater). Some authors propose that *Batrachichnus* and *Limnopus* are ontogenetic variants (Haubold 2000; Tucker and Smith 2004; Stimson *et al.* 2012), the smaller *Batrachichnus* size suggesting that it was produced by juveniles. Haubold (1971, 1996, 2000), Fichter (1979), Voigt (2005), Stimson *et al.* (2012) and others assigned *Batrachichnus* to small temnospondyl tracemakers, and this interpretation has been widely accepted in the literature. However, some authors have also informally postulated and speculated that "microsaurs" were potential tracemakers of *Batrachichnus* (e.g., Stimson *et al.* 2012; Petti *et al.* 2014; Cisneros *et al.* 2020).

The Minto trackway exhibits several diagnostic characteristics of *Batrachichnus salamandroides*: (i) tetradactyl manus, pentadactyl pes; (ii) manus and pes wider than long; (iii) manus slightly smaller than pes; (iv) small size (pes length <35 mm); and (v) relative digit lengths (manus:1-2-3-2; pes:1-2-3-4-2). Following the parameters developed by Marchetti *et al.* (2019), the footprint preservational value of the Minto trackway is 2.0 (semi-optimal), permitting a confident assignment to the ichnogenus. The trackway pattern of NBMG 21591 differs from other trackways of *Batrachichnus* in its evenly spaced arrangement and

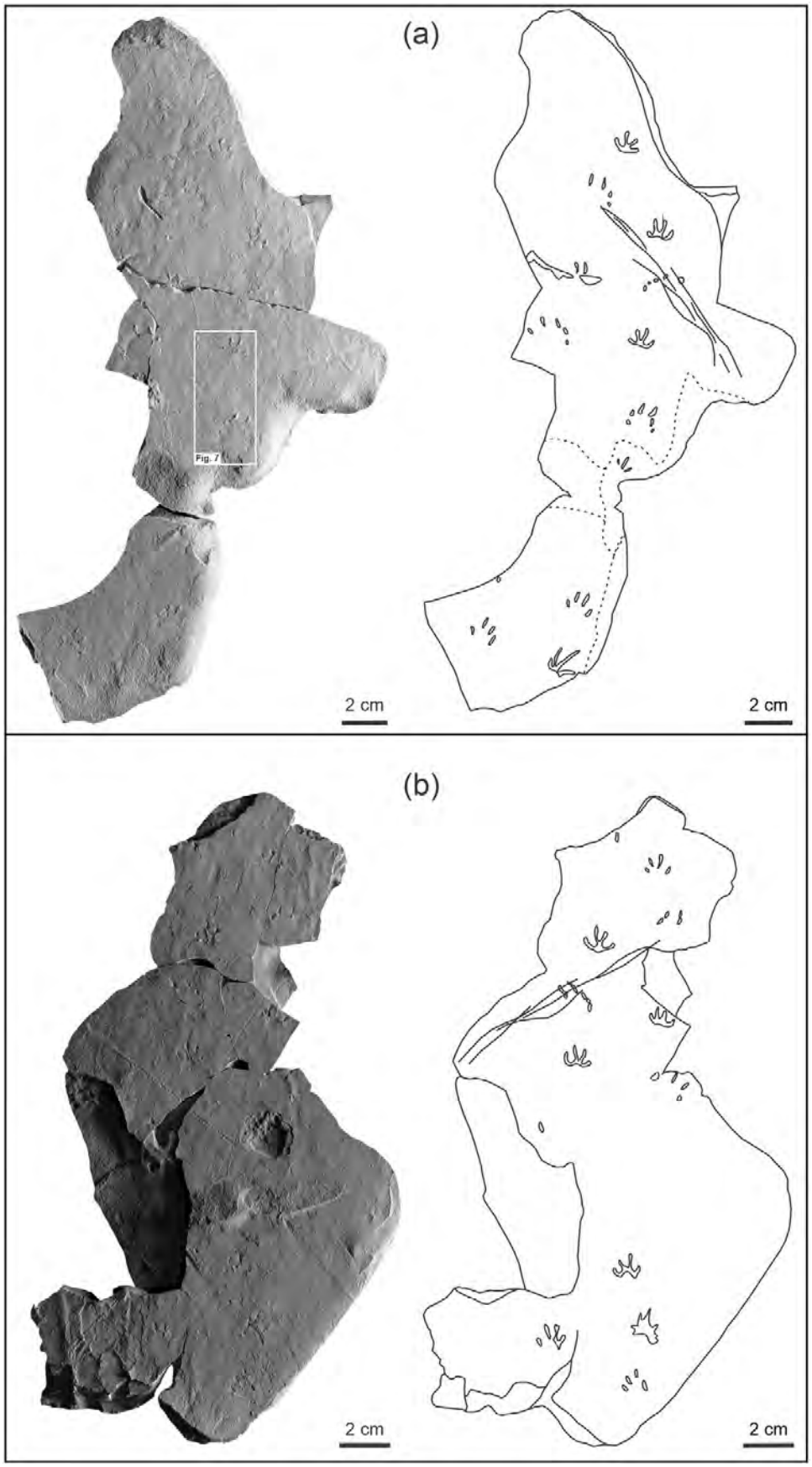

Figure 6. Trackway specimen NBMG 21591. (a) Photograph of NBMG 21591a (left) and interpretive sketch of the same (right). (b) Photography of counter part of NBMG 21591b (left) and interpretive sketch of the same (right).

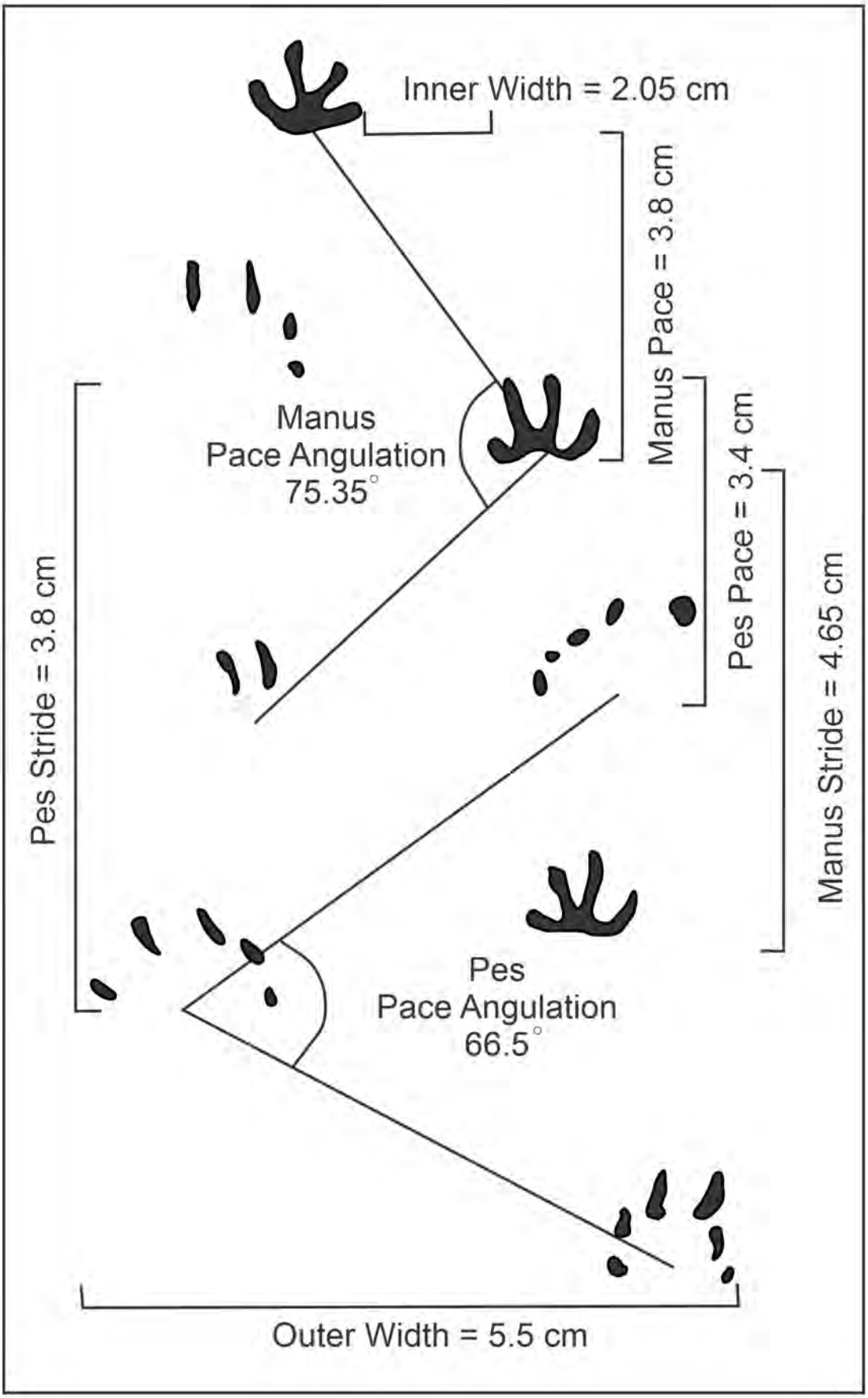

Figure 7. Interpretive sketch of NBMG 21591a with trackway measurements.

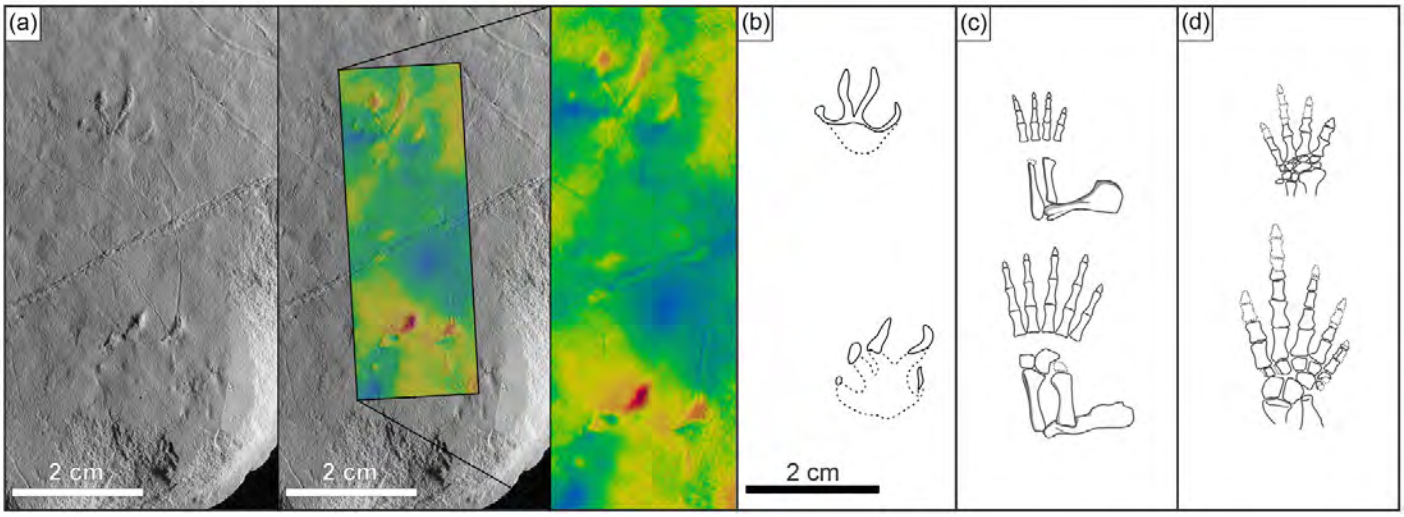

Figure 8. Details of best manus and pes set. (a) Photograph (left) and photogrammetry with false colour relief (middle and right); and (b) interpretive sketch of NBMG 21591a. (c and d) Comparisons with generic temnospondyl (c) and "microsaurian" (d) manus and pes based on reconstructions by Holmes *et al.* (1998) and Carroll (1968), respectively.

undefined manus–pes sets. The low pace angulation, long distance between manus and pes, short stride length, and wide trackway width are indicative of a slow-moving gait. Similar trackway patterns occur frequently in *Matthewichnus caudifur*, which have been attributed to more elongated tracemakers, most notably "microsaurs" (Kohl and Bryan 1994; Voigt and Lucas 2015). Furthermore, when experimenting with modern salamanders, Peabody (1959) noted that tracemaker size also affects trackway pattern. Taking a complementary approach to Kohl and Bryan (1994), we recognize two potential GAD measurements pertaining to both groups of Carboniferous tetrapods. Alongside temnospondyls, we therefore consider "microsaurs" as potential tracemakers of NBMG 21591 based on abnormal trackway parameters that are suggestive of an elongated bauplan commonly associated with "microsauria".

Analysis of candidate tracemakers. No terrestrial vertebrates have yet been documented from New Brunswick, making it necessary to make interpretations from material found elsewhere in Atlantic Canada and other coeval localities in Euramerica. Traditionally, the ichnogenus *Batrachichnus salamandroides* was interpreted to have been produced by temnospondyl amphibians (Fichter 1979; Voigt 2005; Stimson *et al.* 2012). An articulated specimen of *Dendrerpeton* described from Joggins, Nova Scotia (Holmes *et al.* 1998), provides the only articulated temnospondyl skeleton found in the Pennysylvanian succession of Atlantic Canada (Fig.10a). Measurements extracted from this articulated specimen of result in a GAD of 144 mm. The skull measures 94 mm in length (65.28% of the GAD), the presacral vertebral series measures 175 mm (121.53% of the GAD), the caudal vertebral series, though incomplete, is estimated as 144 mm (100% of the GAD), and the complete body length is thus estimated to be 413 mm (Fig.10a). The GAD of *Dendrerpeton* can subsequently be represented as 34.87% of the total body length. *Amphibamus grandiceps* from the early Moscovian of the Mazon Creek Lagerstätte (Bolt 1979; Mann and Gee 2019) and *Platyrhinops lyelli* from Linton, Ohio (Clack and Milner 2009), are additional examples of the classic (short-bodied) temnospondyl bauplan. When the 54 mm GAD interpretation of trackway NBMG 21591 is implemented, a total tracemaker body length of 155 mm is estimated.

Though typically rare in comparison to temnospondyl amphibians, numerous disarticulated "microsaur" remains have been discovered from Nova Scotia. The famous Joggins Fossil Cliffs have yielded a diverse "microsaur" fauna within the interiors of hollow lycopsid trunks (Dawson 1894; Steen 1934; Carroll 1966; Carroll and Gaskill 1978). However, recent work (Mann *et al.* 2020) reduced the faunal list to only four accepted "microsaur" taxa: *Hylerpeton dawsoni* and *Leiocephalikon problematicum* (gymnarthrids), *Steenerpeton silvae* (ostodolepid or rhynchonkid), and *Trachystegos megalodon* (pantylid). All other "microsaur" material at Joggins represent either indeterminate tetrapods or have been reassigned to a different tetrapod lineages. A less diverse "microsaur" assemblage is found at the slightly

Figure 9. (next page) Quantitative comparison of skeletal proportions between the inferred measurements of NBMG 21591 (top measurements in each panel) with estimated glenoacetabular distances (GAD) plotted as temnospondyl (a) and "microsaur" (b and c) body morphologies. (a) Following a short-bodied temnospondyl (*Dendrerpeton* sp.) using an interpreted 54 mm GAD; (b) following a short-bodied "microsaur" (*Pantylus*) using an interpreted GAD of 54 mm; (c) following a longer-bodied "microsaur" (*Steenerpeton*) using a long interpreted GAD of 99 mm.

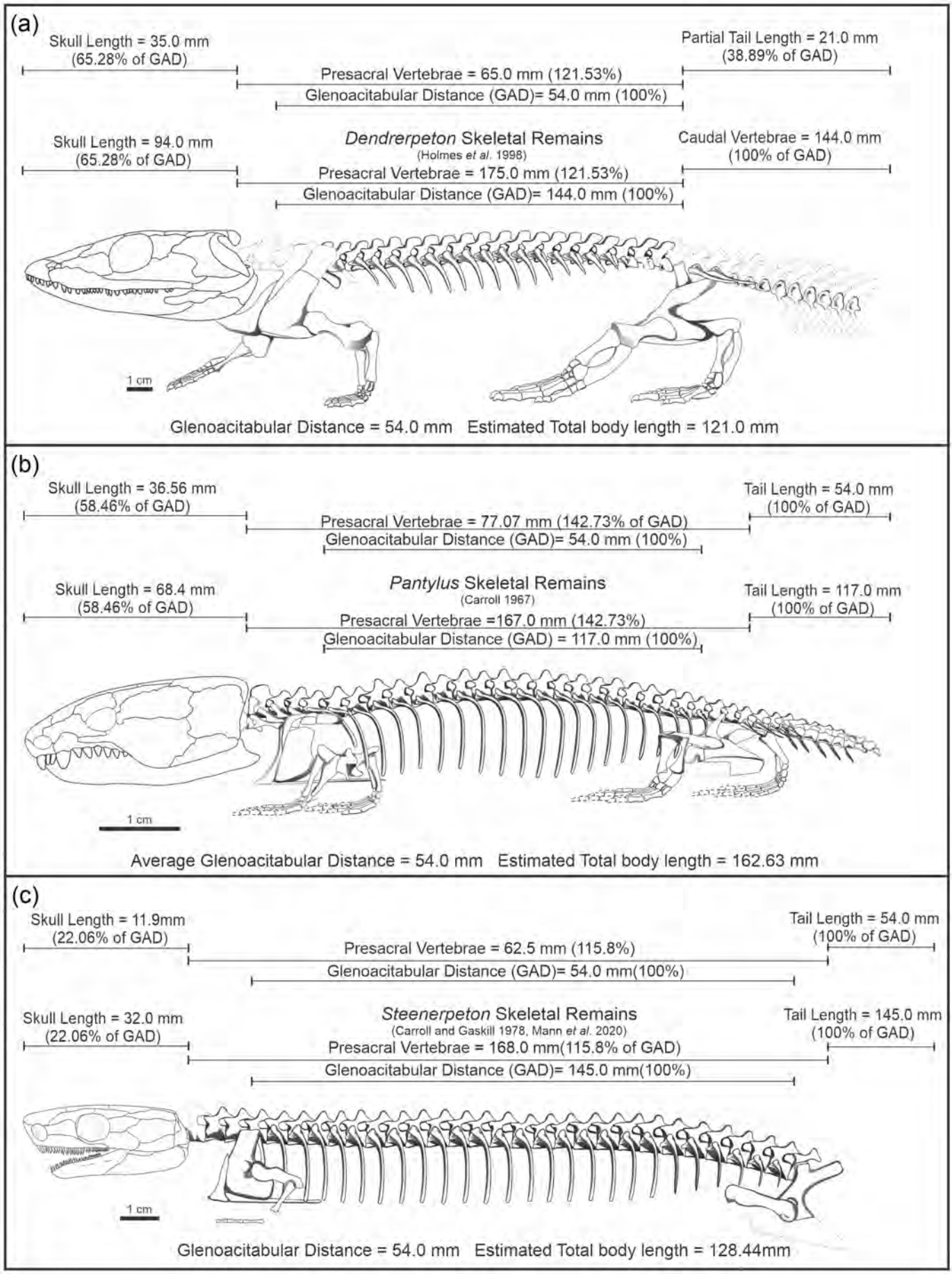

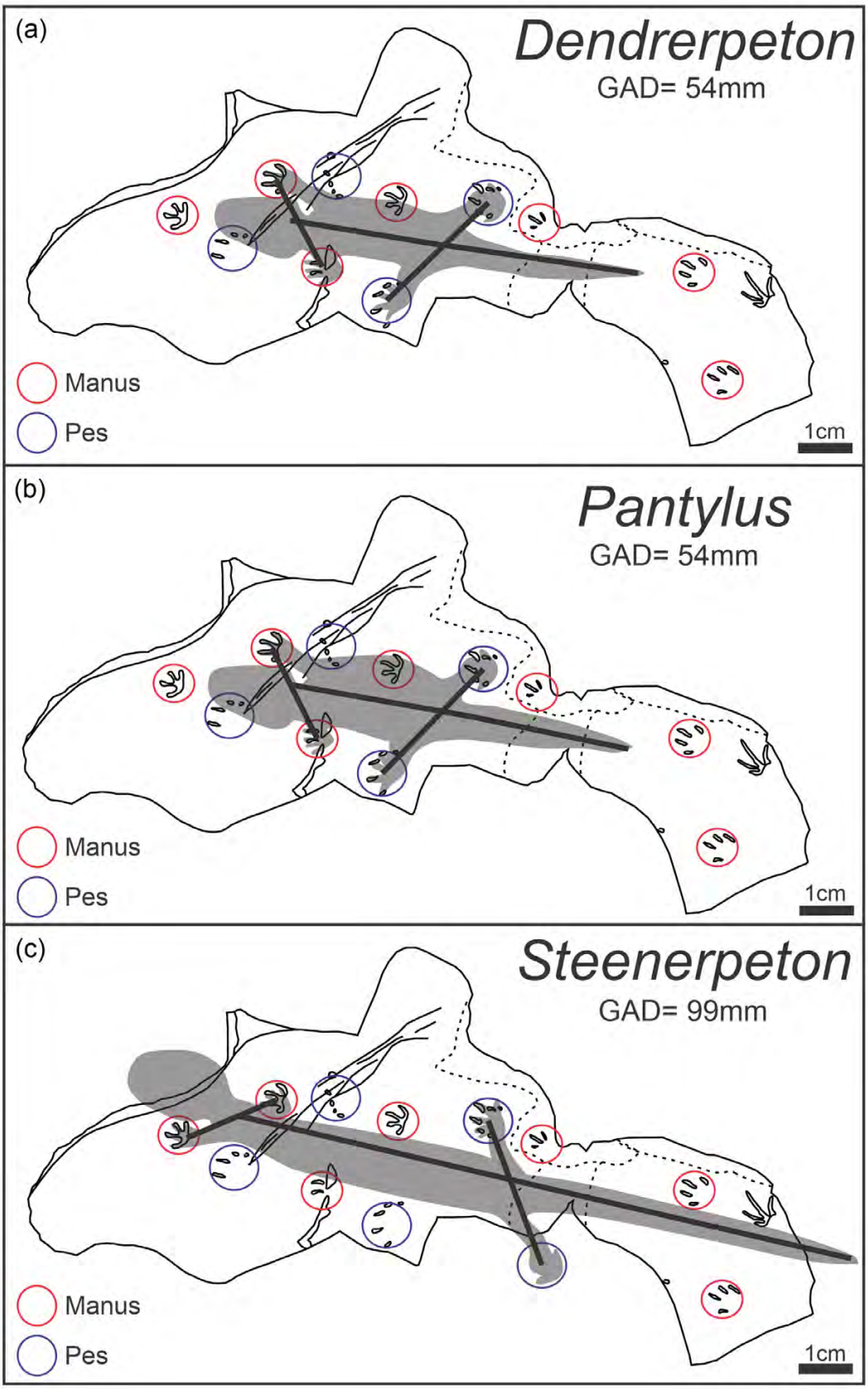

Figure 10. Skeletal measurements of a temnospondyl and select "microsaurs", calculated as percentages of their respective GADs to estimate potential tracemaker body sizes. The short-bodied temnospondyl *Dendrerpeton* (a) using a GAD of 54 mm; (b) The short-bodied "microsaur" *Pantylus*, using an interpreted GAD of 54 mm; and (c) the elongated "microsaur" *Steenerpeton* using an interpreted GAD of 99 mm.

younger (late Moscovian) Florence locality in Nova Scotia (Carroll 1969; Reisz 1971). The rare taphonomy associated with the Joggins tree fauna is also observed at Florence, and involves the remains of temnospondyls (Rieppel 1980; Holmes *et al.* 1995), embolomeres (Klembara 1985), synapsids (Reisz 1971; Mann and Paterson 2020; Mann and Reisz 2020), a "protorothyridid" eureptile (Carroll 1969), and a "microsaur" (Carroll and Gaskill 1978) preserved within in-situ *Sigillaria* stumps. The only "microsaur" taxon recognized from this site is an unidentified gymnarthrid (Carroll and Gaskill 1978). Outside of Atlantic Canada, the Mazon Creek Lagerstätte in Illinois, USA, contains one of the most diverse "microsaur" assemblages of similar age to the Minto Formation (Moscovian). Diverse "microsaur" faunas from the Middle Pennsylvanian are present in the upper Moscovian deposits of Linton, Ohio, and Nyrany in the Czech Republic (Hook and Baird 1986, 1988; Carroll and Gaskill 1978). We do not regard "microsaurs" occurring outside the Maritimes Basin as relevant tracemaker candidates for specimen NBMG 21591. However, the ichnological record reveals the presence of tetrapod taxa in the Minto Formation that are currently not known from the skeletal records, the latter being incomplete due to taphonomic factors (Lucas *et al.* 2022). Furthermore, no tetrapod remains have yet been discovered at Robertson Point, leaving candidates from these nearby assemblages open to consideration.

Based on their relative geographic proximity and stratigraphic position to the Minto Formation, pantylids (*Trachystegos megalodon*) and ostodolepids/rhynchonkids (*Steenerpeton silvae*) are possible "microsaurian" tracemakers for specimen NBMG 21591. Carroll (1968) observed a notable correlation between disarticulated remains of *Trachystegos* from Joggins and the postcranial skeleton of the Permian pantylid, *Pantylus*, from Texas. Based on the availability of skeletal reconstructions, for this study we use *Pantylus* as a skeletal archetype for short-bodied "microsaurs". Lesser-known, short-bodied "microsaurs" include *Diablorotter bolti* (Mann and Maddin 2019) and *Batropetes* (Carroll 1991). *Pantylus* is described from the Wichita Group (lower Permian) of Texas and represents a fully terrestrial form with a short trunk length (24 presacral vertebrae) and robust fore- and hindlimbs (Carroll 1968; Carroll and Gaskill 1978). Measurements taken from the articulated skeletal reconstruction of *Pantylus* (Carroll 1968) provide a GAD of 117 mm. The skull measures 68.4 mm (59% of the GAD), the presacral vertebral series measures 167 mm (142% of the GAD), and the caudal vertebral series, though lacking several elements, is estimated as 117 mm (100% of the GAD). Assuming the reconstruction was correctly interpreted and to scale, the total body length of *Pantylus* is consequently 352.4 mm. The GAD can thus be represented as 33.2% of the total body length. By applying this GAD value to the potential trackway GAD of 54 mm, a total body length of the tracemaker of 162.65 mm is estimated (Fig. 10b).

Steenerpeton silvae is a newly recognized "microsaur" from the Joggins Fossil Cliffs described by Mann *et al.* (2020), following the re-examination of material previously assigned to *Asaphestera intermedium* (Steen 1934; Carroll 1966). The fine-toothed recumbirostran was described as being possibly related to ostodolepids or rhynchonkids (Mann *et al.* 2020), and likely occupied a terrestrial to semi-terrestrial habitat (Carroll and Gaskill 1978). The limbs are relatively large and well-ossified; however, the body length is currently indeterminate due to inadequate preservations of the vertebral column. Following the approach of Carroll and Gaskill (1978), the presacral vertebral count of *Tuditanus* (29) is used to estimate that of *Steenerpeton silvae*. Although largely conjectural, this interpretation, supported by a mosaic of anatomical features shared between the two 'tuditanimorphs', reveals *Steererpeton* to be of a more elongated body plan. Other examples of "microsaurs" with semi-elongated bodies include *Joermungandr bolti* from Mazon Creek, Illinois (Mann *et al.* 2021), *Trihecaton howardinus* from the Late Pennsylvanian of Colorado (Vaughn 1972; Carroll and Gaskill 1978), and *Pelodosotis* from the lower Permian of Texas (Carroll and Gaskill 1978). The GAD of *Steenerpeton silvae* (Mann *et al.* 2020) is found to be 144 mm. The skull measures 44.1 mm (30.63% of the GAD), the presacral vertebral series, possessing 29 elements, measures 171 mm (118.8% of the GAD), and the caudal vertebral series, not included in the reconstruction due to the paucity of preserved elements, is be estimated to be 144 mm (100% of the GAD). The GAD can thus be represented at 40.1% of the total body length of 359.1 mm (Fig. 10c). The formula was subsequently applied to the potential trackway of 99 mm resulting in a total tracemaker body length of 246.9 mm (Fig. 10c).

DISCUSSION

Tracemaker candidates for the ichnogenus *Batrachichnus* have hitherto been attributed to temnospondyl amphibians (Haubold *et al.* 1995, 2005; Voigt 2005; Stimson *et al.* 2012). This consensus was made through recognition of a tetradactyl manus and pentadactyl pes corresponding with autopodium reconstructions of contemporaneous temnospondyl amphibians in close proximity to known *Batrachichnus* localities, for example Joggins (Dawson 1863, 1895; Holmes *et al.* 1998; Stimson *et al.* 2012). Though assigning zoological correlatives to a fossil trace is commonly a challenging task, Voigt (2005) suggested that the temnospondyl *Dendrerpeton* was the most likely tracemaker for *Batrachichnus* due to morphological congruence. However, the significant morphological variability attributed to small amphibian footprints has been noted (Haubold *et al.* 1995), raising the possibility of *Batrachichnus* having been produced by multiple late Paleozoic tetrapod taxa. For example, some authors (Stimson *et al.* 2012; Petti *et al.* 2014; Cisneros *et al.* 2020) proposed that *Batrachichnus* could have additionally been produced by other groups of tetrapods, namely "microsaurs". However, this hypothesis has received little attention subsequently in the literature.

"Microsaurs" represent a taxonomically problematic group of small-bodied tetrapods that first appeared in the

Mississippian (Carroll *et al.* 1991; Lombard and Bolt 1999; Clack 2011), diversified during the Pennsylvianian (Mann *et al.* 2020; Mann and Maddin 2019; Mann *et al.* 2019; Mann *et al.* 2021; Carroll and Gaskill 1978), and persisted through to the early Permian (Carroll 1968; Daly 1973; Carroll and Gaskill 1978). Traditionally "microsaurs" have been considered to be stem-amniotes and part of the group Lepospondyli (Zittel 1888; Romer 1950; Baird 1965; Carroll 1966, 1998; Carroll and Chorn 1995); however, recent taxonomic and phylogenetic studies have found this group to be a polyphyletic assemblage (Anderson 2007; Pardo *et al.* 2017; Pardo and Mann 2018; Clack *et al.* 2019). Study of the anatomy and systematics of "microsaurs" has recently undergone a revival, using new imaging techniques (micro-CT) and methods to reveal stereotypical fossorial adaptations among the group (Maddin *et al.* 2011; Huttenlocker *et al.* 2013; Pardo *et al.* 2015; Szostakiwskyj *et al.* 2015; Pardo and Anderson 2016; Mann and Maddin 2019; Mann *et al.* 2019.) These studies have led to the emergence of a well-supported, fossorially adapted clade called Recumbirostra (Anderson 2007), which includes a core-group of some "microsaurs" and lysorophians (Pardo and Anderson 2016; Pardo *et al.* 2017; Mann *et al.* 2019). The most recent phylogenetic analyses including recumbirostrans retrieve the clade within crown-group amniotes, specifically as early-diverging reptiles (Pardo *et al.* 2017; Mann and Maddin 2019; Mann *et al.* 2019; Mann *et al.* 2021). Despite the recent surge in research on recumbirostran "microsaurs", further work is still needed to confirm the exact phylogenetic placement of the group (involving some or all of its members).

Limitations concerning trackway preservation restrict the production of small tetrapod tracks, including *Batrachichnus*, to terrestrial, semi-aquatic paleoenvironments. Tetrapod footprints preserved in shallow, subaqueous conditions exhibit morphological inaccuracies consisting of a reduced number of digits, distorted digit position, and a parallel digit orientation attributed to the fact that the tracemaker would have been buoyed up by the water (Brand and Kramer 1996). Distortions generated under these conditions hinder the ability to confidently distinguish between walking ichnotaxa (*Batrachichnus salamandroides*) and swimming variants (*Characichnos*, *Lunichnium*). Aside from a rare instance where the limbs were used as stabilizers when swimming directly above the substrate (Minter and Braddy 2006), diagnostic tetrapod trackways produced in deep-water contexts are seldom preserved in the late Paleozoic fossil record. The presence of the fish ichnotaxon *Undichna* on the same surface as the *Batrachichnnus salamandroides* trackway studied here suggests a close proximity, at least periodically, to aquatic environments.

The paleoenvironmental constraints on *Batrachichnus* footprints exclude the aquatic microbrachomorph "microsaur" groups such as Hyloplesiontidae and Microbrachidae. The tetrapod trackway under discussion is a shallow underprint of plantigrade impressions that are spaced at regular intervals (stride and pace) on the same surface as a surface impression of *Undichna*. The co-occurrence of these two ichnogenera does not suggest that this tetrapod trackway was registered into sediments that were deposited under subaquatic settings. Instead, the traces were registered on different sedimentary surfaces, with tetrapod trackway being registered into a slightly younger stratum at millimetre scale above the exposed surface. The tetrapod trackway penetrated into an underlying surface that preserved the *Undichna*, which was obviously deposited under subaquatic conditions. On this basis, it is feasible to narrow down "microsaur" candidates to terrestrially adapted recumbirostrans (e.g., pantylids, hapsidopariieds, gymnarthrids, brachystelechids, ostodolepids, and rhynchonkids) and the currently unrevised forms, such as *Tuditanus* and *Trihecaton*. Some of these terrestrial "microsaurs" bear significant resemblance to small-bodied temnospondyls in bauplan, and can be found in similar environmental settings (Carroll and Gaskill 1978). These settings include coal swamps (Lyell and Dawson 1853; Dawson 1894, 1896; Calder 1998; Calder *et al.* 2006; Davies *et al.* 2005), shallow lakes or ponds (Rayner 1971), channel flanks (Vaughn 1972; Hook and Ferm 1985, 1988), and delta floodplains (Rayner 1971). They are thus viable contenders as producers of *Batrachichnus* footprints.

This conclusion is additionally supported by observations that the autopodium of terrestrial "microsaurs" and temnospondyls share a similar morphology (Carroll 1968; Stimson *et al.* 2012; Fig. 10). The diagnostic tetradactyl manus of *Batrachichnus* is consistent with both groups, as are identical digit proportions (e.g., 1-2-3-2 in the manus), and slightly wider than long dimensions. The Minto trackway exhibits a slightly longer digit IV; however, morphological variation within the ichnogenus is quite extensive, dismissing this feature as a viable extramorphological discrepancy (Haubold *et al.* 1995). Furthermore, the factors relevant in the evaluation of footprint morphology, as discussed by Milàn and Bromley (2006, 2007), have been erected to compensate for some of the extramorphological variability that occurs during trackway registration. The effects of substrate condition, water saturation, taphonomy, erosion, and undertrack preservation must all be taken into consideration as factors that influence footprint morphology (Haubold *et al.* 1995; Melchor and Sarjeant 2004). It is thus interpreted that the footprints produced by "microsaurs" and temnospondyls could be rendered virtually indistinguishable on an ichnotaxonomic level.

The diversity in recumbirostran "microsaur" body proportions, particularly that of the trunk region, provides the potential for high levels of variation in certain aspects of trackway morphology, specifically the estimated GAD. Furthermore, Haubold (1971) noted that the trackway pattern will alter in respect to the tracemaker's body size. The body size of the tracemaker of NBM 21591 is equivocal, as two GAD interpretations are considered valid: (1) a GAD measuring 99 mm, attributed to an overstepping gait of a semi-elongated recumbirostran "microsaur", and (2) GAD measuring 54 mm consistent with known temnospondyls in the region, but also consistent with short-bodied "microsaurs" (e.g., *Pantylus*, *Tuditanus*, and brachystelechids). The

latter interpretation is favoured based on the cogent trackway parameters discussed above. "Microsaur"-produced trackways are thus interpreted to encompass a range of GAD values ranging from lengths only achievable by elongated recumbirostran "microsaurs" to those of temnospondyl affinity. This observation raises the possibility of past tracemaker misidentifications, as the GAD of temnospondyls and short-bodied "microsaurs" would overlap, resulting in a dubious zone of tracemaker identity. Despite being helpful in determining potential tracemaker candidates, the GAD of specimen NBMG 21591 is open to various measurements and cannot be heavily relied on to distinguish between a temnospondyl or "microsaur" tracemaker. Furthermore, additional discoveries of tetrapod body fossils are needed to aid in resolving the true identities of Carboniferous trackways.

CONCLUSIONS

Based on prior studies, the original interpretation that *Batrachichnus* was produced by temnospondyls is regarded as a valid hypothesis. However, the results of this study support those of Stimson *et al.* (2012) in expanding possible tracemakers for *Batrachichnus* to include terrestrial recumbirostran "microsaurs". "Microsaurs" frequented the equatorial regions of Pangea during the Pennsylvanian and were a common component in the terrestrial ecosystems alongside temnospondyls (Carroll and Gaskill 1978). The body lengths of terrestrial recumbirostran "microsaurs" and temnospondyls overlap, and together with indistinguishable manus and pes morphology, complicate the process of discerning between the two groups as potential tracemakers. A more equivocal approach to selecting associated tracemakers for the ichnogenus is encouraged, which may inspire subsequent re-examinations of biota inferred from *Batrachichnus* populated ichnoassemblages. This approach pertains especially to fossil localities where either tetrapod skeletal remains are absent and tetrapod communities are being inferred solely from the ichnological record, or where both "microsaurs" and temnospondyls are present in the skeletal record in addition to tetrapod ichnofossils, for example at Joggins (Dawson 1882, 1896; Carroll 1964, 1966, 1967; Stimson *et al.* 2012; Mann *et al.* 2020; Calder *et al.* 2006).

ACKNOWLEDGMENTS

LA would like to thank Danny, Sarah, and Rachael Allen for their moral and financial support during the drafting of this manuscript. LA would like to thank the community at Robertson Point for supporting our research, including their help and willingness to donate specimens. We thank Andrew MacRae for assistance with generating the false colour relief topographic maps. RN would like to thank Donny and Kate Norrad for their moral and financial support during the drafting of this manuscript. MS acknowledges the support of the Natural Sciences and Engineering Research Council of Canada (NSERC, funding reference number 547631). MS also acknowledges the financial and academic support of the New Brunswick Geological Surveys Branch. He would like to thank the continued academic, financial and moral support of Nancy Jacques and David Wagner over many years. MS also acknowledges the financial and academic support of Christopher Taylor and Marion Homer during the course of his graduate degree. MS would like to thank the staff at "Cask & Kettle" in Saint John, New Brunswick for their continuous support during the drafting and editing of this manuscript. MM thanks Greg MacInnis and Jason Raworth for volunteering their time and equipment to acquire the drone images.

The authors would like to thank Adrian Hunt and one anonymous reviewer for careful reviews and editorial comments that greatly improved the manuscript.

REFERENCES

Anderson J.S. 2007. Incorporating ontogeny into the matrix: a phylogenetic evaluation of developmental evidence for the origin of modern amphibians. *In* Major transitions in vertebrate evolution. *Edited by* J.S. Anderson and H.-D. Sues. Bloomington, Indiana Univ. Press, pp. 182–227.

Baird, D. 1952. Revision of the Pennsylvanian and Permian footprints *Limnopus, Allopus* and *Baropus*. Journal of Paleontology, 26, pp. 832–840.

Baird, D. 1965. Paleozoic lepospondyl amphibians. American Zoologist, 5, pp. 287–294. https://doi.org/10.1093/icb/5.2.287

Ball, F.D., Sullivan, R.M., and Peach, A.R. 1981. Carboniferous drilling project. New Brunswick Department of Natural Resources; Mineral Resources Branch, Report of Investigation 18, 109 pp.

Bell, W.A. 1944. Carboniferous rocks and fossil floras of northern Nova Scotia, Geological Survey of Canada, Memoir 238, 277 pp. https://doi.org/10.4095/119859

Bell, W.A. 1962. Flora of the Pennsylvanian Pictou Group of New Brunswick, Geological Survey of Canada, Bulletin 87, 71 pp. https://doi.org/10.4095/100605

Béthoux, O., Norrad, R.E., Stimson, M.R., King, O.A., Allen, L.F., Deregnaucourt, I., Hinds, S.J., Lewis, J.H., and Schneider, J.W. 2021. A unique, large-sized stem-Odonata (Insecta) found in the early Pennsylvanian of New Brunswick (Canada). Fossil Record, 24, pp. 207–221. https://doi.org/10.5194/fr-24-207-2021

Bolt, J. R. 1979. *Amphibamus grandiceps* as a juvenile dissorophid: evidence and implications. *In* Mazon Creek Fossils. *Edited by* M. H. Nitecki. Academic Press, New York, pp. 529–563. https://doi.org/10.1016/B978-0-12-519650-5.50025-4

Brand, L.R. and Kramer J. 1996. Underprints of vertebrate and invertebrate trackways in the Permian Coconino Sandstone in Arizona. Ichnos, 4, pp. 225–230. https://doi.org/10.1080/10420949609380129

Calder, J.H. 1998. The Carboniferous evolution of Nova Scotia. Geological Society, London, Special Publications, 143, pp. 261–302. https://doi.org/10.1144/GSL.SP.1998.143.01.19

Calder, J.H., Gibling, M.R., Scott, A.C., Davies, S.J., and Hebert, B.L. 2006. A fossil lycopsid forest succession in the classic Joggins section of Nova Scotia: paleoecology of a disturbance-prone Pennsylvanian wetland. *In* Wetlands through time. *Edited by* S.F. Greb and W.A. DiMichele. Geological Society of America Special Paper 399, pp. 169–195. https://doi.org/10.1130/2006.2399(09)

Carroll, R.L. 1964. The earliest reptiles. Zoological Journal of the Linnean Society, 45, pp.61–83. https://doi.org/10.1111/j.1096-3642.1964.tb00488.x

Carroll, R.L. 1966. Microsaurs from the Westphalian B of Joggins, Nova Scotia. Proceedings of the Royal Society of London, 177, pp. 63–97. https://doi.org/10.1111/j.1095-8312.1966.tb00952.x

Carroll, R.L. 1967. Labrynthodonts from the Joggins Formation. Journal of Paleontology, 4, pp. 111–142.

Carroll, R.L. 1968. The postcranial skeleton of the Permian microsaur *Pantylus*. Canadian Journal of Zoology, 46, pp. 1175–1192. https://doi.org/10.1139/z68-168

Carroll, R.L. 1969. A Middle Pennsylvanian captorhinomorph, and the interrelationships of primitive reptiles. Journal of Paleontology, 43, pp. 151–170.

Carroll, R.L. 1991. *Batropetes* from the Lower Permian of Europe — a microsaur, not a reptile. Journal of Vertebrate Paleontology, 11, pp. 229–242. https://doi.org/10.1080/02724634.1991.10011390

Carroll, R. L. 1998. Order Microsauria. *In* Encyclopedia of paleoherpetology, Part 1, Lepospondyli. *Edited by* P. Wellnhofer. Dr. Friedrich Pfeil, Munich, Germany, pp. 133–148.

Carroll, R.L. and Chorn, J. 1995. Vertebral development in the oldest microsaur and the problem of "lepospondyl" relationships. Journal of Vertebrate Paleontology, 15, pp. 37–56. https://doi.org/10.1080/02724634.1995.10011206

Carroll R.L. and Gaskill P. 1978. The order Microsauria. Memoir of the American Philosophical Society, 126, 211 pp.

Carroll, R.L., Bybee, P. and Tidwell, W.D. 1991. The oldest microsaur (Amphibia). Journal of Paleontology, 65, pp. 314–322. https://doi.org/10.1017/S0022336000020552

Cisneros, J.C., Day, M.O., Groenewald, J., and Rubidge, B.S. 2020. Small footprints expand middle Permian amphibian diversity in the South African Karoo. Palaios, 35, pp. 1–11. https://doi.org/10.2110/palo.2018.098

Clack, J.A. 2011. A new microsaur from the Early Carboniferous (Visean) of East Kirkton, Scotland, showing soft tissue evidence. Studies on Fossil Tetrapods, 86, pp. 45–55.

Clack, J.A. and Milner, A.R. 2009. Morphology and systematics of the Pennsylvanian amphibian *Platyrhinops lyelli* (Amphibia: Temnospondyli). Earth and Environmental Science Transactions of the Royal Society of Edinburgh, 100, pp. 275–295. https://doi.org/10.1017/S1755691010009023

Clack, J.A., Ruta, M., Milner, A.R., Marshall, J.E., Smithson, T.R., and Smithson, K.Z. 2019. *Acherontiscus caledoniae*: the earliest heterodont and durophagous tetrapod. Royal Society Open Science, 6, 182087. 6 pp. https://doi.org/10.1098/rsos.182087

Cotton, W., Hunt, A.P., and Cotton, J. 1995. Paleozoic vertebrate tracksites in eastern North America. *In* Early Permian footprints and facies. *Edited by* S.G Lucas and A.B.Heckett, New Mexico Museum of Natural History and Science Bulletin, 6, pp. 189–217.

Daly, E. 1973. A Lower Permian vertebrate fauna from southern Oklahoma. Journal of Paleontology, 43, pp. 562–589.

Davies, S., Gibling, M., Rygel, M., Calder, J., and Skilliter, D. 2005. The Pennsylvanian Joggins Formation of Nova Scotia: sedimentological log and stratigraphic framework of the historic fossil cliffs. Atlantic Geology, 41, pp. 87–102. https://doi.org/10.4138/182

Dawson, J.W. 1863. Air-breathers of the Coal Period: a descriptive account of the remains of land animals found in the Coal Formation of Nova Scotia, with remarks on their bearing on theories of the formation of coal and of the origin of species. Dawson Brothers, Montréal, 81.pp. https://doi.org/10.5962/bhl.title.167425

Dawson, J.W. 1882. On the results of recent explorations of erect trees containing reptilian remains in the Coal Formation of Nova Scotia. Proceedings of the Royal Society, 33, pp. 254–256.

Dawson, J.W. 1894. Preliminary note on recent discoveries of batrachians and other air-breathers in the Coal Formation of Nova Scotia. Canadian Record of Science. 6, pp. 1–7.

Dawson, J. W. 1895. Synopsis of the air-breathing animals of the Paleozoic in Canada up to 1894. Transactions of the Royal Society of Canada, 12, pp. 71–88.

Dawson, J.W. 1896. Additional report on erect trees containing animal remains in the Coal Formation of Nova Scotia. Proceedings of the Royal Society of London. 59, pp. 362–366. https://doi.org/10.1098/rspl.1895.0107

Dietrich, J., Lavoie, D., Hannigan, P., Pinet, N., Castonguay, S., Giles, P., and Hamblin, A. 2011. Geological setting and resource potential of conventional petroleum plays in Paleozoic basins in eastern Canada. Bulletin of Canadian Petroleum Geology, 59, pp. 54–84. https://doi.org/10.2113/gscpgbull.59.1.54

Dunne, E.M., Close, R.A., Button, D.J., Brocklehurst, N., Cashmore, D.D., Lloyd, G.T., and Butler, R.J. 2018. Diversity change during the rise of tetrapods and the impact of the 'Carboniferous rainforest collapse'. Proceedings of the Royal Society B: Biological Sciences, 285, 8 pp. https://doi.org/10.1098/rspb.2017.2730

Dyer, W.S. 1926. Minto Coal Basin, New Brunswick. Geological Survey of Canada Memoir 151, 40 pp., 2 map sheets, scale 1:63 360.

Falcon-Lang, H.J. and Miller, R.F. 2007. Palaeoenvironments and palaeoecology of the Early Pennsylvanian Lancaster Formation ('Fern Ledges') of Saint John, New Brunswick, Canada. Journal of the Geological Society, 164, pp. 945–

957. https://doi.org/10.1144/0016-76492006-189
Falcon-Lang, H.J., Benton, M.J., and Stimson, M. 2007. Ecology of earliest reptiles inferred from basal Pennsylvanian trackways. Journal of the Geological Society, 164, pp. 1113–1118. https://doi.org/10.1144/0016-76492007-015
Falcon-Lang, H.J., Gibling, M.R., Benton, M.J., Miller, R.F., and Bashforth, A.R. 2010. Diverse tetrapod trackways in the Lower Pennsylvanian Tynemouth Creek Formation, near St. Martins, southern New Brunswick, Canada. Palaeogeography, Palaeoclimatology, Palaeoecology, 296, pp. 1–13. https://doi.org/10.1016/j.palaeo.2010.06.020
Fichter, J. 1979. Aktuopaläontologische Studien zur Lokomotion rezenter Urodelen und Lacertilier sowie paläontologische Untersuchungen an Tetrapodenfährten des Rotliegenden (Unter-Perm) SW-Deutschlands. Unpublished Ph.D. thesis, Johannes Gutenberg Universität, Mainz, 425 pp.
Geinitz, H.B. 1861. Dyas oder die Zechsteinformation und das Rhotliegende. Heft I. Wilhelm Engelmann, Leipzig.130 pp., 23 plates. https://doi.org/10.5962/bhl.title.44568
Gibling, M.R., Culshaw, N., Pascucci, V., Waldron J.W.F., and Rygel, M.C. 2019. Chapter 6: The Maritimes Basin of Atlantic Canada: basin creation and destruction during the Paleozoic assembly of Pangea. *In* The sedimentary basins of the United States and Canada (second edition), Elsevier, pp. 267–314. https://doi.org/10.1016/B978-0-444-63895-3.00006-1
Grabau, A.W. and Shimer, H.W. 1910. North American index fossils, 2, pp. 818–819.
Hacquebard, P.A. 1972. The Carboniferous of eastern Canada. Compte Rendu: 7th International Congress of Carboniferous Stratigraphy and Geology, Krefeld 1971, 1, pp. 69–90. https://doi.org/10.4095/130351
Hacquebard, P.A. and Barss, M.S. 1970. Paleogeography and facies aspects of the Minto coal seam, New Brunswick, Canada. Compte Rendu: 6th International Congress on Carboniferous Stratigraphy and Geology, Sheffield 1967, pp. 861–872.
Hamilton, J.B. 1960. Geological Notes – Chipman-Harcourt Area, New Brunswick Department of Natural Resources and Energy Preliminary Map 60-01, 8 pp., 1 sheet, scale 1:63 360.
Hamilton, J.B. 1962a. Geological Notes – Codys, Queens and Kings Counties, New Brunswick Department of Natural Resources and Energy Preliminary Map 59-05, 21 pp., 1 sheet, scale 1:63 360.
Hamilton, J.B. 1962b. Geological Notes – Salisbury [West], Queens, Kings and Westmorland Counties, New Brunswick Department of Natural Resources and Energy Preliminary Map 60-05, 16 pp., 1 sheet, scale 1:63 360.
Hamilton, J.B. 1962c. Geological Notes – Chipman [East], Queens County, New Brunswick Department of Natural Resources and Energy Preliminary Map 60-06, 16 pp., 1 sheet, scale 1:63 360.
Haubold, H. 1971. Ichnia amphibiorum et reptiliorum fossilium. Handbuch der Paläoherpetologie, 18, pp. 1–124.
Haubold, H. 1996. Ichnotaxonomie und Klassifikation von Tetrapodenfahrten aus dem Perm. Hallesches Jahrbuch fur Geowissenschaften, B18, pp. 23–88.
Haubold, H. 2000. Tetrapodenfährten aus dem Perm — Kenntnisstand und Progress 2000. Hallesches Jahrbuch für Geowissenschaften, B22, pp. 1–16.
Haubold, H., Hunt, A.P, Lucas, S.G., and Lockley, M.G. 1995. Wolfcampian (Early Permian) vertebrate tracks from Arizona and New Mexico. *In* Early Permian footprints and facies. *Edited by* S.G, Lucas and A.B. Heckert. New Mexico Museum of Natural History and Science Bulletin, 6, pp. 135–165.
Haubold, H., Allen, A., Atkinson, T.P., Buta, R., Lacefield, J., Minkin S.C., and Relihan, B.A. 2005. Interpretation of the tetrapod footprints from the Early Pennsylvanian of Alabama. *In* Pennsylvanian footprints in the Black warrior basin of Alabama. *Edited by* R.J. Buta, A.K. Kindsberg, and D.C. Kopaska-Merkel. Alabama Paleontological Society Monograph, 1, pp. 75–111.
Holmes R., Godfrey S., and Baird D. 1995. Tetrapod remains from the late Mississippian Pomquet Formation near Grand Étang, Nova Scotia. Canadian Journal of Earth Sciences, 32, pp. 913–921. https://doi.org/10.1139/e95-076
Holmes, R.B., Carroll, R.L., and Reisz, R.R. 1998. The first articulated skeleton of *Dendrerpeton acadianum* (Temnospondyli, Dendrerpetontidae) from the Lower Pennsylvanian locality of Joggins Nova Scotia and a review of its relationships. Journal of Paleontology, 18, pp. 64–79. https://doi.org/10.1080/02724634.1998.10011034
Hook, R.W. and Baird D. 1986. The Diamond Coal Mine of Linton, Ohio, and its Pennsylvanian-age vertebrates. Journal of Vertebrate Paleontology. 6, pp. 174–190. https://doi.org/10.1080/02724634.1986.10011609
Hook, R.W. and Baird, D. 1988. An overview of the Upper Carboniferous fossil deposit at Linton, Ohio. Ohio Journal of Science, 88, pp. 55–60.
Hook, R.W. and Ferm, J.C. 1985. A depositional model for the Linton tetrapod assemblage (Westphalian D, Upper Carboniferous) and its palaeoenvironmental significance. Philosophical Transactions of the Royal Society of London, B, 311, pp. 101–109. https://doi.org/10.1098/rstb.1985.0142
Hook, R.W. and Ferm, J.C. 1988. Paleoenvironmental controls on vertebrate-bearing abandoned channels in the Upper Carboniferous. Palaeogeography, Palaeoclimatology, Palaeoecology. 63, pp. 159–181. https://doi.org/10.1016/0031-0182(88)90095-8
Huttenlocker, A.K., Pardo, J.D., Small, B.J., and Anderson, J.S. 2013. Cranial morphology of recumbirostrans (Lepospondyli) from the Permian of Kansas and Nebraska, and early morphological evolution inferred by micro-computed tomography. Journal of Vertebrate Paleontology, 33, pp. 540–552. https://doi.org/10.1080/02724634.2013.728998
Jutras, P., MacRae, R.A., and Utting, J. 2007. Visean tectonostratigraphy and basin architecture beneath the Pennsylvanian New Brunswick Platform of eastern Can-

ada. Canadian Petroleum Geology Bulletin, 55, pp. 217–236. https://doi.org/10.2113/gscpgbull.55.3.217

Kalkreuth W., Marchioni D., and Utting J. 2000. Petrology, palynology, coal facies, and depositional environments of an Upper Carboniferous coal seam, Minto Coalfield, New Brunswick, Canada. Canadian Journal of Earth Sciences. 37, pp. 1209–1228. https://doi.org/10.1139/e00-039

Keough, B.M., King, O.A., Stimson, M.R., Quinton, P.C., and Rygel, M.C. 2020. Sequence stratigraphy of the late Carboniferous Clifton Formation, New Brunswick. Canadian Journal of Earth Sciences. 57, pp. 1289–304. https://doi.org/10.1139/cjes-2019-0223

Klembara J. 1985. A new embolomerous amphibian (Anthracosauria) from the Upper Carboniferous of Florence, Nova Scotia. Journal of Vertebrate Paleontology. 5, pp. 293–302. https://doi.org/10.1080/02724634.1985.10011867

Kohl, M.S. and Bryan, J.R. 1994. A new middle Pennsylvanian (Westphalian) amphibian trackway from the Cross Mountain Formation, east Tennessee Cumberlands. Journal of Paleontology, 68, pp. 655–663. https://doi.org/10.1017/S002233600002597X

Lavoie, D., Pinet, N., Dietrich, J., Hannigan, P., Castonguay, S., Hamblin, A.P., and Giles, P. 2009. Petroleum resources assessment, Paleozoic successions of the St. Lawrence Platform and Appalachians of eastern Canada. Geological Survey of Canada Open File 6174, 273 pp. https://doi.org/10.4095/248071

Leonardi, G. 1987. Glossary and manual of tetrapod footprint palaeoichnology. Departamento Nacional da Produçao Mineral, 75 pp., 19 plates.

Lombard, R.E. and Bolt, J.R. 1999. A microsaur from the Mississippian of Illinois and a standard format for morphological characters. Journal of Paleontology, 73, pp. 908–923. https://doi.org/10.1017/S0022336000040749

Lucas, S.G., Hunt, A.P., Calder, J.H., Reid, D.R., Hebert, B.L., and Stimson, M.R. 2005. Tetrapod footprints from Joggins Nova Scotia: a template for understanding Carboniferous tetrapod footprints. Geological Association of Canada Annual Meeting, Halifax, Abstracts, 30, pp. 116–117.

Lucas, S.G., Stimson, M.R., King, O.A., Calder, J.H., Mansky, C.F., Hebert, B.L., and Hunt, A.P. 2022. Carboniferous tetrapod footprint biostratigraphy, biochronology and evolutionary events. Geological Society, London, Special Publications, 512, pp. 933–963. https://doi.org/10.1144/SP512-2020-235

Lyell C. and Dawson J.W. 1853. On the remains of a reptile (*Dendrerpeton acadianum*, Wyman and Owen) and of a land shell discovered in the interior of an erect fossil tree in the Coal Measures of Nova Scotia. Quarterly Journal of the Geological Society of London, 9, pp. 58–63. https://doi.org/10.1144/GSL.JGS.1853.009.01-02.20

Maddin, H.C., Olori, J.C., and Anderson, J.S. 2011. A redescription of *Carrolla craddocki* (Lepospondyli: Brachystelechidae) based on high-resolution CT, and the impacts of miniaturization and fossoriality on morphology. Journal of Morphology, 272, pp. 722–743. https://doi.org/10.1002/jmor.10946

Mann, A. and Gee, B.M. 2019. Lissamphibian-like toepads in an exceptionally preserved amphibamiform from Mazon Creek. Journal of Vertebrate Paleontology, 39. https://doi.org/10.1080/02724634.2019.1727490

Mann, A. and Maddin, H.C. 2019. *Diabloroter bolti*, a short-bodied recumbirostran "microsaur" from the Francis Creek Shale, Mazon Creek, Illinois. Zoological Jour-nal of the Linnean Society, 187, pp. 494–505. https://doi. org/10.1093/zoolinnean/zlz025

Mann, A. and Paterson, R.S. 2020. Cranial osteology and systematics of the enigmatic early 'sail-backed' synapsid *Echinerpeton intermedium* Reisz, 1972, and a review of the earliest 'pelycosaurs'. Journal of Systematic Palaeontology, 18, pp. 529–539. https://doi.org/10.1080/14772019.2019.1648323

Mann, A. and Reisz, R.R. 2020. Antiquity of "sail-backed" neural spine hyper-elongation in mammal forerunners. Frontiers in Earth Science, 8, p. 83. https://doi.org/10.3389/feart.2020.00083

Mann, A., Pardo, J.D., and Maddin, H.C. 2019. *Infernovenator steenae*, a new serpentine recumbirostran from the 'Mazon Creek' Lagerstätte further clarifies lysorophian origins. Zoological Journal of the Linnean Society, 187, pp. 506–517. https://doi.org/10.1093/zoolinnean/zlz026

Mann, A., Gee, B.M., Pardo, J.D., Marjanović, D., Adams, G.R., Calthorpe, A.S., Maddin, H.C., and Anderson, J.S. 2020. Reassessment of historic 'microsaurs' from Joggins, Nova Scotia, reveals hidden diversity in the earliest amniote ecosystem. Papers in Palaeontology. 6, pp. 605–625. https://doi.org/10.1002/spp2.1316

Mann, A., Calthorpe, A.S., and Maddin, H.C. 2021. *Joermungandr bolti*, an exceptionally preserved 'microsaur' from the Mazon Creek Lagerstätte reveals patterns of integumentary evolution in Recumbirostra. Royal Society Open Science, 8. https://doi.org/10.1098/rsos.210319

Mansky, C.F. and Lucas, S.G. 2013. Romer's Gap revisited: continental assemblages and ichno-assemblages from the basal Carboniferous of Blue Beach, Nova Scotia, Canada. New Mexico Museum of Natural History and Science Bulletin, 60, pp. 244–273.

Marchetti, L., Belvedere, M., Voigt, S., Klein, H., Castanera, D., Díaz-Martínez, I., Marty, D., Xing L., Feola, S., Melchor, R.N., and Farlow, J.O. 2019. Defining the morphological quality of fossil footprints. Problems and principles of preservation in tetrapod ichnology with examples from the Palaeozoic to the present. Earth-Science Reviews, 193, pp. 109–145. https://doi.org/10.1016/j.earscirev.2019.04.008

Marchetti, L., Voigt, S., Lucas, S.G., Stimson, M.R., King, O.A., and Calder J.H. 2020. Footprints of the earliest reptiles: *Notalacerta missouriensis* — ichnotaxonomy, potential trackmakers, biostratigraphy, palaeobiogeography and palaeoecology. Annales Societatis Geologorum Poloniae, 90, pp. 271–290. https://doi.org/10.14241/asgp.2020.13

Matthew, G.F. 1903. On batrachian and other footprints

from the Coal Measures of Joggins, NS. Natural History Society of New Brunswick Bulletin, 21, pp. 103–108.

Matthew, G. F. 1904. New species and a new genus of batrachian footprints of the Carboniferous System in eastern Canada. Transaction of the Royal Society of Canada, 4, pp. 77–121.

Matthew, G.F. 1910. Remarkable forms of the Little River Group. Transactions of the Royal Society of Canada, 3, pp. 115–133.

Melchor, R.N. and Sarjeant, W.A.S, 2004. Small amphibian and reptile footprints from the Permian Carapacha Basin, Argentina. Ichnos, 11, pp. 57–78. https://doi.org/10.1080/10420940490428814

Milàn, J.E. and Bromley, R.G. 2006. True tracks, undertracks and eroded tracks, experimental work with tetrapod tracks in laboratory and field. Palaeogeography, Palaeoclimatology, Palaeoecology, 231, pp. 253–264. https://doi.org/10.1016/j.palaeo.2004.12.022

Milàn, J. and Bromley, R.G. 2007. The impact of sediment consistency on track and undertrack morphology: experiments with emu tracks in layered cement. Ichnos, 15, pp. 19–27. https://doi.org/10.1080/10420940600864712

Miller, R.F. and Forbes, W.H. 2001. An Upper Carboniferous trigonotarbid, *Aphantomartus pustulatus* (Scudder, 1884), from the Maritimes Basin (Euramerican Coal Province), New Brunswick, Canada. Atlantic Geology, 37, pp. 191–196. https://doi.org/10.4138/1979

Minter N.J. and Braddy, S. 2006. The fish and amphibian swimming traces *Undichna* and *Lunichnium* with examples from the Lower Permian of New Mexico, USA. Palaeontology, 49, pp. 1123–1142. https://doi.org/10.1111/j.1475-4983.2006.00588.x

Muller, J.E. 1951. Geology and coal deposits of the Minto and Chipman map-areas, New Brunswick. Geological Survey of Canada Memoir 260, 47 pp., 3 map sheets, scale 1:63 360. https://doi.org/10.4095/101597

Ó Gogáin, A., Falcon-Lang, H.J., Carpenter, D.K., Miller, R.F., Benton, M.J., Pufahl, P.K., Ruta, M., Davies, T.G., Hinds, S.J., and Stimson, M.R. 2016. Fish and tetrapod communities across a marine to brackish salinity gradient in the Pennsylvanian (early Moscovian) Minto Formation of New Brunswick, Canada, and their palaeoecological and palaeogeographical implications. Palaeontology, 59, pp. 689–724. https://doi.org/10.1111/pala.12249

Pardo, J.D. and Anderson, J.S. 2016. Cranial morphology of the Carboniferous-Permian tetrapod *Brachydectes newberryi* (Lepospondyli, Lysorophia): new data from μCT. PLOS One, 11. https://doi.org/10.1371/journal.pone.0161823

Pardo, J.D. and Mann, A. 2018. A basal aïstopod from the earliest Pennsylvanian of Canada, and the antiquity of the first limbless tetrapod lineage. Royal Society Open Science, 5. https://doi.org/10.1098/rsos.181056

Pardo, J.D., Szostakiwskyj, M., and Anderson, J.S. 2015. Cranial morphology of the brachystelechid 'microsaur' *Quasicaecilia texana* Carroll provides new insights into the diversity and evolution of braincase morphology in recumbirostran 'microsaurs'. PLOS One, 10. https://doi.org/10.1371/journal.pone.0130359

Pardo, J.D., Szostakiwskyj, M., Ahlberg, P.E., and Anderson, J.S. 2017. Hidden morphological diversity among early tetrapods. Nature, 546, pp. 642–645. https://doi.org/10.1038/nature22966

Pardo, J.D., Small, B.J., Milner, A.R., and Huttenlocker, A.K. 2019. Carboniferous–Permian climate change constrained early land vertebrate radiations. Nature Ecology and Evolution, 3, pp. 200–206. https://doi.org/10.1038/s41559-018-0776-z

Peabody, F.E. 1959. Trackways of living and fossil salamanders. University of California Publications in Zoölogy, 63, pp. 1–71. pl. 1–11.

Petti, F.M., Bernardi, M,, Ashley-Ross, M.A., Berra, F., Tessarollo, A., and Avanzini, M. 2014. Transition between terrestrial-submerged walking and swimming revealed by Early Permian amphibian trackways and a new proposal for the nomenclature of compound trace fossils. Palaeogeography, Palaeoclimatology, Palaeoecology, 410, pp. 278–289. https://doi.org/10.1016/j.palaeo.2014.05.032

Prescott, Z.M., Stimson, M.R., Dafoe, L.T., Gibling, M.R., MacRae, R.A., Calder, J.H., and Hebert, B.L. 2014. Microbial mats and ichnofauna of a fluvial-tidal channel in the Lower Pennsylvanian Joggins Formation, Canada. Palaios, 29, pp. 624–645. https://doi.org/10.2110/palo.2013.073

Rayner, D.H. 1971. Data on the environment and preservation of late Palaeozoic tetrapods. Proceedings of the Yorkshire Geological Society, 38, pp. 437–495. https://doi.org/10.1144/pygs.38.4.437

Reisz, R. 1971. Pelycosaurian reptiles from the middle Pennsylvanian of North America. Bulletin of the Museum of Comparative Zoology, 144, pp. 27–61.

Rieppel, O. 1980. The edopoid amphibian *Cochleosaurus* from the middle Pennsylvanian of Nova Scotia. Palaeontology 23, pp. 143–149.

Romer, A.S. 1950. The nature and relationships of the Paleozoic microsaurs. American Journal of Science, 248, pp. 628–654. https://doi.org/10.2475/ajs.248.9.628

Sahney, S., Benton, M.J., and Falcon-Lang, H.J. 2010. Rainforest collapse triggered Carboniferous tetrapod diversification in Euramerica. Geology, 38, pp. 1079–1082. https://doi.org/10.1130/G31182.1

Sarjeant, W.A.S. and Mossman, D.J. 1978. Vertebrate footprints from the Carboniferous sediments of Nova Scotia: a historical review and description of newly discovered forms. Palaeogeography, Palaeoclimatology, Palaeoecology, 23, pp. 279–306. https://doi.org/10.1016/0031-0182(78)90097-4

St. Peter, C.J. 1997a. Revisions to Upper Carboniferous stratigraphy in the Grand Lake area, New Brunswick. Abstracts: 22nd Annual Review of Activities. New Brunswick Department of Natural Resources and Energy, Mineral Resources, Information Circular 97-4, pp. 13–14.

St. Peter, C.J. 1997b. Bedrock geology of Chipman–Canaan River map area (parts of NTS 21 I/04 and 21 H/13), Sun-

bury, Queens and Kings counties, New Brunswick. New Brunswick Department of Natural Resources and Energy, Mineral Resources, plate 97-34, scale 1:20 000.

St. Peter, C.J. 2000. Carboniferous geology of the southwestern New Brunswick platform (Maugerville Subbasin). New Brunswick Department of Natural Resources and Energy, Mineral Resources, plate 2000-16.

St. Peter, C.J. and Johnson, S.C. 2009. Stratigraphy and structural history of the late Palaeozoic Maritimes Basin in southeastern New Brunswick, Canada. New Brunswick Department of Natural Resources; Minerals, Policy and Planning Division, Memoir 3, 348 pp.

Steen, M.C. 1934. The amphibian fauna from the south Joggins, Nova Scotia. Proceedings of the Zoological Society of London, 104, pp. 465–504. https://doi.org/10.1111/j.1096-3642.1934.tb01644.x

Sternberg, C.M. 1933. Carboniferous tracks from Nova Scotia. Geological Society of America Bulletin, 44, pp. 951–964. https://doi.org/10.1130/GSAB-44-951

Stimson, M., Lucas, S.G., and Melanson, G. 2012. The smallest known tetrapod footprints: *Batrachichnus salamandroides* from the Carboniferous of Joggins, Nova Scotia, Canada. Ichnos, 19, pp. 127–140. https://doi.org/10.1080/10420940.2012.685206

Stimson, M.R., Calder, J.H., and Hebert, B.L. 2015. The top predator of Joggins and its tracker Donald Reid. Atlantic Geoscience Society, Annual Colloquium 2015. (Also published as Atlantic Geology, 51, p. 143).

Stimson, M., Miller, R., and Lucas, S. 2016a. Reassignment of vertebrate ichnotaxa from the Upper Carboniferous 'Fern Ledges', Lancaster Formation, Saint John, New Brunswick, Canada. Atlantic Geology, 52, pp. 20–34. https://doi.org/10.4138/atlgeol.2016.002

Stimson, M., Miller, R., Lucas, S., Park, A., and Hinds, S. 2016b. Redescription of tetrapod trackways from the Mississippian Mabou Group, Lepreau Falls, New Brunswick, Canada. Atlantic Geology, 52, pp. 1–19. https://doi.org/10.4138/atlgeol.2016.001

Stimson, M.R., King, O.A., MacRae, R.A., Miller, R.F., Hinds, S.J., and Park, A.F. 2018. Ichnological, palynological, and biomarker studies on the Devonian–Carboniferous (Mississippian and Pennsylvanian) strata of New Brunswick: implications for continental biodiversity during Romer's Gap. Energy, Mines, Petroleum Geoscience Project Summaries and Other Activities, pp. 90–102.

Stimson, M.R., King, O. A., Macrae, R.A., Gastaldo, R., Glasspool, I., Gensel P.G., Basinger, J.F., Miller, R.F., Hinds, S.J, Park, A.F., and Allan, L. 2019. The first evidence of terrestrial vertebrates from the Lower Mississippian Albert Formation of New Brunswick. Implications for the invasion of continental lacustrine ecosystems and biodiversity during Romer's Gap in Atlantic Canada in the western Moncton Subbasin. Energy, Mines, Petroleum Geosci-ence Project Summaries and Other Activities, pp. 70–71.

Szostakiwskyj, M., Pardo, J.D., and Anderson, J.S. 2015. Micro-CT study of *Rhynchonkos stovalli* (Lepospondyli, Recumbirostra), with description of two new genera. PLOS One, 10. https://doi.org/10.1371/journal.pone.0127307

Teichert, C.A. 1948. Simple device for coating fossils with ammonium chloride. Journal of Paleontology, 22, pp. 102–104.

Tucker, L. and Smith, M. P. 2004. A multivariate taxonomic analysis of the Late Carboniferous vertebrate ichnofauna of Alveley, southern Shropshire, England. Palaeontology, 47, pp. 679–710. https://doi.org/10.1111/j.0031-0239.2004.00377.x

Ulrich, E.O. and Bassler, R.S. 1923. Paleozoic Ostracoda: their morphology, classification and occurrence. Maryland Geological Survey, Silurian. pp. 281–283.

van de Poll, H.W., Gibling, M.R., and Hyde, R.S. 1995. Introduction. *In* Chapter 5. Upper Paleozoic rocks. *In* Geology of the Appalachian-Caledonian Orogen in Canada and Greenland. *Edited by* H. Williams; Geological Survey of Canada, Geology of Canada, no. 6, pp. 449-455 (also Geological Society of America, The Geology of North America, v. F-1).

Vaughn, P.P. 1972. More vertebrates, including a new microsaur, from the Upper Pennsylvanian of central Colorado. Natural History Museum, Los Angeles County. pp. 1-29. https://doi.org/10.5962/p.241208

Voigt, S. 2005. Die Tetrapodenichnofauna des kontinentalen Oberkarbon und Perm im Thuringer Wald: Ichnotaxonomie, Paläoökologie und Biostratigraphie. Cuvillier Verlag, Göttingen, 305 pp.

Voigt, S. and Lucas, S.G. 2015. Permian tetrapod ichnodiversity of the Prehistoric Trackways National Monument (south-central New Mexico, USA). New Mexico Museum of Natural History and Science Bulletin, 65, pp. 153–167.

Williams, E.P. 1974. Geology and petroleum possibilities in and around Gulf of St. Lawrence. American Association of Petroleum Geologists Bulletin, 58, pp. 1137–1155. https://doi.org/10.1306/83D9162D-16C7-11D7-8645000102C1865D

Woodworth, J.B. 1900. Vertebrate footprints on Carboniferous shales of Plainville, Massachusetts. Bulletin of the Geological Society of America, 11, pp. 449–454. https://doi.org/10.1130/GSAB-11-449

Zittel, K. A. 1888. Palaeozoologie. Vertebrata (Pisces, Amphibia, Reptilia, Aves). Handbuch der Palaeontologie, Abtheilung 1, Band 3. R. Oldenbourg, Munich and Leipzig, 900 pp.

Editorial responsibility: Robert A. Fensome

Discussion of "The 'lost' islands of Cardigan Bay, Wales, UK: insights into the post-glacial evolution of some Celtic coasts of northwest Europe" by Simon K. Haslett and David Willis[1]

CATHERINE DELANO-SMITH[1,2], PHIL BRADFORD[3,2], AND WILLIAM SHANNON[2]

1. Institute of Historical Research, University of London, Malet Street, London WC1 7HU, United Kingdom
2. Gough Map Research Project (Leverhulme Trust, RPG-2019-070), The Bodleian Library, University of Oxford, Broad Street, Oxford OX 1BH, United Kingdom
3. Department of History, University of York, Heslington, York YO10 5DD, United Kingdom
*Corresponding author: <c.delano-smith@qmul.ac.uk>

Date received: 22 September 2022 ¶ Date accepted 12 October 2022

DISCUSSION

In their article 'The 'lost' islands of Cardigan Bay, Wales, UK: insights into the post-glacial evolution of some Celtic coasts of northwest Europe', Simon K. Haslett and David Willis argue that two islands off the coast of Cardigan Bay were lost to erosion by the mid-sixteenth century. Taking as their starting point medieval Welsh folklore about these islands, the authors use the medieval map of Britain known as the Gough Map as evidence that these islands still existed above sea level in the later Middle Ages. They then turn to a copy of the Gough map made in the sixteenth century by Thomas Butler as proof that the islands had disappeared by the middle of the sixteenth century. Moreover, they claim that Ptolemy's Geographia shows that 'the mouth of the Afon Ystwyth in the 2nd century CE [was] 10–15 km to the west of its present position' (p. 141). Unfortunately, these arguments are based upon a fundamental misunderstanding of early maps and, as the present note shows, not one of the arguments presented stands up to scrutiny.

There is no reason to doubt the authors' understanding that during the Pleistocene the Cardigan Bay area was occupied by Irish Sea ice from the north and west, and Welsh ice from the east. Nor that the Pleistocene left a land surface covered by unconsolidated deposits that subsequently disappeared as a result of the Holocene sea-level rise (which coincided with the Mesolithic archaeological period). It is not unreasonable to maintain, as the authors do, that a 'memory' of this land was retained in various historical and folkloric sources relating how this 'Cantre'r Gwaelod' (the Lowland Hundred) was overrun by the sea at some time in the past, although the extent to which such myths and legends can be relied upon to identify and date the lost lowlands of Cardigan Bay might be a matter for speculation. Such legends are far from unique. There are plenty of myths of lost lands and sunken cities around the British Isles, many supported by botanical and archaeological evidence of the large scale loss of real areas (Pennick 1987). One has only to consider Doggerland, the great land-mass between Britain and the continent that was finally submerged around 6500 BCE, or well-documented cases of settlements lost to storms and coastal erosion more recently such as Ravenser Odd at the mouth of the Humber, a prosperous port abandoned and overwhelmed in the mid-fourteenth century. However, it is abundantly clear that early maps, including the three cited by Haslett and Willis, cannot be used in the way they do to provide details of coastal erosion, still less to date the existence and disappearance of particular islands.

Haslett and Willis attempt to use Ptolemy's Geography (compiled ca. 150 AD) to argue that roughly 1900 years ago, the coast of Wales was some eight miles to the west of its current position. This is to misunderstand the original source completely. Claudius Ptolemy, based in Alexandria, did a brilliant job of pulling together disparate sources to produce a map of the known world. That map has not survived. What does survive are his instructions for making it, and a series of regional maps in the form of lists of coordinates or grid references. It is probable that the latitudes of a small number of Ptolemy's places were located from astronomical observation. But no secure method existed for estimating longitude, and the position of most places given by Ptolemy from his sources would have been derived from statements of the approximate distance and direction between them (as in itineraries). For Britain, it may be that Ptolemy was using

[1]Appears in Atlantic Geoscience, 58, pp. 131–146: this issue

doi: 10.4138/atlgeo.2022.011
2564-2987|22|00261–266 $1.90|0

three or more independent sources, perhaps one for the inland places and two for the coastline, written down several generations before Ptolemy's own time. The opportunities for error, both in the original sources and in later written copies, are enormous; the whole of Scotland is tipped away from pointing north to pointing due east, possibly as a result of an error in copying and transmission, as is readily appreciated from the earliest surviving maps (thought to have been constructed from Ptolemy's figures in Byzantium). Within Britain, many places are mislocated (Shannon 2012). It is also important to note that Ptolemy makes no attempt to describe coasts. Instead, he gives us a series of points in space, between which the coastlines have to be interpolated as straight lines. It is impossible, in short, to work out from Ptolemy's data where the coast of Wales might have been in his day. To imagine that a Ptolemaic map can be interpreted as evidence that the coast was in his day some thirteen kilometres (eight miles) from its present position is far-fetched in the extreme; to go on to use this position to calculate the 'mean rate of removal of the depositional landscape between the recording of Ptolemy's coordinates and the drafting of the Gough Map' (p. 142) is stretching the evidence well beyond breaking point.

Yet it is the Gough Map on which the Haslett and Willis thesis relies most heavily and that is used to show that the two lost islands in which they are interested must have still existed when it was compiled (Fig.1).

Since it came to light in the mid-eighteenth century, the Gough map has attracted considerable interest but the conclusions reached by individual commentators have tended to vary, often considerably and sometimes misleadingly. Notwithstanding, the authors of 'The 'lost' islands of Cardigan Bay' have selected from this literature the parts they find supportive rather than showing an understanding of the problems its (often incompatible) diversity presents. Since 2012, the Gough Map has been intensively studied by a multi-disciplinary team of historians and scientists. Some provisional conclusions were published in 2017 (Delano-Smith *et al*. 2017) but ongoing research (funded by the Leverhulme Trust, RPG-2019-070) is shedding new light and sharpening our understanding of this unique historical document. From this, it can be stated with a reasonable degree of confidence that the extant map dates from approximately 1400 and not from ca.1360 as in the older scholarship (e.g., Parsons 1958).

Although the Gough Map is the finest example of a map of Britain pre-dating 1500, the statement by Haslett and Willis that it is 'the earliest known map of Great Britain' (p.132) is not true. A century and a half before the Gough Map, the St Albans monk Matthew Paris had drawn four maps of Great Britain, improving them as he went along. The basic outline that Paris used was taken from a *mappa mundi*, or world map, where the British Isles are generally shown, with little detail, at the extremity of the known world. Hundreds of these world maps survive from the Middle Ages, from small diagrams on the pages of ecclesiastical chronicles and other

Figure 1. The Gough Map of Britain. ca. 1400. East at the top. ca. 55 × 116 cm. Parchment (two skins joined), Oxford, Bodleian Library, Gough Gen. Top. 16 (Bodleian Libraries, University of Oxford).

books to large stand-alone detailed compilations for display, such as that of ca. 1300 in Hereford Cathedral. A map dating from two centuries before Matthew Paris, now in the British Library and known as the Cotton or Anglo-Saxon map, depicts a recognizable British Isles, albeit with Wales shown as a separate island (probably a miscopying of the rivers Dee and Severn). This map was almost certainly derived from an earlier map which has not survived but which may have dated from the ninth century and that, in turn, owed its origins to late classical maps, also long lost. However, it is clear from the early literature that, for more than a thousand years before the Gough map, the general size and shape of Britain was known; Julius Caesar's figure of 800 miles in length was repeated by medieval authors, including Matthew Paris, and the island was traditionally described as triangle or lozenge in shape.

The most significant of the sources cited by the authors in support of that contention that the Gough Map is the first of its kind, E.J.S. Parsons' important study of 1958, says no such thing and, moreover, explicitly acknowledges the influence of the *mappae mundi* and of Matthew Paris (Parsons, 1958, pp. 1–5). The most that can be said for the Gough Map is that it is the earliest extant depiction of the British Isles in large format. On even the largest *mappa mundi* (Hereford, Ebstorf) Britain was shown tucked away on the periphery of the whole (known) world; while Matthew Paris' maps were in books; and all these early representations of Britain are restricted in size and detail. The Gough Map, by contrast, focuses entirely on Britain (with a token recognition of Ireland and Continental Europe), and was drawn on two sheepskins stitched together to give the required dimensions of 56 by 115 cm. It was produced not for display but as a working document, to be updated as necessary.

Haslett and Willis are correct in noting that the Gough Map was derived from an earlier or predecessor map. The mapmaker had pricked through that predecessor to mark the new made-to-measure parchment to help lay out the replacement map. With few exceptions, the pinholes served also to indicate the different classes of signs for the settlements to be portrayed on the new map. One or two mark the source of a river, to help with locating places. Almost no pinholes are found on the coastline, and while some places on islands were pricked, no island was indicated in this way.

It is not surprising, then, to find in the specific case of the two islands off West Wales, no pinholes at all, making it impossible to say whether those islands were on the predecessor map or whether they appeared for the first time on the extant map. The suggestion that the predecessor map dates from around 1280 — as accepted by the authors when talking about the '13th–14th-century Gough Map' (Haslett and Willis 2022, pp. 133, 141) — derives solely from the arguments of Daniel Birkholz (2004). Birkholz's view, however, has not been widely accepted by other scholars, and ongoing research for the Gough Map project suggests that a date in the fourteenth century is a much more likely date.

Pinholes are absent too from large parts of the east and south-east of England on the Gough Map, suggesting that, as had long been held, new information had become available to the copier of the predecessor map regarding the shape of East Anglia (Andrews 1926). The information would have come from navigation charts (portolan charts) carried on board the ships from the Mediterranean that in the fourteenth century were regularly coming through the Channel and into the North Sea to trade at ports along the east coast of England before heading across the sea to Flanders. The copier was accordingly able to show a probably much-improved coastal outline for this part of England – although not for the west coast of Britain, which remained largely unknown to the Mediterranean chart-makers. Crucially, though, whereas the shape of the south-eastern coast depicted on the Gough Map is familiar to the modern eye, and we know from the geomorphologists that 'the low-lying coastal zones of the North Sea basin have changed dramatically over the centuries', we are warned that 'our knowledge of those changes is weak' (Bailey *et al.* 2021, p. 86). Even for so intensively studied an area as the Suffolk coastlands, for which significant changes are well documented, the Gough Map was found to be of no use when seeking an 'accurate' idea of what the coastline might have been like around ca. 1400. If this is the case for places, ports and inlets along as well-travelled a shore as that of southeast England, how much more cautious and skeptical we should be when faced with regions about which the compiler of the Gough Map obviously possessed far less information.

The idea that a scale can be determined from the Gough Map, to be used to calculate distances and dimensions (Haslett and Willis 2022, pp. 133–134) is also fundamentally misguided. The Gough Map is not a scale map. Maps to mathematical scale were not drawn at this time and remained rare before the later sixteenth century. There are far too many problems and errors to argue for the 'apparent geographical truthfulness' of the Gough map, as the authors do with reference to Lloyd and Lilley (Lloyd and Lilley 2009, p. 29; see also Lilley and Lloyd 2009; Haslett and Willis 2022, p. 133). The red lines that have intrigued previous commentators on the Gough Map are not roads but a construct, not drawn to mathematical scale, devised to help map users to understand the shape and size of the kingdom and the interrelationships between a mass of places; they were reader aids, in other words (Delano-Smith 2002, pp. 81–82).

Nor was the Gough Map the product of any sort of 'survey'. The information that word conveys is far too variegated and inconsistent for that to have been the case. Moreover, any extensive official fourteenth-century survey would have left some trace in the abundant records of England's highly centralised administration, as did those of 1086 (Domesday Book) and of 1279–1280 (the Hundred Roll

enquires; see Roffe 2000; Raban 2004). Rather, the achievement of the Gough Map was to improve upon its predecessor using the latest knowledge as part of an intellectual process that had been going on (in effect) for a thousand years and more.

There is no doubt that the depiction of Britain on the Gough Map is better than anything that had gone before. Inevitably, though, it could be no better than the information available to its compiler(s). It was an English map, after all, reflecting a fundamentally English perspective, which means that the more remote (from the compilers' perspective) fringes of Britain contain some notable errors. Scotland is glossed over as an elongated blip, with little internal detail and with the whole of the country north of Stirling depicted as a separate island, joined to the mainland by a bridge (another tradition found in Matthew Paris). Settlements marked as 'Ross', 'Caithness' and 'Sutherland' were not towns but the names of lordships. North-west England appears to be one of the better-known regions but even here the coast trends north-west in a straight line, with no sign of the bulge of Cumbria. Most cogently, Wales is a rough rectangle, with no hint of Cardigan Bay or the Llŷn Peninsula, and an almost empty interior apart from the error of a large lake at Plynlimon instead of the mountain that was undoubtedly shown on the predecessor map.

All in all, the unavoidable conclusion has to be the compilers of the Gough Map were not at all interested in producing a mathematically accurate depiction of the geography and topography of the island. What mattered was to display the distribution of some 650 places within an outline of the island of Britain. The Gough Map is primarily a map of places set out to show how each related to its neighbours and to an impressive network of rivers. The fifty or so islands surrounding Britain are arbitrarily distributed and all are depicted notionally as rough circles or ellipses. Most are over-sized and lack any hints of physical realism. Thus, the score or so Orkney Islands of tradition are represented as a single, large feature (Insula de Orkeney) lying far off the eastern coast of Scotland instead of close to the northern coast. The Scilly islands are likewise shown as a single island (Celly), whereas the western Isles are identified in the plural as 'Les Outislez' but shown as singular. About half the islands have one or more settlement signs, many of which, especially on the unnamed islands around Scotland, do not appear to be intended to represent specific places so much as to heighten in a general way the well-known point that there are many occupied islands off the Scottish coast.

This allusion to context brings us to consider the two islands with which Haslett and Willis are concerned. Of the ten islands off the Welsh coast, Priestholm and Bardsey are each shown as considerably larger than one would expect. In the latter case, this allowed space for a mytho-historical note about the presence of 'the soothsayers of the Britons', one of a number of adventitious 'folkloric' items found on the map (others include the location of Brutus the Trojan's landing in Cornwall and various myths connected with Loch Tay in Scotland). What underlies the selection of myths and legend is uncertain, but we can say firmly that no reference is made on the Gough Map to the lost lowland of Cantre'r Gwaelod. We can also say that the proportions of the islands shown in Cardigan Bay Island are wholly unrealistic.

Bardsey alone, in reality a mere 179 hectares, is shown as larger than Haslett and Willis' two 'lost' islands together. To the south of these, another similarly sized island labelled 'Ramesey' obviously represents Ramsey Island, off Pembroke, which in fact totals 259 hectares. What, however, the makers of the Gough Map intended by inserting the intervening pair of small islands is less clear. For the much-reduced reproduction of the map published in British Topography (1780), Richard Gough's engraver left the circles empty, but Parsons thought he could read '…l…n' and '… well' and took them to be Gwylan (two islets off Aberdaron, not far from Bardsey) and St Tudwal's Island (two islets off Abersoch, also not far from Bardsey) (Parsons 1958, p. 27). At the time of writing, the missing letters have not yet been deciphered on the recent high-resolution photography scanned for the Gough Map Research Project but there is no reason to doubt Parsons' reading and still less to assume they refer to two islands in the lost land of Cantre'r Gwaelod.

The obvious unfamiliarity of western and central Wales to the distant compilers of the Gough Map would also caution against accepting their map as an 'accurate' presentation of the topography and geography of the area in the late Middle Ages and trying to use it in scientific research into coastal change. Whoever sketched out the coasts of Wales was clearly unaware of the sweeping indentation of Cardigan Bay and drew instead the western Welsh coast as a roughly straight north-south-line broken only by river mouths. Notwithstanding, Haslett and Willis argue that 'the lack of curvature of Cardigan Bay on the Gough Map does not cast significant doubt in itself on the distinct occurrence of the two "lost" islands depicted on the map offshore the Cardigan Bay coast' (p. 133). This is surely incorrect. If the mapmaker was unaware of Cardigan Bay, how can we be sure that these two islands were intended to lie off the coast of Cardigan Bay? Knowing how geographical outlines were drawn on medieval maps in general at this date (even charts), and bearing in mind that the Gough Map represents effectively the very first attempt to trace the details of the coastline of the whole of Britain on a single large surface, it is far more hard-headed to accept that the islands in question, like so many of the other small islands scattered about the map, are (as noted above) representative, not naturalistic, icons of real islands. It is simply not possible to use the Gough Map to 'prove' the existence of these two islands in the way the authors claim.

Finally, the leap that Haslett and Willis then make to their next conclusion is equally invalid. They say that, because these two islands do not appear on Butler's Map, dated to ca. 1547, they must have vanished — submerged—in the intervening century or so. However, this is to misunderstand Butler's

map. Butler was a merchant (Birkholz 2006). His map, which occupies a double page spread in his commonplace book, was copied directly from the Gough map or, more likely, from another copy of that map (Fig. 2). It has far less room for detail (Scotland is not included, although Ireland is expanded). Like the Gough Map compilers, Butler's interest was also in places, although with less space he had to be more selective as to what he could show, and the fact that he did not bother to include the two islands on his pocket-sized copy proves nothing. They were simply irrelevant to his commercial interests and the purpose for which he sketched his map (he drew only four of the eight Channel Islands marked on the Gough Map). Not only did he omit the two Cardigan Bay islands but he also left off nearby Bardsey, shown so disproportionately large on the Gough Map. Bardsey has obviously not been eroded and is still very much there. The logic the authors apply, that something appearing on the Gough Map but not on Butler's Map means that it had been submerged in the intervening period, is therefore ridiculous, as the case of Bardsey (and plenty of other islands present on Gough but not on Butler, such as the Channel Islands) demonstrates.

Another map of approximately the same period, the larger and much more elaborate *Angliae Figura* (1536–1537) is likewise a derivative of the Gough Map. It too retains the Welsh coastline lacking Cardigan Bay and omits the two islands in question. Like Butler, it also omits Bardsey. Exactly the same is true of other sixteenth-century derivatives of the Gough Map, including Sebastian Münster's of 1540 and George Lily's from 1546. All retain Anglesey, Priestholm and Ramsey but omit Bardsey and the two other islands. Nor do they tell us anything about changes to the coastline or the disappearance of small islands in general.

Rather, these Tudor-era maps provide evidence only that those who used the Gough Map to create their derivatives (or made derivatives from other derivatives) omitted things which were not relevant to their reason for redrawing the map,

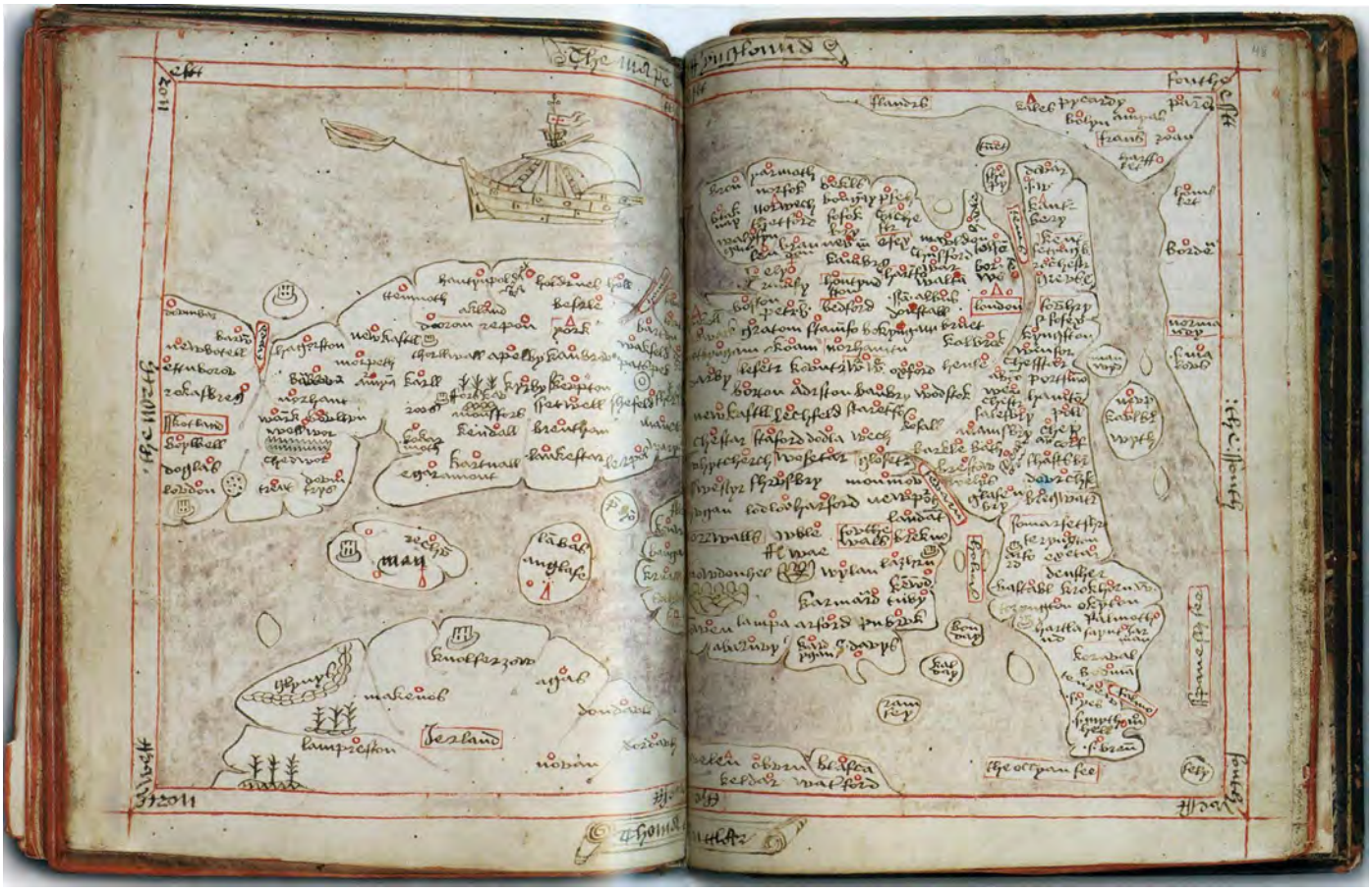

Figure 2. Thomas Butler, The Mape off Ynglonnd. c.1547–1554. East at the top. 18 × 26 cm. Ink on paper in his commonplace book bound into a compendium of astronomical and astrological treatises. Newhaven, Connecticut, Beinecke Library MS 558, fols 47v-48r. (Beinecke Rare Book and Manuscript Library, Yale University.)

be it a whole country (Scotland) or some obscure islands off the Welsh coast. That they did not include Haslett and Willis' two 'lost islands' does not prove that these physical features had disappeared any more than that the Gough Map proved their existence. It simply shows us that they were not regarded as significant to the mapmakers.

In sum, the conclusions reached by Haslett and Willis concerning the 'evidence' of these maps are unsupportable. None of the maps they cite can be used to 'prove' the existence of 'lost' islands, still less to make calculations about their size or location, date of emergence and disappearance. This observation applies to any ancient, medieval or early modern map.

The Gough Map has no place in a geomorphological discussion of post-glacial coastal evolution, and it is to be regretted that the authors did not seek the advice of cartographic historians before publishing their findings.

ACKNOWLEDGEMENTS

The authors are most grateful to colleagues in the Gough Map Research Project (Leverhulme Trust RPG-2019-070) for their supportive comments on early drafts of this article. The authors are thankful to two anonymous reviewers and the journal's editorial comments that improved the manuscript.

[NOTE: The ongoing Gough Map Research Project is due to publish its findings in full, in a book edited by Catherine Delano-Smith and Nick Millea and published by Brill, at the earliest opportunity after 2024.]

REFERENCES

Andrews, M.C. 1926. 'The British Isles in the Nautical Charts of the XIVth and XVth Centuries'. The Geographical Journal, 68, pp.474–480. https://doi.org/10.2307/1782003

Bailey, M., Wain, P., and Sear, D. 2001. 'The Transformation of the Suffolk Coast c.1200 to c.1600: From Orford Ness to Goseford'. Proceedings of the Suffolk Institute of Archaeology and History 45, pp. 86–114.

Birkholz, D. 2004. The King's Two Maps: Cartography and Culture in Thirteenth-Century England. Routledge, London. 254 p. https://doi.org/10.4324/9780203505427

Birkholz, D. 2006. 'The Gough Map Revisited: Thomas Butler's The Mape off Ynglonnd, c.1547–1554', Imago Mundi: The International Journal for the History of Cartography, 58:1, pp. 23–47. https://doi. org/10.1080/03085690500362298

Delano-Smith, C. 2022. 'Who produced the medieval Gough Map of Britain, why and how?'. *In* Pour une Histoire des Cartes Locales en Europe au Moyen Âge et à la Renaissance. *Edited by* J. Dumasy-Rabineau, C. Serchuk, and E. Vaugnon. Paris and New York, Le Passage Editions, pp.71–87.

Delano-Smith, C., Barber, P., Bove, D., Clarkson, C., Harvey, P.D.A., Millea, N., Saul, N., Shannon, W., Whittick, C., and Willoughby, J. 2017. 'New Light on the Medieval Gough Map', Imago Mundi: The International Journal for the History of Cartography, 69:1. pp. 1–36, plates 1–5. https://doi. org/10.1080/03085694.2017.1242838

Haslett, S.K. and Willis. D. 2022. 'The 'lost' islands of Cardigan Bay, Wales, UK: insights into the post-glacial evolution of some Celtic coasts of northwest Europe', Atlantic Geoscience, 58, pp.131–146. https://doi.org/10.4138/atlgeo.2022.005

Lilley, K.D. and Lloyd, C.D. 2009. 'Mapping the Realm: A New Look at the Gough Map of Britain (c. 1360), *Imago Mundi*: The International Journal for the History of Cartography, 61:1, pp 1–28. https://doi.org/10.1080/03085690802456228

Lloyd. C.D. and Lilley, K.D. 2009. 'Cartographic veracity in medieval mapping: analyzing geographical variation in the Gough map of Great Britain', Annals of the Association of American Geographers, 99:1, pp. 27–48. https://doi.org/10.1080/00045600802224638

Parsons, E.J.S. 1958. The Map of Great Britain circa A.D. 1360 known as the Gough Map. University Press of Oxford for the Bodleian Library and the Royal Geographical Society, Oxford. 38 p.

Pennick, N. 1987. Lost Lands and Sunken Cities. Fortean Tomes, London. 96 p.

Raban, S. 2004. A Second Domesday?:The Hundred Roll Enquiries of 1279-80. Oxford University Press, Oxford, 229 p. https://doi.org/10.1093/acprof:oso/9780199252879.001. 0001

Roffe, D. 2000. Domesday: The Inquest and the Book. Oxford University Press, Oxford, 289 p.

Shannon, W.D. 2012. 'From Morikambe to Morecambe: Antiquarians, Periploi and Eischuses', Transactions of the Cumberland and Westmorland Antiquarian and Archaeological Society, Third Series, 12, pp. 37–54.

Editorial responsibility: Denise Brushett

Overview of age constraints for gold mineralization in central and western Newfoundland and new $^{40}Ar/^{39}Ar$ ages for muscovite from selected auriferous zones

Hamish A.I. Sandeman[1], Ian W. Honsberger[2] and Alfredo Camacho[3]

1. Geological Survey Division, Department of Industry, Energy and Technology, Government of Newfoundland and Labrador, St. John's, Newfoundland and Labrador A1B 3J5, Canada
2. Geological Survey of Canada, Ottawa, Ontario K1A 0E8, Canada
3. University of Manitoba, Department of Geological Sciences, Winnipeg, Manitoba R3T 2N2, Canada
*Corresponding author: <hamishsandeman@gov.nl.ca>

Date received:19 May 2022 ¶ Date accepted 25 October 2022

ABSTRACT

This contribution presents new $^{40}Ar/^{39}Ar$ laser step-heating data for muscovite associated with four significant orogenic gold-mineralized zones in central and western Newfoundland to build upon existing geochronological constraints for orogenic gold mineralization across much of the Newfoundland Appalachians. Additionally, we provide the first $^{40}Ar/^{39}Ar$ laser step-heating data for detrital muscovite from gold-mineralized sandstone of the Wigwam Formation (Botwood Group) at the Moosehead gold prospect. Most known gold zones on the isIand occur in proximity to reactivated crustal-scale faults and related structures, and are commonly localized within competent, rigid lithological units (e.g., granitoid rocks); although, some vein systems cut less competent, clastic sedimentary rock sequences. Host rocks range in age from Neoproterozoic to Devonian and may extend into the Carboniferous. Robust Pragian to Emsian (ca. 410–375 Ma) rutile, muscovite and zircon ages constrain the timing of gold mineralization in parts of the Exploits Subzone, whereas less precise age estimates for gold mineralization in the Notre Dame Subzone and Laurentian margin range from Wenlock to Emsian (ca. 433–375 Ma). Collectively, the geochronological data suggest that fluid-pressure cycling associated with gold mineralization in central and western Newfoundland occurred during progressive Siluro-Devonian tectonics associated with the waning stages of the Salinic orogenic cycle and spanning the Acadian and Neoacadian orogenic cycles. Multiple, polyphase, overlapping orogenic events allowed for repeated, gold mineralizing fluid flow events, particularly in proximity to long-lived, reactivated crustal-scale fault zones.

RÉSUMÉ

La présente contribution fait état de nouvelles données obtenues par chauffage échelonné au laser $^{40}Ar/^{39}Ar$ de muscovite associée à quatre zones minéralisées aurifères orogéniques stratégiques dans le centre et l'ouest de Terre-Neuve permettant de mieux préciser les limites géochronologiques existantes de la minéralisation aurifère orogénique dans la majeure partie des Appalaches terre-neuviennes. Nous fournissons de plus les premières données par chauffage échelonné au laser $^{40}Ar/^{39}Ar$ de muscovite détritique provenant de grès minéralisé aurifère de la Formation de Wigwam (groupe de Botwood) dans la zone d'intérêt aurifère de Moosehead. La majorité des zones aurifères connues sur l'île se trouve à proximité de failles d'échelle crustale et de structures connexes, et elles se situent communément à l'intérieur d'unités lithologiques rigides parallèles (p. ex. des roches granitiques), bien que certains réseaux filoniens recoupent des séquences de roches sédimentaires clastiques moins parallèles. L'âge des roches hôtes varie du Néoprotérozoïque au Dévonien et peut s'étendre au Carbonifère. Des datations robustes du Praguien à l'Emsien (env. 410 à 375 Ma) de rutile, de muscovite et de zircon limitent le moment de la minéralisation de l'or dans des parties de la sous-zone Exploits, alors que des estimations moins précises de l'âge de la minéralisation aurifère dans la sous-zone Notre-Dame et de la marge laurentienne varient du Wenlock à l'Emsien (env. 433 à 375 Ma). Les données géochronologiques laissent collectivement supposer que les cycles de pression hydraulique associés à la minéralisation d'or dans le centre et l'ouest de Terre-Neuve se sont manifestés durant la progression tectonique siluro-dévonienne associée aux stades de ralentissement du cycle orogénique salinique et s'étendant aux cycles orogéniques acadien et néoacadien. Plusieurs phénomènes orogéniques polyphasés se chevauchant ont permis des écoulements de fluides minéralisateurs aurifères répétés, en particulier à proximité de zones de failles d'échelle crustale réactivées persistantes.

[*Traduit par la redaction*]

doi:10.4138/atlgeo.2022.012

INTRODUCTION

Prior to the late 1980s, the vast majority of gold produced in the Newfoundland Appalachians was derived as a by-product from auriferous volcanic massive sulphide deposits such as the Rambler, Ming and in particular, Buchans deposits of the central Newfoundland Dunnage Zone (see Piercey 2007; Galley *et al* 2007). Positive market conditions and the introduction of flow through shares stimulated an Island-wide gold exploration boom in the late 1980s that led to the discovery of many of the gold deposits that are past producers (Fig. 1) (e.g., Hope Brook Deposit, Big Ridge Resources; Hammerdown and Orion, Maritime Resources) and are currently in production (e.g., Stog'er Tight deposit, Anaconda Mining). In addition to these deposits, prospective gold deposits and occurrences seeing renewed exploration today include: (1) Valentine Lake Project, Marathon Gold Corporation; (2) Cape Ray Deposits, Matador Mining; (3) Appleton-JBP linears (now Queensway Project), New Found Gold; (4) Little River Prospects (now Golden Baie), Canstar Resources; and (5) Moosehead, Sokoman Minerals.

The geoscientific knowledge base related to gold mineralized zones in central and western Newfoundland is lean compared to other global gold producing districts. Early gold-related studies, subsequent to the explosion of exploration in the late 1980s, provided some of the first descriptive and comparative documentation of the gold occurrences on the Island (e.g., Tuach 1987; Tuach *et al* 1988; Evans 1991, 1993, 1999, 2004; Churchill *et al* 1993; Wilson and Evans 1994). Extant geochronological investigations on gold zones are limited to those from the Hope Brook (Dubé *et al* 1995) and Cape Ray deposits (Dubé *et al* 1996; Dubé and Lauzière 1997) and select geochronological studies at the Nugget Pond (Sangster *et al* 2008) and Hammerdown (Ritcey *et al* 1995) deposits. Subjects of more recent gold-related, paragenetic, lithogeochemical and geochronological studies include: the Rattling Brook (Kerr and van Breemen 2007) and Thor prospects (Minnett *et al* 2012) in western Newfoundland (White Bay); the Pine Cove (Ybarra 2020) and Ming (Au-rich VMS) deposits of Baie Verte Peninsula (Pilote *et al* 2020); and the central Newfoundland gold district (Valentine Lake deposit and Wilding Lake prospect; Honsberger *et al* 2022a).

Robust U–Pb geochronological constraints on gold mineralization are largely restricted to the Neoproterozoic (ca. 570–585 Ma) epithermal prospects of eastern Newfoundland (e.g., O'Brien *et al* 2001; Sparkes *et al* 2005; 2016; Sparkes and Dunning 2014), with fewer constraints on the timing of orogenic gold mineralization in central and western Newfoundland (e.g., ca. 374 Ma muscovite, Sandeman and Dunning 2016; ca. 410 Ma rutile, Honsberger *et al* 2022a). Kerr and Selby (2012) summarized many of the earlier geochronological data for gold mineralization, mostly on the Baie Verte Peninsula, and this contribution builds upon their compilation. We review existing age constraints on gold mineralization in the context of our new $^{40}Ar/^{39}Ar$ geochronological data for muscovite from four gold-mineralized zones across western and central Newfoundland and discuss the data with respect to Paleozoic orogenesis.

CRUSTAL-SCALE ARCHITECTURE OF NEWFOUNDLAND

Williams *et al* (1988) subdivided the Newfoundland Appalachians into four major pre-Silurian tectonic-stratigraphic domains including, from west to east, the Humber, Dunnage, (including the Notre Dame and Exploits subzones), Gander and Avalon zones. The Gander Zone was further divided into Meelpaeg, Mount Cormack and Gander Lake subzones. These zones broadly correspond to (also from west to east): the Laurentian margin (Humber); the Dashwoods terrane (extended Laurentian margin and Notre Dame Subzone); Ganderia (peri-Gondwana terranes including all Gander subzones and overthrust intraoceanic Exploits Subzone rocks); and Avalonia (e.g., van Staal *et al* 1996; van Staal and Barr 2012; Fig. 1). The Bras d'Or terrane of Cape Breton Island may extend to the Cinq-Cerf and Grey River areas in southern Newfoundland and its basement may underlie all the Exploits Subzone (Barr *et al* 2014).

The geographic/aerial extent of the Exploits Subzone and its boundaries in northeast-central Newfoundland is misrepresented on most extant compilation maps, particularly its interpreted southeastern termination at the former Gander River Ultrabasic Belt (GRUB Line), now known as the Gander River Complex (cf. O'Neill and Blackwood 1989). The Exploits Subzone includes Ordovician volcanic and sedimentary rocks of the Baie Du Nord Group that are structurally interleaved with Ganderian basement in the Meelpaeg Subzone (e.g., Valverde-Vaquero and van Staal 2002). The correlated Ordovician Baie D'Espoir and Davidsville groups in central Newfoundland stratigraphically overlie and are imbricated with Cambrian ophiolites and Gander zone basement (e.g., Blackwood and Green 1983; Colman-Sadd *et al* 1992). Moreover, brachiopod and trilobite-bearing strata of Late to Middle Ordovician (Darriwilian) age, comparable to other Exploits Subzone fauna, are exposed ~30 km east of the Gander River Complex at Indian Bay Big Pond (Fig. 1) in the Gander Lake Subzone (Wonderly and Neumann 1984). The latter are spatially accompanied by pillow basalt, siltstone, conglomerate, and minor gabbro along northeast-trending curvilinear magnetic highs that likely represent klippe of Exploits Subzone assemblages structurally above and interleaved with Ganderian margin sedimentary strata (Miller and Weir 1982; Wonderly and Neumann 1984; O'Neill and Colman-Sadd 1993). Exploits Subzone rocks occur sporadically across parts of the poorly exposed Gander Lake subzone and are likely tectonically intercalated with Gander Zone rocks. Emplacement of these klippe is constrained to Middle Ordovician (Colman-Sadd *et al* 1992; Sandeman and Dickson 2019); thus, the Exploits Subzone and Gander Zone were amalgamated by that time and were no longer independent terranes after the Middle

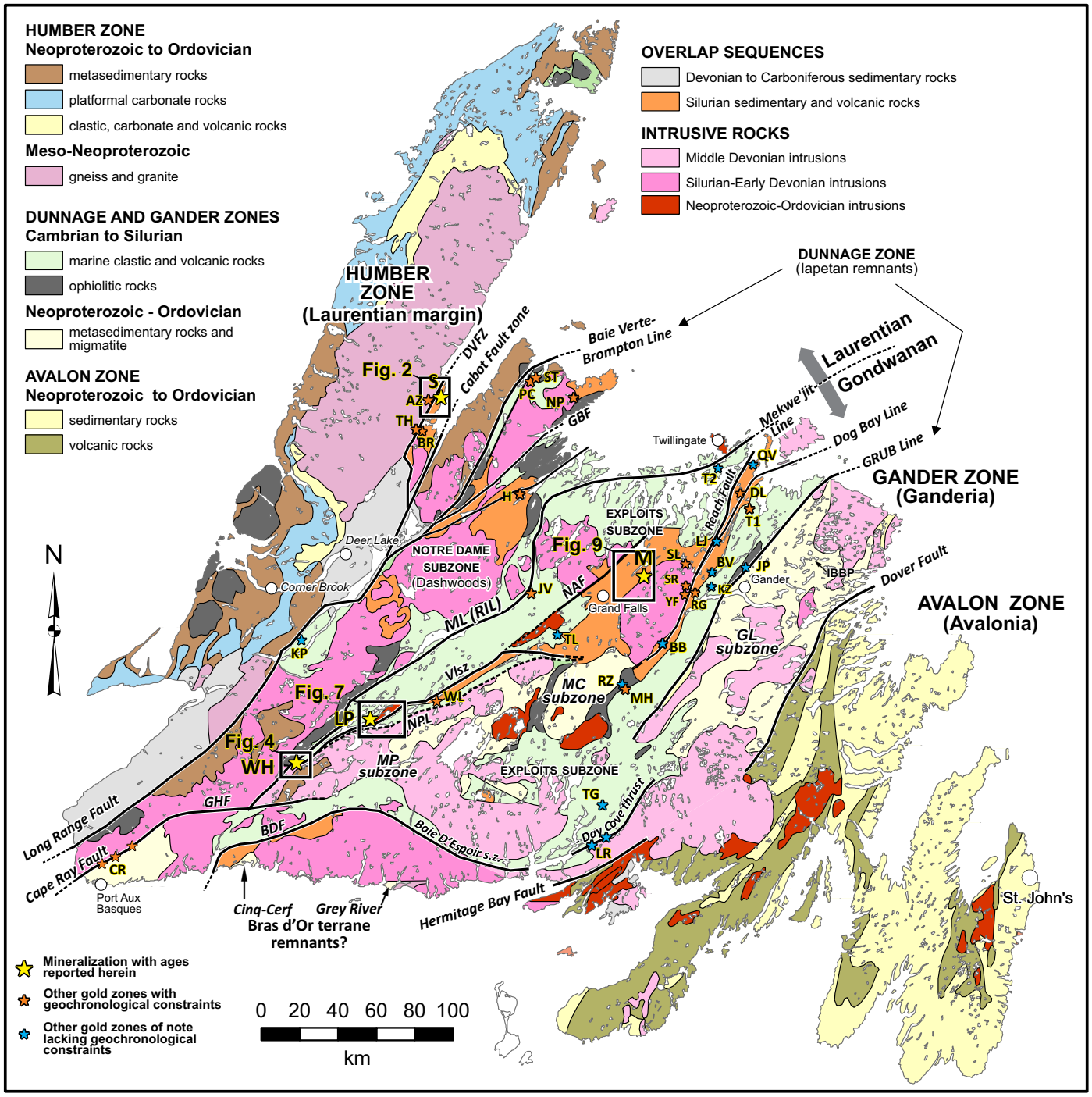

Figure 1. Simplified geological map of the Island of Newfoundland showing the major geological terranes, tectonic boundaries and faults (modified after Colman-Sadd *et al* 1990) and the locations of the gold mineralized zones discussed in this report. AZ–Apsy zone; BB–Beaverbrook; BR–Browning; BV–Big Vein; CR–Cape Ray; DL–Duder Lake; DVFZ–Doucers Valley Fault zone; GBF–Green Bay Fault; GHF–Gunflap Hills Fault; GL Subzone–Gander Lake Subzone; H–Hammerdown; IBBP–Indian Bay Big Pond; JP–Jonathons Pond; JV–Jaclyn Vein; KP–Kettle Pond; KZ–Keats Zone; LJ–Little Joanna; LP–Leprechaun Pond; LR–Little River; M–Moosehead; MC Subzone–Mount Cormack Subzone; MH–Mosquito Hill; MP Subzone–Meelpaeg Subzone; NAF–Northern Arm Fault; NP–Nugget Pond; NPL–Noel Paul's Line; PC–Pine Cove; QV–Quinlan Veins; RG–Road Gabbro; RZ–Reid Zone; S–Shrik; SL–The Slip; SR–Salmon River; ST–Stoger'tite; T1–Titan east; T2–Titan west; TG–True Grit; TH–Thor; TW–Twilite; VLsz–Victoria Lake shear zone; WH–Woods Lake and Hill Top; WL–Wilding Lake; YF–Yellow Fox.

Ordovician. Gander River Complex and other linear strongly magnetic anomalies in Gander Zone represent remnant overthrust Ordovician ophiolitic rocks, and Ordovician to Silurian cover rocks of Ganderia that were subsequently structurally modified during younger orogenic events.

The four major pre-Silurian terranes (Laurentian margin, Dashwoods terrane, composite Ganderian terranes, and Avalonia: van Staal and Barr 2014) are separated and transected by several major, long-lived polyphase fault zones. Progressing eastwards, the terrane-bounding fault zones include: the Baie Verte–Brompton Line separating the Laurentian margin from Dashwoods terrane; the Mekwe'jit Line (formerly Red Indian Line; RIL: see White and Waldron 2022) separating Dashwoods terrane from arcs and backarcs of the leading Ganderian margin; the Noel Paul's Line, Dog Bay Line, and Gander River Complex separating allochthonous blocks of composite Ganderia and; the Dover-Hermitage Bay Fault Zone separating Ganderia and Avalonia (e.g., Blackwood and Kennedy 1975; van Staal *et al* 2009; van Staal and Barr 2012; van Staal *et al* 2014, and references therein).

Despite the prevalence of terrane-bounding faults, orogenic gold mineralization in Newfoundland tends to be associated with crustal-scale fault zones that transect the pre-Silurian terranes. In the west, for example, the Silurian to Carboniferous Cabot–Doucers Valley fault system (Lock 1969; Tuach 1987) merges with the Baie Verte–Brompton Line (Fig. 1) to separate the Laurentian margin from Dashwoods terrane (Waldron and van Staal 2001). Furthermore, splays of the Baie Verte–Brompton Line must have been active post-Ordovician accretion to form Silurian vein-hosted gold mineralization (Dubé *et al* 1993; Poulsen *et al* 2000). In central Newfoundland, the approximately five-million-ounce gold deposit at Valentine Lake and numerous gold prospects along strike (e.g., Wilding Lake prospect) are hosted along an Early Devonian thrust-backthrust system (Honsberger *et al* 2022a) that imbricated rocks of the Exploits Subzone and Gander Zone and uplifted the Meelpaeg nappe along the Noel Paul's Line.

The new $^{40}Ar/^{39}Ar$ geochronology samples in the present study are from: (1) the White Bay area along the Doucer's Valley–Cabot Fault system of the Laurentian margin (Jacksons Arm, Shrik prospect); (2) the southwestern confluence of the Exploits and Meelpaeg subzones with Dashwoods terrane (Wood Lake South zone and Hill Top showing; Leprechaun Pond deposit, Valentine Lake); and (3) the northeastern Exploits Subzone of central Newfoundland (Moosehead prospect; Fig. 1). Existing geochronological constraints for additional auriferous zones are also illustrated in Figure 1.

AURIFEROUS ZONES INVESTIGATED WITH ^{40}AR/^{39}AR GEOCHRONOLOGY

Jacksons Arm trend (Shrik prospect)

The Jacksons Arm gold trend (Shrik, Boot n Hammer, and Stocker zones) occur ~ 4 km north of the community of Jacksons Arm on the Coney Head Peninsula in western White Bay (Fig. 1; Reid and Myllyaho 2012; Myllyaho 2013; English *et al* 2017). The showings occur in a curvilinear zone along the margin of the Ordovician Coney Head Complex (ca. 478 Ma; Dunning 1987; Fig. 2), an ophiolite-related tonalite and marginal basaltic and sedimentary units. The Coney Head Complex is unconformably overlain by syntectonic, clastic sedimentary and bimodal volcanic rocks of the orogenic gold-mineralized Silurian Sops Arm Group (e.g., Heyl 1937; Betz 1948; Kerr 2006a and b; Sandeman and Dunning 2016). The unconformity and the volcanic-sedimentary rocks of the Sops Arm Group are thrust imbricated with tonalite of the Coney Head Complex along broadly north-striking, east-dipping fault zones (this study; Magna Terra Minerals 2022). A sample of altered tonalite and adhering quartz vein (HS12-200C), weakly anomalous in Bi (3.9 ppm), As (24 ppm), Ag (0.1 ppm), and Au (4650 ppb), was collected from the Shrik trench where fine- to medium-grained, variably foliated, sericite-altered, pyritic and quartz-veined tonalite of the Coney Head Complex is exposed over a ~10 m × ~30 m area (Figs. 3a and b). The tonalite is locally cut by irregular, pinch and swell quartz veins with rare pyrite, but the relationships between deformation, veining, and gold mineralization remain unresolved. The tonalite wall rock contains quartz, sericitized plagioclase, mats of intergrown fine-grained muscovite and sparse pyrite and goethite (Fig. 3c).

Wood Lake South (Main) zone - Hill Top showing

The Wood Lake South (Main) gold zone and Hill Top showing occur in central-western Newfoundland near the confluence of the Exploits, Meelpaeg, and Notre Dame subzones (Figs 1 and 4). The Hill Top gold showing consists of two narrow (1–10 cm wide), southeast-northwest-trending, steeply dipping, pinch and swell pyrite + arsenopyrite-bearing quartz veins that cut Ordovician (ca. 467 Ma) Peter Strides monzogranite (e.g., van Egmond 2004; van Staal *et al* 2005a; Valverde-Vaquero *et al* 2006; Sandeman *et al* 2014; Sandeman 2014a) of the Meelpaeeg nappe and extend sporadically along strike for ~50 m. The quartz veins are hosted in an inferred northwest-trending mineralized fracture zone that cuts the monzogranite (Figs. 4 and 5). The host granite is strongly foliated, with a strong quartz mineral lineation, and is cut by translucent-white, foliated and lineated, barren quartz veins oriented sub-parallel to the foliation. The $^{40}Ar/^{39}Ar$ geochronology sample from Hill Top (HS10-59A) is a light grey to pink, fine- to medium-grained, quartz-veined, foliated and lineated monzogranite adjacent to the two quartz veins (Figs. 5a and 5b). In thin section, polyhedral and sutured quartz porphyroclasts (≤1.5 mm) are surrounded by fine-grained intergrown anhedral albite, quartz, and sericite (Fig. 5c). Rare euhedral monazite and subhedral rutile are intergrown with quartz and sericite in the groundmass (Fig. 5d).

Gold-mineralized quartz veins of the Wood Lake South (Main) zone are hosted by massive to brecciated and/or(?)

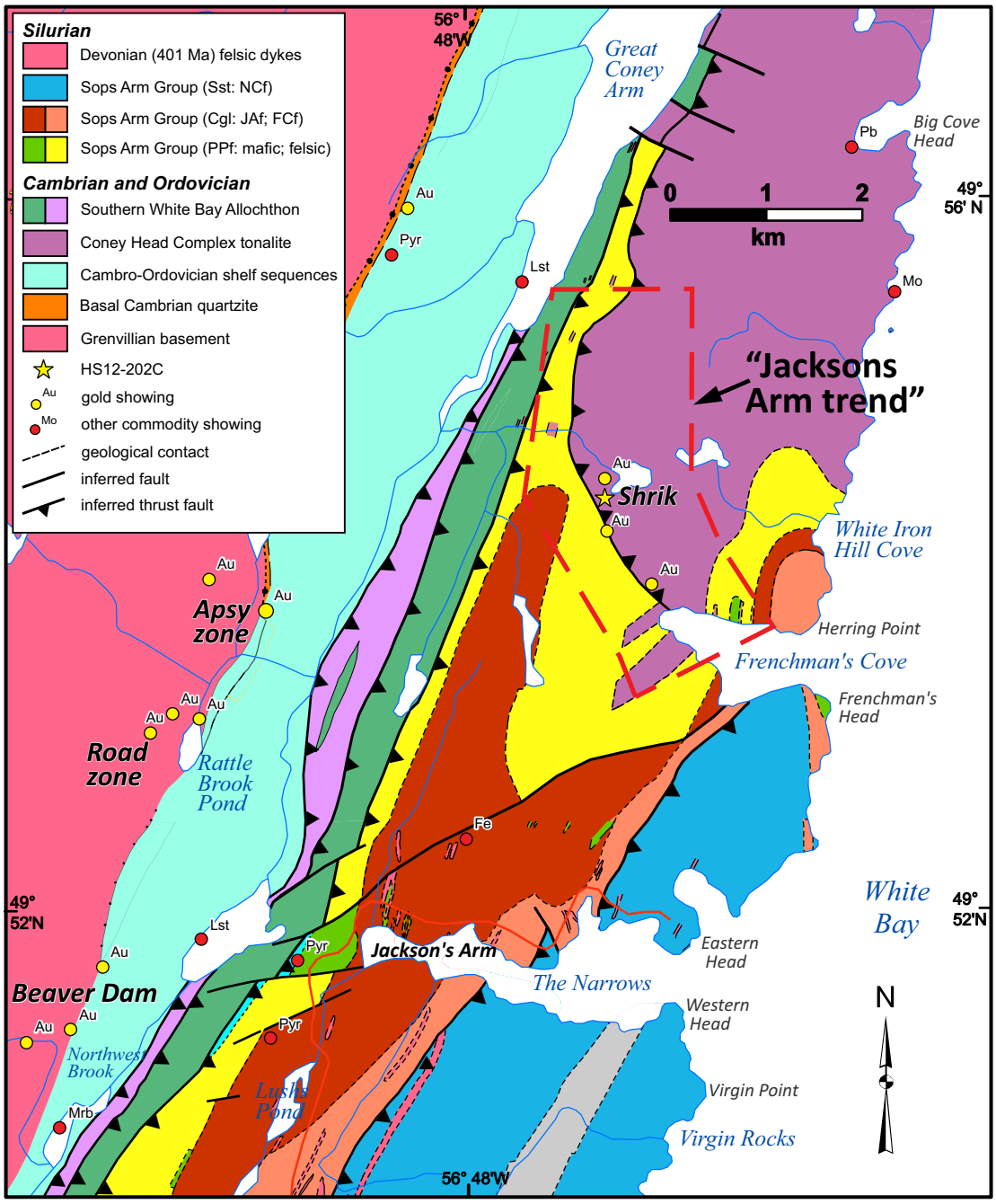

Figure 2. Simplified geology of part of the western White Bay area, northwestern Newfoundland (modified after Kerr 2006b; Sandeman and Dunning 2016), showing the approximate location of $^{40}Ar/^{39}Ar$ muscovite sample HS12-200C (yellow star), as well as the locations of precious- and base-metal showings of the region (Geoscience Atlas 2022)

mylonitic, orange-pink monzogranitic rocks of the Peter Strides Granite Suite. In the main trench (Fig. 6a), intensely deformed monzogranite is intruded by a less deformed, fine- to medium-grained, sericitic monzogranite. The less intensely deformed monzogranite is cut by an extensive array of steeply dipping irregular fractures and anastomosing, pinch and swell quartz veins (≤10 cm). Both the veins and fractures have minor pyrite + hematite ± arsenopyrite, accompanied by adjacent wall rock sericitization, albitization and silicification. Muscovite locally forms randomly oriented clumps and masses in the matrix of brecciated monzogranite, but occurs more typically as wispy platelets along fractures (Figs. 6b and 6c). Further details of the geology of the main trench and associated auriferous zones are provided by van Egmond and Cox (2005) and Sandeman *et al* (2014).

The $^{40}Ar/^{39}Ar$ geochronology sample (HS13-063A) from the Wood Lake South (Main) zone trench consists of an orange-pink, medium-grained, brecciated, and foliated monzogranite exposed below a strand of mylonitic monzogran-

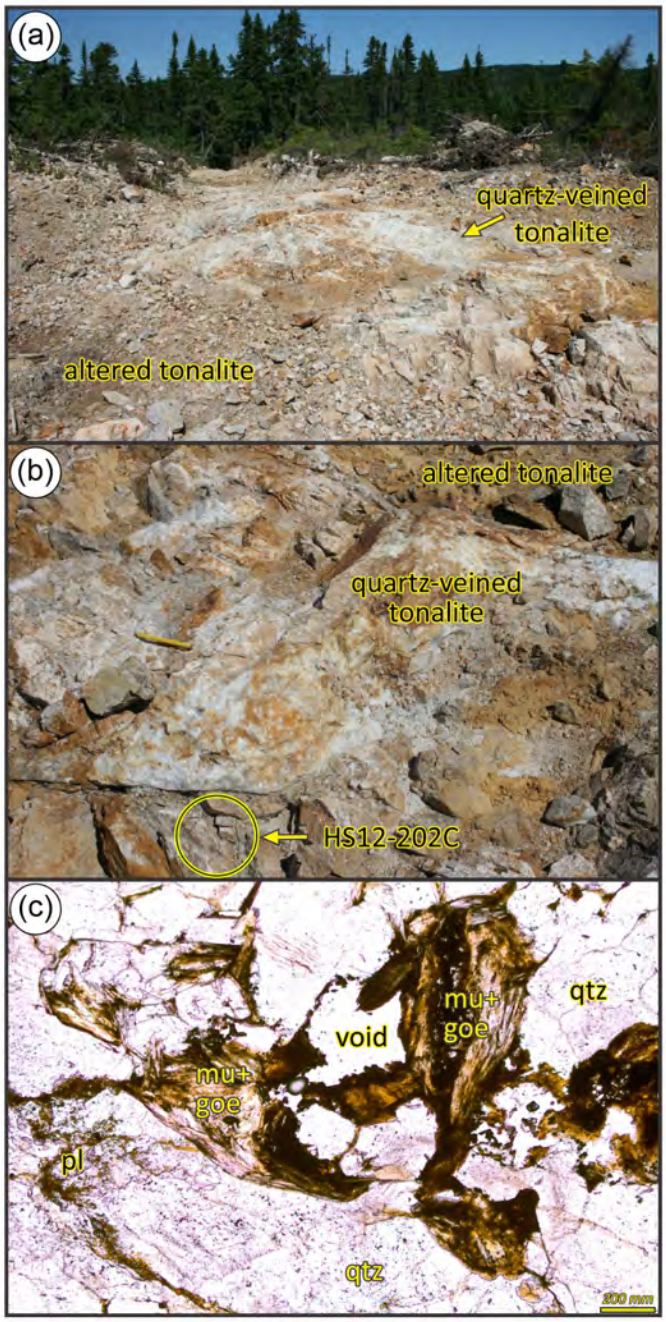

Figure 3. Photographs and photomicrographs of Shrik Showing sample HS12-200C. (a) Photograph of the Shrik discovery trench looking north with quartz-veined, altered tonalite in the centre, bounded to the north and south by sericite altered tonalite. The field of view is 10 m. (b) Close-up of the Shrik trench with quartz veined tonalite mantled by altered tonalite, and the location of sample HS12-200C. Field of view is 15 cm. (c) Photomicrograph in plane polarized light (PPL) showing the mineralogy of the altered tonalite and the random, mat-like nature of the muscovite in the sample. The brown tint of the muscovite is because of goethite staining. Mineral abbreviations after Whitney and Evans (2010).

ite (Figs. 4 and 6). In thin section, large (≤2 mm) polyhedral and sutured quartz grains are surrounded by fine-grained albite, sericite, and quartz. Subhedral pyrite and arsenopyrite are dispersed throughout and locally concentrated in vugs and fractures (Fig. 6b). Relatively large (≤1 mm), weakly to non-aligned muscovite grains are common (Figs. 6c and d).

Leprechaun Pond deposit (Valentine Lake)

The Leprechaun Pond deposit of the Valentine Lake gold property in central-western Newfoundland occurs within the Exploits Subzone near the boundary with the Meelpaeg Subzone (Figs. 1 and 7). The Neoproterozoic to Silurian rocks of the Valentine Lake area trend northeasterly and are bisected by the Victoria Lake shear zone (Valverde-Vaquero *et al* 2006; van Staal *et al* 2005b). This major northeast-trending, variably southeast-dipping, crustal-scale shear zone extends from the Gunflap Hills Fault in the southwest, through central Newfoundland along the northern margin of the Meelpaeg nappe (Figs. 1 and 7). The northeastern trace of the Victoria Lake shear zone is poorly constrained, and it may continue north-eastward to the Bay of Exploits, or alternatively, it may bifurcate and verge to the east along the northern margin of the Mount Cormack Subzone (Honsberger *et al* 2022a).

To the northwest, in the structural footwall of the Victoria Lake shear zone, Neoproterozoic (ca. 570 Ma) orogenic gold-mineralized basement granitoid rocks of the Valentine Lake Intrusive Suite (Evans and Kean 2002; Rogers and van Staal 2002; Rogers *et al* 2006), are uplifted and juxtaposed against the orogenic gold-mineralized Rogerson Lake Conglomerate (Kean and Jayasinge 1980) along the northwest-dipping Valentine Lake shear zone. The Valentine Lake shear zone hosts an approximately five-million-ounce orogenic gold resource, including the Leprechaun Pond deposit, where bleached and altered Neoproterozoic trondhjemite-tonalite and associated rocks contain a stacked array of fault-fill and extensional quartz-tourmaline-pyrite (QTP) vein sets (Lincoln *et al* 2018). The Rogerson Lake Conglomerate crops out southeast of the Valentine Lake shear zone, and is an aerially extensive latest Silurian, syntectonic, clastic sedimentary unit of central Newfoundland that delineates the southwest-northeast-trending fault system that is host to many of the gold occurrences in the central Newfoundland gold district (Honsberger *et al* 2022b; this volume).

At the Wilding Lake gold property, ~36 km northeast along strike of the Leprechaun Pond deposit, orogenic gold mineralization is hosted within both the Rogerson Lake Conglomerate and the associated ca. 422 Ma felsic subvolcanic and volcanic rocks in the footwall of the northeastern extension of the Valentine Lake shear zone (WL on Fig. 1; Honsberger *et al* 2019a; 2019b; 2020a; 2020b; 2022a). Overlapping ca. 410 Ma ID-TIMS U–Pb ages for hydrothermal rutile in quartz veins from both the Leprechaun Pond deposit and the Elm Prospect of the Wilding Lake property (Honsberger *et al* 2022a) indicate an Early Devonian (late

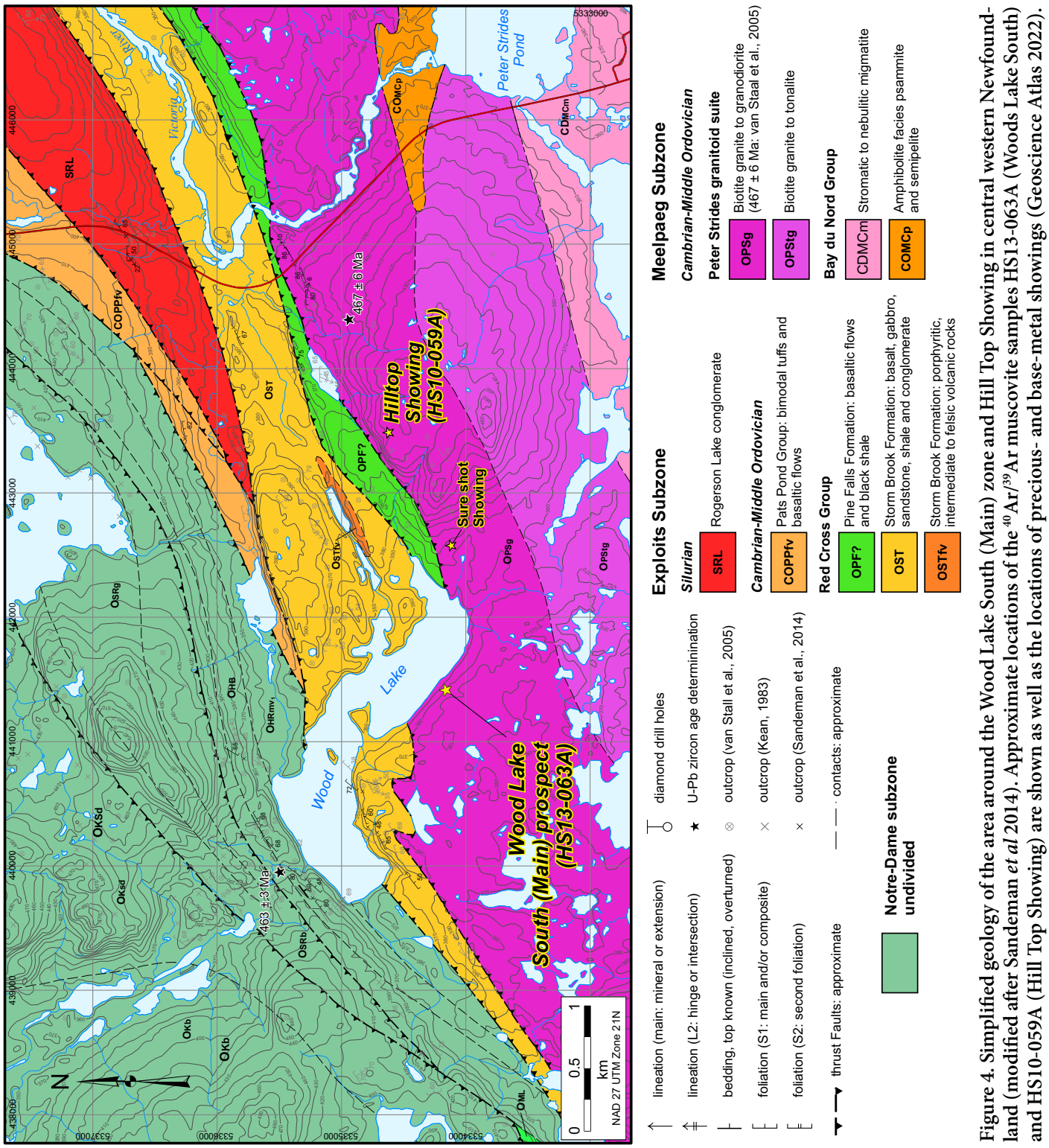

Figure 4. Simplified geology of the area around the Wood Lake South (Main) zone and Hill Top Showing in central western Newfoundland (modified after Sandeman *et al* 2014). Approximate locations of the $^{40}Ar/^{39}Ar$ muscovite samples HS13-063A (Woods Lake South) and HS10-059A (Hill Top Showing) are shown as well as the locations of precious- and base-metal showings (Geoscience Atlas 2022).

Lochkovian) age for quartz vein emplacement associated with orogenic gold mineralization.

The $^{40}Ar/^{39}Ar$ geochronology sample from the Leprechaun Pond deposit, VL-24-62.1m, is a weakly auriferous, bleached, fine-grained, foliated and quartz-veined tourmaline-muscovite-bearing trondhjemite from drillcore (62.1–63.0 metres depth: Figs. 8a, b, c). Large (≤6 mm) polyhedral sutured quartz grains and extensively altered plagioclase are surrounded by fine-grained albite, sericite and quartz. Subhedral pyrite is dispersed throughout the rock but concentrated near the margins of quartz veins (Fig. 8c). Tourmaline occurs as needles in or along vein margins. Relatively large (≤0.6 mm) muscovite grains are common and occur as plates in the groundmass and in primary feldspar grains

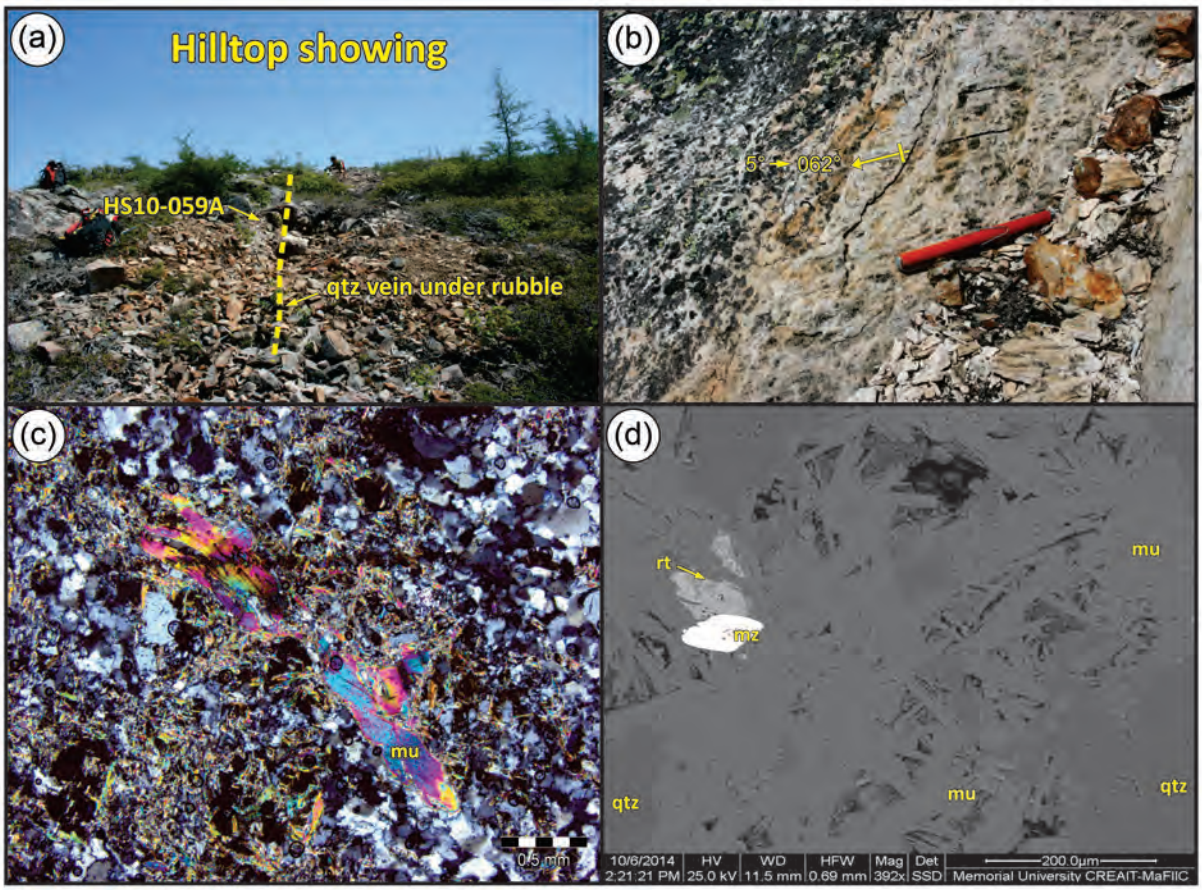

Figure 5. Photographs and photomicrographs of Hill Top Showing sample HS10-059A. (a) Photograph viewed southeast at the narrow Hill Top veins. Note person in background. (b) Photograph of a foliation surface on the wall rock adjacent to the Hill Top vein, illustrating the strong L-fabric in the Peter Strides monzogranite defined by aligned quartz and muscovite. (c) Photomicrograph in crossed polars of the monzogranite wall rock illustrating the disseminated subhedral pyrite, the altered sericitic groundmass and the large, secondary muscovite grains. (d) Backscattered electron image illustrating the minerals and their detailed relationships. Note the subhedral rutile and euhedral monazite, targets for future geochronology.

(Fig. 8c); a 250–450 µm fraction was extracted for $^{40}Ar/^{39}Ar$ geochronology.

Moosehead prospect (North Pond trench; TRMH15-3)

The Moosehead Prospect occurs southeast of the town of Bishops Falls in north-central Newfoundland (Figs. 1 and 9; Morgan 2016; Froude 2019, 2021). It lies within the latest Silurian–Early Devonian, intraorogenic Botwood Basin, ~4 km west of the ca. 425–418 Ma Mount Peyton Intrusive Suite (Sandeman *et al* 2017) in the north-central Exploits Subzone (Figs. 1 and 9). Mineralization consists of extensional, auriferous, sulphide-sulfosalt-bearing quartz veins and breccias that cut mainly muscovite-bearing sandstone and siltstone of the Wigwam Formation of the Botwood Group (i.e., Botwood basin; Williams 1969; Dickson *et al* 2000; O'Brien 2003; Morgan 2016). Mafic volcanic rocks of the lower Botwood Group (Laurenceton Formation) occur immediately south and southeast of the prospect. Gabbroic and fine-grained mafic dykes locally cut the sedimentary rocks and are themselves locally bleached, silicified and carbonate + pyrite ± sericite altered (e.g., Clark 1999; Morgan 2016). Trenching uncovered medium-bedded muscovite-bearing sandstone, southwest-dipping in the north, and south-dipping in the south, with weakly sulphidic, highly disrupted, quartz-veined, sandstone-quartz breccia in between (Figs. 9a, b and 10). The sandstone is variably mineralized, and quartz veins are more abundant in the northern part of the trench. Mineralization occurs in the hanging wall of a discrete east-west fault zone (Figs. 9b and 10). Bedding and crosscutting quartz veins are deflected into the fault zone, consistent with dextral rotation and reverse(?) slip. Further description and assay information for the Moosehead prospect are presented in Morgan (2016).

The $^{40}Ar/^{39}Ar$ geochronology sample from the Moosehead trench is a beige-grey, medium-grained, medium-bedded, quartz-veined muscovite-bearing sandstone of the Wigwam Formation from immediately north of the east-west fault near the centre of the trench (Figs. 9b and 10a). In thin section, large (≤0.4 mm) quartz and muscovite grains are surrounded by fine-grained matrix of albite, sericite, and quartz with subhedral pyrite dispersed throughout (Fig. 10b).

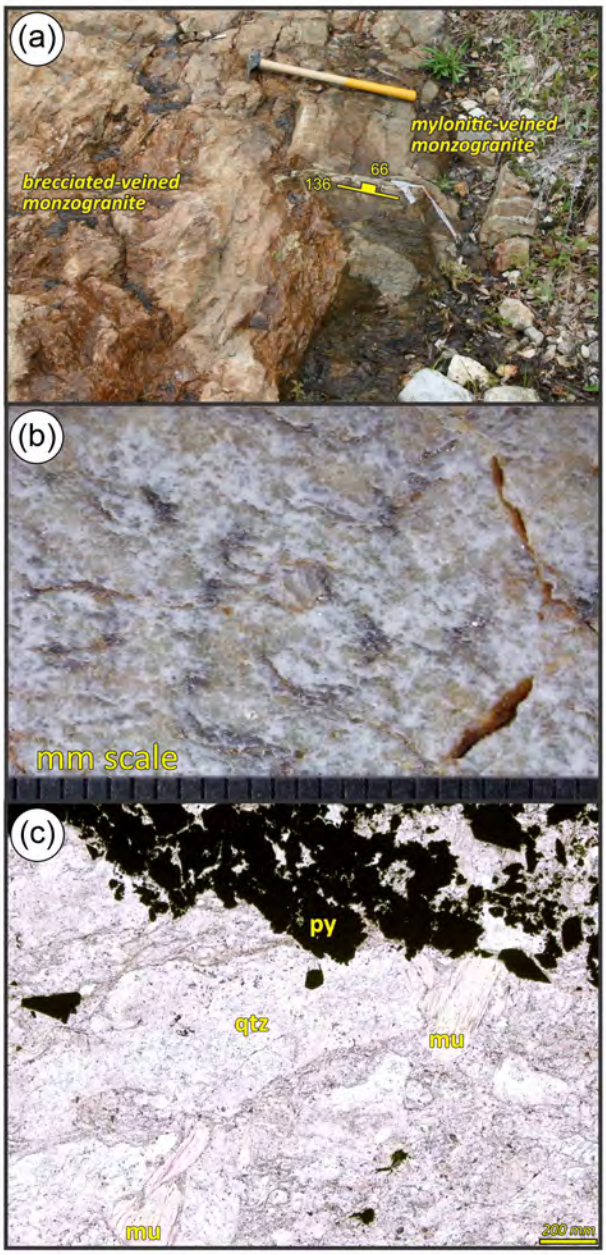

Figure 6. Photographs and photomicrographs of Wood Lake South Main zone sample HS13-063A. (a) Photograph from the main trench with massive and brecciated, quartz-veined and sericite + pyrite ± arsenopyrite mineralized monzogranite cutting mylonitic monzogranite having fabric-parallel, sulphide-poor, internally deformed quartz veins. The location of sample HS13-063A is shown and the Geotul is 54 cm in length. Mylonitic fabric trends 136° and dips 66° to the southwest. (b) Cut slab photograph of sample HS13-063A. White is altered feldspar, grey is quartz and reflective silver grains are muscovite. (c) Photomicrograph in PPL of the brecciated altered monzogranite illustrating the disseminated subhedral pyrite, the altered sericite groundmass and the large, secondary muscovite grains.

Relatively large (≤1 mm), bedding-parallel muscovite grains are common, and appear to be detrital in origin (Fig. 10c).

^{40}AR/^{39}AR GEOCHRONOLOGY

Methods

Geochronology samples were collected during 2010–2015 from selected gold-mineralized zones and drill core across central and western Newfoundland (e.g., Sandeman *et al* 2013; Sandeman 2014b; Sandeman and Dunning 2016). Kilogram-sized hand samples or ~ 40 cm long pieces of split drill core were cut and cleaned of all weathered surfaces and crushed to ~ 1 cm chips. About 100 grams of each sample was gently hand pulverised with pestle and mortar and sieved to two size fractions, 250–420 µm and 180–250 µm. The grain separates were washed repetitively in deionized water and the solute drained. Cleaned and dried samples were then gently cleaned in dilute (~0.5N) HNO_3 to remove adhering sulphides and carbonates from the grain separates. The cleaned separates were re-sieved and muscovite was hand-picked under a binocular microscope for laser step-heating analyses. Muscovite from the Shrik Showing (HS12-200C) was of poor quality, fine-grained, and only a single muscovite–rich (180–250 µm) grain separate was extracted.

The ^{40}Ar/^{39}Ar age data were obtained in the ^{40}Ar/^{39}Ar Thermochronology Laboratory at Queen's University. Mineral separates and flux-monitors (standards) are wrapped in Al-foil, stacked sequentially into an 8.5-cm-long and 2.0-cm-diameter Al irradiation capsule, and then irradiated with fast neutrons in position 8D of the McMaster Nuclear Reactor (Hamilton, Ontario) for a duration of 72 h (at 3 MWH). Packets of flux monitors are located at ~0.5 cm intervals along the irradiation container and the J-value for an individual sample is determined by least-squares, second-order polynomial interpolation using replicate analyses of splits for each monitor position in the capsule. The samples are loaded into flat-bottomed pits in a copper sample-holder and placed beneath the ZnS view-port of a small, bakeable, stainless-steel chamber connected to an ultra-high vacuum purification system. Following bake out at 100°C, a 30 watt New Wave Research MIR 10-30 CO_2 laser with a faceted lens is used to heat samples for ~3 minutes at increasing percent power settings (2 to 45%; beam diameter 3 mm). After purification using hot and cold SAESC50 getters (for ~5 minutes), the evolved gas is admitted to an MAP 216 mass spectrometer, with a Bäur Signer source and an analog electron multiplier (set to a gain of 100 over the Faraday detector). Measured argon-isotope peak heights are extrapolated to zero-time and corrected for discrimination using a ^{40}Ar/^{36}Ar atmospheric ratio of 295.5 and measured ratios of atmospheric argon. Blanks, measured routinely, are subtracted from the subsequent sample gas-fractions. The extraction blanks are typically <10 x 10–13, <0.5 x 10–13, <0.5 x 10–13, and <0.5 x 10–13 cm-3 STP for masses 40,

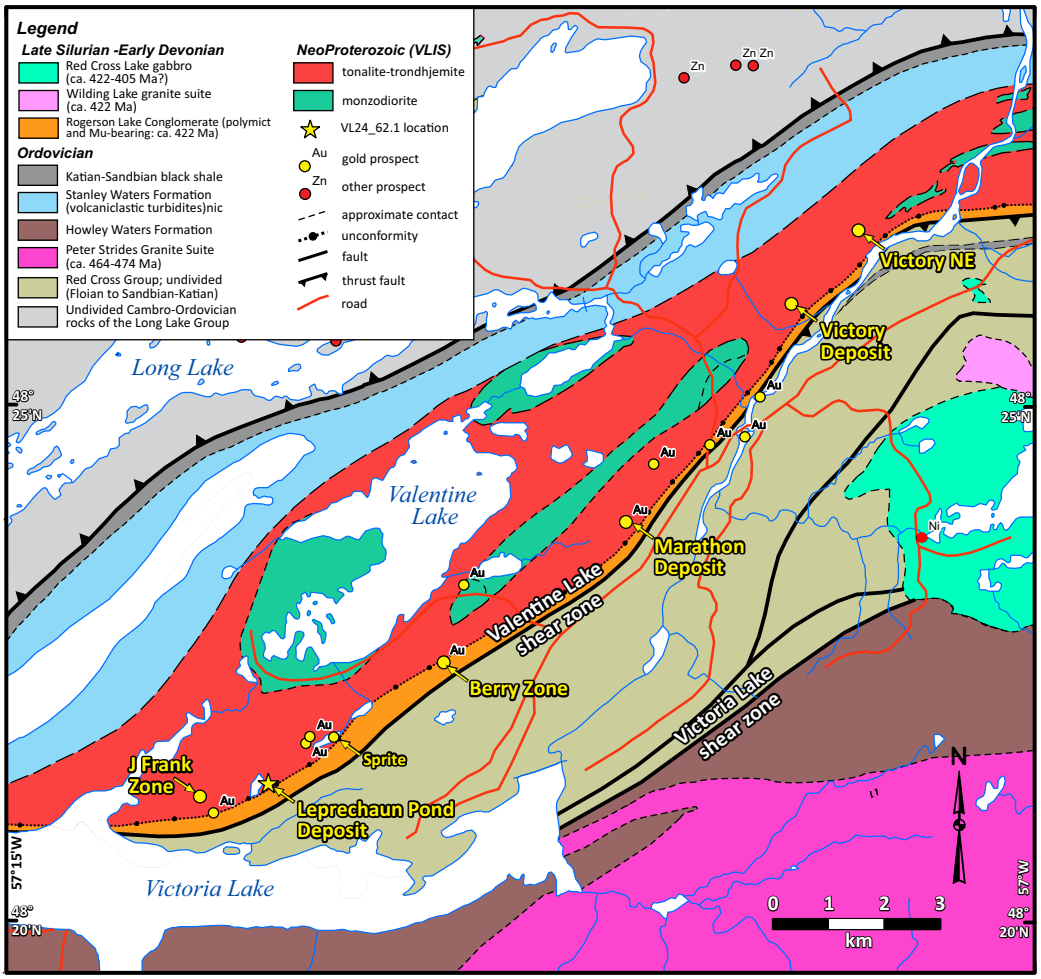

Figure 7. Simplified geology of the area around the Leprechaun Deposit (modified after van Staal *et al* 2005b) showing the approximate locations of the $^{40}Ar/^{39}Ar$ muscovite sample and the recently dated CA-TIMS U–Pb titanite sample (VL335-245; Honsberger *et al* 2022) at the Leprechaun Pond deposit. The locations of precious- and base-metal showings are from the Geoscience Atlas (2022).

39, 37, and 36, respectively. The ^{39}Ar and ^{37}Ar are corrected for radioactive decay during and after irradiation. Corrections are made for neutron-induced ^{40}Ar from potassium, ^{39}Ar and ^{36}Ar from calcium, and ^{36}Ar from chlorine (Roddick 1983; Onstott *et al* 1991). Dates and errors are calculated using the procedure of Dalrymple *et al* (1981) and the constants of Steiger and Jäger (1977). Plateau and inverse isotope correlation dates are calculated using ISOPLOT v. 3.60 (Ludwig 2012). A plateau is herein defined as 3 or more contiguous steps containing >50% of the ^{39}Ar released, with a probability of fit >0.01 and MSWD <2. Errors shown in Supplementary data Table S1 and in Figure 11 represent the analytical precision at 2σ, assuming that the errors in the ages of the flux monitors are zero. This is suitable for comparing within-spectrum variation and determining which steps form a plateau (e.g., McDougall and Harrison 1988, page 89). The dates and J-values are referenced to GA-1550biotite (98.5 Ma; Spell and McDougall 2003) and Hb-3Grhornblende (PP-20; 1073.6 Ma; Jourdan *et al* 2006). The complete $^{40}Ar/^{39}Ar$ dataset is in Supplementary data Table S1, whereas the laser step-heating results are illustrated in Figure 11. Sample coordinates are NAD27 datum, zone 21.

Results

Shrik Showing (HS12-200C: UTM Zone 21, 516037 E, 5527889 N: muscovite)

Altered tonalite wall rock from this sample was crushed, sieved, cleaned, and small (≤0.5 mm), weakly to non-aligned, goethite-dusted muscovite grains were concentrated into a 180–250 µm grain separate for $^{40}Ar/^{39}Ar$ dating. The muscovite separate yielded a complex age spectrum (Fig. 11a). The initial low-T (power) step (1.43% of ^{39}Ar released) yielded an anomalously young age (ca. 336 Ma) but the next 6 steps (30.3% of ^{39}Ar released) yielded anomalously old ages ranging from ca. 390 to 428 Ma and are attributed to the incorporation of excess argon. The higher temperature (power) steps, excluding the final young gas fraction, form a relatively flat segment representing 58.9 % of the ^{39}Ar%

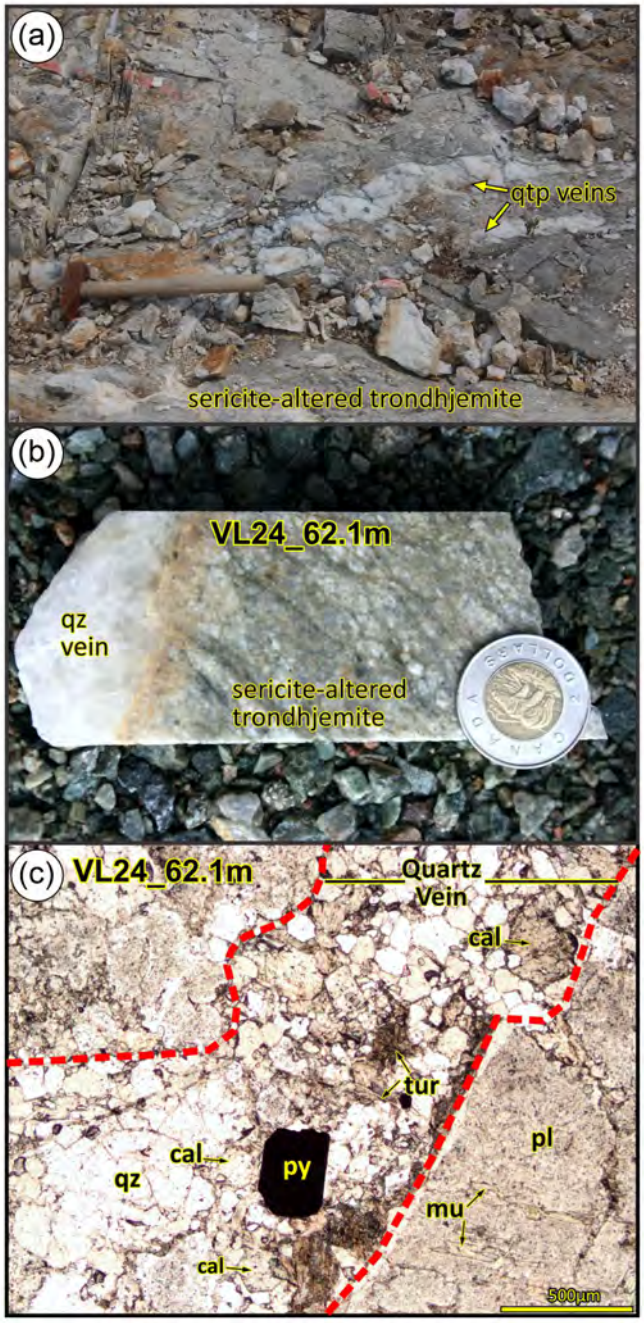

Figure 8. Photographs and photomicrograph of Leprechaun Pond deposit. (a) Photograph from the main trench to the northwest of Leprechaun Pond illustrating the sericite-altered trondhjemite-tonalite of the Valentine Lake Intrusive Suite cut by quartz-tourmaline-pyrite veins. (b) Cut core photograph of quartz-tourmaline vein cutting bleached trondhjemite (DDH VL-24-62.1m). (c) Photomicrograph in PPL of a quartz-tourmaline vein containing pyrite, calcite and muscovite cutting altered trondhjemite host rock composed of saussuritized plagioclase and quartz. Muscovite forms coarse plates along fractures in plagioclase and in vein margins.

released and yield an age of 379.7 ± 1.4 Ma (2σ; POF = 0.36; MSWD = 1.10). The volume of ^{39}Ar released is slightly less than the suggested convention of >60% volume for a plateau age (McDougall and Harrison 1988; Ludwig 2012; Schaen *et al* 2021), but the quasi-plateau appears to have geological significance.

Hill Top Showing (HS10-59A: UTM Zone 21, 443526 E, 5334700 N: muscovite)

Analyses of relatively large (250–425 µm) muscovite grains yielded a relatively simple ^{40}Ar/^{39}Ar age spectrum (Fig. 11b). The nine higher temperature (power) steps formed a relatively flat segment representing 91.4% of the ^{39}Ar released and gave a plateau age of 409.1 ± 1.3 Ma (2σ; POF = 0.77; MSWD = 0.42).

Wood Lake South (Main) zone (HS13-063A: UTM Zone 21, 500450 E, 5504824 N: muscovite)

Two fractions (250–425 µm and 180–250 µm) of muscovite were extracted for ^{40}Ar/^{39}Ar analysis. The nine highest (out of 15) temperature (power) steps of the 250–425 µm fraction, representing 91.4 % of the ^{39}Ar released gives a plateau age of 403.1 ± 1.2 Ma (2σ; POF = 0.91; MSWD = 0.42; Fig. 11c). The second 180–250 µm aliquot (Fig. 11d) yielded a quasi-plateau age of 398.4 ± 1.3 Ma, representing 56.9% of the ^{39}Ar released (2σ; MSWD = 0.74; POF = 0.65), due largely to an unfortunately large-volume last step. The plateau age of 403.1 ± 1.2 Ma is considered the best estimate of the age of the muscovite.

Leprechaun Pond Deposit (Valentine Lake: VL-24_62.1m: UTM Zone 21, 486400 E, 5355880 N: muscovite)

The muscovite at the Leprechaun Pond deposit yielded a somewhat jagged age spectrum (Fig. 11e), but five of the steps formed a flat segment, comprising 59.9% of the ^{39}Ar released, and yielded a quasi-plateau age of 384.2 ± 1.6 Ma (2σ; POF = 0.57; MSWD = 0.74) and is interpreted as the best estimate of the age of the muscovite.

Moosehead Prospect (HS15-137; 613561E, 5428182N: muscovite)

Two muscovite fractions (250–425 µm and 180–250 µm) were extracted for ^{40}Ar/^{39}Ar geochronology and yielded two similar age spectra (Figs. 11f, g). The coarse-grained (250–425 µm) aliquot yielded a well-defined ^{40}Ar/^{39}Ar plateau age of 457.3 ± 1.2 Ma (2σ; POF = 0.94; MSWD = 0.44), representing 91.4% of the ^{39}Ar released (Fig. 11f). The 180–250 µm grain-size fraction (Fig. 11g), similarly yielded a well-defined ^{40}Ar/^{39}Ar plateau age of 453.5 ± 1.1 Ma (2σ; POF = 0.48; MSWD = 0.97), representing 97.0% of the ^{39}Ar released. The older age of 457.3 ± 1.2 Ma for the coarser-grained 250–450 µm fraction is interpreted as the best estimate of the ^{40}Ar/^{39}Ar age of the muscovite.

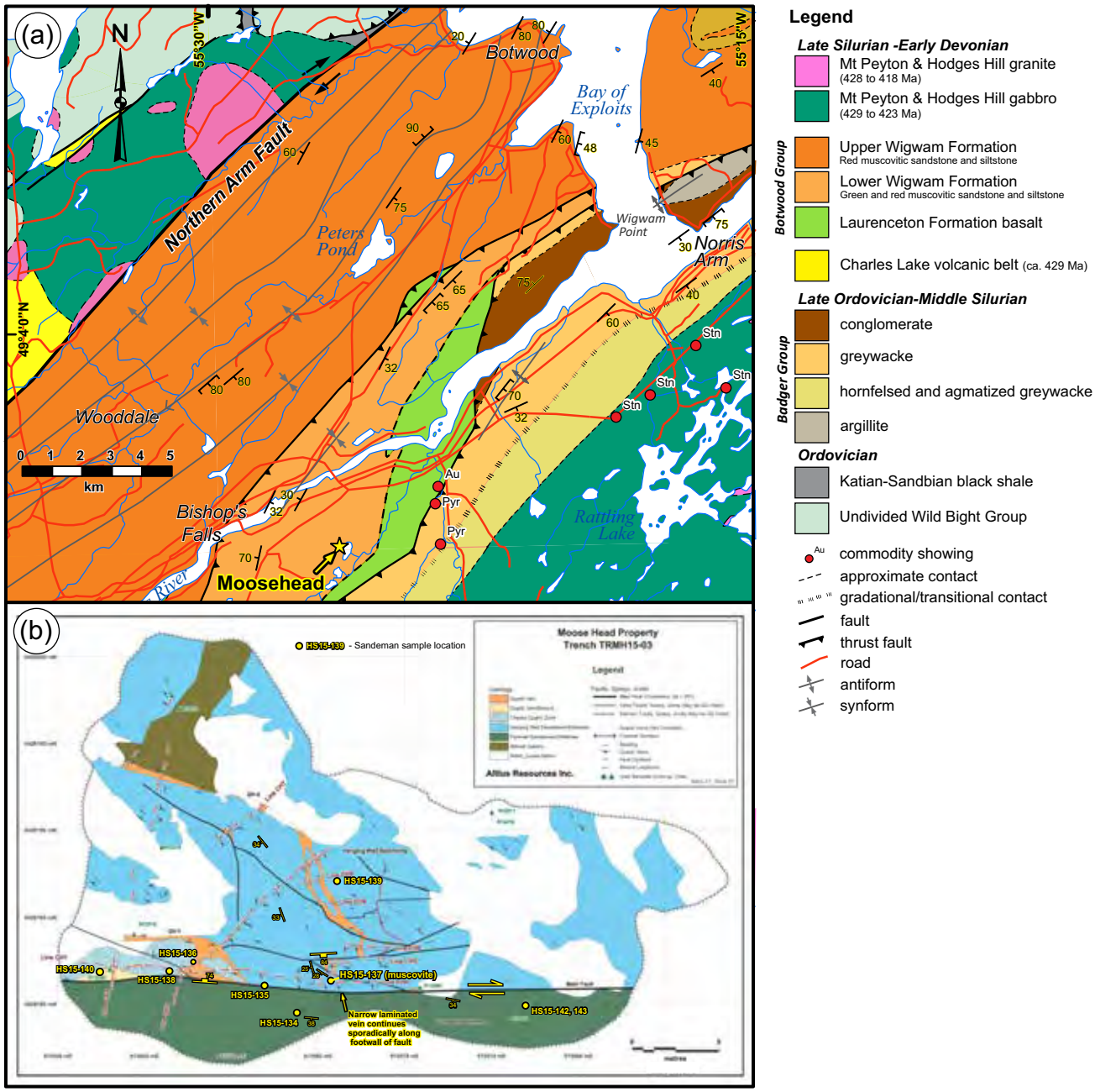

Figure 9. (a) Simplified geology of the northeastern Botwood Basin and the location of the Moosehead Prospect and other local mineral occurrences (modified after the Geoscience Atlas (2022). (b) Geological map of trench TRMH15-3 at the Moosehead Prospect with the locations of the $^{40}Ar/^{39}Ar$ muscovite sample, other lithogeochemical samples and the location of DDH MH-02-15 (see Morgan 2016).

DISCUSSION

Integration of these new $^{40}Ar/^{39}Ar$ geochronological data with existing regional geochronological constraints on gold mineralized zones and magmatic events elucidates deformational, metamorphic, and tectonic intervals that were favourable for gold-mineralization across Newfoundland (Fig. 12). The collective compiled data are diverse as they include age constraints determined via different radiometric methods on various phases/mineral species: some of which are more robust than others. These include studies applying $^{40}Ar/^{39}Ar$ cooling ages on dynamo-metamorphism and mineralization-associated potassic alteration; Re–Os ages on sulphide minerals; implied maximum ages based on U–Pb ages of host rocks and direct U–Pb CA-TIMS dating of the minerals coeval with quartz vein emplacement. For example, the interpreted age of the Hammerdown gold deposit (Springdale Peninsula) comes from U–Pb (zircon) thermal ionization mass spectrometry (TIMS), which yielded an age of 437 ± 4 Ma for a felsic dyke cut by an auriferous vein

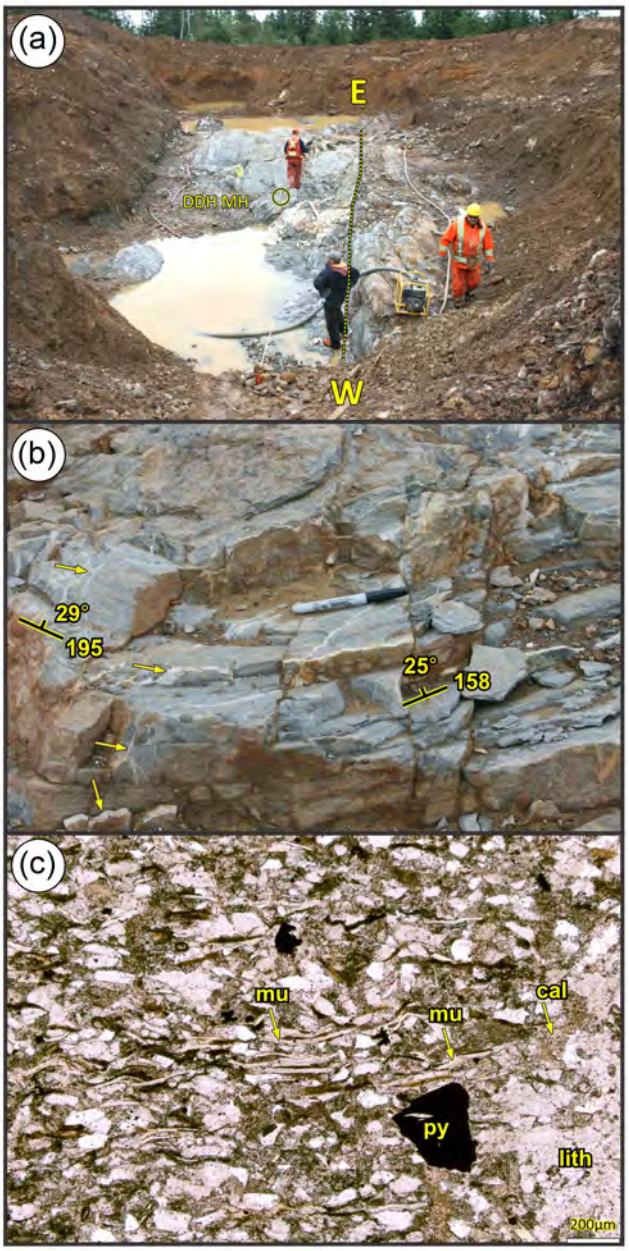

Figure 10. Photographs and photomicrographs of the Moosehead Prospect trench. (a) Photograph looking north from the east-west fault with decimetre-scale bedded muscovitic sandstone cut by an array of narrow, weakly sulphidic quartz veins. These veins largely trend northwest-southeast and are rotated into an east-west orientation near the main fault, indicating this is a dextral fault. (b) Close up of the warped bedding and crosscutting quartz veins at sample location HS15-137. Note the folding of bedding and the small yellow arrows pointing to quartz veins. (c) Photomicrograph in PPL of the sandstone showing disseminated subhedral pyrite, carbonate-sericite-altered groundmass and large, bedding-parallel muscovite grains.

(Ritcey *et al* 1995). This is therefore a maximum age constraint for gold mineralization. In contrast, the ca. 410 Ma chemical abrasion (CA) TIMS ages for rutile from auriferous quartz veins at the Wilding Lake gold prospect and Leprechaun Pond gold deposit (Honsberger *et al* 2022a) provide high-precision maximum constraints on the age of orogenic gold-mineralized quartz vein emplacement. Detailed investigations of vein and alteration mineral parageneses, their relationships to gold deposition and systematic geochronological study of different mineral species are required to better understand the timing of gold mineralization in Newfoundland.

The collective geochronological data outline two distinct, broad age-ranges for orogenic-style gold mineralization in the central and western Newfoundland Appalachians (Fig. 12). These include an older, Wenlock (middle Silurian) to Lochkovian (Lower Devonian) ca. 440 to ca. 405 Ma event, and a younger, Middle Devonian event at ca. 400–375 Ma. The former includes muscovite growth/resetting intervals for gold-bearing zones of the Laurentian margin, Dashwoods terrane, western Exploits subzone and along the Meelpaeg–Exploits subzones boundary; the latter includes muscovite from gold-bearing zones across the Laurentian Margin, Dashwoods terrane, Exploits Subzone, and Gander Zone (Fig. 12).

The muscovite from the Shrik showing occurs in an Ordovician, intraoceanic arc-related tonalite that has a strongly metaluminous composition (Sandeman, unpublished data 2022). The muscovite is spatially associated with quartz veining and bleaching of the tonalite resulting from hydrothermal fluid flow; therefore, it formed as a result of metasomatism, opposed to by igneous or dynamothermal metamorphic processes. Accordingly, the $^{40}Ar/^{39}Ar$ geochronological result of 379.7 ± 1.4 Ma is interpreted as a maximum age constraint for gold mineralization.

The host rocks of the Hill Top and Woods Lake South zones are muscovite-biotite-bearing, strongly peraluminous granitoid rocks of the Ordovician Peter Strides suite (part of the Meelpaeg Subzone) that comprise the hanging wall of the Victoria Lake-Valentine Lake fault system. The northern portion of the Meelpaeg Subzone records metamorphic U–Pb monazite and titanite ages and $^{40}Ar/^{39}Ar$ hornblende, muscovite and biotite cooling ages that range from ca. 418 to 400 Ma (Valverde-Vaquero *et al* 2003). Muscovite from the Hill Top (409.1 ± 1.3 Ma) and Woods Lake zones (403.1 ± 1.2 Ma) therefore likely represent Acadian metamorphic cooling temperatures in the immediate hanging wall of the Victoria Lake Shear Zone, which represent best approximations of maximum ages of gold mineralization.

Metaluminous tonalite and trondhjemite of the Valentine Lake Intrusive Suite host the Leprechaun Pond gold deposit. These rocks do not contain primary muscovite and the white mica is hydrothermal in origin. However, the relationship between the muscovite and deformation of the auriferous quartz-tourmaline-pyrite veins is ambiguous. The hydrothermal rutile age of ca. 410 Ma (see Honsberger *et al* 2022a) is significantly older than the muscovite plateau

age of 384.2 ± 1.6 Ma (this study), suggesting either a single protracted alteration and mineralization event, or multiple discrete events.

In contrast to the other dated samples, muscovite from the sandstone of the Moosehead prospect (ca. 457.3 ± 1.2 Ma and 453.5 ± 1.1 Ma) is detrital in origin and oriented parallel to bedding. Therefore, these ages represent metamorphic cooling ages for the metasedimentary or granitoid sources for the sandstone. One proximal potential Ordovician (Darriwillian: Cohen *et al* 2013) source terrane for the detrital muscovite is the Mount Cormack Complex (Gander Zone) of central Newfoundland (Fig. 1; Williams *et al* 1988; Colman-Sadd *et al* 1992). The Mount Cormack Complex preserves a central core of foliated, upper amphibolite-grade migmatitic psammite and pelite that were metamorphosed and intruded by garnet-muscovite syenogranite (Through Hills granite) at ca. 465–464 Ma (Colman-Sadd *et al* 1992; Valverde-Vaquero *et al* 2006). Metamorphic ages from the complex include: a monazite age of 462 ± 1 Ma; a titanite age of 460 ± 3 Ma; a $^{40}Ar/^{39}Ar$ hornblende plateau age of 465.7 ± 6.4 Ma; and a $^{40}Ar/^{39}Ar$ biotite plateau age of 439.4 ±2.4 Ma (Valverde-Vaquero *et al* 2003, 2006). The hornblende and biotite ages bracket the interval defined by the Moosehead trench muscovite ages and support the suggestion of the Mount Cormack Complex as a possible detrital muscovite source. Muscovite from the Meelpaeg nappe yield younger, Devonian regional metamorphic cooling ages ranging from ca. 418 to 394 Ma (Valverde-Vaquero *et al* 2003), similar to those obtained in the Gander Lake Subzone (ca. 404 to 388 Ma: O'Neill and Lux 1989; O'Neill and Colman-Sadd 1993). The apparent absence of older, Ordovician muscovite in these areas does not entirely preclude them as possible sources, however, this appears to be the case. To the west of the Botwood Basin, an alternative Ordovician, muscovite-bearing source might be represented by the muscovite-biotite-psammite of the reworked Laurentian margin (e.g., Fleur de Lys Supergroup, Baie Verte Peninsula).

The Early Devonian muscovite ages from central Newfoundland (Hill Top showing and Wood Lake South zone) are similar to, but slightly younger than, the ca. 410 Ma ages determined along strike to the northeast for hydrothermal rutile in gold-mineralized veins from the Leprechaun Pond deposit (Valentine Lake) and Wilding Lake prospect (Honsberger *et al* 2022a). This may reflect a lower $^{40}Ar/^{39}Ar$ closure temperature for muscovite relative to the U–Pb closure temperature for rutile (ca. 600°C; Vry and Baker 2006). The ca. 410 Ma rutile ages are interpreted to provide the best minimum estimates for quartz vein emplacement and initial orogenic gold mineralization along the Victoria Lake-Valentine Lake fault corridor (Fig. 1), whereas the muscovite ages provide the best estimates for potassic alteration associated with quartz vein emplacement. Furthermore, the ca. 403 and 409 Ma muscovite ages are also in broad agreement with two identical 406 ± 2 Ma $^{40}Ar/^{39}Ar$ plateau ages for alteration-related muscovite from the Mosquito Hill gold prospect along the southeastern margin of the Mount Cormack Complex (Fig. 1; Sandeman *et al* 2013).

Early Devonian metamorphism, metasomatism and orogenic gold mineralization along the Victoria Lake–Valentine Lake fault corridor is compatible with the timing of initial Acadian thrusting after ca. 418 Ma in southcentral Newfoundland (Dunning *et al* 1990; Valverde-Vaquero and van Staal 2001; van der Velden *et al* 2004; Valverde-Vaquero *et al* 2006). Furthermore, Early Devonian mineralization coincides with ca. 415 to 410 Ma Acadian ductile deformation in north-central and southwestern Newfoundland (Dunning *et al* 1990; Dubé *et al* 1996; McNicoll *et al* 2006). In southwestern–central Newfoundland, $^{40}Ar/^{39}Ar$ geochronology of white mica provides evidence for low-*P* – low-*T* Acadian metamorphism between ca. 408 and 390 Ma (Willner *et al* 2018). On the Baie Verte Peninsula, orogenic gold mineralization may have been initiated earlier than in central Newfoundland as Re–Os pyrite geochronology yielded ages of 420 ± 7 Ma and 411 ± 7 Ma for the Stog'er Tight and Pine Cove deposits (Kerr and Selby 2012), respectively. Similarly, hydrothermal zircon from the Stog'er Tight deposit was dated at 420 ± 5 Ma (Fig. 1; Ramezani *et al* 2002).

The new Middle–Upper Devonian muscovite ages for the Leprechaun deposit (ca. 384 Ma) at Valentine Lake and Shrik showing at White Bay (ca. 380 Ma), contrast with Early Devonian orogenic gold-bearing vein formation documented in both locations (ca. 410 Ma rutile; Honsberger *et al* 2022a; ca. 419 to ca. 408 Ma; Kerr and van Breemen 2007; Minnett *et al* 2012). However, the new data are compatible with a previous age determination for secondary muscovite at White Bay (ca. 374 Ma, Sandeman and Dunning 2016), as well as with ca. 374 ± 8 Ma hydrothermal xenotime from a gold-mineralized vein at the Nugget Pond deposit on the Baie Verte Peninsula (Sangster *et al* 2008). Moreover, a gold-mineralized mafic sill/dyke that cuts the Late Silurian Indian Islands Group near Gander Bay at the Titan prospect (Fig. 1; McNicoll *et al* 2006) yielded a SHRIMP U–Pb zircon age of 381 ±5 Ma, providing a maximum, late Devonian age for the gold mineralization. All these data support the existence of a Middle–Upper Devonian gold mineralization event that is superimposed on Early Devonian quartz vein systems in western, west–central, and central Newfoundland.

All geochronologically constrained orogenic gold occurrences in central and western Newfoundland are Late

Figure 11. (next page) $^{40}Ar/^{39}Ar$ age spectra for muscovite grain separates from the samples under investigation. (a) Shrik Showing muscovite HS12-200C (250–425 μm). (b) Hill Top Showing muscovite HS10-059A (250–425 μm). (c) Wood Lake South (Main) zone muscovite HS13-063A-1 (250–425 μm). (d) Wood Lake South (Main) zone muscovite HS13-063A-2 (180-250μm). (e) Leprechaun Pond Deposit muscovite VL-24-62.1m (250–425 μm). (f) Moosehead Prospect detrital muscovite HS15-137-1 (250–425 μm). (g) Moosehead Prospect detrital muscovite HS15-137-2 (180–250 μm).

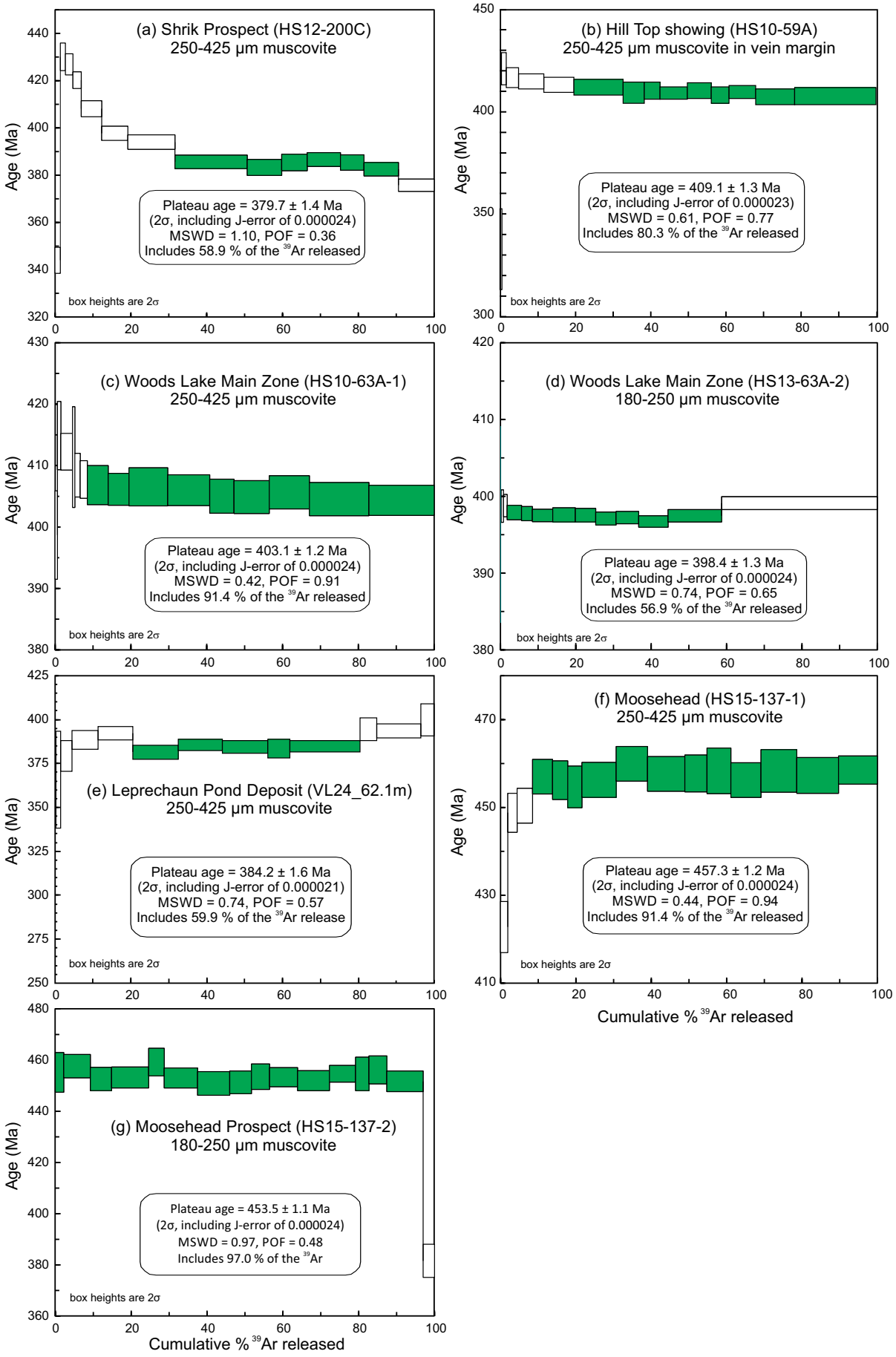

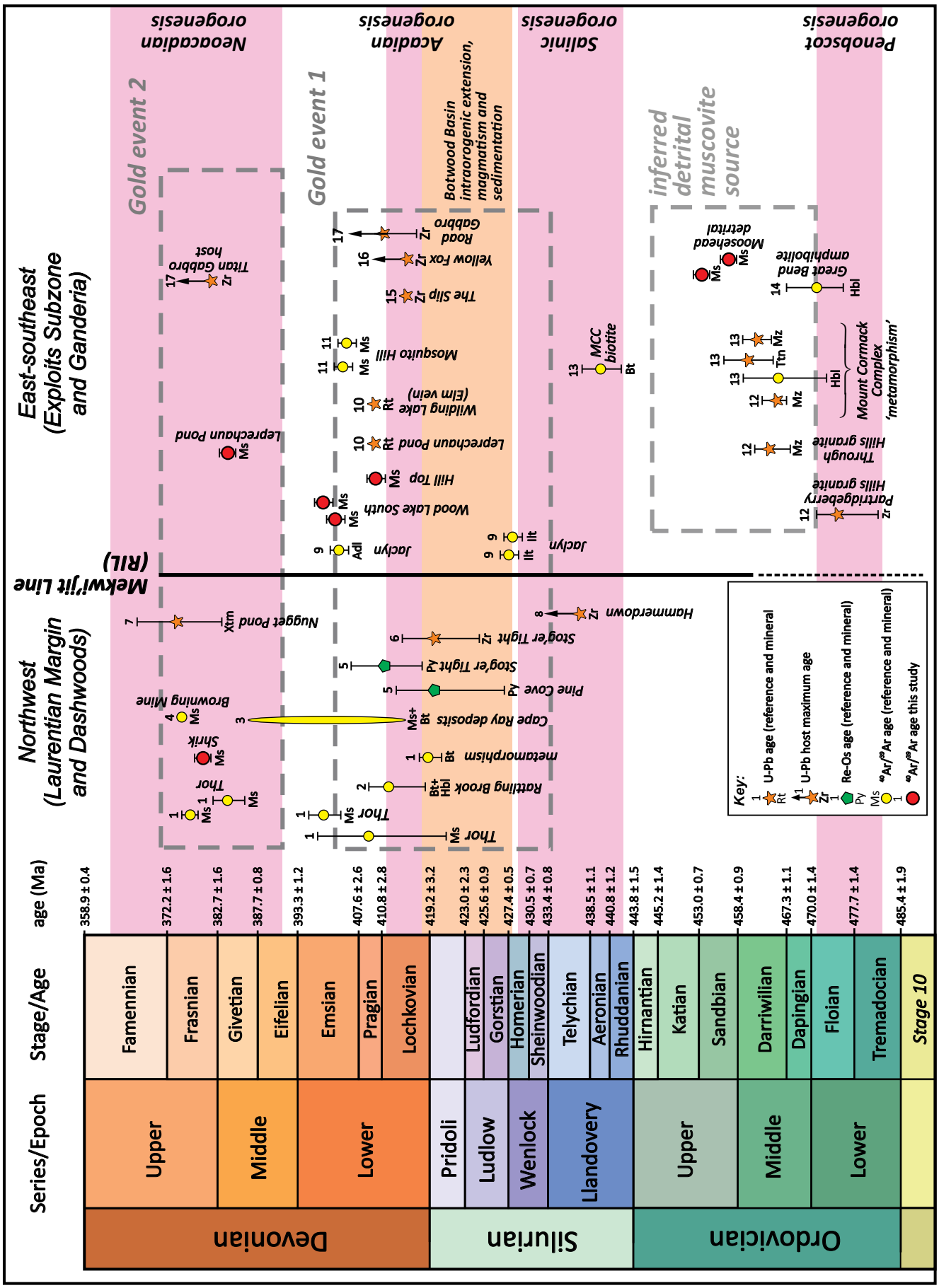

Figure 12. Diagram summarizing geochronological constraints on gold mineralized zones of central and western Newfoundland. Timescale from the International Commission on Stratigraphy stratigraphic chart (Cohen *et al* 2013: updated 2021). Also outlined are the approximate estimates for the orogenic events of the Newfoundland Appalachians (e.g., van Staal and Barr 2012). The orogenic-style mineralization occurs in two broad intervals, one in the latest Silurian to Early Devonian and a second in the Middle to Late Devonian. The latter may be synchronous with, and immediately postdate accretion of the Meguma terrane. Data sources: 1- Minnett et al (2012); 2- Kerr and van Breemen (2007); 3- Dubé *et al* (1996); 4- Sandeman and Dunning (2016); 5- Kerr and Selby (2012); 6- Ramezani *et al* (2002); 7- Sangster *et al* (2008); 8- Ritcey *et al* (1995); 9- Sandeman (2014d); 10- Honsberger *et al* (2022); 11- Sandeman *et al* (2013); 12- Colman-Sadd *et al* (1992); 13- Valverde-Vaquero *et al* (2003); 14- Sandeman and Dickson (2019); 15- Sandeman *et al* (2017); 16- Sandeman and Spurrell (2020); 17- McNicoll *et al* (2006).

Silurian to Middle–Upper Devonian and define two gold-forming intervals broadly between ca. 433 and 405 Ma and ca. 390 and 372 Ma. Spatiotemporal coincidence of orogenesis, metamorphism, magmatism and precious metal mineralization occurs across much of the Laurentian margin, Dashwoods terrane, the western Exploits Subzone and selected parts of the eastern Exploits Subzone. The oldest orogenic gold deposits occur in the west along the Laurentian margin and eastern Dashwoods terrane and are associated with the terminal stages of the Middle to Late Silurian Salinic orogenic cycle (ca. 435–427 Ma: e.g., van Staal and Barr 2012). Moreover, regional magmatic, sedimentary, metamorphic, and structural events indicate that although terrane accretion progressed oceanward (present-day east) throughout the Paleozoic (e.g., van Staal *et al* 2014), earlier accreted terranes were affected by mineralizing events related to subsequent accretion of outboard terranes (e.g., Honsberger *et al* 2022a). Thus, mineralized zones in central and western Newfoundland yield Middle–Late Silurian to Middle Devonian ages that post-date accretion of the encompassing terrane. For example, accretion of Dashwoods to the Laurentian margin took place in the Ordovician (Waldron and van Staal 2001), but gold mineralization at White Bay (Humber Zone, Fig. 1) is Late Silurian to Early or Middle Devonian (Fig. 12). Furthermore, ca. 410 Ma orogenic gold mineralization along the Victoria Lake–Valentine Lake fault corridor post-dates ca. 435 Ma accretion of the composite Gander Zone/Exploits Subzone (Ganderia) to the Dashwoods terrane and composite Laurentia (e.g., Honsberger *et al* 2022a). These relationships indicate that other tectonic processes in addition to accretion, such as oroclinal bends and orogen-parallel along strike temporal variations in the kinematics of orogenic accommodation, were critical to generating the orogenic gold-mineralized faults in central and western Newfoundland, as is presumed elsewhere along the Iapetan suture zone of the Appalachian mountain belt (Romer and Kroner 2018).

CONCLUSIONS

1. New $^{40}Ar/^{39}Ar$ geochronological constraints across central and western Newfoundland are consistent with two distinct intervals of orogenic gold mineralization between ca. 433 and 405 Ma and ca. 390 and 372 Ma.

2. The late Silurian–Early Devonian event includes muscovite growth/resetting intervals for gold-bearing zones of the Laurentian Margin, Dashwoods terrane, western Exploits subzone and along the Meelpaeg–Exploits subzones boundary, whereas the younger Devonian interval includes muscovite from gold-bearing zones across the Laurentian Margin, Dashwoods terrane, Exploits Subzone, and Gander Zone.

3. $^{40}Ar/^{39}Ar$ plateau ages for detrital muscovite from Wigwam Formation sandstone at the Moosehead prospect (ca. 457.3 ± 1.2 to 453.5 ± 1.1 Ma) suggest the Mount Cormack Complex is an erosional source for the sedimentary units of

the Botwood Basin.

4. Detailed investigations of quartz vein and alteration mineral parageneses, their relationships to gold deposition and systematic geochronological investigations of a number of different mineral species at select auriferous zones is necessary to better constrain the timing of gold mineralization in central and western Newfoundland.

ACKNOWLEDGEMENTS

H. Sandeman wishes to acknowledge the capable field assistance of Matthew Minnett, Jonathon Hull and Kendra Power along with the staff of the Geological Survey of Newfoundland and Labrador for making the research happen smoothly. Dr. Doug Archibald (formerly of Queen's University) provided much early technical assistance with the $^{40}Ar/^{39}Ar$ geochronology. Jeremy Powell and two anonymous reviewers provided constructive comments. This is Natural Resources Canada contribution number 20220066.

REFERENCES

Barr, S. M., Dehler, S. A., and Zsámboki, L. 2014. Connecting Cape Breton Island and Newfoundland, Canada: geophysical modeling of pre-Carboniferous 'basement' rocks in the Cabot Strait area. Geoscience Canada, 41, pp. 186–206. https://doi.org/10.12789/geocanj.2014.41.041

Betz, F.J. 1948. Geology and mineral deposits of southern White Bay. Newfoundland Geological Survey Bulletin, 24, 26 p.

Blackwood, R.F. and Green, L. 1983. Great Gull Lake, Fortune Bay District, Newfoundland. Government of Newfoundland and Labrador, Department of Mines and Energy, Mineral Development Division, Map 82-071, scale 1:50 000.

Blackwood, R.F. and Kennedy, M.J. 1975. The Dover Fault: western boundary of the Avalon Zone in northeastern Newfoundland. Canadian Journal of Earth Sciences, 12, pp. 320–325. https://doi.org/10.1139/e75-027

Churchill, R.A., Wilton, D.H.C., and Evans, D.T.W. 1993. Geology, alteration assemblages and geochemistry of the Duder Lake Gold showings, northeastern Newfoundland. *In* Current Research, Government of Newfoundland and Labrador, Department of Mines and Energy, Geological Survey Branch, Report 93-01, pp. 317–333.

Clark, D. 1999. First, third and fifth year assessment report on geophysical and diamond drilling exploration for licence 4821 on claim block 8377 and claims 17325 and 17327 in the Bishops Falls area, 3 reports. Newfoundland and Labrador Geological Survey, Assessment File NFLD/2928, 170 p.

Cohen, K.M., Finney, S.C., Gibbard, P.L., and Fan, J.X. 2013. Updated 2021: The ICS International Chronostratigraphic Chart. Episodes, 36, pp. 199–204. https://doi.org/10.18814/epiiugs/2013/v36i3/002

Colman-Sadd, S., Hayes, J.P., and Knight, I. 1990. Geology of the Island of Newfoundland. Government of Newfoundland and Labrador, Department of Mines and Energy, Geological Survey Branch, Map 90-01, scale: 1:1 000 000.

Colman-Sadd, S.P., Dunning, G.R., and Dec, T. 1992. Dunnage–Gander relationships and Ordovician orogeny in central Newfoundland: a sediment provenance and U/Pb age study. American Journal of Science, 292, pp. 317–355. https://doi.org/10.2475/ajs.292.5.317

Dalrymple, G.B., Alexander, Jr., E.C., Lanphere, M.A., and Kraker, G.P. 1981. Irradiation of samples for $^{40}Ar/^{39}Ar$ dating using the Geological Survey TRIGA Reactor. U.S. Geological Survey, Professional Paper 1176, 55 p. https://doi.org/10.3133/pp1176

Dickson, W.L., O'Brien, B.H., and Colman-Sadd, S.P. 2000. Geology of the Botwood map area [NTS 2E/3], central Newfoundland. Government of Newfoundland and Labrador, Department of Mines and Energy, Geological Survey, Open File 2E/03/1067 Version 2.0, map 2000-11, scale 1:50 000.

Dubé, B. and Lauzière, K. 1997. Gold metallogeny of the Cape Ray fault zone, southwest Newfoundland. Geological Survey of Canada, Bulletin 508, 90 p. https://doi.org/10.4095/209256

Dubé, B., Lauzière, K., and Poulsen, H.K. 1993, The Deer Cove deposit: an example of 'thrust' related breccia-vein type gold mineralization in the Baie Verte Peninsula, Newfoundland: *In* Current Research, Part D, Geological Survey of Canada, Paper 93-1D, p. 1–10. https://doi.org/10.4095/134265

Dubé, B., Dunning, G., and Lauzière, K. 1995. Geology of the Hope Brook Mine, Newfoundland, Canada: A preserved Late Proterozoic high-sulfidation epithermal gold deposit and its implications for exploration. Economic Geology, 93, pp 405–436. https://doi.org/10.2113/gsecongeo.93.4.405

Dube, B., Dunning, G.R., Lauziere, K., and Roddick, J.C. 1996. New insights into the Appalachian Orogen from geology and geochronology along the Cape Ray fault zone, southwest Newfoundland. Geological Society of America Bulletin, 108, pp. 101–116. https://doi.org/10.1130/0016-7606(1996)108<0101:NIITAO>2.3.CO;2

Dunning, G.R. 1987. U/Pb geochronology of the Coney Head Complex, Newfoundland. Canadian Journal of Earth Sciences, 24, pp. 1072–1075. https://doi.org/10.1139/e87-104

Dunning, G.R., O'Brien, S.J., Colman-Sadd, S.P., Blackwood, R.F., Dickson, W.L., O'Neill, P.P., and Krogh, T.E. 1990. Silurian Orogeny in the Newfoundland Appalachians. Journal of Geology, 98, pp. 895–913. https://doi.org/10.1086/629460

English, M., Sparrow, B., Walsh, M., and Copeland, D.A. 2017. First and seventh year assessment report on data compilation and interpretation for licences 22503M, 23772M, 23774M, 24522M, 24523M and 24524M on claims in the White Bay area, Newfoundland and Labrador. Newfoundland and Labrador Geological Survey, As-

sessment File 12H/15/2320, 31 p.

Evans, D.T.W. 1991. Gold metallogeny, eastern Dunnage Zone, central Newfoundland. *In* Current Research, Government of Newfoundland and Labrador, Department of Mines and Energy, Geological Survey Branch, Report 91-01, pp. 301–318.

Evans, D.T.W. 1993, Gold mineralization in the eastern Dunnage Zone, central Newfoundland. *In* Current Research, Government of Newfoundland and Labrador, Department of Mines and Energy, Geological Survey Branch, Report 93-01, pp. 339–349.

Evans, D.T.W. 1999. Epigenetic gold mineralization, Baie Verte Peninsula, Newfoundland. *In* Current Research, Government of Newfoundland and Labrador, Department of Mines and Energy, Geological Survey, Report 99-01, pp. 163–182.

Evans, D.T.W. 2004. Epigenetic gold occurrences, Baie Verte Peninsula, [NTS 12H/09, 16 and 12I/01], Newfoundland. Government of Newfoundland and Labrador, Department of Natural Resources, Geological Survey, Mineral Resource Report 11, 176 p.

Evans, D.T.W. and Kean, B.F. 2002. The Victoria Lake Supergroup, central Newfoundland – its definition, setting and volcanogenic massive sulphide mineralization. Newfoundland and Labrador Department of Natural Resources, Geological Survey Open File NFLD/2790, 80 p.

Froude, T. 2019. Sokoman Iron Acquires a 100% Interest in Moosehead Gold Project. Sokoman Iron URL: <https://sokomanmineralscorp.com/2019/02/01/sokoman-iron-acquires-a-100-interest-in-moosehead-gold-project/> Press release, February 1, 2019.

Froude, T. 2021. Sokoman reports first barge-based drill results Moosehead Gold Project, Central Newoundland; Phase 6 drill Program doubled to 100,000 m. Sokoman Minerals Corp. URL: <https://sokomanmineralscorp.com/2021/11/10/sokoman-reports-first-barge-based-drill-results-moosehead-gold-project-central-newfoundland/> Press release November 10, 2021.

Galley, A.G., Hannington, M.D., and Jonasson, I.R. 2007. Volcanogenic massive sulphide deposits. *In* Mineral Deposits of Canada: A Synthesis of Major Deposit-Types, District Metallogeny, the Evolution of Geological Provinces, and Exploration Methods. *Edited by* W.D. Goodfellow. Geological Association of Canada, Mineral Deposits Division, Special Publication, 5, pp. 141–161.

Geoscience Atlas. 2022. Newfoundland and Labrador Department of Industry, Energy and Technology, Geological Survey. URL <https://geoatlas.gov.nl.ca/Default.htm>, 9 May 2022.

Heyl, G.R. 1937. The geology of the Sop's Arm area, White Bay, Newfoundland. Newfoundland Department of Natural Resources, Geology Section, Bulletin 8, 42 p.

Honsberger, I.W., Bleeker, W., Kamo, S.L., Evans, D.T.W., and Sandeman, H.A.I. 2019a. A Neoproterozoic age for granodiorite underlying Rogerson Lake Conglomerate; Confirmed Ganderian basement in the Wilding Lake area, central Newfoundland gold district. Government of Newfoundland and Labrador, Department of Natural Resources, Geological Survey, St. John's, Open File 12A/07/1774, 12 p.

Honsberger, I.W., Bleeker, W., Sandeman, H.A.I., and Evans, D.T.W. 2019b. Structural geology of a gold-bearing quartz vein system, Wilding Lake region, central Newfoundland. In Current Research, Newfoundland and Labrador Department of Natural Resources Geological Survey, Report 19-1, pp. 23–38.

Honsberger, I.W., Bleeker, W., Sandeman, H.A.I, Evans, D.T.W., and Kamo, S.L. 2020a. The Wilding Lake gold prospect, central Newfoundland: a lithological and structural synthesis. Geological Survey of Canada, Open File 8658, 2 sheets. https://doi.org/10.4095/321490

Honsberger, I.W., Bleeker, W., Sandeman, H.A.I., Evans, D.T.W., and Kamo, S.L. 2020b. Vein-hosted gold mineralization in the Wilding Lake area, central Newfoundland: Structural geology and vein evolution. *In* Targeted Geoscience Initiative 5: Contributions to the Understanding of Canadian Gold Systems. *Edited by* P. Mercier-Langevin, C.J.M. Lawley, and S. Castonguay. Geological Survey of Canada, Open File 8712, pp. 179–192. https://doi.org/10.4095/326020

Honsberger, I.W. Bleeker, W., Kamo, S.L., Sandeman, H.A.I., Evans, D.T.W., Rogers, N., van Staal, C.R., and Dunning, G.R. 2022a. Latest Silurian syntectonic sedimentation and magmatism and Early Devonian orogenic gold mineralization, central Newfoundland Appalachians, Canada: Setting, structure, lithogeochemistry, and high-precision U–Pb geochronology. Geological Society of America Bulletin. https://doi.org/10.1130/GSAB.S.18858221.v1

Honsberger, I.W., Wouter, B., Kamo, S.L., Sutcliffe, C.N., and Sandeman, H.A.I. 2022b. U–Pb geochronology of Late Silurian (Wenlock to Pridoli) volcanic and sedimentary rocks, central Newfoundland Appalachians: targeting the timing of transient extension as a prelude to Devonian orogenic gold mineralization. Atlantic Geoscience, 58, pp. 215–237. https://doi.org/10.4138/atlgeo.2022.009

Jourdan, F., Verati, C., and Féraud, G. 2006. Intercalibration of the Hb3gr $^{40}Ar/^{39}Ar$ dating standard. Chemical Geology, 231, pp. 77–189. https://doi.org/10.1016/j.chemgeo.2006.01.027

Kean, B.F. and Jayasinghe, N.R. 1980. Geology of the Lake Ambrose [12A/10]-Noel Pauls Brook [12A/9] map areas, central Newfoundland. Government of Newfoundland and Labrador, Department of Mines and Energy, Mineral Development Division, Report 80-02, 1980, 34 p, 2 maps, scale 1: 50 000.

Kerr, A. 2006a. Silurian rocks of the Sops Arm group, western Newfoundland: some new food for future digestion. In Current Research. Government of Newfoundland and Labrador, Department of Natural Resources, Geological Survey, Report 06-1, pages 91–117.

Kerr, A. 2006b. Mesothermal gold mineralization in the Silurian Sops Arm group, western Newfoundland: a descriptive and historical overview. In Current Research. Government of Newfoundland and Labrador, Depart-

ment of Natural Resources, Geological Survey, Report 06-1, pages 61–90.

Kerr, A. and Selby, D. 2012. The timing of epigenetic gold mineralization on the Baie Verte Peninsula, Newfoundland, Canada: new evidence from Re–Os pyrite geochronology. Mineralium Deposita, 47, pp. 325–337. https://doi.org/10.1007/s00126-011-0375-2

Kerr, A. and van Breemen, O. 2007. The timing of gold mineralization in White Bay, western Newfoundland: Evidence from $^{40}Ar/^{39}Ar$ studies of mafic dykes that predate and postdate mineralization. Atlantic Geology, 43, pp. 148–162. https://doi.org/10.4138/5623

Lincoln, N., Farmer, R., Eccles, R., and Deering, P. 2018. NI 43-101 Technical Report preliminary economic assessment of the Valentine Lake gold project Newfoundland, NL, Canada. Prepared by Lycopodium Minerals Canada Ltd in accordance with the requirements of National Instrument 43-101, "Standards of Disclosure for Mineral Project", of the Canadian Securities Administrators Qualified Persons. Lycopodium Minerals Canada, 5060 Spectrum Way, Suite 400, Mississauga, Ontario L4W 5N5.

Lock, B.E. 1969. Paleozoic Wrench Faults in Canadian Appalachians: Chapter 55: Late Orogenic Stratigraphy and Structure: Discussion. *In* North Atlantic: Geology and Continental Drift, AAPG Memoir M 12, 789–790.

Ludwig, K.R. 2012. Isoplot 4.15: A Geochronological Toolkit for Microsoft Excel: Berkeley Geochronological Center. URL <http://www.bgc.org/isoplot_etc/isoplot/Isoplot4_15files.zip> 19 May 2022.

Magna Terra Minerals 2022. Maps and Figures -Great Northern. URL <https://www.magnaterraminerals.com/MTT/great_northern_and_viking_projects/4932>, 19 May 2022.

McDougall, I. and Harrison, T.M. 1988. Geochronology and thermochronology by the $^{40}Ar/^{39}Ar$ method. Oxford Monographs on Geology and Geophysics #9, Oxford, United Kingdom, Oxford University Press, 212 p.

McNicol, V., Squires, G.C., Wardle, R.J., Dunning, G.R., and O'Brien, B.H. 2006. U-Pb geochronological evidence for Devonian deformation and gold mineralization in the eastern Dunnage Zone, Newfoundland. In Current Research. Newfoundland and Labrador Department of Natural Resources, Geological Survey, Report 06-1, pp. 43–60.

Miller, H.G. and Weir, C. 1982. The northwest portion of the Gander Zone — a geophysical interpretation. Canadian Journal of Earth Sciences, 19, pp. 1371–1381. https://doi.org/10.1139/e82-119

Minnett, M., Sandeman, H., and Wilton, D. 2012. Geochemistry of the host rocks and timing of gold-electrum mineralization at the Viking Property, Newfoundland. In Current Research, Newfoundland Department of Mines and Energy Geological Survey, Report 12-1, pp. 61–84.

Morgan, J. 2016. First year assessment report on geological, geochemical and trenching exploration for licences 22789M-22800M and 23582M-23587M on claims in the Bishops Falls area, central Newfoundland. Newfoundland and Labrador Geological Survey, Assessment File NFLD/3360, 317 p.

Myllyaho, J. 2013. First and second year assessment report on prospecting and geochemical and trenching exploration for licences 19543M, 19546M, 19902M, 20193M, 20197M, 20382M and 20417M on claims in the Jacksons Arm area, White Bay, Newfoundland. Newfoundland and Labrador Geological Survey, Assessment File 12H/15/2091, 192 s.

O'Brien, B.H. 2003. Geology of the central Notre Dame Bay region, northeastern Newfoundland. Government of Newfoundland and Labrador, Department of Mines and Energy, Geological Survey, Report 3-03, 170 p.

O'Brien, S.J., Dunning, G.R., Dubé, B., O'Driscoll, C.F., Sparkes, B., Israel, S., and Ketchum, J. 2001. New insights into the Neoproterozoic geology of the central Avalon Peninsula (parts of NTS map areas 1N/6, 1N/7 and 1N/3), eastern Newfoundland. *In* Current Research, Government of Newfoundland and Labrador, Department of Mines and Energy, Geological Survey, Report 1-1, pp. 169–189.

O'Neill, P. and Blackwood, F. 1989. A proposal for revised stratigraphic nomenclature of the Gander and Davidsville groups and the Gander River Ultrabasic Belt, of northeastern Newfoundland. *In* Current Research. Government of Newfoundland and Labrador, Department of Mines, Geological Survey, Report 89-01, pp. 127–130.

O'Neill, P.P. and Colman-Sadd, S.P. 1993. Geology of the eastern Gander (NTS 2D/15) and western Gambo (NTS 2D/16) map areas, Newfoundland. Government of Newfoundland and Labrador, Department of Mines and Energy, Geological Survey Branch, Report 93-2, 53 p.

O'Neill, P. and Lux, D. 1989. Tectonothermal history and $^{40}Ar–^{39}Ar$ geochronology of the northeastern Gander Zone, Weirs Pond area (2E/1). *In* Current Research. Government of Newfoundland and Labrador, Department of Mines, Geological Survey, Report 89-1, pp. 131–139.

Onstott, T.C., Phillips, D., and Pringle-Goodell, L. 1991. Laser microprobe measurement of chlorine and argon zonation in biotite. Chemical Geology, 90, pp. 145–168. https://doi.org/10.1016/0009-2541(91)90040-X

Piercey, S.J. 2007. Volcanogenic massive sulphide (VMS) deposits of the Newfoundland Appalachians: An overview of their setting, classification, grade-tonnage data, and unresolved questions. *In* Current Research, Newfoundland and Labrador Department of Natural Resources. Geological Survey, Report 07-1, pp. 169–178.

Pilote, J-L., Piercey, S., and Mercier-Langevin, P. 2020. Evolution of the subseafloor hydrothermal system associated with the Ming VMS deposit, Newfoundland Appalachians, and its controls on base and precious metal distribution. Mineralium Deposita, 55. https://doi.org/10.1007/s00126-019-00899-z

Poulsen, K.H., Robert, F., and Dubé, B. 2000. Geological classification of Canadian gold deposits: Geological Survey of Canada, Bulletin 540, 106 p. https://doi.org/10.4095/211094

Ramezani, J., Dunning, G.R., and Wilson, M.R. 2002. Geologic setting, geochemistry of alteration, and U-Pb age of hydrothermal zircon from the Silurian Stog'er Tight gold prospect, Newfoundland Appalachians, Canada. Exploration and Mining Geology, 9, pp.171–188. https://doi.org/10.2113/0090171

Reid, W. and Myllyaho, J. 2012. First year assessment report on prospecting, geochemical and trenching exploration for licences 18403M, 19525M, 19530M and 19542M on claims in the Jacksons Arm area, White Bay, Newfoundland. Newfoundland and Labrador Geological Survey, Assessment File 12H/15/2066, 84 p.

Ritcey, D.H., Wilson, M.R., and Dunning, G.R. 1995. Gold mineralization in the Paleozoic Appalachian Orogen: Constraints from geologic, U-Pb and stable isotope studies of the Hammerdown prospect, Newfoundland. Economic Geology, 90, pp. 1955–1965. https://doi.org/10.2113/gsecongeo.90.7.1955

Roddick, J.C. 1983. High precision intercalibration of $^{40}Ar/^{39}Ar$ standards. Geochimica et Cosmochimica Acta, 47, pp. 887-898. https://doi.org/10.1016/0016-7037(83)90154-0

Rogers, N. and van Staal, C. 2002. Toward a Victoria Lake Supergroup: a provisional stratigraphic revision of the Red Indian to Victoria lakes area, central Newfoundland. *In* Current Research, Government of Newfoundland and Labrador, Department of Mines and Energy, Geological Survey, Report 2-1, pages 185–195.

Rogers, N., van Staal, C.R., McNicoll, V.J., Pollock, J., Zagorevski, A., and Whalen, J. 2006. Neoproterozoic and Cambrian arc magmatism along the eastern margin of the Victoria Lake Supergroup: A remnant of Ganderian basement in central Newfoundland? Precambrian Research, 147, pp. 320–341. https://doi.org/10.1016/j.precamres.2006.01.025

Romer, R.L. and Kroner, U. 2018, Paleozoic gold in the Appalachians and Variscides. Ore Geology Reviews, 92, pp. 475–505. https://doi.org/10.1016/j.oregeorev.2017.11.021

Sandeman, H.A.I. 2014a. South Wood Lake (Staghorn) gold prospect lithogeochemical database (map area NTS 12A/04). Government of Newfoundland and Labrador, Department of Natural Resources, Geological Survey, Open File 012A/04/1563, 12 p.

Sandeman, H.A.I. 2014b. The timing of mineralization at the Jaclyn zone gold deposit, central Newfoundland: constraints from $^{40}Ar/^{39}Ar$ studies of white mica alteration adjacent to auriferous quartz veins. *In* Current Research, Newfoundland and Labrador Department of Natural Resources Geological Survey, Report 14-1, pp. 63–77.

Sandeman, H.A.I. and Dickson, W.L. 2019. An Ordovician, $^{40}Ar/^{39}Ar$ step-heating age for fabric-forming hornblende in amphibolite, the Great Bend Complex, central Newfoundland (NTS 2D/5). *In* Current Research, Newfoundland and Labrador Department of Natural Resources Geological Survey, Report 19-1, pp. 85–96.

Sandeman, H.A.I. and Dunning, G.R. 2016. Preliminary U–Pb geochronology and petrochemistry of volcanic rocks and felsic dykes of the Silurian Sops Arm Group, White Bay, western Newfoundland (NTS 2H/10 and 15). *In* Current Research, Newfoundland and Labrador Department of Natural Resources Geological Survey, Report 16-1, pp. 39–69.

Sandeman H.A.I. and Spurrell, C. 2020. The Yellow Fox showing: monzogranite-hosted, fracture related antimony–silver–gold mineralization near the eastern margin of the Mount Peyton Intrusive Suite, central Newfoundland (NTS map area 2d/14). *In* Current Research, Newfoundland and Labrador Department of Natural Resources Geological Survey, Report 20-1, pp. 179–205.

Sandeman, H.A.I., Wilton, D.H.C., Conliffe, J., Froude, T. and O'Driscoll, J.M. 2013. Geological setting, geochronological constraints and the nature of mineralization at the Mosquito Hill (Huxter Lane) gold deposit, central Newfoundland. In Current Research, Newfoundland Department of Mines and Energy Geological Survey, Report 13-1, pp. 167–188.

Sandeman, H.A., Hull, J.R., and Wilton, D.H.C. 2014. Geology, lithogeochemistry and mineralization at the South Wood Lake gold prospect (Staghorn property), Exploits–Meelpaeg subzones boundary, western-central Newfoundland. *In* Current Research, Newfoundland and Labrador Department of Natural Resources Geological Survey, Report 14-1, pp. 79–98.

Sandeman, H.A.I., Dunning, G.R., McCullough, C.K., and Peddle, C. 2017. U–Pb geochronology, petrogenetic relationships and intrusion-related precious-metal mineralization in the northern Mount Peyton intrusive suite: implications for the origin of the Mount Peyton Trend, central Newfoundland (NTS 2D/04). *In* Current Research, Newfoundland and Labrador Department of Natural Resources Geological Survey, Report 17-1, pages 189–217.

Sangster, A.L., Douma, S.L., and Lavigne, L. 2008. Base metal and gold deposits of the Betts Cove Complex, Baie Verte Peninsula, Newfoundland. *In* Mineral Deposits of Canada: A Synthesis of Major Deposit Types, District Metallogeny, the Evolution of Geological Provinces and Exploration Methods. *Edited by* W.D. Goodfellow. Geological Survey of Canada, Mineral Deposits Division, Special Volume 5, pp. 703–723.

Schaen, A.J., and 34 others. 2021. Interpreting and reporting $^{40}Ar/^{39}Ar$ geochronologic data. Geological Society of America Bulletin, 133, pp. 461–487. https://doi.org/10.1130/B35560.1

Sparkes, G.W. and Dunning, G.R. 2014. Late Neoproterozoic epithermal alteration and mineralization in the western Avalon Zone: A summary of mineralogical investigations

Sparkes, G.W., O'Brien, S.J., Dunning, G.R., and Dubé, B. 2005. U-Pb geochronological constraints on the timing of magmatism, epithermal alteration and low-sulphidation gold mineralization, eastern Avalon Zone, Newfoundland. *In* Current Research, Government of Newfoundland and Labrador, Department of Natural Resources, Geological Survey, Report 5-1, pp.115–130.

and new U/Pb geochronological results. *In* Current Research, Government of Newfoundland and Labrador, Department of Natural Resources, Geological Survey, Report 14-1, pp. 99–128.

Sparkes, G.W., Ferguson, S.A., Layne, G.D., Dunning, G.R., O'Brien, S.J., and Langille, A. 2016. The nature and timing of Neoproterozoic high-sulphidation gold mineralization from the Newfoundland Avalon Zone: Insights from new U–Pb ages, ore petrography and spectral data from the Hickey's Pond prospect. *In* Current Research, Government of Newfoundland and Labrador, Department of Natural Resources, Geological Survey, Report 16-1, pp. 91–116.

Spell T.L. and McDougall, I. 2003. Characterization and calibration of $^{40}Ar/^{39}Ar$ dating standards. Chemical Geology, 198, pp. 189–211. https://doi.org/10.1016/S0009-2541(03)00005-6

Steiger, R.H. and Jäger, E. 1977. Subcommission on geochronology: Convention on the use of decay constants in geo- and cosmochronology. Earth and Planetary Science Letters, 36, pp. 359–362. https://doi.org/10.1016/0012-821X(77)90060-7

Tuach, J. 1987. Mineralized environments, metallogenesis, and the Doucers Valley Fault Complex, western White Bay: a philosophy for gold exploration in Newfoundland. *In* Current Research, Government of Newfoundland and Labrador, Department of Mines and Energy, Mineral Development Division, Report 87-01, pp. 129–144.

Tuach, J., Dean, P.L., Swinden, H.S., O'Driscoll, C.F., Kean, B.F., and Evans, D.T.W. 1988. Gold mineralization in Newfoundland: a 1988 review. *In* Current Research, Government of Newfoundland and Labrador, Department of Mines, Mineral Development Division, Report 88-01, pp. 279–306.

Valverde-Vaquero, P. and van Staal, C. 2001. Relationships between the Dunnage-Gander zones in the Victoria Lake-Peter Strides Pond area. *In* Current Research, Government of Newfoundland and Labrador, Department of Mines and Energy, Geological Survey, Report 1-1, pp. 159–167.

Valverde-Vaquero, P. and van Staal, C. 2002. Geology and magnetic anomalies of the Exploits-Meelpaeg boundary zone in the Victoria Lake area (central Newfoundland): regional implications. *In* Current Research, Government of Newfoundland and Labrador, Department of Mines and Energy, Geological Survey, Report 2-1, pp. 197–209.

Valverde-Vaquero, P., van Staal, C.R., van der Velden, A., and Dunning, G.R. 2003. Acadian orogenesis and high-grade metamorphism in the Central Mobile Belt of central Newfoundland. Geological Society of America, Northeastern Section Annual Meeting, Abstracts with Programs, 35(2), 23 p.

Valverde-Vaquero, P., van Staal, C.R., McNicoll, V., and Dunning, G.R. 2006. Mid–Late Ordovician magmatism and metamorphism along the Gander margin in central Newfoundland. Journal of the Geological Society, London, 163, pp. 347–362. https://doi.org/10.1144/0016-764904-130

van der Velden, A.J., van Staal, C.R., and Cook, F.A. 2004. Crustal structure, fossil subduction, and the tectonic evolution of the Newfoundland Appalachians: Evidence from a reprocessed seismic reflection survey. Geological Society of America Bulletin, 116, pp. 1485–1498. https://doi.org/10.1130/B25518.1

van Egmond, R. 2004. Second, third, fifth and sixth year assessment report on geological, geochemical and geophysical exploration for licences 6333M, 8378M, 8490M, 8516M and 9162M on claims in the Wood Lake area, southwestern Newfoundland, 2 reports. Newfoundland and Labrador Geological Survey, Assessment File 12A/04/1135, 133 p.

van Egmond, R. and Cox, E. 2005. Third year supplementary and seventh year assessment report on diamond drilling exploration for licences 6333M and 10608M on claims in the Wood Lake area, central Newfoundland. Newfoundland and Labrador Geological Survey, Assessment File 12A/04/1274, 226 p.

van Staal, C. and Barr, S.M. 2012. Lithospheric architecture and tectonic evolution of the Canadian Appalachians and associated Atlantic margin. *In* Tectonic Styles in Canada: the Lithoprobe Perspective. *Edited by* J.A. Percival, F.A. Cook, and R.M. Clowes. Geological Association of Canada, Special Paper, 49, pp. 41–95.

van Staal, C.R., Sullivan, R.W., and Whalen, J.B. 1996. Provenance and tectonic history of the Gander Margin in the Caledonian/Appalachian Orogen: Implications for the origin and assembly of Avalonia. *In* Avalonian and related Peri-Gondwanan terranes of the Circum-North Atlantic. Edited by R.D. Nance and M.D. Thompson. Geological Society of America Special Paper, 304, pp. 347–367. https://doi.org/10.1130/0-8137-2304-3.347

van Staal, C.R., Valverde-Vaquero, P., Zagorevski, A., Pehrsson, S., Boutsma, S., and van Noorden, M.J. 2005a. Geology, King George IV Lake, Newfoundland and Labrador. Geological Survey of Canada, Open File 1665, scale 1:50 000. https://doi.org/10.4095/221286

van Staal, C.R., Valverde-Vaquero, P., Zagorevski, A., Rogers, N., Lissenberg, C.J., and McNicoll, V.J. 2005b. Geology, Victoria Lake, Newfoundland and Labrador; Geological Survey of Canada, Open File 1667, scale 1:50 000. https://doi.org/10.4095/221287

van Staal, C.R., Whalen, J.B., Valverde-Vaquero, P., Zagorevski, A., and Rogers, N. 2009. Pre-Carboniferous, episodic accretion-related, orogenesis along the Laurentian margin of the northern Appalachians. Geological Society, London, Special Publications, 327, pp. 271–316. https://doi.org/10.1144/SP327.13

van Staal, C. R., Zagorevski, A., McNicoll, V. J., and Rogers, N. 2014. Time-transgressive Salinic and Acadian orogenesis, magmatism and Old Red Sandstone sedimentation in Newfoundland. Geoscience Canada, 41(2), pp. 138–164. https://doi.org/10.12789/geocanj.2014.41.031

Vry, J.K. and Baker, J.A. 2006. LA-MC-ICPMS Pb–Pb dating of rutile from slowly cooled granulites: confirmation of

the high closure temperature for Pb diffusion in rutile. Geochimica et Cosmochimica Acta, 70, pp. 1807–1820. https://doi.org/10.1016/j.gca.2005.12.006

Waldron, J. W.F. and van Staal, C. R. 2001. Taconian orogeny and the accretion of the Dashwoods block: A peri-Laurentian microcontinent in the Iapetus Ocean. Geology 29, 811–814. https://doi.org/10.1130/0091-7613(2001)029<0811:TOATAO>2.0.CO;2

White, S.E. and Waldron, J.W.F. 2022, Along-strike variations in the deformed Laurentian margin in the Northern Appalachians: Role of inherited margin geometry and colliding arcs. Earth Science Reviews, 226. https://doi.org/10.1016/j.earscirev.2022.103931

Whitney, D.L. and Evans, B.W. 2010. Abbreviations for names of rock-forming minerals. American Mineralogist, 95, 185–187. https://doi.org/10.2138/am.2010.3371

Williams, H. 1969. Stratigraphy of Botwood Map - Area, Northeastern Newfoundland. Geological Survey of Canada, Open File 113, 104 p. https://doi.org/10.4095/130357

Williams, H., Colman-Sadd, S.P., and Swinden, H.S. 1988. Tectonicstratigraphic subdivisions of central Newfoundland. *In* Current Research, Part B. Eastern and Atlantic Canada, Geological Survey of Canada, Paper 881B, pp. 91-98. https://doi.org/10.4095/122425

Willner, A.P., van Staal, C.R., Zagorevski, A., Glodnye, J., Romere, R.L., and Sudof, M. 2018, Tectonometamorphic evolution along the Iapetus suture zone in Newfoundland: Evidence for polyphase Salinic, Acadian and Neoacadian very low- to medium-grade metamorphism and deformation: Tectonophysics, 742–743, p. 137–167. https://doi.org/10.1016/j.tecto.2018.05.023

Wilson, M. and Evans, D.T.W. 1994. Epigenetic gold occurrences in the eastern Dunnage Zone, Newfoundland: preliminary stable-isotope results. *In* Current Research, Government of Newfoundland and Labrador, Department of Mines and Energy, Geological Survey Branch, Report 94-01, pp. 211–223.

Wonderly, P.F., and Neuman, R.B. 1984. The Indian Bay Formation: fossiliferous Early Ordovician volcanogenic rocks in the northern Gander Terrane, Newfoundland, and their regional significance. Canadian Journal of Earth Sciences, 21, pp. 525–532. https://doi.org/10.1139/e84-057

Ybarra, S. 2020. Lithogeochemistry and hydrothermal alteration of the Pine Cove orogenic gold deposit, Baie Verte Peninsula, Newfoundland, Canada. Unpublished M.Sc. thesis Memorial University of Newfoundland and Labrador, St. John's, Newfoundland and Labrador, 112 p.

Editorial responsibility: Mitchell Kerr

Atlantic Universities Geoscience Conference 2022

ABSTRACTS

October 27–29, 2022

72ND ANNUAL CONFERENCE HOSTED BY:
FLETCHER GEOLOGY CLUB, ACADIA UNIVERSITY
WOLFVILLE, NOVA SCOTIA

Abstracts from the Atlantic Universities Geoscience Conference (AUGC) are published annually in Atlantic Geoscience. Such publication provides a permanent record of the abstracts, and also focuses attention on the excellent quality of the oral presentations and posters at the conference and the interesting and varied geoscience topics that they cover. Although abstracts are modified and edited as necessary for clarity and to conform to Atlantic Geoscience format, the journal editors do not take responsibility for their content or quality.

THE EDITORS

ATLANTIC GEOSCIENCE 58, 291-302 (2022)
2564-2987|22|00291-302 $2.80|0
doi: 10.4138/atlgeo.2022.013

Groove casts? More like whose cast? What made these anomalous structures?

Jessica Beckwith, Mo Snyder, and John Waldron

Department of Earth and Environmental Science, Acadia University, Wolfville, Nova Scotia B4P 2R6, Canada <153914b@acadiau.ca>

The Meguma terrane is home to the metasandstone-rich Goldenville Group. This Cambrian unit contains many sedimentary structures including but not limited to flute casts, wave and current ripples, sand volcanoes, and large enigmatic groove casts. The origin of these large groove casts is currently unknown, but given the consistency and size of the grooves, it is speculated that they may have been formed from a biogenic source such as a large organism being dragged across the sediment surface. Analysis of the structures is made more complex because the rocks within the Goldenville Group have been deformed, causing structures within these rocks to be strained. Reversing strain is an important step in determining the possible origin of the large groove casts. One method to reverse strain is to examine sedimentary structures, such as equant sand volcanoes and circular and meandering trace fossils and determine an overall strain ratio and then apply an inverse strain value to the groove casts. A 3D model of the groove casts created using photogrammetry software will then be compared to various large objects or organisms that were present in the Cambrian to find a potential match for the groove casts. The results of this investigation have implications including the size and abundance of animals from the Cambrian in Nova Scotia. *[Poster presentation]*

Where's the carbon? Spatially mapping carbon on the seafloor

Catherine Brenan

Department of Earth and Environmental Sciences, Dalhousie University, Halifax, Nova Scotia B3H 4R2, Canada <ct477992@dal.ca>

Coastal sediments contain the largest stocks of organic carbon and play a vital role in influencing the carbon cycle. Protecting organic carbon hotspots is essential to mitigating climate change because development and bottom trawling can disturb the seafloor, driving the remineralization of organic carbon into carbon dioxide. Terrestrial carbon stocks are well studied and mapped, but our knowledge of standing stocks of marine sedimentary carbon and the role that it can play in minimizing the effects of climate change are poorly understood. One of the challenges in mapping the seafloor environment is the issue of characterizing spatial heterogeneity of different substrata, which is critical in estimating organic carbon standing stocks in the marine environment. In this study, we use high-resolution multibeam echosounder (MBES) data from the Eastern Shore Islands off Nova Scotia to predict the distribution of percent organic carbon in surface sediments. We applied benthic habitat mapping approaches, utilizing high-resolution continuous coverage environmental variables (bathymetry, backscatter, current velocity, bottom salinity, bottom temperature, ruggedness, slope, Euclidean distance) combined with subsea video and ground truthing to generate thematic maps of sediment types for the area. We then compared those to the measurements of organic carbon from the samples, which were spatially modelled using different methodologies to estimate organic carbon standing stocks in the area by substrate type. These high-resolution sedimentary organic carbon maps can help determine the best approach for using MBES surveys to map carbon and identify carbon hotspots, which are essential for seabed management and climate mitigation strategies. *[Oral presentation]*

Pebble provenance across a syn-tectonic braided fluvial to alluvial fan transition, Flatrock Cove Formation, Flatrock, Newfoundland

Juvani Bryce and Dave Lowe

Department of Earth Sciences, Memorial University of Newfoundland, St. John's Newfoundland and Labrador A1B 3X7, Canada <jobryce@mun.ca>

The Ediacaran Flatrock Cove Formation in the Avalon Zone, eastern Newfoundland, is composed of the Knobby Hill Member conformably overlain by the Piccos Brook Member. These units record syn-tectonic sedimentation and a change from a braided fluvial to alluvial fan environments during progressive folding and thrusting along the proximal margin of the Signal Hill Basin, coinciding with the Avalonian Orogeny (ca. 600–545 Ma). This project aims to constrain the provenance of clasts in conglomerates of the Knobby Hill and Piccos Brook members to identify changes in sources and sediment routing coinciding with Avalonian deformation in sediment hinterlands. Point counting of clasts in the field from the middle of the Knobby Hill Member upward through to the Piccos Brook Member reveals significant changes in clast compositions. In Knobby Hill, there is an upward change in igneous clast populations from angular black rhyolite, andesite, and granite, to a mainly subrounded to rounded weathered granite. Clasts in the Piccos Brook Member are dominated

by sandstone, mudstone, and siltstone. Based on these data, significant changes in clast hinterlands occurred throughout the Flatrock Cove Formation sedimentation, from mainly volcanic, to plutonic, to sedimentary. Fourteen representative igneous clasts were also selected for bulk major and trace element geochemistry, with a focus on high field strength elements (HFSE), rare earth elements (REE), and Y, which will be used to discriminate the petrogenesis of igneous source areas and provide more detail of the sequence of hinterland uplift and exhumation coinciding with Flatrock Cove Formation sedimentation. *[Oral presentation]*

Chemical characterization of melt inclusions in Blake River Volcanics of the Swayze area, Abitibi Greenstone Belt, Ontario, Canada

Aidan Buyers[1], Jacob Hanley[1], Kevin Neyedley[1], and Thomas Gemmell[2]

1. Mineral Exploration and Ore Fluids Laboratory, Department of Geology, Saint Mary's University, Halifax, Nova Scotia B3H 3C3, Canada <aidan.buyers97@gmail.com>
2. Earth Resources and Geoscience Mapping Section, Ontario Geological Survey, Mines and Minerals Division, Ministry of Mines, Sudbury, Ontario, P3E 6B5, Canada

Volcanogenic massive sulphide (VMS) deposits are important sources of economic concentrations of copper, zinc, lead, gold, silver, and other strategic minerals. The Neoarchean Abitibi Greenstone Belt (AGB) is a world class mining district straddling the Ontario and Quebec border and is host to numerous world-class VMS deposits. In terms of total metal endowment, the Blake River Group (BRG; 2704-2695 Ma) is the most enriched group within the AGB. The megacaldera complex has 31 known VMS deposits, most of which are concentrated around the Noranda and Doyon-Bousquet-LaRonde (DBL) mining camps. However, in the Swayze area of the AGB, no economic VMS deposits are known, despite considerable volumes of BRG rocks present in the area. This raises the question as to what factors control the occurrence of BRG-hosted economic VMS deposits in the AGB. This study will investigate whether the Swayze BRG rocks had the same initial melt compositions as the BRG rocks in the prolific DBL camp, specifically ore metals available to be concentrated by magmatic-hydrothermal systems. To achieve this, the study aims to chemically characterize the BRG rocks in the Swayze area, including a sub-economic VMS occurrence, through lithogeochemical melt inclusion chemical analysis. Integrated with detailed petrography, these geochemical data will be compared to data from temporally and lithologically similar rocks of the DBL mining camp. The use of laser ablation- inductively coupled plasma mass spectrometry on zircon-hosted melt inclusions will enable the base and precious metal fertility of the melts associated with the sub-economic VMS occurrence to be determined. *[Poster presentation]*

Geochronology of the Loki's Castle hydrothermal vent field, Artic Mid-Ocean Ridge

Colin Clancey and John Jamieson

Department of Earth Sciences, Memorial University of Newfoundland, St. John's, Newfoundland and Labrador A1B 3X7, Canada <cdc473@mun.ca>

Loki's Castle is an active high-temperature hydrothermal vent field located on the northern end of the Mohns Ridge, where it transitions into the Knipovich Ridge. The Mohns Ridge is part of the slow spreading ridge system that extends northward from Iceland to Gakkel Ridge in the Arctic Ocean. At 2400 m depth, Loki's Castle consists of black smoker chimney clusters located atop two coalesced hydrothermal mounds that are up to 30 m high and 200 m across. In 2017 and 2019, rock samples were collected from Loki's Castle using a remotely-operated vehicle operated from the Norwegian research vessel G.O. Sars. These samples were collected from hydrothermal mounds, and include an active and an inactive barite chimney, an active chimney flange, and an exposed fault surface. In our study, we will use the ^{226}Ra/Ba isotopic system to date hydrothermal barite from a subset of ten samples from the vent field. Chronological analysis will be completed using gamma spectroscopy combined with bulk geochemical analyses. Sample ages will be used to determine how long this system has been forming. These results will be combined with deposit volume estimates determined from analysis of high-resolution bathymetry, to calculate the rate of deposit formation. The barite ages will be compared to previously determined ^{230}Th/^{234}U ages of pyrite from the same samples to evaluate the accuracy and reproducibility of both methods. Along with this geochronological analysis, a petrographic examination of the samples will be conducted to determine mineral paragenesis as it is related to barite and pyrite. *[Oral presentation]*

You had me at "Reflector": interpretations of seismic data for the earliest formations in the Scotian Basin, Canada

Jesse Demaries-Smith[1], Mo Snyder[1], and Shawna White[2]

1. Department of Earth and Environmental Science, Acadia University, Wolfville, Nova Scotia B4P 2R6, Canada <160297d@acadiau.ca>

2. Department of Geology, Saint Mary's University, Halifax, Nova Scotia B3H 3C3, Canada

The Scotian Basin is a rifted continental margin that began forming in the late Triassic during the breakup of Pangea as the North American and African plates began to separate. Rifting created horsts and grabens which formed a series of depocenters, into which sediment could accumulate, bounded by intervening platforms. The first formation deposited was dominantly sandstone, shale, and siltstone of the Eurydice Formation. Directly overlying the Eurydice Formation is the Argo Formation, which is dominated by halite units and lesser anhydrite evaporite units. These formations represent an underexplored potential reservoir for petroleum systems in the petroleum rich Scotian Basin. The purpose of this project is to investigate these earliest Mesozoic (Eurydice and Argo formations) as potential reservoirs in terms of depocenter connectivity early in the basin history using interpretations of 2D seismic data, and through that gain a better understanding of initial basin architecture from which basin petroleum system elements evolved. The ultimate objective for this project is to produce a 3D model of basin geometry and connectivity between the Mohican Graben Complex and the Shelburne sub-basin. *[Oral presentation]*

Aspects of morphology, taphonomy and growth orientation of *Charnia* sp. from Sword Point, Conception Bay, Little Catalina and Catalina, Newfoundland, Canada

Hayley Fitzgerald and Duncan McIlroy

Department of Earth Sciences, Memorial University of Newfoundland, St. John's, Newfoundland and Labrador A1B 3X7, Canada

Animal-like lifeforms from the Ediacaran period (ca. 635–541Ma) have been preserved as impressions in sedimentary rocks from the Avalon and Bonavista peninsulas of Newfoundland. These lifeforms are better known as the Ediacaran macrobiota and are some of the earliest multicellular life preserved on Earth. *Charnia* is a well-known Ediacaran macrofossil which is a member of the extinct clade, Rangeomorpha: a group of sessile, epibenthic organisms that occupied deep marine environments in the Ediacaran period. The purpose of this study is to describe *Charnia* fossils in their sedimentological context as well as focusing on morphometrically quantifying and explaining asymmetric, tousled, and disrupted specimens. A number of *Charnia* specimens were photographed at several localities to digitally measure length, width, and orientation, using the program imageJ. Sedimentary structures indicating a paleocurrent were observed and noted where possible to analyze fossil orientation with respect to current direction, and several casts were made from well preserved specimens to observe morphological aspects and further understand taphonomy. Further investigation into the morphology, taphonomy, and growth orientation of *Charnia* will help reveal an accurate depiction of this early animal-like lifeform, which can help us further understand animal evolution. *[Oral presentation]*

Composition and origin of xenocrysts in the Eastern Shore lamprophyre dykes, Nova Scotia, Canada

Yuzhe Gan and Sandra Barr

Department of Earth and Environmental Science, Acadia University, Wolfville, Nova Scotia B4P 2R6, Canada <150429g@acadiau.ca>

The Eastern Shore dykes are a swarm of lamprophyric dykes in the Sheet Harbour area of eastern Nova Scotia. Two of the dykes, Pleasant Harbour–Borgles Island and Popes Harbour, contain a huge number of exotic xenoliths and xenocrysts, at least some of which were derived from the deep crust. Hence, they may provide insights about the composition of the deeper crust under the Meguma terrane. Although the xenoliths have been studied previously, no studies have been reported on the xenocrysts, and hence this study was undertaken to determine the petrological characteristics of the xenocrysts, including possible connection to the orogenic gold deposits of the Meguma terrane. Twenty-three samples from the dykes collected by previous workers were examined for xenocrysts, from which one sample each from the Borgles Island and Pleasant Harbour dykes was selected for detailed study, based on the abundance and variety of xenocrysts seen in hand specimen. About twenty thin section-sized chips were cut from those samples, and 14 chips with abundant xenocrysts were made into polished sections and used for major and trace element analysis by electron microprobe and LA-ICP-MS. Based on the petrographic evidence, the xenocrysts are subdivided into three groups: (1) small silicate xenocrysts, including quartz, K-feldspar, garnet, and kyanite, all with reaction rims; (2) large silicate xenocrysts; and (3) sulphide xenocrysts. The sulphide xenocrysts are pyrite, with small inclusions of chalcopyrite. The silicate xenocrysts may have been derived from disaggregated xenoliths in which similar minerals have been reported. However, the origin of the large silicate and sulphide xenocrysts remains uncertain. *[Oral presentation]*

Late Quaternary geochronology and stratigraphy of St. Anns Basin, offshore Nova Scotia, Canada

Cameron Greaves[1], Jordan Eamer[2], Edward King[2], and Ian Spooner[1]

1. Department of Earth and Environmental Science, Acadia University, Wolfville, Nova Scotia B4P 2R6, Canada <camdgreaves@gmail.com>
2. Geological Survey of Canada (Atlantic), Bedford Institute of Oceanography, Dartmouth, Nova Scotia B2Y 4A2, Canada

St. Anns Basin is a Quaternary offshore intrashelf basin located southeast of Cape Breton Island, Nova Scotia. The eastern Scotian Shelf remains a poorly understood area due to its complex physiography and late glacial history. St. Anns Basin has a high frequency of widely distributed mass-failures, yet a complete chronology for the deglacial sediment record has not been developed to date these deposits. Here, we present preliminary results that utilize an archival sediment core of a glaciomarine sediment package on the eastern margin of the basin to revise the St. Anns Basin sediment chronology using radiocarbon dating of benthic foraminifera and shell fragments. The sediment core contains suspected brick red mud layers associated with major deglacial ice-calving events that have been precisely dated in the nearby Laurentian Channel. An updated lithostratigraphic section alongside existing biostratigraphic interpretations will be used to provide a framework for the deglacial chronology of the basin. Additionally, the updated chronology enhances the understanding of the seismostratigraphic framework of the St. Anns Basin. These data will collectively be used to interpret if mass failures found throughout the basin are contemporaneous, possibly constituting a seismically induced event and constraining an assessment of modern geohazard risk in the basin. The revision of the chronology of sediments in St. Anns Basin could also further constrain the timing of shelf-ice cover on the eastern Scotian Shelf. *[Oral presentation]*

Microplastic in beach sediment from Mary's Point, Shepody National Wildlife Area, southeast New Brunswick, Canada*

Claire Gullison and Dave Keighley

Department of Earth Sciences, University of New Brunswick, Fredericton, New Brunswick E3B 3A3, Canada <cgullis1@unb.ca>

The Shepody National Wildlife Area (NWA) hosts 50–95% of the world's Semipalmated Sandpiper population during their >3000 km migration south. The sandpipers rest and feed on a variety of biota, including mud shrimp, other crustacea, molluscs, worms, biofilms, etc., that live on and in the NWA's inter-tidal mudflats backed by sand and gravel beaches. Plastic waste is now widely documented as polluting these environments, where it often breaks down into particles of <1 mm size (microplastic), becoming difficult to collect and remove, while becoming more available for ingestion by biota in the sediment and eventually accumulating progressively up the food chain, potentially in humans or sandpipers. Previous studies investigating the microplastic fraction have focused on the readily visible, surficial sediment (<5 cm depth), disregarding the processes active in sediment that may mix the vertical sediment column, distributing the plastic to a greater depth. This initial study aims to investigate microplastic distribution across and vertically within a sandy beach section at Mary's Point, using a sediment corer. Samples are analyzed in 4 cm depth increments, with microplastics separated and compositionally classified for each increment via a novel procedure using low-cost, non-toxic chemicals: four density separations, involving solutions with increasing densities (fresh water, saline water, and low and high concentration NaH_2PO_4 solutions), followed by an oleophilic separation. Separated microplastics were then further analyzed by microscopy to determine size, shape, colour, and degradation; compositions were validated using Raman Spectroscopy. Preliminary results indicate clear and blue fibres (from fishing gear, potentially) dominate. *[Oral presentation]*

*__Winner of the Science Atlantic Presentation and Communication Award for best overall presentation__

Long-term changes in the Nain landfast sea-ice edge, Labrador, Canada

Brayden Harker[1], Audrey Limoges[1], Nicolas Van Nieuwenhove[1], and Alexandre Normandeau[2]

1. Department of Earth Sciences, University of New Brunswick, Fredericton, New Brunswick E3B 5A3, Canada <bharker@unb.ca>
2. Geological Survey of Canada (Atlantic), Bedford Institute of Oceanography, Dartmouth, Nova Scotia B2Y 4A2, Canada

Since 1971, the Arctic has warmed three times faster than the rest of the world. This warming has led to drastic changes in land and sea-ice environments that are particularly challenging for northern sub-Arctic coastal communities. Sea ice loss due to accelerated Arctic warming is jeopardizing important habitats for ice-dwelling life, as well as areas that have been used for fishing, hunting, and gathering for millennia by the Dorset, Thule, and Inuit cultures. Changing

sea-ice conditions also impact the abundance and diversity of algal communities that form the basis of the marine food web. Many algae, such as dinoflagellates, produce robust resting cysts that are preserved in marine sediments. By analyzing these and other palynomorphs alongside other biogenic proxy indicators and geochemical signals preserved in marine sediment cores, past trends in primary production and sea-ice conditions can be inferred. Understanding past responses to climate fluctuations can provide critical insights into understanding current trends and predicting future changes to primary production and the local environment. Using standard palynological methods this project aims to analyze two gravity cores (7 cm diameter) collected in the Nain area (Nunatsiavut), one located within and the other outside of the present-day landfast sea-ice edge. Each core is approximately 60 cm long, allowing for a comparison of the observed changes in each respective environment. The data resulting from this project will contribute to a larger research program, combining other zooarchaeological and collective knowledge to better understand climate-induced changes in the coastal ecosystem of Nain. *[Oral presentation]*

Pyrite paragenesis and relation to gold-bearing fluid phases in the Lone Star deposit, Yukon Territory, Canada

Arthur Hilliard

Department of Earth and Environmental Sciences, Dalhousie University, Halifax, Nova Scotia B3H 4R2, Canada <hilliard.erin@gmail.com>

The Klondike region of the Yukon Territory, Canada, is famous for extensive placer deposits, recovering over 20 million oz since discovery, but lacks any major defined bedrock resources. As a result of a surge in exploration activity, recent drilling efforts have delineated several new bedrock targets, including the Lone Star deposit near Dawson City, Yukon. The Lone Star deposit is hosted by a suite of Late Permian plutonic, volcanic, and sedimentary units known as the Klondike Assemblage. This assemblage formed as a result of subduction-related arc-magmatism, followed by Late Permian–Early Triassic regional greenschist-amphibolite facies metamorphism during accretion onto Laurentia as part of the Yukon–Tanana terrane. Gold deposition is thought to be middle–late Jurassic, mainly occurring within discordant quartz veins with common pyrite mineralization but overall low sulfidation (galena, sphalerite, chalcopyrite, etc. only trace). This study will add to the overall understanding of the Lone Star deposit by establishing relations between pyrite paragenesis and gold mineralization. This will be done through detailed examination of a suite of ten samples, selected based on differences in pyrite occurrence. Textural relations will be determined using reflected light microscopy and SEM on polished mounts. Following this, samples will be analyzed for major and minor elements by electron microprobe and LA-ICP-MS will be used to measure the 2D distribution of trace chalcophile elements. Correlations between texture type and element distributions will be used to determine if there were discrete pyrite-forming events, and whether these events can be related to the influx of gold-bearing fluids. *[Oral presentation]*

How to measure changes in topography without eroding an undergraduate research budget

Parker Ingham and Mo Snyder

Department of Earth and Environmental Science, Acadia University, Wolfville, Nova Scotia B4P 2R6, Canada <136627i@acadiau.ca>

Quick, efficient, and affordable monitoring of coastal surface erosion is an ongoing challenge for scientists and stakeholders. The current standard, aerial LiDAR surveying, can yield precise surface elevations, even through dense foliage. However, LiDAR surveying is expensive and inaccessible to researchers on a tight budget. Additionally, LiDAR surveying does not collect data on complex steep intertidal and subtidal surfaces with caves or indentations that significantly change through time. In contrast, ground-based technicians can collect photographs from multiple angles to create nuanced, coloured photogrammetry clouds with high temporal frequency. However, stakeholders are unable to pin their photogrammetry clouds to accurate coordinates on a map because consumer GPS accuracy is relatively low. This project provides an opportunity for consumer products and open-source software to be tested with the ultimate goal of decreasing the barrier of entry. Merging GeoNova's open coastal elevation LiDAR point cloud to drone or action camera photo-clouds combines the strength of both techniques described above. This work necessitates an evaluation of point cloud similarity which can be done with the open-source software, Cloud Compare. The methodology of creating photogrammetry point clouds, merging point-clouds with LiDAR data, and overcoming challenges is here described. The area of study is at Kingsport Beach, an area of relatively constant topographic change in short amounts of time. *[Oral presentation]*

Sustainable gold mining: replacing gold mining with novel ionic thiourea ligands for gold extraction

Sam Julien, Jacob Hoare, Liah Christie, Caylee Macdonald, Isaac Carlin, Robert Singer, and Christa Brosseau

Department of Geology, Saint Mary's University, Halifax, Nova Scotia B3H 3C3, Canada <sam.julien@smu.ca>

Cyanidation has been the most widely applied gold extraction method world-wide for over a century. Unfortunately, there have been many accidental releases of toxic cyanide, which have resulted in extensive damage to the environment and surrounding communities. Due to this, various alternatives are being explored in efforts to replace cyanidation but have yet to be implemented due to the high material costs and infrastructure changes that would be needed. The current project is working to develop an alternative to cyanidation using novel ionic thiourea derivatives, which can selectively extract gold and silver. Two imidazolium salts have been functionalized with a thiourea group and a dodecyl sulfate [DS]- anion. Up to 98% extraction of gold(III) from a model leachate solution has been achieved reproducibly to date and future efforts are being made to develop a method of extraction from raw gold-containing ore. *[Poster presentation]*

Petrology and metamorphism of the 'Bright-eyed' Gneiss, Grand Teton, Grand Teton National Park, Wyoming, USA

Abby Kelly

Department of Earth Sciences, University of New Brunswick, Fredericton, New Brunswick E3B 5A3, Canada <akelly4@unb.ca>

The Archean southern Teton range, Wyoming, hosts a unique 'bright-eyed gneiss' unit exposed in Death Canyon, Grand Teton National Park. These rocks are biotite orthogneisses with magnetite ($Fe^{3+}2Fe^{2+}O_4$) porphyroclasts surrounded by lenticular quartzofeldspathic pods. The major minerals are biotite, alkali feldspar, plagioclase, quartz, magnetite, ilmenite and titanite. The accessory minerals are apatite, allanite, some sulfides, and small zircon grains. Evidence suggests that these rocks underwent low degrees of partial melting at amphibolite-facies conditions as recorded by melt pseudomorph microtextures. A variety of analytical techniques were applied to eleven hand samples. These include μXRF mapping, SEM backscattered imagery, optical microscopy, and X-ray CT to obtain central cuts through the magnetite grains. Hypotheses to be tested are whether the rocks formed in an open system involving water-fluxed biotite dehydration melting. Another key step in this experiment is to determine the role of original oxidation of possible protoliths for these gneisses including tonalite-granodiorite. EPMA chemical analyses and laser ablation will also be used in tandem to examine mineral zoning and develop a reaction model to help explain how these rocks formed. The significance of this project is to determine the relative ages of the rock, whether it was metamorphic or magmatic in origin. Therefore, this project will be crucial to understanding the Archean rocks in the Grand Teton, and most importantly, the formation of the 'magnetite eyes'. *[Oral presentation]*

Survey of porewater geochemistry within deep marine hydrocarbon seep sediments of the Scotian Slope, Canada*

Nikita Lakhanpal[1], G. Todd Ventura[1], Venus Baghalabadi[1], Natasha Morrisson[2], and Adam Macdonald[2]

1. Department of Geology, Saint Mary's University, Halifax, Nova Scotia B3H 3C3, Canada <nikita.nikita@smu.ca>
2. Nova Scotia Department of Natural Resources and Renewables, Halifax, Nova Scotia B3J 2T9, Canada

The ocean floor surface sediments of the Scotian Slope, Nova Scotia, are host to a complex network of microbially mediated reactions that knit together the various biogeochemical cycles. Limited diffusion between the upper water column and ocean floor mud pore spaces, coupled with competitive microbial ecological niche partitioning, leads to the formation of biogeochemically controlled redox gradients. These microbial biogeochemical zones change if surface sediments are impregnated by hydrocarbon seepage that migrates up from deeper within the basin. Porewater profiles of F^-, NO^{2-}, NO^{3-}, CO_3^{2-} and SO_4^{2-} were used to reconstruct biogeochemical stratification depth profiles that can provide comparative evidence for anion behaviour in active cold seep sites. A comparative study between two methods of data analysis was applied to the samples. The method of standard addition proved to be a better method than the external calibration curve method to measure porewater anion concentrations of natural samples with complex matrices and a varying range of concentrations. For this reason, porewater anion concentrations were compared using the standard addition method. Sulfate concentration decreases dramatically in both ambient and hydrocarbon impacted marine benthic sediments although, in hydrocarbon impacted sites, it appears to occur at a much shallower depth, suggesting that the redox gradient is much

more pronounced and as much sulfate reduction has not yet transpired with the ambient sediments at the same depth. Nitrate and NO^{2-} trends also show similar pronounced reduction patterns occurring at shallower depths for hydrocarbon impacted sediments suggesting widespread increased microbial and bacterial activity in these regions. *[Poster presentation]*

***Winner of the Canadian Society of Petroleum Geologists Award for the best petroleum geology-related presentation**

Zircon petrochronology of the West Barneys River Plutonic Suite: insights into the origin of a potential critical element (REE and Zn) deposit in Nova Scotia, Canada

Michael Leblanc and Donnelly Archibald

Department of Earth Sciences, Saint Francis Xavier University, Antigonish, Nova Scotia B2G 2W5, Canada <x2020fzv@stfx.ca>

The transition to a green-energy future requires a significant increase in the supply of critical elements. Therefore, it is essential that we advance our knowledge of the processes that concentrate these elements. Of the 31 elements that Canada has deemed to be critical, many of them can be concentrated by igneous rock-forming processes. For example, rare earth elements (REE) are known to be concentrated by magmatic processes associated with the emplacement of alkaline to peralkaline igneous rocks. This research focuses on the West Barneys River Plutonic Suite (WBRPS) in Nova Scotia, which has elevated concentrations of both REE and Zn. The WBRPS is a complex, heterogeneous mix of coeval plutonic lithologies ranging in composition from mafic to felsic. Published U–Pb data indicates a range of crystallization ages between ca. 495 and 460 Ma; however, many knowledge gaps remain related to the origin of these rocks and the associated REE and Zn mineralization. Ten representative samples were collected from the WBRPS that range in composition from gabbro to quartz syenite. Of those, seven samples yielded dateable zircon, with preliminary interpretations of LA-ICP-MS U–Pb data yielding a crystallization age range between ca. 465 and 430Ma. Zircon trace element and hafnium isotope data were also collected and will be analyzed to determine the magmatic processes and magma source(s) involved in the generation of the plutonic suite. These new petrochronological data and interpretations will help to better understand the petrogenesis of the WBRPS and the processes that concentrated the REE and Zn. *[Oral presentation]*

Machine-learning focal mechanism inversion for hydraulic fracking- induced earthquakes*

Megan Macdonald and Miao Zhang

Department of Earth and Environmental Sciences, Dalhousie University, Halifax, Nova Scotia B3H 4R2, Canada <macdonald.m@dal.ca>

Hydraulic fracking has contributed to an increase in induced seismicity in recent years in Fox Creek, Alberta. Earthquake focal mechanisms, relying on polarities of earthquake first motions, provide insight into the state of stresses in a region. Traditional methods for manually determining the polarities of first motions are not suitable for microearthquakes due to the large volume of data and owing to their low signal-noise ratio. Machine learning provides a reliable and efficient way for polarity classification. Using data obtained from the Tony Creek Dual Microseismic Experiment, this study aims to show that machine learning can reliably solve for polarities of earthquake first motions and characterize the focal mechanisms of hydraulic fracking-induced earthquakes. The project will provide greater insights into the state of stresses and geologic structures (such as faults) in the study area and will improve our understanding of earthquake-triggering mechanisms during hydraulic fracking. In this presentation, we are going to introduce the seismic data, proposed methods, and preliminary results. *[Poster presentation]*

***Winner of the Canadian Society of Exploration Geophysics Award for best presentation of a geophysics-related paper**

Coastal erosion study on the Flats Road property in Conception Bay South, Newfoundland, Canada

Anna Malone, Alison Leitch, and Colin Farquharson

Department of Earth Sciences, Memorial University of Newfoundland, St. John's, Newfoundland and Labrador A1B 3X7, Canada <aimalone@mun.ca>

This study focuses on the sensitivity of the Newfoundland coastline to erosion, specifically surrounding the beach located at the end of Flats Road in Conception Bay South, Newfoundland. In this study, various geophysical instruments from the Memorial University equipment pool can be used to locate the bedrock or any other subsurface features that will affect the erosion rate in the area. Thus far, a ground-penetrating radar (GPR) survey, a real-time kinematic positioning survey (RTK), and a direct current

resistivity survey (DCR) have been conducted. This research aims to locate the bedrock or subsurface properties that will affect the rate of erosion happening on the land located at the end of Flats Road in Conception Bay. This information is directly proportional to the effects of climate change on the province of Newfoundland. Currently, the average coastal erosion rate for the region is approximately 20 cm/yr. This number will increase with the rise of climate change and sea levels, as the volume of water increases in the oceans, the speed and strength of coastal erosion grows. Post-glacial rebound in Newfoundland varies from coast to coast. The west coast is rising and the east coast, although no precise numbers are known, is generally sinking slowly with respect to the Earth's center. High winds, hurricanes, and storm surges are all factors that result in the shrinking coastline. This project is going to research the rate of erosion and how changing climate affects it. *[Poster presentation]*

Dating fault motion at the northern Appalachian structural front, western Newfoundland, Canada

Dylan Mckeen[1], Shawna White[1], Dawn Kellett[2], and Catherine Mottram[3]

1. Department of Geology, Saint Mary's University, Halifax, Nova Scotia B3H 3C3, Canada <dylan.mckeen@smu.ca>
2. Geological Survey of Canada (Atlantic), Dartmouth, Nova Scotia B2Y 4A2, Canada
3. School of the Environment, University of Portsmouth, Portsmouth PO1 3QL, United Kingdom

The Appalachians formed during Cambrian through Devonian orogenesis, as a result of multiple microcontinent and terrane accretions which occurred as the Iapetus Ocean episodically closed. In western Newfoundland, folds and faults that formed during the Taconian and Acadian orogenies are preserved. The limit of deformation, or Appalachian structural front, extends along Newfoundland's west coast. This front is defined by a structural triangle zone, the upper detachment of which is marked by the Tea Cove Thrust, a back-thrust that only outcrops in one location on the Port au Port Peninsula, our study area. Timing of motion along the structural front is constrained as Devonian through Visean using structural and stratigraphic relationships largely observed in seismic records. However, previous work suggests that earlier Ordovician (Taconian) movement is likely. Observations and data collected during fieldwork suggest that significant structures associated with the structural front, outcropping along the Port au Port Peninsula, have been reactivated. Faults parallel to the Tea Cove Thrust preserve two generations of motion: NW-directed and SE-directed. Later, cross-cutting NW-directed faults with an orientation consistent with post-Taconian basement faults are present too. These cross-cutting and kinematic relationships, combined with data we aim to collect using in-situ dating of calcite slicken-fibres and mica using U–Pb and Rb/Sr by LA-ICP-MS, respectively, will allow us to determine an absolute age of generation and reactivation of faults defining the structural front. New data will also provide information to petroleum models for active exploration in the region, whereby structures at the structural front are demonstrated petroleum traps. *[Oral presentation]*

Mineralogy and corundum trace element composition at the Hopedale "ruby" occurrence, Labrador, Canada: comparison to till-hosted pink corundum

Emma Mercer[1], Ofure Onodenalore[1], Philippe Belley[1], and Heather Campbell[2]

1. Department of Earth Science, Memorial University of Newfoundland, St. John's, Newfoundland and Labrador A1B 3X5, Canada <ecmercer@mun.ca>
2. Geological Survey of Newfoundland and Labrador, St. John's, Newfoundland and Labrador A1B 4J6, Canada

In the Hopedale Block, Labrador, pink to reddish-purple corundum occurs in gneiss and has also been found as pink detrital grains (0.25–0.50 mm) in till. The till-hosted corundum grains occur 28 km west of the hard rock occurrence; however, the ice flow direction is to the east. This indicates that at least two reddish corundum ("ruby") localities occur in this region, and are separated by a vast distance, making the region attractive to ruby exploration. The hard-rock corundum occurrence consists of weakly foliated corundum-biotite-plagioclase gneiss containing accessory rutile, pyrrhotite, pentlandite, and zircon as well as trace galena, titanite, Bi- Ag telluride, and thortveitite (a rare Sc silicate). Corundum occurs as ~10 mm to ~70 mm porphyroblasts with cross-hatched twining within a finer-grained matrix of corundum, biotite, and plagioclase (An_{50}). Both corundum from the outcrop and the till show minor amounts of diaspore retrograde alteration along fractures. This study will compare the mineral associations and corundum trace element composition in the till-hosted grains with those at the gneiss-hosted occurrence to determine whether they come from geologically similar sources. *[Poster presentation]*

The impacts of historical gold mining on chironomid assemblages in Lake Thomas, Nova Scotia, Canada

Suzan Mhagama, Branaavan Sivarajah, and Joshua Kurek

Environmental Science Department, Mount Allison University, Sackville, New Brunswick E4L 1H3, Canada <sdmhagama@mta.ca>

Gold mining operations were one of the predominant economic activities in Nova Scotia between the late 19th and early 20th centuries. The Waverley gold mine district was active from 1862 to 1940 and mine tailings produced were transported into the local environment that contributed to the pollution of the Shubenacadie Canal drainage basin. In this study, we used paleolimnological approaches to understand the long-term ecological effects of historical gold mining operations on Lake Thomas. Concentrations of mining-related contaminants (arsenic and mercury) were measured from a dated sediment core to track pollution history and subfossil chironomid remains were analyzed to examine biological effects. Sedimentary arsenic and mercury levels were low prior to gold mining activities; however, during the mining era concentrations of both elements increased. Sedimentary arsenic and mercury levels reached concentrations of 980 ppm (dry weight) and 31 400 ppb (dry weight), respectively. Arsenic and mercury levels have decreased in the most recent sediments but continue to be higher than national sediment quality guidelines, arsenic levels are 58× and mercury 65× higher than national guidelines. Notable declines in the number of chironomid head capsules per gram of dry sediments during the mining era suggest biological impacts. Although the Waverley gold mine was closed eight decades ago, elevated contaminant levels may still be affecting aquatic biota. This research contributes to the growing number of environmental assessments that are aiming to understand the long-term ecological consequences of past gold mining operations on aquatic ecosystems. *[Poster presentation]*

Mineralogy of the Boundary volcanogenic massive sulfide (VMS) deposit of the Tally Pond Group, Victoria Lake Supergroup, Newfoundland Appalachians, Canada*

Taylor Mugford and Stephen Piercey

Department of Earth Science, Memorial University of Newfoundland, St. John's, Newfoundland and Labrador A1B 3X5, Canada <taytaymug@yahoo.ca>

The Cambrian Boundary volcanogenic massive sulfide (VMS) deposit is in the Victoria Lake Supergroup in the Newfoundland Appalachians, Canada. The deposit is hosted within chlorite-sericite-quartz–altered rhyolite lapilli tuff and represents one of the best preserved subseafloor-replacement-style VMS deposits globally. The purpose of this study is to provide insights into the mineralogical evolution of the replacement style mineralization in the North Zone of the Boundary deposit using mineral textures, paragenesis, and reflected light microscopy, scanning electron microscopy (SEM), and electron probe microanalysis (EPMA). Initial textural results show that the Boundary deposit is dominated by an assemblage of pyrite, sphalerite, chalcopyrite, galena, and pyrrhotite. Pyrite is the dominate sulfide, displaying many textures disseminated, the latter occurring as sulfide stringers. Pyrrhotite is present as small inclusions in pyrite intergrown with chalcopyrite. Sphalerite is present in majority of the mineral facies, but its abundance varies from disseminated, massive, and sulfide stringers; sphalerite also locally exhibits chalcopyrite disease. Galena occurs as irregular grains commonly intergrown with sphalerite and pyrite. SEM and EPMA work are ongoing. *[Oral presentation]*

*Winner of the Frank S. Shea Memorial Award for best economic geology-related presentation

On the discovery of fossil land snails (*Dendropupa* sp) from the Minto Formation of central New Brunswick, Canada

Rowan Norrad[1], Luke Allen[2], Matt Stimson[3,4], Lynn Dafoe[5], Olivia King[3,4], Spencer Lucas[6], Adrian Park[7], Steven Hinds[3,7], and Brian Herbert[8]

1. Department of Earth and Environmental Science, Acadia University, Wolfville, Nova Scotia B4P 2R6, Canada <renorrad@gmail.com>
2. Department of Earth Sciences, University of New Brunswick, Fredericton, New Brunswick E3B 5A3, Canada
3. Steinhammer Paleontological Laboratories, Geology/Paleontology section, Natural History Department, New Brunswick Museum, Saint John, New Brunswick E2K 1E5, Canada
4. Department of Geology, Saint Mary's University, Halifax, Nova Scotia B3H 3C3, Canada
5. Geological Survey of Canada (Atlantic), Dartmouth, Nova Scotia B2Y 4A2, Canada
6. New Mexico Museum of Natural History, Albuquerque, New Mexico 87104, USA
7. Geological Surveys Branch – New Brunswick Department of Natural Resources and Energy Development, Fredericton, New Brunswick E3B 5H1 Canada
8. Fundy Treasures, Joggins, Nova Scotia B0L 1A0, Canada

The Pennsylvanian (late Bashkirian–early Moscovian) Minto Formation of central New Brunswick was previously studied for its diverse paleofloral, rare invertebrate fauna (*trigonotarbid*), and rare disarticulated vertebrate fauna. The Minto Formation has been interpreted as a peat-forming wetland that experienced occasional euryhaline influence within back-barrier or delta front depositional settings. A recently discovered fossil locality situated along the southern shoreline of Grand Lake yields a diverse array of plant fossils, tetrapod and invertebrate footprints, and invertebrate body fossils from the Sunbury Creek Member of the middle to upper Minto Formation. Recent work has described a new Carboniferous stem dragonfly (*Brunellopteron norradi*) and a new specimen of the tetrapod footprints *Batrachichnus*, the latter with new tracemaker interpretations. Here we describe two new terrestrial gastropod (pupa) shells (NBMG 21521) that broadly conform to the Carboniferous land snail *Dendropupa*, with a similar apex and post-apical whorls. However, the Minto Formation pupa differ from *Dendropupa* by possessing axial (longitudinal) sculpture on the shell. *Dendropupa* exhibits an axial lirae along its shell that is not preserved in the Minto Formation specimens. Both Minto Formation specimens exhibit the same morphology but differ in size, suggesting one is an adult and one a juvenile. The diminutive size of the shells suggests that they may represent the smallest known Carboniferous land snails in the fossil record. The two shells are associated with invertebrate ichnofossils (*Gordia*, *Helminthoidichnites*, and cf. *Helminthopsis*) that are of similar width, implying a trace and trace-maker relationship, and broadening the tracemaker interpretations for those ichnogenera. *[Oral presentation]*

Documenting recent human influences using remote sensing techniques on the Tekes River alluvial fan, Xinjiang, China*

Leila Rashid and Philip Giles

Department of Geology, Saint Mary's University, Halifax, Nova Scotia B3H 3C3, Canada <leila.rashid@smu.ca>

The Tekes River alluvial fan is in Xinjiang Province which has an arid to semi-arid climate as well as a historically unpredictable precipitation rate. Further, increasing population and urbanization means that all water resources must be used efficiently. The Tekes River alluvial fan has had a vast amount of human influence in recent decades in the form of dam construction, irrigation, and agriculture expansion. Although development on and surrounding the Tekes River alluvial fan is apparent, there is a lack of research on how these human impacts have affected the fan. The primary objective of this project is to use remotely sensed image analysis to document the human influence that has occurred to the Tekes River alluvial fan. A 31-year time series (1990–2021) was created using Landsat imagery from 1990–2021. The results have found that four dams have been constructed upstream from the fan, irrigation canal length had increased by approximately 400 km, and agricultural fields had increased by approximately 250 km^2. Average seasonal NDVI values were calculated on agricultural fields and compared to natural vegetation in the area for seven dates in 2021. The results do not show great observable differences between agricultural field and natural vegetation cover. However, these results are limited temporally and spatially. Further research should continue to document and test NDVI as well as consider measuring groundwater levels to build upon this research and provide a greater understanding of the anthropogenic impacts on the fan. *[Poster presentation]*

***Winner of the Imperial Oil Best Poster Award for best overall poster presentation**

Methane flux, source, and lipid biomarkers of serpentinite-hosted groundwater springs at contrasting sites of terrestrial serpentinization*

M. Julianna Whelan and Penny Morrill

Department of Earth Science, Memorial University of Newfoundland, St. John's, Newfoundland and Labrador A1B 3X5, Canada <mjw245@mun.ca>

Serpentinization sites are a point of recent scientific interest because of their implications toward primitive microbial metabolisms and astrobiological exploration. Serpentinization occurs when circulating groundwater hydrates ultramafic rocks, a reaction that is common in submarine environments and on land at ophiolite complexes. Three sites of terrestrial serpentinization were studied through their groundwater springs, which act as windows into the subsurface with respect to geochemistry and microbial activity. Serpentinization causes groundwater springs with unique parameters including ultra-basic pH levels (>10), low redox values, and methane and hydrogen gas enrichment. The Tablelands (Newfoundland, Canada), The Cedars (California, USA), and Aqua de Ney (California, USA), produce groundwater springs which act as endmembers, displaying a range of values with respect to the above properties. These sites have been extensively studied in the past and changes have been observed over the last

decade, proving it imperative to characterize these changes and interpret the temporal variations in these systems, made possible through the present comparison. Through past research it has been determined that the source of methane gas is different at each of the sites, but the flux of methane gas had not been quantified. This study intends to relate the methane flux to their source, aqueous geochemistry, and lipid biosignatures. Through gas chromatography and mass spectrometry, this study contributes to the knowledge around what microbial life consumes, what it produces, and how these things are preserved in terrestrial serpentinization systems. *[Oral presentation]*

[*]**Winner of the Atlantic Geoscience Society Environmental Geoscience Award for the best Environmental Science-related presentation**

Reply to the Discussion of "The 'lost' islands of Cardigan Bay, Wales, UK: insights into the post-glacial evolution of some Celtic coasts of northwest Europe" by Catherine Delano-Smith, Phil Bradford, and William Shannon[1]

SIMON K. HASLETT[1,2] AND DAVID WILLIS[2]

1. Department of Geography, Faculty of Science and Engineering, Swansea University, Singleton Park, Swansea SA2 8PP, United Kingdom
2. . Jesus College, University of Oxford, Turl Street, Oxford OX1 3DW, United Kingdom
*Corresponding author: <s.k.haslett@swansea.ac.uk>

Date received: 15 November 2022 ¶ Date accepted 1 December 2022

REPLY

Delano-Smith *et al.* (2022) provide a useful discussion concerning the use of the Gough Map and associated dating in response to the paper by Haslett and Willis (2022), and their views are informative and welcomed. The opportunity to provide further comment is also welcomed and it is hoped that this Reply addresses points raised and will be of benefit to the reader in further evaluating the research.

The study by Haslett and Willis (2022) was prompted by the depiction on the medieval Gough Map of two apparently 'lost' islands in Cardigan Bay (*Bae Ceredigion* in Welsh) lying offshore the coast of Ceredigion in Wales, UK (see fig. 1 of Haslett and Willis 2022 for locations mentioned herein). Therefore, the "starting point" for the study was not "medieval Welsh folklore about these islands" as stated by Delano-Smith *et al.* (2022, p. 261). Celtic literature and folklore are subsequently considered under geomythological sources but Haslett and Willis (2022) do not present Celtic literature or folklore specifically about 'islands' in Cardigan Bay but rather a lowland. Furthermore, to clarify, Haslett and Willis (2022) do not claim "to 'prove' the existence of 'lost' islands" (Delano-Smith *et al.* 2022, p. 264) but through an examination of historical sources, physical aspects, and geomythological sources conclude that their existence is considered plausible. Through such investigation, Haslett and Willis (2022) present a preliminary post-glacial coastal evolution model to provide a hypothetical framework which may be tested and evaluated through further research (e.g., Haslett and Willis, in press).

Scholarly literature concerning the Gough Map, as mentioned by Delano-Smith *et al.* (2022), presents a diverse range of conclusions. Whilst prefacing their introduction to sources with a general note of caution, Haslett and Willis (2022) present examples, not in support of any conclusions of their own but as a prerequisite for embarking on the study in providing at the outset a level of reassurance that suggests the islands depicted on the Gough Map merit further consideration. However, Delano-Smith *et al.* (2022) provide a welcome clarification to the mistake that the Gough Map is not the earliest known map of Great Britain (Haslett and Willis 2022; National Library of Scotland 2022) but rather is more correctly described, for example, as the "earliest known surviving map of Britain drawn on a separate sheet" (Delano-Smith *et al.* 2017, p. 3) and the "the earliest map to show Britain in recognizable form" (Nurse 2022, p. 50).

The possibility that islands once existed in Cardigan Bay, as depicted on the Gough Map, prompted Haslett and Willis (2022) to reconsider Ptolemy's coordinates as corrected by North (1957). The coordinate for the mouth of the River Teifi (*Afon Teifi*) at the southern end of Cardigan Bay is near its present-day location. A geomorphological explanation for an unchanged position is possible in that a radiocarbon date of 9539-10 154 cal. BP suggests that the Trawling Grounds bathymetric feature offshore of the river mouth may have been open to marine conditions and possibly a seaway for several thousand years, which may conceivably have been accessible to early seafarers (see fig. 4 of Haslett and Willis 2022). Northward along the coast, however, the next coordinate, for the mouth of the River Ystwyth (*Afon Ystwyth*), lies some 8 miles (ca. 13 km) west of the present-day location of the river mouth. While fully appreciating the comments of Delano-Smith *et al.* (2022), the depiction of offshore islands on the Gough Map appears consistent with

[1]Appears in Atlantic Geoscience, 58, pp. 261–266: this issue

doi: 10.4138/atlgeo.2022.014
2564-2987|22|00303–305 $1.45|0

Ptolemy's coordinates and it is based on these two strands of independent evidence taken together that Haslett and Willis (2022), perhaps not unreasonably, consider the implications for coastal evolution.

Delano-Smith *et al.* (2022) state that "the Gough Map is not a scale map" (p. 263) and, indeed, Haslett and Willis (2022) acknowledge this. However, the configuration of the middle section of the north-south orientated coast of Cardigan Bay, when compared with the present-day coastline, appears similar overall (Fig. 1) with the main exceptions that, relative to the position of mouths of the Rivers Ystwyth and Mawddach (*Afon Mawddach*), the mouth of the River Dovey (*Afon Dyfi*) is positioned north of its present-day location and, of course, that two islands are depicted lying offshore which are not present today. In describing these islands, as depicted on the Gough Map, Haslett and Willis (2022) provide measurements relative to the length of coastal segments immediately adjacent to each island and strongly advise that "these measurements must be viewed with extreme caution" (p. 135). Notwithstanding this caveat, given the overall similarity between the Gough Map and the present-day configuration of this part of the Cardigan Bay coastline, it may not be unreasonable to attempt illustrative measurements of physical features as part of a geographical description.

In relation to the wider Cardigan Bay, Bower (2015) considered that the absence of the overall embayed configuration of Cardigan Bay may be attributable to poor combination of separate 'surveys' used to construct the Gough Map. Based on this view, Haslett and Willis (2022) considered that "the lack of curvature of Cardigan Bay on the Gough Map does not cast significant doubt in itself on the distinct occurrence of the two 'lost' islands" (p. 133) because the lack of curvature may be due to the "poor combination of three regional surveys" rather than, necessarily, the accuracy of individual 'surveys' themselves, suggesting that local configuration and feature assemblages may be in places more reliable. Indeed, Bower's (2015) evidence suggests that such separate 'surveys' "were individually more accurate than the resultant map of England and Wales overall" (p. 145).

With regard to describing the location of the islands, Delano-Smith *et al.* (2022) state that "the fifty or so islands [depicted on the Gough Map] surrounding Britain are arbitrarily distributed" (p. 264). This may be the case but the location of the two islands considered by Haslett and Willis (2022) in Cardigan Bay do not appear to be arbitrarily positioned because they occur offshore of segments of coast lying between river outlets and the channel between the islands lies directly seaward of the mouth of the River Dovey. If these islands had been arbitrarily distributed then one or more islands may have been expected to have been drafted obscuring a river mouth and that they may not have been drafted each at a similar distance from the shore. Furthermore, as noted in the Haslett and Willis (2022) study, the islands depicted on the Gough Map are approximately coincident with bathymetric highs and the

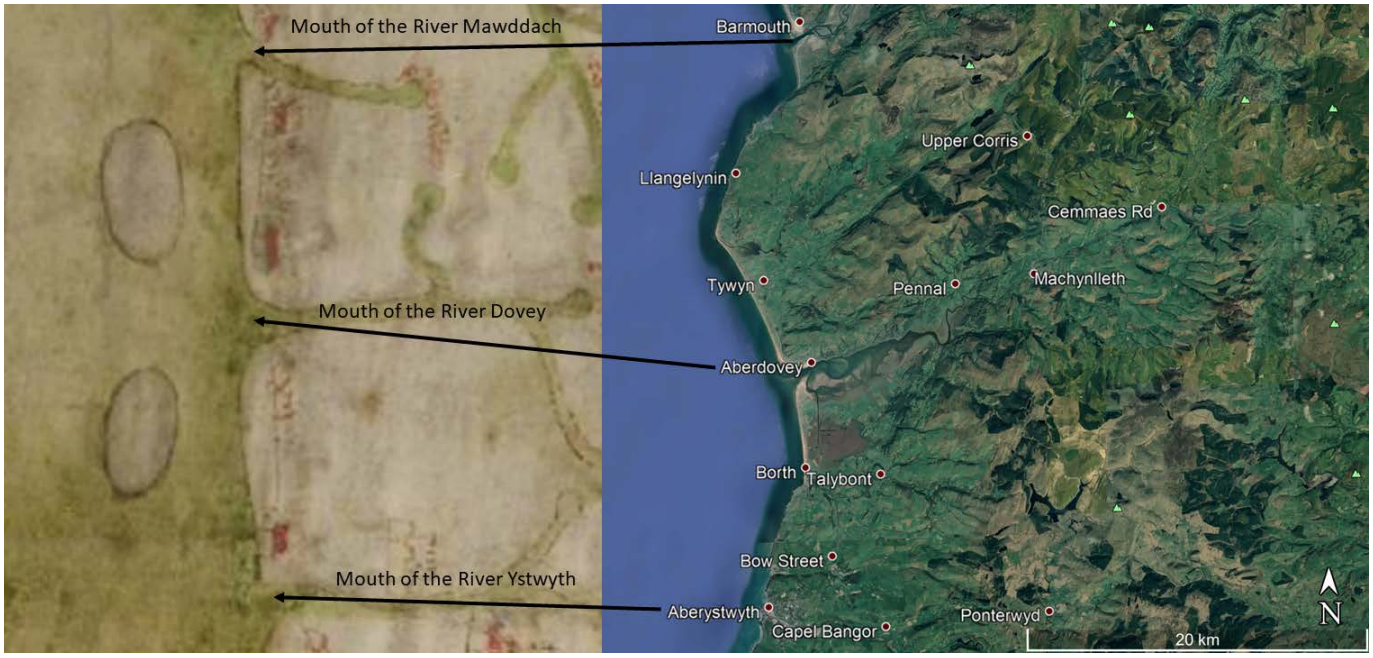

Figure 1. A comparison of the Gough Map (extract left) and the present-day coastline of the middle section of Cardigan Bay (reproduced under the Bodleian Library's, Oxford, and Google Earth's terms of use).

occurrence of accumulations of coarse boulders and gravel on the seabed known as sarns. As suggested by Delano-Smith *et al.* (2022), it may be that these islands represent grossly mislocated islets, such as Gwylan and/or St Tudwal's Islands; however, the position of the 'lost' islands is consistent with, and explainable by, the geology, bathymetry, and physical processes as considered by Haslett and Willis (2022) in the coastal evolution model they present.

Lastly, with regards to geomythological aspects, the view of Delano-Smith *et al.* (2022) "that no reference is made on the Gough Map to the lost lowland of Cantre'r Gwaelod" (p. 264) does not contradict Haslett and Willis (2022), who do not claim otherwise. However, the reference to Cantre'r Gwaelod, or Maes Gwyddno, in Celtic literature and folklore lends support to a general notion that a landscape may have previously existed seaward of parts of the present-day coastline in Cardigan Bay, an idea which is not at odds with the possible occurrence of islands as depicted on the Gough Map.

ACKNOWLEDGEMENTS

We thank an anonymous journal reviewer and Sandra Barr for comments that have improved the clarity of this Reply.

REFERENCES

Bower, D.L. 2015. The Medieval Gough Map, its settlement geography and the inaccurate representation of Wales. Imago Mundi, 67, pp, 145–167. https://doi.org/10.1080/03085694.2015.1027548

Delano-Smith, C., Barber, P., Bove, D., Clarkson, C., Harvey, P.D.A., Millea, N., Saul, N., Shannon, W., Whittick, C., and Willoughby, J. 2017. New Light on the Medieval Gough Map, Imago Mundi: The International Journal for the History of Cartography, 69:1. pp. 1–36, plates 1–5. https://doi. org/10.1080/03085694.2017.1242838

Delano-Smith, C., Bradford, P., and Shannon, W. 2022. Discussion of "The 'lost' islands of Cardigan Bay, Wales, UK: insights into the post-glacial evolution of some Celtic coasts of northwest Europe" by Simon K. Haslett and David Willis. Atlantic Geoscience, 58, pp. 261–266. https://doi.org/10.4138/atlgeo.2022.011

Haslett, S.K. and Willis. D. 2022. 'The 'lost' islands of Cardigan Bay, Wales, UK: insights into the post-glacial evolution of some Celtic coasts of northwest Europe', Atlantic Geoscience, 58, pp.131–146. https://doi.org/10.4138/atlgeo.2022.005

Haslett, S.K. and Willis. D. in press. Exploring the post-glacial history of the Cardigan Bay coast and sites of sediment accumulation. Ceredigion: Journal of the Ceredigion Historical Society.

National Library of Scotland 2022. Mapping Great Britain. URL <https://www.nls.uk/exhibitions/maps/great-britain/> 15 November 2022.

North, F.J. 1957. Sunken cities: some legends of the coast and lakes of Wales. University of Wales Press, Cardiff, 256 p.

Nurse, B. 2022. "Painful Exactness": the publications of the Society of Antiquaries of London during the directorship of Richard Gough (1771–1797). Modern Philology, 120, pp. 49–64. https://doi.org/10.1086/ 720073

Editorial responsibility: Denise Brushett

Devonian palynoevents in the circum-Arctic region

John E. A. Marshall[1*], Gunn Mangerud[2], Manuel Bringué[3] and Jonathan Bujak[4]

1. School of Ocean and Earth Science, University of Southampton, National Oceanography Centre, Southampton SO14 3ZH, UK
2. Department of Earth Science, University of Bergen, Allégaten 41, N-5007 Bergen, Norway
3. Geological Survey of Canada, 3303–3333 Street NW, Calgary, Alberta T2L 2A7, Canada
4. Bujak Research (International), Burbage Lodge, Blackpool, Lancashire FY2 9JS, UK
*Corresponding author: <jeam@soton.ac.uk>

Date received: 11 December 2021 ¶ Date accepted: 19 June 2022

ABSTRACT

Devonian strata of the present-day Arctic contain abundant and diverse assemblages of terrestrial palynomorphs, particularly from Middle and Upper Devonian sections; few intervals of Lower Devonian and Silurian strata have been palynologically studied, and these demonstrate strong palynofloral similarities across the region. Based on published records, we present a compilation of six last occurrence events (LOs), 44 first occurrence events (FOs) and one acme event that have proven of value in correlation in the present-day Arctic. Although their chronostratigraphic resolution is relatively low, and a scarcity of independent age control hampers precise age assignments, palynology is the only biostratigraphic discipline available for confident chronostratigraphic correlation of most Arctic Devonian strata.

RÉSUMÉ

Les strates dévoniennes de l'Arctique d'aujourd'hui abritent des assemblages abondants et diversifiés de palynomorphes, terrestres, en particulier des sections du Dévonien moyen et supérieur. Quelques intervalles de strates du Dévonien inférieur et du Silurien ont fait l'objet d'études palynologiques et celles-ci ont révélé des similarités palynoflorales marquées à l'échelle de la région. Nous basant sur des documents publiés, nous présentons une compilation des six dernières occurrences (DO), des 44 premières occurrences (PO) et d'un phénomène d'abondance s'étant avérés utiles pour la corrélation dans l'Arctique d'aujourd'hui. Même si leur résolution chronostratigraphique est relativement faible et que la rareté des contrôles indépendants de la datation gêne l'attribution d'âges précis, la palynologie est la seule discipline biostratigraphique dont nous disposons pour l'établissement d'une corrélation chronostratigraphique sûre de la majorité des strates dévoniennes arctiques.

[*Traduit par la redaction*]

INTRODUCTION

This article is a contribution to the Circum-Arctic Palynological Events (CAPE) project, providing a scheme of selected events for the Devonian in the present-day Arctic. The Devonian Period, extending from 419 to 359.3 Ma (Becker *et al*. 2020), is a particularly interesting time in Earth history: it saw the establishment of the terrestrial carbon cycle with the origin and spread of the first forests; their deeply rooting plants had many implications for the Earth System. In addition, it witnessed the world's largest-known and most geographically widespread reefs, together with two first order mass extinctions, the later episode terminating the Devonian Period (Becker *et al*. 2020). The Devonian is divided into three series and seven stages: the Lower Devonian comprises the Lochkovian, Pragian and Emsian stages; the Middle Devonian includes the Eifelian and Givetian stages; and the Upper Devonian is composed of the Frasnian and Famennian stages. The Devonian, like the Silurian, had its stages defined early in the development of the modern geological time scale, the last-designated Global Boundary Stratotype Section and Point (GSSP) being for the base of the Emsian (Yolkin *et al*. 1998). Two of these stages are abnormally long: the Emsian and Famennian are 16.21 and 11.8 myr respectively.

The fossils most commonly used for stratigraphic correlation in the Devonian are conodonts and, following their earliest occurrence in the lower Emsian, ammonoids. Spores have also been widely employed in the Devonian, particularly in terrestrial and nearshore marine facies. Only two spore zonal schemes cover the entire Devonian. That by Richardson and McGregor (1986), which is based on assemblages and marker taxa, is particularly relevant here as it incorporates many sections from Arctic Canada. That of

doi:10.4138/atlgeo.2022.015

Streel *et al.* (1987) is of higher resolution but is based on the classic European sections. In addition, that by Avkhimovitch *et al.* (1993) covers the late Emsian to late Famennian interval and includes many near-Arctic sections. Devonian palynological assemblages also include acritarchs, prasinophytes and chitinozoans, and these have proved very useful in stratigraphy. This is evident from the single comprehensive study of Devonian acritarchs by Playford (1977) from the sub-Arctic, which was done in parallel to that of McGregor and Camfield (1976) from the same samples.

The present Devonian compilation will complement those for other periods in the CAPE series. When all papers in the series are complete, the data will be provided as a "CAPE datapack" in Time Scale Creator (TSC; https://timescalecreator.org/index/index.php) and thus can be used with other data in TSC to make plots like that shown in Figure 1 (Bujak *et al*. 2021). Figure 1 includes the age calibration in millions of years (Ma) according to the 2020 version of TSC and Gradstein *et al.* (2020).

The events compiled herein include last occurrences (LOs), first occurrences (FOs), and an abundance event. Where possible, each event is correlated with the base of a chronostratigraphic unit, for example an ammonoid zone or a stage. If the event is not equivalent to the base of such a unit, then an estimation is given as a percentage above the base of the chronostratigraphic unit relative to the entire unit. Details of how a biostratigraphic datapack is constructed in TSC from such information are given in Bringué *et al.* (in press). Localities used for the present compilation are shown in Figure 2. Figure 1 gives a summary of zonation schemes discussed in the following section and referenced in the Palynoevents section.

PALYNOSTRATIGRAPHY

Devonian spore assemblages from the Arctic represent equatorial paleolatitude assemblages and differ from those from higher paleolatitudes where most of the calibration with marine invertebrate faunas (conodonts and ammonoids) has been based. Apart from parts of northern Russia, invertebrate zonations with zone index range bases tied to concurrent palynological zones have not been developed, and available information is generally restricted to single samples. In addition, conodont faunas are limited due to a lack of the favourable facies. This is not from lack of effort, as McGregor (1979), Streel *et al*. (1987) and others have emphasized the importance of independent age control.

A problem is a lack of studied sections from the Silurian and Early Devonian from the Arctic. Such sections exist — for example, the Silurian marine margin basin in North Greenland (Christiansen 1989). Reconnaissance studies by Nøhr-Hansen and Koppelhus (1988) and Nøhr-Hansen (1989) show that this basin contains Late Ordovician and Silurian spores, acritarchs and chitinozoans, but detailed studies are lacking. Early Devonian sections in Arctic Canada with spores have been studied (McGregor 1974; McGregor and Narbonne 1978). Also, thick Early Devonian sections exist in Svalbard, but early workers (Allen 1967) struggled to get good palynological recovery from them. This situation is now being rectified, with good spore recovery from the Lochkovian and clear potential for the establishment of a local zonation scheme (Wellman *et al.* 2022). Early Devonian sections are unknown in East Greenland and the Timan (Komi Republic) in Russia as the sedimentary basins from these regions only developed to any extent in the Middle Devonian (Larsen *et al.* 2008; O'Leary *et al*. 2004), primarily following upper Middle Devonian tectonic extension.

Devonian spores of Arctic Canada

In the Canadian Arctic Islands palynological research began with the separation of megaspores (Chaloner 1959) and spores (McGregor 1960) from single coal samples held in the archives of the Geological Survey of Canada, leading to the description of several important new taxa. Papers describing Canadian Arctic assemblages (McGregor and Owens 1966; McGregor 1967) include several early stratigraphical applications (Kerr *et al*. 1965), and they illustrated the microfloras before their formal taxonomic documentation was established. In addition, McGregor (1969) provided a significant contribution on the important and related microspore and megaspore genera *Archaeoperisaccus* and *Nikitinsporites*. The first substantive monograph (Owens 1971) was based on 20 samples Eifelian to Frasnian samples, describing new stratigraphically important genera and species. These taxa included the distinctive grapnel-tipped spore *Ancyrospora*, subsequently reviewed by Owens *et al.* (2022) in a pan-Arctic study incorporating specimens of related Russian species unavailable for the original monograph.

Significant work was also done on sections on Melville Island, with parallel studies on conodonts (McGregor and Uyeno 1972); the palynological work appeared as partial range charts (McGregor 1981), a monograph (McGregor and Camfield 1982), and a stratigraphic summary in McGregor (1994), with additional information in Richardson and McGregor (1986). Although not found in a continuous section, the *Elenisporis biformis* Subzone was recognized from Ellesmere Island (Arkhangelskaya *et al*. 1990). The latter zone, dated as early Eifelian, was originally defined from western Russia and Belarus (Arkhangelskaya 1985). A contribution by Whiteley (1980) was based on cuttings samples from the Key Point well on the Parry Islands. Of the two assemblages identified, the upper assemblage containing *Archaeoperisaccus* spp. and bifurcate tipped spores was broadly assigned a Frasnian age, and the lower assemblage, dominated by the larger zonate and camerate spores such as *Grandispora* spp., assigned a late Givetian age.

The first stratigraphic study of megaspores was by Hills *et al*. (1971) from northeastern Banks Island, now in Nunavut. This theme was further developed in a major taxonomic study of megaspores (Chi and Hills 1976a, b) from multiple sections on Banks, Melville and Prince Patrick islands, partly from the same intervals covered by McGregor and

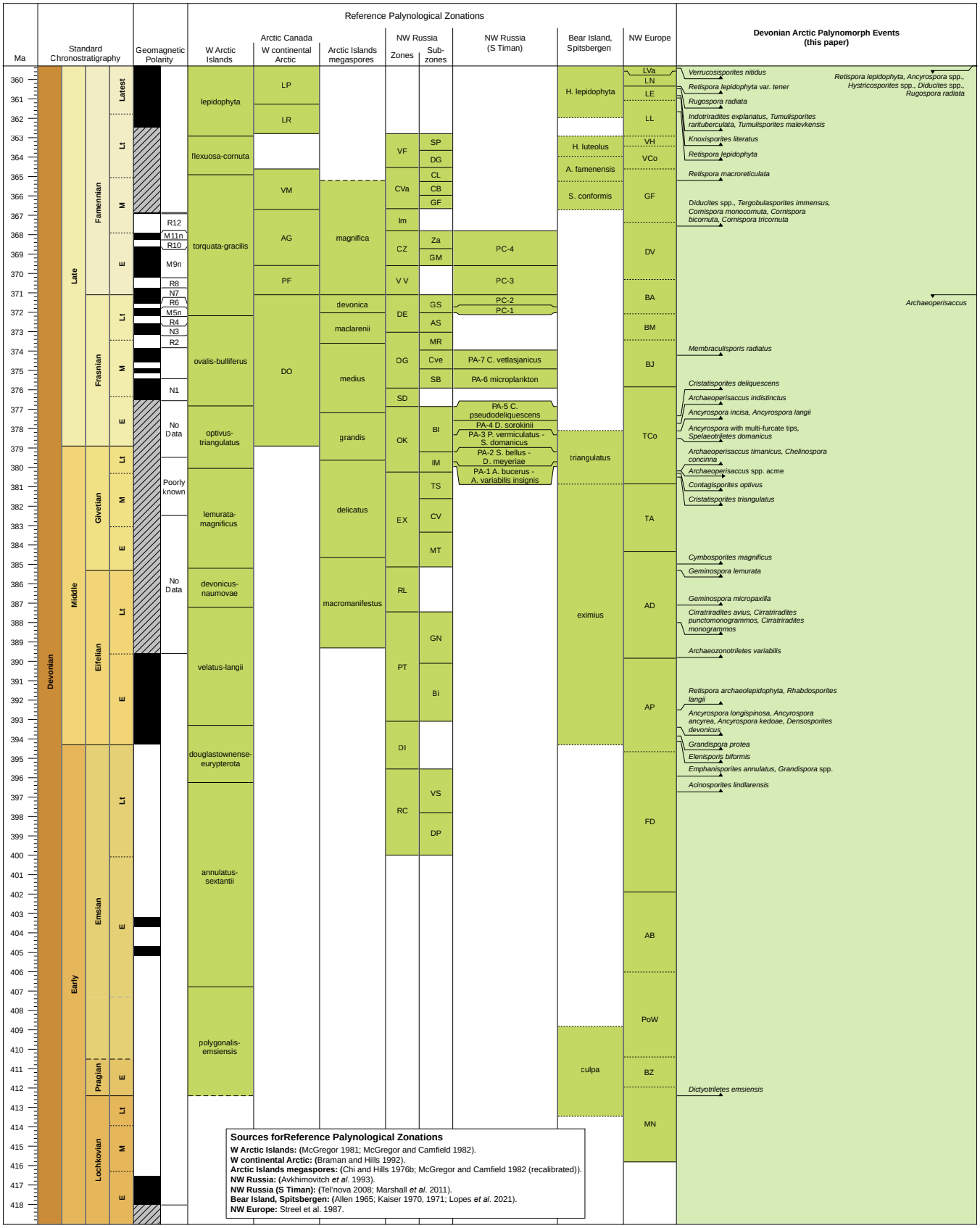

Figure 1. Chronostratigraphic plot generated using TSC showing stratigraphically significant Devonian palynological events together with Arctic and a northeastern European palynological zonation. Columns to the left of the "Reference Palynological Zonations" column are from TSC: broken lines suggest degrees of uncertainty (dashed = probable and dotted = possible). W = western; NW = northwestern; S = southern.

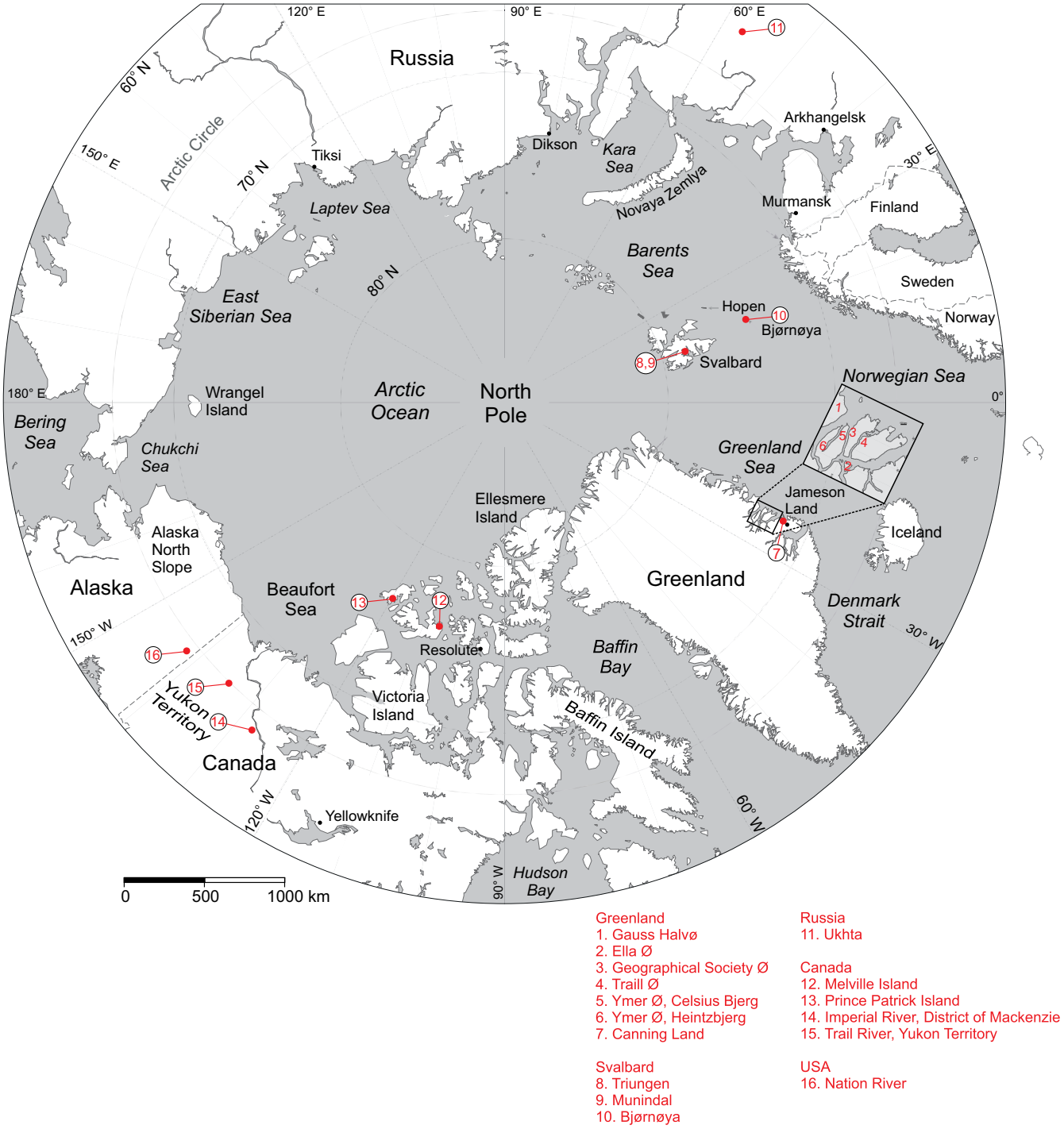

Figure 2. Circumpolar projection map showing the main Devonian localities discussed herein.

Camfield 1982). Chi and Hills (1976) erected seven megaspore zones for the Middle and early Late Devonian. These are shown in Figure 1, which also includes the important chronostratigraphic recalibration of these zones by McGregor and Camfield (1982). Subsequently, a series of taxonomic and stratigraphic papers from northern Canada (from locations now in Nunavut and the Northwest Territories sensu stricto — the latter formerly District of Mackenzie) by Chi and Hills (1974), Hyslop and Hills (1982) and Hills *et al.* (1984) used the same zonation. A major monograph (Braman and Hills 1992) included multiple sections from the Frasnian to Tournaisian in the Northwest Territories (sensu stricto) and Yukon. Braman and Hills proposed six Devonian spore zones, albeit with a middle to late Famennian stratigraphic gap. They recognized the significance of a middle Famennian zone (VM) with *Cornispora* spp. that puts in context the earlier contribution of Van der Zwan and Walton (1981). In addition Braman and Hills (1985) produced a largely

taxonomic paper on the zonally important and distinctive monolete spore *Archaeoperisaccus*, which is generally restricted to the Frasnian Stage and the present-day Arctic. No Devonian/Carboniferous boundary sections are preserved in the Canadian Arctic Islands, there being a general stratigraphic gap from about the middle Famennian up into the Visean (Utting *et al.* 1989). The Yukon sections of Braman and Hills (1992) do have a Devonian/Carboniferous boundary section but with a late Famennian stratigraphic gap between their VM and LR spore zones, consequently involving a delayed range base to *Retispora lepidophyta*.

Devonian spores of Alaska

A single data point from Alaska (Scott and Doher 1967), Frasnian in age, includes such distinctive spores as *Archaeoperisaccus* cf. *timanicus*, *Cristatisporites triangulatus*, *Contagisporites optivus* and possibly *Cymbosporites*.

Devonian spores of Greenland

Initial palynological studies from East Greenland by K.C. Allen were included in a review in Friend *et al.* (1983). Other publications focused on megaspores, including seed-megaspores and their paleobiological significance (Allen 1972). This seed-megaspore work was continued by Marshall and Hemsley (2003) who described an important early seed-mega-spore from the Givetian of Ella Ø (Ø means island), and the accompanying spore assemblage. Marshall and Astin (1996) gave a brief account of Eifelian and Givetian spores from Canning Land, including recognition of the first occurrence of the base-Givetian marker *Geminospora lemurata*. Vigran *et al.* (1999) published a palynostratigraphic scheme for the Carboniferous of East Greenland that included two zones (the *Retispora lepidophyta* Abundance Zone and the *Spelaeotriletes* spp. – *Lophozonotriletes malevkensis* Concurrent Range Assemblage) within the latest Devonian. Marshall *et al.* (1999) reported on additional palynological assemblages from the late Famennian that resolved a dating controversy involving East Greenland early tetrapods. The Devonian/Carboniferous boundary was picked within the Obrutschew Formation and further defined by Streel and Marshall (2006) and Marshall (2021). A much more detailed account was provided in the Supplementary Material (SM) of Marshall *et al.* (2020); their discussion of the Devonian/Carboniferous boundary terrestrial mass extinction was accompanied by a range chart and spore illustrations for the latest Famennian inter-val, including recognition of the spore LL, LE, LN* and VI zones.

Devonian spores of Svalbard

The first Devonian palynological work, spanning the period, was from Spitsbergen, Svalbard (Høeg 1942). This study was unusual for its time in that spores were described both from within sporangia and dispersed in the enclosing sedimentary rocks. The first specifically palynological paper was by Vigran (1964), who described spore assemblages from five late-Middle Devonian samples from the Mimerdalen area of Dickson Land, including a number of important new species (e.g., *Lycospora svalbardiae* — now *Geminospora svalbardiae*). These species have tended to be overlooked in synonymies, but their publication predates both Richardson (1965) and Allen (1965). Allen (1965, 1967, 1973) made a significant contribution in a study of both Early and Middle Devonian spores from Dickson Land (including Mimerdalen) in central Vestspitsbergen. In addition, Allen (1967) sampled numerous localities in Andrée Land, but found only rare, poorly preserved spores.

The Mimerdal sections were later investigated via a series of boreholes (Pčelina *et al.* 1986) from which several palynological assemblages were documented. Results from this work were later incorporated into Piepjohn and Dallman (2014).

Additional spores, including the first assemblages from Andreé Land, were illustrated in Schweitzer's (1999) review of the Spitsbergen Devonian flora. These later contributions concluded that the Mimerdal sequence was as young as latest Famennian based on the occurrence of *Retispora lepidophyta*. This conclusion was challenged by Berry and Marshall (2015) based on detailed resampling through the Planteryggen and Plantekløfte formations. These authors noted that the specimen of *Retispora lepidophyta* (now lost, but illustrated in Schweitzer 1999, Plate 6, fig. 10, Plate 7, fig. 1) was much larger than typical specimens, and that it had square fovea that were in fact pits caused by pyrite cubes in a specimen of *Grandispora*. Berry and Marshall (2015) also demonstrated that, from their detailed palynological and palaeobotanical analyses of the Mimerdal successions, robust correlations could be drawn to established conodont-controlled sections in Poland (Turnau and Racki 1999), as well as to the PA-3 Zone from the Timan, Russia (Tel'nova 2008) (Fig. 1). Berry and Marshall also noted that the black mudstone unit 6 of Vogt (1941), now at the base of the Fiskekløfte Member of Piepjohn and Dallman (2014), was equivalent to the late Givetian Taghanic Onlap.

The age of the Hørbyebreen Formation has been difficult to establish, estimates ranging from Famennian to Visean (Dallmann *et al.* 1999). However a key section, rediscovered during a search for early tetrapods on Triungen is a thin (~45 m) succession unconformably overlying the Emsian Wood Bay Group, and was found to contain a diversity of *Cornispora* spp. that correlate with CB Subzone of the CVa Zone (Avkhimovitch *et al.* 1993) of middle Famennian age (Marshall *et al.* 2015). This key section is unconformably succeeded by a Visean section (Lopes *et al.* 2019). A single sample from a similarly thin sequence was reported from Lomfjorden by Scheibner *et al.* (2012), and this again contained the middle Famennian *Cornispora*/*Cyrtospora* assemblage.

Palynological work on the Devonian of Bjørnøya began with descriptions of megaspores by Nathorst (1902), updated and refigured by Sen (1958). The Bjørnøya sequence has always attracted interest as it includes the then-earliest-

known commercially mined coals, which were well documented in a monograph by Horn and Orvin (1928). Spores from Bjørnøya were initially studied by Playford (1962), and were subsequently monographed by Kaiser (1970, 1971) and integrated with the paleobotanical studies of Schweitzer (1967, 1969). The spores are at a high level of thermal maturity and are not well preserved, having mineral damage. The important Bjørnøya section was resampled and restudied by Lopes *et al.* (2021), who reinterpreted the palynological assemblages with the advantage of decades of palynological studies on Devonian/Carboniferous boundary sections. These authors were able to identify and revalidate Kaiser's (1970, 1971) zonation, and also recognized the parallel zonation developed within both eastern and western Europe. Lopes *et al.* found that the *Cornispora* assemblage was present and thus permitted recognition of the Cva Zone (Avkhimovitch *et al.* 1993), together with the overlying VF Zone. Above this zone level, correlations are with western Europe, and the section includes the first occurrence of *Retispora lepidophyta* and forms allowing recognition of the upper LL to LN zones. The latter zonal attribution is based on the presence of *Indotriradites explanatus* in some sections, together with *Retispora lepidophyta* var. *minor*, which is characteristic of the *tener* event (Prestianni *et al.* 2016). Some differences in the Bjørnøya section are apparent, with *Tumulispora malevkensis* having an apparent earlier first occurrence than in western Europe. It remains unclear whether this difference is related to the more humid conditions in this paleoequatorial location.

Devonian spores of Russia

Spore assemblages from Russia occupy a special place in the study of Devonian palynology, particularly with respect to the Arctic. The systematic study of Devonian spores, motivated by the need to improve understanding of Devonian hydrocarbon reservoirs, started in Russia. A series of significant monographs, starting with that by Naumova (1953), has resulted in a unified zonation scheme (Avkhmovitch *et al.* 1993) for the Russian Platform. The scheme incorporates the same paleoequatorial palynological assemblages as found in Arctic Canada, Greenland and Svalbard. Moreover, these sections include prolific faunas of ammonoids (Becker *et al.* 2000; House *et al.* 2000) and conodonts (Ovnatanova and Kononova 2008); these two key Devonian fossil groups are central to Devonian biostratigraphy and have been continually revised and updated (Ovnatanova *et al.* 2017). The zonation in the Timan region (Sennova 1972; Durkina 1984; Avkhimovitch *et al.* 1993) extends from the late Middle Devonian to the early Famennian. In addition to regional schemes, higher resolution palynological zonations have been developed within the Timan region (Fig. 1) includ-ing seven zones (PA-1 to PA-7) through the late Givetian to middle Frasnian interval (Tel'nova 2008), and a further four zones (PC-1 to PC-4) spanning the Frasnian/Famennian boundary (Marshall *et al.* 2011).

ARCTIC DEVONIAN PALYNOEVENTS

All taxon names with authorship are listed in Appendix A and a summary of the following Devonian palynoevents is provided as Appendix B.

FO of *Dictyotriletes emsiensis*

Dictyotriletes emsiensis was originally described from short stratigraphic sections from Vestspitsbergen, Svalbard, and regarded as Emsian, but without independent age evidence apart from fossil fish. The only section from northern higher latitudes where it occurs in a long section is that from the Moose River Basin in Ontario, Canada (McGregor and Camfield 1976), where it defines the base of the *caperatus-emsiensis* Zone of late Pragian age; this section has been independently dated using conodonts (Uyeno and Bultynck 1993). The age of *Dictyotriletes emsiensis* was confirmed with a similarly faunal-controlled first occurrence in northwestern Europe. This taxon is an important spore inception, commonly used to define a zone across a wide area, including Gondwana (Melo and Loboziak 2003; Breuer and Steemans 2013), northern Europe (Streel *et al.* 1987) and Canada (McGregor 1977).

The FO of *Dictyotriletes emsiensis* is taken here as the base of the Pragian based on correlations in the Ardenne–Rhenish region (Streel *et al.* 1987).

FO of *Acinosporites lindlarensis*

Acinosporites lindlarensis has a possible first occurrence at the base of the section on Melville Island and assigned an early Eifelian age. It is the in situ spore of the lycopod *Leclercqia*, which has a late Emsian first occurrence (Richardson *et al.* 1993). Note that this spore has a densely sculptured outer wall layer that spalls off from an inner body such that it can resemble *Geminospora*, and some occurrences were initially placed in this genus — e.g., *Geminospora treverica* of Riegel (1973). In the Jaab Lake No. 1 well, the base of *Acinosporites lindlarensis* appears immediately below that of the inception of *Emphanisporites annulatus* (McGregor and Camfield 1976).

The FO of *Acinosporites lindlarensis* is taken here as 85% up from the base of the Emsian.

FO of *Emphanisporites annulatus*

Emphanisporites annulatus is a very distinctive, biostratigraphically significant spore. It has very few published occurrences in the Arctic, with only a single unequivocal specimen from Melville Island (McGregor and Camfield 1982); this record is from within the Eifelian and above its range base as defined elsewhere. However, the range base occurs in the Moose River Basin (McGregor and Camfield 1976), where conodonts indicate an upper Emsian inception above the incomplete range of the conodont *serotinus* Zone (Uyeno and Bultynck 1993).

The FO of *Emphanisporites annulatus* is taken here as 90% up from the base of the Emsian.

FO of *Grandispora* spp.

This event marks the first occurrences of the wider group of camerate spores that are zonate — i.e., have an equatorial extension. They all have well-spaced sculpture that varies from small coni to long spines, normally bearing simple tips. They have no documented first occurrences in the Arctic, but occur in the latest Emsian in the Moose River Basin (McGregor and Camfield 1976). Sporadic earlier occurrences occur in Gondwana (Melo and Loboziak 2003).

The FO of *Grandispora* spp. is taken here as 90% up from the base of the Emsian.

FO of *Elenisporis biformis*

This event is defined on the inception of *Elenisporis biformis* a spore characterized by prominent ribs on the proximal contact face. It has been widely recognized across western Russia and Belarus, where it has been incorporated into regional spore zonations (Arkhangelskaya 1985). Subsequently it has been recognized at a single level from Ellesmere Island (Arkhangelskaya *et al*. 1990). Its associated palynological assemblage and a conodont assemblage higher in a correlative section places it in the early Eifelian.

The FO of *Elenisporis biformis* is taken here as 2% up from the base of the Eifelian stage.

FO of *Grandispora protea*

On Melville Island (McGregor and Camfield 1976) *Grandispora protea* has a first occurrence in the earliest Eifelian, above that of *Rhabdosporites langii*; but in western Europe *Grandispora protea* appears earlier.

The FO of *Grandispora protea* occurs in the early Eifelian and is taken here as 5% above the base of the Eifelian.

FOs of *Ancyrospora longispinosa*, *Ancyrospora ancyrea*, *Ancyrospora kedoae* and *Densosporites devonicus*

Important from the latest Early Devonian to the Devonian-Carboniferous boundary are a group of spores with processes that have bifurcate tips. Those with an extended zona are placed in *Ancyrospora*. *Ancyrospora longispinosa* has long bifurcate tipped processes and an early Eifelian first occurrence on Melville Island (McGregor and Camfield 1976), more or less synchronous with the first occurrence of the much smaller (in size and spine length) *Ancyrospora ancyrea*. However, *Ancyrospora ancyrea* has a longer range, and both species are more typical of the Eifelian.

Ancyrospora kedoae is representative of a distinctive group of species within *Ancyrospora* that have relatively small bifurcate tipped spines on an otherwise relatively large spore. Others within the group are *Ancyrospora eurypterota*, *Ancyrospora loganii* and *Ancyrospora nettersheimensis*. On Melville Island (McGregor and Camfield 1976) all species in this group have early Eifelian first occurrences at the base of the studied section. In the Ardenne–Rhenish region of northwestern Europe they have earlier first occurrences, in the latest Emsian, and form a distinctive assemblage (Riegel 1982).

Densosporites devonicus has a distinctive annular thickening within a thinner equatorial cingulum. Although it is assigned to *Densosporites*, it is quite dissimilar to the diverse group of Carboniferous densospores (Staplin and Jansonius 1964)

The FOs of *Ancyrospora longispinosa*, *Ancyrospora ancyrea, Ancyrospora kedoae* and *Densosporites devonicus* occur in the early Eifelian and are taken here as 10% above the base of the Eifelian.

FO of *Retispora archaeolepidophyta*

This species consists of camerate spores with an exoexine that forms a reticulate mesh. Although placed appropriately within *Retispora*, it appears unrelated to *Retispora lepidophyta*, and a considerable range gap occurs between their occurrences. The exoexine of *Retispora archaeolepidophyta* is more like to a mesh, whereas in *Retispora lepidophyta* it has the form of an outer wall perforated by foveae. On Melville Island *Retispora archaeolepidophyta* is persistent through the Eifelian and early Givetian (McGregor and Camfield 1976). Although rarely reported, the species does occur in the Eifelian of both Shetland (at 60°N; Marshall 1988) and Caithness (personal observations) in northern Scotland. The species was originally described from Belarus (Kedo 1955), and Plax *et al*. (2016) included more recent late Eifelian records that are independently dated with conodonts.

The FO of *Retispora archaeolepidophyta* occurs in the early Eifelian and is taken here as 20% above the base of the Eifelian.

FO of *Rhabdosporites langii*

This spore is known in situ from the aneurophytalean progymnosperms and is particularly abundant in the late Eifelian and early Givetian. It is distinctively camerate and covered by closely packed coni. Its first occurrence in Melville Island is below the base of the studied section (McGregor and Camfield 1982). In the Moose River Basin (Jaab Lake No. 1 well) it has a delayed first occurrence (McGregor and Camfield 1976) above an interval with poor spore recovery.

The FO of *Rhabdosporites langii* is taken here as 60% above the base of the conodont *costatus* Zone based on its first occurrence in the Ardenne–Rhenish area (Riegel 1982). This equates with 20% above the base of the Eifelian.

FO of *Archaeozonotriletes variabilis*

Archaeozonotriletes variabilis is a somewhat unusual spore in having a distinctive distal thickening or patina. It is widely distributed paleogeographically and is present in

many Arctic sections. It has a middle Eifelian first occurrence on Melville Island (McGregor and Camfield 1982) that is partially age-controlled by conodont assemblages (McGregor 1981).

The FO of *Archaeozonotriletes variabilis* is taken here as 50% above the base of the Eifelian.

FO *Cirratriradites avius*, *Cirratriradites punctomonogrammos* and *Cirratriradites monogrammos*

Cirratriradites avius was described by Allen (1965) from Svalbard but may be a heterotypic junior synonym of *Cirratriradites punctomonogrammos*. *Cirratriradites avius* is a distinctive flattened zonate spore with a prominent triangular shape. *Cirratriradites monogrammos* is identical but has a distal sculpture in the form of a flattened reticulum. All forms are widely distributed paleogeographically (Xu *et al*. 2014).

In Svalbard *Cirratriradites avius* has a Givetian age but, as it occurs in a short stratigraphic section, its true range remains unknown. However, data from Lithuania, Russia and Belarus (the RL Zone of Avkhimovitch *et al.* 1993; Plax *et al*. 2016), all south of the Arctic, indicate a late Eifelian first occurrence. The range of *Cirratriradites avius* and related species includes the conodont *kockelianus* and *ensis* zones, which are late Eifelian.

The FOs of *Cirratriradites avius*, *Cirratriradites punctomonogrammos* and *Cirratriradites monogrammos* occur in the late Eifelian and are taken here as 70% above the base of the Eifelian.

FO of *Geminospora micropaxilla*

Geminospora is a genus of small camerate spores, often with a subtle separation between a thin walled intexine and a patinate or thickened exoexine. It contains a number of related forms sometimes separated into distinct species, but the variation can be circumscribed broadly under the name *Geminospora lemurata* (McGregor and Camfield 1982). The surface beyond the contact face is covered with closely packed coni. The species is the in situ microspore of archaeopteridalean progymnosperms, an important group of plants with a Givetian first occurrence that formed the first deeply rooted forests (Stein *et al.* 2019). Some authors (e.g., Tel'nova 2007) recognize several species of *Geminospora* based on both specimens found in situ from fertile *Archaeopteris* fronds and dispersed spores. On Melville Island (McGregor and Camfield 1982) the earliest species of *Geminospora* to occur is *Geminospora micropaxilla* (originally *Rhabdosporites micropaxillus*); compared to other species in the genus, this species is larger in diameter and has a wider separation between intexine and exoexine. It is thus closer in morphology to the *Rhabdosporites* spores of the aneurophytalean progymnosperms, the group into which this species was originally assigned. Other species of *Geminospora* appear higher in the section on Melville Island, above the range of *Cymbosporites magnificus*.

The FO of *Geminospora micropaxilla* occurs in the latest Eifelian and is taken here as 80% above the base of the Eifelian.

FO of *Geminospora lemurata*

A stratigraphically higher group of *Geminospora* includes *Geminospora tuberculata* and *Geminospora micromanifesta*. The latter is probably a heterotypic junior synonym of *Geminospora svalbardiae* (D.C. McGregor, pers. comm.), first described by Vigran (1964) from Svalbard or more generally within *Geminospora lemurata*. *Geminospora svalbardiae* is abundant within the Mimerdalen Subgroup but no clear range base was determined from the limited sections available to Allen (1965, 1967). However, the range base of *Geminospora lemurata* is present within the Nathorst Fjord Group in Canning Land, East Greenland (Marshall and Astin 1996) although not constrained by any independent faunal evidence apart from some rather ambiguously dated fish.

On Melville Island (McGregor and Camfield 1982) the situation is more problematic as five species and varieties of *Geminospora* were identified, all of which could probably be placed within *Geminospora lemurata*. Their appearance may mark the base of the Givetian stage, but there is insufficient conodont data to be more specific.

The FO of *Geminospora lemurata* occurs at the base of the Givetian based on conodont correlations in Germany (Loboziak *et al.* 1991).

FO of *Cymbosporites magnificus*

Cymbosporites magnificus is a spore distinguished by a patinate or thickened exoexine covered with closely packed verrucae. It probably derives from the arborescent lycopod *Protolepidodendropsis* and is abundant in Givetian and early Frasnian sections in the Arctic (Berry and Marshall 2015). It has long been known to occur in Arctic coals (McGregor 1960) where its dominance demonstrates that its parent plant formed paleoequatorial wetland forests at that time (Marshall *et al*. 2019). The first occurrence of *Cymbosporites magnificus* on Melville Island postdates that of *Geminospora micropaxilla*. It occurs widely across the Arctic — in Svalbard, the sub-polar Urals, and as far south as the Volga River area, where it has been called *Archaeozonotriletes vorobjensis* and *Archaeozonotriletes tamilii* (V.N. Mantsurova, pers. comm. 2014). The parent plant is heterosporous and has a much larger, but morphologically similar, megaspore referred to *Verrucisporites submamillarius*. This megaspore is widely known from Arctic Canada (Chi and Hills 1976a). However, it does not occur across the entirety of the Arctic, being absent from sections in East Greenland that are either too distant from the paleoequator or too arid, being deep within the Old Red Sandstone Continent (Torsvik and Cocks 2017). It is also absent from both western Europe (including Shetland at 60°N) and southern North America.

The FO of *Cymbosporites magnificus* occurs in the early Givetian and is taken here as 5% above the base of the Givetian.

FO of *Cristatisporites triangulatus*

Cristatisporites triangulatus is a distinctive species that has some biostratigraphic significance and has been used to define a zone base in several schemes. Allen (1982) revised the species description using additional material, including further Arctic occurrences. The species consists of small lightly sculptured spores with a circular inner body and a distinctly triangular equatorial cingulum that is extended along the trilete rays but thins to almost nothing in the interradial areas. In Arctic Canada McGregor (1981) assigned it a late Givetian first occurrence, whereas in western Europe it has an early Givetian conodont-controlled first occurrence (Loboziak *et al.* 1991); however, the identity of these much earlier specimens is the subject of discussion (Turnau and Narkiewicz 2011).

The FO of *Cristatisporites triangulatus* on Melville Island is placed high in the Givetian based on its co-occurrence with *Archaeoperisaccus timanicus*, and beneath the occurrence of the influx of *Archaeoperisaccus* spp. In terms of conodont stratigraphy this event occurs in the middle of the conodont *triangularis* Zone (McGregor 1981, 1994). This placement is supported by the appearance of *Cristatisporites triangulatus* in the late Givetian of Russia in or slightly below the TS Subzone (Avkhimovitch *et al.* 1993).

The FO of *Cristatisporites triangulatus* is taken here as 75% above the base of the Givetian.

FO of *Contagisporites optivus*

Contagisporites optivus is the megaspore pairing with the microspore *Geminospora lemurata*. It occurs widely across the Arctic, in Arctic Canada, Alaska, East Greenland, Svalbard and the Timan. Regarding its range base, the best study was by Chi and Hills (1976a), which was exclusively on mega spores. Importantly these authors studied the identical section on Melville Island as that examined by McGregor and Camfield (1982).

Contagisporites optivus is rare at its range base. It usually only becomes abundant in the latest Givetian, above the Taghanic Event and coincident with the Geneseo Taghanic Onlap. Spore extinctions occur at the Taghanic Event, and both *Geminospora* and *Contagisporites* become more dominant at and above this level; hence the latter's appearance in zonal schemes at this horizon (e.g., the OK Zone of Avkhimovitch *et al.* 1993 with the O referring to *optivus*). Before the definition of the base Frasnian GSSP, the stage base was considered coincident with the latest Givetian Geneseo Onlap, and this was a much more obvious level at which to place the boundary. This history explains why older zonations give *Contagisporites optivus* a Frasnian range base. On Melville Island the first occurrence of *Contagisporites optivus* is not coincident with that of either *Geminospora micropaxilla* or *Geminospora tuberculata*/*micromanifestus*, but 200 m higher and above a sample gap. But it should be noted that earlier occurrences of *Contagisporites optivus* can be somewhat morphologically different from typical specimens of the species (Marshall 1996). No range base for *Contagisporites optivus* is known in other Arctic sections, although the species occurs in Canning Land. The sections in the Timan probably start just above its range base (Tel'nova 2008).

The FO of *Contagisporites optivus* occurs at the base of the late Givetian at the Geneseo Onlap and coincident with the base of the conodont *Schmidtognathus hermanii* Zone. It is taken here as the base of the late Givetian.

FO of *Chelinospora concinna*

A prominent group of Givetian small spores with a thick distal patina centre around *Archaeozonotriletes variabilis*. In northwestern Europe this group is given an early Givetian first occurrence, but has been recorded as having a somewhat earlier late Eifelian first occurrence from the Melville Island section (McGregor and Camfield 1982). *Archaeozonoriletes variabilis* is widely distributed across the Arctic and is well known from Spitsbergen and northern Russia (Allen 1965, 1967; Avkhimovitch *et al.* 1993). *Chelinospora concinna* is similar to *Archaeozonotriletes variabilis* in having a much reduced distal patina dissected to a reticulum. Together with related species, *Chelinospora concinna* occurs in profusion (Allen 1965, 1967) in the Givetian of Spitsbergen.

The FO of *Chelinospora concinna* is placed 80% above the base of the Givetian.

FO *Archaeoperisaccus timanicus* and the acme of *Archaeoperisaccus* spp.

This group of sculptured monolete spores characterize the Frasnian of the Arctic regions; they have been recorded in Canada, Alaska, northern Russia, Greenland and Spitsbergen, but have not been found farther south than the northern North Sea, the Baltic area (Latvia) and Siberia (Marshall *et al.* 1996). Spores in this group have first occurrences in the latest-Givetian BI Subzone of Avkhimovitch *et al.* (1993), with *Archaeoperisaccus timanicus* being a typical and common species. These first occurrences were often placed in the early Frasnian because the latest Givetian OK Zone was assigned to the early Frasnian prior to definition of the base-Frasnian GSSP. A significant number of *Archaeoperisaccus* species have been described and an attempt was made to discriminate between them by Braman and Hills (1985). They reach an acme in the OG Zone of Avkhimovitch *et al.* (1993), then declining and becoming extinct in the very latest Frasnian, at the Frasnian/Famennian mass extinction. *Archaeoperisaccus* species have range bases on Melville Island (McGregor 1981) that were also placed in the latest Givetian and broadly coincident with that of *Chelinospora concinna*, but in a widely spaced set of samples and without independent age control.

The FO of *Archaeoperisaccus timanicus* is taken here as 80% above the base of the Givetian. The acme is in the middle Frasnian, 50% above the base of the stage.

FO of *Ancyrospora* with multifurcate tips

Most species of *Ancyrospora* and *Hystricosporites* have spines with bifurcate or grapnel tips. But in the Frasnian, including in the Arctic (McGregor and Owens 1966; Owens 1971) the trend is for more species to have multifurcate tips, the grapnels having been reduced to a number of spines. These species with multifurcate tips have a conodont-controlled earliest-Frasnian first occurrence (Turnau and Narkiewicz 2011); they all became extinct at the Devonian/Carboniferous boundary.

The FO of *Ancyrospora* with multi-furcate tips is taken here as 5% above the base of the Frasnian.

FO of *Spelaeotriletes domanicus*

A plexus of robust species of *Spelaeotriletes* with well-spaced sculpture consists of *Spelaeotriletes krestovnikovii*, *Spelaeotriletes bellus* and *Spelaeotriletes domanicus*. *Spelaeotriletes krestovnikovii* has a range base at basement in the Timan, where it occurs with abundant *Contagisporites optivus* and *Ancyrospora incisa* (Tel'nova 2008). There then follow the successive appearances of *Spelaeotriletes bellus* and *Spelaeotriletes domanicus*. The most distinctive species is *Spelaeotriletes domanicus*, with a coarse net or reticulum on the surface of the exoexine, which has nodes at the bases of the spines. *Spelaeotriletes domanicus* was recorded as *Hymenozonotriletes domanicus* in the Frasnian of Arctic Canada (the DO Zone of Braman and Hills 1992), but again at the base of the studied section; so the first occurrence is not known. The species also occurs at 58.8°N in BP well 14/6-1 in the North Sea (Marshall *et al*. 1996). Avkhimovitch *et al*. (1993) noted the increasing abundance of the species in their IM Subzone.

The FO of *Spelaeotriletes domanicus* is taken here as 5% above the base of the Frasnian.

FOs of *Ancyrospora incisa* and *Ancyrospora langii*

Ancyrospora incisa is an important biostratigraphic indicator that marks the base of the *incisa-micromanifesta* Zone that has a conodont-controlled first occurrence in the latest Givetian (Turnau and Racki 1999). It has been recorded mostly from Russia and Poland. The closely related *Ancyrospora langii* was first described from France and then in the Arctic, in Spitsbergen and Canada (McGregor 1981; Braman and Hills 1992; Owens *et al*. 2022). Allen (1965) considered that *Ancyrospora langii* would be conspecific with *Ancyrospora incisa* if the latter was shown to have bifurcate tips although these were not evident from its original description and illustration. It is now known to possess bifurcate tips (Kedo and Obukhovskaya 1981; Avkhimovitch *et al*. 1993). *Ancyrospora langii* has a first occurrence in the late-Early Frasnian DO Zone in Yukon (Braman and Hills 1992) and occurs above *Archaeoperisaccus timanicus* in Melville Island (McGregor 1981).

The FOs of *Ancyrospora incisa* and *Ancyrospora langii* are taken here as 10% above the base of the Frasnian.

FO of *Archaeoperisaccus indistinctus*

Archaeoperisaccus indistinctus has a somewhat surprising first occurrence within the Frasnian of East Greenland. It is a distinctive species of *Archaeoperisaccus*, first described from China and northern Australia as *Archaeoperisaccus indistinctus* or *Archaeoperisaccus rhacodes*. (Lu 1988; Hashemi and Playford 2005). It was earlier considered to be restricted to Australasia but appears in the early Frasnian in East Greenland (JEAM personal observations).

Its FO is uncertain, but it occurs with *Cristatisporites deliquescens* and *Membraculisporis radiatus*. It is taken as 15% above the base of the Frasnian.

FO of *Cristatisporites deliquescens*

Cristatisporites deliquescens is an important component of Frasnian spore assemblages, having a first occurrence in the early Frasnian SD Zone of Avkhimovitch *et al*. (1993) and an extinction at the Frasnian/Famennian boundary. Braman and Hills (1992) recorded its first occurrence at the base of the DO Zone and the base of their section. In the Timan (Tel'nova 2008) the first occurrence is in the PA-5 assemblage of the Ust'-Yarega Formation, which contains the goniatite *Hoeninghausia nalivkini* (Becker *et al*. 2000), equivalent to the conodont MN3 Zone of early Frasnian age.

The FO of *Cristatisporites deliquescens* is taken here as 20% above the base of the Frasnian.

FO of *Membraculisporis radiatus*

Membraculisporis radiatus is a very distinctive spore with three clearly distinguishable wall layers, the outer one being covered with radial folds. It is a typical species in the middle to late Frasnian in the Arctic, occurring in East Greenland, Yukon (Braman and Hills 1992), with a range base coincident with the middle DO Subzone. The species was first recognized in Russia, occurring in the Timan (Avkhimovitch *et al*. 1993), where it it has an inception and sporadic occurrence in the conodont CVe Zone (with lower *Palmatolepis gigas* Zone conodonts), but becomes more abundant upwards and defines the MR zone, where it is abundant; its abundance is a characteristic that continues into the overlying DE Zone.

The FO of *Membraculisporis radiatus* is taken here as 60% above the base of the Frasnian.

LO of *Archaeoperisaccus*

The mass extinction at the Frasnian/Famennian boundary includes spore disappearances, although this aspect is not particularly well understood because of a general absence of high-resolution studies. The mass extinction is, in fact, a pair of extinction events, each characterized by a black mudstone (the Lower and Upper Kellwasser; Becker *et al*. 2020)

within each of which multiple taxa become extinct among conodonts, ammonoids, trilobites and cnidarians. The only high-level clade to become extinct was the tentaculoids (Bond 2006), and this can be recognized palynologically (Marshall and Tel'nova 2017) through the disappearance of the internal linings of these otherwise calcareous microfossils. The current consensus, as evidenced by the mercury proxy (Racki *et al.* 2018) and geochronological dating (Ernst *et al.* 2020), is that the cause of the Frasnian–Famennian mass extinction was the the destabilization of the Earth System by two major phases of eruption from a large igneous province. The only detailed record through "Arctic" Frasnian–Famennian spore assemblages is that by Braman and Hills (1992). In their account, the boundary is placed on an older conodont definition (within the conodont *triangularis* Zone) rather than at the conodont *gigastriangularis* Zone boundary. Palynological assemblages across the boundary were reviewed by Streel *et al.* (2000), who replotted data, including those from Braman and Hills 1992) so as to show last occurrences. As for the invertebrates, the compilation by Streel *et al.* shows a series of spore extinctions somewhat below the level of the Frasnian/Famennian boundary and coincident with the PF/DO zonal boundary of Braman and Hills (1992). Notable extinctions include all species of *Archaeoperisaccus*, the only clade that appears to become extinct (but see Marshall 2021). Other notable extinctions are *Spelaeotriletes domanicus*, *Membraculisporis radiatus* and a several species of *Ancyrospora* and *Hystricosporites*. Braman and Hills (1992) defined the boundary as the replacement in a lineage of *Vallatisporites preanthoideus* by *Vallatisporites anthoideus* at their spore PF/AG Zone boundary.

Many of the Frasnian/Famennian boundary sections are in marginal marine sedimentary successions and include hiatuses above both of the Kellwasser black mudstones. This situation is present throughout much of the Timan (Obukhovskaya *et al.* 2000). However, a science borehole at Sosnogorsk was drilled through a more complete Frasnian/Famennian boundary section that enabled the recognition of four palynocomplexes (PC 1–4), with the disappearance of characteristic Frasnian taxa occurring in PC-2 (Marshall *et al.* 2011). In addition, the PC-2 assemblage was also characterized by the incoming of highly variable species, *Grandispora pseudodeliquescens* (Tel'nova and Marshall 2009).

The LO of of *Archaeoperisaccus* is taken as the base of the Famennian.

FOs of *Tergobulasporites immensus* and *Diducites* spp.

The first occurrence of the megaspore *Tergobulasporites immensus*, formerly known as *Lagenoisporites immensus*, was used to define the base of the lm Zone of Avkhimovitch *et al.* (1993). This event coincides with the first occurrence of the distinctive group of Famennian species of *Diducites* (e.g., *Diducites poljessica* and *Diducites versabilis*), characterized with an external diaphanous third wall layer of outer exoexine. These species appear in East Greenland, but above their range base (Marshall *et al.* 2020). The lm Zone is placed in the latest early Famennian.

The FOs of *Tergobulasporites immensus* and *Diducites* spp. are taken here as 30% above the base of the Famennian.

FOs of *Cornispora monocornuta*, *Cornispora bicornuta* and *Cornispora tricornuta*

This very distinctive plexus of spores are characterized by the variable development of one, two or three irregularly developed horns on an otherwise simple spore. They are characteristic of assemblages across the Arctic (Streel 1986) and have a middle Famennian first occurrence. However, they do not occur further south until the delayed latest Devonian first occurrence of the related *Cyrtospora cristifera*. In the Timan the three species are used to define two subzones of the CVa Zone, with a maximum proliferation and diversity of 1–3 horned forms defining the CB Subzone. In Canada, *Cornispora bicornuta* and *Cornispora tricornuta* are grouped as the *Cornispora varicornuta* morphon (Van der Zwan and Walton 1981) and used to define the VM Zone (Braman and Hills 1992). They are also present in both Vestspitsbergen (Scheibner *et al.* 2012) and Bjørnøya. Importantly, the Bjørnøya section (Kaiser 1971; Lopes *et al.* 2021) is continuous with overlying latest Famennian strata characterized by *Retispora lepidophyta*.

The FO of *Cornispora monocornuta* is coincident with that of *Tergobulasporites immensus* and *Diducites* spp., so the FOs of *Cornispora monocornuta*, *Cornispora bicornuta* and *Cornispora tricornuta* are taken here as 30% above the base of the Famennian, although in Russia they are reported as occurring in the sequential order of *Cornispora monocornuta*, *Cornispora bicornuta* and *Cornispora tricornuta* (Avkhimovitch *et al.* 1993; Sennova 1972).

FO of *Retispora macroreticulata*

This species is similar to *Retispora lepidophyta* but with a much larger overall size (average 150 μm) and with larger foveae. It has a first occurrence before that of *Retispora lepidophyta* and the two species have a partial range overlap. The species and range overlap occur in East Greenland, but the range bases are not seen there (Marshall *et al.* 2020). In Avkhimovitch *et al.* (1993), *Retispora macroreticulata* has a first occurrence in the DG Zone, and co-occurs with foraminifera of the *Quasiendothyra communis* Zone.

The FO of *Retispora macroreticulata* is taken here as 50% above the base of the Famennian.

FO of *Retispora lepidophyta*

Retispora lepidophyta is the most significant latest Famennian spore; it appears to be globally distributed and has a short range and a distinctive morphology. Outside the Arctic it has a FO just below the base of the conodont upper *exp-*

ansa Zone (Streel 2009). It is a component of all latest Famennian zonations. Braman and Hills (1992) reported it above a stratigraphic gap in their LR and LP Zones in Yukon. It is also abundant in many localities in Bjørnøya but, as shown by Lopes *et al.* (2021), these represent short sections that are difficult to correlate. The sections probably start high in the LL Zone, so the range base of *Retispora lepidophyta* is not present.

In East Greenland the best section with *Retispora lepidophyta* is on Stensiö Bjerg on Gauss Halvø (Marshall *et al.* 2020). Here the first occurrence of *Retispora lepidophyta* occurs in the upper part of the Britta Dal Formation, above some 500 m of section barren of spores. This event accompanies a change in the paleoclimate from a long interval of sustained aridity to one of higher seasonality that included humid episodes. The first occurrence *Retispora lepidophyta* is some 100 m below the first occurrence of *Indotriradites explanatus*, so a significant fraction of its total range must be present. *Retispora lepidophyta* was also used by Vigran *et al.* (1999) to define the *Retispora lepidophyta* Abundance Zone and the *Spelaeotriletes* spp. – *Lophozonotriletes malevkensis* Assemblage Zone. The first occurrence of *Retispora lepidophyta* has been extensively studied (e.g., Streel 2009) although the event appears not to have been independently dated in the Arctic.

The FO of *Retispora lepidophyta* is taken here as 80% above the base of the Famennian.

FO of *Knoxisporites literatus*

In East Greenland (Marshall *et al.* 2020, Supplementary Material) *Knoxisporites literatus* has a FO in the uppermost LL Zone, immediately beneath that of *Indotriradites explanatus*. So its FO is taken here as 86% above the base of the Famennian.

FOs of *Indotriradites explanatus*, *Tumulispora rarituberculata* and *Tumulispora malevkensis*

Indotriradites explanatus is a widely distributed spore with a distinctive zona, including a thickened inner ring. It occurs in the latest Famennian of Bjørnøya (Lopes *et al.* 2021), which supports the general late LL to LE age given to the sections there. In East Greenland it occurs in both the Stensiö Bjerg and Nathorst Bjerg sections (Marshall *et al.* 2020), where its first occurrence is coincident with strata representing a stratified lake deposit that reflects a short interval of warmer, more humid climate.

Streel (2009) placed the base of *Indotriradites explanatus* at about the base of the conodont lower *presulcata* Zone, some 1.6 myr below the Devonian/Carboniferous boundary and 13% into the estimated duration of the Famennian; thus, the FO of *Indotriradites explanatus* is taken here as 87% above the base of the Famennian.

Tumulispora rarituberculata and *Tumulispora malevkensis* are distinctive spores that have been used in zonation schemes by, for example, Higgs *et al.* (1988), which specify a first occurrence at the base of the LN Zone. However, in Bjørnøya the two species have an earlier first occurrence (Lopes *et al.* 2021); and in East Greenland (Marshall *et al.* 2020), their first occurrences are coincident with the base of the LE Zone. So the presence of humid conditions was appears to have controlled the first occurrence of these spores.

The FOs of *Tumulispora rarituberculata* and *Tumulispora malevkensis* coincide with that of *Indotriradites explanatus* and are taken here as at 87% above the base of the Famennian.

FO of *Rugospora radiata*

Rugospora radiata has a first occurrence in East Greenland above that of *Indotriradites explanatus* (Marshall *et al.* 2020). It was not recorded in the Yukon sections of Braman and Hills (1992), or from Bjørnøya by Lopes *et al.* (2021). In terms of section thickness, it lies at 25% into the interval between the first occurrence of *Indotriradites explanatus* and the Devonian/Carboniferous boundary; so the FO of *Rugospora radiata* is taken here as is 90% above the base of the Famennian.

FO of *Retispora lepidophyta* var. *tener*

This first occurrence is the *tener* event of Prestianni *et al.* (2016), defined by the occurrence of a small variant of *Retispora lepidophyta*. The event was reported from Bjørnøya by Kaiser (1970, 1971) as the *Hymenozonotriletes lepidophytus* var. *minor* Zone and this identification as the *tener* event was corroborated by Lopes *et al.* (2021). In East Greenland small specimens of *Retispora lepidophyta* occur after the first occurrences of both *Indotriradites explanatus* and *Rugospora radiata* (JEAM, personal observations). In age, this event occurs one-third up in the section between the FO of *Indotriradites explanatus* and the Devonian/Carboniferous boundary: hence, the FO of *Retispora lepidophyta* var. *tener* is taken here as 91% above the base of the Famennian.

FO of *Verrucosisporites nitidus*

The first occurrence of *Verrucosisporites nitidus* defines the base of the LN Zone. Difficulties in its application have arisen because spores that are variably verrucate have been placed in the species. Turnau *et al.* (1994) gave a more tightly circumscribed definition, restricting the species to spores with a continuous cover of hemispherical verrucae. In addition, the first occurrence has also caused problems as it appears to be absent in some sections. Differences in the timing of inception have been variously attributed to ecological control or, by Prestianni *et al.* (2016), to differential spore transport to distal environments. The section from East Greenland clarified this situation, with Marshall (2021) finding a distinct increase in diversity, including *Verrucosisporites nitidus*, some 1.5 m below the Devonian/Carboniferous boundary, associated with the humidification that accompanied the flooding of the basin by the deep,

stratified and wide lake represented by the Obrutschew Formation. This change reflected the climatic amelioration that accompanied the collapse of the terminal latest Famennian glaciation. Hence, the first appearance of *Verrucosisporites nitidus* is controlled by climate — specifically relatively more humid conditions. This increase in spore diversity immediately beneath the VI zone has been recognized in other sections and referred to as the LN transitional zone (notation as LN*) of Higgs *et al.* (1993).

The FO of *Verrucosisporites nitidus* in East Greenland occurs within the Obrutschew lake cycle that is coincident with the Devonian/Carboniferous boundary (Marshall *et al.* 2020). This orbitally forced lacustrine cycle represents either precession or obliquity, i.e., a fraction of 20 or 40 kyr. With a Famennian duration conservatively estimated at some 12 myr (Becker *et al.* 2020), the lacustrine cycle represents less than 1% of that total duration. So the FO of *Verrucosisporites nitidus* is taken here as 99% above the base of the Famennian.

LOs of *Retispora lepidophyta*, *Ancyrospora* spp., *Hystricosporites* spp., *Diducites* spp. and *Rugospora radiata*

High resolution sampling across the Devonian/Carboniferous boundary from sections in East Greenland (Marshall *et al.* 2020; Marshall 2021) show that the distinctive, abundant and globally distributed spore species, *Retispora lepidophyta*, becomes extinct over a short time interval; the event is coincident with the disappearance of *Diducites*, all the grapnel tipped spores (*Ancyrospora* and *Hystricosporites*), and *Rugospora radiata*. The event marks the LN*/VI zonal boundary. This combined last appearance is seen in other Arctic sections, most notably at the LP/VB zonal boundary of Braman and Hills (1992). In Bjørnøya, no stratigraphic sections with continuous palynological recovery occur across the Devonian/Carboniferous boundary, but there is a clear extinction of *Retispora lepidophyta* and related forms (Kaiser 1970). The extinction of *Retispora lepidophyta* has also been recognized in a number of sections in the Timan (Sennova 1972; Durkina 1984).

We note here that *Vallatisporites pusillites and Vallatisporites verrucosus* are important first occurrences in latest Famennian zonations from lower latitudes (e.g., New York State, USA). However, these species are absent or rare in Arctic assemblages below the earliest Carboniferous VI spore assemblage (Mangerud *et al.* 2021).

The LOs of *Retispora lepidophyta*, *Ancyrospora* spp., *Hystricosporites* spp., *Diducites* spp. and *Rugospora radiata* are taken here as the base of the Tournaisian.

ACKNOWLEDGEMENTS

John Marshall gratefully acknowledges the contribution of Olga Tel'nova (Syktyvkar, Komi Republic) for productive collaboration and providing an insight into Russian Devonian spores. We thank Gilda Lopes and Geoffrey Playford for their helpful reviews of the manuscript.

REFERENCES

Allen, K.C. 1965. Lower and Middle Devonian spores of North and Central Vestspitsbergen. Palaeontology, 8, pp. 687–748.

Allen, K.C. 1967. Spore assemblages and their stratigraphical application in the Lower and Middle Devonian of North and Central Vestspitsbergen. Palaeontology, 10, pp. 280–297.

Allen, K.C. 1972. Devonian megaspores from East Greenland: their bearing on the development of certain trends. Review of Palaeobotany and Palynology, 14, pp. 7–17. https://doi.org/10.1016/0034-6667(72)90004-8

Allen, K.C. 1973. Further information on the Lower and Middle Devonian spores from Dickson Land, Spitsbergen. Norsk Polarinstitutt Årbok 1971, pp. 43–54.

Allen, K.C. 1982. *Samarisporites triangulatus* Allen, 1965, an important Devonian miospore, and its synonymous species. Pollen et Spores, 24, pp. 157–166.

Arkhangelskaya, A.D. 1963. New species of spores from Devonian deposits of the Russian Platform, Trudy VNIGRI, 37, pp. 18–30, 122–153.

Arkhangelskaya, A.D. 1985. Zonal spore assemblages and stratigraphy of the Lower and Middle Devonian in the Russian Plate. *In* Atlas of spores and pollen from the Phanerozoic petroleum formations in the Russian and Turanian plates. *Edited by* V.V. Menner and T.V. Byvsheva. Trudy Vsesoiuznogo Nauchno Issledovatel'skogo Geologo-razvedochnogo Neftianogo Institute (VNIGNI), Moscow, pp. 5–21.

Arkhangelskaya, A.D. 1987. New genus and some species of spores from the Frasnian stage of the Volgograd Region. Paleontology Journal 1987, 3, pp. 84–91.

Arkhangelskaya, A.D., McGregor, D.C., and Richardson, J.B. 1990. Correlation of the lower Middle Devonian *Elenisporis biformis* spore subzone in Arctic Canada and the U.S.S.R. *In* Current Research Part D. Geological Survey of Canada, Paper 90-ID, pp. 213–217. https://doi.org/10.4095/131357

Avkhimovitch, V.I., Tchibrikova, E.V., Obukhovskaya, T.G., Nazarenko, A.M., Umnova, V.T., Raskatova, L.G., Mantsurova, V.N., Loboziak, S., and Streel, M. 1993. Middle and Upper Devonian miospore zonation of Eastern Europe. Bulletin des Centres de Recherches Exploration–Production Elf–Aquitaine, 17, pp. 79–147.

Balme, B.E. 1962. Upper Devonian (Frasnian) spores from the Carnarvon Basin, Western Australia. The Palaeobotanist, 9, pp. 1–10. https://doi.org/10.54991/jop.1960.590

Becker, R.T., House, M.R., Menner, V.V., and Ovnatanova, N.S. 2000. Revision of ammonoid biostratigraphy in the Frasnian (Upper Devonian) of the southern Timan (Northeast Russian Platform). Acta Geologica Polonica, 50, pp. 67–97.

Becker, R.T., Marshall, J.E.A., and Da Silva, A.-C. 2020. The Devonian Period. *In* The Geological Time Scale 2020. *Edited by* F.M. Gradstein, J.G. Ogg, M.D. Schmitz, and G.M. Ogg, 2, pp. 733–810. https://doi.org/10.1016/B978-0-12-

824360-2.00022-X

Berry, W. 1937. Spores from the Pennington Coal, Rhea County, Tennessee. The American Midland Naturalist, 18 (1), pp. 155–160. https://doi.org/10.2307/2420626

Berry, C.M. and Marshall, J.E.A. 2015. Lycopsid forests in the early Late Devonian paleoequatorial zone of Svalbard. Geology, 43, pp. 1043–1046. https://doi.org/10.1130/G37000.1

Bond, D. 2006. The fate of homoctenids (Tentaculitoidea) during the Frasnian–Famennian mass extinction (Late Devonian). Geobiology, 4, pp. 167–177. https://doi.org/10.1111/j.1472-4669.2006.00078.x

Braman, D.R. and Hills, L.V. 1985. The spore genus *Archaeoperisaccus* and its occurrence within the Upper Devonian Imperial Formation, District of Mackenzie, Canada. Canadian Journal of Earth Sciences, 22, pp. 1118–1132. https://doi.org/10.1139/e85-114

Braman, D.R. and Hills, L.V. 1992. Upper Devonian and Lower Carboniferous miospores, western District of Mackenzie and Yukon Territory, Canada. Palaeontographica Canadiana, 8, pp. 1–97.

Breuer, P. and Steemans, P. 2013. Devonian spore assemblages from northwestern Gondwana. Special Papers in Palaeontology, 89, pp. 1–163.

Bringué, M., Fensome, R.A., Poulton, T.P., Galloway, J.M., Bujak, J.P., Golding, M.L., Orchard, M.J., and Williams, G.L. in press. The 2020 Canada datapack for TimeScale Creator: a new tool for Mesozoic–Cenozoic stratigraphy of the Canadian North. Geological Survey of Canada, Bulletin 609. https://doi.org/10.1130/abs/2020AM-353274

Bujak, J., Fensome, R., Mangerud, G., and Williams, G. 2021. Introduction to the "Circum-Arctic Palynological Event Stratigraphy" (CAPE) series of papers. Atlantic Geology, 57, pp. 1–5. https://doi.org/10.4138/atlgeol.2021.001

Byvscheva, T.V. 1985. Spores of the Tournaisian and Visean deposits around the Russian Platform. Zonal spore assemblages and stratigraphy of the Lower and Middle Devonian in the Russian Plate. *In* Atlas of spores and pollen from the Phanerozoic petroleum formations in the Russian and Turanian plates. *Edited by* V.V. Menner and T.V. Byvsheva. Trudy Vsesoiuznogo Nauchno Issledovatel'skogo Geologo-razvedochnogo Neftianogo Institute (VNIGNI), Moscow, pp. 80–158.

Chaloner, W.G. 1959. Devonian megaspores from Arctic Canada. Palaeontology, 1, pp. 321–332.

Chi, B.I. and Hills, L.V. 1974. Stratigraphic and paleoenvironmental significance of Upper Devonian megaspore type section of the Imperial Formation, Northwest Territories, Canada. *In* Proceedings of a Symposium on Canadian Arctic Geology, *Edited by* J.D. Aitken and D.J. Glass. Geological Association of Canada – Canadian Society of Petroleum Geologists Symposium, Saskatoon, Saskatchewan, pp. 241–257.

Chi, B.I. and Hills, L.V. 1976a Biostratigraphy and taxonomy of Devonian megaspores, Arctic Canada: Bulletin of Canadian Petroleum Geology, 24, pp. 640–818.

Chi, B.I. and Hills, L.V. 1976b. Morphological variation and stratigraphic significance of *Triangulatisporites rootsii* Chaloner. Canadian Journal of Earth Sciences, 13, pp. 847–861. https://doi.org/10.1139/e76-088

Chibrikova E.V. 1959. Spores from the Devonian and older rocks from Bashkiria. Academy of Sciences of USSR, Bashkir Branch, Data on Palaeontology and Stratigraphy of Devonian and Older Deposits of Bashkiria, pp. 3–116.

Christiansen, F.G. 1989. Petroleum geology of North Greenland. Grønlands Geologiske Undersøgelse, 158, pp. 1–92. https://doi.org/10.34194/bullggu.v158.6700

Dallmann, W.K., Gjelberg, J.G., Harland, W.B., Johannessen, E.P., Keilen, H.B., Lønøy, A., Nilsson, I., and Worsley, D. 1999. Upper Palaeozoic lithostratigraphy. *In* Lithostratigraphic lexicon of Svalbard. Review and recommendations for nomenclature use. Upper Palaeozoic to Quaternary bedrock. *Edited by* W.K. Dallmann. Norsk Polarinstitutt, pp. 25–126.

Dolby, G. and Neves, R. 1970. Palynological evidence concerning the Devonian–Carboniferous boundary in the Mendips, England. Compte rendu 6e Congrès de Stratigraphie et de Géologie du Carbonifère (Sheffield, 1967) 2, pp. 631–646.

Durkina, A.V. 1984. Biostratigraphy of the Devonian–Carboniferous Boundary, 3, Timan–Pechora Province. Akademii Nauk, USSR, pp. 1–68.

Eisenack, A. 1944. Über einige pflanziche Funde in geschieben, nebst Bemerkungen, zum Hystrichosphaerideen-Problem. Zeitschrift für Geschiebeforsch, 19, pp. 103–124.

Ernst, R.E., Rodygin, S.A., and Grinev, O.M. 2020. Age correlation of Large Igneous Provinces with Devonian biotic crises. Global and Planetary Change, 185. https://doi.org/10.1016/j.gloplacha.2019.103097

Filippova, M.F., Aronova, S.N., Afremova, M.F. 1958. Devonian sediments of the central regions of the Russian Platform. VNIGNI, Gostop Techizdat.

Friend, P.F., Alexander-Marrack, P.D., Allen, K.C., Nicholson, J., and Yeats, A.K. 1983. Devonian sediments of East Greenland, VI. Review of results. Meddelelser om Grønland, 206, pp. 1–96.

Gradstein, F.M., Ogg, J.G., Schmitz M.D., and Ogg, G.M. 2020. The Geological Time Scale 2020, Elsevier, 1357 pp.

Hacquebard, P. A. 1957. Plant spores in coal from the Horton Group (Mississippian) of Nova Scotia. Micropaleontology, 3, pp. 301–324. https://doi.org/10.2307/1484439

Hashemi, H. and Playford, G. 2005. Devonian miospore assemblages of the Adavale Basin, Queensland (Australia): descriptive systematics and stratigraphic significance. Revista Española de Micropaleontologia, 7, pp. 317–417.

Higgs, K., Clayton, G., and Keegan, J.B. 1988. Stratigraphic and systematic palynology of the Tournaisian rocks of Ireland. The Geological Survey of Ireland, Special Paper Number 7, pp. 1–93.

Higgs, K.T., Streel, M., Korn, D., and Paproth, E. 1993. Palynological data from the Devonian–Carboniferous boundary beds in the new Stockum Trench II and the Hasselbachtal borehole, Northern Rhenish Massif, Ger-

many. Annales de la Société Géologique de Belgique, 115, pp. 551–557.

Hills, L.V., Smith R.E., and Sweet, A.R. 1971. Upper Devonian megaspores, northeastern Banks Island, N.W.T. Bulletin of Canadian Petroleum Geology, 19, pp. 799–811.

Hills, L.V., Hyslop, K., and Braman, D.R. 1984. Megaspores, Imperial Formation (Upper Devonian), Mountain River, District of Mackenzie. Bulletin of Canadian Petroleum Geology, 32, pp. 233–236.

Høeg, O.A. 1942. The Downtonian and Devonian flora of Spitsbergen. Norges Svalbard-og Ishavs-Undersøkelser, 83, pp. 1–229.

Hoffmeister, W.S., Staplin, F.L., and Malloy, R.E. 1955. Mississippian plant spores from the Hardinsburg Formation of Illinois and Kentucky. Journal of Paleontology, 29, pp. 372–399.

Horn, G. and Orvin, A. 1928. Geology of Bear Island. Skrifter om Svalbard og Ishavet 15, pp. 1–152.

House, M.R., Menner, V.V., Becker, R.T., Klapper, G., Ovnatanova, N.S., and Kuz'min, V. 2000. Reef episodes, anoxia and sea-level changes in the Frasnian of the southern Timan (NE Russian Platform). *In* Carbonate Platform Systems: components and interactions. *Edited by* E. Insalaco, P.W. Skelton, and T.J. Palmer. Geological Society of London Special Publication, 178, pp. 147–176. https://doi.org/10.1144/GSL.SP.2000.178.01.11

Hyslop, K. and Hills, L.V. 1982. *Lagenicula validespinosa*, Imperial Formation, District of Mackenzie. Bulletin of Canadian Petroleum Geology, 30, pp. 230–235.

Kaiser, H. 1970. Die Oberdevon-Flora der Bäreninsel. 3. Mikroflora des höheren Oberdevons und des Unterkarbons. Palaeontographica Abteilung B, 129, pp. 71–124.

Kaiser, H. 1971. Die Oberdevon-Flora der Bäreninsel 4. Mikroflora der Misery-Serie und der flözleered Sandstein-Serie. Palaeontographica Abteilung B, 135, pp. 127–164.

Kedo, G.I. 1955. Spores of the Middle Devonian of the northeastern Byelorussian SSR. Academy of Sciences of BSSR, Institute of Geological Sciences, Palaeontology and Stratigraphy of BSSR, Sbornik, 1, pp. 5–59.

Kedo, G. I. 1957. Spores from the supra-salt Devonian deposits of the Pripyat Depression and their stratigraphic significance. Paleontology and Stratigraphy, B.S.S.R. Minsk, Akad Nauk B.S.S.R., 1, 5–47.

Kedo, G.I. 1963. Spores of the Tournaisian Stage of the Pripyat Depression and their stratigraphic significance. Academy of Sciences of BSSR, Institute of Geological Sciences, Palaeontology and Stratigraphy of BSSR, Sbornik, 4, pp. 3–131.

Kedo, G. I. 1974. The Devonian-Carboniferous Boundary in the Pripyatskaya Vpadina (Depression) as revealed by palynological data. *In* Palynology of the Proterophyte and Paleophyte, Nauka, 86–92.

Kedo, G.I. and Obukhovskaya, T.G. 1981. Middle Devonian of Baltic and northeast Belarus. *In* Devonian and Carboniferous of Baltic. Zinatne, Riga, 502 pp.

Kedo, G.I., Nazarenko, A.M., Nekriata, N.C., Raskatova, L.G., Sennova, V.F., and Chibrikova, E.V. 1971. New species of spores from Famennian deposits of the Pripyat Depression, central regions of the Russian Platform, Volga–Ural oil and gas province and Timan. *In* BelNIGRI, The palynology research in the Byelorussia and other regions of the USSR. *Edited by* G.I. Kedo, pp. 172–205.

Kerr, J.W., McGregor, D.C., and McLaren, D.J. 1965. An unconformity between Middle and Upper Devonian rocks of Bathurst Island, with comments on Upper Devonian faunas and microfloras from the Parry Islands. Bulletin of Canadian Petroleum Geology, 13, pp. 409–431.

Larsen, P-H., Olsen, H., and Clack, J.A. 2008. The Devonian basin in East Greenland—Review of basin evolution and vertebrate assemblages. *In* The Greenland Caledonides: evolution of the northeast margin of Laurentia. *Edited by* A.K. Higgins, J.A. Gilotti and M.P. Smith. Geological Society of America, Memoir 202, pp. 273–292. https://doi.org/10.1130/2008.1202(11)

Loboziak, S., Streel, M., and Weddige, K. 1991. Miospores, the *lemurata* and *triangulatus* levels and their faunal indices near the Eifelian/Givetian boundary in the Eifel (F.R.G.). Annales de la Société Géologique de Belgique, 113, pp. 299–313.

Lopes, G., Mangerud, G., and Clayton, G. 2019. The palynostratigraphy of the Mississippian Birger Johnsonfjellet section, Spitsbergen, Svalbard, Palynology, 43 (4), pp. 631–649, https://doi.org/10.1080/01916122.2018.1518849

Lopes, G., Mangerud, G., Clayton, G., and Vigran, J.O. 2021. Palynostratigraphic reassessment of the Late Devonian of Bjørnøya, Svalbard. Review of Palaeobotany and Palynology, 286. https://doi.org/10.1016/j.revpalbo.2020.104376

Lu Lichang. 1988. Middle Devonian microflora of the Haickou Formation at Shijiapo in Zhanyi of Yunnan, China. Memoirs of the Nanjing Institute of Geology and Palaeontology, Academica Sinica, 24, pp. 109–222.

Luber, A.A. and Waltz, I.E. 1938. Classification and stratigraphic value of spores of some Carboniferous coal deposits in the USSR. Trudy Vsesoyuznyy Nauchno-Issleologorazvedochniy Neftyanoy Institut (VNIGRI), 105, pp. 1–46.

Luber, A.A. and Waltz, I.E. 1941. Atlas of microspores and pollen grains of the Paleozoic of the U.S.S.R. Soviet Union Geological Institute Transactions, VSEGEI, 139, 107 pp.

Mangerud, G., Paterson, N.W., and Bujak, J. 2021. Triassic palynoevents in the circum-Arctic region. (CAPE) series of papers. Atlantic Geology, 57, pp. 71–101. https://doi.org/10.4138/atlgeol.2021.005

Marshall, J.E.A. 1988. Devonian miospores from Papa Stour, Shetland. Transactions of the Royal Society of Edinburgh: Earth Sciences, 79, pp. 13–18. https://doi.org/10.1017/S0263593300014073

Marshall, J.E.A. 1996. *Rhabdosporites langii*, *Geminospora lemurata* and *Contagisporites optivus*: an origin for heterospory within the Progymnosperms. Review of Palaeobotany and Palynology, 93, pp. 159–189. https://doi.org/10.1016/0034-6667(95)00125-5

Marshall, J.E.A. 2021. A terrestrial Devonian–Carboniferous boundary section in East Greenland. Palaeobiodiver-

sity and Palaeoenvironments, 101, pp. 541–559. https://doi.org/10.1007/s12549-020-00448-x

Marshall, J.E.A. and Astin, T.R. 1996. An ecological control on the distribution of the Devonian fish *Asterolepis*. Newsletters in Stratigraphy, 33, pp. 133–144. https://doi.org/10.1127/nos/33/1995/133

Marshall, J.E.A. and Hemsley A.R. 2003. A Mid Devonian seed-megaspore from East Greenland and the origin of the seed plants. Palaeontology, 46, pp. 647–670. https://doi.org/10.1111/1475-4983.00314

Marshall, J.E.A. and Tel'nova, O.P. 2017. The 'last' tentaculitoids. Palynology, 41, pp. 178–188. https://doi.org/10.1080/01916122.2017.1362215

Marshall, J.E.A., Rogers, D.A., and Whiteley, M.J. 1996. Devonian marine incursions into the Orcadian Basin, Scotland. Journal of the Geological Society of London, 153, pp. 451–466. https://doi.org/10.1144/gsjgs.153.3.0451

Marshall, J.E.A., Astin, T.R., and Clack, J.A. 1999. The East Greenland tetrapods are Devonian in age. Geology, 27, pp. 637–640. https://doi.org/10.1130/0091-7613(1999)027<0637:EGTADI>2.3.CO;2

Marshall, J.E.A., Tel'nova, O.P., and Vetoshkina, O.S. 2011. Ecosystem crisis at the Frasnian–Famennian boundary (southern Timan). Doklady Earth Sciences, 440, pp. 1396–1398. https://doi.org/10.1134/S1028334X11100217

Marshall, J., Lindemann, F.J., Finney, S., and Berry, C. 2015. A mid Famennian (Late Devonian) spore assemblage from Svalbard and its significance. *In* CIMP Meeting 2015, Abstract Book, 25. *Edited by* G. Mangerud, G. Lopes, M. Vecoli, and R. Wicander, 1 p.

Marshall, J.E.A., Tel'nova, O.P., and Berry, C.M. 2019. Devonian and Early Carboniferous coals and the evolution of wetlands. Vestnik IG Komi SC UB RAS, 2019, (10), pp. 12–15. https://doi.org/10.19110/2221-1381-2019-10-12-15

Marshall, J.E.A., Lakin, J., Troth, I., and Wallace-Johnson, S.M. 2020. UV-B radiation was the Devonian–Carboniferous terrestrial extinction kill mechanism. Science Advances, 6. https://doi.org/10.1126/sciadv.aba0768

McGregor, D.C. 1960. Devonian spores from Melville Island, Canadian Arctic Archipelago. Palaeontology, 3, pp. 26–44.

McGregor, D.C. 1961. Spores with proximal radial pattern from the Devonian of Canada. Geological Survey of Canada Bulletin, 76, pp. 1–11. https://doi.org/10.4095/100594

McGregor, D.C. 1967. Composition and range of some Devonian spore assemblages of Canada. Review of Palaeobotany and Palynology, 1, pp. 173–183. https://doi.org/10.1016/0034-6667(67)90119-4

McGregor, D.C. 1969. Devonian plant fossils of the genera *Kryshtofovichia*, *Nikitinsporites*, and *Archaeoperisaccus*. Geological Survey of Canada, Bulletin, 182, pp. 91–93. https://doi.org/10.4095/100900

McGregor, D.C. 1973. Lower and Middle Devonian spores of eastern Gaspé, Canada. I. Systematics. Palaeontographica Abteilung B, 142, pp. 1–77.

McGregor, D.C. 1974. Early Devonian spores from central Ellesmere Island, Canadian Arctic. Canadian Journal of Earth Sciences, 11, pp. 70–78. https://doi.org/10.1139/e74-006

McGregor, D.C. 1977. Lower and Middle Devonian spores of eastern Gaspé, Canada. II. Biostratigraphy. Palaeontographica Abteilung B, 163, pp. 111–142.

McGregor, D.C. 1979. Devonian miospores of North America. Palynology, 3, pp. 31–52. https://doi.org/10.1080/01916122.1979.9989183

McGregor, D.C. 1981. Spores and the Middle–Upper Devonian boundary. Review of Palaeobotany and Palynology, 34, pp. 25–47. https://doi.org/10.1016/0034-6667(81)90064-6

McGregor, D.C. 1994. Palynological correlation of the Middle and Upper Devonian rocks of Melville Island, Arctic Canada. Geological Survey of Canada Bulletin, 450, pp. 111–120. https://doi.org/10.4095/194018

McGregor, D.C. and Camfield, M. 1976. Upper Silurian? to Middle Devonian spores of the Moose River Basin, Ontario. Geological Survey of Canada, Bulletin, 263, pp. 1–63. https://doi.org/10.4095/103961

McGregor, D.C. and Camfield, M. 1982. Middle Devonian miospores from the Cape de Bray, Weatherall, and Hecla Bay formations of northeastern Melville Island, Canadian Arctic. Geological Survey of Canada, Bulletin, 348, pp. 1–105. https://doi.org/10.4095/119434

McGregor, D.C. and Narbonne, G.M. 1978. Upper Silurian trilete spores and other microfossils from the Read Bay Formation, Cornwallis Island, Canadian Arctic. Canadian Journal of Earth Sciences, 15, pp. 1292–1303. https://doi.org/10.1139/e78-136

McGregor, D.C. and Owens, B. 1966. Illustrations of Canadian fossils: Devonian spores of eastern and northern Canada. Geological Survey of Canada Paper, 1966, 66, no. 30, pp. 1–66. https://doi.org/10.4095/100965

McGregor, D.C. and Uyeno, T.T. 1972. Devonian spores and conodonts of Melville and Bathurst Islands, District of Franklin. Geological Survey of Canada, Paper 71-13, pp. 1–36. https://doi.org/10.4095/100693

Melo, J.H.G. and Loboziak, S. 2003. Devonian–Early Carboniferous miospore biostratigraphy of the Amazon Basin, northern Brazil. Review of Palaeobotany and Palynology, 124, pp. 131–202. https://doi.org/10.1016/S0034-6667(02)00184-7

Moreau-Benoit, A. 1980. Les spores du Dévonien de Libye, deuxième partie. Cahiers de Micropaléontologie, 1.1980, pp. 1–53.

Nathorst, A.G. 1902. Zur oberdevonischen Flora der Bären-Insel. Kungliga Svenska Vetenskapsakademiens Handlingar, 366, 60 pp. https://doi.org/10.5962/bhl.title.7637

Naumova, S.N. 1953. Upper Devonian spore–pollen assemblages of the Russian Platform and their stratigraphic significance. Transactions of the Institute of Geological Sciences, Academy of Sciences of the USSR, 143 (Geological Series no. 60), pp. 1–204.

Nazarenko, A.M., Kedo, G.I., Araslanova, R.M., Zhadanova, L.R., Lomaeva, E.T., Raskatova, L.G., Sennova, V.F.,

Sergeeva, L.A., Umnova, V.T., and Shishova, G.M. 1971. New species from the Frasnian Stage of the Russian Platform and Altai. *In* Palynological Research in Byelorussia and other regions of the USSR. BEINIGRI, pp. 155–172.

Neves, R. and Owens, B. 1966. Some Namurian camerate miospores from the English Pennines. Pollen et Spores, 8, pp. 337–360.

Nøhr-Hansen, H. 1989. Palynological studies of the organic matter. *In* Petroleum geology of North Greenland. *Edited by* F.G. Christiansen, Grønlands Geologiske Undersøgelse, 158, pp. 27–31. https://doi.org/10.34194/bullggu.v158.6703

Nøhr-Hansen, H. and Koppelhus, E.B. 1988. Ordovician spores with trilete rays from Washington Land, North Greenland. Review of Palaeobotany and Palynology, 56, pp. 305–311. https://doi.org/10.1016/0034-6667(88)90062-0

Obukhovskaya T.G., Avkhimovitch V.I., Streel M., and Loboziak, S. 2000. Miospores from the Frasnian–Famennian boundary deposits in Eastern Europe (the Pripyat Depression, Belarus and the Timan–Pechora Province, Russia) and comparison with Western Europe (northern France). Review of Palaeobotany and Palynology, 112, pp. 229–246. https://doi.org/10.1016/S0034-6667(00)00045-2

O'Leary, N., White, N., Tull, S., Bashilov, V., Kuprin, V., Natapov, L., and Macdonald, D. 2004. Evolution of the Timan–Pechora and South Barents Sea basins. Geological Magazine, 141, pp. 141–160. https://doi.org/10.1017/S0016756804008908

Ovnatanova, N.S. and Kononova, L.I. 2008. Frasnian conodonts from the eastern Russian Platform. Paleontological Journal, 42, pp. 997–1166. https://doi.org/10.1134/S0031030108100018

Ovnatanova, N.S., Kononova, L.I., Kolesnik, L.S., and Gatovsky, Y.A. 2017. Upper Devonian conodonts of northeastern European Russia. Paleontological Journal, 51, pp. 973–1165. https://doi.org/10.1134/S003103011710001X

Owens, B. 1971. Miospores from the Middle and early Upper Devonian rocks of the western Queen Elizabeth Islands, Arctic Archipelago. Geological Survey of Canada, Paper, 70-38, pp. 1–157. https://doi.org/10.4095/100689

Owens, B., Marshall, J.E.A., Tel'nova, O.P., and Wellman, C.H. 2022. Morphological relationships of *Ancyrospora* species from the Givetian and Frasnian deposits of the Pan-Arctic Region. Paleontology Journal, 56, pp. 58–80.

Pashkevitch, N.G. 1964. New species of *Archaeoperisaccus* (Gymnospermae) from northern Timan. Paleontology Journal, 1964. pp. 126–129.

Pčelina, T.M., Bogač, S.I., and Gavrilov B.P. 1986. New data on the lithostratigraphy of the Devonian deposits of the region of Mimerdalen of the Svalbard Archipelago. *In* Geology of the sedimentary blanket of the archipelago of Spitsbergen. *Edited by* A.A. Krasil'ščikov and M.N. Mirzaev, Leningrad, Sevmorgeologija, pp. 7–19.

Piepjohn, K. and Dallmann, W.K. 2014. Stratigraphy of the uppermost Old Red Sandstone of Svalbard (Mimerdalen Subgroup): Polar Research, 33:1. https://doi.org/10.3402/polar.v33.19998

Plax, D.P., Kruchek, S.A., and Obukhovskaya, V.Y. 2016. Stratigraphy of Eifelian Stage deposits of the Middle Devonian in the western part of the Pripyat Trough. Litasphera, 2 (45), pp. 29–47.

Playford, G. 1962 Lower Carboniferous microfloras of Spitsbergen. Palaeontology, 5, pp. 550–618.

Playford, G. 1963. Lower Carboniferous microfloras of Spitsbergen. Palaeontology, 5, pp. 619–678.

Playford, G. 1964. Miospores from the Mississippian Horton Group, eastern Canada. Geological Survey of Canada, Bulletin, 107, pp. 1–47. https://doi.org/10.4095/120064

Playford G. 1976. Plant microfossils from the Upper Devonian and Lower Carboniferous of the Canning Basin, Western Australia. Palaeontographica, Abteilung B, 158, pp. 1–71.

Playford, G. 1977. Lower to Middle Devonian acritarchs of the Moose River Basin, Ontario. Geological Survey of Canada, Bulletin, 279, pp. 1–87. https://doi.org/10.4095/102867

Playford, G. 1983. The Devonian miospore genus *Geminospora* Balme 1962: a reappraisal based upon topotypic *G. lemurata* (type species). Memoirs of the Association of Australasian Palaeontologists, 1, pp. 311–325.

Playford, G. 1991. Australian Lower Carboniferous miospores relevant to extra-Gondwanic correlations: an evaluation. Courier Forschungsinstitut Senckenberg, 130, pp. 85–125.

Prestianni, C., Sautois, M., and Denayer, J. 2016. Disrupted continental environments around the Devonian–Carboniferous Boundary: introduction of the *tener* event. Geologica Belgica, 19, pp. 135–145. https://doi.org/10.20341/gb.2016.013

Racki, G., Rakociński, M., Marynowski, L., and Wignall, P.B. 2018. Mercury enrichments and the Frasnian–Famennian biotic crisis: a volcanic trigger proved? Geology, 46, pp. 543–546. https://doi.org/10.1130/G40233.1

Richardson, J.B. 1960. Spores from the Middle Old Red Sandstone of Cromarty, Scotland. Palaeontology, 3, pp. 45–63.

Richardson, J.B. 1962. Spores with bifurcate processes from the Middle Old Red Sandstone of Scotland. Palaeontology, 5, pp. 171–194.

Richardson, J.B. 1965. Middle Old Red Sandstone spore assemblages from the Orcadian basin north-east Scotland. Palaeontology, 7, pp. 559–605.

Richardson, J.B. and McGregor, D.C. 1986. Silurian and Devonian spore zones of the Old Red Sandstone continent and adjacent regions. Geological Survey of Canada, Bulletin, 364, pp. 1–79. https://doi.org/10.4095/120614

Richardson, J.B., Bonamo, P., and McGregor, D.C. 1993. The spores of *Leclercqia* and the dispersed spore morphon *Acinosporites lindlarensis* Riegel: a case of gradualistic evolution. Bulletin of the Natural History Museum, London, Geology Series, 49, pp. 121–155. https://doi.org/10.5962/p.313808

Riegel, W. 1968. Die Mitteldevon-Flora von Lindlar (Rhein-

land) 2. Sporae dispersae. Palaeontographica Abteilung B, 123, pp. 76–96.

Riegel, W. 1973. Sporenformen aus den Heisdorf-, Lauch- und Nohn-Schichten (Emsium und Eifelium) der Eifel, Rheinland. Palaeontographica, Abteilung B, 142, pp. 78–104.

Riegel, W. 1982. Palynological aspects of the Lower/Middle Devonian transition in the Eifel Region. Courier Forschungsinstitut Senckenberg, 55, pp. 279–292.

Scheibner, C., Hartkopf-Fröder, C., Blomeir, D., and Forke, H. 2012. The Mississippian (Lower Carboniferous) in northeast Spitsbergen (Svalbard) and a re-evaluation of the Billefjorden Group. Zeitschrift der Deutschen Gesellschaft für Geowissenschaften, 163/3, pp. 293–308. https://doi.org/10.1127/1860-1804/2012/0163-0293

Schweitzer, H.-J. 1967. Die Oberdevon-Flora der Bareninsel. 1. *Pseudobornia ursina* Nathorst. Palaeontographica Abteilung B, 120, pp. 116–137.

Schweitzer, H.-J., 1969. Die Oberdevon-Flora der Bareninsel 2. Lycopodinae. Palaeontographica Abteilung B, 126, pp. 101–137.

Schweitzer, H.-J. 1999. Die Devonflores Spitzbergens. Palaeontographica Abteilung B., 252, pp. 1–222.

Scott, R.A. and Doher, L.I. 1967. Palynological evidence for Devonian age of the Nation River Formation, east-central Alaska. United States Geological Survey, Professional Paper 375B, pp. B45–B49.

Sen, J. 1958. On the megaspores described by Nathorst from the Upper Devonian of Bear Island. Geologiska Föreningen i Stockholm Förhandlingar, 80, 2, pp. 141–148. https://doi.org/10.1080/11035895809447224

Sennova, V.F. 1972. Upper Devonian spore and pollen assemblages in the Timan–Pechora Province. *In* Geology and petroleum potential in the north-east of the European USSR. Syktyvkar, 2, pp. 99–108.

Staplin, F.L. 1960. Upper Mississippian plant spores from the Golata Formation, Alberta, Canada. Palaeontographica, Abteilung B, 107 (1), pp. 1–40.

Staplin, F.L. 1961. New plant spores similar to *Torispora* Balme. Journal of Paleontology, 35, pp. 1227–1231.

Staplin, F.L. and Jansonius, J. 1964. Elucidation of some Paleozoic densospores. Palaeontographica Abteilung B. 114, pp. 95–117.

Stein, W.E., Berry, C.M., Morris, J.L., Hernick, L.V., Mannolini, F., Ver Straeten, C., Landing, E., Marshall, J.E.A., Wellman, C.H., Beerling, D.J., and Leake, J.R. 2019. Mid-Devonian *Archaeopteris* roots signal revolutionary change in earliest fossil forests. Current Biology, 30, pp. 1–11. https://doi.org/10.1016/j.cub.2019.11.067

Streel, M. 1986. Miospore contribution to the upper Famennian–Strunian event stratigraphy. Annales de la Société géologique de Belgique, 109, pp. 75–92.

Streel, M. 2009. Upper Devonian miospore and conodont zone correlation in western Europe. *In* Devonian change: case studies in palaeogeography and palaeoecology. *Edited by* P. Königshof, Special Publication of the Geological Society of London, 314, pp. 163–176. https://doi.org/10.1144/SP314.9

Streel, M. and Marshall, J.E.A. 2006. Devonian–Carboniferous boundary global correlations and their paleogeographic implications for assembly of Pangaea. *In* Proceedings of the XVth International Congress on Carboniferous and Permian Stratigraphy. Utrecht, the Netherlands, 10–16 August 2003. *Edited by* T.E. Wong, Royal Netherlands Academy of Arts and Sciences, pp. 481–496.

Streel, M., Higgs, K., Loboziak, S., Riegel, W., and Steemans, P. 1987. Spore stratigraphy and correlation with faunas and floras in the type marine Devonian of the Ardenne–Rhenish regions. Review of Palaeobotany and Palynology, 50, pp. 211–229. https://doi.org/10.1016/0034-6667(87)90001-7

Streel, M., Caputo, M.V., Loboziak, S., and Melo, J.H.G. 2000. Late Frasnian–Famennian climates based on palynomorph analyses and the question of the Late Devonian glaciations. Earth-Science Reviews, 52, pp. 121–173. https://doi.org/10.1016/S0012-8252(00)00026-X

Taugourdeau-Lantz, J. 1960. Sur la microflore du Frasnien Inférieur de Beaulieu (Boulonnais). Revue de Micropaléontologie, 3, pp. 144–154.

Tel'nova, O.P. 2007. Miospores in Middle to Upper Devonian sediments of the Timan–Pechora oil and gas province. Russian Academy of Science, Uralian Division, Komi Science Centre, Institute Geology, Ekaterinburg, pp. 1–133.

Tel'nova, O.P. 2008. Palynological characterization of the Givetian–Frasnian deposits in the reference borehole Section 1—Balneologicheskaya (southern Timan). Stratigraphy and Geological Correlation, 16, pp. 41–58. https://doi.org/10.1134/S0869593808020044

Tel'nova, O.P. and Marshall, J.E.A. 2009. New biostratigraphical subdivision at the Frasnian/Famennian boundary on the East European platform. Doklady, 429, pp. 1270–1272. https://doi.org/10.1134/S1028334X09080078

Torsvik, T.H. and Cocks L.R.M. 2017. Earth History and Palaeogeography, Cambridge University Press, 317 pp. https://doi.org/10.1017/9781316225523

Turnau, E. 1974. Microflora from core samples of some Palaeozoic sediments from beneath the flysch Carpathians (Bielsko–Wadowice area, southern Poland). Rocznik Polskiego Towarzystwa Geologicznego, 44, pp. 143–169.

Turnau, E. 1978. Spore zonation of uppermost Devonian and Lower Carboniferous deposits of western Pomerania (N. Poland). Mededelingen Rijks Geologische Dienst, 30-1, pp. 1–35.

Turnau, E. 2002. Two new Devonian spore genera from Euramerica and their stratigraphic and geographic distribution. Review of Palaeobotany and Palynology, 118, pp. 261–268. https://doi.org/10.1016/S0034-6667(01)00118-X

Turnau, E. and Narkiewicz, K. 2011. Biostratigraphical correlation of spore and conodont zonations within Givetian and ?Frasnian of the Lublin area (SE Poland). Review of Palaeobotany and Palynology, 164, pp. 30–38. https://doi.org/10.1016/j.revpalbo.2010.07.003

Turnau, E. and Racki, G. 1999. Givetian palynostratigraphy

and palynofacies: new data from the Bodzentyn Syncline (Holy Cross Mountains, central Poland). Review of Palaeobotany and Palynology, 106, pp. 237–271. https://doi.org/10.1016/S0034-6667(99)00011-1

Turnau, E., Avchimovitch, V.I., Byvscheva, T.V., Clayton, G., Higgs, K.T., and Owens, B. 1994. Taxonomy and stratigraphic distribution of *Verrucosisporites nitidus* Playford, 1964 and related species. Review of Palaeobotany and Palynology, 81, pp. 289–295. https://doi.org/10.1016/0034-6667(94)90113-9

Utting, J., Jachowicz, M., and Jachowicz, A. 1989. Palynology of the Lower Carboniferous Emma Fjord Formation of Devon, Axel Heiberg, and Ellesmere Islands, Canadian Arctic Archipelago. Contributions to Canadian Paleontology, 396, pp. 145–159. https://doi.org/10.4095/127721

Uyeno, T.T. and Bultynck, P. 1993. Lower to Middle Devonian conodonts of the Jaab Lake well, Moose River Basin, northern Ontario. Geological Survey of Canada, Bulletin, 444, pp. 7–35. https://doi.org/10.4095/183978

Van der Zwan, C.J. 1979. Aspects of Late Devonian and Early Carboniferous palynology of southern Ireland, I. The *Cyrtospora cristifer* morphon. Review of Palaeobotany and Palynology, 28, pp. 1–20. https://doi.org/10.1016/0034-6667(79)90020-4

Van der Zwan, C.J. and Walton, H.S. 1981. The *Cyrtospora cristifer* morphon: inclusion of *Cornispora varicornata* and *C. monocornata*. Review of Palaeobotany and Palynology, 33, pp. 139–152. https://doi.org/10.1016/0034-6667(81)90045-2

Van Veen, P.M. 1981. Aspects of Late Devonian and Early Carboniferous palynology of southern Ireland, IV morphological variation within *Diducites*, a new form genus to accommodate camerate spores with two layered outer wall. Review of Palaeobotany and Palynology, 31, pp. 261–287. https://doi.org/10.1016/0034-6667(80)90031-7

Vigran, J.O., 1964. Spores from Devonian deposits, Mimerdalen, Spitsbergen. Norsk Polarinstitutt Skrifter, 132, pp. 1–33.

Vigran, J.O., Stemmerik, L., and Piasecki, S. 1999. Stratigraphy and depositional evolution of the uppermost Devonian–Carboniferous (Tournaisian–Westphalian) non-marine deposits in North-East Greenland. Palynology, 23, pp. 115–152. https://doi.org/10.1080/01916122.1999.9989525

Vogt, T. 1941. Geology of a Middle Devonian cannel coal from Spitsbergen. Norsk Geologisk Tidsskrift, 21, pp. 1–12.

Wellman, C.H., Berry, C.M., Davies, N.S., Lindemann, F-J., Marshall, J.E.A., and Wyatt, A. 2022. Low tropical diversity during the adaptive radiation of early land plants. Nature Plants. https://doi.org/10.1038/s41477-021-01067-w

Whiteley, M.J. 1980. Givetian and Frasnian spores from the Key Point Well, Parry Islands, Arctic Canada. Review of Palaeobotany and Palynology, 29, pp. 301–311. https://doi.org/10.1016/0034-6667(80)90066-4

Winslow, M.R. 1962. Plant spores and other microfossils from Upper Devonian and Lower Mississippian rocks of Ohio. United States Geological Survey, Professional Paper 364, pp. 1–93. https://doi.org/10.3133/pp364

Xu, H-H, Marshall, J.E.A., Wang, Y., Zhu, H-C., Berry, C.M., and Wellman, C.H. 2014. Devonian spores from an intra-oceanic volcanic arc, West Junggar (Xinjiang, China) and the palaeogeographical significance of the associated fossil plant beds. Review of Palaeobotany and Palynology, 206, pp. 10–22. https://doi.org/10.1016/j.revpalbo.2014.03.002

Yolkin, E.A., Kim, A.I., Weddige, K., Talent, J.A., and House, M.R. 1998. Definition of the Pragian/Emsian Stage Boundary. Episodes, 20, pp. 235–240. https://doi.org/10.18814/epiiugs/1997/v20i4/005

Yushko, L.A. 1960. New species of microspores from the Cherepetsk deposit of the Tournaisian Stage from the Moscow Basin. *In* Data on geology and useful minerals of the central regions of the European part of the USSR. Paleontologiya i Regional'naya Geologiya Geologich Eskoe Upravlenie Tsentral'nykh Raionov, 3, pp. 121–137.

Editorial responsibility: Robert A. Fensome

APPENDIX A: TAXON NAMES WITH AUTHORSHIP CITATIONS

Note: we acknowledge that combinations by Avkhimovitch *et al* . 1993 have not been validly published, but to validate them is beyond the scope of the present work.

Acinosporites lindlarensis Riegel 1968
Ancyrospora Richardson 1960
Ancyrospora ancyrea (Eisenack 1944) Richardson 1962
Ancyrospora eurypterota Riegel 1973
Ancyrospora incisa (Naumova 1953) Raskatova and Obukovskaya in Avkhimovitch *et al* . 1993
Ancyrospora kedoae (Riegel 1973) Turnau 1974
Ancyrospora langii (Taugourdeau-Lantz 1960) Allen 1965
Ancyrospora loganii McGregor 1973
Ancyrospora longispinosa Richardson 1962
Ancyrospora nettersheimensis Riegel 1973
Archaeoperisaccus (Naumova 1953) McGregor 1969
Archaeoperisaccus indistinctus Lu 1988
Archaeoperisaccus rhacodes Hashemi and Playford 2005
Archaeoperisaccus timanicus Pashkevitch 1964
Archaeozonotriletes tamilii Filippova *et al.* 1958 (name not validly published — no description or illustration; synonym of *Cymbosporites magnificus* according to V.N. Mantsurova personal communication to JEAM 2014)
Archaeozonotriletes variabilis (Naumova 1953) Allen 1965
Archaeozonotriletes vorobjensis Naumova (name not validly published; synonym of *Cymbosporites magnificus* according to V.N. Mantsurova personal communication to JEAM 2014)
Chelinospora concinna Allen 1965
Cirratriradites avius Allen 1965
Cirratriradites monogrammos (Arkhangelskaya 1963) Arkhangelskaya 1985
Cirratriradites punctomonogrammos (Arkhangelskaya 1963) Arkhangelskaya 1985
Contagisporites Owens 1971
Contagisporites optivus (Chibrikova 1959) Owens 1971 (megaspore pairing to *Geminospora lemurata*)
Cornispora Staplin and Jansonius in Staplin 1961
Cornispora bicornata Nazarenko in Kedo *et al* . 1971
Cornispora monocornata Nazarenko in Kedo *et al* . 1971
Cornispora tricornata Nazarenko in Kedo *et al* . 1971
Cristatisporites deliquescens (Naumova 1953) Arkhangelskaya 1987
Cristatisporites triangulatus (Allen 1965) McGregor and Camfield 1982
Cymbosporites Allen 1965
Cymbosporites magnificus (McGregor 1960) McGregor and Camfield 1982
Cyrtospora Winslow 1962
Cyrtospora cristifera (Luber in Luber and Waltz 1941) Van der Zwan 1979
Densosporites Berry 1937
Densosporites devonicus Richardson 1960
Dictyotriletes emsiensis (Allen 1965) McGregor 1973
Diducites Van Veen 1981
Diducites poljessica (Kedo 1957) Van Veen 1981
Diducites versabilis (Kedo 1957) Van Veen 1981
Elenisporis biformis (Arkhangelskaya 1963) Arkhangelskaya 1985
Emphanisporites annulatus McGregor 1961
Geminospora Balme 1962
Geminospora lemurata (Balme 1962) Playford 1983
Geminospora micromanifesta (Naumova 1953) Arkhangelskaya 1985
Geminospora micropaxilla (Owens 1971) McGregor and Camfield 1982 (originally *Rhabdosporites micropaxillus*)
Geminospora svalbardiae (Vigran 1964) Allen 1965 (originally *Lycospora svalbardiae*)
Geminospora treverica Riegel 1973 (now *Acinosporites lindlarensis*)

APPENDIX A: continued.

Geminospora tuberculata (Kedo 1955) Allen 1965
Grandispora Hoffmeister *et al.* 1955
Grandispora protea (Naumova 1953) Moreau-Benoit 1980
Grandispora pseudodeliquescens Tel'nova and Marshall 2009.
Hymenozonotriletes domanicus Naumova 1953
Hymenozonotriletes lepidophytus var. *minor* Kedo 1963
Hystricosporites McGregor 1960
Indotriradites explanatus (Luber in Luber and Waltz 1941) Playford 1991
Knoxisporites literatus (Waltz in Luber and Waltz 1938) Playford 1963
Lagenoisporites immensus Nazarenko and Nekriata in Kedo *et al.* 1971
Lophozonotriletes malevkensis Naumova in Kedo 1963
Lycospora svalbardiae Vigran 1964 (now *Geminospora svalbardiae*)
Membraculisporis radiatus (Naumova 1953) Arkhangelskaya 1985
Nikitinsporites Chaloner 1959
Retispora Staplin 1960
Retispora archaeolepidophyta (Kedo 1955) McGregor and Camfield 1982
Retispora lepidophyta (Kedo 1957) Playford 1976
Retispora lepidophyta var. *minor* Kedo 1971
Retispora lepidophyta var. *tener* Prestianni *et al.* (2016)
Retispora macroreticulata (Kedo 1974) Byvsheva 1985
Rhabdosporites Richardson 1960
Rhabdosporites langii (Eisenack 1944) Richardson 1960
Rhabdosporites micropaxillus Owens 1971 (now *Geminospora micropaxilla*)
Rugospora radiata (Yushko 1960) Byvsheva 1985
Spelaeotriletes Neves and Owens 1966
Spelaeotriletes bellus (Naumova 1953) Obukhovskaya in Avkhimovitch *et al* . 1993
Spelaeotriletes domanicus (Naumova 1953) Obukhovskaya in Avkhimovitch *et al.* 1993
Spelaeotriletes krestovnikovii (Naumova 1953) Obukhovskaya in Avkhimovitch *et al.* 1993
Tergobulasporites immensus (Nazarenko and Nekriata in Nazarenko *et al.* 1971) Turnau 2002
(previously *Lagenoisporites immensus*)
Tumulispora malevkensis (Kedo 1957) Turnau 1978
Tumulispora rarituberculata (Luber in Luber and Waltz 1941) Playford 1991
Vallatisporites Hacquebard 1957
Vallatisporites anthoideus (Sennova in Nazarenkœt *al.* 1971 Braman and Hills 1992
Vallatisporites preanthoideus Braman andHills 1992
Vallatisporites pusillites (Kedo 1957) Dolby and Neves 1970
Vallatisporites verrucosus Hacquebard 1957
Verrucisporites submamillarius (McGregor 1960) Chi and Hills 1976a
Verrucosisporites nitidus (Naumova 1953) Playford 1964

APPENDIX B: SPREADSHEET SUMMARIZING PALYNOEVENTS

Event	Calibration
FO of *Dictyotriletes emsiensis*	Base of the Pragian
FO of *Acinosporites lindlarensis*	85% up the Emsian
FO of *Emphanisporites annulatus*	90% up the Emsian
FO of *Grandispora* spp.	90% up the Emsian
FO of *Elenisporis biformis*	2% up the Eifelian
FO of *Grandispora protea*	5% up the Eifelian
FO of *Ancyrospora ancyrea*	10% up the Eifelian
FO of *Ancyrospora k* edoae	10% up the Eifelian
FO of *Ancyrospora longispinosa*	10% up the Eifelian
FO of *Densosporites devonicus*	10% up the Eifelian
FO of *Retispora archaeolepidophyta*	20% up the Eifelian
FO of *Rhabdosporites langii*	20% up the Eifelian
FO of *Archaeozonotriletes variabilis*	50% up the Eifelian
FO of *Cirratriradites avius*	70% up the Eifelian
FO of *Cirratriradites monogrammos*	70% up the Eifelian
FO of *Cirratriradites punctomonogrammos*	70% up the Eifelian
FO of *Geminospora micropaxilla*	80% up the Eifelian
FO of *Geminospora lemurata*	Base of the Givetian
FO of *Cymbosporites magnificus*	5% up the Givetian
FO of *Cristatisporites triangulatus*	75% up the Givetian
FO of *Contagisporites optivus*	Base of the late Givetian
Acme of *Archaeoperisaccus* spp.	80% up the Givetian
FO of *Archaeoperisaccus timanicus*	80% up the Givetian
FO of *Chelinospora concinna*	80% up the Givetian
FO of *Ancyrospora* with multi-furcate tips	5% up the Frasnian
FO of *Spelaeotriletes domanicus*	5% up the Frasnian
FO of *Ancyrospora incisa*	10% up the Frasnian
FO of *Ancyrospora langii*	10% up the Frasnian
FO of *Archaeoperisaccus indistinctus*	15% up the Frasnian
FO of *Cristatisporites deliquescens*	20% up the Frasnian
FO of *Membraculisporis radiatus*	60% up the Frasnian
LO of *Archaeoperisaccus*	Base of the Famennian
FO of *Diducites* spp.	30% up the Famennian
FO of *Tergobulasporites immensus*	30% up the Famennian
FO of *Cornispora bicornuta*	30% up the Famennian
FO of *Cornispora monocornuta*	30% up the Famennian
FO of *Cornispora tricornuta*	30% up the Famennian
FO of *Retispora macroreticulata*	50% up the Famennian
FO of *Retispora lepidophyta*	80% up the Famennian
FO of *Knoxisporites literatus*	86% up the Famennian
FO of *Indotriradites explanatus*	87% up the Famennian
FO of *Tumulisporites malevkensis*	87% up the Famennian
FO of *Tumulisporites rarituberculata*	87% up the Famennian
FO of *Rugospora radiata*	90% up the Famennian
FO of *Retispora lepidophyta* var. *tener*	91% up the Famennian
FO of *Verrucosisporites nitidus*	99% up the Famennian
LO of *Ancyrospora* spp.	Base of the Tournaisian
LO of *Diducites* spp.	Base of the Tournaisian
LO of *Hystricosporites* spp.	Base of the Tournaisian
LO of *Retispora lepidophyta*	Base of the Tournaisian
LO of *Rugospora radiata*	Base of the Tournaisian

Reviewers

The Editors thank the following individuals who reviewed manuscripts (in some cases more than one) submitted to or published in Atlantic Geology in 2022, as well as nine others who chose to remain anonymous.

T. Burbery
J. A. D'Angelo
K. Dybkjaer
C. Eble
R. Hartlieb
A. Hunt
Graham Layne
D. Lentz
G. Lopes
Brendan Murphy
Kevin Neyedley
Geoff Playford
J. Powell
D. Shaw
Ryan Taylor
John Waldron
D. West